BEILSTEIN JOURNAL OF ORGANIC CHEMISTRY

Supramolecular chemistry II

Edited by Christoph A. Schalley

Imprint

Beilstein Journal of Organic Chemistry
www.bjoc.org
ISSN 1860-5397
Email: journals-support@beilstein-institut.de

The *Beilstein Journal of Organic Chemistry* is published by the Beilstein-Institut zur Förderung der Chemischen Wissenschaften.

Beilstein-Institut zur Förderung der Chemischen Wissenschaften
Trakehner Straße 7–9
60487 Frankfurt am Main
Germany
www.beilstein-institut.de

Beilstein Journal of Organic Chemistry

Supramolecular chemistry II

Christoph A. Schalley

Editorial

Open Access

Address:
Institut für Chemie und Biochemie - Organische Chemie, Freie Universität Berlin, Takustr. 3, 14195 Berlin, Germany

Email:
Christoph A. Schalley - schalley@chemie.fu-berlin.de

Beilstein J. Org. Chem. **2011,** *7,* 1541–1542.
doi:10.3762/bjoc.7.181

Received: 31 October 2011
Accepted: 04 November 2011
Published: 22 November 2011

This article is part of the Thematic Series "Supramolecular chemistry II".

Guest Editor: C. A. Schalley

Supramolecular chemistry is a rapidly growing field, which has had remarkable impact on the life sciences on one hand and on materials sciences on the other. In the life sciences, the networks of noncovalent interactions between the constituents of cells, for example, have shifted into the current focus. Self-assembly, templation, self-sorting and multivalent binding all contribute to setting up the extremely complex architecture of a cell. But the same concepts are useful for generating materials with function, when for example the building blocks are programmed appropriately to find their places in a larger, noncovalent architecture. The basis for all these concepts is molecular recognition. Recently, many studies have been devoted to quantifying host–guest interactions, aiming at a more profound understanding of the subtle entropic and enthalpic effects that govern the interactions between host and guest.

A first Thematic Series devoted to supramolecular chemistry was assembled about two years ago and published by the Beilstein Journal of Organic Chemistry [1]. This first series of articles had quite a broad scope ranging from encapsulation and carbohydrate, peptide, anion and ammonium ion binding, through chiral recognition, the formation of pseudorotaxanes and template effects, all the way to allosteric binding to synthetic receptors, crystallographic studies of halogen bonding and the use of polymers for protein binding.

The second series again has a broad scope, as you will discover in the coming months as the series develops. With the second Thematic Series on supramolecular chemistry, we wish to contribute to the endeavor to investigate noncovalently bound complexes and aggregates of every possible kind, thus highlighting the importance of the above-mentioned concepts.

With the now well-known Thematic Series, the Beilstein Journal of Organic Chemistry provides an excellent platform for this aim, in particular since it is a true open access journal.

I would like to thank warmly all authors who have accepted the invitation to contribute to this series and sincerely hope that the readers will enjoy reading the articles that are published within this Thematic Series.

Christoph A. Schalley

Berlin, October 2011

Reference

1. Schalley, C. A. *Beilstein J. Org. Chem.* **2009,** *5,* No. 76. doi:10.3762/bjoc.5.76
See for the editorial of the first Thematic Series on supramolecular chemistry in this journal.

Beilstein Journal of Organic Chemistry

NMR studies of anion-induced conformational changes in diindolylureas and diindolylthioureas

Damjan Makuc[1,2], Jennifer R. Hiscock[3], Mark E. Light[3], Philip A. Gale[*3] and Janez Plavec[*1,2,4]

Full Research Paper

Open Access

Address:
[1]Slovenian NMR Centre, National Institute of Chemistry, Hajdrihova 19, SI-1000 Ljubljana, Slovenia, [2]EN→FIST Centre of Excellence, Dunajska 156, SI-1000 Ljubljana, Slovenia, [3]Chemistry, University of Southampton, Southampton SO17 1BJ, United Kingdom and [4]Faculty of Chemistry and Chemical Technology, University of Ljubljana, SI-1000 Ljubljana, Slovenia

Email:
Damjan Makuc - damjan.makuc@ki.si; Jennifer R. Hiscock - J.Hiscock@soton.ac.uk; Mark E. Light - m.e.light@soton.ac.uk; Philip A. Gale* - philip.gale@soton.ac.uk; Janez Plavec* - janez.plavec@ki.si

* Corresponding author

Keywords:
anion recognition; conformation analysis; host–guest systems; NMR spectroscopy

Beilstein J. Org. Chem. **2011,** *7,* 1205–1214.
doi:10.3762/bjoc.7.140

Received: 31 May 2011
Accepted: 03 August 2011
Published: 02 September 2011

This article is part of the Thematic Series "Supramolecular chemistry II".

Guest Editor: C. A. Schalley

Abstract

The conformational properties of 1,3-diindolylureas and thioureas were studied by a combination of heteronuclear NMR spectroscopy and quantum mechanics calculations. NOE experiments showed that the *anti–anti* conformer along the C7–N7α bonds was predominant in DMSO-d_6 solution in the absence of anions. Anion-induced changes in the ^{1}H and ^{15}N chemical shifts confirm the weak binding of chloride anions with negligible conformational changes. Strong deshielding of ureido protons and moderate deshielding of indole NH was observed upon the addition of acetate, benzoate, bicarbonate and dihydrogen phosphate, which indicated that the predominant hydrogen bond interactions occurred at the urea donor groups. Binding of oxo-anions caused conformational changes along the C7–N7α bonds and the *syn–syn* conformer was preferred for anion–receptor complexes. The conformational changes upon anion binding are in good agreement with energetic preferences established by ab initio calculations.

Introduction

In the last two decades, remarkable efforts have been made in the field of the development of synthetic anion receptors, motivated by prospective applications in recognition, separation, guest inclusion and catalysis [1-13]. The fundamental role of anions in biological and chemical processes drives much of this research. Biomolecules such as the sulfate binding protein [14] and phosphate binding protein [15] employ hydrogen bonds as the key driving force to bind or transport anions through cell membranes. Hydrogen bonding interactions are extensively employed in synthetic anion receptors comprising groups such

as amides, pyrroles, indoles, ureas and triazoles, as well as in ammonium, guanidinium and imidazolium moieties used as hydrogen bond donors [16-23]. Amongst neutral anion receptor systems, indole and related heterocycles, such as carbazole, 2,2'-biindole and indolo[1,2-*b*]carbazoles, have recently attracted significant attention [24-31]. Indole contains a single hydrogen bond donor group, which is employed in biological systems to bind anions such as chloride [32] and sulfate [14].

We have recently analyzed the conformational preferences of several 2,7-disubstituted indoles with amide substituents at C2 and urea substituents at C7, which showed preference for distinct conformations in the presence and in the absence of anions [33-35]. In addition, indole and urea groups were strongly involved in hydrogen-bonding interactions with the bound anionic guest, whilst the amide group interacted only weakly with the bound anion. These observations led to the design of diindolylureas and diindolylthioureas [36-38]. These compounds have remarkably high affinities for oxo-anions such as phosphate and sulfate for neutral receptors in DMSO-d_6/0.5% water and have been shown to perturb the pK_a of bound guests (Table 1) [38,39]. X-ray crystal structures of a variety of complexes with anions revealed the adoption of the *syn–syn* conformation in the solid state upon anion complexation. With the urea analogues, such as **1**, this is accompanied by higher order complex formation with oxo-anions in the solid state. For example, with dihydrogen phosphate, three equivalents of receptor complex to a single anion, which has doubly deprotonated, resulting in the formation of a complex in which twelve hydrogen bonds stabilize the PO_4^{3-} anion. In solution, the thiourea analogues such as compound **2** show significantly lower affinities for oxo-anions than do the urea analogues. We had previously proposed that this may be due to the larger size of the sulfur atom resulting in a lower propensity of these systems to adopt a planar conformation. Whilst the conformational properties of these compounds have been explored by single crystal X-ray diffraction in the solid-state, a detailed analysis of the conformational properties of the these compounds in solution, in the absence and presence of oxo-anions, has yet to be performed and may help shed light on the high affinity of these systems for oxo-anions. Therefore, in the current work the conformational preorganization of bis-indole receptors **1**–**4** (Figure 1), as well as the conformational changes of these systems upon binding of chloride and several oxo-anions, were studied by NMR spectroscopy and supported by energetic preferences established from ab initio calculations.

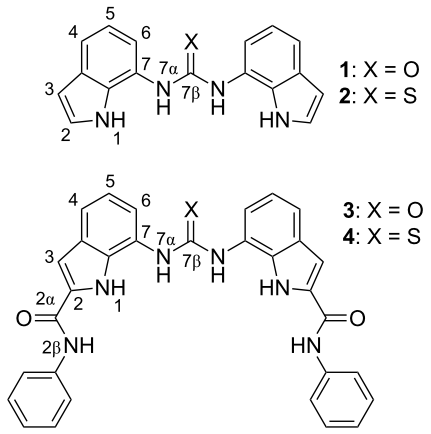

Figure 1: Anion receptors **1**–**4** together with their atomic numbering scheme.

Results and Discussion

Synthesis

Compounds **1**–**3** were synthesized following a previously reported methodology [36-39]. Compound **4** was prepared by reaction of 7-amino-*N*-phenyl-1*H*-indole-2-carboxamide (0.27 g, 1.07 mM) with 7-isothiocyanato-*N*-phenyl-1*H*-indole-2-carboxamide (0.31 g, 1.07 mM) in pyridine in 27% yield (see Supporting Information File 1 for details).

Structural features and NMR chemical shifts

The conformational properties of diindolylureas and diindolylthioureas **1**–**4**, shown in Figure 1, were evaluated by means of NMR spectroscopy. Proton and ^{13}C NMR resonances were

Table 1: Stability constants of compound **1** measured in DMSO-d_6/0.5% water, DMSO-d_6/10% water and DMSO-d_6/25% water and compound **2** in DMSO-d_6/0.5% water at 298 K by ^{1}H NMR titration techniques [37].

Anion[a]	Compound **1** in DMSO-d_6/0.5% water	Compound **1** in DMSO-d_6/10% water	Compound **1** in DMSO-d_6/25% water	Compound **2** in DMSO-d_6/0.5% water
Cl^-	128	17	–	74
$CH_3CO_2^-$	>10^4	774	20	1620
$C_6H_5CO_2^-$	>10^4	521	precipitate	477
$H_2PO_4^-$	>10^4	5170	160	1630

[a]Anions added as tetrabutylammonium salts.

assigned through 1D and 2D spectra, while ^{15}N chemical shifts were determined by ^{1}H–^{15}N correlations in HSQC and HMBC spectra. Notable ^{1}H and ^{15}N NMR chemical shifts of **1**–**4** are shown in Table 2. It should be noted that only one set of signals was observed for both indole rings in all four receptors, due to the symmetry of the compounds. The full NMR data set together with ^{13}C NMR chemical shifts is reported in Supporting Information File 1.

Indole NH proton resonances were found between 10.8 and 11.7 ppm. Thioureido containing compounds **2** and **4** exhibited slight downfield shifts of H1 and H7α with respect to ureido receptors **1** and **3** (Table 2). N1 chemical shifts showed only minor variations as a result of structural differences in **1**–**4**. The most significant differences in chemical shifts between the ureido and thioureido functionalized receptors were observed for H7α and N7α atoms ($\Delta\delta_H$ = 0.8 and $\Delta\delta_N$ = 22 ppm, Table 2). Compounds **3** and **4** contain phenylamide substituents at C2 and hence two more NH groups (Figure 1). Considerable deshielding of the H3 and H6 resonances was observed in **3** and **4** with respect to the nonsubstituted indole moieties in **1** and **2**. The downfield shift of δ_{H3} was attributed directly to the presence of the phenylamide group at C2. Deshielding of H6 (Δδ 0.4–0.5 ppm) in **3** and **4** with respect to **1** and **2**, respectively, was much larger than the deshielding of H4 (Δδ 0.1 ppm), possibly due to a more efficient conjugation.

^{1}H and ^{15}N NMR chemical shift changes in **1** upon addition of anions

Figure 2 shows ^{1}H chemical shift changes of **1** in the presence of one equivalent of chloride, acetate, benzoate, bicarbonate and dihydrogen phosphate anions. The protons that are most affected by anion–receptor interaction were found to be H1, H6 and H7α. Only minor $\Delta\delta_{H7\alpha}$ and negligible differences of δ_{H1} and δ_{H6} were observed in the presence of chloride anions (Figure 2a and Figure 2b). The very weak interactions between chloride and **1** could be due to competing interactions of the polar DMSO molecules for the hydrogen bond donor groups of the receptor, and the weak basicity of the chloride. This is supported by the stability constant determinations previously reported, and presented in Table 1. Considerable downfield shifts of $\delta_{H7\alpha}$ were observed upon addition of acetate, benzoate and bicarbonate anions (Δδ ≈ 2 ppm, Figures 2c–2e), which suggested strong interaction of ureido NH protons with these anions. In addition, the strong deshielding of indolyl H1 protons corroborates its participation in the hydrogen bond formation with carboxylate and bicarbonate moieties (Δδ ≈ 1 ppm). Planar oxo-anions interact both with H1 and H7α due to their Y-shaped geometry. The tetrahedral geometry of the dihydrogen phosphate anion allows strong interaction with all four hydrogen bond donor groups, which is reflected in the substantial deshielding of the H1 and H7α protons (Figure 2f). Interestingly, one set of signals was observed for each type of anion on

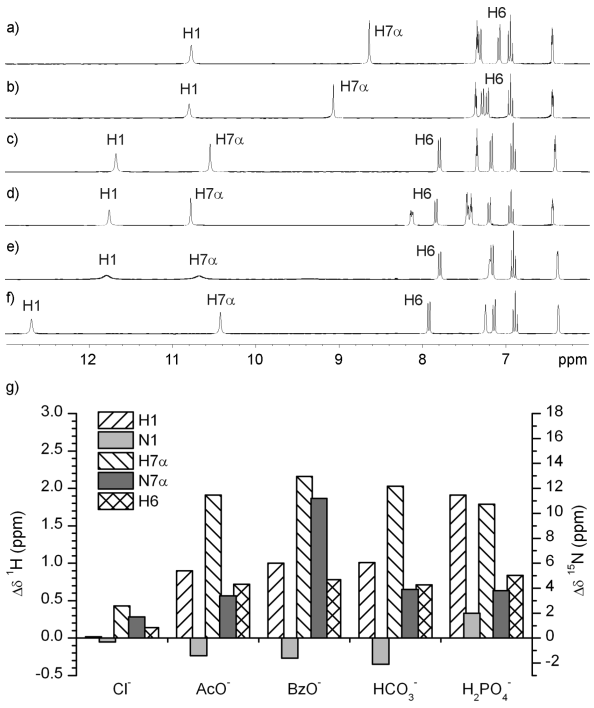

Figure 2: ^{1}H NMR spectra of **1** in the absence of anions (a) and upon addition of one equivalent of the following anions: Chloride (b), acetate (c), benzoate (d), bicarbonate (e) and dihydrogen phosphate (f). All spectra were recorded in DMSO-d_6 at 298 K. (g) ^{1}H and ^{15}N NMR chemical shift changes, Δδ = δ (in the presence of anion) – δ (in the absence of anions), induced by addition of one equivalent of different anions to receptor **1**.

Table 2: Selected ^{1}H and ^{15}N NMR chemical shifts for **1**–**4** (in ppm).[a]

	H1	H2β	H7α	H2	H3	H6	N1	N2β	N7α
1	10.78	–	8.64	7.35	6.44	7.08	136.5	–	102.7
2	11.03	–	9.48	7.36	6.46	7.03	136.3	–	124.9
3	11.62	10.29	8.97	–	7.49	7.59	134.5	128.6	104.6
4	11.68	10.26	9.72	–	7.48	7.39	134.9	129.0	126.6

[a]In DMSO-d_6 at 298 K.

the NMR timescale, which suggested that the symmetry of the receptor **1** is preserved upon interactions with anions. The stability constant determinations presented in Table 1 also support the finding that this compound interacts selectively with oxo-anions.

Anion–receptor interactions assessed by ^{1}H chemical shift changes were corroborated by ^{15}N NMR data. Weak shielding of N1 in **1** was observed upon addition of acetate, benzoate and bicarbonate anions, whereas addition of dihydrogen phosphate anions led to deshielding of N1 (Figure 2g). In contrast, N7α was deshielded upon addition of anions (Figure 2g). The strongest deshielding of 11.2 ppm was observed for the **1**·BzO^{-} complex.

Conformational properties of **1** and its complexes with anions

The rotational flexibility of the ureido moiety allows numerous conformations of receptor **1**. Among them three major, energetically preferred, conformers are likely to be observed (Figure 3). The *syn–syn* conformer, where NH protons form a convergent hydrogen-bonding array, is expected to be adopted in the presence of bound anionic guests, based on the previous solid-state studies. On the other hand, this conformer is unlikely to be abundant in the absence of anions, due to repulsion between the hydrogen bond donor groups. The other two rotamers, namely *anti–anti* and *syn–anti*, can be stabilized by intramolecular NH–CO hydrogen bonds, which represent competition to anion–receptor interactions and therefore make conformational studies even more appealing.

The conformational characteristics of diindolylurea **1** were assessed by the use of 1D difference NOE experiments in the absence and in the presence of anions. The orientation along the C7–N7α bonds was established by comparative evaluation of NOE enhancements of H7α with H1 and H6 protons. The saturation of H7α in **1** gave strong NOE at H6 (10.4%) and moderate NOE at H1 (4.3%), which suggested that the *anti* orientation prevails along the linkage between ureido moiety and indole ring (Figure 4a). As the observed NOE enhancements are primarily a function of the H6–H7α and H1–H7α distances, we compared their values in the optimized *anti–anti* (d(H6–H7α) = 2.28 Å) and *syn–syn* (d(H1–H7α) = 2.32 Å) structures and established a minor difference of 0.04 Å which would be reflected in a 1% change in the NOE enhancements. The observed difference between NOE enhancements in the uncomplexed form of receptor **1** was over 6%, which led us to conclude that the *anti–anti* conformer is predominant in the DMSO-d_6 solution. In addition, the *anti–anti* conformer of **1** with its plane of symmetry along the carbonyl bond is in agreement with the single set of resonances in the NMR spectra. On the other hand, the *syn–anti* rotamer shows a twofold rotational

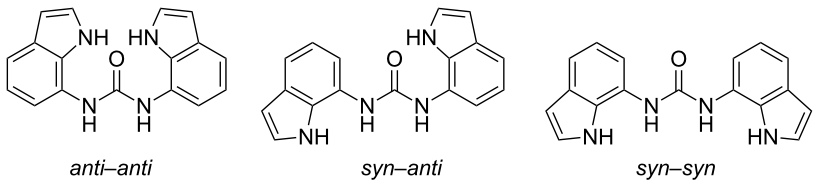

Figure 3: Three representative conformational families of rotamers of **1**. Notations refer to the orientations along [C6–C7–N7α–C7β] fragments.

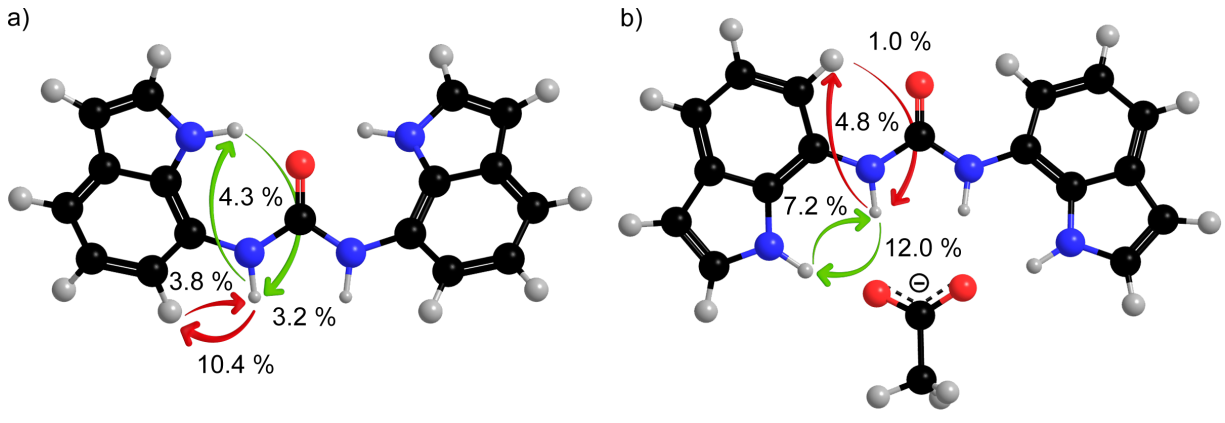

Figure 4: NOE enhancements of **1** in the absence of anions (a) and upon addition of one equivalent of acetate anions (b).

symmetry and is expected to exhibit distinct shielding of nuclei, imposed by the orientations of H6 and H1 protons in the two indole rings with respect to the carbonyl group. However, the populations of the two distinct conformational families are averaged on the NMR time scale.

Only minor changes in the NOE enhancements were observed upon addition of chloride anions to **1**. The strongest NOE was observed between H7α and H6 (9.9%), which was of comparable magnitude to the NOE between the same protons in the absence of anions (Table 3). On the other hand, stronger NOE enhancement between H7α and H1 (7.0%) suggested predominance of the *syn–anti* rotamer of **1** in the presence of chloride anions in DMSO-d_6 solution. Interestingly, the *syn–syn* rotamer was observed in the crystal structure, where conformational preferences are dictated by other forces, such as crystal packing. These observations are in agreement with minute ^{1}H chemical shift changes and the weak stability constant of **1** for the binding of chloride anions.

Table 3: Selected NOE enhancements for **1** in the absence and in the presence of different anions (in %).

Saturated:	H1	H6	H7α	
Enhanced:	H7α	H7α	H1	H6
no anion	3.2	3.8	4.3	10.4
Cl^-	4.2	2.2	7.0	9.9
AcO^-	7.2	1.0	12.0	4.8
BzO^-	7.2	0.9	10.4	4.8
HCO_3^-	–[a]	0.0	–[a]	4.7
$H_2PO_4^-$	4.2	0.0	5.3	2.8

[a]Broad NH signals in the baseline.

Considerable changes in the NOE enhancements were observed upon addition of acetate anions to **1**. The saturation of H7α resulted in a much stronger NOE at H1 (12.0%) with respect to H6 (4.8%), which suggested that addition of acetate anions led to conformational changes along the C7–N7α bond (Table 3). The *syn–syn* conformer is preferred for the **1**·AcO^- complex in solution (Figure 4b). In a similar manner, significant changes in the NOEs were observed upon addition of benzoate anions. The saturation of H7α gave much stronger NOE at H1 (10.4%) with respect to H6 (4.8%, Table 3). Broad NH proton signals prevented the study of the conformation of the **1**·HCO_3^- complex through NOE experiments. NOE enhancements between H1 and H7α (4.2–5.3%) were considerably stronger with respect to NOE between H7α and H6 (0–2.8%) upon addition of dihydrogen phosphate to **1**. The observed NOE enhancements for **1**·$H_2PO_4^-$ complex suggest a preference for the *syn–syn* conformer in DMSO-d_6.

Conformational analysis of **1** and its anion complexes by quantum mechanics calculations

The observations on the conformational equilibria in the absence and in the presence of anions were corroborated by quantum mechanical calculations at the B3LYP/6-311+G(d,p) level of theory by means of the Gaussian 03 [40] and Gaussian 09 [41] programs. Indole rings represent the rigid part of the anion receptors, while the substituents on the ureido moiety in **1** exhibit conformational freedom. [C6–C7–N7α–C7β] torsion angles were defined to follow energetic changes induced by reorientation of the indolyl moieties along the C7–N7α bonds. The energy surface for the [C6–C7–N7α–C7β] torsion angles, with 30° resolution, shows that the conformer with the lowest energy is in the *anti–anti* region (Figure 5).

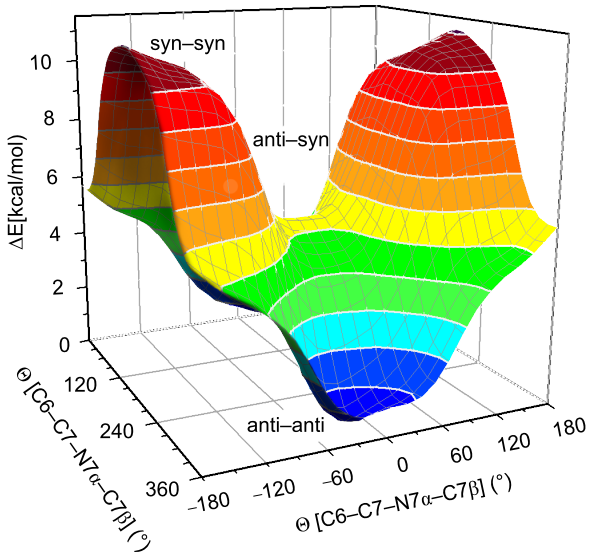

Figure 5: Surface plot of the relative potential energy of **1** as a function of the two constitutive [C6–C7–N7α–C7β] torsion angles. Individual geometries were optimized at the B3LYP/6-311+G(d,p) level of theory at 30° resolution.

Energy minimization of the *anti–anti* conformer of **1** was performed without any constraints, whereas *syn* orientations in the *syn–anti* as well as the *syn–syn* cases were restrained along the [C6–C7–N7α–C7β] torsion angle, while other degrees of freedom were freely optimized. The relative energies for the three representative conformers are reported in Table 4. The *anti–anti* conformer of **1** was found to be the lowest in energy, while the *syn–syn* conformer showed considerably higher energy (11.6 kcal·mol^{-1}). The angle between the two indolyl rings in the freely optimized *anti–anti* conformer was 53.9° (Figure 6a). The relative energies of the three representative conformers were also computed for complexes of **1** with chloride, acetate and bicarbonate anions. The *syn–syn* conformer exhibited the lowest relative energy for all three anion–receptor

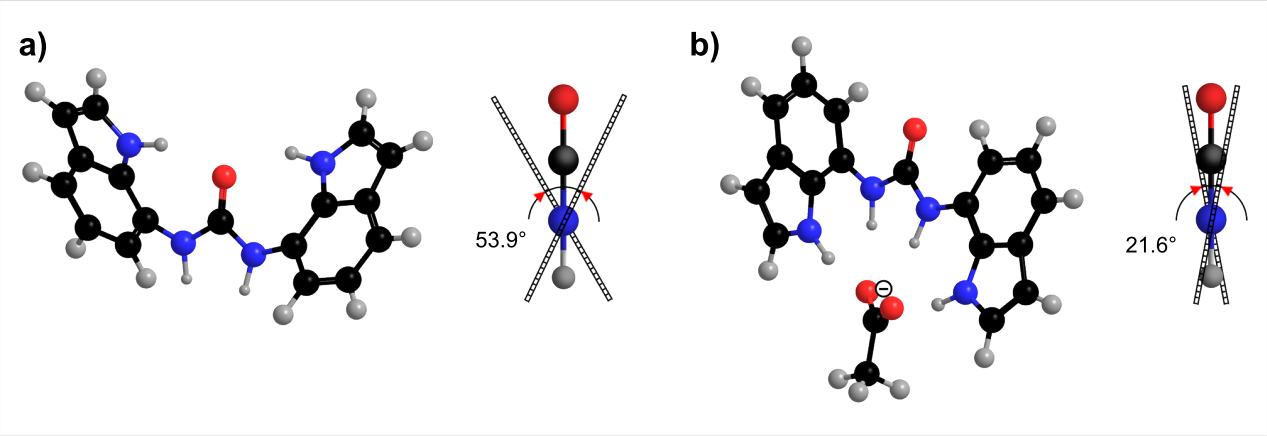

Figure 6: Freely optimized structure at the B3LYP/6-311+G(d,p) level of theory and side view showing deviation from coplanarity defined by the angle between the indolyl rings of receptor **1** in the absence of anions (a) and for the **1**·AcO⁻ complex (b).

complexes (Table 4). The *anti–anti* conformers of anion–receptor complexes exhibited considerably higher energies between 6.2 and 7.3 kcal·mol^{-1}. The angle between the two indolyl rings in the freely optimized *syn–syn* conformer of the **1**·AcO⁻ complex was found to be 21.6° (Figure 6b). The optimized structure, shown in Figure 6b, shows a single acetate anion bound to the four NH groups in the receptor **1** with N···O distances in the range from 2.75 to 2.95 Å and N–H···O angles in the range 170–176°.

Table 4: Relative energies[a] (in kcal·mol^{-1}) of receptor **1** in vacuo and in DMSO, in the absence and in the presence of anions.

anion	conformer	in vacuo	in DMSO
no anion	*anti–anti*	0.00	0.00
	syn–anti	5.09	2.74
	syn–syn	11.61	6.60
Cl⁻	*anti–anti*	6.50	1.20
	syn–anti	1.84	0.12
	syn–syn	0.00	0.00
AcO⁻	*anti–anti*	7.26	3.75
	syn–anti	2.82	1.74
	syn–syn	0.00	0.00
HCO_3^-	*anti–anti*	6.21	2.97
	syn–anti	2.02	1.31
	syn–syn	0.00	0.00

[a]Relative energies are reported with respect to the lowest energy (arbitrarily set to 0.00 kcal/mol) in the absence and in the presence of anions. Geometry optimizations were carried out at B3LYP/6-311+G(d,p).

In order to evaluate the role of DMSO on the energetic preferences of rotamers, relative energies were calculated with the use of Tomasi's polarized continuum model [42,43]. Preferences amongst the three rotamers were retained (Table 4). Only small differences below 1.2 kcal·mol^{-1} were found between the three distinct conformers in the case of the **1**·Cl⁻ complex. In particular, the negligible energy differences between *syn–syn* and *syn–anti* rotamers are in agreement with the NOE data that suggested predominance of the *syn–anti* conformer upon addition of chloride. The energetic preference of the *syn–syn* over the *anti–anti* conformer of 3.8 and 3.0 kcal·mol^{-1} was observed for the **1**·AcO⁻ and the **1**·HCO_3^- complexes, respectively (Table 4). The energetic preferences of the **1**·AcO⁻complex are in excellent agreement with the NOE experiments, which showed conformational reorganizations of **1** upon addition of acetate anions.

Conformational features of receptors 2–4

The choice of thio (**2** and **4**) versus oxo (**1** and **3**) ureido functionalities, as well as the C2 functionalization of the indole scaffolds with pendant phenyl amides in **3** and **4**, allows tuning of the binding affinities of the receptors. Negligible Δδ values were observed for **2** upon interaction with chloride anions (Figure 7a), which suggests a very weak interaction between chloride and **2**, similar to the weak interactions observed between chloride and **1**. Chemical shift changes showed that the main interaction between receptor **2** and trigonal planar anions (acetate, benzoate and bicarbonate) occurred at the H7α protons (Figure 7a). Addition of dihydrogen phosphate anions caused considerable deshielding of the H1 and H7α protons. Comparison of the Δδ values for **1** and **2** upon interaction with the anions showed that the urea derivative **1** exhibited a higher preference for anion binding relative to thiourea **2** (the data were supported by the stability constant determinations performed previously and shown in Table 1). The larger sulfur atom can prevent the receptor **2** from adopting a planar conformation, which may reduce the affinity of this receptor for anionic

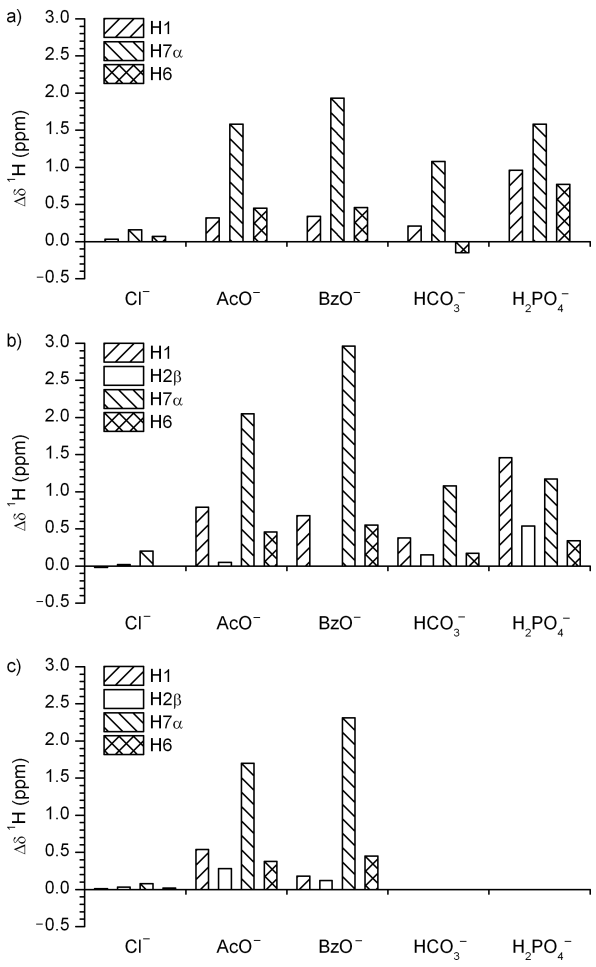

Figure 7: ^{1}H NMR chemical shift changes, Δδ = δ (in the presence of anions) – δ (in the absence of anions), induced by addition of one equivalent of different anions to receptors **2** (a), **3** (b) and **4** (c). Note, there is no H2β proton in **2**.

guests. Conformational studies of **2** with the use of NOE enhancements showed that the *anti–anti* conformer is the preferred conformation in the absence of anions. No apparent conformational changes were observed upon addition of chloride anions to **2**. The overlap of the proton signals as well as the broad line-width of the H1 and H7α NMR resonances prevented conformational analysis of **2** upon addition of other anions used in the study. The conformational preferences of **2** were evaluated by quantum mechanical calculations at the B3LYP/6-311+G(d,p) level of theory. The freely optimized *anti–anti* conformer of **2** exhibited the lowest energy and the *syn–syn* conformer was 8.0 kcal·mol^{-1} higher in energy, in vacuo. Interestingly, the two indolyl rings were not coplanar, with the angle between the two indolyl planes found to be 98.9° (Figure 8a). In the case of **2**·AcO$^-$ complex the *syn–syn* conformer exhibited the lowest energy, while the *anti–anti* conformer was 7.4 kcal·mol^{-1} higher in energy, in vacuo. The optimized structure of **2**·AcO$^-$ complex is shown in Figure 8b, where the two acetate oxygen atoms are hydrogen bonded to the four NH groups, with N···O distances in the range from 2.76 to 2.94 Å and N–H···O angles in the range 168–177°. The angle between the indolyl rings in the freely optimized *syn–syn* conformer of the **2**·AcO$^-$ complex was 68.0°.

Bis-amide functionalized diindolylurea **3** exhibits two extra NH groups, which introduces additional possibilities for interactions with anions. The addition of chloride anions to **3** induced negligible chemical shifts, suggesting only weak interactions with this anion (Figure 7b). The strong deshielding of H7α and moderate deshielding of H1 protons in the **3**·AcO$^-$ and **3**·BzO$^-$ complexes suggests a significant interaction between the anions and the ureido functionality. Interestingly, negligible deshielding of H2β in **3** was observed and this suggests that the amide protons do not participate in the interaction with acetate

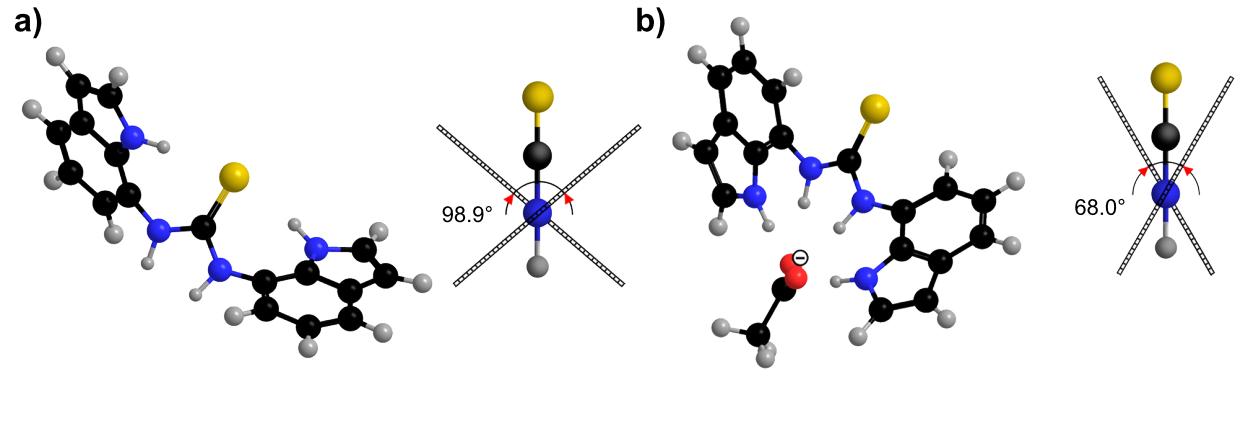

Figure 8: Freely optimized structures at the B3LYP/6-311+G(d,p) level of theory and side view showing deviation from coplanarity defined by the angle between the indolyl rings of **2** (a) and **2**·AcO$^-$ complex (b).

and benzoate (Figure 7b). The observed Δδ values support the idea that carboxylates were strongly bound to the urea H7α protons which prevented interaction between the anions and the amide H2β protons. Analogously, large chemical shift changes of up to 1 ppm were observed for the H7α and H1 protons upon the addition of bicarbonate anions to **3**. Strong deshielding of H1, H2β and H7α protons in the **3**·$H_2PO_4^-$ complex suggests that all the NH donor groups are involved in interactions with the dihydrogen phosphate anions (Figure 7b).

The conformational properties of **3** and of its complexes with different anions were studied by NOE measurements. The saturation of the H1 protons resulted in moderately negative NOEs at the H7α and H2β protons. The cross peaks in the 2D NOESY spectra between the NH protons and bulk water suggest chemical exchange that complicated the conformational study along the C2–C2α and C7–N7α bonds. Nevertheless, strong NOE enhancements between the H2β and H3 protons suggest an orientation along the C2–C2α bond where the H2β and H3 protons are spatially close and the C2α carbonyl group is oriented towards the indole H1 proton. NOE enhancements between H2β and H3 protons were observed also in the **3**·AcO^- and **3**·BzO^- complexes, which suggests that the orientation of the carboxamide group along the C2–C2α bond is retained in **3** upon addition of carboxylate anions. This observation was supported by negligible Δδ values for the H2β protons in the **3**·AcO^- and **3**·BzO^- complexes with respect to **3**. The conformational preferences and the proposed binding mode in the **3**·AcO^- complex are shown in Figure 9. A conformational study of **3** in the presence of bicarbonate and dihydrogen phosphate anions was hindered by the broadened and overlapped ^{1}H signals. In the solid state compound **3** crystallized with tetrabutylammonium dihydrogen phosphate as the monohydrogen phosphate complex [38].

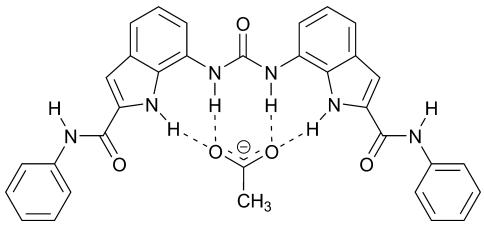

Figure 9: Conformational preferences and proposed binding mode for the **3**·AcO^- 1:1 complex.

Only negligible chemical shifts were observed for **4** upon addition of chloride anions (Figure 7c). Considerable deshielding of H7α protons in **4** by up to 2.3 ppm in the **4**·AcO^- and **4**·BzO^- complexes suggested that the major interactions between carboxylates and receptor **4** occurred at the ureido functionality (Figure 7c). The conformational properties of the **4**·AcO^- and **4**·BzO^- complexes could not be determined due to the broad and overlapped proton signals. Unfortunately, excessively broad and overlapped ^{1}H signals for the **4**·HCO_3^- and **4**·$H_2PO_4^-$ complexes prevented unambiguous assignment of the NMR resonances and hence the conformational studies of these complexes. In the solid state compound **4** crystallized with tetrabutylammonium dihydrogen phosphate as the monohydrogen phosphate complex (see Supporting Information File 2 for more details).

Conclusion

The bis-indole receptors **1**–**4** were characterized by heteronuclear NMR spectroscopy. NOE based conformational analysis was supported by quantum mechanics calculations and revealed that diindolylurea **1** exhibited conformational preorganization in DMSO-d_6 solution. The *anti–anti* conformer, which could be stabilized by intramolecular hydrogen bonds between the C7β carbonyl group and indole NH proton, was predominant for **1** in the absence of anions. The energetically minimized structure of *anti–anti* conformer showed a plane of symmetry along the ureido carbonyl group and deviation from coplanarity amongst the indolyl rings. Anion-induced chemical shift changes suggested weak binding of chloride anions and negligible conformational changes for **1**. Addition of acetate, benzoate, bicarbonate and dihydrogen phosphate resulted in strong deshielding of the ureido protons and moderate deshielding of the indole H1, which indicated that the main hydrogen bond interaction occurred at the urea donor groups of **1**. Furthermore, binding of anions caused conformational changes along the C7–N7α bonds, and the *syn–syn* conformer was predominant in the anion–receptor complexes according to both NOE enhancements and ab initio calculations in solution. The freely optimized *syn–syn* conformer of the **1**·AcO^- complex retained a plane of symmetry along the carbonyl bond and showed a smaller deviation from indole ring coplanarity than did the *anti–anti* conformer of **1**. The conformational preferences for **2** were analogous to those observed for receptor **1**. Unfortunately, excessively broad and overlapped ^{1}H signals prevented a detailed conformational analysis of the anion–receptor complexes for **3** and **4**.

Experimental

NMR experiments

^{1}H, ^{13}C and ^{15}N NMR spectra were acquired on a Varian Unity Inova 300 MHz NMR spectrometer. All data were recorded in DMSO-d_6 at 298 K. Chemical shifts were referenced to the residual solvent signal of DMSO-d_6 at δ 2.50 ppm for ^{1}H (297.801 MHz) and δ 39.50 ppm for ^{13}C (76.190 MHz), while ^{15}N (30.188 MHz) chemical shifts were referenced relative to external benzamide (δ 103.55 ppm). Individual resonances were

assigned on the basis of their chemical shifts, signal intensities, multiplicity of resonances, H–H coupling constants as well as by means of a series of 2D NMR experiments (COSY, gHSQC and gHMBC). The saturation delay in the 1D difference NOE experiment was 5.0 s. All anions were added as tetrabutylammonium salts except bicarbonate which was added as a tetraethylammonium salt. NOESY spectra were acquired with mixing time of 100 and 300 ms.

Ab initio calculations

Initial structures were generated by Chem3D Pro 10.0 software and energy minimization at the B3LYP/6-311+G(d,p) level was performed for **1** and **2** without any constraints for the *anti–anti* conformers, by means of Gaussian 03 [40] and Gaussian 09 [41]. *Syn* orientations in the *syn–anti* as well as the *syn–syn* conformers of **1** and **2** were restrained along the [C6–C7–N7α–C7β] torsion angle while other degrees of freedom were freely optimized. Ab initio calculations of anion–receptor complexes were carried out without any constraints for the *syn–syn* conformers, where anions were placed initially at the expected equilibrium distance to the H1 and H7α protons. The positions of the anions were freely optimized. Energy minimizations of the *syn–anti* and *anti–anti* conformers of the anion–receptor complexes were restrained along the [C6–C7–N7α–C7β] torsion angle while other degrees of freedom were freely optimized. The tetrabutylammonium countercation was omitted in the geometry optimization of the anion–receptor complexes. Frequency calculations verified that the optimized geometries were stable points on the potential energy surface. Relative energies in solution were calculated by means of Tomasi's polarized continuum model, where the dielectric constant of DMSO was used (ε = 46.7).

Supporting Information

Supporting Information File 1

Experimental for the synthesis of compound **4** and details of the crystal structure of the HPO_4^{2-} complex of **4**, ^1H and ^{13}C NMR data for **1**–**4**, 1D difference NOE spectra for **1** in the absence and upon addition of one equivalent of acetate anions.
[http://www.beilstein-journals.org/bjoc/content/supplementary/1860-5397-7-140-S1.pdf]

Supporting Information File 2

Crystallographic data of the complex of compound **4** with tetrabutylammonium dihydrogen phosphate (**4**·TBA_2·HPO_4).
[http://www.beilstein-journals.org/bjoc/content/supplementary/1860-5397-7-140-S2.cif]

Acknowledgements

We gratefully acknowledge the financial support of the Slovenian Research Agency (ARRS, program no. P1-0242), COST D-31, EAST-NMR (grant no. 228461) and Bio-NMR (grant no. 261863) FP7 projects. PAG thanks the EPSRC for support and the access to the crystallographic facilities at the University of Southampton.

References

1. Bianchi, A.; Bowman-James, K.; García-España, E., Eds. *Supramolecular Chemistry of Anions;* Wiley-VCH: New York, 1997.
2. Schmidtchen, F. P.; Berger, M. *Chem. Rev.* **1997,** *97,* 1609. doi:10.1021/cr9603845
3. Beer, P. D. *Acc. Chem. Res.* **1998,** *31,* 71. doi:10.1021/ar9601555
4. Kavallieratos, K.; Bertao, C. M.; Crabtree, R. H. *J. Org. Chem.* **1999,** *64,* 1675. doi:10.1021/jo982382l
5. Beer, P. D.; Gale, P. A. *Angew. Chem., Int. Ed.* **2001,** *40,* 486. doi:10.1002/1521-3773(20010202)40:3<486::AID-ANIE486>3.0.CO;2-P
6. Wiskur, S. L.; Ait-Haddou, H.; Lavigne, J. J.; Anslyn, E. V. *Acc. Chem. Res.* **2001,** *34,* 963. doi:10.1021/ar9600796
7. Vilar, R. *Angew. Chem., Int. Ed.* **2003,** *42,* 1460. doi:10.1002/anie.200200551
8. Bowman-James, K. *Acc. Chem. Res.* **2005,** *38,* 671. doi:10.1021/ar040071t
9. Gale, P. A. *Acc. Chem. Res.* **2006,** *39,* 465. doi:10.1021/ar040237q
10. Sessler, J. L.; Gale, P. A.; Cho, W. S. *Anion Receptor Chemistry;* Royal Society of Chemistry: Cambridge, 2006.
11. Albrecht, M. *Naturwissenschaften* **2007,** *94,* 951. doi:10.1007/s00114-007-0282-7
12. Lankshear, M. D.; Beer, P. D. *Acc. Chem. Res.* **2007,** *40,* 657. doi:10.1021/ar7000217
13. Vilar, R. *Eur. J. Inorg. Chem.* **2008,** 357. doi:10.1002/ejic.200701017
14. Pflugrath, J. W.; Quiocho, F. A. *Nature* **1985,** *314,* 257. doi:10.1038/314257a0
15. Luecke, H.; Quiocho, F. A. *Nature* **1990,** *347,* 402. doi:10.1038/347402a0
16. Bondy, C. R.; Loeb, S. J. *Coord. Chem. Rev.* **2003,** *240,* 77. doi:10.1016/S0010-8545(02)00304-1
17. Gómez, D. E.; Fabbrizzi, L.; Licchelli, M.; Monzani, E. *Org. Biomol. Chem.* **2005,** *3,* 1495. doi:10.1039/b500123d
18. Kang, S. O.; Begum, R. A.; Bowman-James, K. *Angew. Chem., Int. Ed.* **2006,** *45,* 7882. doi:10.1002/anie.200602006
19. Gale, P. A.; García-Garrido, S. E.; Garric, J. *Chem. Soc. Rev.* **2008,** *37,* 151. doi:10.1039/b715825d
20. Caltagirone, C.; Gale, P. A. *Chem. Soc. Rev.* **2009,** *38,* 520. doi:10.1039/b806422a
21. Gale, P. A. *Chem. Commun.* **2005,** 3761. doi:10.1039/b504596g
22. Gale, P. A. *Chem. Soc. Rev.* **2010,** *39,* 3746. doi:10.1039/c001871f
23. Gale, P. A. *Chem. Commun.* **2011,** *47,* 82. doi:10.1039/c0cc00656d
24. Chmielewski, M. J.; Charon, M.; Jurczak, J. *Org. Lett.* **2004,** *6,* 3501. doi:10.1021/ol048661e
25. Piatek, P.; Lynch, V. M.; Sessler, J. L. *J. Am. Chem. Soc.* **2004,** *126,* 16073. doi:10.1021/ja045218q
26. Chang, K.-J.; Moon, D.; Lah, M. S.; Jeong, K.-S. *Angew. Chem., Int. Ed.* **2005,** *44,* 7926. doi:10.1002/anie.200503121
27. Curiel, D.; Cowley, A.; Beer, P. D. *Chem. Commun.* **2005,** 236. doi:10.1039/b412363h

28. Pfeffer, F. M.; Lim, K. F.; Sedgwick, K. J. *Org. Biomol. Chem.* **2007,** *5,* 1795. doi:10.1039/b702804k
29. Chmielewski, M. J.; Zhao, L. Y.; Brown, A.; Curiel, D.; Sambrook, M. R.; Thompson, A. L.; Santos, S. M.; Felix, V.; Davis, J. J.; Beer, P. D. *Chem. Commun.* **2008,** 3154. doi:10.1039/b804941f
30. Suk, J.-m.; Chae, M. K.; Kim, N.-K.; Kim, U.-I.; Jeong, K.-S. *Pure Appl. Chem.* **2008,** *80,* 599. doi:10.1351/pac200880030599
31. Zhao, L.; Mullen, K. M.; Chmielewski, M. J.; Brown, A.; Bampos, N.; Beer, P. D.; Davis, J. J. *New J. Chem.* **2009,** *33,* 760. doi:10.1039/b818854h
32. Verschueren, K. H. G.; Seljée, F.; Rozeboom, H. J.; Kalk, K. H.; Dijkstra, B. W. *Nature* **1993,** *363,* 693. doi:10.1038/363693a0
33. Makuc, D.; Lenarčič, M.; Bates, G. W.; Gale, P. A.; Plavec, J. *Org. Biomol. Chem.* **2009,** *7,* 3505. doi:10.1039/b908947k
34. Makuc, D.; Triyanti; Albrecht, M.; Plavec, J.; Rissanen, K.; Valkonen, A.; Schalley, C. A. *Eur. J. Org. Chem.* **2009,** *2009,* 4854. doi:10.1002/ejoc.200900721
35. Makuc, D.; Albrecht, M.; Plavec, J. *Supramol. Chem.* **2010,** *22,* 603. doi:10.1080/10610278.2010.506544
36. Caltagirone, C.; Gale, P. A.; Hiscock, J. R.; Brooks, S. J.; Hursthouse, M. B.; Light, M. E. *Chem. Commun.* **2008,** 3007. doi:10.1039/b806238b
37. Caltagirone, C.; Hiscock, J. R.; Hursthouse, M. B.; Light, M. E.; Gale, P. A. *Chem.–Eur. J.* **2008,** *14,* 10236. doi:10.1002/chem.200801639
38. Gale, P. A.; Hiscock, J. R.; Moore, S. J.; Caltagirone, C.; Hursthouse, M. B.; Light, M. E. *Chem.–Asian J.* **2010,** *5,* 555. doi:10.1002/asia.200900230
39. Gale, P. A.; Hiscock, J. R.; Jie, C. Z.; Hursthouse, M. B.; Light, M. E. *Chem. Sci.* **2010,** *1,* 215. doi:10.1039/c0sc00202j
40. *Gaussian 03,* Revision B.3; Gaussian, Inc.: Pittsburgh PA, 2004.
41. *Gaussian 09,* Revision A.5; Gaussian, Inc.: Wallingford CT, 2009.
42. Miertus, S.; Scrocco, E.; Tomasi, J. *Chem. Phys.* **1981,** *55,* 117. doi:10.1016/0301-0104(81)85090-2
43. Miertus, S.; Tomasi, J. *Chem. Phys.* **1982,** *65,* 239. doi:10.1016/0301-0104(82)85072-6

License and Terms

Beilstein Journal of Organic Chemistry

Highly efficient cyclosarin degradation mediated by a β-cyclodextrin derivative containing an oxime-derived substituent

Michael Zengerle[1], Florian Brandhuber[2], Christian Schneider[1], Franz Worek[2], Georg Reiter[2] and Stefan Kubik[*1]

Full Research Paper

Open Access

Address:
[1]Fachbereich Chemie - Organische Chemie, Technische Universität Kaiserslautern, Erwin-Schrödinger-Straße, D-67663 Kaiserslautern, Germany, Fax: +49-631-205-3921 and [2]Institut für Pharmakologie und Toxikologie der Bundeswehr, Neuherbergstraße 11, D-80937 München, Germany

Email:
Stefan Kubik[*] - kubik@chemie.uni-kl.de

* Corresponding author

Keywords:
acetylcholinesterase; cyclodextrins; cyclosarin; neurotoxic organophosphonates; oximes

Beilstein J. Org. Chem. **2011,** *7,* 1543–1554.
doi:10.3762/bjoc.7.182

Received: 28 September 2011
Accepted: 08 November 2011
Published: 22 November 2011

This article is part of the Thematic Series "Supramolecular chemistry II".

Guest Editor: C. A. Schalley

Abstract

The potential of appropriately substituted cyclodextrins to act as scavengers for neurotoxic organophosphonates under physiological conditions was evaluated. To this end, a series of derivatives containing substituents with an aldoxime or a ketoxime moiety along the narrow opening of the β-cyclodextrin cavity was synthesized, and the ability of these compounds to reduce the inhibitory effect of the neurotoxic organophosphonate cyclosarin on its key target, acetylcholinesterase, was assessed in vitro. All compounds exhibited a larger effect than native β-cyclodextrin, and characteristic differences were noted. These differences in activity were correlated with the structural and electronic parameters of the substituents. In addition, the relatively strong effect of the cyclodextrin derivatives on cyclosarin degradation and, in particular, the observed enantioselectivity are good indications that noncovalent interactions between the cyclodextrin ring and the substrate, presumably involving the inclusion of the cyclohexyl moiety of cyclosarin into the cyclodextrin cavity, contribute to the mode of action. Among the nine compounds investigated, one exhibited remarkable activity, completely preventing acetylcholinesterase inhibition by the (−)-enantiomer of cyclosarin within seconds under the conditions of the assay. Thus, these investigations demonstrate that decoration of cyclodextrins with appropriate substituents represents a promising approach for the development of scavengers able to detoxify highly toxic nerve agents.

Introduction

Cyclodextrins, cyclic oligosaccharides composed of α-1,4-linked D-glucose units, represent one of the most important classes of host systems in supramolecular chemistry [1]. Their easy availability, their ability to include organic nonpolar molecules into the cavity made up by the cyclically arranged glucose units in aqueous solution, their predictable and controllable

binding properties, and their relatively straightforward chemical modification have made cyclodextrins indispensable tools in applications such as sensing [2], nanotechnology [3,4], polymer chemistry [5-8], medicinal chemistry [9,10], food chemistry [11], and others. Importantly, the scope of cyclodextrins goes beyond molecular recognition since the recognition event can in some cases be coupled with the chemical transformation of a substrate. This property was already realized in 1959 when it was shown that native cyclodextrins accelerate the cleavage of some acetic acid esters [12]. Subsequent work then established cyclodextrins containing appropriate substituents or dimeric cyclodextrins as a potent class of enzyme mimics [13,14]. Interestingly, it was also demonstrated relatively early in the field of cyclodextrin chemistry that native cyclodextrins are able to accelerate the cleavage of phosphates and phosphonates [15-18], including the highly neurotoxic organophosphonates (OP) sarin and soman [19-21]. While α-cyclodextrin, the cyclodextrin containing six anhydroglucose units along the ring, was shown to be most effective for sarin [17,22], the larger β-cyclodextrin with the seven-membered ring was demonstrated to also mediate soman degradation [19,20]. Moreover, the cyclodextrins were shown to act enantioselectively, being more effective for the more toxic (*R*)-(−)-enantiomer of sarin, for example [17,22]. Surprisingly, this work has largely been overlooked despite the fact that it provided strong indications for the potential applicability of cyclodextrins for the detoxification of chemical warfare agents. Only very recently has the use of cyclodextrins to induce degradation of neurotoxic OPs been addressed again. These investigations showed that β-cyclodextrin derivatives with a substituent along the wider rim of the cavity, bearing a nucleophilic group in the form of an iodosylbenzoate [23-25] or an oxime [26], efficiently react with paraoxon, cyclosarin (**GF**), and tabun thus reducing the inhibitory effects of these OPs on the key target of OP toxicity, acetylcholinesterase (AChE). Moreover, the results indicate that the mode of action of these cyclodextrin derivatives involves the formation of an inclusion complex with the OP.

The question thus arises as to whether suitable cyclodextrin derivatives could also be used in vivo as antidotes against OP poisonings. Such compounds should be able to act as scavengers by rapidly decomposing the OP into nontoxic byproducts before inhibition of AChE occurs. Catalytic action of the scavenger is desirable, reducing the necessary dose of the drug, but is not required if the toxicity is low. Since the amount of data currently available is too low to assess whether this approach has a realistic prospect of success, we initiated a research program aimed at the synthesis of a large number of structurally diverse cyclodextrin derivatives and the evaluation of their effect on OP degradation. In terms of structure, these compounds follow a common design principle, involving three distinct subunits each of which has a characteristic function (Figure 1):

- A cyclodextrin ring, which forms the basis of each compound. Complex formation between this subunit and the substrate should bring the P-atom of the substrate into spatial proximity with the substituent on the ring, thus facilitating the attack by the reactive group on the substituent. The type of cyclodextrin in this subunit (α, β, γ) controls the substrate affinity.
- The linking unit between the cyclodextrin ring and the reactive part of the substituent. This group should be chosen to allow straightforward synthetic access to the cyclodextrin derivatives, ideally allowing the synthesis to proceed in a modular fashion.
- The reactive unit bearing a functional group that should be able to specifically cleave the P–X bond on the substrate. In the case of **GF** (Scheme 1), for example, the most labile P–F bond is the one that is most prone to cleavage. In general, the functional group contains a suitable nucleophilic center, with α-effect nucleophiles possessing particularly promising activities [27,28]. Accordingly, the first step of OP deactivation is expected to consist of the phosphonylation of this nucleophilic group, similar to the phosphonylation of the serine residue in the active site of AChE during OP-mediated inhibition of this enzyme. If the compound thus formed is hydrolytically unstable, it will be cleaved in the aqueous medium, releasing the original reactive unit and allowing it to mediate another reaction.

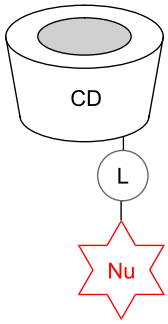

Figure 1: Schematic representation of the general structural design of the investigated cyclodextrin derivatives (CD = cyclodextrin ring, L = linking unit, Nu = reactive nucleophilic unit).

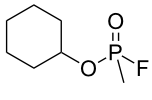

GF

Scheme 1: Structure of cyclosarin (**GF**).

Here, we describe our first results in this project, involving a series of β-cyclodextrin derivatives with substituents on the primary face of the cyclodextrin ring, containing oximes as nucleophilic groups. Oximes are well-known antidotes for the treatment of OP poisonings. Their mode of action involves reactivation of the OP-inhibited acetylcholinesterase [29], yet previous work has also indicated that certain oximes are able to cleave OPs directly [30]. We show that some of our cyclodextrin derivatives efficiently reduce **GF** concentrations in solution under physiological conditions within seconds, thus preventing the OP from inhibiting AChE. The observed correlation of structural and electronic parameters of the cyclodextrin derivatives with their activity strongly indicates that the interaction between the cyclodextrin ring and the substrate plays a decisive role in the mode of action.

Results and Discussion

Synthesis. The cyclodextrin derivatives investigated in this study are shown in Scheme 2. All compounds derive from the seven-membered β-cyclodextrin and contain the substituent in the 6-position of a glucose unit, i.e., along the narrower rim of the cyclodextrin cavity.

These products were prepared by following two different routes. Cyclodextrins **1a**–**e** derive from mono-6-(*p*-tolylsulfonyl)-β-cyclodextrin (**3**), which can be expediently prepared from β-cyclodextrin and *p*-tolylsulfonyl chloride [31]. Reaction of **3** with an appropriate nucleophile then afforded the functionalized products (Scheme 3, route A). Compound **1a** was prepared by the reaction of **3** with 3-(aminomethyl)benzaldehyde oxime (**5**) (Scheme 4), the latter of which was synthesized

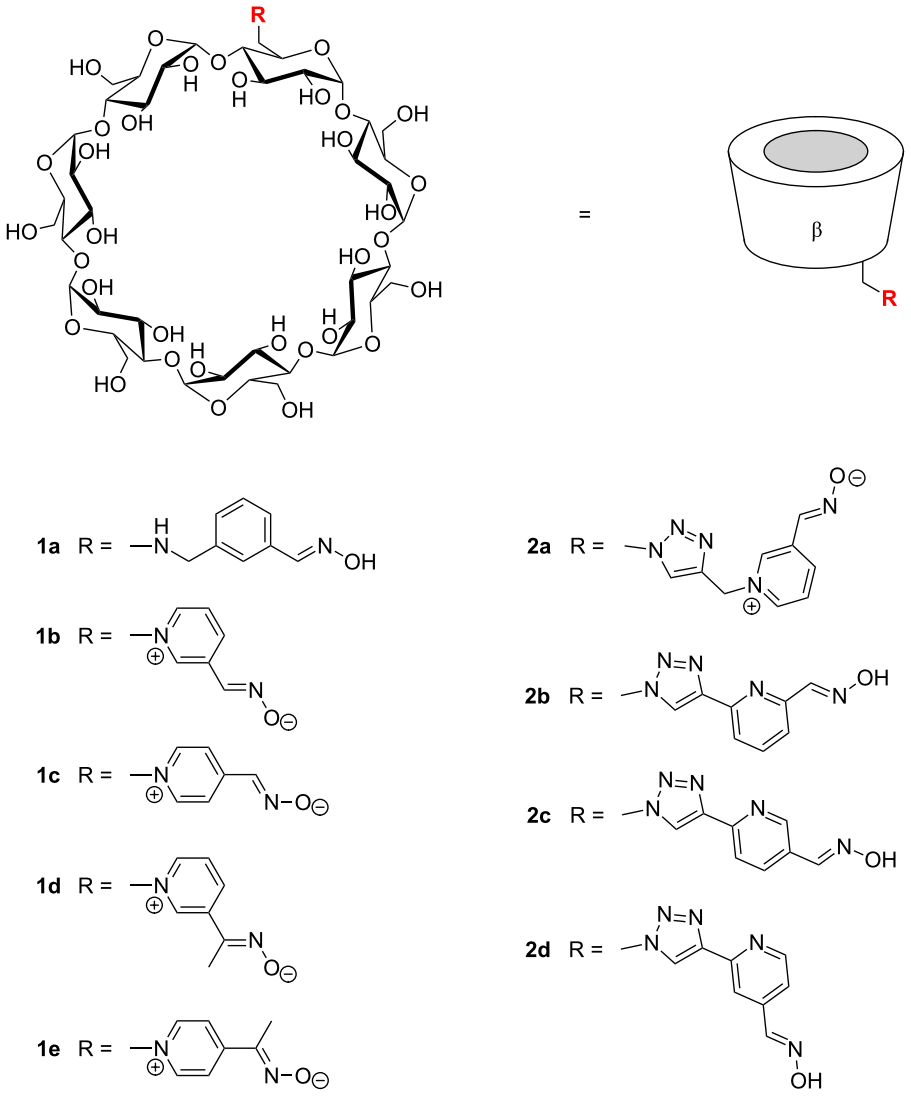

Scheme 2: Cyclodextrin derivatives tested as potential **GF** scavengers.

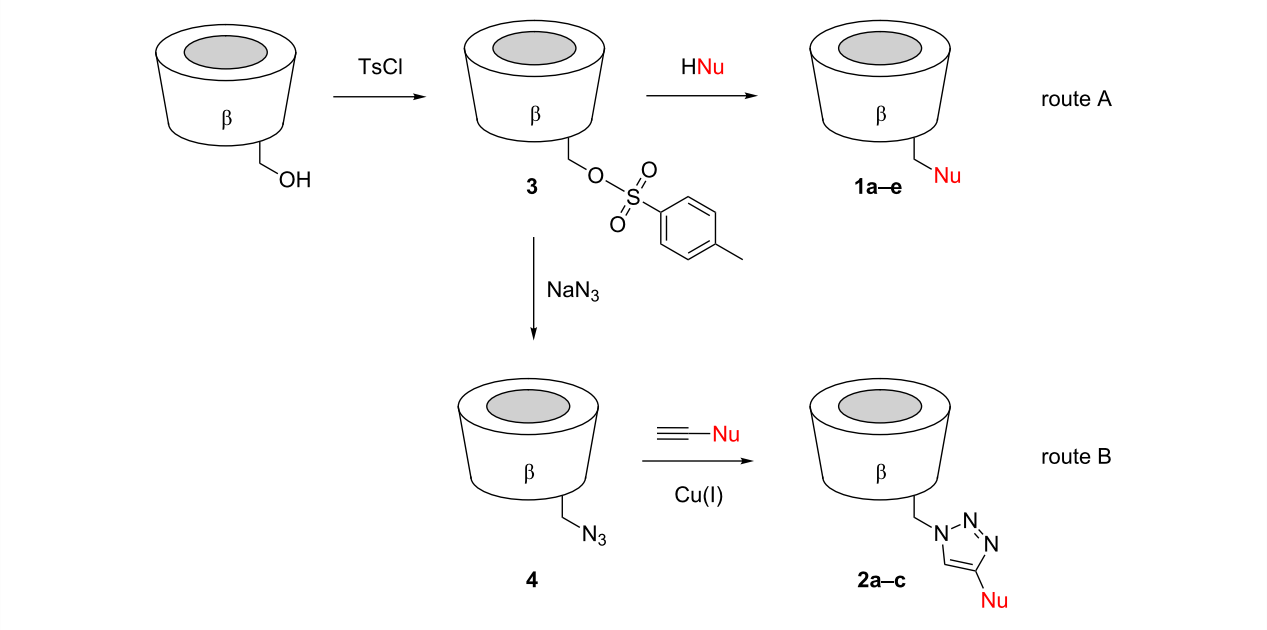

Scheme 3: General strategies used for the preparation of the investigated cyclodextrin derivatives.

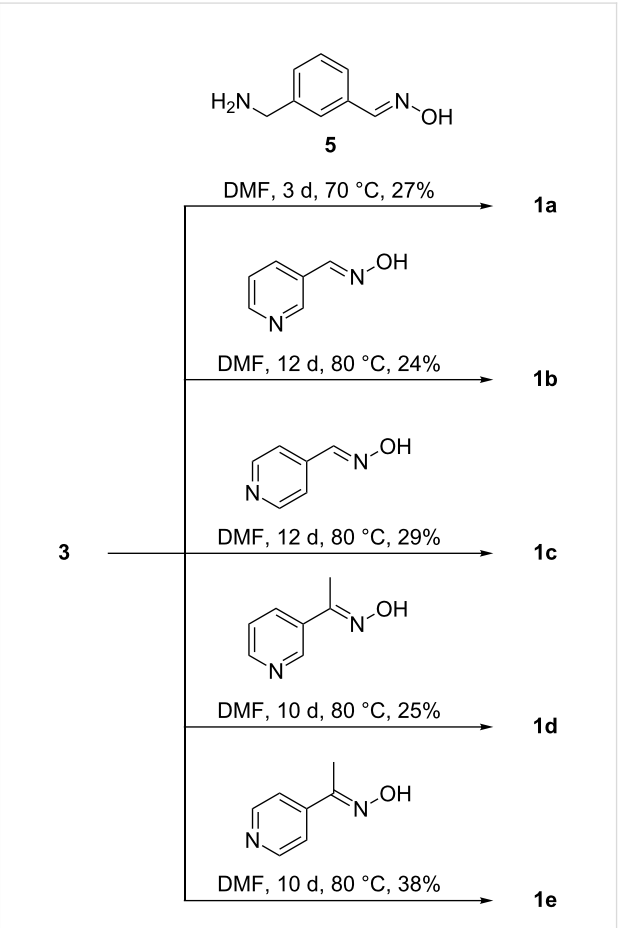

Scheme 4: Reaction conditions used for the preparation of cyclodextrin derivatives **1a–e** from tosylate **3**.

from isophtalaldehyde, as shown in Scheme 5. Compounds **1b–e** were obtained from **3** and the corresponding pyridine aldoximes or ketoximes (Scheme 4) all of which are easily accessible from the commercially available aldehydes or ketones by reaction with hydroxylamine [32]. Attempts to also prepare the analogous derivative with the oxime group in the 2-position of the pyridinium ring, by reaction of **3** with 2-formylpyridine oxime or 2-acetylpyridine oxime, unfortunately failed to produce the desired products.

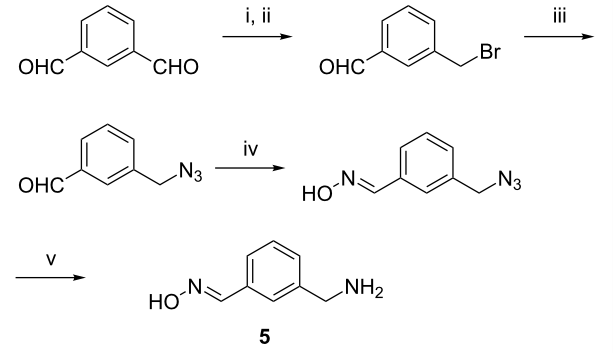

Scheme 5: Synthesis of 3-(aminomethyl)benzaldehyde oxime (**5**). Reagents and conditions: i. $NaBH_4$, EtOH, 1 h, 25 °C; ii. HBr/HOAc, 2 h, 25 °C, 38% (2 steps); iii. NaN_3, EtOH, 4 h, reflux, 94%; iv. $NH_2OH{\cdot}HCl$, NEt_3, EtOH, 1.5 h, 25 °C, 87%; v. PPh_3, H_2O/MeOH, 18 h, 25 °C, 80%.

The cyclodextrin derivatives **2a–d** contain 1,4-disubstituted 1,2,3-triazole moieties as the linking units. Accordingly, they were prepared by copper(I)-catalyzed azide–alkyne cycload-

dition ("click-reaction") [33] from mono-6-azido-6-deoxy-β-cyclodextrin (**4**) and a functionalized alkyne (Scheme 3, route B). Conjugations by copper(I)-catalyzed azide–alkyne cycloadditions have become popular in many different fields of chemistry [33,34], including cyclodextrin chemistry [35-41]. The alkyne **6** required for the synthesis of **2a** was obtained from propargyl bromide and 3-formylpyridine oxime (Scheme 6), and those for **2b**, **2c**, and **2d**, following the routes shown in Scheme 7. Reaction of these alkynes with **4** in the presence of copper(II) sulfate, sodium ascorbate and tris[(1-benzyl-1*H*-1,2,3-triazol-4-yl)methyl]amine (TBTA) [42] afforded the corresponding coupled products (Scheme 8).

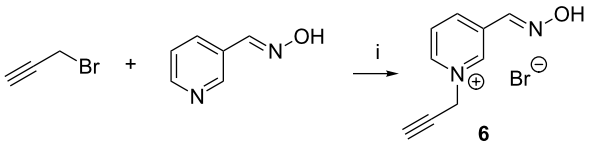

Scheme 6: Synthesis of 3-((hydroxyimino)methyl)-1-(prop-2-ynyl)pyridinium bromide (**6**). Reagents and conditions: i. KI, DMF/toluene, 3 h, 25 °C, 39%.

All functionalized cyclodextrins **1a**–**e** and **2a**–**d** were purified by preparative HPLC. To this end, a universal method was developed that involves the use of a reversed-phase C18 column and a gradient of a binary solvent mixture, acetonitrile/0.025% aqueous ammonia. All products were thus obtained in analytically pure form, which is necessary to ensure that the subsequent evaluation of activity yields reliable results. Elemental analyses and NMR spectroscopy indicated that the pyridinium-containing cyclodextrins do not contain a counterion and that they therefore most probably represent the betaine forms depicted in Scheme 2.

Qualitative assay. In a first step, the ability of the prepared cyclodextrin derivatives to reduce **GF** concentration in solution and, as a consequence, the inhibitory effect of this OP on AChE was estimated by using a fully automated high-throughput screening assay recently developed for the characterization of potential nerve agent detoxifying materials [43]. This test involves incubation of the nerve agent with an excess of a

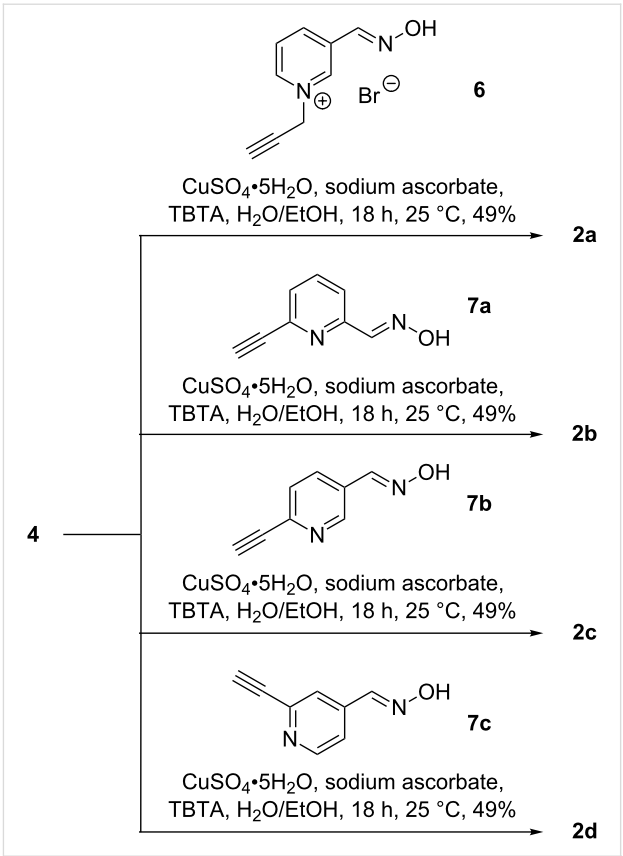

Scheme 8: Reaction conditions used for the preparation of cyclodextrin derivatives **2a**–**d** from azide **4**.

respective cyclodextrin derivative at 37.0 °C in an aqueous TRIS-HCl buffer (pH 7.40). Aliquots of this solution were added to a solution containing human acetylcholinesterase (hAChE, EC 3.1.1.7), acetylthiocholine (ATCh) and 5,5'-dithiobis-(2-nitrobenzoic acid) (DTNB) immediately after mixing and after 30 and 60 min. The inhibitory effect of **GF** on the enzyme was then quantified photometrically by following the rate of formation of the 2-nitro-5-thiobenzoate dianion (Ellman assay) [44,45]. A first order rate constant k_1 was derived from these curves by nonlinear regression analysis, which is a measure of the extent of enzyme inhibition: The larger the value of k_1 the stronger the inhibitory effect of the nerve agent on the enzyme activity. By relating k_1 to k_1^{ref}, the

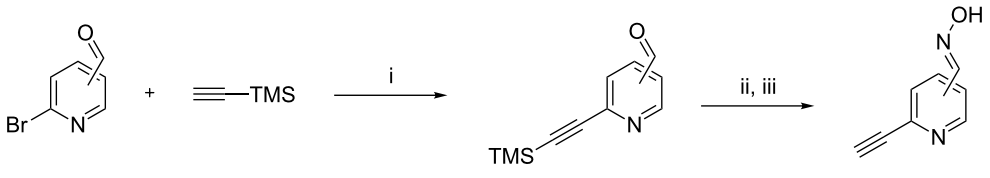

Scheme 7: Syntheses of 6-ethynyl-formylpyridine oximes (**7a**–**c**). Reagents and conditions: i. CuI, $(PPh_3)_2PdCl_2$, DPEphos, NEt_3, 18–20 h, 25 °C, 71-87%; ii. NH_2OH, H_2O, 30 min, 80 °C; iii. TBAF, THF, 1 h, 0 °C, 68–83%.

rate constant determined in the absence of the cyclodextrin, and to k_1^{native}, the rate constant determined in a preliminary assay in the absence of both cyclodextrin and **GF**, one obtains $(k_1^{ref}–k_1)/(k_1^{ref}–k_1^{native})\cdot100\% = \Delta k_1$, a term which correlates with the activity of the cyclodextrin. If the extent of enzyme inhibition is the same in the absence and the presence of the cyclodextrin ($k_1^{ref} = k_1$) the cyclodextrin is inactive and $\Delta k_1 = 0\%$. If, however, the nerve agent is decomposed faster in the presence of the cyclodextrin than during the background reaction, k_1 becomes smaller with respect to k_1^{ref} until it approaches the value of k_1^{native}. As a consequence Δk_1 increases up to 100% for full enzymatic activity ($k_1 = k_1^{native}$). The results of this assay obtained for cyclodextrin derivatives **1a**–**e** and **2a**–**d** are summarized in Figure 2.

Figure 2 shows that even native β-cyclodextrin exhibits a substantial activity, consistent with the results of previous investigations [19,20]. The reduction of AChE inhibition is clearly visible after 30 min, and the enzyme is fully active when **GF** was incubated with β-cyclodextrin for 1 h prior to the Ellman assay. Notably, all substituted cyclodextrin derivatives already exhibit an effect in the first measurement, thus clearly demonstrating the enhancement of activity caused by the substituents. While this effect is small for most cyclodextrins, it is significant for **1d**, and the activity of **1b** is so high that no enzyme inhibition is observable even in the first measurement.

The correlation between the type of substituent on the cyclodextrin and the reduction of AChE inhibition, which is evidenced in Figure 2, indicates that the activity of these cyclodextrin derivatives depends sensitively on the structural parameters of the substituents in combination with the electronic properties. The generally larger activity of the pyridinium derivatives such as **1b**–**e** and **2a** with respect to compounds containing a neutral pyridine ring can most probably be attributed to the higher acidity of the aldoxime proton in pyridinium aldoximes, for example. For reference, the pK_a of the aldoxime proton in 3-formylpyridine oxime amounts to 10.36 and that of the corresponding proton in the 1-methiodide of 3-formylpyridine oxime to 9.22. Correspondingly, the pK_a of the aldoxime proton in 4-formylpyridine oxime (9.99) also decreases by more than one order of magnitude to 8.57 upon methylation of the ring nitrogen [46]. Thus, oximes on pyridinium rings are deprotonated more easily, which renders them more nucleophilic.

The influence of structural effects on the activity becomes evident when comparing **1b** and **2a**, both of which have the oxime moiety in the same position on the aromatic ring. The significantly larger activity of **1b** is an indication that the positioning of the nucleophilic group closer to the cavity of the cyclodextrin facilitates the reaction with **GF**. Interestingly, even small structural variations such as shifting the substituent on the pyridinium ring from the 3- into the 4-position (**1b** versus **1c**) or replacing the aldoxime with a ketoxime (**1b** versus **1d**) are associated with a significant loss of activity. While the latter effect is presumably due to the lower acidity of ketoximes with respect to aldoximes by ca. one order of magnitude [32], the higher activity of **1b** with respect to **1c** is more likely to be a structural effect, since on the basis of the pK_a values of 1-methiodides of 3-formylpyridine oxime (9.22) and 4-formylpyridine oxime (8.57) one would expect the opposite trend.

The pronounced activity of the investigated cyclodextrin derivatives, in particular of **1b**, also indicates that noncovalent interactions, most probably the inclusion of the apolar cyclohexyl moiety of **GF** into the cyclodextrin cavity, are an important aspect of the mode of action. Assuming that the affinity of **GF**

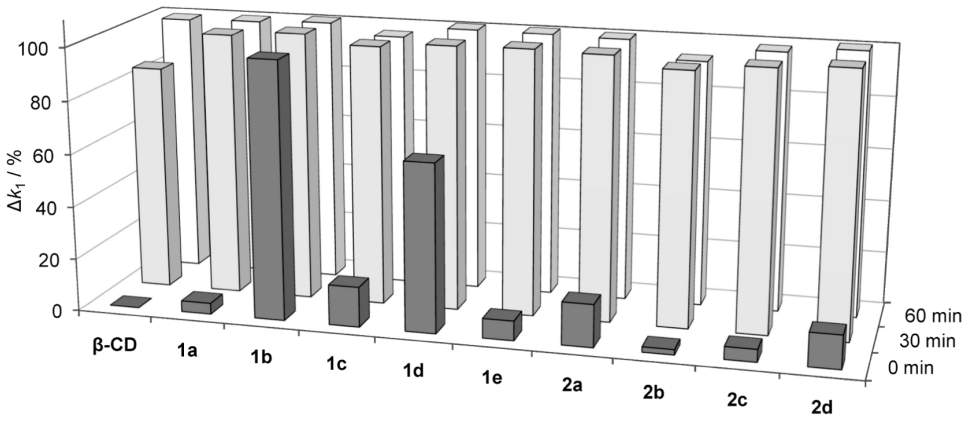

Figure 2: Diagram summarizing the observed Δk_1 values for cyclodextrins **1a**–**e** and **2a**–**d**. For comparison, the results obtained for native β-cyclodextrin are also included in the diagram. Large bars indicate low enzyme inhibition and, consequently, high activity of the corresponding cyclodextrin. The results are averages over three independent measurements.

to β-cyclodextrin in water is similar to that of cyclohexanol (687 M^{-1} at 30 °C) [47,48], and that it is approximately independent of the type of substituent, ca. 25% of the substrate molecules are estimated to reside in the cyclodextrin cavity under the conditions of the assay (500 μM cyclodextrin and 1 μM **GF**). This value presumably represents a lower limit, because hydrogen-bonding interactions between the OH-groups along the rim of the cyclodextrin cavity and the P=O group of the substrate can cause the **GF**complex to be more stable than that of cyclohexanol. However, it indicates that complexation of only part of the total substrate amount could ensure efficient conversion, if the oxime group of the cyclodextrin can approach the phosphonate moiety of the substrate in the complex, and if complexation/decomplexation kinetics are fast as is usually the case for cyclodextrin complexes [49]. The remarkable high activity observed for **1b** prompted us to evaluate in more detail the rate with which **GF** is degraded in the presence of this compound. For comparison, the less active isomer of **1b**, 4-substituted derivative **1c**, and the triazole-linked derivative **2a** were also included in this study.

Quantitative assay. The kinetic parameters for the reduction of **GF** concentration in solution mediated by **1b**, **1c**, and **2a** were determined as described previously for other cyclodextrin derivatives [23]. Briefly, a buffered solution (pH 7.40) containing the nerve agent was incubated at 37.0 °C and an aliquot was taken to determine the initial concentration of **GF**, c_0(**GF**). After the addition of a thermostatted cyclodextrin solution, aliquots were taken at defined intervals. These samples were immediately extracted with hexane and subjected to GC–MS analysis by using d_{11}-**GF** (**GF** with a perdeuterated cyclohexyl residue) as the internal standard. The use of a chiral stationary phase allowed independent evaluation of the effect of the cyclodextrin on both **GF** enantiomers. The results of these measurements are shown in Figure 3.

One important aspect that becomes immediately apparent when looking at the graphs in Figure 3 is that the cyclodextrins act enantioselectively, with the (−)-enantiomer of **GF** being the one that disappears faster, independent of the cyclodextrin derivative used. This result, which is consistent with those of previous investigations [22,23], is another indication of the involvement of the chiral cyclodextrin residue in the reaction. The top left graph shows that under the standard conditions of this measurement (−)-**GF** is consumed so quickly, with conversion being complete after ca. 5 s, that no reliable kinetic analysis could be performed. Decomposition of the corresponding (+)-enantiomer is slower, but also complete after ca. 4 min. In order to follow the rate with which (−)-**GF** disappears, the concentration of cyclodextrin during incubation with **GF** was reduced to

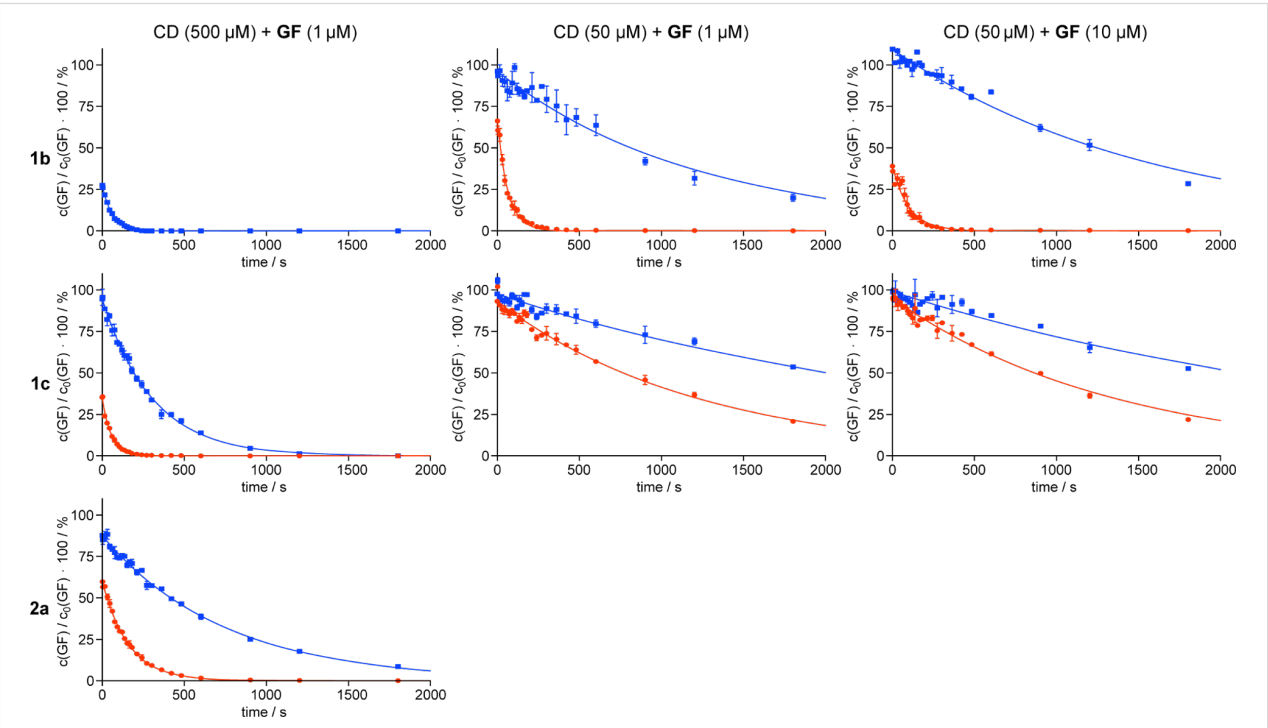

Figure 3: Time-dependent decrease of **GF** concentration in the presence of **1b** (top row), **1c** (middle row), and **2a** (bottom row). The measurements were performed at different concentrations of cyclodextrin (CD) and nerve agent, which are indicated at the top of each column. The data points (means ± SD, n = 2) denote the experimental results normalized to the initial concentration of **GF**, c_0(**GF**). The curves show the results of fitting the data points to a first-order rate reaction. Disappearance of the (−)-enantiomer of **GF** is shown in red and that of the (+)-enantiomer in blue.

50 μM. As expected, this modification of conditions caused a reduced rate of conversion for both enantiomers, presumably because the amount of **GF** molecules bound inside the cyclodextrin cavity decreases by a factor of ca. 10. Performing the analysis at 50 μM of cyclodextrin and 10 μM of **GF** does not have a large effect on the rate of reaction, which is consistent with the fact that increasing the **GF** concentration does not shift the complex equilibrium to a large extent. It should be noted that this assay currently does not allow us to ascertain whether the action of the cyclodextrins is stoichiometric or catalytic, because the cyclodextrin derivatives were used in excess with respect to **GF**.

Similar trends were observed for the other cyclodextrin derivatives, although their overall rates of conversion were consistently lower than those of **1b**. Quantitative information in terms of the observed rate constants k_{obs} and half-lives $t_{1/2}$was obtained by fitting the experimentally obtained decay curves to a first order rate reaction and subtracting the effect of spontaneous **GF** hydrolysis under these conditions ($1.5 \cdot 10^{-4}$ s^{-1}) [23]. The results thus obtained are summarized in Table 1.

Comparison of these rate constants with ones obtained previously under similar conditions for native β-cyclodextrin and 2-*O*-(carboxy-iodosobenzyl)-β-cyclodextrin leads to the conclusion that the substituted cyclodextrins investigated here enhance the **GF** decomposition by at least one order of magnitude more efficiently than native β-cyclodextrin does [23]. Degradation of (+)-**GF** is ca. twice as fast in the presence of **1b** than in the presence of 2-*O*-(carboxy-iodosobenzyl)-β-cyclodextrin. Because of the relatively low enantioselectivity observed for 2-*O*-(carboxy-iodosobenzyl)-β-cyclodextrin, the activity of cyclodextrin **1b** is estimated to be at least one order of magnitude higher. More detailed information about the kinetics and thermodynamics of the reaction could be obtained by following the dependency of the rate of reaction on the **GF** concentration (Michaelis–Menten kinetics). These measurements are, however, demanding in light of the complexity of the currently used kinetic assay and have therefore not yet been performed.

Conclusion

These investigations demonstrate that appropriately substituted cyclodextrin derivatives can efficiently reduce the inhibitory effect of **GF** on AChE under physiological conditions. The relatively strong effect of the cyclodextrin derivatives on **GF** degradation and, in particular, the observed enantioselectivity are good indications for noncovalent interactions between the cyclodextrin ring and the substrate, presumably involving the inclusion of the cyclohexyl moiety of cyclosarin into the cyclodextrin cavity, which contribute to the mode of action. In addition, the correlation between structural parameters and activity can be rationalized on the basis of the distance of the substituents from the cyclodextrin cavity, where OP binding presumably takes place, and the expected nucleophilicity of the oxime groups of the substituents. With **1b** a compound could be identified that, to the best of our knowledge, currently represents the most active cyclodextrin derivative mediating **GF** degradation in solution. These results make us optimistic that substituted cyclodextrins represent a very promising platform for the development of scavengers for highly toxic organophosphonates, including also ones that are more persistent than **GF**, such as tabun or VX. Work in this context is ongoing in our group.

Experimental

General details. The synthesized compounds were characterized as follows: Melting points, Müller SPM-X 300; NMR, Bruker Avance 600, Bruker DPX 400; MALDI-TOF-MS,

Table 1: Kinetic constants determined for **GF** degradation mediated by cyclodextrins **1b**, **1c**, and **2a** (k_{obs} in s^{-1}, $t_{1/2}$ in s).

cyclodextrin concentration	cyclodextrin		(−)-**GF**	(+)-**GF**	(−)-**GF**	(+)-**GF**
			1 μM		10 μM	
500 μM	**1b**	k_{obs}	n.d.[a]	$1.6 \cdot 10^{-2}$		
		$t_{1/2}$	n.d.[a]	43		
	1c	k_{obs}	$1.8 \cdot 10^{-2}$	$3.1 \cdot 10^{-3}$		
		$t_{1/2}$	39	211		
	2a	k_{obs}	$6.1 \cdot 10^{-3}$	$1.2 \cdot 10^{-3}$		
		$t_{1/2}$	114	583		
50 μM	**1b**	k_{obs}	$1.5 \cdot 10^{-2}$	$6.5 \cdot 10^{-4}$	$9.6 \cdot 10^{-3}$	$4.7 \cdot 10^{-4}$
		$t_{1/2}$	46	1071	72	1465
	1c	k_{obs}	$6.6 \cdot 10^{-4}$	$1.8 \cdot 10^{-4}$	$5.9 \cdot 10^{-4}$	$1.7 \cdot 10^{-4}$
		$t_{1/2}$	1053	3857	1179	4143

[a]no reliable rate constant and half-life could be determined.

Bruker Ultraflex TOF/TOF; ESI–MS, Bruker Esquire 3000; IR, FT-IR System Spectrum BX, Perkin-Elmer; elemental analysis, Elementar vario Micro cube. All chemicals, unless other stated, are commercially available and were used without further purification. Cyclosarin and deuterated cyclosarin (d_{11}-cyclosarin, d_{11}-**GF**) (>98% by GC–MS, ^{1}H NMR, and ^{31}P NMR) were made available by the German Ministry of Defense (All experiments with cyclosarin were performed at the Institut für Pharmakologie und Toxikologie der Bundeswehr). Hemoglobin-free erythrocyte ghosts as a source for human erythrocyte acetylcholinesterase (AChE, EC 3.1.1.7) were prepared according to the procedure of Dodge et al. [50] with minor modifications [51]. AChE activity was adjusted to 4000 U/l by dilution with phosphate buffer (0.1 M, pH 7.40). Aliquots were stored at a temperature of −80 °C. Prior to use, ghosts were homogenized with a Sonoplus HD 2070 ultrasonic homogenator (Bandelin electronic, Berlin, Germany) twice for 5 s with a 20 s interval to achieve a homogeneous matrix. For the preparative HPLC the following conditions were used: HPLC, Dionex UltiMate 3000; column, Thermo Fisher, BetaBasic-18, 250 × 21.2 mm, 5 µm particle size; flow, 12 mL/min; eluent, aqueous: 0.025% aqueous ammonia, organic: acetonitrile; for the separation of neutral compounds (**1a**, **2b**–**2d**) the following gradient was used: 0–6 min, 0% organic; 6–27 min, linear increase of organic to 40%; 27–33 min, 40% organic; 33–39 min, linear decrease to 0% organic; 39–45 min, 0% organic; charged compounds (**1b**–**1e**, **2a**) were purified by employing a slightly different gradient: 0–6 min, 0% organic; 6–22 min, linear increase to 15% organic; 22–25 min, linear increase to 50% organic; 25–30 min, 50% organic; 30–37 min, linear decrease to 0% organic; 37–45 min, 0% organic.

Qualitative assay. The qualitative test was performed by using a Tecan Freedom EVO liquid handling system (Männedorf, Switzerland) [43]. A solution of cyclodextrin (500 µM) and **GF** (1 µM) was prepared and incubated in TRIS-HCl buffer (0.1 M, pH 7.40) at 37.0 °C (Scheme 9). Immediately after mixing, a sample (25 µL) was transferred to a measuring plate prefilled with buffer (2400 µL, 0.1 M TRIS-HCl, pH 7.40 and 0.3 mM DTNB) and human AChE (10 µL) and preheated to 37.0 °C. ATCh (50 µL, 49.7 mM) was added immediately, the microplate was transferred to a photometer and the absorption was measured at 436 nm for 30 min while the temperature was maintained at 37.0 °C. Further aliquots of the test mixture were taken after 30 min and 60 min and treated analogously. The rate constants k_1 were determined by nonlinear regression analysis of the resulting curves by using Prism 5.0 (GraphPad Software, San Diego, CA, USA) as described previously [43]. All results shown are mean values of n = 3 experiments. The value for k_1^{native} was determined in independent experiments to be $8.56 \cdot 10^{-5}$ s^{-1}.

Quantitative assay. The quantitative assay was performed in a stirred 2.0 ml cryo vial (Wheaton Science Products, Millville, NJ, USA) positioned in a temperature controlled water bath. Buffer (1850 µL, TRIS-HCl 0.1 M, pH 7.40) containing **GF** (1.1 µM) was incubated at 37.0 °C and an aliquot (50 µL) was removed to determine the initial concentration of **GF**, c_0(**GF**) (Scheme 10). After preheated cyclodextrin solution (200 µL, final concentration 500 µM) was added, aliquots (50 µL) were taken at defined time points. These samples were transferred into a tube containing sodium formate buffer (20 µL, 300 µM, pH 3.5) and a solution of the internal standard d_{11}-**GF** in 2-propanol (2.5 µL, 10 µg/mL). Afterward, ice-cold hexane (500 µL) was immediately added, and the mixture was shaken vigorously and stored on ice. Each sample was centrifuged as soon as possible (10.000 rpm, 10 min, 4 °C), and the organic layer was removed immediately and transferred to GC vials for analysis. The experimental results were normalized to the initial concentration of **GF** in the absence of cyclodextrin, c_0(**GF**). The kinetic constants k_{obs} were determined by, first, nonlinear regression analysis of the resulting decay curves (using GraphPad Prism 5.0, San Diego, CA, USA) on the basis of the following equation: $c_{(+/-)\mathbf{GF},t} = c_{(+/-)\mathbf{GF},0*} \cdot \exp(-k_{obs} \cdot t)$, in which $c_{(+/-)\mathbf{GF},t}$ denotes the concentration of (+)-**GF** or (−)-**GF** at a certain time t and $c_{(+/-)\mathbf{GF},0*}$ the concentration of (+)-**GF** or (−)-**GF**immediately after cyclodextrin addition, followed by subtracting the effect of spontaneous **GF** hydrolysis ($1.5 \cdot 10^{-4}$ s^{-1}) [23]. All data shown are the mean values of n = 2 experiments.

Quantification of GF enantiomers by PCI MS. Quantification of **GF** enantiomers was performed by GC–MS, as described before but with slight modifications [52]. In brief, a gas chromatographic system 6890N coupled with a mass spectrometer detector 5973 with positive chemical ionization

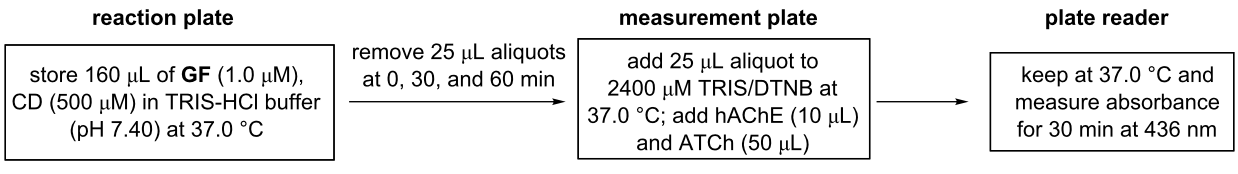

Scheme 9: Schematic protocol for the qualitative assay.

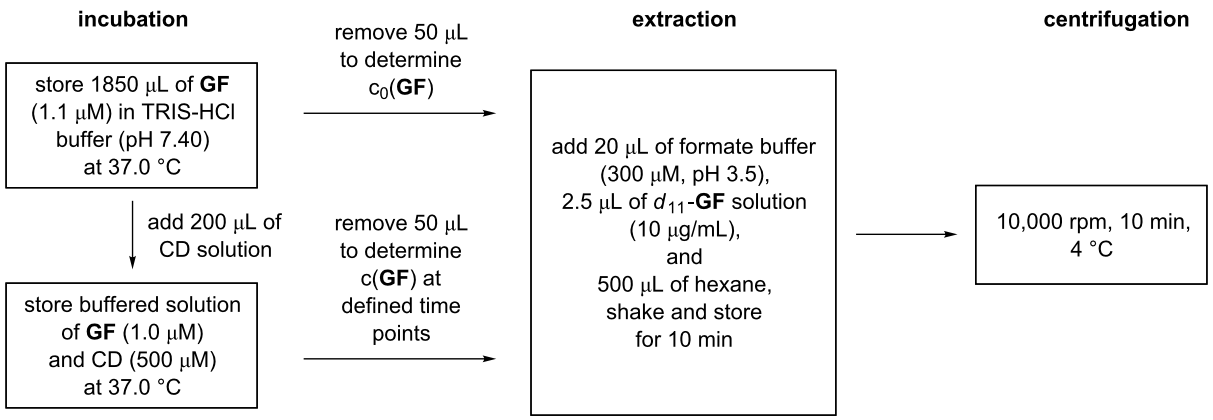

Scheme 10: Schematic protocol of the quantitative assay.

(PCI) (Agilent Technologies, Waldbronn, Germany), large volume injection (LVI), and a GAMMA DEX^{TM} 225 GC column (30 m × 0.25 mm, 0.25 μm film thickness, Sigma–Aldrich Chemie, Taufkirchen, Germany) was used (Table 2). CI quantification was performed by applying ammonia 6.0 as reactant gas with a flow rate of 2.0 mL/min and helium as carrier gas with a flow rate of 1.3 mL/min. The following oven temperature program was applied: 50 °C for 4.5 min, increase to 100 °C at 40 °C/min and subsequently to 135 °C at 3 °C/min, maintain this temperature for 2 min, further increase to 170 °C at 40 °C/min. The limit of quantification was estimated to be 2.5 pg per enantiomer.

Supporting Information

Supporting Information File 1

Detailed experimental procedures and physical data for all newly prepared compounds.
[http://www.beilstein-journals.org/bjoc/content/supplementary/1860-5397-7-182-S1.pdf]

Acknowledgements

This research was supported by a contract of the German Armed Forces (E/UR3G/9G127/9A803). The generous funding is gratefully acknowledged.

References

1. Dodziuk, H., Ed. *Cyclodextrins and Their Complexes: Chemistry, Analytical Methods, Applications;* Wiley-VCH: Weinheim, 2006.
2. Ogoshi, T.; Harada, A. *Sensors* **2008,** *8,* 4961–4982. doi:10.3390/s8084961
3. Ling, X. Y.; Reinhoudt, D. N.; Huskens, J. *Pure Appl. Chem.* **2009,** *81,* 2225–2233. doi:10.1351/PAC-CON-09-07-04
4. Ludden, M. J. W.; Reinhoudt, D. N.; Huskens, J. *Chem. Soc. Rev.* **2006,** *35,* 1122–1134. doi:10.1039/b600093m
5. Chen, G.; Jiang, M. *Chem. Soc. Rev.* **2011,** *40,* 2254–2266. doi:10.1039/c0cs00153h
6. Harada, A.; Takashima, Y.; Yamaguchi, H. *Chem. Soc. Rev.* **2009,** *38,* 875–882. doi:10.1039/b705458k
7. Wenz, G.; Han, B.-H.; Müller, A. *Chem. Rev.* **2006,** *106,* 782–817. doi:10.1021/cr970027+
8. Ritter, H.; Tabatabai, M. *Prog. Polym. Sci.* **2002,** *27,* 1713–1720. doi:10.1016/S0079-6700(02)00022-9

Table 2: GC–MS parameters for PCI analysis of **GF**.

injection program		MS parameters	
injection volume	50 μL	detected mass	*m*/*z* 198, *m*/*z* 209
injection speed	20 μL/min	dwell time	125 ms
initial temperature	40 °C, hold for 0.05 min	solvent delay	13.00 min
initial end temperature	260 °C, hold for 2 min		
initial time	2.70 min		
vent time	2.60 min		
vent flow	10.0 mL/min		
purge time	4.60 min		

9. Aniskevich, S.; Leone, B. J.; Brull, S. J. *Expert Rev. Neurother.* **2011,** *11,* 185–198. doi:10.1586/ern.11.2
10. Loftsson, T.; Brewster, M. E. *J. Pharm. Pharmacol.* **2010,** *62,* 1607–1621. doi:10.1111/j.2042-7158.2010.01030.x
11. Szente, L.; Szejtli, J. *Trends Food Sci. Technol.* **2004,** *15,* 137–142. doi:10.1016/j.tifs.2003.09.019
12. Cramer, F.; Dietsche, W. *Chem. Ber.* **1959,** *92,* 1739–1747. doi:10.1002/cber.19590920804
13. Marinescu, L.; Bols, M. *Trends Glycosci. Glycotechnol.* **2009,** *21,* 309–323. doi:10.4052/tigg.21.309
14. Breslow, R.; Dong, S. D. *Chem. Rev.* **1998,** *98,* 1997–2012. doi:10.1021/cr970011j
15. Mochida, K.; Matsui, Y.; Ota, Y.; Arakawa, K.; Date, Y. *Bull. Chem. Soc. Jpn.* **1976,** *49,* 3119–3123. doi:10.1246/bcsj.49.3119
16. Brass, H. J.; Bender, M. L. *J. Am. Chem. Soc.* **1973,** *95,* 5391–5399. doi:10.1021/ja00797a046
17. van Hooidonk, C.; Groos, C. C. *Recl. Trav. Chim. Pays-Bas* **1970,** *89,* 845–856. doi:10.1002/recl.19700890810
    Interestingly, this work contains an early application of an indicator displacement assay, a sensing technique whose usefulness in supramolecular chemistry was demonstrated in recent years particularly by the Anslyn group, see: Wiskur, S. L; Aït-Haddou, H.; Lavigne, J. J.; Anslyn, E. V. *Acc. Chem. Res.* **2001,** *34,* 963–972. doi:10.1021/ar9600796
18. Hennrich, N.; Cramer, F. *J. Am. Chem. Soc.* **1965,** *87,* 1121–1126. doi:10.1021/ja01083a032
19. Désiré, B.; Saint-André, S. *Experientia* **1987,** *43,* 395–397. doi:10.1007/BF01940424
20. Désiré, B.; Saint-André, S. *Fundam. Appl. Toxicol.* **1986,** *7,* 646–657. doi:10.1016/0272-0590(86)90114-4
21. van Hooidonk, C. *Recl. Trav. Chim. Pays-Bas* **1972,** *91,* 1103–1109. doi:10.1002/recl.19720910910
22. van Hooidonk, C.; Breebaart-Hansen, J. C. A. E. *Recl. Trav. Chim. Pays-Bas* **1970,** *89,* 289–299. doi:10.1002/recl.19700890309
23. Müller, S.; Koller, M.; Le Provost, R.; Lafont, O.; Estour, F.; Wille, T.; Thiermann, H.; Worek, F.; Reiter, G. *Toxicol. Lett.* **2011,** *200,* 53–58. doi:10.1016/j.toxlet.2010.10.014
24. Wille, T.; Tenberken, O.; Reiter, G.; Müller, S.; Le Provost, R.; Lafont, O.; Estour, F.; Thiermann, H.; Worek, F. *Toxicology* **2009,** *265,* 96–100. doi:10.1016/j.tox.2009.09.018
25. Masurier, N.; Estour, F.; Froment, M.-T.; Lefèvre, B.; Debouzy, J.-C.; Brasme, B.; Masson, P.; Lafont, O. *Eur. J. Med. Chem.* **2005,** *40,* 615–623. doi:10.1016/j.ejmech.2005.02.008
26. Le Provost, R.; Wille, T.; Louise, L.; Masurier, N.; Müller, S.; Reiter, G.; Renard, P.-Y.; Lafont, O.; Worek, F.; Estour, F. *Org. Biomol. Chem.* **2011,** *9,* 3026–3032. doi:10.1039/c0ob00931h
27. Smith, B. M. *Chem. Soc. Rev.* **2008,** *37,* 470–478. doi:10.1039/b705025a
28. Morales-Rojas, H.; Moss, R. A. *Chem. Rev.* **2002,** *102,* 2497–2522. doi:10.1021/cr9405462
29. Marrs, T. C.; Rice, P.; Vale, J. A. *Toxicol. Rev.* **2006,** *25,* 297–323.
30. Louise-Leriche, L.; Păunescu, E.; Saint-André, G.; Baati, R.; Romieu, A.; Wagner, A.; Renard, P.-Y. *Chem.–Eur. J.* **2010,** *16,* 3510–3523. doi:10.1002/chem.200902986
31. McNaughton, M.; Engman, L.; Birmingham, A.; Powis, G.; Cotgreave, I. A. *J. Med. Chem.* **2004,** *47,* 233–239. doi:10.1021/jm030916r
32. Ginsburg, S.; Wilson, I. B. *J. Am. Chem. Soc.* **1957,** *79,* 481–485. doi:10.1021/ja01559a067
33. Meldal, M.; Tornøe, C. W. *Chem. Rev.* **2008,** *108,* 2952–3015. doi:10.1021/cr0783479
34. Lallana, E.; Riguera, R.; Fernandez-Megia, E. *Angew. Chem., Int. Ed.* **2011,** *50,* 8794–8804. doi:10.1002/anie.201101019
    Angew. Chem. **2011,** *123,* 8956–8966. doi:10.1002/ange.201101019
35. Ward, S.; Ling, C.-C. *Eur. J. Org. Chem.* **2011,** 4853–4861. doi:10.1002/ejoc.201100445
36. Böhm, I.; Ritter, H. *Macromol. Chem. Phys.* **2011,** *212,* 1080–1085. doi:10.1002/macp.201100006
37. Christensen, H. S.; Sigurskjold, B. W.; Frihed, T. G.; Marinescu, L. G.; Pedersen, C. M.; Bols, M. *Eur. J. Org. Chem.* **2011,** 5279–5290. doi:10.1002/ejoc.201100671
38. Jazkewitsch, O.; Ritter, H. *Macromolecules* **2011,** *44,* 375–382. doi:10.1021/ma102456n
39. Méndez-Ardoy, A.; Guilloteau, N.; Di Giorgio, C.; Vierling, P.; Santoyo-González, F.; Ortiz Mellet, C.; García Fernández, J. M. *J. Org. Chem.í* **2011,** *76,* 5882–5894. doi:10.1021/jo2007785
40. Tran, D. N.; Blaszkiewicz, C.; Menuel, S.; Roucoux, A.; Philippot, K.; Hapiot, F.; Monflier, E. *Carbohydr. Res.* **2011,** *346,* 210–218. doi:10.1016/j.carres.2010.11.024
41. Trellenkamp, T.; Ritter, H. *Macromolecules* **2010,** *43,* 5538–5543. doi:10.1021/ma100812q
42. Chan, T. R.; Hilgraf, R.; Sharpless, K. B.; Fokin, V. V. *Org. Lett.* **2004,** *6,* 2853–2855. doi:10.1021/ol0493094
43. Wille, T.; Thiermann, H.; Worek, F. *Toxicol. in Vitro* **2010,** *24,* 1026–1031. doi:10.1016/j.tiv.2009.11.023
44. Eyer, P.; Worek, F.; Kiderlen, D.; Sinko, G.; Stuglin, A.; Simeon-Rudolf, V.; Reiner, E. *Anal. Biochem.* **2003,** *312,* 224–227. doi:10.1016/S0003-2697(02)00506-7
45. Worek, F.; Mast, U.; Kiderlen, D.; Diepold, C.; Eyer, P. *Clin. Chim. Acta* **1999,** *288,* 73–90. doi:10.1016/S0009-8981(99)00144-8
46. Mason, S. F. *J. Chem. Soc.* **1960,** 22–26. doi:10.1039/JR9600000022
47. Rekharsky, M. V.; Inoue, Y. *Chem. Rev.* **1998,** *98,* 1875–1918. doi:10.1021/cr970015o
48. Rekharsky, M. V.; Schwarz, F. P.; Tewari, Y. B.; Goldberg, R. N.; Tanaka, M.; Yamashoji, Y. *J. Phys. Chem.* **1994,** *98,* 4098–4103. doi:10.1021/j100066a032
49. Connors, K. A. *Chem. Rev.* **1997,** *97,* 1325–1358. doi:10.1021/cr960371r
50. Dodge, J. T.; Mitchell, C.; Hanahan, D. J. *Arch. Biochem. Biophys.* **1963,** *100,* 119–130. doi:10.1016/0003-9861(63)90042-0
51. Worek, F.; Reiter, G.; Eyer, P.; Szinicz, L. *Arch. Toxicol.* **2002,** *76,* 523–529. doi:10.1007/s00204-002-0375-1
52. Reiter, G.; Koller, M.; Thiermann, H.; Dorandeu, F.; Mikler, J.; Worek, F. *J. Chromatogr., B* **2007,** *859,* 9–15. doi:10.1016/j.jchromb.2007.08.040

Beilstein Journal of Organic Chemistry

Impact of the level of complexity in self-sorting: Fabrication of a supramolecular scalene triangle

Kingsuk Mahata and Michael Schmittel*

Letter

Open Access

Address:
Center of Micro- and Nanochemistry and Engineering, Organische Chemie I, Universität Siegen, Adolf-Reichwein-Straße, D-57068 Siegen, Germany

Email:
Michael Schmittel* - schmittel@chemie.uni-siegen.de

* Corresponding author

Keywords:
copper; metallosupramolecular chemistry; phenanthroline; self-assembly; self-sorting

Beilstein J. Org. Chem. **2011,** *7,* 1555–1561.
doi:10.3762/bjoc.7.183

Received: 12 September 2011
Accepted: 24 October 2011
Published: 22 November 2011

This article is part of the Thematic Series "Supramolecular chemistry II".

Guest Editor: C. A. Schalley

Abstract

The impact of the level of complexity in self-sorting was elaborated through the fabrication of various scalene triangles. It turned out that the self-sorting system with a higher level of complexity was far superior to less complex sorting algorithms.

Introduction

Self-assembly guided by self-sorting algorithms has received considerable attention over the past two decades as such protocols pave the way for intricate supramolecular assemblies [1-19]. However, despite its wide use, the definition of self-sorting remains vague with no precise guidelines provided in the literature. It has been widely reported that self-sorting operates when the numerical outcome of a chemical system is lower than the plausible number of potential aggregates (assemblies) estimated on the basis of statistical, chemical, and geometrical arguments [20,21]. This definition has drawbacks, and levelling effects [22] have been observed among various self-sorting systems. To numerically grasp the difference between different self-sorting processes, we defined the degree of self-sorting M as $M = P/P_0$ with P representing the number of possibilities and P_0 representing the number of experimentally observed aggregates in the mixture [8]. For example, the degree of the self-sorting process realised with ligands **1**–**4** in the presence of both Cu^+ and Zn^{2+}, as described in Scheme 1, is $M = 10$, as only two complexes formed out of twenty possible ones [8].

In contrast, when ligands **1**–**4** were treated with either Cu^+ or Zn^{2+}, the observed experimental outcome was four complexes (Supporting Information File 1, Figures S1 and S2), which has to be evaluated in light of the ten possible products (Scheme 2). Thus, for this process $M = 2.5$. Is this difference in M of any relevance, for example in the fabrication of intricate entities, or not? Herein, we investigate the utility of both self-sorting algorithms, from Scheme 1 and Scheme 2, for the fabrication of supramolecular scalene triangles. Importantly, we are able to demonstrate that the clean formation of a scalene triangle is only possible with the algorithm exhibiting the higher degree of self-sorting.

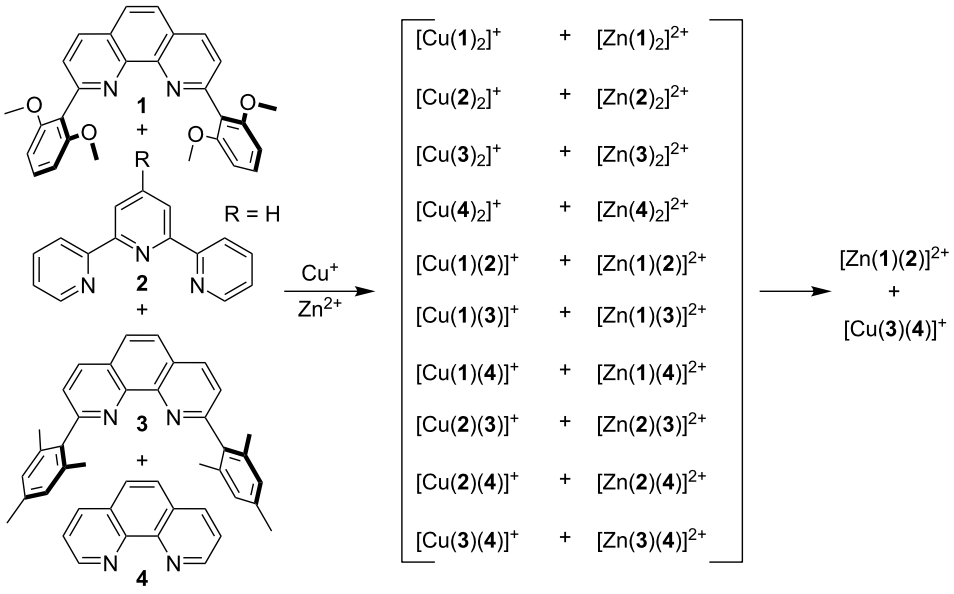

Scheme 1: Self-sorting in a six-component library [8].

Among the triangular assemblies, the scalene triangle is found to be the most difficult to fabricate. Hence, it comes as no surprise that there is only one report on a scalene triangle so far [16]. To design a further scalene triangle we modified a design already probed in the preparation of a geometrically isosceles triangle [15], and we implemented the coordination motifs of **1**–**4** into the three different multitopic ligands **5**–**7** [15,23], integrating twice the $[Cu(\mathbf{3})(\mathbf{4})]^+$ [24-26] and once the $[Zn(\mathbf{1})(\mathbf{2})]^{2+}$ motif [8,16] (Figure 1). The coordination behaviour of molecular component **3** was integrated into **5**, the latter being synthesised in a Sonogashira homocoupling reaction [27]. The information stored in **1** and **4** was instated in the unsymmetrical bisphenanthroline **6**, readily accessible by stepwise Sonogashira cross-coupling reactions [15]. A known procedure was followed to prepare the terpyridine–phenanthroline hybrid **7** [8]. The lengths of the ligands were chosen in such a way that they provide the geometrically different sides of a scalene triangle.

Results and Discussion

We tested both self-sorting algorithms as described earlier (Scheme 1 and Scheme 2). In a first round of experiments, we combined the ligands **5**, **6**, and **7** in equimolar ratio and made them react with one equivalent of Zn^{2+} and two equivalents of Cu^+ in acetonitrile at 60 °C for 3 h. At the end, a clear red solution was furnished, which was characterised as received, by means of mass spectrometry, ^{1}H NMR, diffusion-ordered spectroscopy (DOSY), differential pulse voltammetry (DPV) and elemental analysis. The electrospray ionisation mass spectrum (ESI-MS) of the reaction mixture suggests clean formation of the triangular species **T** = $[Cu_2Zn(\mathbf{5})(\mathbf{6})(\mathbf{7})](OTf)_2(PF_6)_2$ (Scheme 3). In the accessible spectral region of m/z = 150–2000 only three intense peaks were observed, all of them corresponding to triangle **T** (Figure 2). The most abundant peak at m/z = 666.8 can be assigned to $[Cu_2Zn(\mathbf{5})(\mathbf{6})(\mathbf{7})]^{4+}$, whereas the triply charged one at m/z = 938.5 is attributed to $[Cu_2Zn(\mathbf{5})(\mathbf{6})(\mathbf{7})](OTf)^{3+}$, and the doubly charged one at

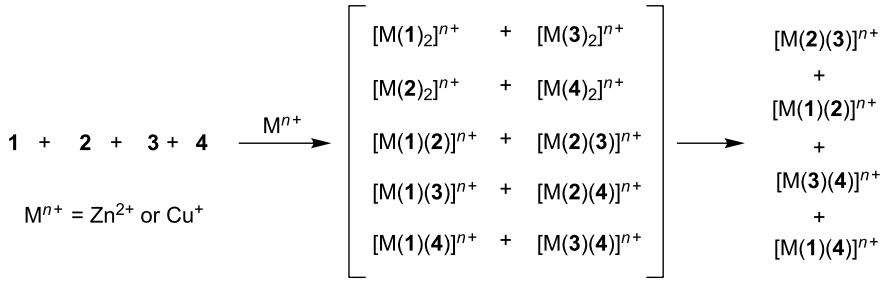

Scheme 2: Self-sorting in a five-component library. We used **2** in a slightly different form with Zn^{2+} (R = 4-C_6H_4I) and Cu^+ (R = H).

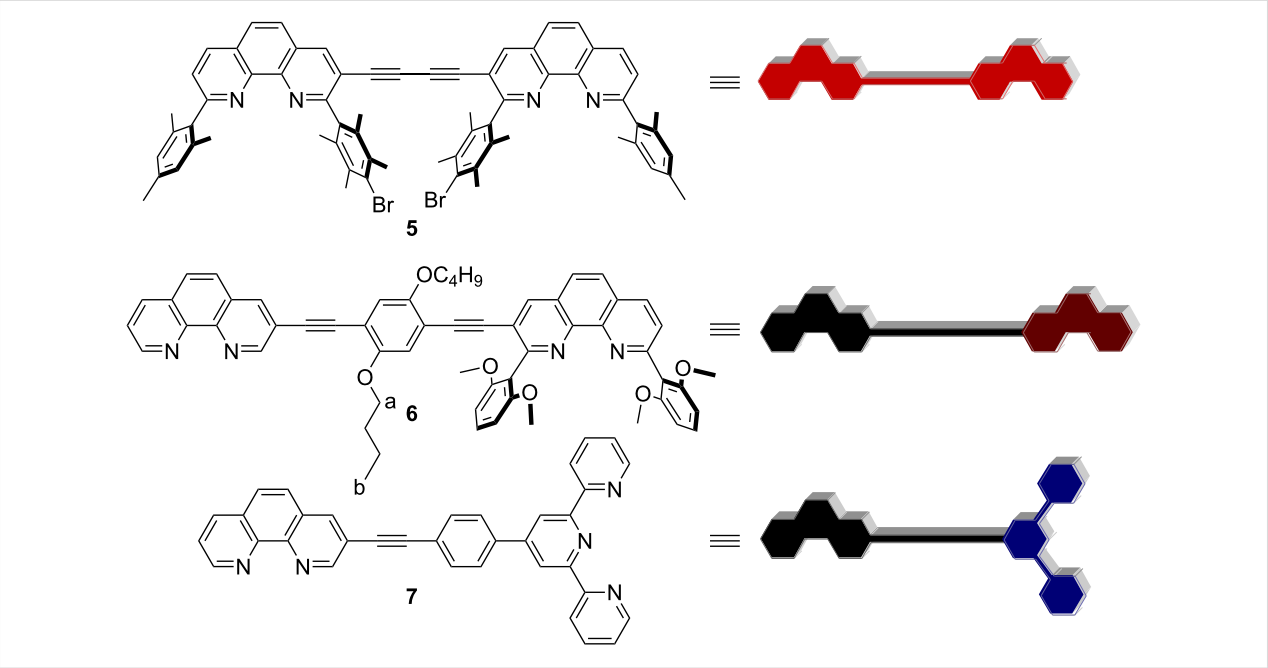

Figure 1: Ligands used in the present study.

m/z = 1481.1 to $[Cu_2Zn(\mathbf{5})(\mathbf{6})(\mathbf{7})](OTf)_2^{2+}$. All peaks were isotopically resolved, showing full agreement with the theoretically expected isotopic distribution.

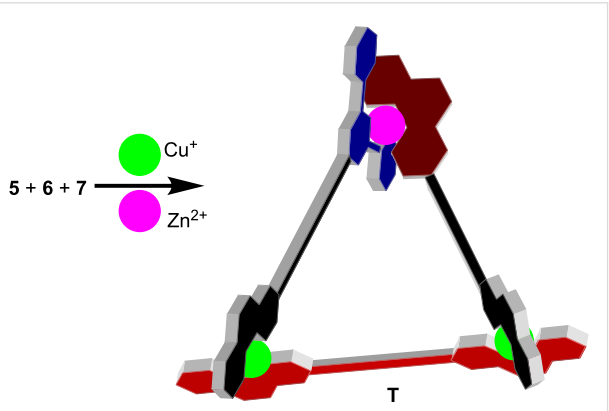

Scheme 3: Synthesis of the triangular assembly **T** (only *syn* shown).

To corroborate the clean self-assembly process, we carefully examined the DOSY and ^{1}H NMR of **T**. As in the ESI-MS, both sets of data unambiguously supported the presence of only one species, i.e., the DOSY spectrum showed only a single diffusion coefficient (Supporting Information File 1, Figure S4). Additional information was derived from the ^{1}H NMR signals of the methoxy protons, as these appear in a diagnostic region. In **T**, up to eight singlets are expected for the four methoxy groups due to their constitutional differences and the occurrence of two diastereomers (*syn* and *anti*). Diastereomers form as a result of two stereogenic heteroleptic copper(I) complex motifs $[Cu(\mathbf{3})(\mathbf{4})]^+$ in **T** [8,28,29]. The ^{1}H NMR of the assembly indeed showed seven singlets (one peak is merged with the others) between 2.73–3.10 ppm (Figure 3c). From NMR integration the ratio of the diastereomers was found to be approximately 3:1. The finding of further characteristic ^{1}H NMR shifts for protons of **6** (H–a and H–b) additionally supports the formation of **T** as a mixture of two diastereomers. Four triplets (two for each diastereomer) were observed for protons H–a between 3.53–3.97 ppm, and the same number of triplets was seen for H–b in the region of 0.57–1.00 ppm (Supporting Information File 1). Elemental analysis of the assembly also confirmed the exclusive formation of **T**.

We further evaluated the structure using DPV, because this analytical method provides valuable information about redox active units (here Cu^+). It is well known that copper(I) shows distinct oxidation potentials in different complex environments. Thus, the DPV measurements should allow us to analyse the number and ligand sphere of copper(I) centres in **T**. In the mononuclear complex $[Cu(\mathbf{1})(\mathbf{4})](PF_6)$ the copper(I) oxidation is observed at +0.29 V_{SCE}, whereas for $[Cu(\mathbf{3})(\mathbf{4})](PF_6)$ and $[Cu(\mathbf{1})(\mathbf{2})](PF_6)$ the oxidation is placed at +0.44 V_{SCE} and −0.21 V_{SCE}, respectively [8]. In **T**, only one type of copper(I) complex is present. As two values were expected for the two diastereomers, the broad peak was deconvoluted for two copper(I) oxidation waves (Figure 4) resulting in two values at +0.59 and +0.64 V_{SCE}. The values agree with those reported for a similar copper(I) complex (+0.61 and +0.67 V_{SCE}) in a

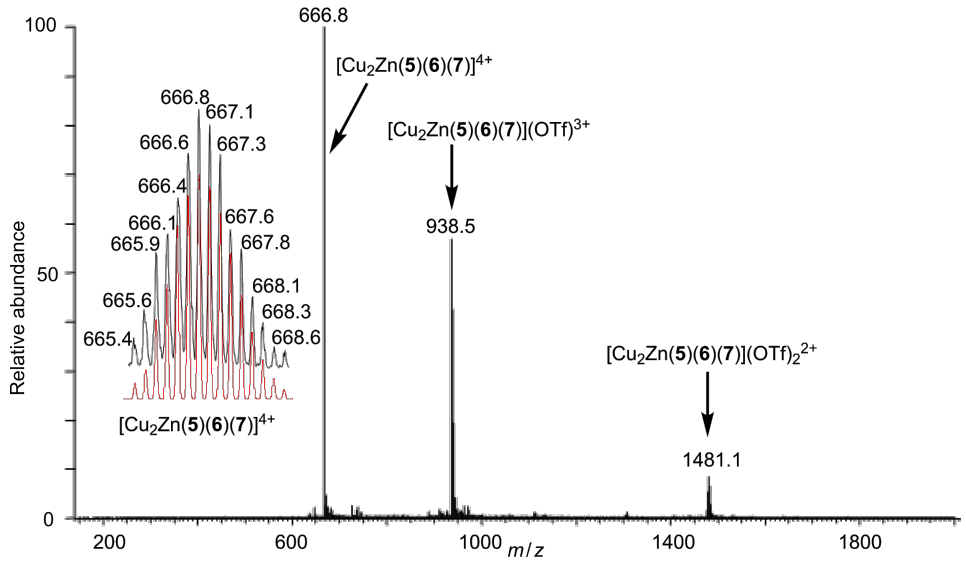

Figure 2: ESI-MS of triangle **T** in acetonitrile along with the isotopically resolved peak at 666.8 (black: Experimental; red: Calculated for $[Cu_2Zn(\mathbf{5})(\mathbf{6})(\mathbf{7})]^{4+}$). See also Figure S5 in Supporting Information File 1.

recently reported supramolecular trapezoid [8]. The population of the two diastereomers as determined from the deconvoluted DPV spectrum (Supporting Information File 1) was roughly 3:1, in full agreement with the ratio derived from ^{1}H NMR results.

We then focused on the self-sorting protocol mentioned in Scheme 2. We reacted three equivalents of copper(I) ions with an equimolar mixture of all three ligands **5**–**7**. After 3 h, at similar conditions as for **T**, a dark red solution was afforded, which was characterised by ^{1}H NMR without any further purification. The ^{1}H NMR spectrum was found to be broad (Figure 3a). The broadening of the signals is partly due to the presence of a phenanthroline–Cu^+–terpyridine complex. Due to the tetrahedral coordination behaviour of Cu^+, one pyridine nitrogen atom of the terpyridine unit is left uncoordinated [30], and thus it undergoes rapid exchange leading to broad NMR signals. The experiment was also carried out in the presence of three equivalents of Zn^{2+}. A clear yellow solution was produced after exposure to similar reaction conditions. Unlike the other experiment with Cu^+, only sharp signals were observed in the ^{1}H NMR (Figure 3b), but the many signals in the region

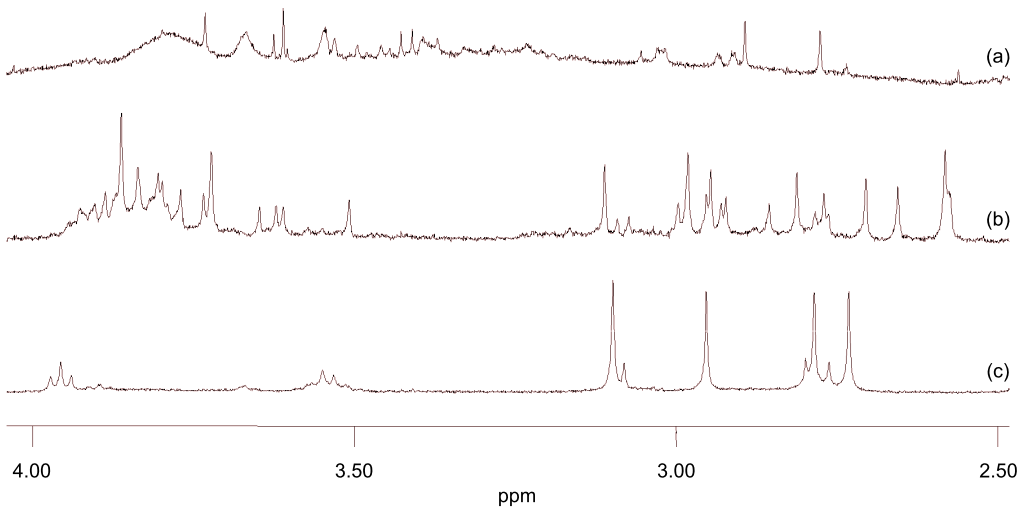

Figure 3: Partial ^{1}H NMR (400 MHz, 298 K, CD_3CN) spectra of an equimolar mixture of **5**, **6**, and **7** in the presence of (a) 3 equivalents of Cu^+, (b) 3 equivalents of Zn^{2+} and (c) 3 equivalents of a metal-salt mixture (Cu^+:Zn^{2+} = 2:1).

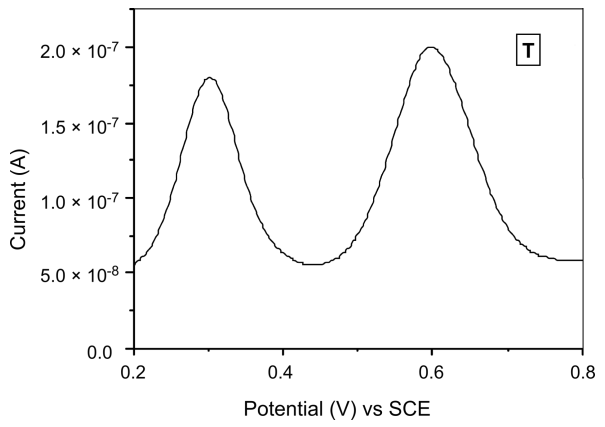

Figure 4: Differential pulse voltammogram of **T** in acetonitrile (0.1 M *n*-Bu_4NPF_6 as electrolyte, Ag wire as a quasi-reference electrode, 1,1'-dimethylferrocene as internal standard, scan rate = 20 mV s^{-1} and a pulse height of 2 mV).

2.5–4.0 ppm suggest formation of several species. Thus, a comparison among the NMR spectra nicely demonstrated that the self-assembly process was only clean in the case of the mixed-metal scenario, whereas the situation turned out to be complicated in both homometallic cases.

The observations can be rationalised in the following way. In the homometallic cases selectivity was less, because the ligands may organise into ≥2 competing triangular arrays with different connectivities (constitutions). In the all-copper situation, the linkage between **5** and **6** is only possible by $[Cu(\mathbf{3}^5)(\mathbf{4}^6)]^+$ coordination [31]. The triangle is completed through a bridging with **7**. However, the connectivity of **7** is not defined. The ligand may arrange itself in either of the two possible ways, $[Cu(\mathbf{3}^5)(\mathbf{4}^7)]^+$ and $[Cu(\mathbf{1}^6)(\mathbf{2}^7)]^+$ or $[Cu(\mathbf{2}^7)(\mathbf{3}^5)]^+$ and $[Cu(\mathbf{1}^6)(\mathbf{4}^7)]^+$, as demonstrated in Scheme 2, resulting in the formation of two different triangular species. Hence, the number of constitutional isomers increases in the case of the all-copper triangle. A related explanation may be given for the all-zinc triangle. The hindered phenanthroline of **6**, i.e., unit **1**, has four methoxy groups available for coordination in addition to its two bisimine nitrogens. Thus, unit **1** may either act as a strong bidentate, tridentate or tetradentate binding site for zinc(II) ions, and there is no large thermodynamic difference between a $[Zn(\mathbf{1}^6)(\mathbf{2}^7)]^+$-type connection and a $[Zn(\mathbf{1}^6)(\mathbf{4}^7)]^+$-type link. The outcomes are similar to those observed with copper(I) ions. On the other hand, in the mixed-metal scenario the terpyridine prefers to connect with terminus **1** as embedded in **6**, which is nicely illustrated from the self-sorting described in Scheme 1. Thus, the self-assembly process was constitutionally clean when self-sorting occurred along the algorithm with the higher level of complexity (Scheme 1). Due to the beauty of self-sorting, the five-component assembly (five different starting materials, mixed metal scenario) was flawless as compared to the four-component assembly (four different starting materials, homometallic cases).

As all attempts to obtain a crystal structure of **T** were unsuccessful, MM^+ force-field computations and molecular dynamics on **T** (Hyperchem 7.52®, Hypercube, Inc.) provided some insight to their structure as scalene triangles. Taking the metal–metal distance as a measure, the three metal corners of **T** (*syn*) are separated by 1.27, 1.58 and 1.63 nm in the energy-minimised structure (Figure 5) and by 1.36, 1.58 and 1.63 nm in **T** (*anti*) (Supporting Information File 1), nicely illustrating the scalene triangle arrangement of **T**.

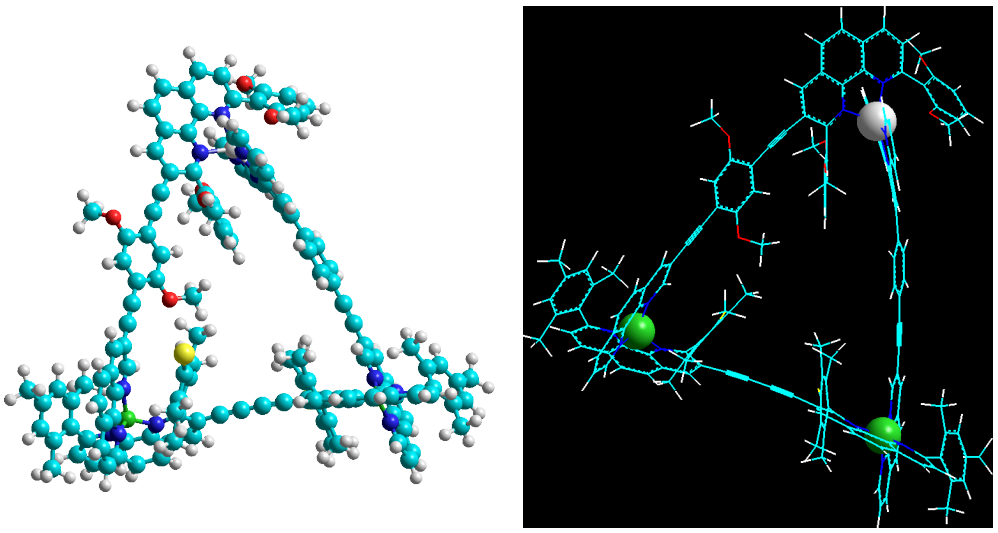

Figure 5: Two representations of the energy-minimised structure of the scalene triangle **T** (*anti*); copper(I) ions – green, zinc(II) ion – white.

Conclusion

We have been able to establish that our strategy to fabricate an isosceles triangle [15] can equally be applied to the preparation of a supramolecular scalene triangle and thus is tolerant to changes at the angles (of the vertices) and to variations of the lengths of the sides. Moreover, we have demonstrated with a study on homo- versus heterometallic scalene triangles that the level of complexity of self-sorting is important for the fabrication of intricate supramolecular assemblies [32,33].

Experimental

General

All commercial reagents were used without further purification. The solvents were dried with appropriate desiccants and distilled prior to use. NMR measurements were carried out on a Bruker Avance 400 MHz spectrometer with the deuterated solvent as the lock and residual solvent as the internal reference. Electrospray ionisation mass spectra (ESI-MS) were recorded on a Thermo-Quest LCQ Deca. Differential pulse voltammetry (DPV) was measured on a Parstat 2273 in dry acetonitrile. The melting point was measured on a Büchi SMP-20 and is uncorrected. The infrared spectrum was recorded on a Varian 1000 FT-IR instrument and the elemental analysis measurement was performed with a EA 3000 CHNS. Compound **5** [27], **6** [15], and **7** [8] were synthesised according to known procedures.

Synthesis of scalene triangle T

6 (1.49 mg, 1.65 μmol), **5** (1.76 mg, 1.65 μmol), **7** (0.85 mg, 1.65 μmol), $Zn(OTf)_2$ (0.60 mg, 1.66 μmol) and $[Cu(MeCN)_4]PF_6$ (1.23 mg, 3.31 μmol) were heated under reflux in a mixture of dichloromethane (10 mL) and acetonitrile (25 mL) for 2 h. The solvents were evaporated under reduced pressure and the solid was characterised as such. Yield quantitative; mp >260 °C; IR (KBr) ν: 3448, 3068, 2953, 2931, 2869, 2362, 2209, 1617, 1602, 1589, 1549, 1499, 1475, 1427, 1406, 1383, 1277, 1255, 1223, 1159, 1111, 1030, 1019, 912, 843, 791, 767, 725, 639; ESI-MS *m*/*z* (%): 666.8 (100) $[M - 2PF_6, 2OTf]^{4+}$, 938.5 (70) $[M - 2PF_6, OTf]^{3+}$, 1481.1 (20) $[M - 2PF_6]^{2+}$; Anal. calcd for $C_{161}H_{127}Br_2Cu_2F_{18}N_{13}O_{12}P_2S_2Zn{\cdot}3CH_2Cl_2$: C, 56.10; H, 3.82; N, 5.19; S, 1.83; found: C, 56.36; H, 3.27; N, 5.35; S, 1.91.

Supporting Information

Supporting Information File 1

^{1}H NMR spectra of self-sorting mixtures and of **T**. DOSY, ESI and DPV spectra of **T**.
[http://www.beilstein-journals.org/bjoc/content/supplementary/1860-5397-7-183-S1.pdf]

Acknowledgements

We are indebted to the DFG for the continued financial support of our work (Schm 647/15-1).

References

1. Krämer, R.; Lehn, J.-M.; Marquis-Rigault, A. *Proc. Natl. Acad. Sci. U. S. A.* **1993,** *90,* 5394–5398. doi:10.1073/pnas.90.12.5394
2. Caulder, D. L.; Raymond, K. N. *Angew. Chem., Int. Ed. Engl.* **1997,** *36,* 1440–1442. doi:10.1002/anie.199714401
3. Lehn, J.-M. *Science* **2002,** *295,* 2400–2403. doi:10.1126/science.1071063
4. Liu, S.; Ruspic, C.; Mukhopadhyay, P.; Chakrabarti, S.; Zavalij, P. Y.; Isaacs, L. *J. Am. Chem. Soc.* **2005,** *127,* 15959–15967. doi:10.1021/ja055013x
5. Nitschke, J. R. *Acc. Chem. Res.* **2007,** *40,* 103–112. doi:10.1021/ar068185n
6. Xu, S.; Giuseppone, N. *J. Am. Chem. Soc.* **2008,** *130,* 1826–1827. doi:10.1021/ja710248q
7. Wang, F.; Han, C.; He, C.; Zhou, Q.; Zhang, J.; Wang, C.; Li, N.; Huang, F. *J. Am. Chem. Soc.* **2008,** *130,* 11254–11255. doi:10.1021/ja8035465
8. Mahata, K.; Schmittel, M. *J. Am. Chem. Soc.* **2009,** *131,* 16544–16554. doi:10.1021/ja907185k
9. Barboiu, M.; Dumitru, F.; Legrand, Y.-M.; Petit, E.; van der Lee, A. *Chem. Commun.* **2009,** 2192–2194. doi:10.1039/b900155g
10. Ulrich, S.; Lehn, J.-M. *J. Am. Chem. Soc.* **2009,** *131,* 5546–5559. doi:10.1021/ja809828g
11. Zheng, Y.-R.; Yang, H.-B.; Ghosh, K.; Zhao, L.; Stang, P. J. *Chem.–Eur. J.* **2009,** *15,* 7203–7214. doi:10.1002/chem.200900230
12. Ajami, D.; Hou, J.-L.; Dale, T. J.; Barrett, E.; Rebek, J., Jr. *Proc. Natl. Acad. Sci. U. S. A.* **2009,** *106,* 10430–10434. doi:10.1073/pnas.0809903106
13. Jiang, W.; Schalley, C. A. *Proc. Natl. Acad. Sci. U. S. A.* **2009,** *106,* 10425–10429. doi:10.1073/pnas.0809512106
14. Northrop, B. H.; Zheng, Y.-R.; Chi, K.-W.; Stang, P. J. *Acc. Chem. Res.* **2009,** *42,* 1554–1563. doi:10.1021/ar900077c
15. Schmittel, M.; Mahata, K. *Chem. Commun.* **2010,** *46,* 4163–4165. doi:10.1039/c0cc00191k
16. Mahata, K.; Saha, M. L.; Schmittel, M. *J. Am. Chem. Soc.* **2010,** *132,* 15933–15935. doi:10.1021/ja108419k
17. Johnson, A. M.; Hooley, R. J. *Inorg. Chem.* **2011,** *50,* 4671–4673. doi:10.1021/ic2001688
18. Jiang, W.; Wang, Q.; Linder, I.; Klautzsch, F.; Schalley, C. A. *Chem.–Eur. J.* **2011,** *17,* 2344–2348. doi:10.1002/chem.201003194
19. Jiang, W.; Sattler, D.; Rissanen, K.; Schalley, C. A. *Org. Lett.* **2011,** *13,* 4502–4505. doi:10.1021/ol201618f
20. Chas, M.; Gil-Ramírez, G.; Ballester, P. *Org. Lett.* **2011,** *13,* 3402–3405. doi:10.1021/ol201146r
21. Dumitru, F.; Petit, E.; van der Lee, A.; Barboiu, M. *Eur. J. Inorg. Chem.* **2005,** 4255–4262. doi:10.1002/ejic.200500463
22. No differences among various self-sorting processes.
23. We use here a simplification to denote the ligand setting. While ligand **3** is not identical with the 2-bromoduryl-9-mesitylphenanthroline ligand site in **5**, our investigations over 10 years have revealed an analogous coordination behaviour of both ligands.
24. Schmittel, M.; Ganz, A. *Chem. Commun.* **1997,** 999–1000. doi:10.1039/a701509g

25. Schmittel, M.; Lüning, U.; Meder, M.; Ganz, A.; Michel, C.; Herderich, M. *Heterocycl. Commun.* **1997,** *3,* 493–498. doi:10.1515/HC.1997.3.6.493
26. Schmittel, M.; Ammon, H.; Kalsani, V.; Wiegrefe, A.; Michel, C. *Chem. Commun.* **2002,** 2566–2567. doi:10.1039/b207801e
27. Schmittel, M.; Michel, C.; Wiegrefe, A.; Kalsani, V. *Synthesis* **2001,** 1561–1567. doi:10.1055/s-2001-16093
28. Schmittel, M.; Kalsani, V.; Fenske, D.; Wiegrefe, A. *Chem. Commun.* **2004,** 490–491. doi:10.1039/b312807e
29. Schmittel, M.; Mahata, K. *Chem. Commun.* **2008,** 2550–2552. doi:10.1039/b801462k
30. Medlycott, E. A.; Hanan, G. S. *Chem. Commun.* **2007,** 4884–4886. doi:10.1039/b711765e
31. We use here a short notation: [Cu(**35**)(**46**)]$^+$-type linkage: The copper complex is made from the phenanthroline terminus **3** embedded in **5** and the phenanthroline terminus **4** embedded in **6**.
32. Funeriu, D. P.; Rissanen, K.; Lehn, J.-M. *Proc. Natl. Acad. Sci. U. S. A.* **2001,** *98,* 10546–10551. doi:10.1073/pnas.191362998
33. Funeriu, D. P.; Lehn, J.-M.; Fromm, K. M.; Fenske, D. *Chem.–Eur. J.* **2000,** *6,* 2103–2111. doi:10.1002/1521-3765(20000616)6:12<2103::AID-CHEM2103>3.0.CO;2-S

License and Terms

Beilstein Journal of Organic Chemistry

Planar-bilayer activities of linear oligoester bolaamphiphiles

Jonathan K. W. Chui, Thomas M. Fyles* and Horace Luong§

Full Research Paper

Open Access

Address:
Department of Chemistry, University of Victoria, Victoria BC, Canada

Email:
Jonathan K. W. Chui - jkwchui@uvic.ca;
Thomas M. Fyles* - tmf@uvic.ca

* Corresponding author
§ Current address: Department of Chemistry, University of Manitoba, Winnipeg MB, Canada

Keywords:
activity grid; single-molecule studies; synthetic ion channels; voltage clamp experiment

Beilstein J. Org. Chem. **2011,** *7,* 1562–1569.
doi:10.3762/bjoc.7.184

Received: 22 August 2011
Accepted: 26 September 2011
Published: 22 November 2011

This article is part of the Thematic Series "Supramolecular chemistry II".

Guest Editor: C. A. Schalley

Abstract

Voltage-clamp experiments of eight oligoester bolaamphiphiles in two subclasses are described. Syntheses of three new terephthalate-based compounds were achieved in three linear steps. Together with five previously described, related compounds, the ion transport activity was assessed by means of the voltage-clamp technique. All of the compounds show multiple types of conductance behavior in planar bilayers, a subset of which was exponentially voltage-dependent. The varied and irregular activities were summarized with the aid of a recently developed "activity-grid" method.

Introduction

Ion channels modulate conductance in cell membranes, and form the basic elements from which action potentials and other complex electrophysiological behaviors are constructed [1]. With recent technological breakthroughs, such as stochastic sensing [2] and the construction of ionic networks [3,4], the control and understanding of ion-channel attributes at a single-molecule level takes on a new urgency. By being able to tailor molecular features through synthesis, and potentially being accessible in far larger quantity than membrane proteins, de novo channels promise to be useful entities for structure–activity studies as well as practical "ionic components" of more complex systems. Since the pioneering report by Tabushi [5] some three decades ago, hundreds of disparate synthetic compounds have been shown to behave as ion channels, by ensemble and/or single-molecule techniques [6,7]. Ensemble techniques refer to the many variations of vesicle-based assays [8]; the results obtained are comparable under identical conditions, but often incommensurate with different variants of the method.

The voltage-clamp technique, on the other hand, reports absolute flux under defined conditions [9]. In this method, a

planar bilayer is formed in an aperture between two electrically connected aqueous compartments; this forms an insulator between the electrodes, and no current flows despite an applied potential across the electrodes. Upon addition of the compound forming the active channel, a current on the order of pA can be detected corresponding to the activity of single or small groups of molecules, and this current can be monitored with millisecond time resolution or faster. Thus, this method can report not only the flux but also the structural dimensions and dynamic properties of the channel with high sensitivity; however, the voltage-clamp experiment suffers from a need for specialized equipment, as well as the daunting task of making sense of all but the most regular of activities.

We have recently developed an empirical classification scheme for summarizing the range of voltage-clamp activities [10]. This "activity grid" represents the conductance of an event as a vertical position on a logarithmic scale in half log-unit steps from 3 to 3000 pS, the duration of these events as horizontal position on a logarithmic scale from 10 ms to 100 sec, and the pattern of activity as a different color shading (green for discrete "square-top" behavior, yellow for "flickering", blue for discrete transitions with irregular opening, red for short duration spikes, purple for "erratic" activities from which no pattern was discerned, and grey for regions of the grid where the experimental setup precludes detection of events). A systematic evaluation of published synthetic-ion-channel conductance records revealed an underlying commonality over the wide range of structural types. However, published records are typically a brief excerpt of full activities and we wondered how the methodology would fare in the real world. How would the method apply to full sets of unabridged records? And are there phenomena that are beyond the scope of this representation?

To provide a suitably focused yet sufficiently diverse suite of molecules in order to answer these questions, two classes of bolaamphiphiles were selected (Scheme 1). Both the phthalate and solid-phase derived alkyl compounds derive from the de-macrocyclization of an earlier active channel [11]. Structurally they similarly consist of a linear topology linked by internal esters (Es); the classes differ by the presence of multiple aromatic rings in the phthalates, and the lack of centrosymmetry in the alkyl compounds. These were expected to be active in voltage-clamp experiments, as close analogues to the phthalate compounds were found to be active in vesicles and planar bilayers [12], and the activities of the solid-phase compounds in vesicle experiments were previously established [13].

Results and Discussion

Synthesis of new compounds

The solid-phase synthesis of the alkyl oligoesters was previously reported [14]. The phthalate compounds were prepared by a modular methodology (Scheme 2), beginning by reacting terephthaloyl chloride or compound **9** (prepared by a method adapted from [15]) with α,ω-bromoalcohols prepared by monobrominating the corresponding diols as described [16]. This gave the bis-bromides, which were subsequently displaced by the protected carboxylate anion of BOC-protected aniline **14** to give precursors **15**, **16** and **17**.

Deprotection of the carbamate protecting groups under various acidic conditions also resulted in cleavage of internal esters in **15**. Selective cleavage was ultimately achieved by use of a TMSCl–phenol reagent [17] in dichloromethane to give the desired targets in three linear steps with modest overall yields. All three products were white solids that are freely soluble in chloroform; compounds **2** and **3** are soluble in methanol

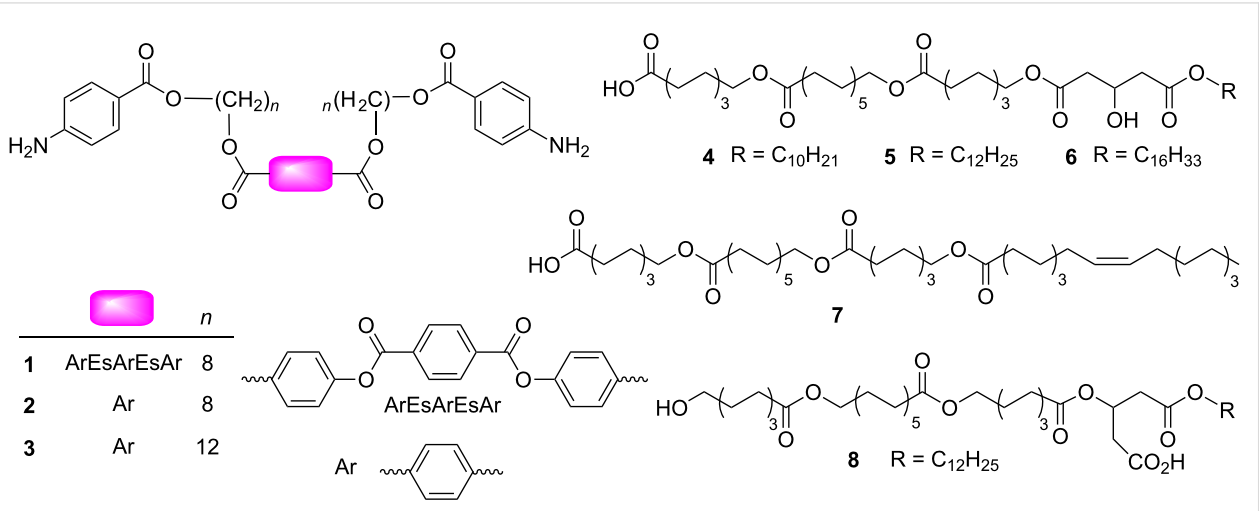

Scheme 1: Compounds studied with the voltage-clamp experiment.

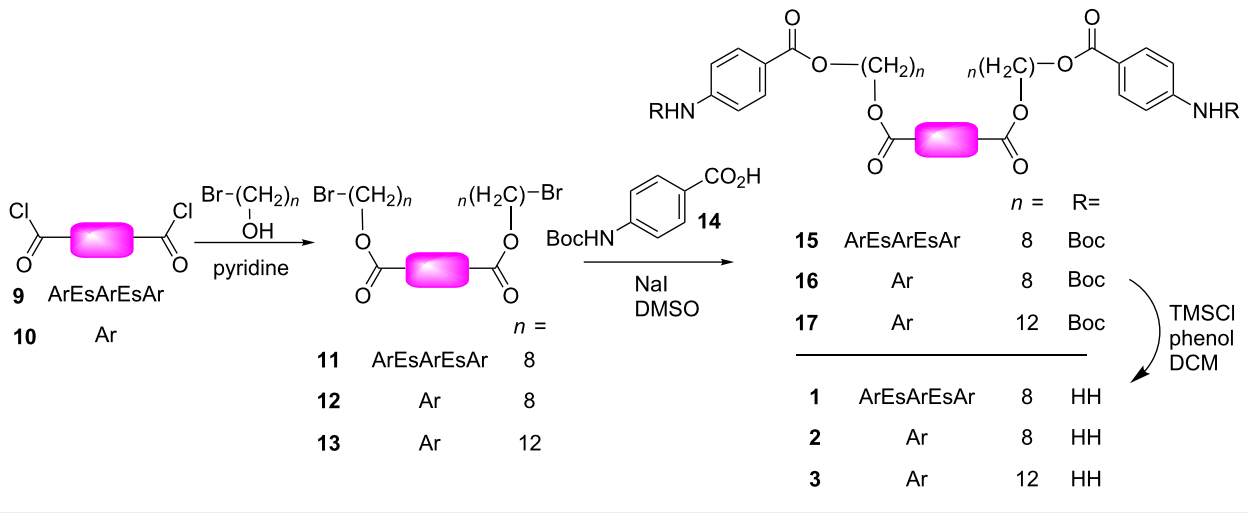

Scheme 2: Synthesis of phthalate compounds.

whereas **1** is only sparingly soluble. All three compounds precipitate from water at micromolar concentration or above.

Voltage-clamp results

Voltage-clamp studies were performed as previously described [12]. The method of introducing the compounds is limited by their solubility: Water-soluble compounds (**4**–**8**) were generally introduced as a solution to the bathing electrolyte, sparingly soluble **2** and **3** by injection close to the proximity of the bilayer, and the insoluble compound **1** was added by physical transfer from a brush. Physical transfer often results in membrane rupture, and the integrity of the membrane cannot be guaranteed; nonetheless, an analysis of different methods of compound introduction showed no substantial differences in compound activity [18].

Excerpts of experimental data are shown in Figure 1 and Figure 2 for compounds **1** and **2**, respectively. These two figures establish that a great variety of activities coexist for these two compounds, and that the regular "square top" behavior is a minority-type among many different types of irregular behavior. Complete experimental summaries are given in the Supporting Information File 1, from which it is clear that we could have made similar representations as Figure 1 and

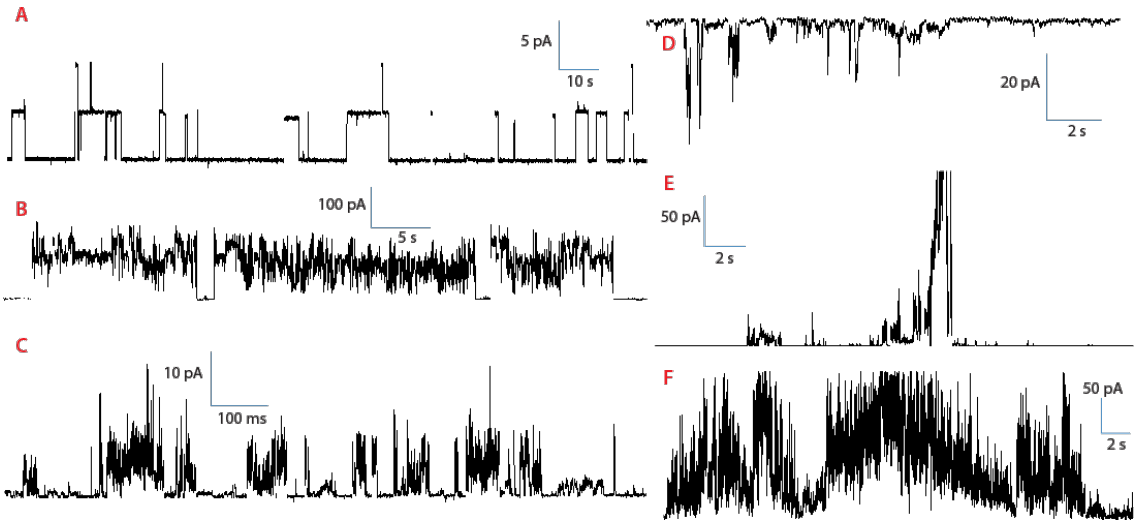

Figure 1: Channel activities of compound **1**. **A**: Regular "square-top" activity. Conditions: 1 M KCl buffered to pH 4.5, +200 mV; **B**: Large semiregular activity. Conditions: 1 M CsCl unbuffered, +130 mV; **C**: Short-lived semiregular openings. Conditions: 1 M KCl unbuffered, +100 mV; **D**: Short-lived, low-conductance bursts. Conditions: 1 M CsCl unbuffered, −50 mV; **E**: High-conductance bursts. Conditions: 1 M CsCl unbuffered, +120 mV; **F**: Continuous erratic activity. Conditions: 1 M CsCl unbuffered, +160 mV.

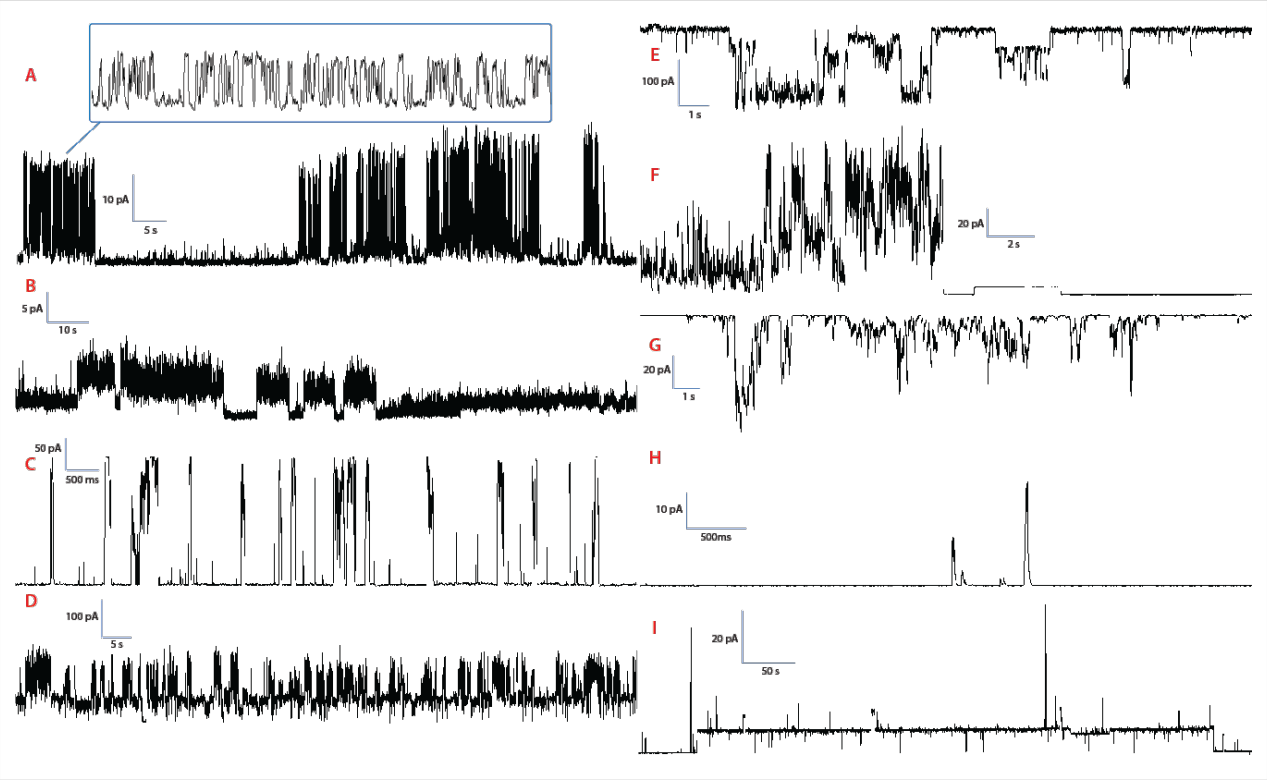

Figure 2: Channel activities of compound **2**. **A**: Rapid flickering. Conditions: 1 M CsCl, +100 mV; **B**: Semiregular openings. Conditions: 1 M CsCl, +100 mV; **C**: Regular high-conductance bursts. Conditions: 1 M CsCl, +120 mV; **D**: Long-lived opening punctuated by regular bursts. Conditions: 1 M CsCl, +100 mV; **E**: High-conductance, quasiregular activity. Conditions: 1 M CsCl, −120 mV; **F**: Abrupt closure following sustained bursts. Conditions: 1 M CsCl, pH 7, +120 mV; **G**: Short-lived, high-conductance bursts. Conditions: 1 M CsCl, pH 7, −120 mV; **H**: Brief spikes. Conditions: 1 M CsCl, pH 7, +180 mV; **I**: Long-lived regular opening, with conductance sublevels. Conditions: 1 M CsCl, pH 7, +170 mV.

Figure 2 with any other pair of compounds. Erratic behaviors may be aesthetically unappealing but should come as no surprise: The hydrocarbon chains that are present in every compound have significant conformational freedom; a variety of aggregation states are accessible, and an anisotropic membrane presents different local environments and other time-dependent degrees of freedom, which can be aptly collected under the umbrella term "dynamic supramolecular polymorphism" [8].

A theoretical framework and tools for extracting mechanistic information from the modeling of ideal "square-top" opening/closing events is well-developed, and statistical approaches may be appropriate when large numbers of events ($> 10^4$) are at hand [19]. The majority of the observations made in this study conform to neither of these criteria, and we were unable to visually discern any obvious patterns; for this reason we turned to the summary activity grids as a (potentially) model-independent method for recording diverse behaviors.

Preparing the "activity grid" from empirical current–time traces was facilitated by a suite of custom software, the development of which was described elsewhere [18]. There are two steps involved. The first involves the systematic conversion of current–time profiles, such as those given in Figure 1 and Figure 2, into conductance–time profiles from the known applied potentials. A simple example is given in Figure 3 which, when viewed from the experimental current–time perspective (top panel), shows (i) negative currents initially and positive currents over time, that (ii) events **A** and **B** are visually of lower magnitude than events **D**–**G**, and (iii) events **D**–**G** are of decreasing magnitude. Correcting for changes in the applied potential (middle panel) allows direct comparisons to be made, and it is clear from the bottom panel of Figure 3 that events **A** and **B** have a conductance at least twice as large as events **D**–**G**, and that the unit conductance of events **D**–**G** are in fact identical. Simple cases such as this could be resolved by a skilled observer, but more complex cases require full conversion to a conductance–time representation.

The second step involves a systematic inspection over several orders of magnitude in time and conductance in order to recognize and classify the conductance events that are encoded on the activity grid of each record. A single experiment consists of several records from a single day. Experiments were conducted over a period of time, with varying conditions of electrolyte, sequence of applied potentials, etc. The entire dataset of activity

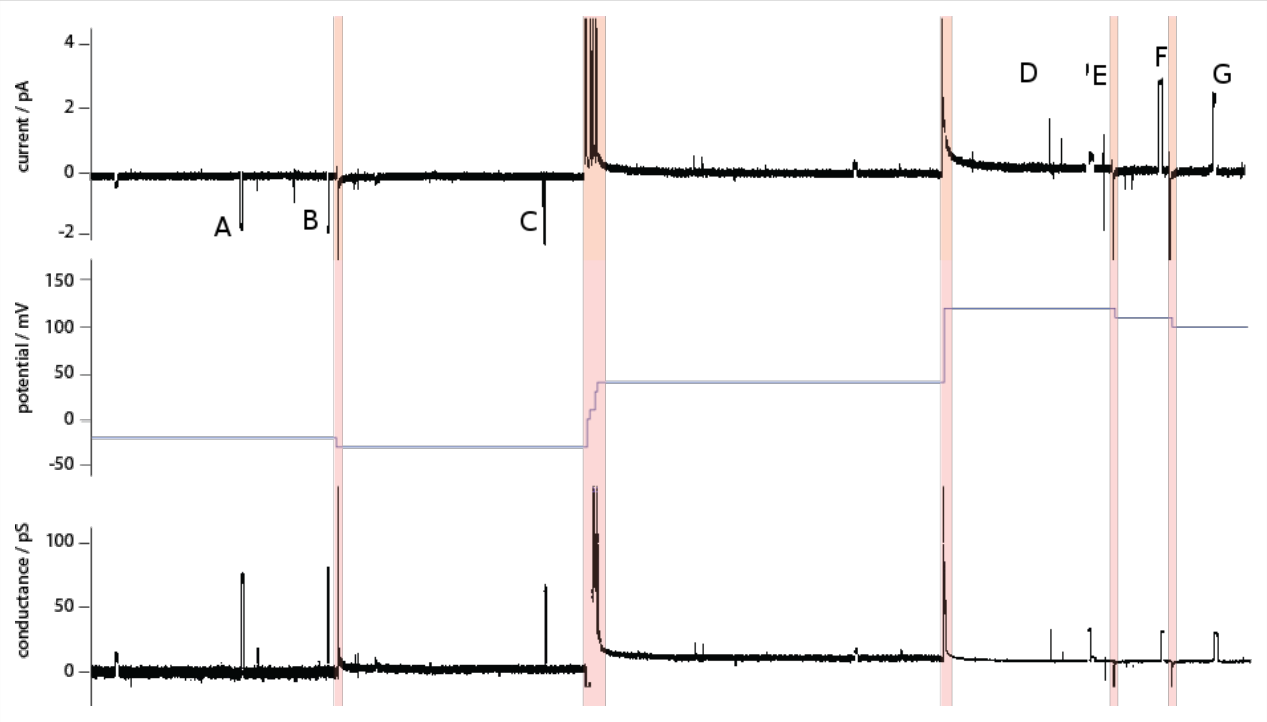

Figure 3: Conversion of a current–time profile of compound **5** (top) into conductance–time profile (bottom) by use of the applied potential (middle). (Red bands indicate changes of the potential; the spikes appearing in these periods are the capacitive currents from the instrument. The conductance is undefined when the applied potential is 0 mV, and thus this results in a break in the centre of the conductance–time profile.)

grids for a given compound was then summarized in a single set of grids. This procedure answers the question: Was a particular behavior of a particular conductance–duration ever observed? It does not provide information on the frequency of any particular type of activity or conductance–duration. This results in an activity profile for each compound, representative of the types of activity that were observed and their magnitude, from which a coarse-grained structure–activity can be mapped out (Figure 4).

The derived profiles are certainly consistent with our observations that almost every compound exhibits multiple types of activity. In this form it lacks a metric for the frequency of observation and is thus susceptible to both false positives (e.g., instrumental artifacts) as well as false negatives (i.e., absence of evidence is not evidence of absence). Nonetheless, the profiles reveal some interesting features when scrutinized through pairwise comparisons, and then from a "bird's eye view".

Specific pairwise comparisons are revealing in two senses. The first is that trends that were not obvious upon browsing through current–time traces stand out: For example, the comparison of the activity grids between the chain-reversed pair **5** and **8** shows that they are capable of forming "square-tops" of similar duration and conductance, but the latter also has other modes of irregular or erratic activity that are simply not observed in the former. The second is that, despite being able to point out empirical activity differences, these are almost impossible to rationalize in any simple way as the activities themselves are multifacetted and do not admit simple explanations.

In our systematic application of the "activity-grid" method to published records we found that, from the great number of unique architectures, there is an overall clustering characteristic for the type of activity [10]. What we find here is preliminary evidence that these relatively flexible molecules each individually also give rise to clusters of activity types. The extent of the clusters, as well as their magnitude in terms of duration and conductance, seem to be conserved between different linear bolaamphiphiles and correspond to the influence of each unique architecture on the overall system behavior. This is experimental support for the proposal [10] that there is some underlying energetic landscape that is as much a property of the system (lipid, water, and compound) as it is a property of the compounds we prepare and introduce.

Voltage dependence

Two types of voltage dependence have been reported previously. The first is a rectifying behavior, where ionic current passes preferentially for one polarity of the applied potential in comparison to the other polarity [20,21]. The second is a nonlinear current response to the applied potential, such as the

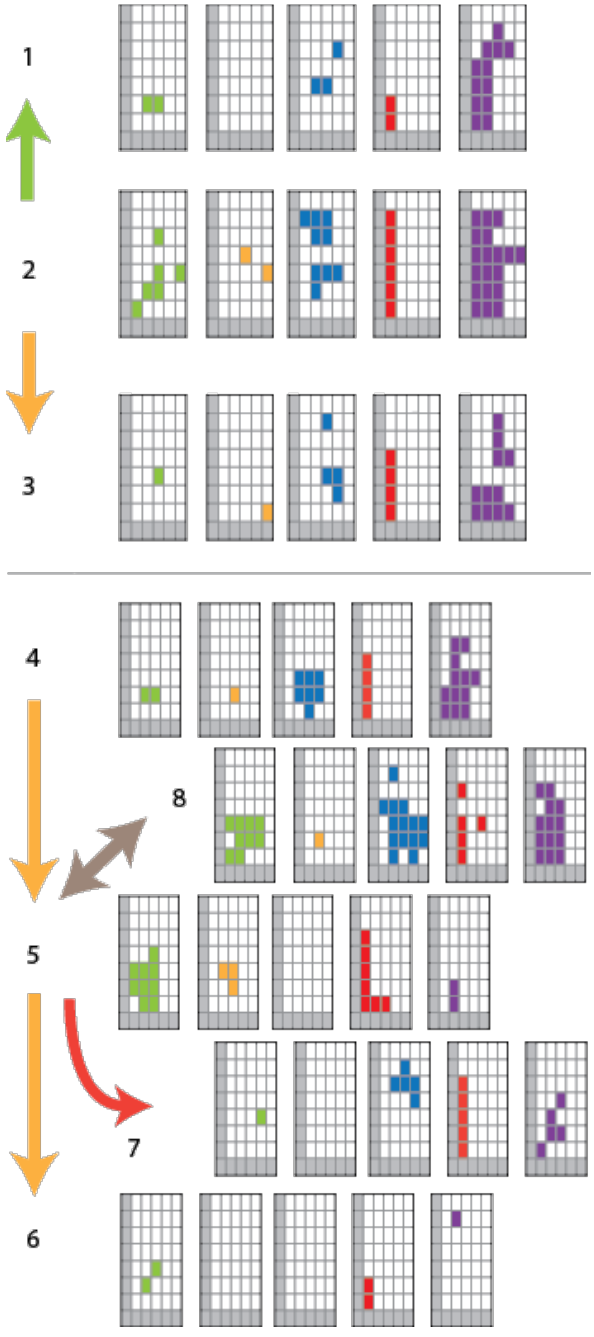

Figure 4: Single-molecule structure–activity relationships for compounds **1**–**8**. Grids are given in the following sequence in each case: Square-top (green); flicker (yellow); multiple-opening (blue); spike (red); erratic (purple). Yellow arrows indicate hydrocarbon homologs; green arrows indicate expansion of aromatic units; red arrows indicate the removal of a polar head group; the beige arrow indicates the reversal of chain polarity.

exponential dependence seen in alamethicin [22,23] or in a synthetic channel [24]. Two of the compounds in the terephthalate series, **1** and **2**, exhibit voltage dependence in the second sense (Figure 5).

The current–time behavior is irregular, and therefore the current was averaged over a 200 second interval. A plot of average current as a function of applied potential appeared symmetrical about zero, so the two branches for a given experiment were combined as the average current as a function of the absolute applied potential. Fits to a single exponential were adequate given the erratic activity ($r^2 > 0.9$), but both pre-exponential and exponential terms varied considerably between different experiments (Table 1). The exponent term of the fits can be used to derive an apparent gating charge, corresponding in an idealized model to the number of elementary charges required to move in response to the applied potential [25]. The observed values lie in the range from 1.2 to 3.5, with a cluster around 1.5. A physical interpretation of these values requires a detailed model, but it is clear that several charged species, presumed to be the protonated anilinium head groups, must move in response to the applied potential through some significant portion of the bilayer thickness. Neither the pre-exponential nor the exponent appears to be a characteristic solely of the compound. Concentration of the compound in the membrane presumably plays a large role, but the general lack of suitable solubility precludes additional studies.

Table 1: Voltage-dependent current (averaged over 200 s) for compounds **1** and **2**. **A** is the pre-exponential of the fitting, whereas **b** is the exponent.

Compound	A	b	r^2	Apparent gating charge
1	0.0285	0.0645	0.9795	2.5
1	0.2062	0.0386	0.9671	1.5
1	0.4802	0.030	0.9702	1.2
1	0.0170	0.0422	0.9499	1.6
2	1.1919	0.0896	0.9199	3.5
2	0.0983	0.0382	0.9709	1.5
2	0.1655	0.032	0.9562	1.2

Qualitatively, both the open probability as well as unit conductance (of the somewhat regular “blue” multilevel openings) appears to be enhanced at higher potentials. What could be the underlying mechanism? One line of possibilities relates to the underlying “system property” mentioned earlier. It is known that pure lipids near their phase transitions can show single-channel conductance activities; while the specific mode of action depends on the identity of the lipid, discrete conductance events indistinguishable from channels are possible [26]. It was recently reported that an applied potential can effect lipid phase transitions [27], one consequence of which is the creation of voltage-dependent lipid ion channels at the phase-transition temperature. Pure diphytanoyl phosphatidylcholine is normally stable to potentials exceeding 400 mV and does not show any

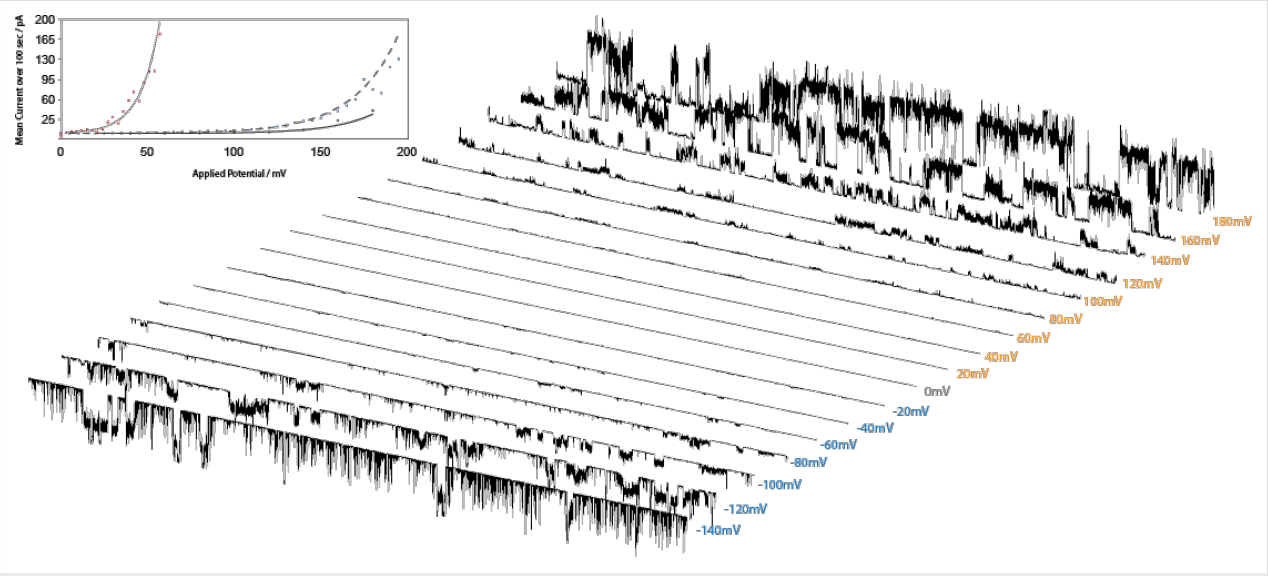

Figure 5: Voltage-dependent opening of compound **1**. Inset: Exponential dependence of the mean current on the potential. The solid line fits the trace shown in the figure.

detectible phase transitions [28,29]. It is conceivable that our introduction of "impurities" creates local disorder akin to domain separation at the melting transition and that fluctuations at the domain boundaries would give rise to voltage-dependent channel activity.

Conclusion

Two subclasses of linear oligoester bolaamphiphiles, comprising a total of eight compounds, were tested for conductance activity in diphytanoyl phosphatidylcholine planar bilayers. All compounds were active; most of them showed discrete "square-top" activity considered as a benchmark for the formation of single-channels. One of these compounds **5** has "square-top" activity as its predominant mode of activity, and two compounds in the terephthalate subclass show an exponential potential dependence of the ionic currents. Aside from the potential-dependent activity, the other types of conductance events can be documented in a standardized fashion by means of the "activity grid" method. From these individual profiles a (sparse) structure–activity map was constructed, and from this map two conclusions were drawn.

Firstly, the observations of clustered profiles match those that emerged from our systematic literature survey [10]. Note however, that the statistical support for this conclusion is very weak due to the very small number of observations (fewer than 200 on each side). Moreover, the irregular potential-dependence of the ion channels observed is similar in characteristic to the voltage-dependent lipid-only channels. These two parallels suggest that these simple bolaamphiphile compounds are not acting as channels on their own but rather in concert with a loosely defined "system" comprising lipid, compound, water, and electrolyte. A more focused investigation along these lines will be necessary to advance our understanding of how these simple channels "work".

The second conclusion concerns the "what compounds ought we to think about" question. Many synthetic ion channels require heroic synthetic efforts, and one of the enduring motivations in various research groups is to find structures that are synthetically accessible such that structural variations are possible. This often translates into smaller "minimalist" channel molecules, and our suite of compounds was built along these lines. This makes sense only if there is a defined and simple activity, such as the observed "square-top" events. In this study, we provided evidence that, although regular activities are not rare, their presence does not exclude other types of activity. The frequent presence of other types of activity calls into question our ability to draw simple structure–function correlations. Rather, our attention should be focused on the entire range of different activities, and the activity profiles give us a means to do that. However, no obvious trend emerged from the pairwise comparisons of this study. One possible reason is that, as compounds become smaller, more individual molecules must come together for active self-interactions or interactions with the lipid, and site-specific changes are less able to target only a single molecular parameter (rather than a confounding host of them). If this is true, then it suggests that "as small as possible" is not the optimal size for future investigations, and a larger study involving species with higher molecular weights may thus lead to both more unique behaviors (with less dependence on "system" properties) and deeper structure–activity insights.

Supporting Information

Supporting Information File 1

Synthesis procedures, spectroscopic characterization of new compounds and voltage-clamp summary activity records
[http://www.beilstein-journals.org/bjoc/content/supplementary/1860-5397-7-184-S1.pdf]

Acknowledgements

The ongoing support of the Natural Sciences and Engineering Research Council of Canada is gratefully acknowledged.

References

1. Hille, B. *Ionic Channels of Excitable Membranes,* 3rd ed.; Sinauer Associates Incorporated: Sunderland, 2001; p 383.
2. Lu, S.; Li, W.-W.; Rotem, D.; Mikhailova, E.; Bayley, H. *Nat. Chem.* **2010,** *2,* 921–928. doi:10.1038/nchem.821
3. Hwang, H. L.; Chen, M.; Cronin, B.; Holden, M. A.; Bayley, H. *J. Am. Chem. Soc.* **2008,** *130,* 5878–5879. doi:10.1021/ja802089s
4. Hwang, H. L.; Holden, M. A.; White, S.; Bayley, H. *J. Am. Chem. Soc.* **2007,** *129,* 11854–11864. doi:10.1021/ja074071a
5. Tabushi, I.; Kuroda, Y.; Yokota, K. *Tetrahedron Lett.* **1982,** *23,* 4601–4604. doi:10.1016/S0040-4039(00)85664-6
6. Sisson, A. L.; Shah, M. R.; Bhosale, S.; Matile, S. *Chem. Soc. Rev.* **2006,** *35,* 1269–1286. doi:10.1039/b512423a
7. Matile, S.; Som, A.; Sordé, N. *Tetrahedron* **2004,** *60,* 6405–6435. doi:10.1016/j.tet.2004.05.052
8. Matile, S.; Sakai, N. The characterization of synthetic ion channels and pores. In *Analytical Methods in Supramolecular Chemistry;* Schalley, C. A., Ed.; Wiley-VCH: Weinheim, 2007; pp 381–418.
9. Fyles, T. M. *Chem. Soc. Rev.* **2007,** *36,* 335–347. doi:10.1039/b603256g
10. Chui, J. K. W.; Fyles, T. M. *Chem. Soc. Rev.* **2011**. doi:10.1039/c1cs15099e
11. Fyles, T. M.; Loock, D.; van Straaten-Nijenhuis, W. F.; Zhou, X. *J. Org. Chem.* **1996,** *61,* 8866–8874. doi:10.1021/jo961267c
12. Eggers, P. K.; Fyles, T. M.; Mitchell, K. D. D.; Sutherland, T. *J. Org. Chem.* **2003,** *68,* 1050–1058. doi:10.1021/jo026415f
13. Luong, H.; Fyles, T. M. *Org. Biomol. Chem.* **2009,** *7,* 733–738. doi:10.1039/b816649h
14. Luong, H.; Fyles, T. M. *Org. Biomol. Chem.* **2009,** *7,* 725–732. doi:10.1039/b816648j
15. Mehdipour-Ataei, S.; Akbarian-Heizi, L. *Eur. Polym. J.* **2005,** *41,* 1280–1287. doi:10.1016/j.eurpolymj.2004.12.007
16. Chong, J. M.; Heuft, M. A.; Rabbat, P. *J. Org. Chem.* **2000,** *65,* 5837–5838. doi:10.1021/jo000291u
17. Kaiser, E.; Picart, F.; Kubiak, T.; Tam, J. P.; Merrifield, R. B. *J. Org. Chem.* **1993,** *58,* 5167–5175. doi:10.1021/jo00071a028
18. Chui, J. K. W. A New Paradigm for Voltage-Clamp Studies of Synthetic Ion Channels. Ph.D. Thesis, University of Victoria, Victoria, Aug 20, 2011.
19. Chui, J. K. W.; Fyles, T. M. *Chem. Commun.* **2010,** *46,* 4169–4171. doi:10.1039/c0cc00366b
20. Goto, C.; Yamamura, M.; Satake, A.; Kobuke, Y. *J. Am. Chem. Soc.* **2001,** *123,* 12152–12159. doi:10.1021/ja010761h
21. Fyles, T. M.; Loock, D.; Zhou, X. *J. Am. Chem. Soc.* **1998,** *120,* 2997–3003. doi:10.1021/ja972648q
22. Hall, J. E.; Vodyanoy, I.; Balasubramanian, T. M.; Marshall, G. R. *Biophys. J.* **1984,** *45,* 233–247. doi:10.1016/S0006-3495(84)84151-X
23. Sansom, M. S. P. *Eur. Biophys. J.* **1993,** *22,* 105–124. doi:10.1007/BF00196915
24. Sakai, N.; Ni, C.; Bezrukov, S. M.; Matile, S. *Bioorg. Med. Chem. Lett.* **1998,** *8,* 2743–2746. doi:10.1016/S0960-894X(98)00481-8
25. Sakai, N.; Houdebert, D.; Matile, S. *Chem.–Eur. J.* **2003,** *9,* 223–232. doi:10.1002/chem.200390016
26. Blicher, A.; Wodzinska, K.; Fidorra, M.; Winterhalter, M.; Heimburg, T. *Biophys. J.* **2009,** *96,* 4581–4591. doi:10.1016/j.bpj.2009.01.062
27. Heimburg, T. *Biophys. Chem.* **2010,** *150,* 2–22. doi:10.1016/j.bpc.2010.02.018
28. Fyles, T. M.; Knoy, R.; Müllen, K.; Sieffert, M. *Langmuir* **2001,** *17,* 6669–6674. doi:10.1021/la0105937
29. Lindsey, H.; Petersen, N. O.; Chan, S. I. *Biochim. Biophys. Acta* **1979,** *555,* 147–167. doi:10.1016/0005-2736(79)90079-8

License and Terms

Beilstein Journal of Organic Chemistry

Structural conditions required for the bridge lithiation and substitution of a basic calix[4]arene

Conrad Fischer, Wilhelm Seichter and Edwin Weber*

Full Research Paper

Open Access

Address:
Institut für Organische Chemie, TU Bergakademie Freiberg, Leipziger Str. 29, 09596 Freiberg, Germany

Email:
Edwin Weber* - Edwin.Weber@chemie.tu-freiberg.de

* Corresponding author

Keywords:
calixarene; lithiation; methylene bridge; supramolecular chemistry; X-ray structure

Beilstein J. Org. Chem. **2011,** *7,* 1602–1608.
doi:10.3762/bjoc.7.188

Received: 07 October 2011
Accepted: 10 November 2011
Published: 30 November 2011

This article is part of the Thematic Series "Supramolecular chemistry II".

Guest Editor: C. A. Schalley

Abstract

Lithiation and subsequent reaction with CO_2 was applied to calix[4]arenes with different, equal or mixed, ether functions at the lower-rim site as well as *tert*-butylated or non-*tert*-butylated upper-rim positions. Whereas this reaction fails for symmetric calix[4]arene ethers with alkoxy residues greater than methoxy, the carboxylation of mixed methoxy-propoxy calixarene ethers is possible. In connection with this, several new monobridge-substituted calix[4]arenes were characterized with respect to their conformational behaviour in solution and the X-ray crystal structure of one key intermediate is taken into consideration.

Introduction

Besides the huge progress made in the modification of the upper- and lower-rim positions of basic calix[4]arenes such as **1** in Scheme 1, the substitution of at least one methylene bridge of the chalice opens up a perspective for the vertical expansion of the molecule [1,2]. Thus, during the past decade two main preparative routes for the methylene-bridge substitution of *p*-*tert*-butyltetramethoxycalix[4]arene have been established: A protocol described by Biali et al. yields a stabilized methylene carbocation through bromination that is ready for electrophilic substitution under S_N1 conditions [3], whereas we follow a route involving the formation of a methylene carbanion through lithiation, which by nucleophilic substitution forms the desired bridge-substituted calixarenes [4,5]. While the number of

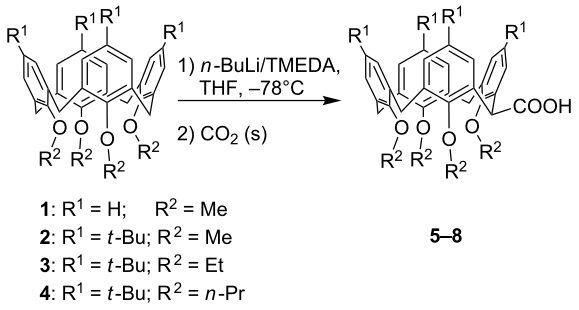

1: R^1 = H; R^2 = Me
2: R^1 = *t*-Bu; R^2 = Me
3: R^1 = *t*-Bu; R^2 = Et
4: R^1 = *t*-Bu; R^2 = *n*-Pr

5–8

Scheme 1: Calix[4]arene tetraethers **1–4** and corresponding bridge monosubstituted carboxylic acid derivatives **5–8**.

substituted methylene atoms in the first protocol depends clearly on the amount of *N*-bromosuccinimide used, surprisingly only monosubstitution of the chalice is observed by application of the lithiation technique, independent of the amount of *n*-BuLi. However, twofold substitution on opposite methylene bridges can be achieved by successive application of the latter technique [6]. This may suggest that the type of substitution significantly influences the conformation of the calixarene core, which is a versatile and important feature of this compound type (Figure 1). Nevertheless, in all these attempts for the purpose of a bridge substitution, only *p-tert*-butyltetramethoxycalix[4]arene **2** (Scheme 1) has been used as the basic compound. By way of contrast, nothing is known about the corresponding behaviour of upper-rim site unprotected or higher lower-rim site ether homologues as starting materials for a horizontal expansion of the chalice. Thus, within this paper, we present the results of the lithiation of differently upper- and lower-rim-modified calix[4]arenes, allowing us to draw helpful conclusions about the necessary structural requirements for the bridge lithiation and subsequent substitution of a basic calix[4]arene.

Results and Discussion

Since the calixarene **2** is known to undergo lithiation and subsequent carboxylation to yield the carboxylic acid **6** [4], we became interested in the question of whether the upper-rim unsubstituted calix[4]arene **1**, as well as higher ether homologues, such as **3** and **4**, can also be used for this reaction (Scheme 1). While the upper-rim site unprotected calix[4]arene **1** can be similarly converted into the respective acid **5**, this reaction failed for the higher ether homologues **3** and **4**. In the case of **3**, only a few very weak signals in the ^{1}H NMR spectrum suggested traces of the desired acid **7**, whereas upon addition of *n*-BuLi to a solution of the tetrapropyl ether **4** no colour change to cherry red (indicating the anion formation) was observed. Obviously, the lithiation step requires a high degree of conformational flexibility from the calixarene core, giving rise to coordinative interactions of the lithium cation with the methoxy O-atoms. For **1** and **2**, a rotation around the methylene groups is easily possible, thus allowing the conformational flexibility of the chalice, which is beneficial for the lithiation step. Though a rotation through the annulus may also take place in compound **3**, in principle, this conformational adaptation is slow on the timescale of lithiation. After addition of *n*-BuLi to a THF solution of the tetraethyl ether **3**, the colour changed over a period of 40 minutes only to strawberry red, indicating the highly limited reactivity of **3**. Since a rotation of any arene unit in the calix[4]arene **4** is impossible, due to the sterical hindrance of the propyl groups, no reaction with *n*-BuLi and CO_2 was observed.

Considering the aforementioned facts, in a second attempt, we asked the question of whether the lithiation can also be achieved with mixed calix[4]arene ethers containing a combination of

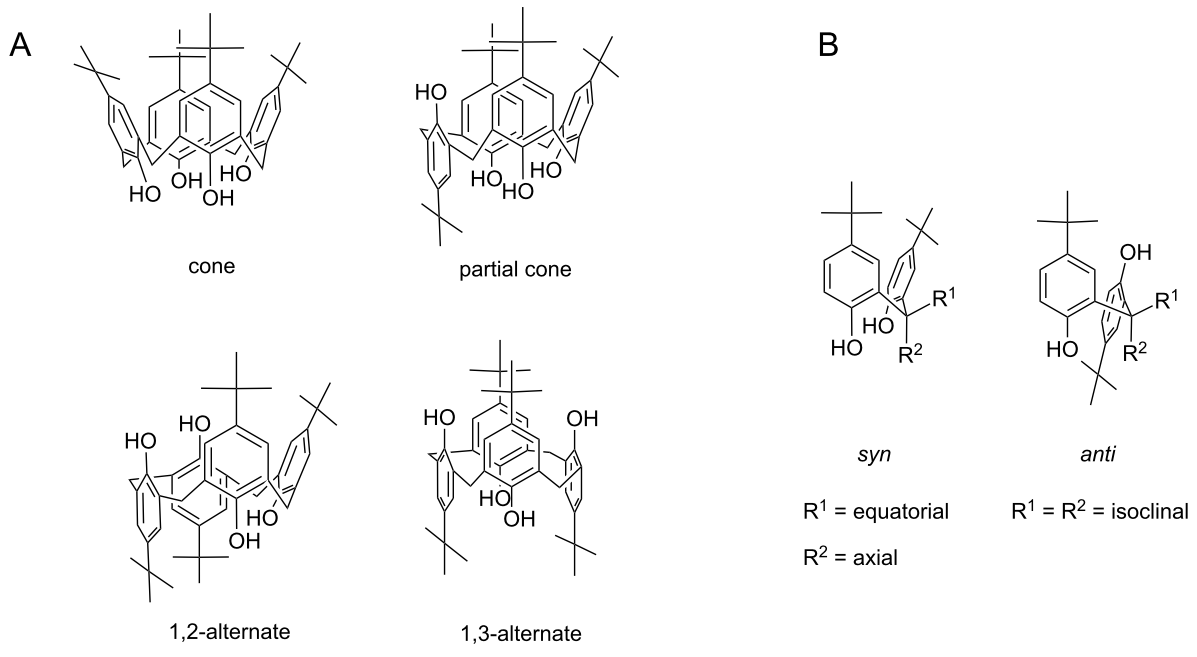

Figure 1: A: Four fundamental conformations of a calix[4]arene. B: Arrangement of the methylene group substituents with respect to the orientation of the neighbouring arene units.

methoxy and propoxy groups at the lower-rim site. Therefore, the proximal and distal dipropoxy-dimethoxy ether derivatives **11** and **12** were synthesized in a two-step procedure by regioselective propylation of the parent tetrahydroxycalix[4]arene [7,8] and subsequent methylation of the intermediates **9** and **10** (Scheme 2). In accordance with a previous description [9], both derivatives show a high conformational flexibility in $CDCl_3$ solution due to the possible rotation of the anisole units through the annulus, whereas the more bulky propoxy-containing arene units remain fixed. However, on the application of an elegant preparation procedure involving the addition of small amounts of NaI and acetronitrile-d_3 to the $CDCl_3$ solution, fixation of the calixarenes in a pure cone conformation was achieved (Figure 2).

Separate lithiation of the two mixed ethers **11** and **12** followed by the addition of CO_2 results in the desired carboxylic acid derivatives **13** and **14**, which again feature high conformational flexibility in $CDCl_3$ solution. Nevertheless, the yield of the acid **13** is much lower than for **14**, which is comprehensible since in compound **13** the lithium cation is always restricted by the steric demand of having one neighbouring propoxy group, limiting an ideal complexation. Again, on the addition of NaI and acetonitrile-d_3 to the $CDCl_3$ solution of **13** the cone conformation is preserved, bearing the lateral COOH group in an equatorial position between neighbouring methoxy and propoxy units, as indicated by NOESY interactions of the remaining methine proton. In contrast, after addition of the fixatives to a $CDCl_3$ solution of **14**, a more complex signal pattern indicates the presence of at least two fixed conformations. One can be related to the expected resonances of the cone conformer, while the resonances of the second species fit best to a 1,2-alternate conformation (Supporting Information File 1, Figure S9). In both conformers, the lateral substituent is located at the equato-

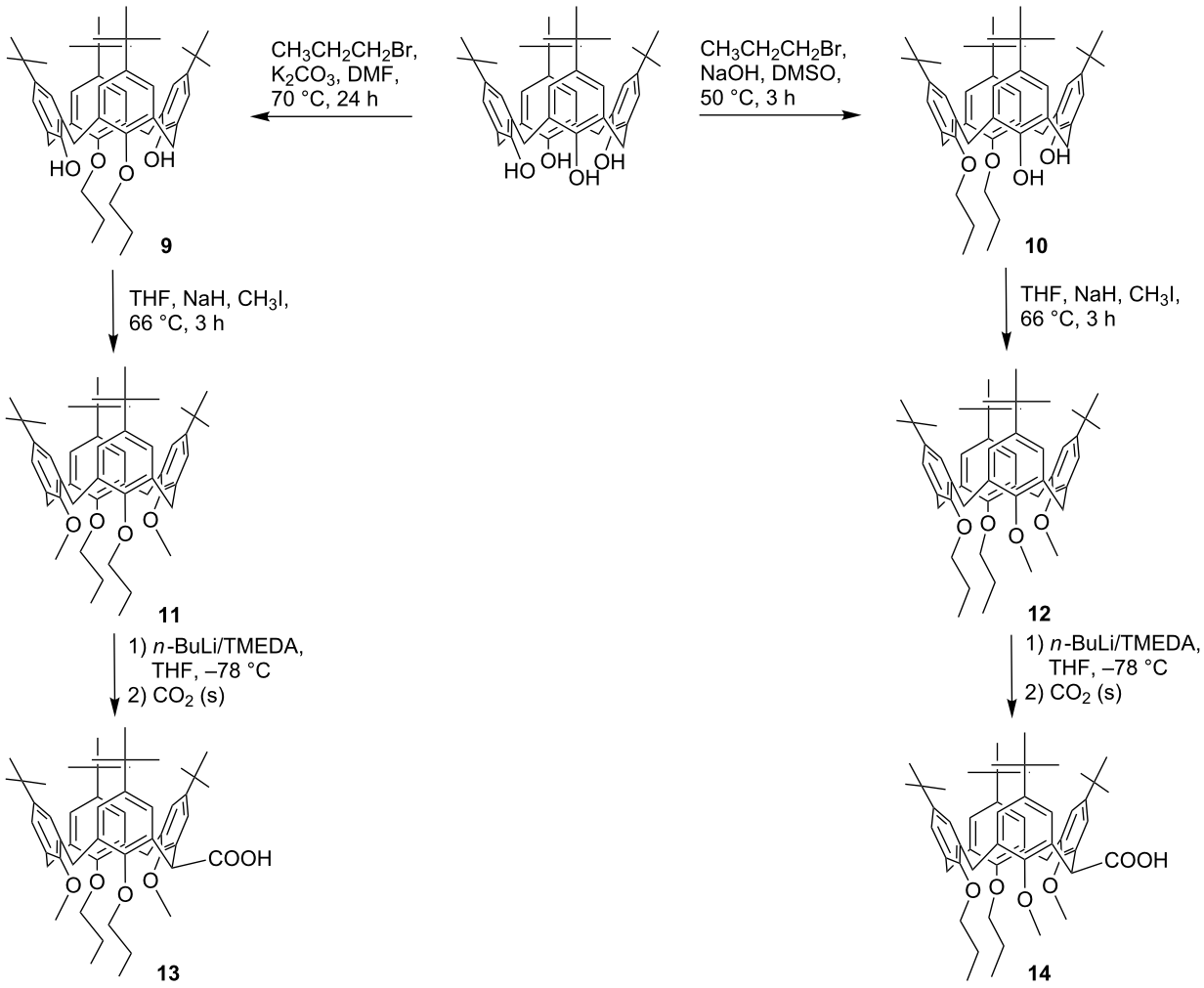

Scheme 2: Pathways to the calixarene acids **13** and **14** bearing mixed ether functions in different fashions.

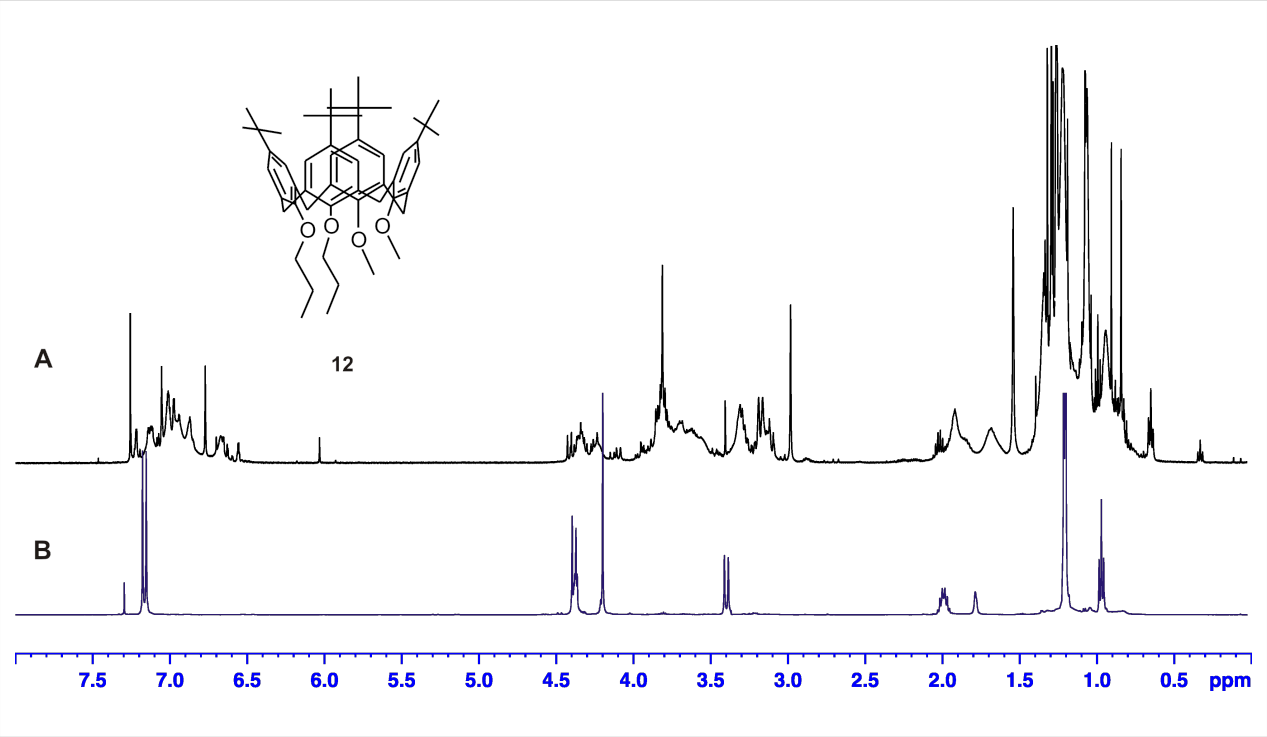

Figure 2: ^{1}H NMR spectrum ($CDCl_3$, 293 K, 500 MHz) of calixarene ether **12** before (**A**) and after the addition of NaI/acetonitrile-d_3 (**B**).

rial position, assuming a rotation of both methoxy groups before the substitution step. Thus, a subsequent rotation of both methoxy groups through the annulus, transferring the 1,2-alternate to the cone conformer, is impossible, since it would ultimately lead to an axial orientation of the COOH group, which is strictly avoided for steric reasons [4,10].

Crystal structure of compound 12

Crystallization of the mixed calixarene ether **12** from ethanol yielded colourless solvent-free crystals featuring two crystallographically independent molecules within the asymmetric unit (Figure 3). Unlike the findings relating to the conformational behaviour in solution, both structurally different calixarene molecules display a partial cone conformation with an anti-arrangement of the two neighbouring methoxy groups (Table 1). Whereas the molecule **12(1)** shows a nearly coplanar arrangement of the opposite arene rings A/C (4.12°), in the molecule **12(2)** these rings are inclined at an angle of 11.80°, which is attributable to packing effects. Remarkably, the two propyl chains seem to have no significant influence on the behaviour of the chalice with reference to related structures of tetramethoxycalix[4]arenes in a partial cone conformation [11-13].

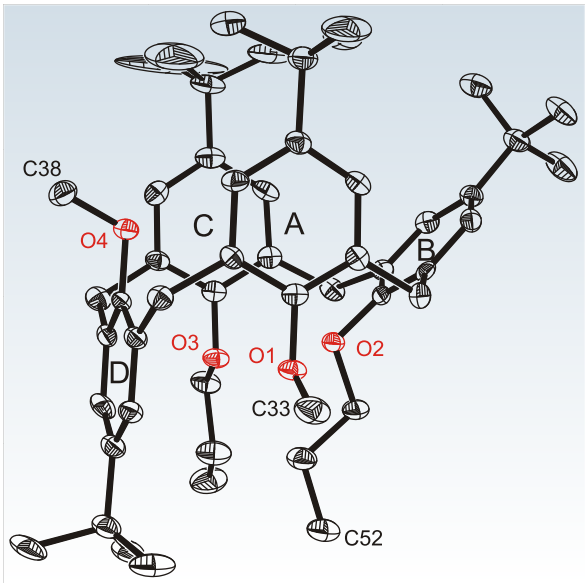

Figure 3: Crystal structure of compound **12**. For clarity only one of the two crystallographically independent molecules is presented; **12(1)** and H-atoms are omitted.

In the packing (Supporting Information File 1, Figure S11), the molecules are stacked along the crystallographic *ab* plane stabilized by weak C–H···π interactions [14] involving methoxy groups and arene units of the neighbouring calixarene molecules (C33A–H33D···centroid *C*: 3.460(6) Å; C38–H38A···centroid *B*: 3.707(6) Å; C52A–H52D···centroid *A*: 3.619(6) Å). The resulting channel-like voids between any two calixarene layers are potentially accessible for guest inclusion,

Table 1: Selected conformational parameters of the mixed ether **12** in comparison with the corresponding tetramethoxycalix[4]arene **2**. Pairs (e.g. **12(1)** and **12(2)**) reflect two crystallographically independent molecules in these structures.

	12(1)	12(2)	2(1)	2(2)
Interplanar angle (°)				
A[a]/mpla[b]	86.21	79.86	88.27	86.20
B/mpla	44.87	42.39	35.35	36.28
C/mpla	89.68	88.36	84.82	84.74
D/mpla	85.17	77.62	88.00	88.39
A/C	4.12	11.80	6.96	9.09
B/D	40.31	35.29	52.65	52.18
KPI	62.9		–	

[a]Aromatic rings: A···C1–C6; B···C8–C13; C···C15–C20 and D···C22–C27. [b]Mean plane through atoms C7, C14, C21 and C28.

which is also reflected by a comparatively low packing index (62.9) of the crystal [15].

Conclusion

It was shown that the bridge monosubstitution of a basic calix[4]arene via lithiation requires a high conformational flexibility of the calixarene, which is the case when the overall lower-rim substitution is not larger than methoxy and/or when the *tert*-butyl groups at the upper-rim site are absent. Moreover, in the case of mixed higher calixarene ethers bearing only two methoxy groups at the lower-rim site, the calixarene undergoes lithiation and substitution as well, indicating that the lithiation takes place favourably in the neighbourhood of the methoxy groups for potential complexation reasons. Once the bridge substitution has taken place in these types of calixarene ethers, a subsequent rotation around the methylene groups seems impossible, as suggested by the presence of two nonconvertible conformers of the calixarene acid **14**.

Experimental

General remarks

Melting points were determined on a microscope heating stage PHMK Rapido (VEB Dresden Analytik) and are uncorrected. IR spectra were measured on a Nicolet FT-IR 510 as KBr pellets. NMR spectra were recorded on a Bruker Avance DPX 500 spectrometer at 500.1 MHz (^{1}H NMR) and 125.7 MHz (^{13}C NMR), in $CDCl_3/CD_3CN$ solution (9:1) with small amounts of NaI. Chemical shifts δ are reported in ppm relative to the internal reference TMS. Mass spectra were measured on a Varian 320 MS. Elemental analyses were perfomed on a Heraeus CHN-Rapid Analyzer. Reagents and chemicals for the synthesis were used as purchased from chemical suppliers. The solvents used were purified or dried according to common literature procedures.

Syntheses

Starting compounds **1** [16], **2** [17], **3** [18] and **4** [7], as well as the intermediates **9** [7] and **10** [8] were prepared according to described protocols. The carboxylic acid **6** was prepared in a similar manner to compound **5**.

25,26,27,28-Tetramethoxycalix[4]arene-2-carboxylic acid (**5**) (*cone*)

A solution of 1.7 mL (11.0 mmol) TMEDA in 100 mL dry THF was cooled down to −78 °C and at this temperature 5.2 mL (8.3 mmol) *n*-BuLi (1.6 M in *n*-hexane) was added. After 30 min a solution of 1.8 g (3.8 mmol) 25,26,27,28-tetramethoxycalix[4]arene (**1**) in 50 ml dry THF was added by syringe. The resulting cherry red solution was allowed to warm up to ambient temperature. After 1 h, solid CO_2 was added, immediately changing the colour of the solution to yellow. Removal of all volatiles resulted in a yellow residue, which was dissolved in a small amount of methanol. By addition of water, a white precipitate was formed giving **5** after recrystallization from methanol as a microcrystalline solid. Yield: 0.9 g (46%); mp 249–251 °C; ^{1}H NMR (500.1 MHz, $CDCl_3/CD_3CN$ 9:1) δ 7.44 (d, J = 7.5 Hz, 2H, ArH), 7.19 (d, J = 7.5 Hz, 2H, ArH), 7.15 (d, J = 7.5 Hz, 4H, ArH), 6.96 (t, J = 7.8 Hz, 2H, ArH), 6.90 (t, J = 7.8 Hz, 2H, ArH), 5.83 (s, 1H, CHCOOH), 4.33 (m, 4H, $ArCH_2Ar$), 4.27 (s, 6H, OCH_3), 4.22 (s, 6H, OCH_3), 3.48 (m, 4H, $ArCH_2Ar$); ^{13}C NMR (125.7 MHz, $CDCl_3/CD_3CN$ 9:1) δ 177.8 (COOH), 152.7, 152.4, 134.9, 134.8, 134.7, 129.8, 129.2, 129.0, 127.6, 126.2, 126.0, 65.7, 65.1, 40.8, 29.4; IR (cm^{-1}): 2931, 2820, 1714, 1588, 1463, 1426, 1326, 1288, 1248, 1206, 1168, 1087, 1009, 897, 838, 771, 685, 612; LC–MS *m*/*z*: 542.2 $[M + NH_4]^+$; Anal. calcd for $C_{33}H_{32}O_6$: C, 71.85; H, 6.40; found: C, 72.00; H, 6.28.

General procedure for the synthesis of **11** and **12** (*O*-methylation)

The given amount of distal and proximal *O*-propoxylated calix[4]arenes **9** and **10** was dissolved in dry THF and NaH (60% in mineral oil) was added. After 1.5 h of reflux, 9 equiv of MeI were added by syringe and heating was continued for 3 h. All volatiles were removed and the crude product was treated carefully with water. The solid was separated and dissolved in 30 mL $CHCl_3$. After addition of MeOH, a white precipitate formed, which was collected and recrystallized from $CHCl_3$/MeOH 1:3.

5,11,17,23-Tetra-*tert*-butyl-25,27-dimethoxy-26,28-dipropoxycalix[4]arene (**11**) (*cone*)

Reagents: 2.85 g (3.9 mmol) **9** in 40 mL dry THF, 1.6 g (40 mmol) NaH, 2.3 mL (5.1 g, 36 mmol) CH_3I. Yield: 1.7 g (58%); mp 203–206 °C; ^{1}H NMR (500.1 MHz, $CDCl_3/CD_3CN$ 9:1) δ 7.18 (s, 4H, ArH), 7.15 (s, 4H, ArH), 4.38 (d, J = 12.4

Hz, 4H, $ArCH_2Ar$), 4.37 (m, 4H, $CH_2CH_2CH_3$), 4.20 (s, 6H, OCH_3), 3.39 (d, J = 12.4 Hz, 4H, $ArCH_2Ar$), 1.99 (m, 4H, $CH_2CH_2CH_3$), 1.21 (s, 18H, $C(CH_3)_3$), 1.20 (s, 18H, $C(CH_3)_3$), 0.97 (t, J = 7.4 Hz, 6H, $CH_2CH_2CH_3$); ^{13}C NMR (125.7 MHz, $CDCl_3/CD_3CN$ 9:1) δ 150.8, 149.9, 148.7, 148.0, 134.8, 134.6, 125.8, 125.7, 79.7, 64.7, 34.2, 34.1, 31.1, 31.0, 30.4, 22.6, 9.3; LC–MS m/z: 778.6 $[M + NH_4]^+$; Anal. calcd for $C_{52}H_{72}O_4 \cdot CH_3OH$: C, 81.14; H, 9.59; found: C, 81.01; H, 9.38.

5,11,17,23-Tetra-*tert*-butyl-25,26-dimethoxy-27,28-dipropoxycalix[4]arene (**12**) (*cone*)

Reagents: 2.2 g (3.0 mmol) **10** in 40 mL dry THF, 1.2 g (30 mmol) NaH, 1.7 mL (3.8 g, 27 mmol) CH_3I. Yield: 1.4 g (61%); mp 154–156 °C; ^1H NMR (500.1 MHz, $CDCl_3/CD_3CN$ 9:1) δ 7.17 (s, 4H, ArH), 7.17 (s, 2H, ArH), 7.16 (s, 2H, ArH), 4.47 (d, J = 12.4 Hz, 1H, $ArCH_2Ar$), 4.39 (d, J = 12.4 Hz, 2H, $ArCH_2Ar$), 4.35 (m, 4H, $CH_2CH_2CH_3$), 4.29 (d, J = 12.4 Hz, 1H, $ArCH_2Ar$), 4.21 (s, 6H, OCH_3), 3.40 (m, 4H, $ArCH_2Ar$), 2.00 (m, 4H, $CH_2CH_2CH_3$), 1.21 (s, 18H, $C(CH_3)_3$), 1.20 (s, 18H, $C(CH_3)_3$), 0.97 (t, J = 7.4 Hz, 6H, $CH_2CH_2CH_3$); ^{13}C NMR (125.7 MHz, $CDCl_3/CD_3CN$ 9:1) δ 150.8, 149.8, 148.6, 148.1, 135.0, 134.7, 134.6, 134.4, 125.9, 125.8, 125.7, 125.6, 79.6, 65.0, 34.2, 34.1, 31.0, 31.0, 30.4, 22.5, 9.3; LC–MS m/z: 778.6 $[M + NH_4]^+$; Anal. calcd for $C_{52}H_{72}O_4$: C, 82.06; H, 9.53; found: C, 82.22; H, 9.67.

5,11,17,23-Tetra-*tert*-butyl-25,27-dimethoxy-26,28-dipropoxycalix[4]arene-2-carboxylic acid (**13**) (*cone*)

Lithiation and subsequent substitution followed the described protocol for compound **5**. Reagents: 0.76 g (1 mmol) mixed ether **11** in 25 mL dry THF, 0.95 mL (6.1 mmol) TMEDA in 40 mL dry THF, 2.85 mL (4.6 mmol) *n*-BuLi. Yield: 0.28 g (36%); mp 147–150 °C; ^1H NMR (500.1 MHz, $CDCl_3/CD_3CN$ 9:1) δ 7.16 (d, J = 12 Hz, 6H, ArH), 7.06 (d, J = 5 Hz, 2H, ArH), 5.86 (s, CHCOOH), 4.38 (d, J = 12.5 Hz, 3H, $ArCH_2Ar$), 4.37 (m, 4H, $CH_2CH_2CH_3$), 4.20 (s, 6H, OCH_3), 3.39 (d, J = 12.5 Hz, 3H, $ArCH_2Ar$), 1.99 (m, 4H, $CH_2CH_2CH_3$), 1.21 (s, 18H, $C(CH_3)_3$), 1.20 (s, 18H, $C(CH_3)_3$), 0.97 (t, J = 7.3 Hz, 6H, $CH_2CH_2CH_3$); ^{13}C NMR (125.7 MHz, $CDCl_3/CD_3CN$ 9:1) δ 179.3 (COOH), 150.8, 150.0, 148.7, 148.1, 134.8, 134.6, 133.7, 132.5, 132.1, 127.8, 125.8, 125.7, 125.5, 125.4, 79.7, 64.8, 64.6, 34.2, 34.1, 31.5, 31.4, 31.1, 30.9, 30.4, 22.6, 9.3; IR (cm^{-1}): 2959, 2905, 2873, 2822, 1707, 1602, 1481, 1462, 1391, 1296, 1245, 1202, 1122, 1067, 1043, 1013, 966, 947, 870, 815, 698, 640, 556; LC–MS m/z: 822.6 $[M + NH_4]^+$; Anal. calcd for $C_{53}H_{72}O_6$: C, 79.06; H, 9.01; found: C, 79.12; H, 9.21.

5,11,17,23-Tetra-*tert*-butyl-25,26-dimethoxy-27,28-dipropoxycalix[4]arene-2-carboxylic acid (**14**)

Lithiation and subsequent substitution followed the described protocol for compound **5**. Reagents: 0.71 g (0.9 mmol) mixed ether **12** in 25 mL dry THF, 0.95 g (6.1 mmol) TMEDA in 40 mL dry THF, 2.85 mL (4.6 mmol) *n*-BuLi. Yield: 0.45 g (60%); mp 130–133 °C; ^1H NMR (500.1 MHz, $CDCl_3/CD_3CN$ 9:1) δ 7.17 (m, 8H, ArH), 5.86 (s, 1H, CHCOOH), 4.53 (d, J = 12 Hz, 1H, $ArCH_2Ar$), 4.43 (d, J = 12.5 Hz, 2H, $ArCH_2Ar$), 4.35 (m, 4H, $CH_2CH_2CH_3$), 4.27 (s, 3H, OCH_3), 4.20 (s, 3H, OCH_3), 3.42 (m, 3H, $ArCH_2Ar$), 2.00 (m, 4H, $CH_2CH_2CH_3$), 1.21 (s, 18H, $C(CH_3)_3$), 1.20 (s, 18H, $C(CH_3)_3$), 0.96 (t, J = 7.3 Hz, 6H, $CH_2CH_2CH_3$); ^{13}C NMR (125.7 MHz, $CDCl_3/CD_3CN$ 9:1) δ 173.9 (COOH), 153.4, 150.6, 150.3, 149.7, 148.7, 134.8, 134.6, 134.2, 133.8, 132.8, 132.6, 132.1, 126.7, 126.4, 126.1, 125.7, 125.5, 79.9, 79.5, 65.5, 65.0, 60.5, 41.3, 41.0, 37.2, 34.3, 34.0, 33.8, 31.4, 31.3, 31.0, 29.6, 22.5, 22.2, 9.9, 9.2; IR (cm^{-1}): 2955, 2904, 2871, 2820, 1707, 1602, 1481, 1463, 1391, 1361, 1287, 1245, 1201, 1121, 1067, 1043, 1018, 967, 948, 869, 789, 677, 637, 554; LC–MS m/z: 822.6 $[M + NH_4]^+$; Anal. calcd for $C_{53}H_{72}O_6$: C, 79.06; H, 9.01; found: C, 78.75; H, 9.03.

Crystallography

The intensity data for the crystals of compound **12** submitted to X-ray diffraction were collected on a Kappa APEX II diffractometer (Bruker-AXS) with graphite-monochromated Mo Kα radiation (λ = 0.71073 Å) using ω- and φ-scans. Reflections were corrected for background, Lorentz and polarization effects. Preliminary structure models were derived by application of direct methods [19] and were refined by full-matrix least-squares calculations based on F^2 for all reflections. An empirical absorption correction based on multiple scans was applied by using the SADABS program [20]. All non-hydrogen atoms were refined anisotropically. All hydrogen atoms were refined as being constrained to bonding atoms.

Crystal data for 12: $C_{52}H_{72}O_4$, crystal system, space group: Monoclinic, $P2_1/c$; unit cell dimensions: a = 17.3537 (8) Å, b = 20.1153 (9) Å, c = 27.2570 (13) Å, β = 91.930° (2); volume: 9509.3 (8) $Å^3$; Z = 8; calculated density: 1.063 mg m^{-3}; absorption coefficient: 0.065; F(000): 3328; θ-range for data collection 1.17–25.03°; refinement method: Full matrix least-square on F^2; data/parameters: 7791/1041; goodness-of-fit on F^2: 1.013; final R indices [$I > 2\sigma(I)$]: R = 0.0944, wR = 0.1970; R-indices (all data): R = 0.2010, wR = 0.2517; final $\Delta\rho_{max}/\Delta\rho_{min}$: 0.49/−0.45 e $Å^{-3}$. CCDC: 847217.

Supporting Information

Supporting Information File 1

^1H NMR and ^{13}C NMR spectra of compounds **5**, **11**–**14** and crystal packing illustration of mixed ether **12**.
[http://www.beilstein-journals.org/bjoc/content/supplementary/1860-5397-7-188-S1.pdf]

Acknowledgements

The authors are grateful for generous financial support to this work from the German Federal Ministry of Economics and Technology (BMWi) under grant No. 16IN0218 'ChemoChips'.

References

1. Fischer, C.; Gruber, T.; Seichter, W.; Weber, E. *Org. Biomol. Chem.* **2011,** *9,* 4347–4352. doi:10.1039/c1ob00028d
2. Fischer, C.; Lin, G.; Bombicz, P.; Seichter, W.; Weber, E. *Struct. Chem.* **2011,** *22,* 433–439. doi:10.1007/s11224-011-9746-7
3. Kuno, L.; Biali, S. E. *J. Org. Chem.* **2011,** *76,* 3664–3675. doi:10.1021/jo200580m
4. Gruber, T.; Gruner, M.; Fischer, C.; Seichter, W.; Bombicz, P.; Weber, E. *New J. Chem.* **2010,** *34,* 250–259. doi:10.1039/b904489b
5. Gruner, M.; Fischer, C.; Gruber, T.; Weber, E. *Supramol. Chem.* **2010,** *22,* 256–266. doi:10.1080/10610270903437044
6. Fischer, C.; Lin, G.; Seichter, W.; Weber, E. *Tetrahedron* **2011,** *67,* 5656–5662. doi:10.1016/j.tet.2011.05.087
7. Iwamoto, K.; Araki, S.; Shinkai, S. *J. Org. Chem.* **1991,** *56,* 4955–4962. doi:10.1021/jo00016a027
8. Boyko, V. I.; Podoprigorina, A. A.; Yakovenko, A. V.; Pirozhenko, V. V.; Kalchenko, V. I. *J. Inclusion Phenom. Macrocyclic Chem.* **2004,** *50,* 193–197. doi:10.1007/s10847-005-5240-4
9. Matthews, S. E.; Saadioui, M.; Böhmer, V.; Barboso, S.; Arnaud-Neu, F.; Schwing-Weill, M.-J.; Carrera, A. G.; Dozol, J.-F. *J. Prakt. Chem.* **1999,** *341,* 264–273. doi:10.1002/(SICI)1521-3897(199904)341:3<264::AID-PRAC264>3.0.CO;2-F
10. Biali, S. E.; Böhmer, V.; Cohen, S.; Ferguson, G.; Grüttner, C.; Grynszpan, F.; Paulus, E. F.; Thondorf, I.; Vogt, W. *J. Am. Chem. Soc.* **1996,** *118,* 12938–12949. doi:10.1021/ja960883n
11. Grootenhuis, P. D. J.; Kollman, P. A.; Groenen, L. C.; Reinhoudt, D. N.; Van Hummel, G. J.; Ugozzoli, F.; Andreetti, G. D. *J. Am. Chem. Soc.* **1990,** *112,* 4165–4176. doi:10.1021/ja00167a010
12. Fischer, C.; Gruber, T.; Seichter, W.; Weber, E. *Acta Crystallogr.* **2007,** *E63,* o4572–o4573. doi:10.1107/S1600536807053925
13. Fischer, C.; Gruber, T.; Seichter, W.; Schindler, D.; Weber, E. *Acta Crystallogr.* **2008,** *E64,* o673. doi:10.1107/S1600536808002304
14. Nishio, M.; Umezawa, Y.; Honda, K.; Tsuboyama, S.; Suezawa, H. *CrystEngComm* **2009,** *11,* 1757–1788. doi:10.1039/b902318f
15. Kitaigorodskii, A. L. *Molecular Crystals and Molecules;* Academic Press: New York, 1973.
16. Harada, T.; Rudziński, J. M.; Shinkai, S. *J. Chem. Soc., Perkin Trans. 2* **1992,** 2109–2115. doi:10.1039/p29920002109
17. Gutsche, C. D.; Dhawan, B.; Levine, J. A.; No, K. H.; Bauer, L. J. *Tetrahedron* **1983,** *39,* 409–426. doi:10.1016/S0040-4020(01)88541-0
18. Araki, K.; Iwamoto, K.; Shinkai, S.; Matsuda, T. *Chem. Lett.* **1989,** *18,* 1747–1750. doi:10.1246/cl.1989.1747
19. Sheldrick, G. M. *Acta Crystallogr.* **2008,** *A64,* 112–122. doi:10.1107/S0108767307043930
20. *SADABS;* Sheldrick, G. M.; University of Göttingen: Göttingen, Germany, 2004.

Beilstein Journal of Organic Chemistry

(How) does 1,3,5-triethylbenzene scaffolding work? Analyzing the abilities of 1,3,5-triethylbenzene- and 1,3,5-trimethylbenzene-based scaffolds to preorganize the binding elements of supramolecular hosts and to improve binding of targets

Xing Wang and Fraser Hof*

Full Research Paper

Open Access

Address:
University of Victoria, Department of Chemistry, Victoria, BC, V8W 3V6, Canada

Email:
Fraser Hof* - fhof@uvic.ca

* Corresponding author

Keywords:
binding affinity; entropy; molecular recognition; scaffolds; supramolecular hosts; triethylbenzene; trimethylbenzene

Beilstein J. Org. Chem. **2012,** *8,* 1–10.
doi:10.3762/bjoc.8.1

Received: 14 October 2011
Accepted: 15 December 2011
Published: 02 January 2012

This article is part of the Thematic Series "Supramolecular chemistry II".

Guest Editor: C. A. Schalley

Abstract

1,3,5-triethylbenzenes have been widely used as supramolecular templates to organize molecular-recognition elements. It is believed that the steric-gearing effect of the 1,3,5-triethylbenzene template directs the binding elements toward the same face of the central ring, hence increasing the binding affinity. At the same time the 1,3,5-trimethylbenzene scaffold, without steric-gearing effects, has also been found to improve the binding affinities of hosts compared to the unsubstituted analogues. By studying experimental data from the literature and the Cambridge Structural Database, as well as by conducting computational studies of representative structures, we concluded that the steric gearing offered by the ethyl groups confers some energetic advantage over the methyl groups, but the size of this advantage can be small and is dependent on the groups involved.

Introduction

Supramolecular hosts use arrays of multiple weak interactions to achieve strong and specific binding to targeted guest molecules. Many important weak interactions are directional and lead to highly ordered host–guest complexes [1,2]. The preorganization of binding elements in a competent binding geometry can have enthalpic effects on binding when considering the energy that must be paid to adopt a (potentially unfavorable) binding conformation, and can also have effects on binding entropy when one considers the degrees of freedom in the host, guest, and solvated host–guest complex. Rigid macrocyclic

hosts are often successful because of their high degree of preorganization [3,4]. As a nonmacrocyclic alternative, 1,3,5-triethylbenzenes are widely used as an easy-to-synthesize and general scaffold for presenting molecular-recognition elements in a convergent manner (Figure 1) [1,5]. These systems were spawned by the work of Mislow, who studied the conformational preferences of hexaethylbenzene by calculation, NMR, and crystallography and concluded that the conformation bearing alternating up-down arrangement of substituents was the global minimum for this system (Figure 1) [6]. This preference arises from steric gearing of adjacent substituents, which are positioned to be as far from their respective neighbors as possible. Even before Mislow's systematic study on this topic, Wilson and co-workers obtained the crystal structure of hexa(thiophenyl)benzene. The six thiophenyl groups are arranged around the central ring in alternating up–down fashion [7]. Raymond first took advantage of this kind of steric gearing by leaving ethyl groups in positions 1,3,5 and replacing the substituents in positions 2,4,6 with metal-coordinating ligands, which by design were directed toward the same face of the central scaffold and therefore preorganized for metal chelation (Figure 2a) [8]. The field has since exploded, with the first all-organic host–guest system of this type constructed by Anslyn [9] (Figure 2b) and over 150 papers reporting on 900 such structures for binding organic and inorganic guests having been published in the last 30 years [10]. The preorganizing effect of 1,3,5-triethylbenzene-based hosts (**1**$_{Et}$) has generally been demonstrated by comparing them to analogues that are unsubstituted at the 1,3,5 positions (**1**$_{H}$). But a parallel set of literature reports describes structures (**1**$_{Me}$) based on the 1,3,5-trimethylbenzene scaffold (700 structures in 300 papers identified by SciFinder substructure searches) [10]. These have no basis for producing the steric gearing that would favor a convergent conformation of binding elements, but their binding affinities can also be improved relative to analogous unsubstituted systems (**1**$_{H}$). The direct comparison of the 1,3,5-triethylbenzene (**1**$_{Et}$) and 1,3,5-trimethylbenzene (**1**$_{Me}$) templates in a single system is very rare (see below), which raises some questions: To what extent do ethyl substituents improve the binding properties of a host? To what extent do methyl substituents improve the binding properties of a host? What evidence exists for different enthalpic and entropic effects that might be responsible for the observed binding data in these families of hosts? In this paper, we report on our efforts to answer these questions using experimental data mined from the literature and from the Cambridge Structural Database, as well as with computational analysis of some representative host systems. We hope that these simple computational approaches might be more broadly useful for predicting the behavior of new supramolecular hosts.

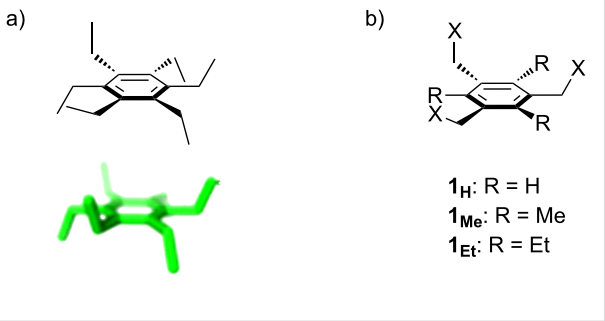

Figure 1: a) The global minimum-energy conformation for hexaethylbenzene reveals the basis for steric gearing in crowded arenes. b) A generalized set of hosts based on 1,3,5-triethylbenzene (**1**$_{Et}$), 1,3,5-trimethylbenzene (**1**$_{Me}$), and an unsubstituted analogue (**1**$_{H}$).

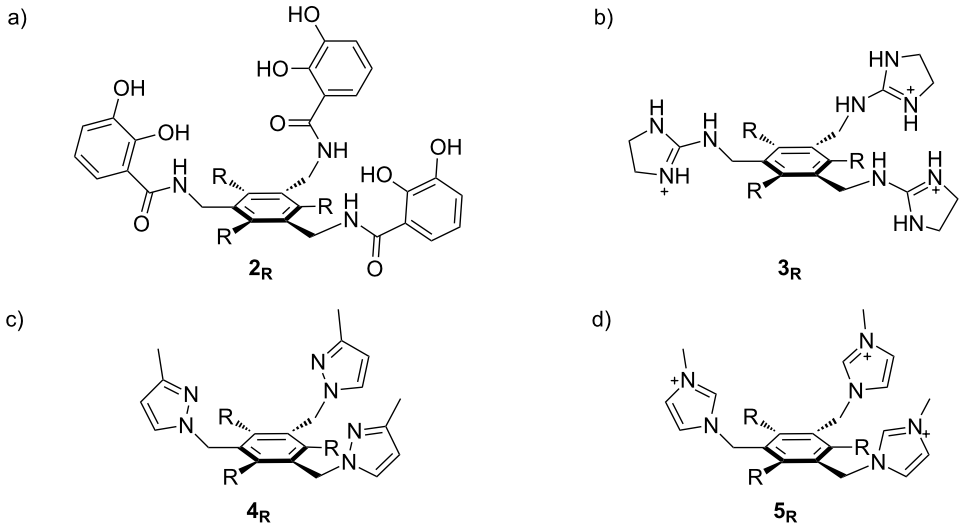

Figure 2: Structures of hosts discussed in this manuscript. R = H, Me, or Et.

Results and Discussion

Literature binding affinities

Chelating ligand $\mathbf{2_{Et}}$, the forerunner of all hosts in this class, displayed $K_{assoc} = 10^{47}$ M^{-1} for Fe, which is 10^4 or 5.4 kcal/mol stronger binding than the control host $\mathbf{2_H}$ ($K_{assoc} = 10^{43}$ M^{-1}) [8]. Anslyn's host $\mathbf{3_{Et}}$, a host that does not rely on strong metal–ligand interactions, binds citrate only 0.6 kcal/mol more strongly than its congener $\mathbf{3_H}$ [9]. One other host in this class that we were able to track down in the literature for direct comparisons of ethyl-substituted and unsubstituted hosts gives $\Delta\Delta G = 2.3$ kcal/mol (Table 1, entry 1). These values provide a mixed picture of the impact of ethyl substitution.

A separate summary of comparisons of methyl-substituted and unsubstituted hosts is presented in Table 2. The average $\Delta\Delta G$ is 0.3 kcal/mol, with a maximum of 2.3 kcal/mol and a minimum of −0.8 kcal/mol.

So is the ethyl substitution better than methyl? We found four papers that directly reported the binding affinities of seven different 1,3,5-triethylbenzene-based and analogous 1,3,5-trimethylbenzene-based tripodal hosts for their respective guests. These results are reported in Table 3. From this limited amount of literature data we see a range of binding-affinity differences for ethyl- and methyl-substituted hosts, which range

Table 1: Affinity comparisons of ethyl-substituted and unsubstituted hosts.

Entry [ref.]	R group	Guest	K_{assoc} values (M^{-1})	$\Delta\Delta G$[a] (kcal/mol)
1 [11]	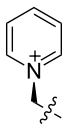	Br^-	$\mathbf{6_{Et}} = 8.5 \times 10^2$ $\mathbf{6_H} = 17$	2.3
2 [8]	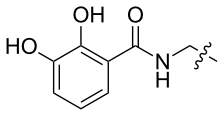	Fe	$\mathbf{7_{Et}} = 10^{47}$ $\mathbf{7_H} = 10^{43}$	5.4
3 [9]	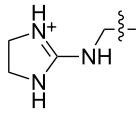	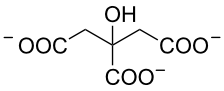	$\mathbf{8_{Et}} = 6.9 \times 10^3$ $\mathbf{8_H} = 2.4 \times 10^3$	0.6

[a]$\Delta\Delta G$ calculated from differences in reported K_{assoc} values. We estimate the errors as ±20%, depending on the measuring technique used in the literature.

Table 2: Affinity comparisons of methyl-substituted and unsubstituted hosts.

Entry [ref.]	R group	Guest	K_{assoc} values (M^{-1})	$\Delta\Delta G$[a] (kcal/mol)
1 [12]	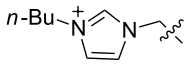	Cl^-	$\mathbf{9_{Me}} = 7.5 \times 10^4$ $\mathbf{9_H} = 1.5 \times 10^3$	2.3
2 [13]	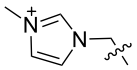	$H_2PO_4^-$	$\mathbf{10_{Me}} = 2.1 \times 10^3$ $\mathbf{10_H} = 2.0 \times 10^3$	0.04
		HSO_4^-	$\mathbf{10_{Me}} = 1.1 \times 10^3$ $\mathbf{10_H} = 1.2 \times 10^3$	−0.05
		Cl^-	$\mathbf{10_{Me}} = 1.1 \times 10^3$ $\mathbf{10_H} = 1.0 \times 10^3$	0.04
		Br^-	$\mathbf{10_{Me}} = 1.8 \times 10^2$ $\mathbf{10_H} = 7.6 \times 10^2$	−0.8

[a]$\Delta\Delta G$ calculated from differences in reported K_{assoc} values. We estimate the errors as ±20%, depending on the measuring technique used in the literature.

Table 3: Direct affinity comparisons of ethyl- and methyl-substituted hosts.

Entry [ref.]	R group	Guest	K_{assoc} values (M^{-1})	$\Delta\Delta G^a$ (kcal/mol)
1 [14]	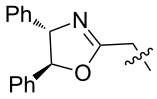	*n*-$BuNH_3^+$	**11**$_{Et}$ = 5.9 × 10^7 **11**$_{Me}$ = 2.0 ×10^6	2.0
		sec-$BuNH_3^+$	**11**$_{Et}$ = 8.3 × 10^5 **11**$_{Me}$= 8.3 × 10^4	1.4
		t-$BuNH_3^+$	**11**$_{Et}$ = 1.5 × 10^4 **11**$_{Me}$ = 4.7 × 10^3	0.7
2 [15]	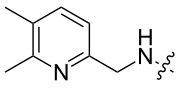	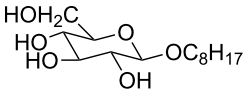	**12**$_{Et}$ = 48630 **12**$_{Me}$ = 20950	0.5
		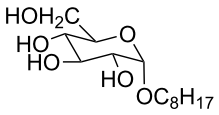	**12**$_{Et}$ = 1310 **12**$_{Me}$ = 800	0.3
3 [15]	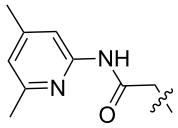	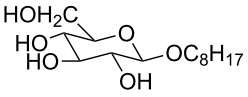	**13**$_{Et}$ = 1230 **13**$_{Me}$ = 650	0.4
5 [15]	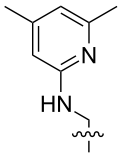	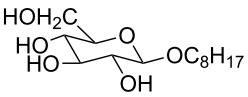	**14**$_{Et}$ = 48630 **14**$_{Me}$ = 20950	0.5
		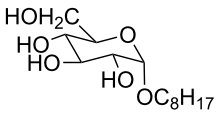	**14**$_{Et}$ = 1310 **14**$_{Me}$ = 800	0.3
		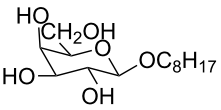	**14**$_{Et}$ = 3070 **14**$_{Me}$ = 1360	0.5
6 [15]	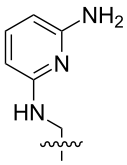	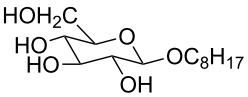	**15**$_{Et}$ = 19590 **15**$_{Me}$ = 9500	0.4
		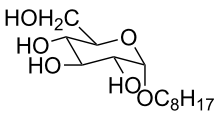	**15**$_{Et}$ = 1100 **15**$_{Me}$ = 620	0.3
7 [15]	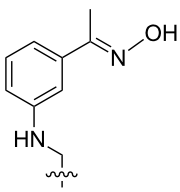	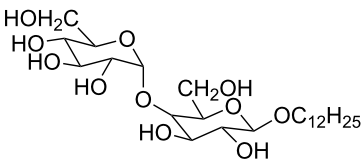	**16**$_{Et}$ = 98900 **16**$_{Me}$ = 96300	0.02

Table 3: Direct affinity comparisons of ethyl- and methyl-substituted hosts. (continued)

	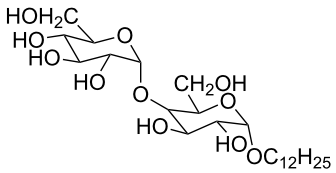	**16**$_{Et}$ = 58600 **16**$_{Me}$ = 62000	0.03
8 [16]	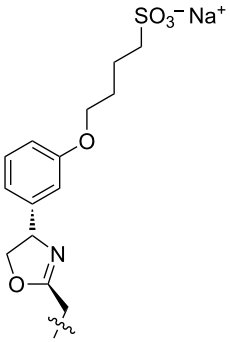	**17**$_{Et}$ = 86 **17**$_{Me}$ = 82	0.03
	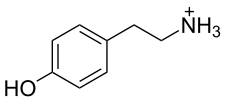	**17**$_{Et}$ = 101 **17**$_{Me}$ = 92	0.06
	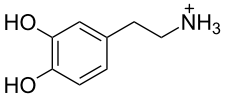	**17**$_{Et}$ = 178 **17**$_{Me}$ = 161	0.06
	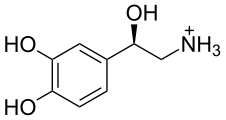	**17**$_{Et}$ = 74 **17**$_{Me}$ = 67	0.06
	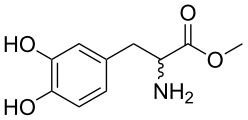	**17**$_{Et}$ = 72 **17**$_{Me}$ = 65	0.06

[a]$\Delta\Delta G$ calculated from differences in reported K_{assoc} values. We estimate the errors as ±20%, depending on the measuring technique used in the literature.

from no difference to a 17-fold difference, with an average $\Delta\Delta G$ of 0.4 kcal/mol in favor of ethyl substitution.

Crystallographic analysis of conformations

We next carried out a survey of the literature data in the Cambridge Structure Database to evaluate the conformations adopted by 1,3,5-triethylbenzene- and 1,3,5-trimethylbenzene-derived hosts in the solid state. One must always be cautious in interpreting crystallographic data on molecular conformations, as it is subject to crystal packing influences, which are not present in solution. However, those artifacts are diminished in surveys that contain many structures, making this a generally reliable way to get a qualitative overview of a class of functional groups. We first used generalized triethylbenzene substructures (Figure 3) to retrieve records for all related organic molecules, and discarded from our analysis those whose conformations were predetermined by macrocyclizations (and that therefore were not under the control of steric gearing). In

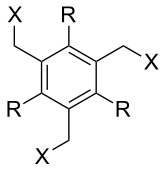

Figure 3: Generalized structural fragments used for mining the Cambridge Structure Database. R = Me and Et, X = N, O, C, Br.

total, 126 such crystal structures of tripodal triethylbenzene-based hosts were found in the database. Among these, 86 (68.3%) were in the up–down alternating conformation in which all ethyl groups are on one face of the central ring and all binding elements are on the other, while the remainder showed some deviation from this ideal. It is also interesting to note in this section that in Mislow's original reports on hexaethylbenzene, the presence of η^6-coordinated $Mo(CO)_3$ or $Cr(CO)_3$ produced crystal structures, showing that the bound metal did not perturb the predicted up–down alternating conformation [6]. The coordination of the larger $Cr(CO)_2PPh_3$ fragment produced instead a crystal structure in which the highly unfavorable all-up conformation of hexaethylbenzene dominated, and it was confirmed by NMR that this conformation persisted in solution [6].

The CSD was also mined for structures of 1,3,5-trimethylbenzene-based hosts, by using a similar search methodology and selection criteria to those described above. Of the total 194 crystal structures of such hosts found in the database, 88 (45.4%) were in a conformation defined as having all three binding elements on the same face of the central benzene ring. Overall, the proportion of triethylbenzene structures in their ideal "binding" conformation is lower than what would be expected based on the energy differences observed in solution (Table 1); however, it is significantly higher than the proportion of trimethylbenzene structures observed to be in the preorganized "binding" conformation, as expected.

Computational analysis

Mislow originally calculated the energy of hexaethylbenzene in all possible conformations [6], and we started by repeating these calculations at the HF/6-31G* level of theory (Table 4). This method, although simple by modern standards, is suitable for conformational analysis and allowed us to calculate the relatively large systems (below) in a short time. Seven conformations including the lowest four conformations were studied and reported here. The results of the calculation in the gas phase were in good agreement with the values reported by Mislow (Table 4). The *ududud* conformer adopted the most stable conformation and the energy level of this conformation was 4.3 kcal/mol lower than the second most stable conformer, namely *uddudd*.

Table 4: Calculated energies for hexaethylbenzene conformations.

Conformation	Relative energy in gas phase (kcal/mol) (Mislow)	Relative energy in gas phase (kcal/mol) (this work)	Relative energy in water (kcal/mol) (this work)
uuuuuu	8.2	10.5	10.1
uuuddd	6.6	8.9	8.8
uddddd	5.9	8.7	7.5
udduud	3.7	4.4	4.4
ududdd	3.7	4.4	4.4
uddudd	3.5	4.3	4.3
ududud	0	0	0

One can expect a significant effect of the nature of the recognition elements on conformational energies. Many recognition elements that vary in shape, functionality, charge, and chirality have been reported. We picked pyrazole-derived hosts **4** (used for cation binding) [17] and imidazolium-based hosts **5** (used for anion binding) [18,19] as instructive systems for computational analysis (Figure 2). These hosts were chosen because (1) they are typical of the kinds of heterocycles often used as recognition elements in this family of hosts; (2) we wished to examine the effects of charge and solvation on conformational energies; and (3) they are nearly isosteric to each other, allowing us to separate out the influences of sterics and charges.

All calculations were carried out both in the gas phase and in the implicit water environment, as implemented in Spartan '10 (SM8 model). These calculations were used to identify the global minimum-energy conformation for each host, and to determine the relative energies for each of the other conformations in each series (Table 5).

Table 5: Calculated energies for conformations of test hosts $\mathbf{4_{Et}}$ and $\mathbf{5_{Et}}$.

Conformation	Host $\mathbf{4_{Et}}$ relative energy in gas phase (kcal/mol)	Host $\mathbf{4_{Et}}$ relative energy in water (kcal/mol)	Host $\mathbf{5_{Et}}$ relative energy in gas phase (kcal/mol)	Host $\mathbf{5_{Et}}$ relative energy in water (kcal/mol)
uuuuuu	12.4	10.4	11.7	9.9
uuuddd	9.9	9.9	4.3	6.2
uddddd	7.8	7.5	2.5	6.1
udduud	4.6	3.1	0.3	4.4
ududdd	4.6	4.3	0.4	4.0
uddudd	2.8	2.9	−0.1	3.8
ududud	0	0	0	0

Unlike simple hexaethylbenzene, the imidazolium groups of $\mathbf{5_{Et}}$ provided a very different result when examined by gas-phase calculations. The conformers *ududud* and *uddudd*, are almost of the same energy and the next two most stable conformers, *ududdd* and *uddduud*, lie only 0.3 and 0.4 kcal/mol above the *ududud* conformer. When the solvent condition is changed to water the trend of the results is much closer to those of hexaethylbenzene. The ideal *ududud* conformation is 3.8 kcal/mol lower than the second lowest conformation. No such change is observed for hexaethylbenzene itself on comparison of gas-phase and water calculations (Table 4). We expect that these differences arise from the overwhelming influence of (inadequately screened) charge–charge repulsion in the gas-phase calculations on $\mathbf{5_{Et}}$.

The calculated results of pyrazole-substituted $\mathbf{4_{Et}}$ are quite similar in the gas phase and water. On comparison of the results of $\mathbf{4_{Et}}$ to hexaethylbenzene, it is seen that the sequential ordering of the conformational energies is the same. But the *ududud* conformer of pyrazole-substituted $\mathbf{4_{Et}}$ is only 2.9 kcal/mol more stable than the second-lowest-energy conformation in water, a gap that is a significant 1.4 kcal/mol smaller than the value calculated for hexaethylbenzene (4.3 kcal/mol). We interpret this difference in terms of the steric clashes between neighboring groups that occur in nonideal conformations such as *uddudd*. Planar, sp^2-hybridized heterocycles on $\mathbf{4_{Et}}$ have reduced steric demand relative to the sp^3-hybridized CH_3 groups that clash with neighboring substituents in hexaethylbenzene. These results show in general that the conformational-energy calculations for hexaethylbenzene cannot be simply applied to all 1,3,5-triethylbezene-based hosts. Although all the calculations in our study showed that *ududud* was the preferred conformation, the energy gap between the ideal conformer and the next most stable conformer depends strongly on the substituents.

The conformational energy landscapes of 1,3,5-trimethylbenzene-based hosts and their unsubstituted analogs are much simpler. There are only two possible conformations to be considered in these systems: "*uuu*," in which all three substituted arms are directed toward the same face of the benzene, and "*uud*," in which one binding arm is directed toward the opposite face of the benzene from the other two. Imidazolium-substituted hosts $\mathbf{5_{Me}}$ and $\mathbf{5_H}$ both show a preference for the nonideal *uud* conformation in the gas phase, which we can again attribute to the mutual repulsion of the positively charged substituents. This difference disappears when the calculation is carried out in water, in which the alike charges are more effectively screened from each other, and the *uuu* conformers are favored by 1.0 kcal/mol (for $\mathbf{5_H}$) and 0.5 kcal/mol (for $\mathbf{5_{Me}}$). The *uuu* conformers that are best suited for binding are favored for the pyrazole-substituted hosts $\mathbf{4_H}$ and $\mathbf{4_{Me}}$, in the gas phase and in water, by values that range from 0.7–1.7 kcal/mol (Table 6). This result is not intuitive. The steric gearing that could possibly be provided by the methyl groups comes only from C–H bonds: A single C–H bond directed toward one face of the central benzene ring and two C–H bonds directed toward the other. Compared to the steric gearing provided by the ethyl groups, we assume that the magnitude of the possible energetic contribution to preorganization from the methyl groups is minor.

These calculations collectively show that, except in the case of exaggerated charge–charge repulsions present in the gas phase, all hosts of types $\mathbf{5_{Et}}$, $\mathbf{5_{Me}}$, and $\mathbf{5_H}$ prefer the conformations in which all binding substituents are directed toward the same face of the central benzene ring. While a complete analysis would take all conformations (and their energies) into account, a simple and useful basis for evaluating these calculations of conformational energy differences is to compare the energy gaps between the lowest energy conformations and their next-highest congeners in each series, as these are the two conformations that would be most heavily populated in solution. The dependence of these gaps on the nature of the recognition substituents (imidazolium, pyrazole, or ethyl groups) is discussed above. But what about comparing the use of either ethyl or methyl groups as interposing or preorganizing elements for a given type of host? We calculate that the energetic preference for the "binding" conformation (defined as *ududud* for ethyl-substituted hosts and *uuu* for methyl-substituted hosts) is greater for ethyl-substituted hosts in general, being 3.8 kcal/mol for imidazolium $\mathbf{5_{Et}}$, (compared to 0.5 kcal/mol for imidazolium $\mathbf{5_{Me}}$) and 2.9 kcal/mol for pyrazole $\mathbf{4_{Et}}$, (compared to 0.8 kcal/mol for imidazolium $\mathbf{4_{Me}}$). This suggests that the steric gearing

Table 6: Calculated energies for conformations of test hosts $\mathbf{4_{Me}}$, $\mathbf{4_H}$, $\mathbf{5_{Me}}$, and $\mathbf{5_H}$.

Conformation	Host $\mathbf{4_{Me}}$ relative energy (kcal/mol)		Host $\mathbf{4_H}$ relative energy (kcal/mol)		Host $\mathbf{5_{Me}}$ relative energy (kcal/mol)		Host $\mathbf{5_H}$ relative energy (kcal/mol)	
	gas	water	gas	water	gas	water	gas	water
uud	0.9	0.8	1.7	0.7	−1.8	0.5	−0.3	1.0
uuu	0	0	0	0	0	0	0	0

offered by the ethyl groups confers some energetic advantage over the methyl groups, but that the size of this advantage is dependent on the groups involved.

Calculated dynamics and rotational barriers

Although kinetics has no bearing on binding thermodynamics, we sought also to understand computationally the dynamics of these different hosts. Molecular-dynamics simulations carried out at 300 K showed little or no dynamic exchange of conformations. Simulations carried out at the artificially elevated temperature of 400 K showed little more in the way of conformational exchange (one change of conformation for pyrazole host $\mathbf{4_{Et}}$ and two for $\mathbf{4_{Me}}$ during 10 ns). The unsubstituted host $\mathbf{4_H}$ is a more mobile system, as indicated by the occurrence of 177 exchanges during the same simulation period. Faced with evidence that the barriers to exchange of "up" and "down" conformers in the sterically congested 1,3,5-triethylbenzene and 1,3,5-trimethylbenzene systems are too high to examine conveniently by MD simulations, we turned instead to a calculation of the barriers to bond rotation for a given set of substituents. These calculations were run on models composed of one of the test substituents (ethyl, pyrazolyl-CH_2, or imidazolium-CH_2) flanked by ethyl groups, methyl groups, or protons at the *ortho* and all other ring positions (Figure 4). The dihedral angle between the central benzene ring and the pendant substituent was constrained at 40° intervals between −180° and +180° and minimized at each stage in order to generate an energy profile for simple bond rotation for each type of host. This type of analysis ignores correlated bond rotations, which are sometimes important in sterically crowded systems. We make this assumption because Mislow's original NMR studies demonstrated experimentally that there are no such correlated motions, even in highly crowded hexaethylbenzene [6]. Exemplary dihedral driving data, and the barriers thus calculated, are presented in Figure 4 and Table 7. The calculated rotation barriers for ethyl directed hosts are in the same range as previously reported values for related systems, which were determined by variable temperature NMR to be 9.3–11.8 kcal/mol [6,20].

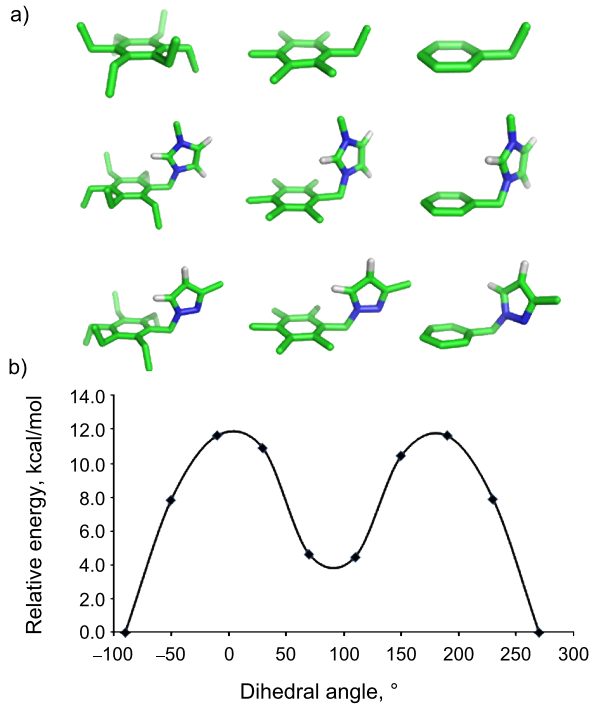

Figure 4: a) Structures used to calculate energy profiles at the starting geometry. b) An example of an energy profile arising from dihedral driving calculations on $\mathbf{1_{Et}}$. The smoothed line is intended to guide the reader's eye.

Table 7: Calculated energy barriers (kcal/mol) to bond rotation, with respect to the rotating functional group and neighboring substituents.

	ortho substituents		
Rotating substituent	Et	Me	H
Et	11.6	9.0	4.3
Pyrazole-CH_2	10.3	7.7	1.0
Imidazolium-CH_2	15.7	9.5	3.5

As with the MD simulations, these results indicate that both ethyl and methyl *ortho* substituents cause high barriers to rotation (7.7–15.7 kcal/mol). Compared to the unsubstituted molecule, the ethyl *ortho* substituent provides 10.3–15.7 kcal/mol and the methyl *ortho* substituent provides 7.7–9.5 kcal/mol. We also find in this data a strong dependence on the nature of the rotating substituent, which is not easily explained by sterics. In general, the lowest barriers are calculated for pyrazole-CH_2, while the nearly isosteric imidazolium-CH_2 has significantly higher barriers across the board. In this result, again, we see that the rotation barriers offered by the ethyl groups confer some energetic advantage over the methyl groups, but the size of this advantage can be small and is dependent on the groups involved.

A consideration of entropic effects

So how do these collective data inform us on the relative abilities of ethyl-, methyl-, and unsubstituted hosts to bind guests? The energies (E) calculated here are most closely akin to enthalpies (ΔH), and neglect differences in entropy (ΔS) from one host type to another. The aspects of host entropy that might contribute to guest binding, i.e., translational, vibrational, solvation, and configurational entropy, are worth separate discussions. Entropic effects arising from translation are not likely to depend strongly on host conformation (i.e., all conformations

experience the same degree of reduced translational freedom upon binding), and we can assume that the presence of ethyl or methyl groups has little effect on translational entropy. We expect that changes in both vibrational entropy and solvent entropy will be highly variable for different systems in this class. While they might yield significant differences, their influence on binding energies cannot be predicted in a general way that depends on ethyl or methyl substitution. But the configurational entropy of "preorganized" systems like these is a fertile ground for discussion. In binding equilibria, the configurational entropy of a host is most frequently discussed in terms of the number of rotatable bonds (N_{rot}) in free and bound states, which is a surrogate for considering the probability that a given conformation is occupied before and after binding [21,22]. Various schemes have been proposed for calculating the energetic contributions of these differences based on differences in N_{rot} between free and bound states; whatever the details of the calculations, a negative value for ΔN_{rot} upon binding (i.e., a transition to a more ordered state) is unfavorable. The unsubstituted hosts, such as $\mathbf{1_H}$, lose three rotatable bonds upon forming a host–guest complex ($\Delta N_{rot} = -3$), as do the methyl-substituted hosts such as $\mathbf{1_{Me}}$. Consideration of the ethyl-substituted hosts, such as $\mathbf{1_{Et}}$, becomes a bit tricky. If one considers that the system is perfectly fixed before and after binding then ΔN_{rot} is 0 (which is more favorable for binding). This kind of analysis was used by Raymond, in which it was estimated that the installation of ethyl groups produced a favorable $T\Delta S$ of 4.5 kcal/mol (of the total of the 5.4 kcal/mol favorable binding energy). However, we have turned up no report that was published since with such a dramatic difference in overall binding energy. While host $\mathbf{3_{Et}}$ has been shown to bind citrate in an entropy-driven manner, no comparison to $\mathbf{3_H}$ or $\mathbf{3_{Me}}$ was made, and the authors posit a significant role of solvent entropy in explaining their experimental data [23]. Overall, no specific measurement exists that correlates a large favorable change in entropy to the installation of ethyl groups.

Some insight is offered by the crystallographic survey we present above, which contains many structures for which either binding arms or ethyl groups (or both) are disordered. Our computational data suggests that these alternate conformations can be disfavored by small energies and may be significantly populated at room temperature (depending on the identity of the substituents). Further, the calculated bond rotation barriers for any of our ethyl-substituted model hosts are low enough that they would be easily surmounted at room temperature. It is interesting, therefore, to consider the possibility that, with a ΔN_{rot} of up to −6 (depending on the number of bonds free in unbound state and frozen in the bound state), some ethyl-substituted hosts may have an entropic disadvantage relative to methyl- and unsubstituted hosts. Given our analyses of existing data, it is likely that the true nature of the configurational entropic contributions lies somewhere between the two extremes. While entropic effects have surfaced in general in some classic studies [23], there is little or no experimental data on the separation of entropic contributions to host behavior in these systems, so this must remain, for now, a hypothesis awaiting experimental conformation.

Conclusion

The picture that emerges from the combined surveys of crystallographic structures and binding affinities measured in solution is that the effect of installing ethyl or methyl groups onto supramolecular hosts is often favorable (as expected), but that the correlations between preorganized structures and binding affinities is nontrivial. Our computational data adds to this survey a basis for understanding the observed differences in energies that are most often invoked when discussing host preorganization, while also contributing additional evidence for variable behaviors that depend on the identities of molecular recognition elements and not purely on the scaffolds. The evidence collected here and elsewhere suggests that the installation of ethyl or methyl groups at 1,3,5 positions leads to consistent but relatively small increases in binding affinity relative to unsubstituted hosts. Given the overall variability we observe (and the desire of most researchers to synthesize only a single host for any given job), we suggest that carrying out the simple, broadly accessible calculations of the types described here may guide researchers in the selection of optimum substituents and scaffolds before synthesis begins.

Acknowledgements

This work was funded by NSERC. FH is a Michael Smith Foundation for Health Research Career Scholar and a Canada Research Chair.

References

1. Anslyn, E. V.; Dougherty, D. A. *Modern physical organic chemistry;* University Science Books, 2005.
2. Tsuzuki, S.; Fujii, A. *Phys. Chem. Chem. Phys.* **2008,** *10,* 2584–2594. doi:10.1039/b718656h
3. Cram, D. J. *Angew. Chem., Int. Ed. Engl.* **1986,** *25,* 1039–1057. doi:10.1002/anie.198610393
4. Seel, C.; Vögtle, F. *Angew. Chem., Int. Ed. Engl.* **1992,** *31,* 528–549. doi:10.1002/anie.199205281
5. Hennrich, G.; Anslyn, E. V. *Chem.–Eur. J.* **2002,** *8,* 2218–2224. doi:10.1002/1521-3765(20020517)8:10<2218::AID-CHEM2218>3.0.CO;2-H
6. Iverson, D. J.; Hunter, G.; Blount, J. F.; Damewood, J. R., Jr.; Mislow, K. *J. Am. Chem. Soc.* **1981,** *103,* 6073–6083. doi:10.1021/ja00410a015
7. MacNicol, D. D.; Hardy, A. D. U.; Wilson, D. R. *Nature* **1977,** *266,* 611–612. doi:10.1038/266611a0

8. Stack, T. D. P.; Hou, Z.; Raymond, K. N. *J. Am. Chem. Soc.* **1993,** *115,* 6466–6467. doi:10.1021/ja00067a094
9. Metzger, A.; Lynch, V. M.; Anslyn, E. V. *Angew. Chem., Int. Ed. Engl.* **1997,** *36,* 862–865. doi:10.1002/anie.199708621
10. Scifinder substructure searches were conducted with 1,3,5-triethylbenzene or 1,3,5-trimethylbenzene bearing 2,4,6 substituents defined as fragments of the type CH_2O-, CH_2N-, CH_2S-, and CH_2Br.
11. Wallace, K. J.; Belcher, W. J.; Turner, D. R.; Syed, K. F.; Steed, J. W. *J. Am. Chem. Soc.* **2003,** *125,* 9699–9715. doi:10.1021/ja034921w
12. Sato, K.; Arai, S.; Yamagishi, T. *Tetrahedron Lett.* **1999,** *40,* 5219–5222. doi:10.1016/S0040-4039(99)00942-9
13. Fahlbusch, T.; Frank, M.; Schatz, J.; Schmaderer, H. *Eur. J. Org. Chem.* **2006,** 1899–1903. doi:10.1002/ejoc.200500825
14. Kim, S.-G.; Ahn, K. H. *Chem.–Eur. J.* **2000,** *6,* 3399–3403. doi:10.1002/1521-3765(20000915)6:18<3399::AID-CHEM3399>3.0.CO;2-M
15. Mazik, M.; Radunz, W.; Boese, R. *J. Org. Chem.* **2004,** *69,* 7448–7462. doi:10.1021/jo048979k
16. Kim, J.; Raman, B.; Ahn, K. H. *J. Org. Chem.* **2006,** *71,* 38–45. doi:10.1021/jo051630s
17. Ahn, K. H.; Kim, S.-G.; Jung, J.; Kim, K.-H.; Kim, J.; Chin, J.; Kim, K. *Chem. Lett.* **2000,** *29,* 170–171. doi:10.1246/cl.2000.170
18. Yoon, J.; Kim, S. K.; Singh, N. J.; Kim, K. S. *Chem. Soc. Rev.* **2006,** *35,* 355–360. doi:10.1039/b513733k
19. Yun, S.; Ihm, H.; Kim, H. G.; Lee, C.-W.; Indrajit, B.; Oh, K. S.; Gong, Y. J.; Lee, J. W.; Yoon, J.; Lee, H. C.; Kim, K. S. *J. Org. Chem.* **2003,** *68,* 2467–2470. doi:10.1021/jo0263519
20. Kilway, K. V.; Siegel, J. S. *Tetrahedron* **2001,** *57,* 3615–3627. doi:10.1016/S0040-4020(01)00248-4
21. Chang, C. A.; Chen, W.; Gilson, M. K. *Proc. Natl. Acad. Sci. U. S. A.* **2007,** *104,* 1534–1539. doi:10.1073/pnas.0610494104
22. Pickett, S. D.; Sternberg, M. J. E. *J. Mol. Biol.* **1993,** *231,* 825–839. doi:10.1006/jmbi.1993.1329
23. Rekharsky, M.; Inoue, Y.; Tobey, S.; Metzger, A.; Anslyn, E. *J. Am. Chem. Soc.* **2002,** *124,* 14959–14967. doi:10.1021/ja020612e

License and Terms

Beilstein Journal of Organic Chemistry

Binding of group 15 and group 16 oxides by a concave host containing an isophthalamide unit

Jens Eckelmann, Vittorio Saggiomo, Svenja Fischmann and Ulrich Lüning*

Full Research Paper

Open Access

Address:
Otto-Diels-Institut für Organische Chemie,
Christian-Albrechts-Universität zu Kiel, Olshausenstr. 40, D-24098
Kiel, Germany

Email:
Ulrich Lüning* - luening@oc.uni-kiel.de

* Corresponding author

Keywords:
anion binding; association constant; estimation of binding constants;
macrocycle; molecular recognition

Beilstein J. Org. Chem. **2012,** *8,* 11–17.
doi:10.3762/bjoc.8.2

Received: 13 September 2011
Accepted: 29 November 2011
Published: 03 January 2012

This article is part of the Thematic Series "Supramolecular chemistry II".

Guest Editor: C. A. Schalley

Abstract

A bi-macrocycle with an incorporated isophthalamide substructure was synthesized by double amide formation between an isophthaloyl dichloride and two equivalents of a bis(alkenyloxy)aniline, followed by ring-closing metathesis and hydrogenation. In contrast to many related isophthalamides, the concave host exhibits a better binding for oxides, such as DMSO or pyridine-*N*-oxide, than for halide anions. A general method for a quick estimation of the strength of binding derived from only a few data points is presented and gives an estimated K_{ass} of pyridine-*N*-oxide of ca. 40 M^{-1}, NMR titration confirms 25 M^{-1}.

Introduction

In the last decade, isophthalamide derivatives have become attractive neutral hosts as anion receptors [1,2]. Some of these derivatives show a high selectivity for one anion over others [3]. Isophthalamide units have also been incorporated into macrocycles [4,5] or bi-macrocycles for ion-pair and ion-triplet recognition [6-9]. During the last few years, it was also shown that the orientation of the amide bonds of the isophthalamides plays an important role in the effectiveness of anion binding and subsequently in applications such as transmembrane anion transport. Rotation along the amide–aryl bonds leads to *syn/anti*, *syn/syn* and *anti/anti* conformers (*syn* and *anti* defined with respect to the relative orientation of the NH atoms), and only the *syn/syn* conformer of an isophthalamide is capable of simultaneously binding an anion by *both* NH groups. The *syn/syn* conformation can be stabilized by using isophthalamide derivatives capable of intramolecular hydrogen bonding to the CO part of the amide groups [10,11], or by other means of bridging [12]. Due to the preorganization of such molecules, the binding constant for chloride is impressively increased with respect to the non-preorganized isophthalamides. However, an intramolecular hydrogen bond can be easily broken in polar solvents, hence destroying the preorganization and thus decreasing the binding affinities for the anions. Herein we describe the facile synthesis and the binding properties of a concave host **1** with a different type of preorganization. This contains an isophthalamide unit in a bi-macrocyclic structure (Figure 1). Concave hosts and especially concave reagents are best envisioned as having the form of a lamp in a lampshade in

which the light bulb is the reactive centre [13-15]. The preorganization and the exact shape of the "lampshade" determine the selectivity and the difference in binding of various guests.

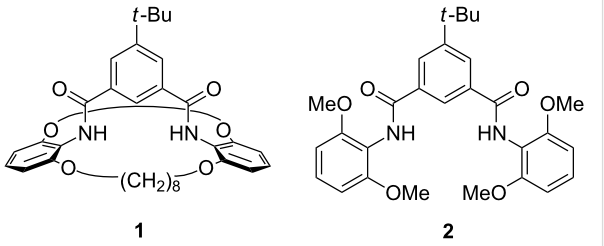

Figure 1: Bi-macrocyclic concave host **1** and its non-macrocyclic model **2**.

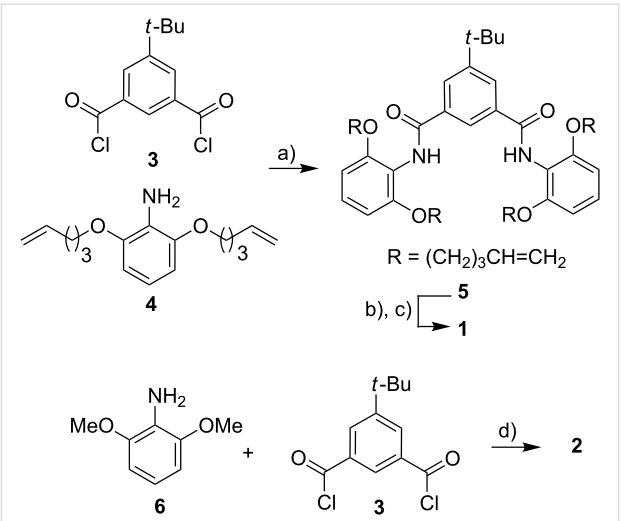

Scheme 1: Synthetic scheme for the syntheses of concave host **1** and non-macrocyclic derivative **2**. a) Et_3N, THF, 16 h, room temp., 61%; b) Grubbs 1st gen. cat., CH_2Cl_2, 24 h, room temp.; c) Pd/C, H_2, MeOH, 24 h, room temp., 77%; d) Et_3N, THF, 18 h, room temp., 97%.

Results and Discussion

Synthesis

Besides the desired bi-macrocycle **1**, isophthalamide **2** was synthesized in order to compare the binding properties of a non-macrocyclic host with the concave host **1**. The syntheses of the concave host **1** and its analogue **2** are depicted in Scheme 1.

The preparation of concave host **1** starts with aniline **4**, which was synthesized as previously published [16]. The reaction of two equivalents of this aniline **4** with isophthaloyl dichloride **3** gave the open diamide **5**. This tetraalkene **5** was then converted to bi-macrocycle **1** by ring-closing metathesis followed by catalytic hydrogenation. Model compound **2** was obtained by reacting isophthaloyl dichloride **3** with 2,6-dimethoxyaniline (**6**). The two products **1** and **2** were isolated and characterized. The preorganization of the binding region was investigated by NOESY experiments. While two cross peaks between the NH protons and both types of protons in the central aromatic region were observed in the case of the more flexible compound **2**, there was only one cross peak of an aromatic proton of the isophthalamide of bi-macrocycle **1** with the NH protons: The *endo*-proton in the 2-position of the isophthalic unit is in close proximity to the NH protons. Thus, the binding region of **1** is preorganized (for details see Supporting Information File 1).

NMR binding studies

Each of the isophthalamides, **1** and **2**, was dissolved in CD_2Cl_2 and ^1H NMR spectra were recorded after addition of five equivalents of different tetrabutylammonium halide salts (TBAHal). The chemically induced shifts (CIS) of the NH and the isophthalamide *endo*-CH protons (i.e., the 2-position of the aromatic ring) were analyzed (Figure 2). Further addition of guests led to larger CIS, but no saturation was observed. The shallow curvature and absence of saturation suggest small

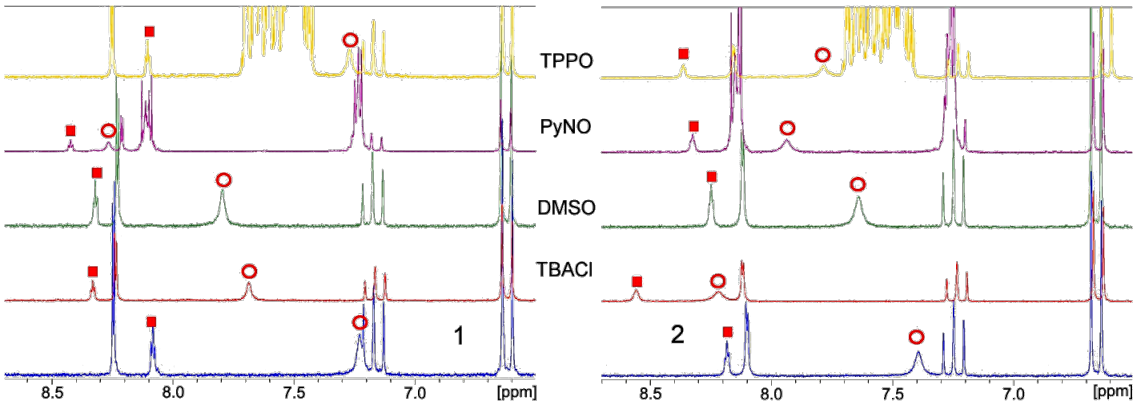

Figure 2: Expansion of a part of the ^1H NMR spectra (200 MHz, 298 K) of pure **1** and **2** in CD_2Cl_2 (bottom) and after addition of TBACl, DMSO, pyridine-*N*-oxide (PyNO), triphenylphosphine oxide (TPPO), from bottom to top, respectively. NH proton (red circles), *endo*-CH proton (red squares).

binding constants. The different magnitudes of the CIS suggest that concave host **1** binds halides with lower affinity than its acyclic relative **2**, although the magnitude of the CIS need not be correlated with the binding constants.

However, when sulfoxides were added as neutral guests, the relative binding of these guests by **1** and **2** showed drastic differences. Dimethyl sulfoxide (DMSO), methylphenyl sulfoxide (MPSO) and diphenyl sulfoxides (DPSO) induced a shift of the *endo*-CH in the concave host **1** of 0.24 ppm, 0.20 ppm and 0.25 ppm, respectively (for DMSO see Figure 2, left, see also Supporting Information File 1), while the addition of these guests had almost no effect on the *endo*-CH of model compound **2** (for DMSO see Figure 2, right). Although there is almost no CIS observed for the *endo*-CH of model compound **2**, a small shift for the NH protons is observed. However, for DMSO, the CIS of the NH is larger for the concave host **1** than for model compound **2** (0.57 ppm for **1** and 0.25 ppm for **2**), in contrast to the results of the anion-binding experiments (see above). To the best of our knowledge, this is the second host capable of binding DMSO in an organic solvent [17]. In this regard, concave host **1** seems to be selective and a better binder for negatively polarized oxygen atoms when compared to acyclic compound **2**.

Next, element oxides other than sulfoxides were chosen as guests, namely pyridine-*N*-oxide (PyNO) [18,19] and triphenylphosphine oxide (TPPO). PyNO showed the same behaviour as DMSO, i.e., large CIS for concave host **1**, and small CIS for the linear compound (Figure 2, PyNO, *endo*-CH, 0.34 ppm for **1** and 0.14 ppm for **2**). In contrast, with TPPO as guest, model compound **2** showed a larger CIS when compared to concave host **1** (Figure 2, TPPO). This may be explained by the large steric bulk of TPPO, which may be too extreme to allow TPPO to fit nicely inside the cavity of concave host **1** but still allows a binding to the sterically less demanding non-macrocyclic host **2**.

In order to reliably determine small binding constants, a titration up to a large excess of guest has to be carried out but, even then, a limiting value for the CIS often is not reached and thus a second parameter besides K_{ass}, namely the maximum of the observed CIS $\Delta\delta_{max}$, has to be obtained by curve fitting, which adds to the overall error. In our host–guest systems, saturation was not reached even when 20 equivalents of guests were used. An even larger excess of guest changed the polarity of the solvent to such an extent that all signals were affected, not only those involved in the binding [20].

If most guests only bind very moderately, an exact (and tedious) determination of all binding constants K_{ass} is not interesting. It would be sufficient if a quick screening of the binding potentials of the hosts were possible and host–guest pairs with significant association constants were identified. Estimation rather than an exact determination of K_{ass} would be fair enough. Once a good candidate is recognized, a standard determination of the association constant, for example, by NMR titration, can be done.

With $\Delta\delta_{max}$ unknown, the magnitude of the CIS cannot distinguish between weak and strong binding. However, when NMR titrations of different host–guest pairs are carried out with identical concentrations, small and large association constants can be differentiated by the different curvatures of the titration graphs. In a titration curve of strong binding, the curvature is more extreme, and the final value of $\Delta\delta_{max}$ is approached faster than in the case of weak binding. Beyond 1:1 stoichiometry, the CIS values converge more the stronger the binding is.

Can this be a method for the quick estimation of binding constants? We have tested this alternative for hosts **1** and **2**. All measured ^{1}H NMR shifts were normalized to a CIS at high guest concentration, but not at saturation: The CIS from all experiments that used ca. 20 equivalents of a given guest were arbitrarily defined as 100%, and the CIS measured for ca. 5 equivalents of the same guest were divided by that CIS value measured with 20 equivalents. The resulting normalized CIS were plotted against the guest equivalents (Figure 3). With a more strongly binding guest, the titration curve possesses a

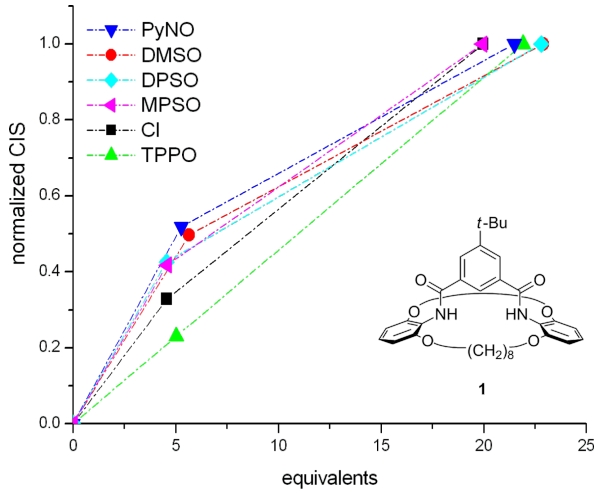

Figure 3: Normalized ^{1}H NMR CIS (see text) for concave host **1** with different anionic and neutral guests. The deviations of the data points at ca. 5 equivalents, from the straight line connecting the origin and the data points at 20 equivalents, describe the strength of binding. The binding strength decreases from top to bottom. The dashed lines have no physical significance but help to demonstrate the deviation from linearity.

more extreme curvature, and thus, in this normalized form, the data points at 5 equivalents lie further away from the linear line that connects the points corresponding to 0 and 20 equivalents.

The validity of this estimation has been checked with calculated titration curves for different association constants K_{ass} and different maximum CIS (see Supporting Information File 1). For an application on host **1**, see Figure 3; for **2**, see Figure 4. For each host, only those guests that are bound most strongly are listed. For the full data set, see Supporting Information File 1. Data points below the straight line are physically meaningless, and simply reflect the large errors for very weak binding (the method of normalizing the shifts should preferably not be carried out for guests with *very* small CIS).

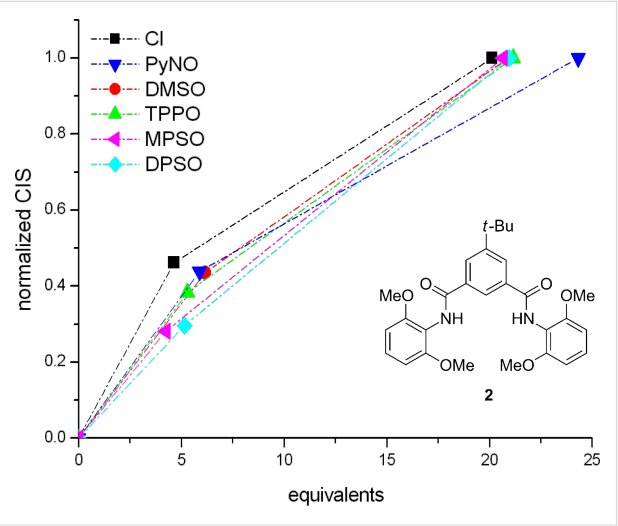

Figure 4: Normalized ^{1}H NMR CIS (see text) for concave host **2** with different anionic and neutral guests. The deviations of the data points at ca. 5 equivalents, from the straight line connecting the origin and the data points at 20 equivalents, describe the strength of binding. The binding strength decreases from top to bottom. The dashed lines have no physical significance but help to demonstrate the deviation from linearity.

In Figures 3 and 4, the relative strengths of binding can be obtained from the vertical deviations of the normalized CIS at ca. 5 equivalents from the straight line connecting the origin and the values at 20 equivalents. The magnitude of the binding decreases from top to bottom.

By using this methodology, it is possible and easy to determine the relative binding strengths of the two hosts **1** and **2** even for weak binding constants and situations where maximal chemically induced shifts $\Delta\delta_{max}$ cannot be determined from only a few measurements. When the two graphs for **1** and **2** with different guests are compared, the different selectivity of the two hosts becomes evident. Concave host **1** shows a better affinity for negatively polarized oxygen atoms than for anions, except in the case of the bulky TPPO. The affinities of concave host **1** lie in the following order: PyNO > DMSO > DPSO = MPSO > Cl^- > TPPO. In contrast, the affinities of the non-macrocyclic analogue **2** are: Cl^- > PyNO = DMSO = TPPO > MPSO = DPSO (see Supporting Information File 1). When the plot was compared with the simulated titration curves (see Supporting Information File 1, page S12), K_{ass} for the best binder to **1**, pyridine-*N*-oxide (PyNO), was estimated to be ca. 40 M^{-1}. A subsequent NMR titration of host **1** with PyNO provided an association constant of 25 M^{-1} (see Supporting Information File 1). Remarkably, chloride ions are only very weakly bound by concave host **1**, and binding constants are moderate anyway. A possible explanation may be a repulsion between the negatively polarized oxygen atoms in the 2- and 6-positions of the bridge heads of **1** and the negatively, or partially negatively charged guests.

Conclusion

1 is a readily synthesized concave host molecule in which the isophthalamide moiety is the central binding unit, and it is preorganized by its incorporation into the bi-macrocyclic structure. This concave host, although it does not exhibit strong binding, is selective for negatively polarized oxygen atoms and selects them according to the steric bulk of the guests. These initial experiments now open the way for the synthesis of new modified concave hosts based on isophthalamide units with improved binding selectivity and/or for organocatalysis [21]. Concave host **1** can also be applied as a carrier in transport experiments. When applied to chloride-loaded liposomes [22], it showed twice as much transmembrane chloride transport with respect to acyclic compound **2** (see Supporting Information File 1). Even if the chloride binding is lower for concave host **1**, the transport through a bilayer membrane is faster. Additional transport experiments are under investigation.

Experimental

General remarks

All reagents were obtained from commercial sources and used without additional purification unless otherwise indicated. 5-*tert*-Butylisophthaloyl dichloride (**3**) was prepared from 5-*tert*-butylisophthalic acid and thionyl chloride according to Vögtle et al. [23]. 2,6-Bis(pent-4-enyloxy)aniline (**4**) was prepared from 2-nitroresorcine according to Winkelmann et al. [16]. 2,6-Dimethoxyaniline (**6**) was synthesized from 2-nitroresorcine according to Mechoulam and Srebnik [24] and was finally reduced to 2,6-dimethoxyaniline (**6**) according to Franck and Kauffmann [25]. THF was freshly distilled from lithium aluminium hydride (triphenylmethane as indicator). All reactions were carried out in an atmosphere of nitrogen. NMR spectra were recorded with Bruker AC 200, DRX 500 or AV 600 instruments. Assignments are supported by COSY, HSQC

and HMBC. All chemical shifts are referenced to TMS or residual solvent peaks. Mass spectra were recorded with Finnigan MAT 8200 or MAT 8230. ESI mass spectra were recorded with an Applied Biosystems Mariner Spectrometry Workstation. IR spectra were recorded with Perkin-Elmer Spectrum 100 spectrometer, equipped with an ATR unit. Elemental analyses were carried out with a EuroEA 3000 Elemental Analyzer from Euro Vector. MALDI-TOF spectra were recorded with Bruker-Daltonics Biflex III. 4-Chloro-α-cyanocinnamic acid (Cl-CCA) was used as the matrix.

^{1}H NMR experiments

Each NMR tube was filled with 600 µL of a stock solution (5 mg/mL) of **1** or **2** in CD_2Cl_2, and subsequently ca. 5, and later ca. 20 equivalents of the respective guest were added. The exact amount was recalculated from the integrals by using Bruker Topspin® 2.1. All experiments were carried out on a Bruker AC 200 NMR equipped with an autosampler at 300 K. The spectra are referenced to the residual solvent peak.

Synthesis of 25^5-*tert*-Butyl-2,11,13,22-tetraoxa-23,27-diaza-1,12 (1,3,2)-25 (1,3)-tribenzenabicyclo[10.10.5]heptacosaphan-24,26-dione (**1**)

A solution of 25^5-*tert*-Butyl-2,11,13,22-tetraoxa-23,27-diaza-1,12(1,3,2)-25(1,3)-tribenzenabicyclo[10.10.5]heptacosaphan-6,17-dien-24,26-dione (186 mg, 284 µmol), Pd/C (10%, 150 mg) and methanol (30 mL) was stirred under an atmosphere of hydrogen for 24 h. The mixture was filtered through a syringe filter (0.450 µm) to remove all Pd/C, and the solvent was removed under reduced pressure to obtain **1** as a white solid (144 mg, 219 µmol, 77%); mp 225 °C (decomp.); ^{1}H NMR (500 MHz, $CDCl_3$) δ 8.30 (s, 2H, 25^{4,6}-H), 8.06 (s, 1H, 25^2-H), 7.24 (br. s, 2H, NH), 7.14 (t, ^3J = 8.4 Hz, 2H, 1^5,12^5-H), 6.59 (d, ^3J = 8.4 Hz, 4H, 1^{4,6},12^{4,6}-H), 4.19 (ddd, ^2J = ca. 9 Hz, ^3J = ca. 9 Hz, ^3J = ca. 2 Hz, 4H, OCH_aH$_b$), 3.85 (ddd, ^2J = 9.7 Hz, ^3J = 9.7 Hz, ^3J = 2.1 Hz, 4H, OCH$_a$$H_b$), 1.79 (m$_c$, 4H, OCH$_2CH_aH_b$), 1.62 (m$_c$, 4H, OCH$_2CH_a$$H_b$), 1.43 (s, 9H, CH$_3$), 1.32 (m$_c$, 8H, CH$_2$), 1.25 (m$_c$, 8H, CH$_2$); ^{13}C NMR (125 MHz, $CDCl_3$) δ 165.4 (s, *C*=O), 154.0 (s, 1^{1,3},12^{1,3}-C), 153.3 (s, 25^5-C), 134.8 (s, 25^{1,3}-C), 129.6 (d, 25^{4,6}-C), 127.1 (d, 1^5,12^5-C), 121.1 (d, 25^2-C), 115.6 (s, 1^2,12^2-C), 105.4 (d, 1^{4,6}, 12^{4,6}-C), 69.2 (t, OCH$_2$), 35.3 (s, *C*(CH$_3$)$_3$), 31.2 (q, CH$_3$), 30.6 (t, OCH$_2$*C*H$_2$), 29.7 (t, O(CH$_2$)$_3$*C*H$_2$), 27.4 (t, O(CH$_2$)$_2$*C*H$_2$); IR (ATR) $\tilde{\nu}$: 3430 (w, NH), 2930, 2848 (2 w, aliph. CH), 1683 (m, C=O), 1589 (w, arom. C=C), 1509 (m, arom. C=C),1392 (s, CH$_3$) cm^{-1}. EIMS (70 eV): *m/z* (% relative intensity) 656 (100) [M]$^{+\bullet}$; CIMS (isobutane): *m/z* (% relative intensity) 657 (30) [M + H]$^+$; ESIMS ($CHCl_3$): *m/z* (% relative intensity) 679 (100) [M + Na]$^+$, 657 (75) [M + H]$^+$; MS (MALDI-TOF, Cl-CCA): *m/z* 695 [M + K]$^+$, 679 [M + Na]$^+$, 656 [M]$^+$; HRMS calcd for $C_{40}H_{52}N_2O_6$ 656.38251; found: 656.38257 (Δ = −0.1 ppm); calcd for $C_{39}{}^{13}CH_{52}N_2O_6$ 657.38586; found: 657.38597 (Δ = −0.2 ppm); Anal. calcd for $C_{40}H_{52}N_2O_6$: C, 73.14; H, 7.98; N, 4.26; found: C, 73.04; H, 8.04; N, 4.39.

Synthesis of 5-*tert*-Butyl-*N,N′*-bis(2,6-dimethoxyphenyl)-isophthalamide (**2**)

A solution of 5-*tert*-butylisophthaloyl dichloride (**3**, 550 mg, 2.12 mmol) in tetrahydrofuran (5.00 mL) was added dropwise over 45 min to a stirred solution of 2,6-dimethoxyaniline (**6**) (650 mg, 4.24 mmol) and triethylamine (2.35 mL, 1.72 g, 17.0 mmol) in tetrahydrofuran (20 mL). The solution was stirred for 24 h. The solvent and excess of triethylamine was evaporated under reduced pressure. The residue was dissolved in chloroform (25 mL) and water (25 mL). The water phase was extracted once with chloroform (25 mL), the combined organic layer was dried with magnesium sulfate and evaporated under reduced pressure to yield a yellow solid, which was purified by column chromatography (silica gel, dichloromethane/methanol, 40:1, R_f = 0.11) to give **2** as a white solid (1.02 g, 2.07 mmol, 97%); mp 122 °C; ^{1}H NMR (500 MHz, $CDCl_3$) δ 8.24 (s, 1H, Ar^1-2-H), 8.14 (s, 2H, Ar^1-4,6-H), 7.43 (br. s, 2H, NH), 7.21 (t, ^3J = 8.4 Hz, 2H, Ar^2-4-H), 6.62 (d, ^3J = 8.4 Hz, 4H, Ar^2-3,5-H), 3.84 (s, 12H, OCH$_3$), 1.38 (s, 9H, CH$_3$); ^{13}C NMR (125 MHz, $CDCl_3$) δ 165.8 (C=O), 155.1 (Ar^2-2,6-C), 152.4 (Ar^1-5-C), 134.7 (Ar^1-1,3-C), 128.2 (Ar^1-4,6-C), 127.6 (Ar^2-4-C), 123.4 (Ar^1-2-C), 114.6 (Ar^2-1-C), 104.4 (Ar^2-3,5-C), 56.0 (OCH$_3$), 35.1 (*C*(CH$_3$)$_3$), 31.3 (q, CH$_3$); IR (ATR) $\tilde{\nu}$: 3387 (w, NH), 3231 (w, arom. CH), 2947 (m, aliph. CH), 1663 (m, C=O), 1593 (m, arom. C=C), 1519 (s, arom. C=C) cm^{-1}; EIMS (70 eV): *m/z* (% relative intensity) 492 (83) [M]$^{+\bullet}$, 340 (100) [M − $C_8H_{10}NO_2$]$^+$; CIMS (isobutane): *m/z* (% relative intensity) 493 (100) [M + H]$^+$. Anal. calcd for $C_{28}H_{32}N_2O_6$·0.1CH_2Cl_2: C, 67.36; H, 6.48; N, 5.59; found: C, 67.42; H, 6.53; N, 5.74.

Synthesis of *N,N′*-Bis(2,6-bis[pent-4-enyloxy]-phenyl)-5-*tert*-butyl-isophthalamide (**5**)

In 20 mL anhydrous tetrahydrofuran, 2,6-bis(pent-4-enyloxy)aniline (4, 1.95 g, 7.46 mmol) and anhydrous triethylamine (4.14 mL, 3.02 g, 29.7 mmol) were dissolved. A solution of 5-*tert*-butylisophthaloyl dichloride (**3**) (970 mg, 3.75 mmol) in anhydrous tetrahydrofuran (10 mL) was added dropwise. The solution was stirred for 16 h at room temperature. The solvent and excess of triethylamine were evaporated under reduced pressure and the residue was dissolved in chloroform (25 mL) and water (25 mL). The aqueous phase was extracted with chloroform (25 mL). The organic layers were collected, dried with magnesium sulfate and the solvent was evaporated under reduced pressure. The product was isolated by column chromatography (silica, cyclohexane/ethyl acetate, 1:1, R_f = 0.34) as a

white solid (1.63 g, 2.30 mmol, 61%); mp 136 °C; ^{1}H NMR (500 MHz, $CDCl_3$) δ 8.18 (s, 1H, Ar^1-2-H), 8.08 (s, 2H, Ar^1-4,6-H), 7.28 (br. s, 2H, NH), 7.16 (t, ^3J = 8.4 Hz, 2H, Ar^2-4-H), 6.59 (d, ^3J = 8.4 Hz, 4H, Ar^2-3,5-H), 5.78 (ddt, ^3J = 16.9 Hz, ^3J = 10.2 Hz, ^3J = 6.6 Hz, 4H, C*H*=CH_2), 4.97 (m_c, 4H, H_Z), 4.91 (m_c, 4H, H_E), 4.01 (t, ^3J = 6.5 Hz, 8H, OCH_2), 2.16 (m_c, 8H, CH_2CH=CH_2), 1.85 (m_c, 8H, OCH_2CH_2), 1.38 (s, 9 H, CH_3).^{13}C NMR (125 MHz, $CDCl_3$) δ 166.1 (s, C=O), 154.8 (s, Ar^2-2,6-C), 152.3 (s, Ar^1-5-C), 137.6 (d, *C*H=CH_2), 135.4 (s, Ar^1-1,3-C), 127.6 (d, Ar^1-4,6-C), 127.6 (d, Ar^2-4-C) 123.3 (d, Ar^1-2-C), 115.1 (t, CH=*C*H_2), 106.2 (s, Ar^2-1-C), 105.4 (d, Ar^2-3,5-C), 68.1 (t, OCH_2), 35.1 (s, *C*$(CH_3)_3$), 31.2 (q, CH_3), 30.1 (t, *C*H_2CH=CH_2), 28.4 (t, OCH_2*C*H_2); IR (ATR) $\tilde{\nu}$: 3207 (br. w, NH), 3076 (w, arom. CH), 2946 (m, aliph. CH), 1669 (m, C=O), 1647 (m, aliph. C=C), 1589 (m, arom. C=C), 1520 (s, arom. C=C) cm^{-1}; EIMS (70 eV): *m/z* (% relative intensity) 709 (49) $[M]^{+\bullet}$, 708 (100) $[M - H]^+$; CIMS (isobutane): *m/z* (% relative intensity) 710 (25) $[M + H]^+$, 709 (59) $[M]^{+\bullet}$, 708 (100) $[M - H]^+$; ESIMS ($CHCl_3$): *m/z* (% relative intensity) 732 (25) $[M + Na]^+$; HRMS: calcd for $C_{44}H_{56}N_2O_6$: 708.41382; found: 708.41390 (Δ = −0.1 ppm); calcd for $C_{43}{}^{13}CH_{56}N_2O_6$: 709.41718; found: 709.41706 (Δ = 0.2 ppm). Anal. calcd for $C_{44}H_{56}N_2O_6{\cdot}0.3C_6H_{12}{\cdot}0.3C_4H_8O_2$: C, 74.18; H, 8.24; N, 3.66; found: C, 73.95; H, 7.93; N, 4.04.

Synthesis of 25^5-*tert*-Butyl-2,11,13,22-tetraoxa-23,27-diaza-1,12(1,3,2)-25(1,3)-tribenzenabicyclo[10.10.5]heptacosaphan-6,17-dien-24,26-dione

Anhydrous dichloromethane (800 mL) was added to a mixture of *N,N*′-bis-(2,6-bis[pent-4-enyloxy]-phenyl)-5-*tert*-butyl-isophthalamide (**5**, 1.00 g, 1.41 mmol) and Grubbs Catalyst 1st gen. (162 mg, 141 µmol). The solution was stirred for 24 h at room temperature. The reaction was quenched with ethyl vinyl ether (2 mL) and the mixture was stirred for 1 h. The solvent was removed under reduced pressure and the crude product was filtered over silica gel (1 cm, dichloromethane/methanol, 40:1). The solvent was removed and cyclohexane/ethyl acetate (150 mL, 1:1, v/v) was added to crystallize the product. The product was filtered off and washed with ethyl acetate (10 mL) to obtain a white solid (186 mg, 284 µmol, 20%). ^{1}H NMR (500 MHz, $CDCl_3$) δ 8.25 (s, 2H, $25^{4,6}$-H), 7.98 (s, 1H, 25^2-H), 7.20 (br. s, 2H, NH), 7.15 (t, ^3J = 8.3 Hz, 2H, 1^5,12^5-H), 6.61 (d, ^3J = 8.3 Hz, 4H, $1^{4,6}$,$12^{4,6}$-H), 5.36–5.27 (m, 4H, C*H*=C*H*), 4.22–3.82 (m, 8H, OCH_2), 2.20–1.60 (m, 16H, CH_2), 1.42 (s, 9H, CH_3) ppm; ^{13}C NMR (125 MHz, $CDCl_3$) δ 154.2 (s, $1^{1,3}$,$12^{1,3}$-C), 153.8 (s, 25^5-C), 134.6 (s, $25^{1,3}$-C), 130.3 (s, *C*H=*C*H), 129.6 (d, $25^{4,6}$-C), 127.0 (d, 1^5,12^5-C), 121.7 (d, 25^2-C), 116.1 (s, 1^2,12^2-C), 105.4 (d, $1^{4,6}$,$12^{4,6}$-C), 69.5 (t, OCH_2), 35.3 (s, *C*$(CH_3)_3$), 31.2 (q, CH_3), 30.7 (t, OCH_2*C*H_2), 24.9 (t, $O(CH_2)_2$*C*H_2); The C=O signal was too weak to be detected in this ^{13}C spectrum. MS (MALDI-TOF, Cl-CCA): *m/z* 676 $[M + Na]^+$, 654 $[M + H]^+$.

Supporting Information

NMR spectra and product analyses for **1** and **2** are available in the Supporting Information as well as details of the NMR CIS titrations, the evaluation of the normalized CIS method, ^{1}H,^{1}H NOESY experiments, and the transport experiments.

Supporting Information File 1

Product analyses and experimental data.
[http://www.beilstein-journals.org/bjoc/content/supplementary/1860-5397-8-2-S1.pdf]

Acknowledgements

We thank Dr. Roberto Quesada, University of Burgos, Spain, for the chloride transport experiments, and the EU for its support through the Marie Curie Research Training Network MRTN-CT-2006-035614 Dynamic Combinatorial Chemistry (DCC).

References

1. Kavallieratos, K.; de Gala, S. R.; Austin, D. J.; Crabtree, R. H. *J. Am. Chem. Soc.* **1997,** *119,* 2325–2326. doi:10.1021/ja964018e
2. Kavallieratos, K.; Bertao, C. M.; Crabtree, R. H. *J. Org. Chem.* **1999,** *64,* 1675–1683. doi:10.1021/jo982382l
3. Bates, G. W.; Gale, P. A.; Light, M. E. *Chem. Commun.* **2007,** 2121–2123. doi:10.1039/b703905k
4. Chmielewski, M. J.; Jurczak, J. *Chem.–Eur. J.* **2005,** *11,* 6080–6094. doi:10.1002/chem.200500232
5. Chmielewski, M. J.; Jurczak, J. *Chem.–Eur. J.* **2006,** *12,* 7652–7667. doi:10.1002/chem.200501471
6. Eckelmann, J.; Saggiomo, V.; Sönnichsen, F. D.; Lüning, U. *New J. Chem.* **2010,** 1247–1250. doi:10.1039/c0nj00160k (Ion triplet receptor).
7. Mahoney, J. M.; Beatty, A. M.; Smith, B. D. *J. Am. Chem. Soc.* **2001,** *123,* 5847–5848. doi:10.1021/ja0156082 (Ion pair receptors).
8. Mahoney, J. M.; Beatty, A. M.; Smith, B. D. *Inorg. Chem.* **2004,** *43,* 7617–7621. doi:10.1021/ic049066b (Ion pair receptors).
9. Bernier, N.; Carvalho, S.; Li, F.; Delgado, R.; Félix, V. *J. Org. Chem.* **2009,** *74,* 4819–4827. doi:10.1021/jo9005798 (Ion pair receptors).
10. Santacroce, P. V.; Davis, J. T.; Light, M. E.; Gale, P. A.; Iglesias-Sánchez, J. C.; Prados, P.; Quesada, R. *J. Am. Chem. Soc.* **2007,** *129,* 1886–1887. doi:10.1021/ja068067v
11. Davis, J. T.; Gale, P. A.; Okunola, O. A.; Prados, P.; Iglesias-Sánchez, J. C.; Torroba, T.; Quesada, R. *Nat. Chem.* **2009,** 138–144. doi:10.1038/nchem.178
12. Hughes, M. P.; Smith, B. D. *J. Org. Chem.* **1997,** *62,* 4492–4499. doi:10.1021/jo9702249

13. Lüning, U.; Müller, M. *Liebigs Ann. Chem.* **1989,** 367–374. doi:10.1002/jlac.198919890163
14. Lüning, U. *Concave Reagents*. In *Encyclopedia of Supramolecular Chemistry;* Atwood, J. L.; Steed, J. W., Eds.; Marcel Dekker: New York, 2004; pp 311–318.
15. Lüning, U. Concave Reagents. In *Molecular Encapsulation: Organic Reactionsin Constrained Systems;* Brinker, U. H.; Mieusset, J.-L., Eds.; John Wiley and Sons: Chichester, UK, 2010; pp 175–199.
16. Winkelmann, O.; Näther, C.; Lüning, U. *Eur. J. Org. Chem.* **2007,** 981–987. doi:10.1002/ejoc.200600843
17. Deetz, M. J.; Shang, M.; Smith, B. D. *J. Am. Chem. Soc.* **2000,** *122,* 6201–6207. doi:10.1021/ja994487r
18. Chen, M.; Han, S.; Jiang, L.; Zhou, S.; Jiang, F.; Xu, Z.; Liang, J.; Zhang, S. *Chem. Commun.* **2010,** *46,* 3932–3934. doi:10.1039/c003118f
A recent investigation of pyridine-*N*-oxide binding.
19. Hancock, L. M.; Beer, P. D. *Chem. Commun.* **2011,** *47,* 6012–6014. doi:10.1039/c1cc11224d
Pyridine-*N*-oxide in a rotaxane.
20. The binding constants were also too weak to be determined by ITC and UV–vis.
21. Kinsella, M.; Duggan, P. G.; Muldoon, J.; Eccles, K. S.; Lawrence, S. E.; Lennon, C. M. *Eur. J. Org. Chem.* **2011,** *6,* 1125–1132. doi:10.1002/ejoc.201001439
A recent example of organocatalysis by an isophthalamide.
22. Saggiomo, V.; Goeschen, C.; Herges, R.; Quesada, R.; Lüning, U. *Eur. J. Org. Chem.* **2010,** 2337–2343. doi:10.1002/ejoc.201000038
Details on the test system.
23. Heim, C.; Affeld, A.; Nieger, M.; Vögtle, F. *Helv. Chim. Acta* **1999,** *82,* 746–759. doi:10.1002/(SICI)1522-2675(19990505)82:5<746::AID-HLCA746>3.0.CO;2-C
24. Srebnik, M.; Mechoulam, R.; Yona, I. *J. Chem. Soc., Perkin Trans. 1* **1987,** 1423–1427. doi:10.1039/P19870001423
25. Kauffmann, H.; Franck, W. *Ber. Dtsch. Chem. Ges.* **1907,** *40,* 3999–4015. doi:10.1002/cber.19070400408

License and Terms

Beilstein Journal of Organic Chemistry

Thermodynamic and kinetic stabilization of divanadate in the monovanadate/divanadate equilibrium using a Zn-cyclene derivative: Towards a simple ATP synthase model

Hanno Sell, Anika Gehl, Frank D. Sönnichsen and Rainer Herges*

Full Research Paper

Open Access

Address:
Otto-Diels Institut für Organische Chemie,
Christian-Albrechts-Universität zu Kiel, Otto-Hahn-Platz 4, 24418 Kiel, Germany

Email:
Rainer Herges* - rherges@oc.uni-kiel.de

* Corresponding author

Keywords:
EXSY NMR; NMR titration; supramolecular chemistry; vanadate condensation; ^{51}V NMR; Zn-cyclene

Beilstein J. Org. Chem. **2012,** *8,* 81–89.
doi:10.3762/bjoc.8.8

Received: 30 September 2011
Accepted: 21 December 2011
Published: 12 January 2012

This article is part of the Thematic Series "Supramolecular chemistry II".

Guest Editor: C. A. Schalley

Abstract

For the condensation of anions such as phosphate and ADP to form ATP and water, nature employs sophisticated supramolecular systems to overcome coulomb repulsion and activation barriers. For an attempt to create a simple, analogous chemical system, the dimerization of vanadate is probably the simplest model. We have investigated Zn-benzylcyclene which favors the dimerization thermodynamically as shown by NMR titration. Moreover, EXSY NMR experiments reveal that the vanadate dimer is also kinetically stabilized with respect to hydrolysis by complexation with Zn-cyclene.

Introduction

Driving endergonic reactions with external energy sources is one of the challenging and so far unsolved problems in supramolecular chemistry. The best known example in nature is probably the condensation of phosphate and ADP to ATP, driven by a proton gradient across a membrane [1]. There are a number of preconditions that have to be met for such an energy driven condensation of inorganic anions. At least three steps (four stages) are required (Figure 1): a) Moving both complexated anions together, b) bond formation (condensation), and c) product release/reactant binding. In the ATP synthase, the energy is put into the system mainly in step c), thus, avoiding product inhibition [2].

In a first attempt towards the very ambitious goal of creating an artificial ATP synthase model, the a) → b) → c) energy profile has to be carefully designed to operate such a system. Here, we focused on step b). To further simplify the system, we chose the dimerization of vanadate as a model for the phosphate condensation for the following reasons: The condensation of phosphate has a very high activation barrier (disodium phosphate

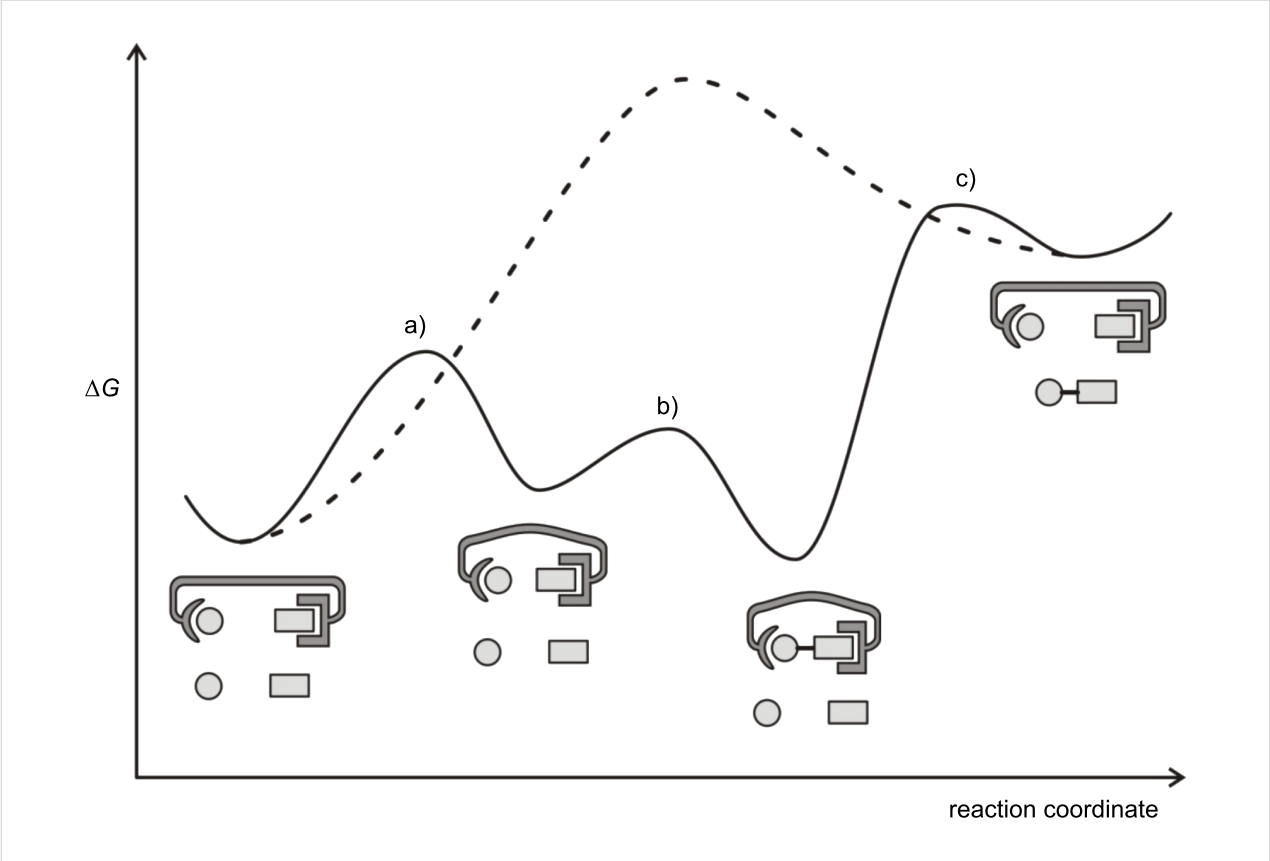

Figure 1: Simplified free energy scheme for driving an endergonic condensation (elimination/addition of water is omitted for simplicity). The non-driven reaction is depicted by a dashed line. a) Moving both complexated anions together, b) bond formation (condensation), and c) product release/reactant binding.

condensates to pyrophosphate at temperatures >250 °C) which is likely difficult to be realized in a prototype artificial system [3]. In contrast to phosphates, mono-, di- and higher vanadates are in equilibrium at room temperature depending on the pH. Moreover, ^{51}V is one of the most sensitive NMR nuclei in the periodic table [4]. The concentration of the different vanadate species can be easily determined even in very diluted solutions by integration of the corresponding NMR peaks [5]. Although vanadates are slightly larger than their corresponding phosphates (V–O bond approximately 0.170 nm, P–O bond approximately 0.152 nm) they exhibit a striking similarity in their chemistry [6]. Vanadates are accepted by a number of phosphatase enzymes [7]. Thus, the plethora of information on both natural and artificial phosphate binding systems can be used to design vanadate coordinating ligands. Vice versa, the vanadate model systems will provide insight into the phosphate condensation, e.g., the formation of ATP [8].

A large number of thoroughly investigated enzymes hydrolyze phosphates and provide insight into conceivable mechanisms of phosphate or vanadate condensations. In phosphatases, kinases and ATP synthase, the catalyzed transfer of phosphate usually requires the presence of metal cations such as Zn^{2+}, Mg^{2+} and Mn^{2+} in the active site [9]. It is generally assumed that the coordination of the metal cations to the phosphate oxygen atoms reduces the Coulomb repulsion in the transition states or in the intermediates, thus, lowering the activation barrier [10]. In tyrosine phosphatase, this role is taken by hydrogen bonding of the phosphate ion to the positively charged arginine side chain [11]. In the key step of the hydrolysis of pyrophosphate by the yeast phosphatase, two Mg^{2+} ions and arginine H-bonds assist the P–O bond cleavage [12]. A number of artificial enzymes that catalyze phosphate ester hydrolysis have been synthesized and investigated [13]. Kimura et al. demonstrated the acceleration of phosphate ester hydrolysis by Zn^{2+} complexes of triazacyclododecane and tetraazacyclododecane (cyclene) [14]. The efficiency was increased by tethering two or three Zn-cyclene units in an appropriate distance to allow multiple coordination to the phosphate oxygen atoms [15]. Brown et al. were able to catalyze the cyclization (hydrolysis/intramolecular condensation) of 2-hydroxypropyl aryl phosphate using a tethered dimeric Zn-triazacyclododecane [16]. Lehn et al. catalyzed the condensation of acetyl phosphate and phosphate to pyrophosphate using a protonated macrocyclic polyamine [17-19].

Results and Discussion

Investigation of the thermodynamic effect

To investigate the fundamental thermodynamic and kinetic effects of metal coordination in inorganic condensation reactions, we focused on the influence of benzyl Zn-tetraazacyclododecane (Zn-benzylcyclene) **1** on the aggregation of vanadate in water.

According to DFT calculations (B3LYP/6-31G*) of a number of different geometries, the monovanadate anion is bound to the Zn-cyclene unit by forming one coordination bond to the Zn^{2+} ion and two hydrogen bonds to the NH groups of the cyclene ring (Figure 2). The formation of a bidentate complex (two vanadate oxygens coordinating with Zn^{2+}) is considerably less favorable. This is also in agreement with X-ray structures of Zn-cyclene phosphate complexes [15].

For the analysis of the multicomponent system, 1-D ^{51}V NMR titrations of Na_3VO_4 with ligand **1** were performed at three different pH values at 25 °C (pH ~9.5 CHES buffer (*N*-cyclohexyl-2-aminoethanesulfonic acid); pH ~8.5 EPPS buffer (3-[4-(2-hydroxyethyl)-1-piperazinyl]propanesulfonic acid); pH ~7.6 HEPES buffer (2-[4-(2-hydroxyethyl)piperazin-1-yl]ethanesulfonic acid)) (Figure 3, see also Supporting Information File 1). These alkaline pH values were chosen because monovanadate is the main species in this range. Like the monovanadate, the di- and tetravanadate exist primarily in the neutral region.

The ^{51}V NMR titration at pH 9.5 is shown in Figure 3 (for the corresponding spectra recorded at pH 7.6 and 8.5 see Supporting Information File 1). The addition of Zn-benzylcyclene **1** leads to an upfield shift of the monovanadate and the divanadate signal at all pH values that were investigated. This shift indicates that Zn-benzylcyclene **1** is capable of complexing both mono- and divanadate. The monovanadate signal remains the main signal throughout the titrations, however, the signal of the divanadate increases upon addition of Zn-benzylcyclene. By raising the concentration of benzylcyclene $\mathbf{1}_t$ from 0 to 7.5 mM in a system with a total concentration of vanadium $[V]_t$ of 1.5 mM at a pH value of 9.5, the ratio of vanadium bound in divanadate species rises from 5% to 23%, while the ratio of vanadium bound in monovanadate decreases from 95% to 77%. Hence, Zn-benzylcyclene **1** favors the condensation of monovanadate to divanadate.

To determine the stoichiometry and stability of the most important species in this system, we included all vanadate oxo-anions that are known to exist in aqueous solution [20,21] and the corresponding complexes with ligand **1** in different stoichiometries as basis of a complex formation model. This model was refined with respect to the experimental data.

In the approach mentioned above, the equilibria of the multi component system were described mathematically by mass balance equations. When the equilibrium species are written

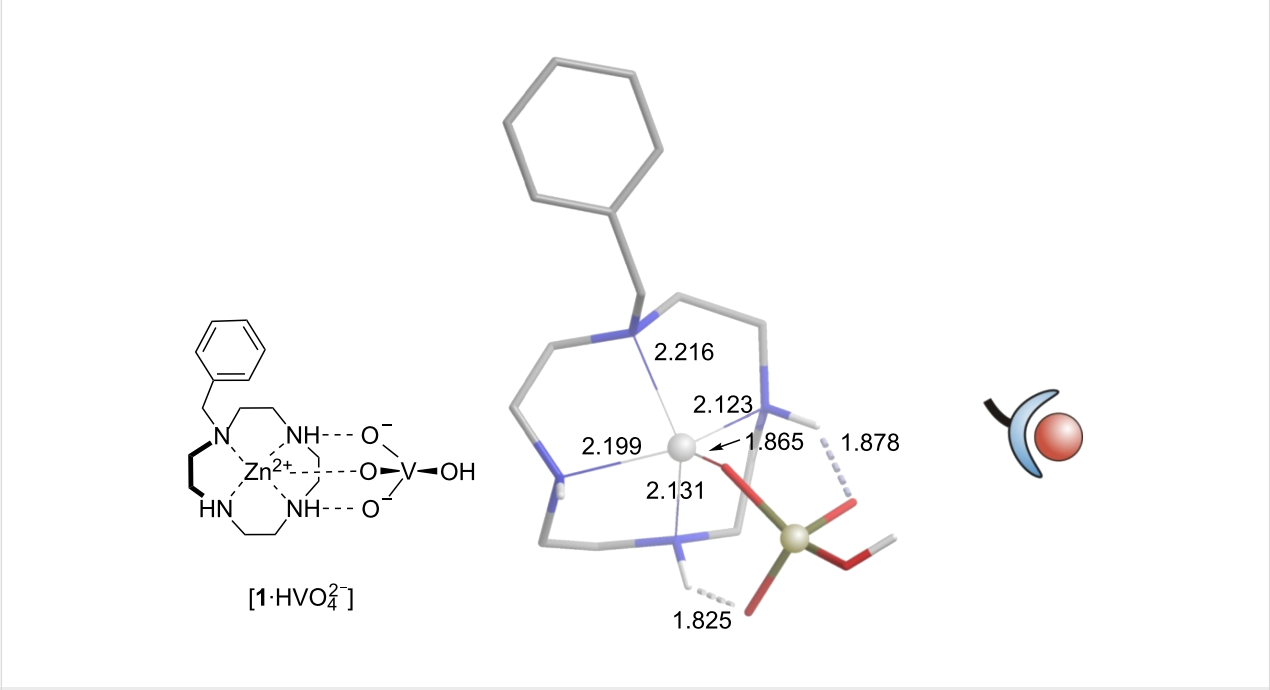

Figure 2: Binding motive of a vanadate zinc benzylcyclene complex (left) as suggested by the results of DFT calculations (B3LYP/6-31G*) (middle). Bond lengths of coordinative bonds and H bridges are given in Å. Metal coordination as well as H–bond formation are operative in binding the oxo-anion to the zinc cyclene unit. The schematic representation (right) is used to improve clarity.

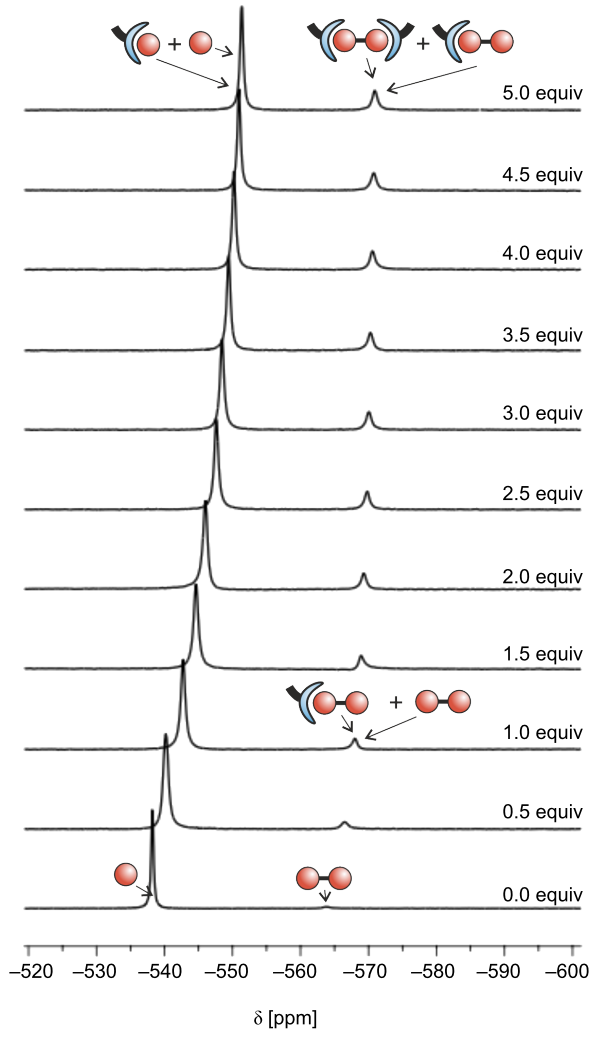

Figure 3: ^{51}V NMR titration at pH 9.5 ([V]$_t$ = 1.5 mM, [**1**]$_t$ = 0 to 7.5 mM (0 to 5 equiv), 100 mM CHES). [V]$_t$ and [**1**]$_t$ are the total molar concentrations of vanadium and Zn-benzylcyclene **1**. The predominant species in equilibrium are represented schematically (Figure 2).

with H^+, VO_4^{3-}, and Zn-benzylcyclene **1** as components, they are formed according to the general expression (Equation 1) [21]:

$$p\,\mathrm{H}^{+} + q\,\mathrm{VO}_4^{3-} + r\,\mathbf{1}^{2+} \rightarrow \mathrm{H}_p(\mathrm{VO}_4)_q\mathbf{1}_r^{(p-3q+2r)} \quad (1)$$

The formation constants of the species β_{pqr} are defined using the concentrations of **1**, VO_4^{3-} and of the protons according to Equation 2.

$$\beta_{pqr} = \frac{\left[\mathrm{H}_p(\mathrm{VO}_4)_q\mathbf{1}_r^{(p-3q+2r)}\right]}{\left[\mathrm{H}^+\right]^p\left[\mathrm{VO}_4^{3-}\right]^q\left[\mathbf{1}^{2+}\right]^r} \quad (2)$$

The substitution of the complex species concentration in the mass balances of the components leads to the mass balance equation system (3). The concentrations of the free components are the variables; the stability constants are the parameters to be optimized.

$$\begin{aligned}\left[\mathrm{H}^+\right]_t &= \sum_{pqr} p\cdot\beta_{pqr}\cdot\left[\mathrm{H}^+\right]^p\left[\mathrm{VO}_4^{3-}\right]^q\left[\mathbf{1}^{2+}\right]^r\\ \left[\mathrm{VO}_4^{3-}\right]_t &= \sum_{pqr} q\cdot\beta_{pqr}\cdot\left[\mathrm{H}^+\right]^p\left[\mathrm{VO}_4^{3-}\right]^q\left[\mathbf{1}^{2+}\right]^r\\ \left[\mathbf{1}^{2+}\right]_t &= \sum_{pqr} r\cdot\beta_{pqr}\cdot\left[\mathrm{H}^+\right]^p\left[\mathrm{VO}_4^{3-}\right]^q\left[\mathbf{1}^{2+}\right]^r\end{aligned} \quad (3)$$

In the ^{51}V NMR titrations for the analysis of the vanadate/Zn-benzylcyclene system the total vanadium concentration [V]$_t$ at each pH value was 1.5 mM, and the total concentration of **1** ([**1**]$_t$) was varied from 0 to 7.5 mM. The NMR data were obtained by careful deconvolution and integration of the signals using routines included in the MestreNova program [22]. The mathematical analysis of the NMR data was performed with the program system LAKE [23] for chemical equilibrium analysis and with MS-Excel [24]. Data of all titrations (78 titration points in total) were included in the calculation. The formation constants for the vanadium oxo-anions of the VO_4^{3-}/H^+-subsystem [21], the pK_a value of Zn-benzylcyclene **1** [14] as well as the pK_a values of the buffers [25] were adopted from literature. The influence of the ionic medium was taken into account in the calculation by means of the Davies equation [26]. The most important ternary species in the equilibrium model that fit the recorded data are presented in Table 1.

Table 1: Stoichiometry and formation constants of the complex species in the proton/vanadium/Zn benzylcyclene system.

p, q, r[a]	formula[b]	lg β_{pqr}[c] (3σ)
1, 1, 1	$HVO_4\mathbf{1}$	16.7 (0.3)
2, 2, 1	$V_2O_7\mathbf{1}^{2-}$	32.2 (0.1)
2, 2, 2	$V_2O_7\mathbf{1}_2$	35.7 (0.8)
3, 2, 1	$HV_2O_7\mathbf{1}^-$	40.6 (0.3)
3, 2, 2	$HV_2O_7\mathbf{1}_2^{2+}$	43.6 (0.4)
8, 4, 2	$V_4O_{12}\mathbf{1}_2$	99.9 (0.7)
8, 4, 4	$V_4O_{12}\mathbf{1}_4^{4+}$	105.6 (1.8)

[a]Stoichiometric coefficients according to the formation from the components H^+, VO_4^{3-} and **1** (Equation 1); [b]formula of the oxo-anion complex. The water formed according to the formation reaction from the components is not given; [c]ionic strength, I = 150 mM, T = 298 K.

According to these data, the association constant for the protonated monovanadate HVO_4^{2-} with **1** is about $10^{3.8}$ M^{-1}, while

the association constant for $V_2O_7^{4-}$ is $K_a = 10^{6.2}$ M^{-1}. The pK_a value for the coordinated divanadate is 8.4 and therewith, 1.9 pK_a units lower than for the uncoordinated $V_2O_7^{4-}$ ion. The binding of a second Zn-benzylcyclene unit proceeds with an association constant of $10^{3.5}$ M^{-1}. Consequently, the affinity of the divanadate for both the proton and the second Zn-benzylcyclene is lowered by the coordination of the first Zn-benzylcyclene unit. A speciation diagram for the titration at pH 9.5 based on these data is given in Figure 4. Fits of calculated and experimental ^{51}V NMR integral data at pH 7.6, 8.5, and 9.5 are given in the Supporting Information File 1.

The formation constants given in Table 1 can be used to calculate the free enthalpy (ΔG_1^0, ΔG_2^0, ΔG_3^0) of the condensation reactions (Equations 4–9):

$$2\ HVO_4^{2-} \underset{}{\overset{K_1}{\rightleftharpoons}} V_2O_7^{4-} + H_2O \qquad (4)$$

$$\lg K_1 = \lg \beta_{220} - 2 \cdot \lg \beta_{110} = 0.15$$
$$\Delta G_1^0 = 0.9\ \text{kJ mol}^{-1} \qquad (5)$$

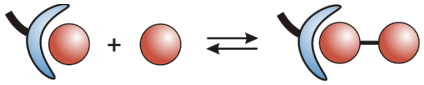

$$HVO_4^{2-} + HVO_4L \overset{K_2}{\rightleftharpoons} V_2O_7L^{2-} + H_2O \qquad (6)$$

$$\lg K_2 = \lg \beta_{221} - \lg \beta_{110} - \lg \beta_{111} = 2.6$$
$$\Delta G_2^0 = -14.8\ \text{kJ mol}^{-1} \qquad (7)$$

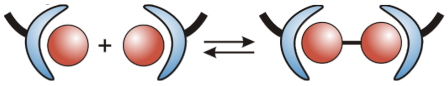

$$2\ HVO_4L \overset{K_3}{\rightleftharpoons} V_2O_7L_2 + H_2O \qquad (8)$$

$$\lg K_3 = \lg \beta_{222} - 2 \cdot \lg \beta_{111} = 2.3$$
$$\Delta G_3^0 = -13.1\ \text{kJ mol}^{-1} \qquad (9)$$

The analysis reveals that the free reaction enthalpy for the condensation of hydrogen monovanadate is lowered by the complexation of the vanadium oxo-anions with Zn- benzylcyclene. In the absence of the ligand, the dimerization of monovanadate

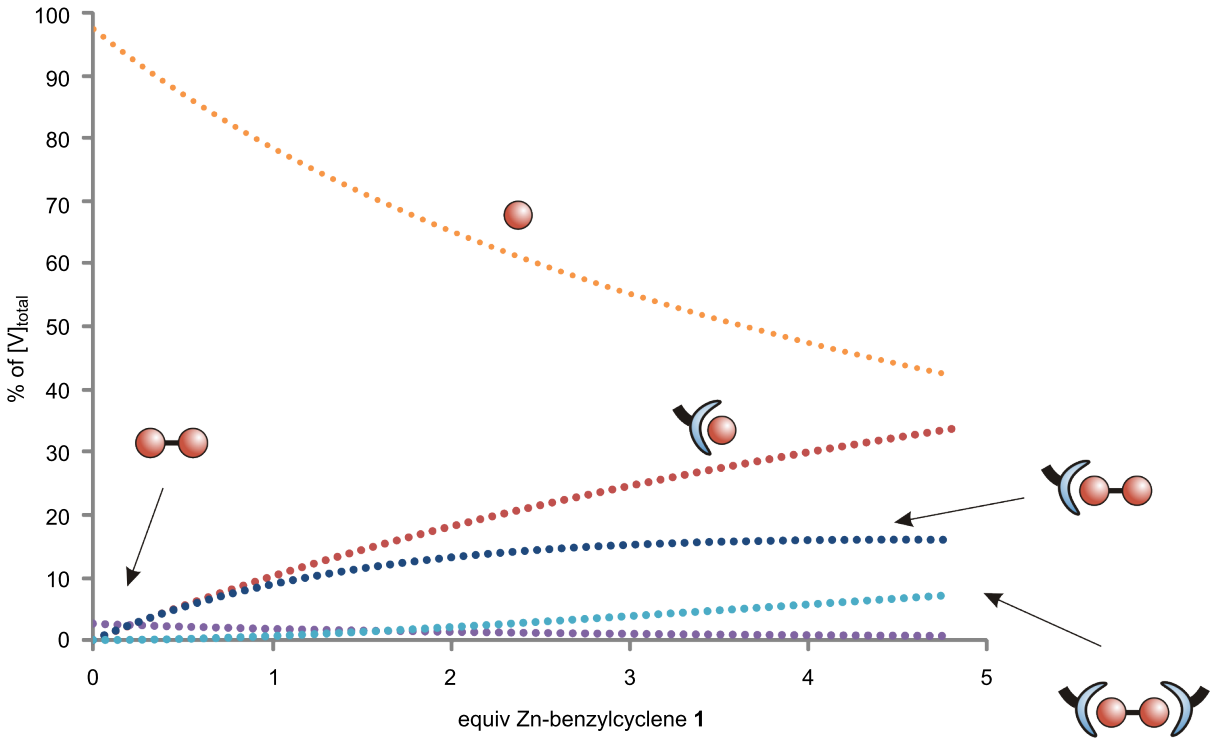

Figure 4: Speciation of vanadium in a solution containing 1.5 mM Na_3VO_4, 100 mM CHES (pH = 9.5) and a Zn-benzylcyclene **1** amount varying from 0 to 5 equiv.

is almost thermoneutral ($\Delta G_1{}^0$ = 0.9 kJ mol^{-1}). However, the condensation of a free monovanadate with a monovanadate bound to Zn-benzylcyclene is exothermic ($\Delta G_2{}^0$ = −14.8 kJ mol^{-1}) and the reaction of two complexed monovanadates is less exothermic ($\Delta G_3{}^0$ = −13.1 kJ mol^{-1}). Hence, the condensation is favored by the complexation with Zn-benzylcyclene and one equiv of the ligand is more effective than two.

Further insight into the stabilization of divanadate by Zn-benzylcyclene is obtained by analyzing the ligand exchange reactions (Equation 10 and Equation 12). While the transfer of a ligand from hydrogenmonovanadate to divanadate is exergonic ($\Delta G_{10}{}^0$ = −13.7 kJ mol^{-1}), the transfer of a second ligand from another hydrogen monovanadate is endergonic ($\Delta G_{12}{}^0$ = 1.1 kJ mol^{-1}).

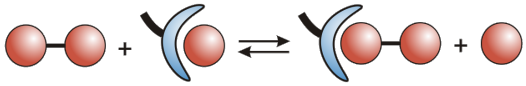

$$V_2O_7^{4-} + HVO_4L \underset{}{\overset{K_{10}}{\rightleftharpoons}} V_2O_7L^{2-} + HVO_4^{2-} \quad (10)$$

$$\begin{aligned} \lg K_{10} &= \lg \beta_{221} + \lg \beta_{110} - \lg \beta_{111} - 2 \cdot \lg \beta_{220} \\ &= 2.4 \\ \Delta G_{10}^0 &= -13.7 \text{ kJ mol}^{-1} \end{aligned} \quad (11)$$

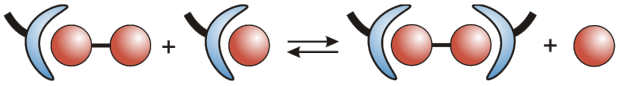

$$V_2O_7L^{2-} + HVO_4L \underset{}{\overset{K_{12}}{\rightleftharpoons}} V_2O_7L_2 + HVO_4^{2-} \quad (12)$$

$$\begin{aligned} \lg K_{12} &= \lg \beta_{222} + \lg \beta_{110} - \lg \beta_{111} - 2 \cdot \lg \beta_{221} \\ &= -0.2 \\ \Delta G_{12}^0 &= 1.1 \text{ kJ mol}^{-1} \end{aligned} \quad (13)$$

Accordingly, a complexed divanadate is destabilized by the coordination of a second ligand.

Investigation of the kinetic effect

The influence of the complexation on the rates of condensation and hydrolysis of the involved vanadium oxo-anions was examined by ^{51}V EXSY NMR experiments [27,28]. ^{51}V EXSY NMR data were collected for solutions buffered with EPPS and HEPES and 1.5 mM total vanadium concentration at 25 °C. For each buffer solution, the amount of Zn-benzylcyclene **1** was varied. The mixing time was 1 ms (Figure 5).

The data show a decrease for the pseudo first order rate constant of the condensation (k_{12} in Equation 14) as well as for the hydrolysis (k_{21} in Equation 15), while the influence on the rate constant of the hydrolysis is stronger.

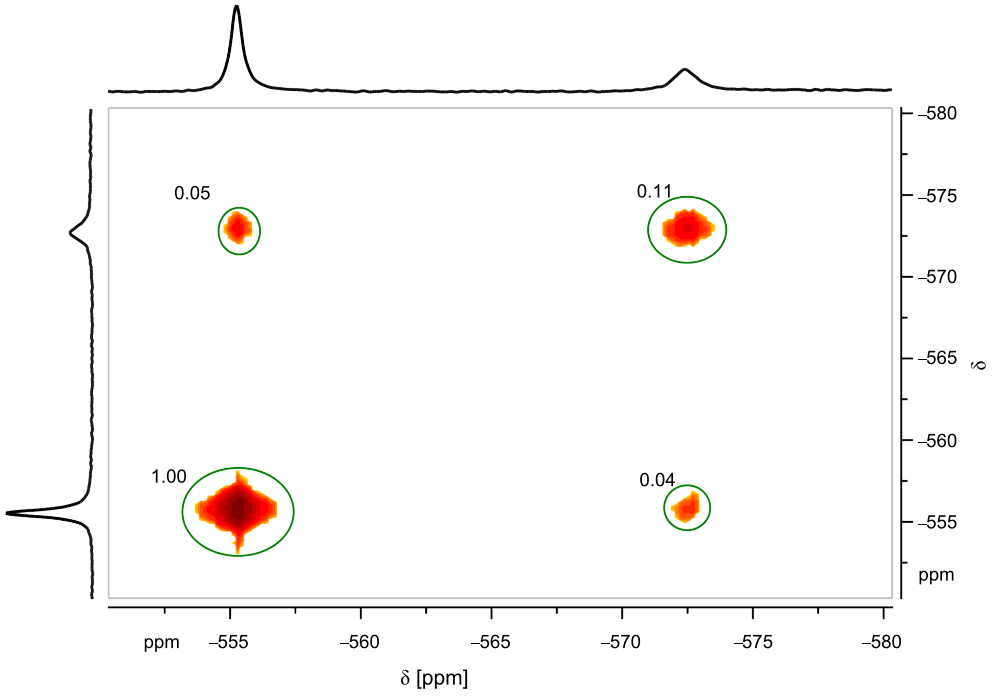

Figure 5: ^{51}V EXSY NMR spectrum (t_{mix} = 1 ms) of a solution containing 1.5 mM Na_3VO_4, 3 mM Zn-benzylcyclene and 100 mM EPPS (pH = 7.9).

$$\frac{d[V_1]}{dt} = -k_{12} \cdot [V_1] \quad (14)$$

$$\frac{d[V_2]}{dt} = -k_{21} \cdot [V_2] \quad (15)$$

In the HEPES buffered solution (pH 7.6), the rate constant for the condensation decreased from 73 s^{-1} to 68 s^{-1} upon the addition of Zn-benzylcyclene (3 mM), while the rate constant for the hydrolysis decreased from 206 s^{-1} to 89 s^{-1}. Compared to that, in the EPPS buffered solution (pH 8.0), the rate constant for condensation decreased from 23 s^{-1} to 14 s^{-1} upon the addition of Zn-benzylcyclene **1** (3 mM), while the rate constant for the hydrolysis decreased from 164 s^{-1} to 70 s^{-1}.

The fact that the condensation of monovanadate is slower in the presence of the ligand is probably due to steric reasons. The nucleophilic attack on the complexed monovanadate is only possible from the non-shielded side. Moreover, the role of the monovanadate acting as the electrophile is defined by complexation which reduces the probability of effective collisions and, thus, decreases the entropy of activation. Both effects, obviously, overcompensate the increased reactivity of the vanadate acting as the electrophile which is induced by complexation (decreased Coulomb repulsion of the two negatively charged reactants). The same arguments are true for the hydrolysis of divanadate (attack of water). However, the thermodynamic stabilization of divanadate further increases the barrier of hydrolysis (provided that the transition state is less effected). Therefore, the rate constant of the divanadate hydrolysis is lowered more strongly by complexation than the rate constant for the condensation of monovanadate.

Conclusion

In conclusion, the condensation of monovanadate to divanadate is considerably favored in the presence of the ligand **1** (Zn-benzylcyclene). In the absence of the ligand at pH 9.5 the condensation is almost thermoneutral (ΔG_1^0 = 0.9 kJ mol^{-1}) whereas upon addition of the ligand the dimerization reaction is exergonic (ΔG_2^0 = −14.8 kJ mol^{-1}). This is mainly due to the fact that the free binding enthalpy of ligand **1** to divanadate is 13.7 kJ mol^{-1} larger than the complex formation with monovanadate.

Complexation with **1** also favors the formation of divanadate kinetically by decreasing its rate of hydrolysis from 164 s^{-1} to 70 s^{-1} upon addition of ligand **1**, as determined by ^{51}V EXSY NMR experiments.

Dimerization, however, is less favorable if both reacting monovanadate units are complexed with ligand **1** (ΔG_3^0 = −13.1 kJ mol^{-1}) compared to the reaction of a complexed vanadate with a free monovanadate (ΔG_2^0 = −14.8 kJ mol^{-1}). For the design of an artificial system driving endergonic condensations (Figure 1), we draw the conclusion that only one of the binding sites should provide metal coordination to the vanadate (or phosphate) and the other binding site should associate the nucleophilic anion by neutral hydrogen bonds.

Similar effects obviously hold for natural systems – particularly ATP synthase, phosphatases and kinases catalyzing the condensation, hydrolysis and phosphate transfer in phosphate esters and phosphate oligomers – which are unsymmetric with respect to metal complexation of the substrates. In the P–O bond forming/cleaving step of yeast pyrophosphatase, the phosphate group acting as the electrophile is activated by coordination to Mg^{2+} as well as by hydrogen bonding to a guanidinium group [12]. The electrophilicity of ADP in ATP synthase is even further increased by electron transfer to Mg^{2+} forming a radical ion pair [29]. Similar to the ATP synthase, a simplified artificial system should prevent product inhibition by actively releasing the product. This could be realized by a (photo)-switchable ligand, see step a) and c) in Figure 1.

Experimental

Synthesis

1-Benzyl-1,4,7,10-tetraazacyclododecane (benzylcyclene): Benzylchloride (1.00 mL, 8.69 mmol) and cyclene (6.00 g, 34.8 mmol) were dissolved in dry chloroform (240 mL). Under nitrogen atmosphere, triethylamine (1.45 mL, 10.4 mmol) was added and refluxed for 20 h. After cooling, chloroform (200 mL) was added, and the organic phase was washed three times with 1 N sodium hydroxide solution (200 mL) and three times with distilled water (200 mL). The organic phase was dried over potassium carbonate and the solvent was removed under reduced pressure [30].

For efficient purification, the crude product (2.27 g) was protected with di-*tert*-butyl dicarbonate (3 equiv) in dry dichloromethane (100 mL). After removal of the solvent the product was purified by column chromatography (cyclohexane:ethylacetate = 1:1, R_f = 0.58). Yield: 4.24 g (87%); ^1H NMR (500 MHz, CD_2Cl_2) δ 7.3–7.2 (m, 5H, CH_{aryl}), 3.65 (s, 2H, Ar-CH_2), 3.52 (br s, 4H, CH_2), 3.4–3.1 (m, 8H, CH_2), 2.60 (br s, 4H, CH_2), 1.41, 1.36 (2 s, 27H, CH_3) ppm; ^{13}C NMR (125 MHz, CD_2Cl_2) δ 155.7 (C=O), 137.5 ($C_{aryl,q}$), 128.5, 127.6, 123.6, (C_{aryl}), 80.0, 79.5, 79.4 ($C(CH_3)_3$), 57.5 (Ar-CH_2), 50.7, 50.1, 48.2 (CH_2), 28.8, 28.6 (CH_3) ppm.

To release the free amine, the boc-protected benzylcyclene (3.76 g, 6.69 mmol) was dissolved in dry dichloromethane (30 mL). Trifluoroacetic acid (5 mL) was added under a

nitrogen atmosphere and the mixture stirred at room temperature for 12 h. Under ice cooling sodium hydroxide (3 g) and distilled water (30 mL) were added. The organic layer was separated, and the aqueous phase extracted five times with 50 mL dichloromethane. The combined organic phases were dried over potassium carbonate and the solvent was removed under reduced pressure to yield a colorless solid (1.52 g, 86%); ^{1}H NMR (500 MHz, CD_2Cl_2) δ 7.3–7.2 (m, 5H, CH_{aryl}), 3.64 (s, 2H, Ar-CH_2), 2.8–2.4 (m, 16H, CH_2) ppm; ^{13}C NMR (125 MHz, CD_2Cl_2) δ 139.9 ($C_{aryl,q}$), 129.5, 128.6, 127.4 (C_{aryl}), 60.1 (Ar-CH$_2$), 51.8, 48.1, 46.6, 46.1 (CH$_2$) ppm.

In order to regain the excess of cyclene used in the first step, the aqueous phase was concentrated under reduced pressure and neutralized with 1 N HCl until a white precipitate formed. The precipitate was filtered to yield pure cyclene (2.8 g). ^{1}H NMR (200 MHz, DCl_3) δ 2.65 (s, 16H, CH_2) ppm.

Zinc-1-benzyl-1,4,7,10-tetraazacyclododecane nitrate (1): 1-Benzyl-1,4,7,10-tetraazacyclododecane (1.00 g, 3.81 mmol) was dissolved in methanol (20 mL). A zinc nitrate solution in water (49.7 mM, 76.6 mL) was added and the solution was stirred for 1 h at room temperature. The solvent was removed under reduced pressure and the colorless solid was dried. Yield: 100 %; ^{1}H NMR (500 MHz, D_2O) δ 7.4–7.3 (m, 5H, CH_{aryl}), 3.94 (s, 2H, CH_2), 3.2–3.0 (m, 4H, CH_2), 2.9–3.0 (m, 12H, CH_2) ppm; ^{13}C NMR (125 MHz, D_2O) δ 138.5 ($C_{aryl,q}$), 131.3, 129.1, 128.7 (C_{aryl}), 56.7 (Ar-CH$_2$), 49.1, 44.5, 43.6, 42.2 (CH$_2$) ppm; ESI *m*/*z* (%): 363.1 (100), 364.1, 365.1, 366.1, 367.1, 368.1 [$C_{15}H_{26}N_4Zn(OH_2)_2$], 326.1 (78), 327.1, 328.1, 329.1, 330.1, 331.1 [$C_{15}H_{25}N_4Zn$].

NMR experiments

NMR titrations

For the NMR titrations three different buffer stock solutions were used: pH 7.6: HEPES (4-(2-hydroxyethyl)piperazine-1-ethanesulfonic acid), pH 8.5: EPPS (4-(2-hydroxyethyl)-1-piperazinepropanesulfonic acid) and pH 9.5: CHES (2-(cyclohexylamino)ethanesulfonic acid). The stock solutions had a total buffer concentration of 100 mM and 50 mM of sodium hydroxide. They were prepared by dissolving the appropriate amount of buffer and sodium hydroxide in 90% deionized water and 10% deuterium oxide. To obtain the vanadate stock solution (50 mM) sodium orthovanadate (92.0 mg) was dissolved in the respective buffer solution (10 mL). For the receptor stock solution (10 mM) the receptor **1** (45.2 mg) was dissolved in 10 mL of the respective buffer solution.

All measurements were carried out at a 1.5 mM total vanadate concentration and a 100 mM buffer concentration. The samples of the ^{51}V NMR titrations were prepared by mixing the appropriate amount of the vanadate stock solution and the receptor **1** stock solution in an NMR tube. Finally, the volume of each sample was brought to a volume of 600 µL by addition of the appropriate amount of the respective buffer stock solution. All NMR spectra were recorded on a Bruker FT-NMR-spectrometer DRX 500. Vanadium chemical shifts are reported relative to the external reference $VOCl_3$ (0 ppm).

EXSY measurements

The EXSY measurements were performed at two different pH values (pH 7.6 and pH 8.0) and at a total vanadate concentration of 1.5 mM. The concentration of **1** was 3.0 mM. For all stock solutions deionized water was used as solvent. The samples were prepared in the following way: The buffer stock solutions had a total buffer concentration of 500 mM (HEPES for pH 7.6, EPPS for pH 8.0) and 250 mM of sodium hydroxide. The vanadate stock solution contained of 50 mM sodium orthovanadate, and the concentration of the Zn-benzylcyclene **1** stock solution was 10 mM. For each experiment 60 µL of the vanadate stock solution, 400 µL of the respective buffer stock solution, and 600 µL of the Zn-benzylcyclene **1** stock solution were mixed with 100 µL deuterium oxide and 840 µL deionized water. The NMR tubes were then filled with 600 µL of the mixture. In all experiments a mixing time of 1 ms was applied.

Supporting Information

Supporting Information File 1

^{51}V NMR spectra and data fitting results.
[http://www.beilstein-journals.org/bjoc/content/supplementary/1860-5397-8-8-S1.pdf]

Acknowledgements

We would like to thank the Deutsche Forschungsgemeinschaft (DFG) for funding via SFB 677 (Function by Switching).

References

1. Boyer, P. D. *Annu. Rev. Biochem.* **1997,** *66,* 717–749. doi:10.1146/annurev.biochem.66.1.717
2. O'Neal, C. C.; Boyer, P. D. *J. Biol. Chem.* **1984,** *259,* 5761–5767.
3. Osterheld, R. K. *Top. Phosphorus Chem.* **1972,** *7,* 103–254.
4. Pregosin, P. S., Ed. *Transition Metal Nuclear Magnetic Resonance;* Elsevier, 1991.
5. Crans, D. C.; Shin, P. K.; Armstrong, K. B. Application of NMR Spectroscopy to Studies of Aqueous Coordination Chemistry of Vanadium(V) Complexes. In *Mechanistic Bioinorganic Chemistry;* Thorp, H. H.; Pecoraro, V. L., Eds.; Advances in Chemistry, Vol. 246; American Chemical Society: Washington, DC, 1995; pp 303–328. doi:10.1021/ba-1995-0246.ch011
6. Chasteen, N. D. *Struct. Bond.* **1983,** *53,* 105–138. doi:10.1007/BFb0111304

7. Crans, D. C.; Keramidas, A. D.; Drouza, C. *Phosphorus, Sulfur Silicon Relat. Elem.* **1996,** *109,* 245–248. doi:10.1080/10426509608545136
8. Ko, Y. H.; Hong, S.; Pedersen, P. L. *J. Biol. Chem.* **1999,** *274,* 28853–28856. doi:10.1074/jbc.274.41.28853
9. Lipscomb, W. N.; Sträter, N. *Chem. Rev.* **1996,** *96,* 2375–2434. doi:10.1021/cr950042j
10. Lahiri, S. D.; Zhang, G.; Dunaway-Mariano, D.; Allen, K. N. *Science* **2003,** *299,* 2067–2071. doi:10.1126/science.1082710
11. Asthagari, D.; Dillet, V.; Liu, T.; Noodleman, L.; Van Etten, R. L.; Bashford, D. *J. Am. Chem. Soc.* **2002,** *124,* 10225–10235. doi:10.1021/ja020046n
12. Oksanen, E.; Ahonen, A.-K.; Tuominen, H.; Tuominen, V.; Lahti, R.; Goldmann, A.; Heikinheimo, P. *Biochemistry* **2007,** *46,* 1228–1239. doi:10.1021/bi0619977
13. Kirby, A. J. *Angew. Chem., Int. Ed. Engl.* **1996,** *35,* 706–724. doi:10.1002/anie.199607061
14. Koike, T.; Kimura, E. *J. Am. Chem. Soc.* **1991,** *113,* 8935–8941. doi:10.1021/ja00023a048
15. Kimura, E.; Aoki, S.; Koike, T.; Shiro, M. *J. Am. Chem. Soc.* **1997,** *119,* 3068–3076. doi:10.1021/ja9640408
16. Bunn, S. E.; Liu, C. T.; Lu, Z.-L.; Neverov, A. A.; Brown, R. S. *J. Am. Chem. Soc.* **2007,** *129,* 16238–16248. doi:10.1021/ja076847d
17. Hosseini, M. W.; Lehn, J.-M. *Chem. Commun.* **1985,** 1155–1157. doi:10.1039/C39850001155
18. Hosseini, M. W.; Lehn, J.-M. *J. Am. Chem. Soc.* **1987,** *109,* 7047–7058. doi:10.1021/ja00257a024
19. Hosseini, M. W.; Lehn, J.-M. *J. Chem. Soc., Chem. Commun.* **1988,** 397–399. doi:10.1039/C39880000397
20. Schmidt, H.; Andersson, I.; Rehder, D.; Pettersson, L. *Chem.–Eur. J.* **2001,** *7,* 251–257. doi:10.1002/1521-3765(20010105)7:1<251::AID-CHEM251>3.0.CO;2-9
21. Cruywagen, J. J.; Heyns, J. B. B. *Polyhedron* **1991,** *10,* 249–253. doi:10.1016/S0277-5387(00)81596-X
22. Willcott, M. R. *J. Am. Chem. Soc.* **2009,** *131,* 13180. doi:10.1021/ja906709t
23. Ingri, N.; Andersson, I.; Pettersson, L.; Yagasaki, A.; Andersson, L.; Holmström, K. *Acta Chem. Scand.* **1996,** *50,* 717–734. doi:10.3891/acta.chem.scand.50-0717
24. Del Piero, S.; Melchior, A.; Polese, P.; Portanova, R.; Tolazzi, M. *Ann. Chim.* **2006,** *96,* 29–49. doi:10.1002/adic.200690005
25. Technical Librarby. Buffer pKa/pH Tables and Formulas. http://www.sigmaaldrich.com/life-science/core-bioreagents/learning-center/technical-library.html#pH (accessed Dec 9, 2011).
26. Davies, C. *Ion Association;* Butterworth: Washington, D.C., 1962; pp 37–53.
27. Crans, D. C.; Rithner, C. D.; Theisen, L. A. *J. Am. Chem. Soc.* **1990,** *112,* 2901–2908. doi:10.1021/ja00164a009
28. Perrin, C. L.; Gipe, R. K. *J. Am. Chem. Soc.* **1984,** *106,* 4036–4038. doi:10.1021/ja00326a027
29. Buchachenko, A. L.; Shchegoleva, L. N.; Breslavskaya, N. N. *Chem. Phys. Lett.* **2009,** *483,* 77–80. doi:10.1016/j.cplett.2009.10.044 (Example for a recent theoretical paper).
30. Massue, J.; Plush, S. E.; Bonnet, C. S.; Moore, D. A.; Gunnlaugsson, T. *Tetrahedron Lett.* **2007,** *48,* 8052–8055. doi:10.1016/j.tetlet.2007.09.022

License and Terms

Beilstein Journal of Organic Chemistry

On the mechanism of action of gated molecular baskets: The synchronicity of the revolving motion of gates and in/out trafficking of guests

Keith Hermann, Stephen Rieth, Hashem A. Taha, Bao-Yu Wang, Christopher M. Hadad and Jovica D. Badjić*

Full Research Paper

Open Access

Address:
Department of Chemistry, The Ohio State University, 100 West 18th Avenue, Columbus OH, 43210, USA

Email:
Jovica D. Badjić* - badjic@chemistry.ohio-state.edu

* Corresponding author

Keywords:
dynamic NMR; host–guest chemistry; linear free-energy relationships; molecular encapsulation; recognition kinetics

Beilstein J. Org. Chem. **2012,** *8,* 90–99.
doi:10.3762/bjoc.8.9

Received: 14 October 2011
Accepted: 13 December 2011
Published: 16 January 2012

This article is part of the Thematic Series "Supramolecular chemistry II".

Guest Editor: C. A. Schalley

Abstract

We used dynamic ^{1}H NMR spectroscopic methods to examine the kinetics and thermodynamics of CH_3CCl_3 (**2**) entering and leaving the gated molecular basket **1**. We found that the encapsulation is first-order in basket **1** and guest **2**, while the decomplexation is zeroth-order in the guest. Importantly, the interchange mechanism in which a molecule of CH_3CCl_3 directly displaces the entrapped CH_3CCl_3 was not observed. Furthermore, the examination of the additivity of free energies characterizing the encapsulation process led to us to deduce that the revolving motion of the gates and in/out trafficking of guests is synchronized, yet still a function of the affinity of the guest for occupying the basket: Specifically, the greater the affinity of the guest for occupying the basket, the less effective the gates are in "sweeping" the guest as the gates undergo their revolving motion.

Introduction

Covalent and self-assembled molecules with a natural cavity, i.e., molecular capsules [1,2], employ several mechanisms to trap and release guests capable of residing in their inner space [3-5]. The so-called "slippage" scenario [6], in which a guest makes its way to and from the host by forcing the expansion of its aperture [7], appears frequently. The "gating" scenario [8], on the other hand, includes a conformational change in the host to create an opening that is large enough for a guest to "squeeze" its way in or out of the host. In the case of self-assembled hosts, however, the slippage, gating and possible partial or full disassembly of the capsule constitute mechanistic alternatives for the exchange of guests [4]. In the last decade, we [9-14] and others [7,8,15-18] have studied gated molecular encapsulation in artificial and natural systems [19].

In particular, we designed gated molecular baskets (Figure 1) and employed both experimental and theoretical methods to gain an understanding of their mechanism of action [4]. These dynamic hosts comprise a semirigid platform with three aromatic gates appended to its rim through CH_2 "hinges" (Figure 1). The gates were set to interact by hydrogen bonding to control the opening and closing of the basket and thereby the rate by which a guest enters or departs the cavity of the basket [12-14]. Indeed, the action mechanism of the basket has been addressed [14], yet the exact role of the gates in the process of the in/out guest exchange necessitates additional scrutiny. In particular, a careful inspection of the additivity of free energies [21] pertaining to the constrictive $\Delta G^{\ddagger}_{in/out}$ and intrinsic $\Delta G°$ binding energies of the guests [11] as well as the racemization of the basket $\Delta G^{\ddagger}_{rac}$ (i.e., opening and closing, see below in Figure 6) reveals a systematic disparity ($\Delta G° + \Delta G^{\ddagger}_{rac} + \Delta G^{\ddagger}_{sterics} \neq \Delta G^{\ddagger}_{out}$, see below in Figure 7). In order to address this conundrum, we have employed methods of experimental (dynamic NMR) and computational chemistry (steered molecular dynamics, SMD) to inspect the relationship between the gates revolving at the rim of the host and the in/out exchange of guests. The results of our study suggest that for guests with a greater propensity to occupy the interior of the basket (i.e., more negative $\Delta G°$) the process of gating is poorly synchronized with the guest exchange. The gates undergo a revolving motion to sweep the space but are concurrently less effective in enforcing the ejection of the guest from the cavity. Moreover, the results of dynamic ^{1}H NMR measurements of CH_3CCl_3 (**2**) entering and departing basket **1** (Figure 1) suggest the absence of an interchange mechanism [22] in which a molecule of CH_3CCl_3 directly displaces another CH_3CCl_3 residing in the interior of the gated basket.

Results and Discussion

The encapsulation stoichiometry and the intrinsic binding ($\Delta G°$)

In an earlier study [13], we reported on the tendency of basket **1** to trap CH_3CCl_3 (**2**) as a guest, and we hereby elaborate on the equilibrium thermodynamics of the recognition event (Figure 2). The incremental addition of **2** to a CD_2Cl_2 solution of **1** (0.67 mM, 298.0 K) caused considerable ^{1}H NMR chemical shifts of the resonances corresponding to the presence of the basket (Figure 2). At 298.0 K, the formation and degradation of [basket–CH_3CCl_3] complex was sufficiently fast on the "NMR time scale": The nonlinear least-squares fitting of the binding isotherm to a 1:1 binding model provided $K_a = 54 \pm 1$ M^{-1} ($R^2 = 0.998$, Figure 2) [23].

Indeed, the results of a variable temperature ^{1}H NMR study (400 MHz, CD_2Cl_2) of **1** (0.67 mM) containing CH_3CCl_3 (**2**) (1.07 mM) was in line with the formation of the 1:1 complex; note that extrapolation of the fitted line gives K_a of 86 ± 16 M^{-1} at 298.0 K, which is akin to the value obtained in the titration experiment. Furthermore, the van't Hoff analysis of the ^{1}H NMR data revealed that the encapsulation is also driven by enthalpy ($\Delta H° = -3.56 \pm 0.06$ kcal/mol, Figure 2). Indeed, the computed electrostatic potential surface (AM1, Spartan) [20] of guest **2** is complementary to the one corresponding to the concave interior of **1** (Figure 1). Furthermore, compound **2** (93 Å^3, Spartan) occupies 42% of the inner space of **1** (221 ± 9 Å^3)

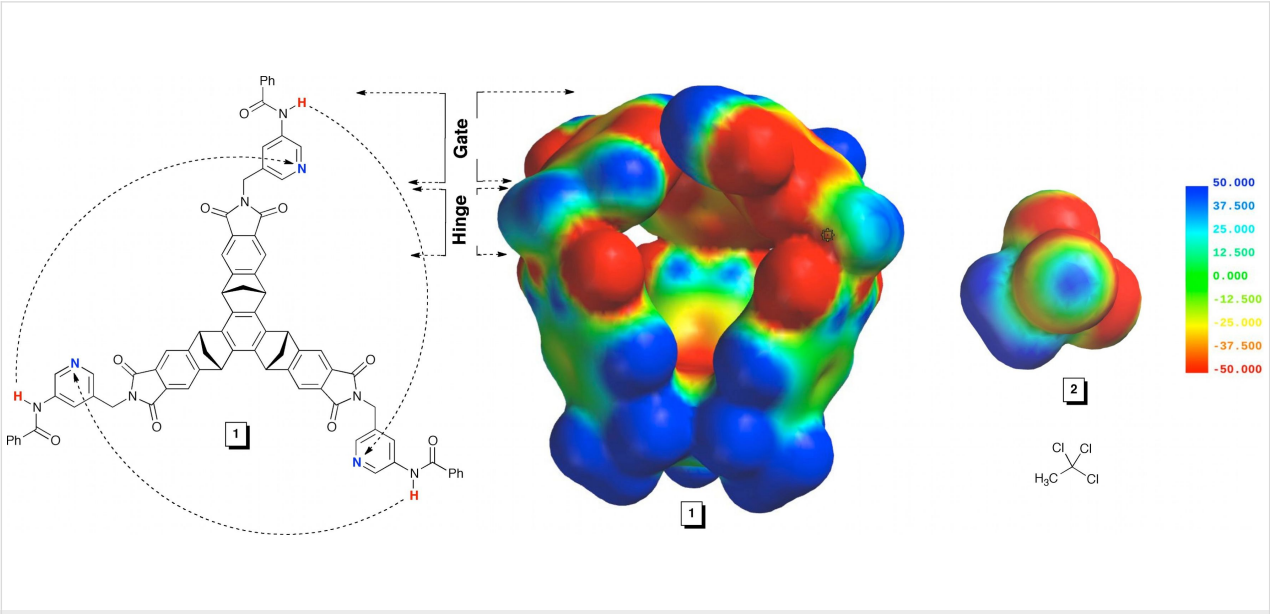

Figure 1: Chemical structure of gated molecular basket **1** and 1,1,1-trichloroethane (**2**). Electrostatic potential surfaces of basket **1** and guest **2** were computed with Spartan (AM1) [20].

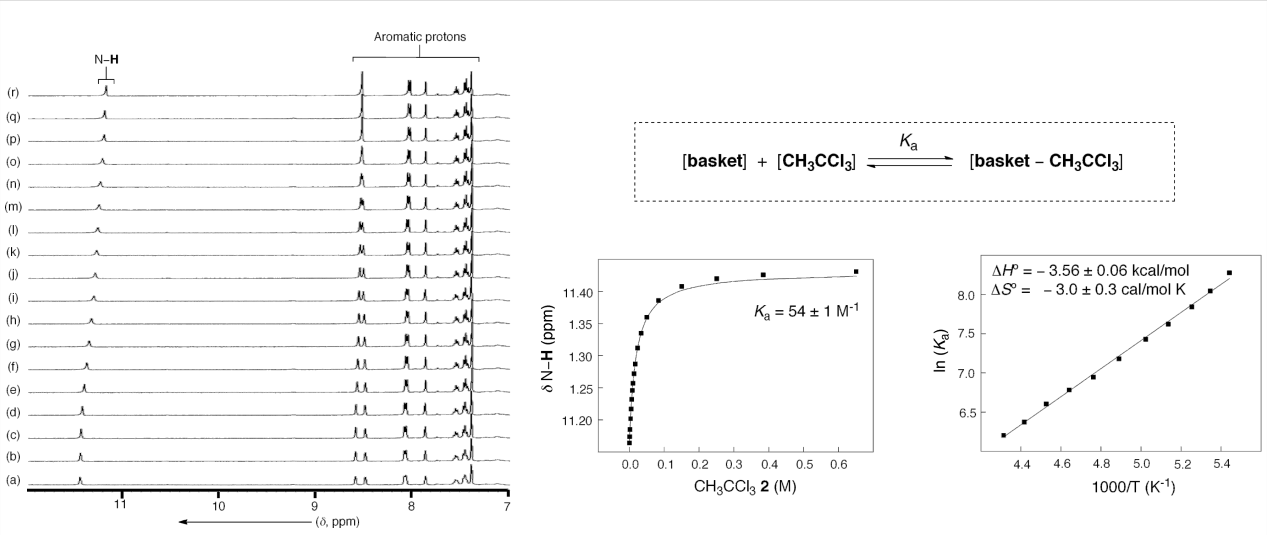

Figure 2: (Left): ^{1}H NMR spectra (400 MHZ, CD_2Cl_2) of **1** (0.67 mM) obtained upon incremental addition of 1,1,1-trichloroethane (**2**) (0.00–0.65 M) at 298.0 K. (Middle): Nonlinear least-squares fitting (SigmaPlot) of the N–**H** chemical shift of **1** as a function of the concentration of **2** gave K_a = 54 ± 1 M^{-1} at 298.0 K [23]. (Right): The van't Hoff plot was generated from variable temperature ^{1}H NMR measurements (400 MHz, 180–250 K) of **1** (0.67 mM) containing CH_3CCl_3 (1.07 mM).

[11], which is close to the packing coefficient of liquids and thereby a good indicator of a stable assembly [24].

The rate law characterizing guest exchange and the constrictive binding ($\Delta G^{\ddagger}_{in/out}$)

We performed ^{1}H,^{1}H-EXSY [25] and selective inversion-transfer [26,27] NMR measurements (400 MHz, CD_2Cl_2) to examine the rate laws characterizing the trafficking of CH_3CCl_3 (**2**) to and from basket **1**. At concentrations of CH_3CCl_3 as a guest comparable to those of host **1**, the EXSY measurements (250.0 ± 0.1 K) allowed us to extract (MNova software) the magnetization rate coefficients k^*_{in} and k^*_{out} (Figure 3).

At higher concentrations of CH_3CCl_3 with respect to host **1**, however, we noticed an intense T_1 noise coinciding with the $[CH_3CCl_3]_{out}$ signal, thus preventing the accurate determination of the volume of the corresponding cross peak. Accordingly, we had to turn to selective inversion-transfer NMR measurements to obtain the values of k^*_{in} and k^*_{out}. The exchange rate constants k^*_{in} and k^*_{out} (characterizing the longi-

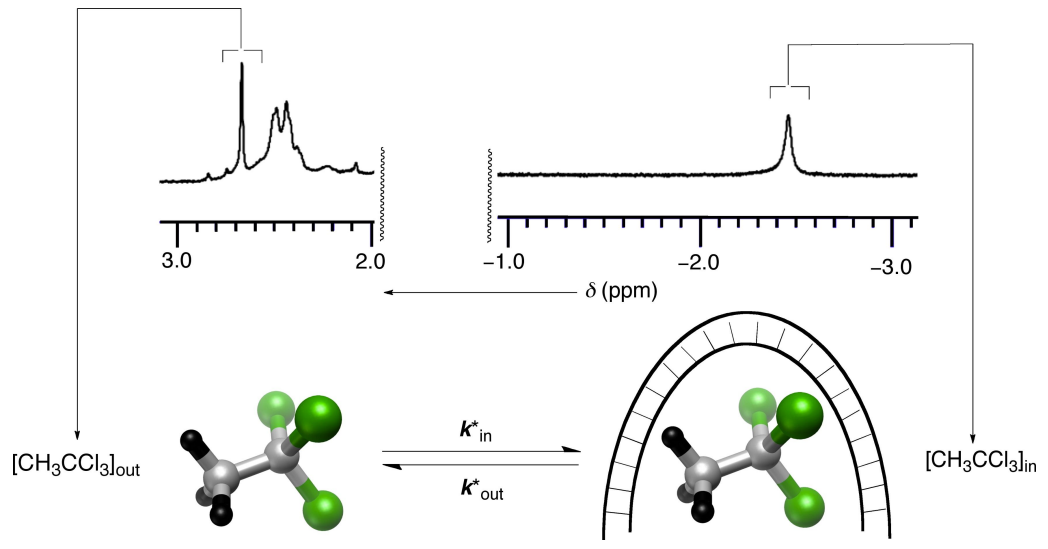

Figure 3: Chemically equivalent CH_3 protons (black) in 1,1,1-trichloroethane (**2**) alter their magnetic environment from 2.70 ppm in bulk solvent to −2.45 ppm inside the basket.

tudinal magnetization of the hydrogen nuclei in C**H**$_3$CCl$_3$ altering the chemical/magnetic environment) are by the nature of the experiment pseudo-first-order in character (see below) [25,26].

On the basis of the reaction stoichiometry (Figure 2), we initially made the assumption that the entrapment is first-order in both [basket] and [CH_3CCl_3]. Accordingly, the rate of the forward reaction is given as:

$$v_{in} = k_{in}\left[\text{basket}\right]\cdot\left[CH_3CCl_3\right] \quad (1)$$

As per the earlier discussion, the pseudo-first-order constant k^*_{in} describes the longitudinal magnetization of the hydrogen nuclei in C**H**$_3$CCl$_3$ transferring from the bulk solvent (δ = 2.70 ppm, Figure 3) to the interior of **1** (δ = −2.45 ppm, Figure 3).

Correspondingly, the rate of the forward reaction (entrapment) can be formulated as:

$$v_{in} = k^*_{in}\left[CH_3CCl_3\right] \quad (2)$$

From Equation 1 and Equation 2, we furthermore derive:

$$k_{in}\left[\text{basket}\right]\cdot\left[CH_3CCl_3\right] = k^*_{in}\left[CH_3CCl_3\right]$$
$$k^*_{in} = k_{in}\left[\text{basket}\right] \quad (3)$$

If the proposed model is valid, then the experimentally determined k^*_{in} will be linearly proportional to the concentration of free basket **1**. Indeed, when the value of k^*_{in} is plotted against the concentration of free basket **1**, there is an apparent linear dependence, with the slope of the fitted curve k_{in} = 2.1 ± 0.3 × 10^3 $M^{-1}\cdot s^{-1}$ (at 250 ± 0.1 K, Figure 4). Using Equation 4, we derive Equation 5, which upon insertion into Equation 3 gives Equation 6:

$$K_a = \left[\text{basket–}CH_3CCl_3\right]/\left(\left[\text{basket}\right]\cdot\left[CH_3CCl_3\right]\right) \quad (4)$$

$$\left[\text{basket}\right] = \left[\text{basket–}CH_3CCl_3\right]/\left(K_a\left[CH_3CCl_3\right]\right) \quad (5)$$

$$k^*_{in} = k_{in}\left[\text{basket–}CH_3CCl_3\right]/\left(K_a\left[CH_3CCl_3\right]\right) \quad (6)$$

This particular dependence suggests that k^*_{in} should be directly proportional to the concentration of the host–guest complex, [basket–CH_3CCl_3], but inversely proportional to the concentration of CH_3CCl_3. At higher concentrations of CH_3CCl_3, however, there should be a negligible variation in the concentration of basket–CH_3CCl_3 and the magnetization rate coefficient k^*_{in} becomes inversely proportional to the concentration of CH_3CCl_3.

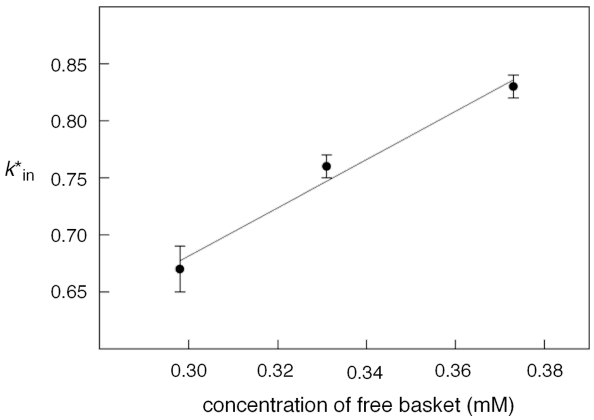

Figure 4: Nonlinear least-squares fitting (SigmaPlot) of magnetization rate constants k^*_{in} (2-D EXSY, 250.0 ± 0.1 K) as a function of the concentration of the free basket to a linear function gives a slope of k_{in} = 2.1 ± 0.3 × 10^3 $M^{-1}\cdot s^{-1}$.

In accordance with this theoretical model, we completed a series of selective inversion-transfer [27] NMR measurements of **1** (1.65 mM) and CH_3CCl_3 (16–200 mM) in CD_2Cl_2 at 250.0 ± 0.1 K (Figure 5). In the experiment, the proton resonance corresponding to $[CH_3CCl_3]_{out}$ was selectively inverted, resulting in the perturbation of the longitudinal relaxation of both $[C\mathbf{H}_3CCl_3]_{out}$ and $[C\mathbf{H}_3CCl_3]_{in}$ due to chemical exchange over the course of variable delay time τ (180° x (selective) – τ – 90° x (nonselective) – τ_d). Upon the integration of both signals (I_{in} and I_{out}), we subjected the data to nonlinear least-squares fitting of $I_{in/out}$ versus τ using the proposed solutions of the McConnell equations [27] describing the relaxation of the hydrogen nucleus residing in two environments (Figure 5A). For the fitting, the longitudinal relaxation rate ($1/T_1$) of hydrogen nuclei in CH_3CCl_3 was determined separately by using a classical selective inversion-recovery NMR pulse sequence. When the experimental k^*_{in} was plotted against the equilibrium concentration of CH_3CCl_3, there indeed appeared a hyperbolic dependence (Figure 5B) in agreement with Equation 6 ($k^*_{in} \propto 1/[CH_3CCl_3]$). The fitting of the data to Equation 6 was inaccurate as only a few experimental points characterize the dependence (Figure 5B), although computing k_{in} from each data point would give a value of this coefficient (~2 × 10^3 $M^{-1}\cdot s^{-1}$) similar to that determined in the EXSY experiment (Figure 4). In accordance with the 2-D EXSY and selective inversion-transfer results, we conclude that the entrapment is first-order in both basket **1** and guest **2**.

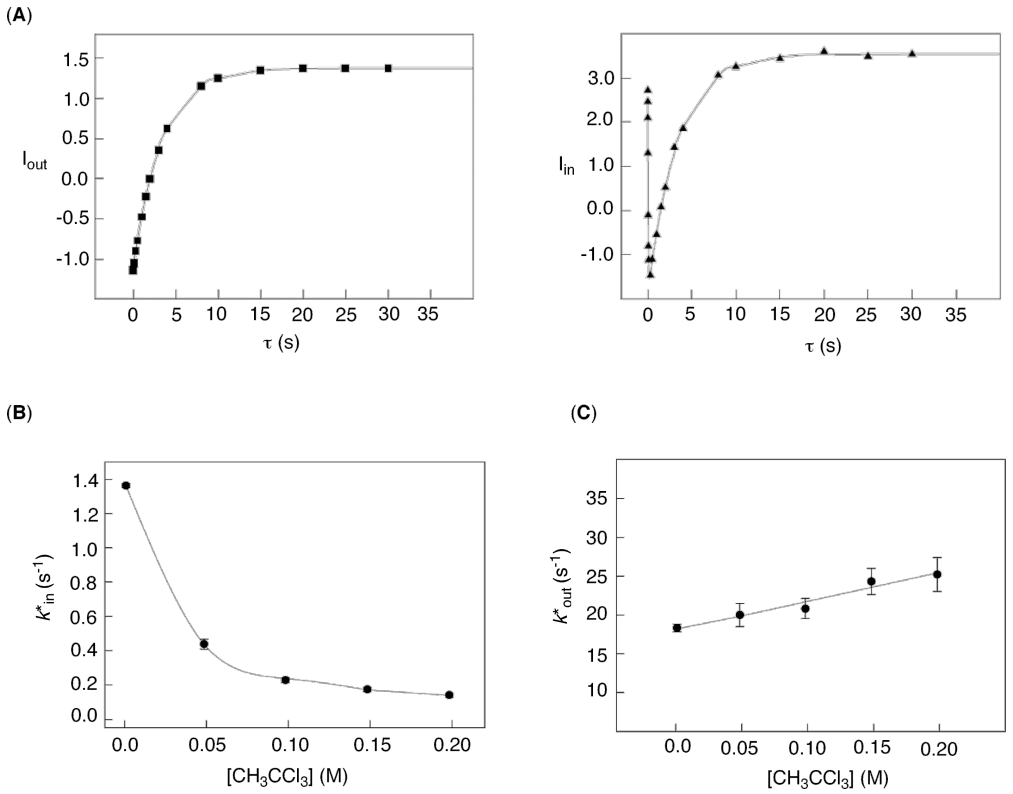

Figure 5: (A): Nonlinear least-squares fitting of ^{1}H NMR signal intensities ($I_{in/out}$) of $[CH_3CCl_3]_{in/out}$ as function of the time variable τ (250.0 ± 0.1 K) was completed with the assistance of the Bloch–McConnell equations [27,28] describing the relaxation of hydrogen nuclei in two different environments; in this particular experiment $[basket]_0$ = 1.65 mM and $[CH_3CCl_3]_0$ = 50.0 mM. Magnetization transfer rate coefficients k^*_{in} (B) and k^*_{out} (C) were further obtained [27,28] from selective inversion-transfer measurements and plotted as a function of the concentration of free CH_3CCl_3.

On the basis of the reaction stoichiometry (Figure 2), the rate law for **2** leaving the encapsulation complex can be described as:

$$v_{out} = k_{out}\left[\text{basket–}CH_3CCl_3\right] \quad (7)$$

Alternatively, the rate of the same process expressed through the NMR magnetization transfer rate coefficient k^*_{out} is:

$$v_{out} = k^*_{out}\left[\text{basket–}CH_3CCl_3\right] \quad (8)$$

As in the case above, the manipulation of Equation 7 and Equation 8 gives Equation 9:

$$k^*_{out} = k_{out} \quad (9)$$

In accordance with this theoretical model, we increased the concentration of guest **2** (16–200 mM) with respect to **1** (1.65 mM) and measured k^*_{out} using the selective inversion-transfer NMR pulse sequence. Markedly, there was essentially no interdependence between k^*_{out} (21 ± 3 s^{-1}) and the concentration of guest **2** (Figure 5C); the curve indeed shows a small slope, but the intercept of 18.1 suggests that this is likely an artifact. 2-D EXSY measurements would give a rate coefficient k^*_{out} = 10 ± 0.1 s^{-1}, which was also found to be independent of the external concentration of the basket/guest (Figure 4). The departure of CH_3CCl_3 from its complexed form [basket–CH_3CCl_3], therefore, follows a dissociative mechanism [4]. Notably, a molecule of solvent CD_2Cl_2 and not another CH_3CCl_3 (interchange mechanism) displaces the encapsulated guest. In fact, the inspection of CPK models as well as molecular dynamics studies (see below) revealed that the departure of CH_3CCl_3 (93 Å^3) demands (a) "opening" of at least two gates, (b) disruption of internal N–H···N hydrogen bonds, and (c) distortion of the framework of the basket. We further reason that in the case of a direct exchange of two CH_3CCl_3 molecules, the departure of CH_3CCl_3 would create an empty host, and therefore vacuum, before another guest of the same kind can take its place. Note that two large compounds (overall ~186 Å^3) cannot simultaneously occupy the interior of **1** (~220 Å^3).

Computational examination of the in/out trafficking

To gain mechanistic insight into the departure of CH_3CCl_3 (**2**) from the interior of basket **1**, we completed a series of steered molecular dynamics (SMD) simulations using the AMBER 10.0 suite of programs [29-32]. Without applying any external force on the entrapped CH_3CCl_3, we first found that this guest would, within 10 ns, adopt many positions inside host **1**, although the one depicted in Figure 6A is obtained after 1 ns (Supporting Information File 1). The N–**H**···**N** hydrogen bond contacts along the top of the basket were also monitored throughout the 10 ns simulation. Importantly, the distance between each pair of amide-hydrogen and pyridine-nitrogen atoms was found to be invariant (~2 Å, see Supporting Information File 1).

In addition, the width of each side aperture (the span between adjacent carbonyl oxygen atoms) also remained constant at ~6.3 Å throughout the simulation (Figure S3, see Supporting Information File 1). We then selected multiple trajectories for "pulling" the guest from the host (Figure 6A). Markedly, the departure of CH_3CCl_3 necessitated the cleavage of at least two intramolecular N–**H**···N hydrogen bonds in **1** (Figure 6B) with a simultaneous expansion of the host (Figure 6B). That is to say, the "slippage" of CH_3CCl_3 (with gates in the "closed" position) does not appear to be a viable mechanistic scenario. Note that our simulation did not include solvent molecules (CD_2Cl_2) displacing the entrapped CH_3CCl_3, as suggested by the kinetic study. The substitution of the guest by the solvent should perhaps cause an even greater distortion of the framework of the basket.

The revolving of the gates and the racemization of basket 1

The aromatic gates in basket **1** interact through hydrogen bonding, as exemplified by a large downfield shift of the signal corresponding to (O=C)N−**H** protons (δ = 11.6 ppm at 298.0 K, Figure 2) [13]. In addition, the aromatic gates are dynamic, each one revolving about its axis to give rise to two enantiomeric conformers $\mathbf{1_A}$ and $\mathbf{1_B}$ (Figure 7A). The interconversion kinetics of the $\mathbf{1_{A/B}}$ racemization can be followed by dynamic NMR spectroscopy in which a singlet corresponding to $\mathbf{H}_a/\mathbf{H}_b$ nuclei at high temperatures is seen to split into two doublets at low temperatures. In particular, the revolving rate of the gates is temperature dependent, thereby governing the lifetime of $\mathbf{H}_a$ or $\mathbf{H}_b$ nuclei, each residing in a particular chemical environment ($\tau = 1/k_{rac}$); the hydrogen nuclei are observed as separate resonances when $\tau >> 1/\Delta\nu(H_{a/b})$ [33]. Accordingly, we performed the classical line-shape analysis of $\mathbf{H}_a/\mathbf{H}_b$ resonances (WinDNMR-Pro software) to obtain the rate constants (k_{rac}) and corresponding activation energies $\Delta G^{\ddagger}_{rac}$ characterizing the racemization of basket **1** (Figure 7B). Evidently, the rate at which the aromatic gates in **1** revolve is a function of the com-

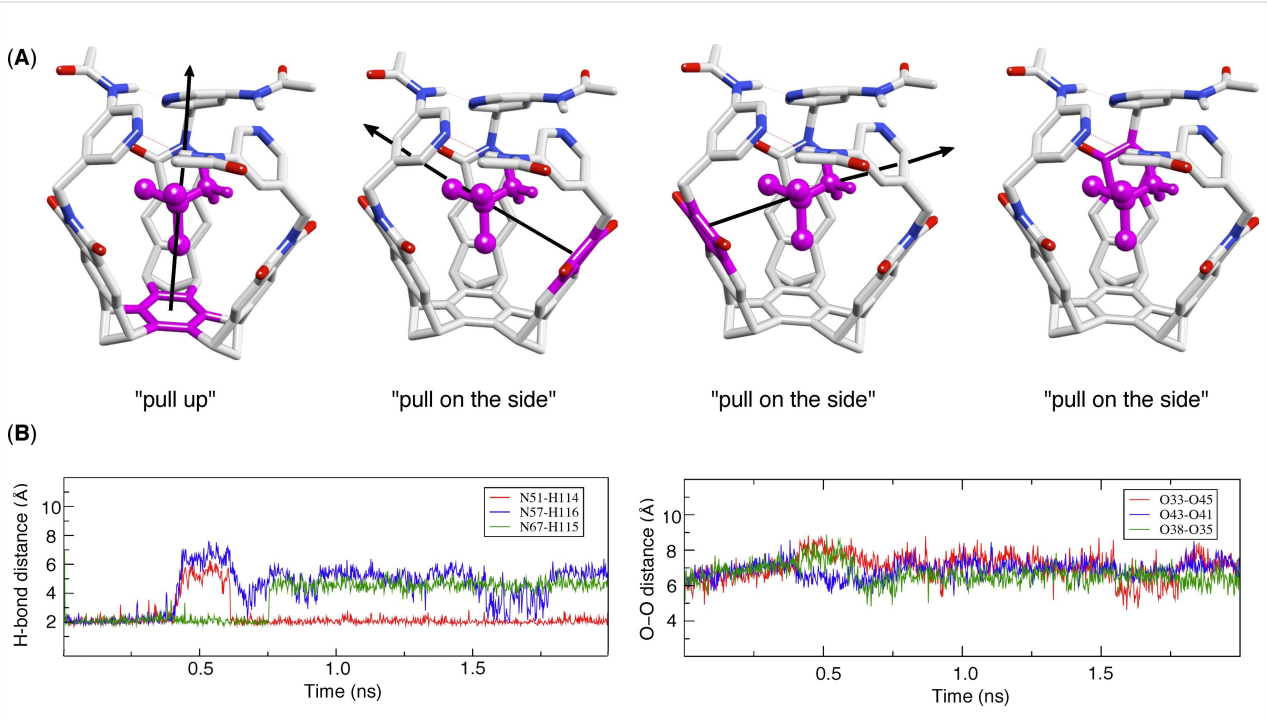

Figure 6: (A) Four different trajectories were used for examining the departure of CH_3CCl_3 guest from basket **1** with steered molecular dynamics. (B) The variation in N–**H**···**N and** –C=**O**···**O**=C– distances during SMD simulation with CH_3CCl_3 being pulled on the side.

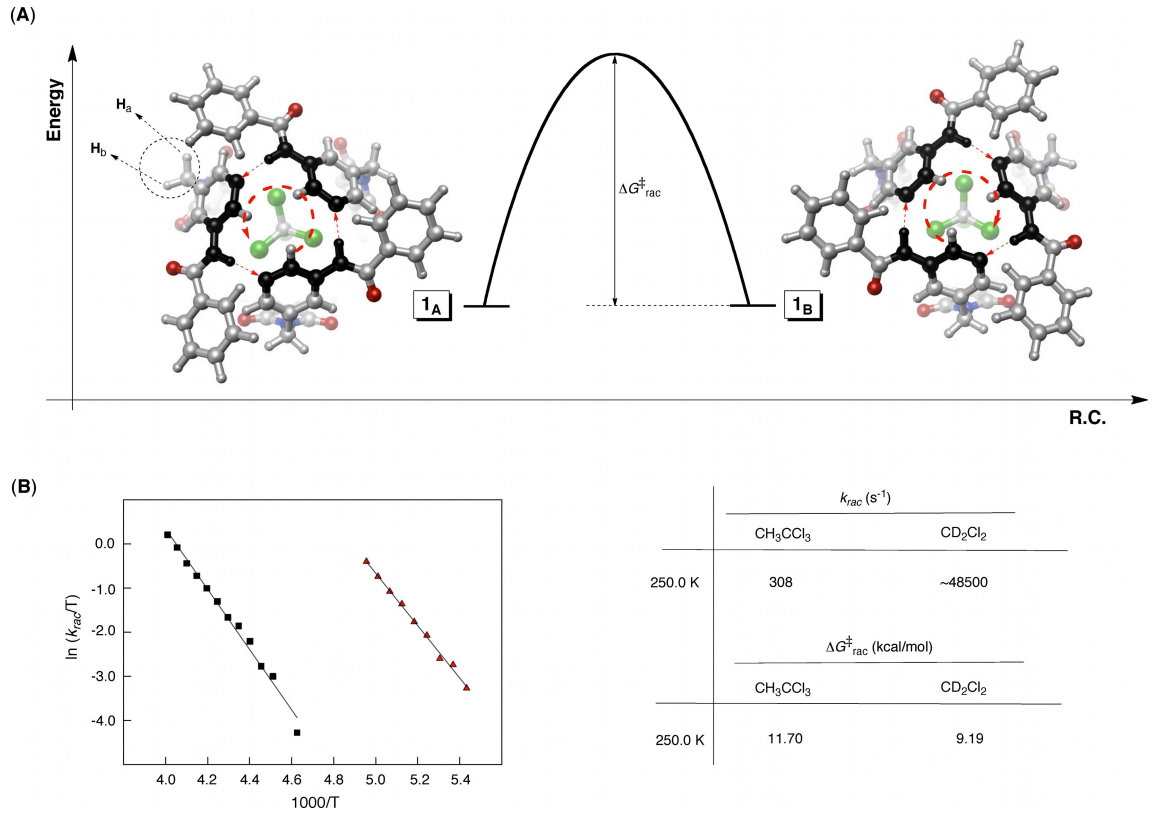

Figure 7: (A) The interconversion of conformational enantiomers $\mathbf{1}_A$ and $\mathbf{1}_B$, having anticlockwise and clockwise senses in the orientation of the intramolecular N–H···N hydrogen bonds, contributes to the process of racemization, i.e., the opening and closing of the basket [13]. (B) Eyring plots describing the linear relationship between ln(k_{rac}/T) and temperature for basket **1** containing CH_3CCl_3 (black squares) and solvent CD_2Cl_2 (red triangles). The plots were generated from the results of the line-shape analysis (WinDNMR-Pro) of ^{1}H NMR $\mathbf{H}_{a/b}$ signals of **1** (1.65 mM, CD_2Cl_2) at variable temperatures.

pound occupying the inner space: With CH_3CCl_3 the gates are less dynamic than with CD_2Cl_2 occupying the cavity (Figure 7B).

On the action mechanism of the basket

Is there a relationship between the aromatic gates sweeping the space and guests trafficking to and from the basket [11]? That is to say, will the gates expel the entrapped guest each time that they alter their propeller-like orientation (Figure 8)? First, our kinetic measurements suggest that guest CH_3CCl_3 (**2**) enters basket **1** by substituting solvent (CD_2Cl_2) molecule(s), while exactly the opposite occurs during the dissociation (Figure 8). Given this exchange scenario, we deduce that $\mathbf{1}_A$–CH_3CCl_3 shall transform into $\mathbf{1}_B$–CH_3CCl_3 via intermediate **1**–CD_2Cl_2 (Figure 8). That is, the formation of **1**–CD_2Cl_2 from $\mathbf{1}_A$–CH_3CCl_3 is accompanied by either reorientation or reinstatement of the gates, and therefore, there is an equal likelihood that **1**–CD_2Cl_2 will yield $\mathbf{1}_A$–CH_3CCl_3 or $\mathbf{1}_B$–CH_3CCl_3 (Figure 8); this reasoning is also supported by the fact that the gates of the solvated basket revolve at a higher rate (Figure 7B). In accordance with such a racemization mechanism, we apply the statistical correction to the measured k_{rac} to obtain $k_{rac'}$ ($k_{rac'} = 2k_{rac} = 616\ s^{-1}$, Figure 7B) [34]. This particular rate coefficient should more precisely describe the process of racemization.

One could describe the free energy characterizing the guest departure ($\Delta G^{\ddagger}_{out}$) as a linear combination of $\Delta G^{\ddagger}_{rac'} + \Delta G° + \Delta G^{\ddagger}_{sterics}$ representing (1) the opening of the gates ($\Delta G^{\ddagger}_{rac'}$), (2) the decomplexation of the guest ($\Delta G°$), and (3) the "slippage" of the guest while exiting the open host ($\Delta G^{\ddagger}_{sterics}$) [8,11,21,35]. The encapsulation kinetics is first-order in guest CH_3CCl_3 suggesting that this species creates van der Waals strain (friction) during the in/out trafficking, thereby justifying the use of the $\Delta G^{\ddagger}_{sterics}$ term.

In addition, the decomplexation of CH_3CCl_3 follows a late transition state [14] whereby its affinity for populating the interior of the basket should decrease to a somewhat smaller value than described by $\Delta G°$. Given the delicacy of the proposed partitioning, will the additivity of free energies and the relationship $\Delta G^{\ddagger}_{rac'} + \Delta G° + \Delta G^{\ddagger}_{sterics} \sim \Delta G^{\ddagger}_{out}$ still hold?

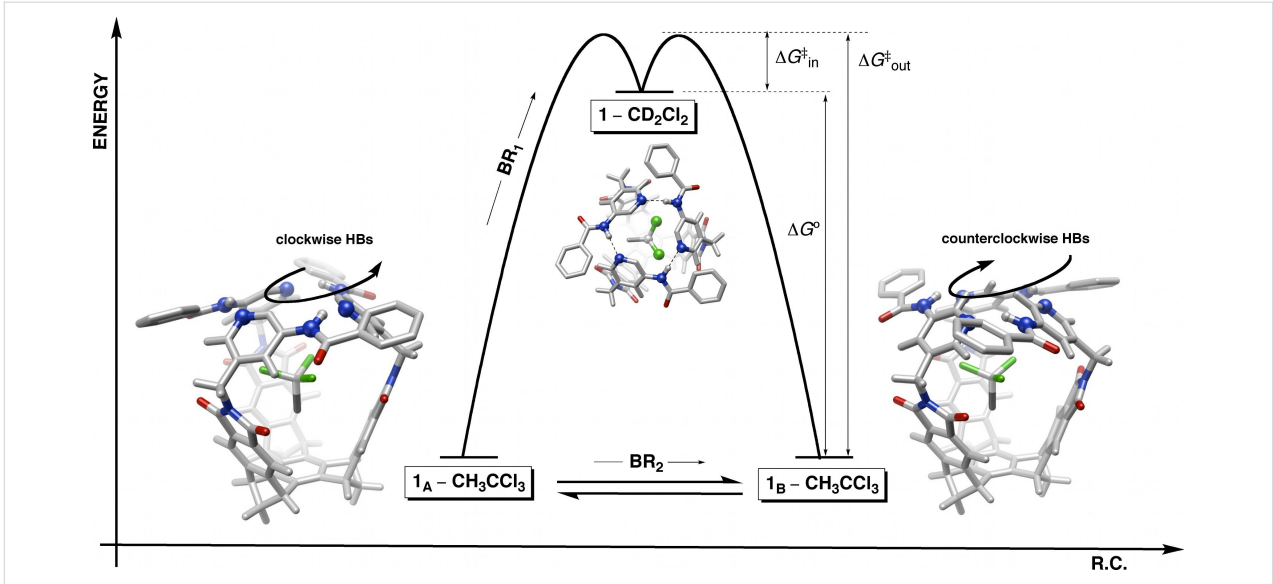

Figure 8: The departure of CH_3CCl_3 from $\mathbf{1}_A$–CH_3CCl_3 gives rise to the less stable **1**–CD_2Cl_2, which upon entrapment of another CH_3CCl_3 gives either $\mathbf{1}_A$–CH_3CCl_3 or $\mathbf{1}_B$–CH_3CCl_3. The $\mathbf{1}_{A/B}$–CH_3CCl_3 interconversion occurs with CH_3CCl_3 departing (BR_1 mechanism) or remaining (BR_2 mechanism) in the cavity.

When $\Delta G^{\ddagger}_{rac'}$ of 11.4 ± 0.1 kcal/mol (at 250.0 ± 0.1 K, Figure 7) is added to the intrinsic binding energy of CH_3CCl_3 ($|\Delta G^{\circ}|$ = 2.79 ± 0.09 kcal/mol at 250.0 ± 0.1 K, Figure 2), a value of 14.2 kcal/mol is obtained. Without even including $\Delta G^{\ddagger}_{sterics}$ (as a positive number), there is an apparent disagreement between the sum value (≥14.2 kcal/mol) and the experimentally determined $\Delta G^{\ddagger}_{out}$ = 13.4 ± 0.1 kcal/mol (from 2-D EXSY, k_{out} = 10 ± 1 s^{-1}). Is there a missing factor needed in order to understand this phenomenon?

In reality, when the internal hydrogen bonds are broken and the gates open up the guest does not have to depart the basket cavity. That is to say, the gates should be able to revolve to allow the interconversion of $\mathbf{1}_A$–CH_3CCl_3 into $\mathbf{1}_B$–CH_3CCl_3 without even ejecting the guest. Accordingly, we hereby propose that the conversion of $\mathbf{1}_A$–CH_3CCl_3 into $\mathbf{1}_B$–CH_3CCl_3 (i.e., racemization) occurs by two routes, BR_1 and BR_2, one with (BR_1) and another without (BR_2) the concomitant guest exchange (Figure 8).

It follows that, during the departure of CH_3CCl_3, the measured racemization of **1** ($\Delta G_{rac'}$) includes energetic contributions from two pathways ($\Delta G^{\ddagger}_{rac'} = \Delta G^{\ddagger}_{BR1} + \Delta G^{\ddagger}_{BR2}$) of which only BR_1 should be incorporated in the additivity assessment. It is therefore convenient to partition the energetic contribution of the two "competing" BR_1 and BR_2 routes to $\Delta G^{\ddagger}_{rac'}$ ($\Delta G^{\ddagger}_{rac'} = \Delta G^{\ddagger}_{BR1} + \Delta G^{\ddagger}_{BR2}$) to corroborate fully the role of the gates. However, this is a difficult task, but for guest molecules holding strongly onto the basket (more negative ΔG°) there should be a greater contribution from the RG_2 pathway during the racemization.

In one of our prior studies [13,14], we measured kinetic and thermodynamic parameters pertaining to the exchange of five isosteric (same-size) guests **3**–**7** to and from basket **1** (Figure 9). When $\Delta G^{\ddagger}_{rac'} + \Delta G^{\circ}$ is computed for each guest and the values plotted against $\Delta G^{\ddagger}_{out}$, a linear relationship appears (R^2 = 0.99, Figure 9A). Note that $\Delta G^{\ddagger}_{sterics}$ is not included in this analysis as it is unknown; however, we anticipate that the value of the parameter should show minimal fluctuations for the series of isosteric guests **3**–**7**. Importantly, the greater the affinity of a particular guest for occupying the interior of the basket (ΔG°), the greater the deviation of the calculated $\Delta G^{\ddagger}_{rac'} + \Delta G^{\circ}$ (black line, Figure 9A) from the experimental $\Delta G^{\ddagger}_{out}$ (red line, Figure 9A). The variation of $\Delta\Delta G = (\Delta G^{\ddagger}_{rac'} + \Delta G^{\circ}) - \Delta G^{\ddagger}_{out}$ with intrinsic binding energies ΔG° of **3**–**7** is shown in Figure 9B. The trend is evident, supporting the notion that for guests having greater propensity to occupy the basket (ΔG°) the BR_2 pathway is more greatly involved in the $\mathbf{1}_A$–CH_3CCl_3/$\mathbf{1}_B$–CH_3CCl_3 racemization. As already discussed, the BR_2 pathway contributes to the measured $\Delta G^{\ddagger}_{rac'}$, yet it is not involved in the exchange of guests.

Conclusion

Describing mechanisms by which dynamic hosts entrap/release guests is a challenging task necessitating experimental and computational scrutiny. Notably, one can use NMR spectroscopic methods for understanding the equilibrium kinetics characterizing the rate law of molecular encapsulation processes. Our study, accordingly, describes the rate law characterizing the encapsulation of guest CH_3CCl_3 by the gated basket **1.** Importantly, the entrapment reaction is first-order in each compound,

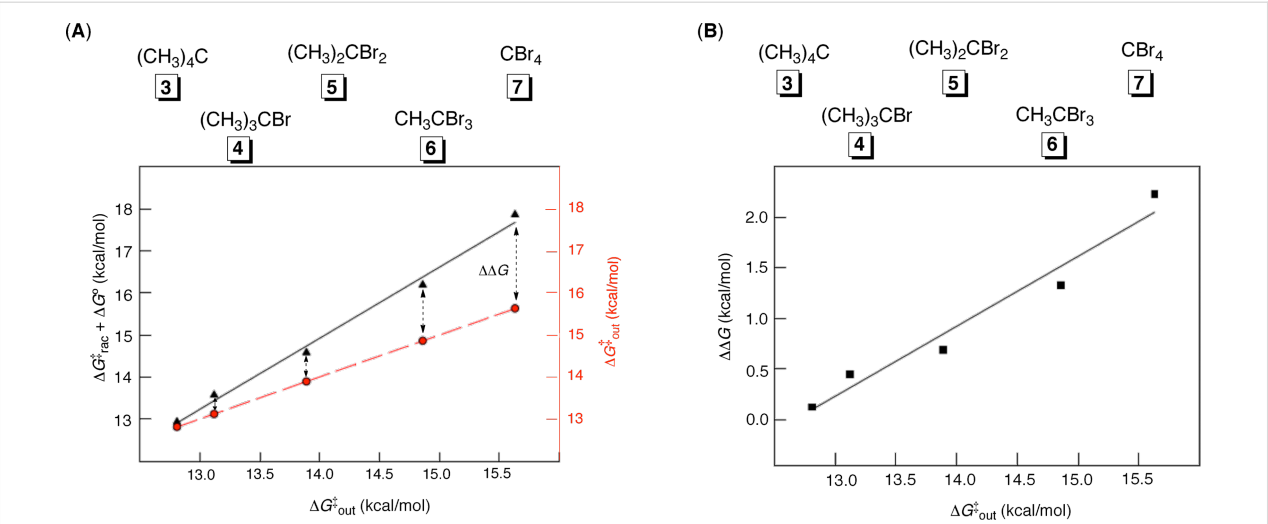

Figure 9: (A): Kinetic and thermodynamic parameters [13,14] characterizing the departure of isosteric guests **3**–**7** from the basket. (B): The computed $\Delta\Delta G = (\Delta G^{\ddagger}_{rac'} + \Delta G^{\circ}) - \Delta G^{\ddagger}_{out}$ is apparently a linear function of $\Delta G^{\ddagger}_{out}$.

while the complex dissociation is zeroth-order in guest CH_3CCl_3. Furthermore, examination of the additivity of free energies corresponding to different molecular events can assist in the understanding of the operation of gated hosts and, in particular, can help to reveal the explicit role of the gates. On the basis of these results, we deduced that the synchronicity in the revolving motion of the gates and in/out trafficking of guests is a function of the affinity of the guest for occupying the gated basket. The greater the affinity, the less effective the gates are in "sweeping" the guest as the gates undergo their revolving motion. This result is important for exploring the utility of gating for controlling the outcome of chemical reactions occurring in confined space but also for the understanding of the effective conversion of energy at the molecular level and the preparation of molecular machines [36,37].

Experimental

Procedure for 2-D EXSY experiments [25]: A solution of basket **1** and guest **2** in CD_2Cl_2 (J. Young NMR tube) was cooled to 250.0 ± 0.1 K inside the NMR probe and allowed to equilibrate for 1.0 h. A series of gradient NOESY experiments was run with a relaxation delay of 5 × T_1 and mixing times (τ_m) of 0 ms and three others ranging from 40 ms to 250 ms, such that the cross-peaks were clearly resolved; the spin–lattice relaxation time (T_1 = 3.30 s) for the free guest was determined by performing a standard inversion-recovery pulse sequence with a relaxation delay (τ_d) of at least 5 × T_1. Each of the 128 F_1 increments represented the accumulation of at least two scans. The corresponding integrals were determined by using MNova software from Mestrelab Research, after phase and baseline corrections in both dimensions. The magnetization exchange rate constants (k^*_{in} and k^*_{out}) were, at each mixing time τ_m, calculated by using the EXSYCalc program (Mestrelab Research). The mean values of k^*_{in} and k^*_{out} are reported with the standard deviation as an experimental error.

Procedure for ^{1}H-selective inversion-transfer experiments [27]: A solution of basket **1** and guest **2** in CD_2Cl_2 (J. Young NMR tube) was cooled to 250.0 ± 0.1 K inside the NMR probe and allowed to equilibrate for 1.0 h. The ^{1}H spin–lattice relaxation time (T_1 = 3.30 s) for the free guest was determined by a standard inversion-recovery pulse sequence with a relaxation delay (τ_d) of at least 5 × T_1. By using a selective 1-D inversion-recovery pulse sequence [180° x (selective) – τ – 90° x (nonselective) – τ_d], 32 transients were obtained for each variable delay time (τ) with a relaxation delay (τ_d) of at least 5 × T_1. The absolute integrals corresponding to encapsulated and free guest molecules were, at each mixing time, determined by using TopSpin software from Bruker, and the resulting data was fitted by using the two-site exchange equations described by Led et al. [27] to obtain magnetization exchange rate constants k^*_{in} and k^*_{out}.

Supporting Information

Supporting Information contains details of the computational studies.

Supporting Information File 1

Details of the computational studies.
[http://www.beilstein-journals.org/bjoc/content/supplementary/1860-5397-8-9-S1.pdf]

Acknowledgements

This work was financially supported with funds obtained from the National Science Foundation under CHE-1012146 (to J.D.B.). We thank the Ohio Supercomputer Center for generous allocations of computational resources.

References

1. Badjić, J. D.; Stojanović, S.; Ruan, Y. *Adv. Phys. Org. Chem.* **2011,** *45,* 1. doi:10.1016/B978-0-12-386047-7.00001-1
2. Hof, F.; Craig, S. L.; Nuckolls, C.; Rebek, J., Jr. *Angew. Chem., Int. Ed.* **2002,** *41,* 1488. doi:10.1002/1521-3773(20020503)41:9<1488::AID-ANIE1488>3.0.CO;2-G
3. Palmer, L. C.; Rebek, J., Jr. *Org. Biomol. Chem.* **2004,** *2,* 3051. doi:10.1039/b412510j
4. Rieth, S.; Hermann, K.; Wang, B.-Y.; Badjić, J. D. *Chem. Soc. Rev.* **2011,** *40,* 1609. doi:10.1039/c005254j
5. Pluth, M. D.; Raymond, K. N. *Chem. Soc. Rev.* **2007,** *36,* 161. doi:10.1039/b603168b
6. Davis, A. V.; Raymond, K. N. *J. Am. Chem. Soc.* **2005,** *127,* 7912. doi:10.1021/ja051037s
7. Raymo, F. M.; Houk, K. N.; Stoddart, J. F. *J. Am. Chem. Soc.* **1998,** *120,* 9318. doi:10.1021/ja9806229
8. Houk, K. N.; Nakamura, K.; Sheu, C.; Keating, A. E. *Science* **1996,** *273,* 627. doi:10.1126/science.273.5275.627
9. Maslak, V.; Yan, Z.; Xia, S.; Gallucci, J.; Hadad, C. M.; Badjić, J. D. *J. Am. Chem. Soc.* **2006,** *128,* 5887. doi:10.1021/ja060534l
10. Wang, B.-Y.; Bao, X.; Stojanovic, S.; Hadad, C. M.; Badjić, J. D. *Org. Lett.* **2008,** *10,* 5361. doi:10.1021/ol802199t
11. Wang, B.-Y.; Bao, X.; Yan, Z.; Maslak, V.; Hadad, C. M.; Badjić, J. D. *J. Am. Chem. Soc.* **2008,** *130,* 15127. doi:10.1021/ja8041977
12. Wang, B.-Y.; Rieth, S.; Badjić, J. D. *J. Am. Chem. Soc.* **2009,** *131,* 7250. doi:10.1021/ja9023868
13. Rieth, S.; Badjić, J. D. *Chem.–Eur. J.* **2011,** *17,* 2562. doi:10.1002/chem.201003138
14. Rieth, S.; Bao, X.; Wang, B.-Y.; Hadad, C. M.; Badjić, J. D. *J. Am. Chem. Soc.* **2010,** *132,* 773. doi:10.1021/ja908436c
15. Helgeson, R. C.; Hayden, A. E.; Houk, K. N. *J. Org. Chem.* **2010,** *75,* 570. doi:10.1021/jo9012496
16. Sheu, C.; Houk, K. N. *J. Am. Chem. Soc.* **1996,** *118,* 8056. doi:10.1021/ja9535423
17. Wang, X.; Houk, K. N. *Org. Lett.* **1999,** *1,* 591. doi:10.1021/ol9900820
18. Hooley, R. J.; Van Anda, H. J.; Rebek, J., Jr. *J. Am. Chem. Soc.* **2006,** *128,* 3894. doi:10.1021/ja058727g
19. Zhou, H.-X.; McCammon, J. A. *Trends Biochem. Sci.* **2010,** *35,* 179. doi:10.1016/j.tibs.2009.10.007
20. Kamieth, M.; Klärner, F.-G.; Diederich, F. *Angew. Chem., Int. Ed.* **1998,** *37,* 3303. doi:10.1002/(SICI)1521-3773(19981217)37:23<3303::AID-ANIE3303>3.0.CO;2-T
21. Dill, K. A. *J. Biol. Chem.* **1997,** *272,* 701. doi:10.1074/jbc.272.2.701
22. Craig, S. L.; Lin, S.; Chen, J.; Rebek, J., Jr. *J. Am. Chem. Soc.* **2002,** *124,* 8780. doi:10.1021/ja025672z
23. Wilcox, C. S. In *Frontiers in supramolecular organic chemistry and photochemistry;* Schneider, H.-J; Dürr, H., Eds.; VCH: Weinheim, Germany, 1991; pp 123 ff.
24. Mecozzi, S.; Rebek, J., Jr. *Chem.–Eur. J.* **1998,** *4,* 1016. doi:10.1002/(SICI)1521-3765(19980615)4:6<1016::AID-CHEM1016>3.0.CO;2-B
25. Perrin, C. L.; Dwyer, T. J. *Chem. Rev.* **1990,** *90,* 935. doi:10.1021/cr00104a002
26. Lian, L. Y. In *NMR of macromolecules : a practical approach;* Roberts, G. C. K., Ed.; IRL Press: Oxford, 1993; pp 153 ff.
27. Led, J. J.; Gesmar, H.; Abildgaard, F. *Methods Enzymol.* **1989,** *176,* 311. doi:10.1016/0076-6879(89)76017-1
28. Hansen, D. F.; Led, J. J. *J. Magn. Reson.* **2003,** *163,* 215. doi:10.1016/S1090-7807(03)00062-4
29. Duan, Y.; Wu, C.; Chowdhury, S.; Lee, M. C.; Xiong, G.; Zhang, W.; Yang, R.; Cieplak, P.; Luo, R.; Lee, T.; Caldwell, J.; Wang, J.; Kollman, P. *J. Comput. Chem.* **2003,** *24,* 1999. doi:10.1002/jcc.10349
30. Wang, J.; Wolf, R. M.; Caldwell, J. W.; Kollman, P. A.; Case, D. A. *J. Comput. Chem.* **2004,** *25,* 1157. doi:10.1002/jcc.20035
31. Isralewitz, B.; Gao, M.; Schulten, K. *Curr. Opin. Struct. Biol.* **2001,** *11,* 224. doi:10.1016/S0959-440X(00)00194-9
32. Sotomayor, M.; Schulten, K. *Science* **2007,** *316,* 1144. doi:10.1126/science.1137591
33. Sandström, J. *Dynamic NMR Spectroscopy;* Academic Press: London, 1982.
34. Bao, X.; Rieth, S.; Stojanović, S.; Hadad, C. M.; Badjić, J. D. *Angew. Chem., Int. Ed.* **2010,** *49,* 4816. doi:10.1002/anie.201000656
35. Christensen, T.; Gooden, D. M.; Kung, J. E.; Toone, E. J. *J. Am. Chem. Soc.* **2003,** *125,* 7357. doi:10.1021/ja021240c
36. Northrop, B. H.; Braunschweig, A. B.; Mendes, P. M.; Dichtel, R. W.; Stoddart, J. F. Molecular Machines. In *Handbook of Nanoscience, Engineering, and Technology,* 2nd ed.; Goddard, W. A.; Brenner, D. W.; Lyshevski, S. E.; Iafrate, G. J., Eds.; CRC Press: Boca Raton, 2007; 11-1–11-50.
37. Saha, S.; Stoddart, J. F. Molecular Motors and Muscles. In *Functional Organic Materials;* Müller, T. J. J.; Bunz, U. H. F., Eds.; Wiley-VCH: Weinheim, Germany, 2007; pp 295 ff.

License and Terms

Beilstein Journal of Organic Chemistry

Fifty years of oxacalix[3]arenes: A review

Kevin Cottet[1,2], Paula M. Marcos[3] and Peter J. Cragg[*1]

Review

Open Access

Address:
[1]School of Pharmacy and Biomolecular Sciences, Huxley Building, University of Brighton, Brighton BN2 4GJ, UK, [2]UFR de Chimie, Université Joseph Fourier Grenoble 1, 301 rue de la Chimie, BP53 - 38041 Grenoble Cedex 9, France and [3]Centro de Ciências Moleculares e Materiais, FCUL, Edifício C8, 1749-016 Lisboa, Portugal and Faculdade de Farmácia da Universidade de Lisboa, Av. Prof. Gama Pinto, 1649-003 Lisboa, Portugal

Email:
Peter J. Cragg[*] - P.J.Cragg@brighton.ac.uk

* Corresponding author

Keywords:
calixarenes; host–guest chemistry; macrocycles; oxacalixarenes

Beilstein J. Org. Chem. **2012,** *8,* 201–226.
doi:10.3762/bjoc.8.22

Received: 15 October 2011
Accepted: 11 January 2012
Published: 07 February 2012

This article is part of the Thematic Series "Supramolecular chemistry II".

Guest Editor: C. A. Schalley

Abstract

Hexahomotrioxacalix[3]arenes, commonly called oxacalix[3]arenes, were first reported in 1962. Since then, their chemistry has been expanded to include numerous derivatives and complexes. This review describes the syntheses of the parent compounds, their derivatives, and their complexation behaviour towards cations. Extraction data are presented, as are crystal structures of the macrocycles and their complexes with guest species. Applications in fields as diverse as ion selective electrode modifiers, fluorescence sensors, fullerene separations and biomimetic chemistry are described.

Introduction

Calixarenes, macrocycles which are widely used in supramolecular chemistry, are 2,6-metacyclophanes with a methylene bridge between their phenolic groups, as shown in Figure 1 [1-3]. In 1994, the term "homocalixarene" was coined by Brodesser and Vögtle to describe analogues of calixarenes with two or more methylene groups between the aromatic moieties [4]. When one or more CH_2 bridges are replaced by CH_2OCH_2 groups the macrocycles are known as homooxacalixarenes, or simply oxacalixarenes. The presence of the heteroatom is reflected in the name of the compound, for example, *p-tert*-butylcalix[4]arene (**1**) with a CH_2OCH_2 group instead of a CH_2 bridge is *p-tert*-butyldihomooxacalix[4]arene (**2**) [5]. "Dihomo" implies two additional atoms in the bridge and "oxa" that one of them is oxygen. The remainder of the calixarene nomenclature denotes any substituents attached to the phenolic oxygens, known as the "lower rim", and substituents found in the *para*-position of the phenols, also known as the "upper rim" (Figure 2). For the purposes of this review the term "oxacalix[*n*]arene" will be used as a generalization for this class of compounds.

Although some aspects of homooxacalixarene chemistry have been reviewed [4,6-8], notably by Shokova and Kovalev in 2004 [9,10], it is timely for the 50th anniversary of Hultzsch's

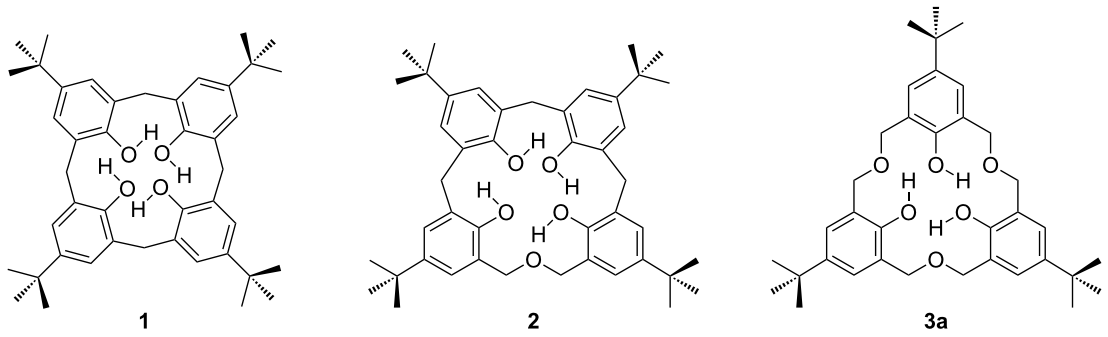

Figure 1: Calixarenes and expanded calixarenes: *p-tert*-Butylcalix[4]arene (**1**), *p-tert*-butyldihomooxacalix[4]arene (**2**), *p-tert*-butylhexahomotrioxacalix[3]arene (**3a**).

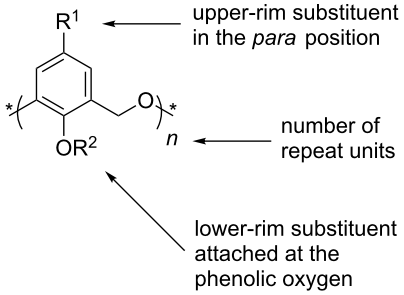

Figure 2: Conventional nomenclature for oxacalix[*n*]arenes.

discovery of *p-tert*-butylhexahomotrioxacalix[3]arene (**3a**) [11] to reflect on the history of these compounds and assess recent advances in the field. Many other expanded calix[*n*]arenes are now known, including the methyl ethers of dihomooxa-, tetrahomodioxa-, hexahomotrioxa- and octahomotetraoxacalix[4]arenes, which have been described in detail by Masci [12]. Despite these advances, the oxacalix[3]arenes have remained the main focus of attention for researchers and are the subject of this review.

Review

1 Synthesis of parent oxacalix[3]arenes

1.1 Thermal dehydration

The first oxacalix[*n*]arenes to be reported were the hexahomotrioxacalix[3]arenes, and these remain the most-studied members of the class. *p-tert*-Butylhexahomotrioxacalix[3]arene (**3a**), initially reported by Hultzsch in 1962, was isolated in less than 1% yield by heating 2,6-bis(hydroxymethyl)-4-*tert*-butylphenol [11]. Elemental analysis gave an empirical formula of $C_{12}H_{16}O_2$ and molecular weight determinations gave values corresponding to a trimer. Despite interest in novel phenol–formaldehyde polymers and macrocycles and characterization of **3a** in 1979 [13], it took a further 20 years for a reproducible synthesis to be published. In 1983, Gutsche reported that the thermally induced dehydration of 2,6-bis(hydroxymethyl)phenols in xylene under reflux gave rise to the formation of homooxacalixarenes, some of them in reasonable yields, as shown in Scheme 1 [14].

Although not discussed by Gutsche, both cyclotrimers and tetramers are usually formed by this method and, in 1991, Vicens and Zerr performed a thermal dehydration of 2,6-bis(hydroxy-

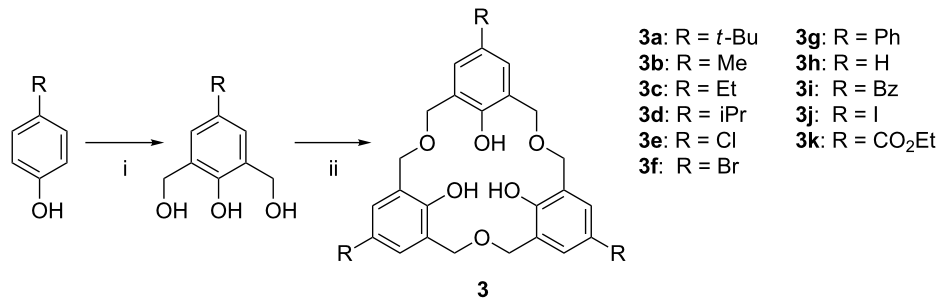

Scheme 1: Synthesis of oxacalix[3]arenes: (i) Formaldehyde (37% aq), NaOH (aq), 1,4-dioxane; glacial acetic acid, acetone; (ii) refluxing *o*-xylene [14] or Na_2SO_4, MsOH, in refluxing DME [15].

methyl)-4-*tert*-butylphenol in xylene under reflux allowing them to isolate *p*-*tert*-butyloctahomotetraoxacalix[4]-arene (**4a**), illustrated in Figure 3, along with **3a** [16].

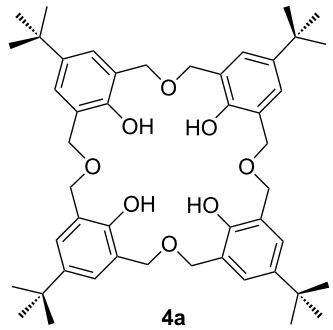

Figure 3: *p*-*tert*-Butyloctahomotetraoxacalix[4]arene (**4a**) [16].

To finally prove that the main product from thermal dehydration was indeed a trimer, Vicens reported the X-ray crystal structure of **3a** in 1992 (Figure 4) demonstrating it to be exclusively in the bowl-shaped *cone* conformation [17].

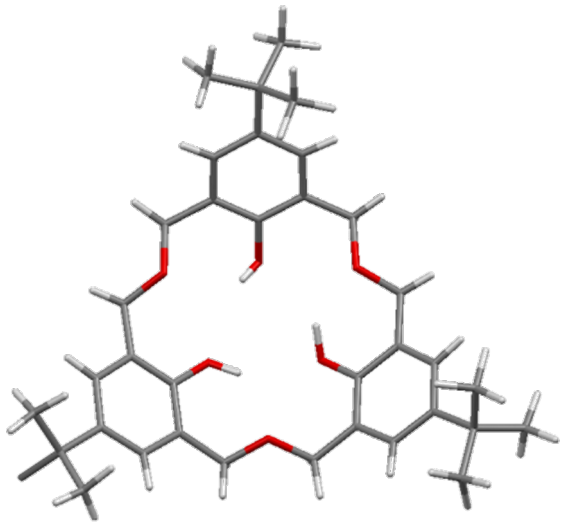

Figure 4: X-ray crystal structure of **3a** showing phenolic hydrogen bonding (IUCr ID AS0508) [17].

In 1994, Hampton et al. used an alternative acid-catalyzed procedure to prepare **3a** and developed a method that improved its purity through the formation of the Na^+ salt and its subsequent neutralization with acid [15]. The process separated **3a** from the cyclic tetramer; the former precipitates as the sodium salt in dry methanol due to complementarity between the arrangement of phenolic groups and the preferred coordination environment of Na^+. Removal of the *tert*-butyl groups through a conventional $AlCl_3$ driven retro-Friedel–Crafts de-*tert*-butylation reaction, as seen in other calixarenes, is unsuccessful in the case of oxacalixarenes, therefore different *para*-substituents must be introduced through the starting phenol in order to obtain derivatives with different groups at the upper rim. A number of other *para*-substituted bis(hydroxymethyl)phenols were therefore also cyclized in the presence of methanesulfonic acid (MsOH) or *para*-toluenesulfonic acid (TsOH) and Na_2SO_4. The corresponding oxacalixarenes were isolated in varying yields: *t*-Bu (**3a**) 32%; Me (**3b**) 21%; Et (**3c**) 21%; iPr (**3d**) 30%; Cl (**3e**)12% [15].

Although conditions were not necessarily optimal, the principles of oxacalix[3]arene syntheses had been established. Monomers react to give the cyclic trimer, predominantly, when heated under reflux in high-boiling-point organic solvents along with an organic acid. Water formed in the dehydration process must be removed through reaction with anhydrous drying agents or be collected in a Dean–Stark trap. In Gutsche's report, and presumably in the work of Hultzsch too, the bis(hydroxymethyl)phenol monomer was isolated as the sodium salt and neutralized with acetic acid. Upon removal of solvent, traces of the acid presumably remained and were taken through to the cyclization step. Cragg noted that acid had to be present for the cyclization to occur, as carefully purified monomers formed calix[4]arenes or dihomooxacalix[4]arenes rather than oxacalix[3]arenes when subjected to standard synthetic methods [18]. To test this theory, the synthesis of **3a** was attempted in *o*-xylene under reflux by using either the freshly prepared crude monomer or the recrystallized monomer. The formation of **3a** was observed in the reaction of the unpurified monomer, but not under acid-free conditions. Moreover, in separate experiments MsOH, TsOH or glacial acetic acid (AcOH) were added to reactions involving the recrystallized monomer. MsOH or TsOH, having complementary threefold symmetry with the lower rim of oxacalix[3]arenes, were expected to increase the yields, but AcOH appeared to be just as effective. Notably, the addition of TsOH gave the oxacalix[3]arene as the sole product.

1.2 Other synthetic methods

Since the initial reports of oxacalix[3]arene syntheses, several procedures have been developed to improve both the reaction conditions and the range of derivatives that can be prepared. The initial strategy to make oxacalix[3]arenes was a single step condensation, which can only lead to C_3-symmetric compounds bearing the same *para*-substituted phenol; however, in host–guest chemistry an asymmetric macrocycle can provide a site for enantioselective molecular recognition. In the case of *p*-*tert*-butylcalix[*n*]arenes the *tert*-butyl substituent can be removed, as mentioned previously, through a retro-Friedel–Crafts acylation, and replaced by other groups, but the dibenzyl ether bridge in the oxacalixarenes is too fragile for this

to be successful. In 1998, Fuji proposed a stepwise synthesis of asymmetric oxacalix[3]arenes based on linear precursors protected with a combination of isopropylidene and methoxymethyl groups [19]. As shown in Scheme 2, the phenolic position of a monomeric precursor is protected with methyl chloromethyl ether (MOMCl). A different monomer is then protected with 2,2-dimethoxypropane, in the presence of TsOH. This links one methylol group to the phenol, leaving the second open to bromination with CBr_4 and PPh_3. The linear trimer is formed between one methoxymethyl protected monomer and two benzyl bromide derivatives in DMF with NaH as the base. Intramolecular cyclization was achieved in 4 h at room temperature with 60% $HClO_4$ in $CHCl_3$ under high-dilution conditions. Pretreatment of the solvent with water was found to be necessary to remove the ethanol stabilizer and to aid deprotection. Yields were up to 50%, and, interestingly, there was no template effect from any alkali metals. An analogous strategy was developed by Georghiou in 2001 to prepare asymmetric oxacalix[3]naphthalene derivatives [20], and this is discussed in greater detail below.

In a later communication, Fuji reported the crystal structure of an unusual byproduct of the reaction, a heptahomotetraoxacalix[3]arene **5** with *t*-Bu, Et and H upper-rim substituents (Figure 5) [21].

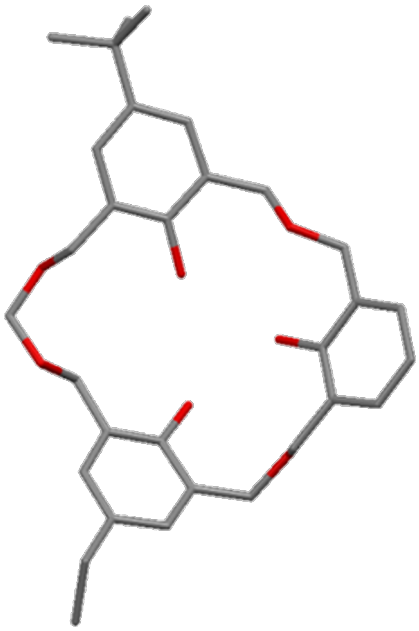

Figure 5: X-ray crystal structure of heptahomotetraoxacalix[3]arene **5** (CCDC ID 166088) [21].

In 2001, Komatsu proposed a different way to access compounds in which two, or all three, units are identical [22]. The method was based on the reductive coupling of silylated derivatives of 2,6-hydroxymethylphenols, in which R is *t*-Bu, Me, benzyl (Bz), phenyl (Ph), or a halide, as shown in Scheme 3. The reaction takes place under conditions of high dilution at −78 °C to favour intramolecular cyclization over polymerization. Coupling reactions are successful, whether the groups in the *para*-position are the same or different, and this method also gives access to oxacalix[4]arenes in modest yields up to 42% for the *p-tert*-butyl derivative.

1.3 Oxacalix[3]naphthalenes

The oxacalix[3]naphthalenes, e.g., **6a** and **6b** reported by Georghiou, have extended aromatic groups with H or *t*-Bu groups in the 6-position and can be considered as close relatives of the oxacalix[3]arenes [20]. The synthesis, shown in

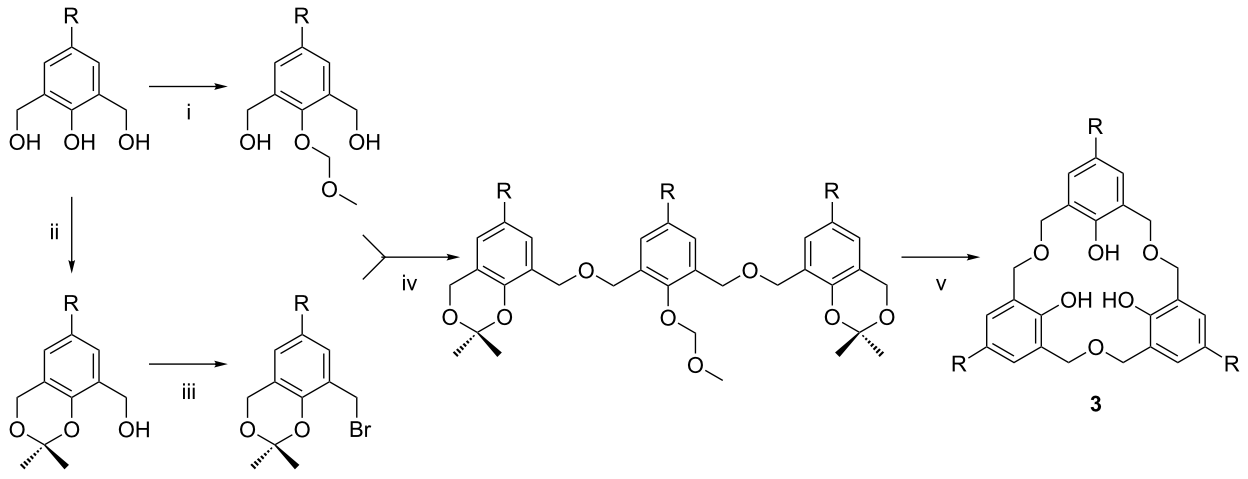

Scheme 2: Stepwise synthesis of asymmetric oxacalix[3]arenes: (i) MOMCl, Adogen®464; (ii) 2,2-dimethoxypropane, *p*-TsOH; (iii) CBr_4, PPh_3, CH_2Cl_2; (iv) NaH, DMF; (v) $HClO_4$ (aq), wet $CHCl_3$ [19].

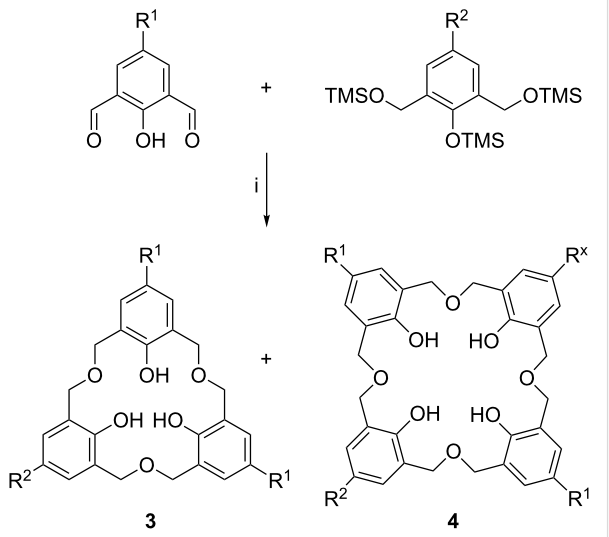

Scheme 3: Oxacalix[3]arene synthesis by reductive coupling: (i) Me_3SiOTf, Et_3SiH, CH_2Cl_2; R^1, R^2 = I, Br, benzyl, *n*-octyl (x = 1 or 2) [22].

Scheme 4, is analogous to Fuji's method for oxacalix[3]arenes [19]. As noted below, this extended aromatic surface is oriented perfectly for C_{60} inclusion [23].

2 Conformational properties

Oxacalix[3]arenes have received significant attention as receptors, mainly due to their structural features: A cavity formed by a 18-membered ring, only two basic conformations (*cone* and *partial-cone*), and a C_3-symmetry [24]. This last feature can provide a suitable binding site for species that require trigonal-planar, tetrahedral or octahedral coordination environments. The flexibility of the macrocycles can allow them to establish ideal bond distances and angles to bind such species. In common with other calix[*n*]arenes, oxacalix[3]arenes containing free OH groups are conformationally mobile, leading to *cone* and *partial-cone* conformers (Figure 6). Without lower-rim substituents there is free rotation of each phenolic unit through the macrocyclic annulus; however, the presence of a hydrogen-bond motif in the *cone* conformer makes it the more stable form.

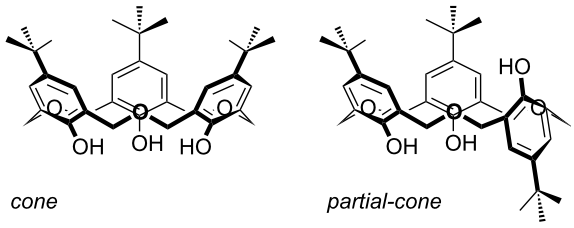

Figure 6: Conformers of **3a**.

In 1985, Gutsche investigated the conformational flexibility of parent calix[*n*]arenes (*n* = 4–8) and oxacalixarenes by temperature-dependent ^{1}H NMR [5]. The *through-the-annulus* rotation barrier for oxacalix[3]arenes was calculated to be much lower than that for other calixarenes, either in non-coordinating or in polar solvents, such as $CDCl_3$ or pyridine, respectively. The ^{1}H NMR spectrum of **3a** in $CDCl_3/CS_2$ only showed a singlet for the CH_2 resonance, even at −90 °C, and the $\Delta G^{\neq}$ barrier for conformational inversion in $CDCl_3$ was <38 kJ mol^{-1}, in contrast with 66 kJ mol^{-1} for the calix[4]arene analogue. To freeze the oxacalix[3]arene conformer, *through-the-annulus* rotation must be prevented. This can be achieved by the introduction of sufficiently large groups on the lower rim of the macrocycle. Upper-rim inversion is less likely to occur when, as in the case of **3a**, it is hindered by the *tert*-butyl group.

3 Oxacalix[3]arene derivatives

3.1 Lower-rim derivatives

Oxacalix[3]arene derivatization at the lower rim has been achieved through alkylation reactions with simple alkyl halides or with functionalized alkylating agents. Lower-rim derivatiza-

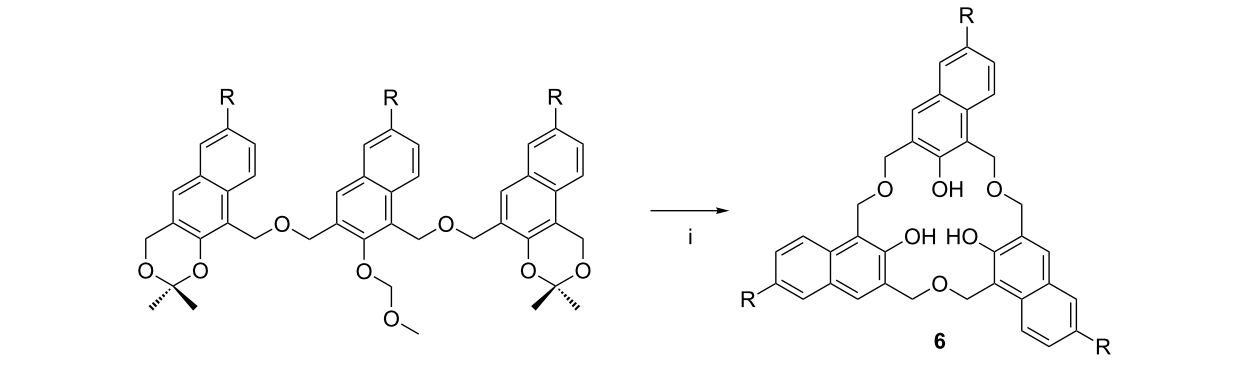

Scheme 4: Oxacalix[3]naphthalene: (i) $HClO_4$ (aq), wet $CHCl_3$ (R = *tert*-butyl, **6a**, H, **6b**) [20].

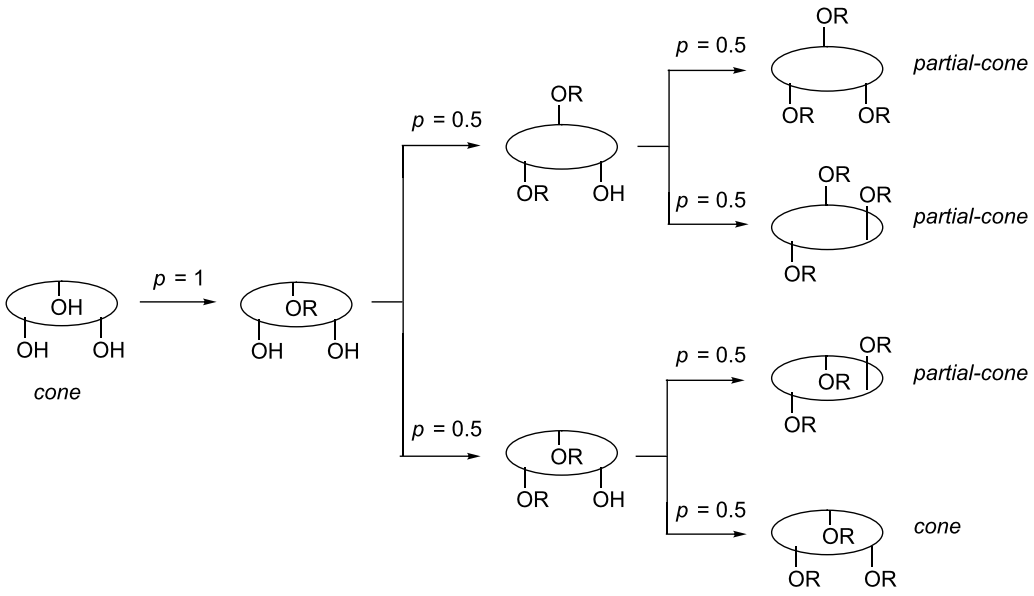

Scheme 5: Origin of the 25:75 *cone*:*partial-cone* statistical distribution of *O*-substituted oxacalix[3]arenes (*p* = probability) [25,26].

tion is relatively straightforward, but conformational control is harder to achieve. The main drawback of lower-rim substitution is that statistically only 25% of the product is formed in the *cone* conformation, as shown in Scheme 5 [25,26].

3.1.1 Alkyl ethers: Classical *O*-alkylation of oxacalix[3]arenes was first achieved by Shinkai et al. in 1993 [24]. Treatment of **3a** with the corresponding alkyl halides in DMF in the presence of NaH afforded Me (**7**), Et (**8**), *n*-Pr (**9**) and *n*-Bu (**10**) derivatives (Scheme 6). Under these conditions, **8** was obtained in the *partial-cone* conformation only. When the reaction was performed in the presence of *t*-BuOK a 1:4 mixture of *cone* and *partial-cone* was obtained and even with Cs_2CO_3 the *cone* conformer could be detected. It seems that K^+ and Cs^+ favourably interact with the three phenolic oxygen atoms placed on the same side, whereas Na^+ preferentially interacts with them across the ring.

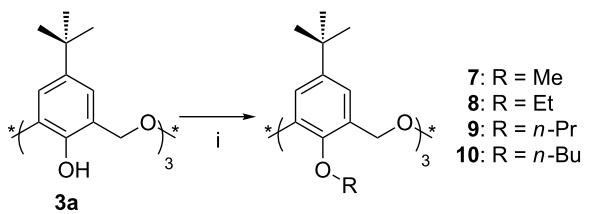

Scheme 6: Synthesis of alkyl ethers **7**–**10**: (i) Alkyl halide, NaH, DMF [24].

Introduction of heteroatoms, such as nitrogen, into the oxacalix[3]arene lower rims can also be achieved by *O*-alkylation. Pyridine is known to be a good ligand towards metals and is widely employed in transition-metal coordination chemistry; therefore, in an attempt to incorporate these binding sites into oxacalix[3]arenes, Yamato [27] and Cragg [26] independently reacted **3a** with 2-(chloromethyl)pyridine, as shown in Scheme 7. The presence of Cs_2CO_3 leads to the formation of the *partial-cone* conformer, whereas K_2CO_3 and NaH increase the yield of the *cone* conformer of **11a** to about 25%. ^{1}H NMR analysis of the *cone* conformer indicates that the nitrogen atoms point away from the macrocyclic cavity [27].

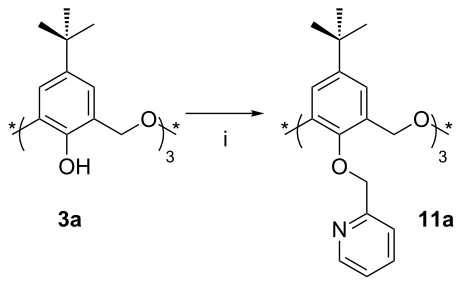

Scheme 7: Synthesis of a pyridyl derivative **11a**: (i) Picolyl chloride hydrochloride, NaH, DMF [26,27].

When 4-(chloromethyl)pyridine was used instead, NaH was ineffectual as a deprotonating agent. Na_2CO_3 yielded the disubstituted product only, K_2CO_3 gave both *cone* (8%) and *partial-*

cone (68%) conformers, and the only isolated product with Cs_2CO_3 was the *partial-cone* conformer (75%) [28].

The X-ray structure of the *partial-cone* conformer (Figure 7), reported by Cragg, shows one pyridyl group to be included within the macrocyclic cavity and the remaining two with their nitrogen atoms pointing away from it [26].

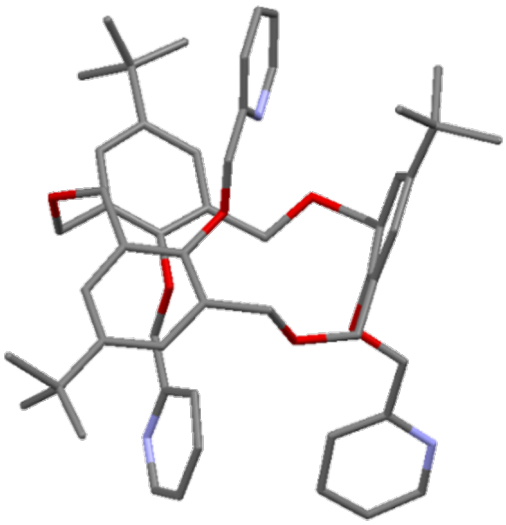

Figure 7: X-ray crystal structure of *partial-cone* **11a** (CCDC ID 150580) [26].

3.1.2 Functionalized alkyl ethers: Functionalized alkyl halides of the type XCH_2Y, where X is a leaving group and Y is a functional group, have also been used to introduce a variety of groups into the lower rim of oxacalix[3]arenes. Thus, derivatives containing carbonyl groups (ester, acid, amide and ketone) and heteroatoms, such as nitrogen and phosphorous, have been obtained.

In 1993, Shinkai et al. [29] reported the synthesis of the first ethyl ester derivative **12a**. In the belief that the alkali-metal template effect would lead preferentially to the *cone* conformer with NaH, the reaction of excess ethyl bromoacetate with **3a** was carried out in acetone under reflux (Scheme 8). The *partial-cone* conformer of **12a** was formed exclusively when weaker bases, K_2CO_3 or Cs_2CO_3, were used. NaH or *t*-BuOK in THF gave a mixture of products, but the yield of the *cone* conformer never exceeded 22%. An experiment with the oxacalix[3]naphthalene analogue was performed in 2003 by Georghiou [30], which also gave the *cone* conformer in 25% yield.

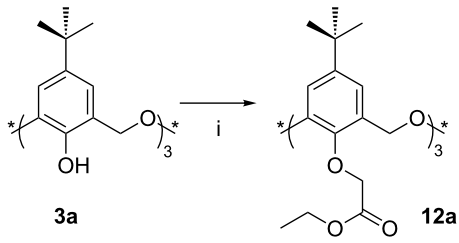

Scheme 8: Lower-rim ethyl ester synthesis: (i) Ethyl bromoacetate, NaH, *t*-BuOK or alkali metal carbonate, THF or acetone [29].

Cone-**12a** was used by Shinkai as the starting point from which to construct the chiral capped oxacalix[3]arene **13** as shown in Scheme 9 [31]. The parent compound was cleaved to form the tris(acid) **14a**, which then reacted with *S*-phenylalanine methyl ester. Deprotection of the methyl ester followed by reduction with $LiBH_4$ gave the chiral amide **15**, which reacted with 1,3,5-benzenetricarbonyl chloride to form the capped species **13**. Compound **13** was shown to bind primary ammonium cations better than an uncapped ester analogue.

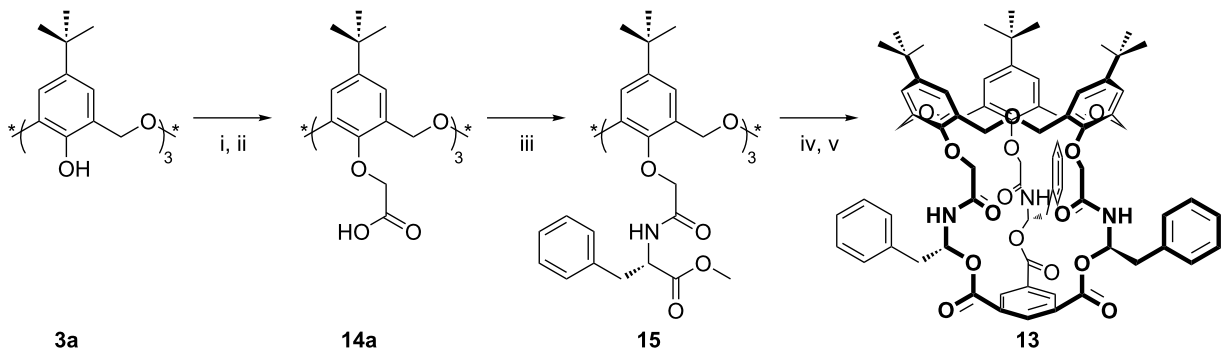

Scheme 9: Forming chiral receptor **13**: (i) Ethyl bromoacetate, NaH, THF; (ii) NaOH, H_2O/1,4-dioxane; (iii) *S*-PheOMe·HCl, DCC, HOBt, NEt_3, CH_2Cl_2; (iv) $LiBH_4$, THF; (v) 1,3,5-benzenetricarbonyl chloride, pyridine, THF [31].

In 1995, Vicens reported the crystal structure of a *partial-cone* triethyl ester derivative of 4-phenyloxacalix[3]arene illustrated as **16** in Figure 8 [32]. Few synthetic details were given; however, it was reported that cyclization of bis(2,5-methylol)-4-phenylphenol to give **3g** was followed by reaction with ethyl-bromoacetate, but no mention of the yield or isolation of a *cone* conformer was made.

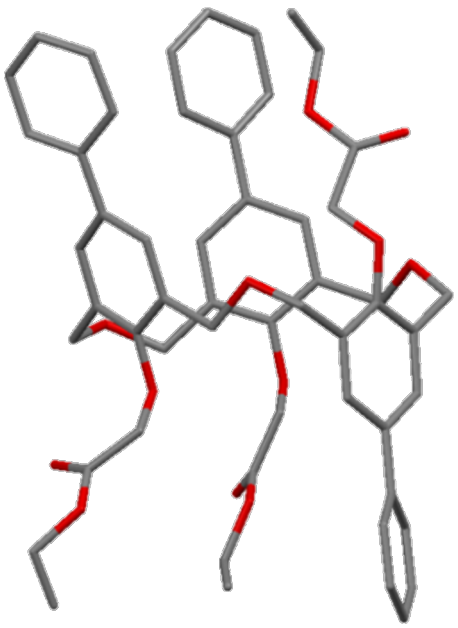

Figure 8: X-ray crystal structure of **16** (IUCr ID PA1110) [32].

The first amide derivative was reported by Shinkai in 1995 [25] through the reaction of **3a** with *N*,*N*-diethylchloroacetamide (Scheme 10). Heating under reflux in THF, with NaH as base, gave *cone* amide **17a** as the only isolated product in 23% yield. Using the same conditions, Cragg reported an improved yield of 44% through a slight modification of the previous procedure (recrystallization from MeCN instead of MeOH) [26], and Yamato later reported a 90% yield [33]. This is in stark contrast to the maximum yield of 25% for the esterification reaction discussed above and points to a subtle, yet essential, difference between the interaction modes of the oxacalixarene, cation and alkylating agent. Despite much speculation, the reason for this is not yet understood. As with the esterification reaction, use of K_2CO_3 or Cs_2CO_3 in place of NaH, and with acetone as the solvent, reverses the conformer preference with *partial-cone*-**17a** isolated in 45% yield with only a trace of the *cone* conformer. This suggests a template effect for both K^+ and Cs^+ that occurs whether an amide or ester is formed, and a function for Na^+ beyond that of a mere template.

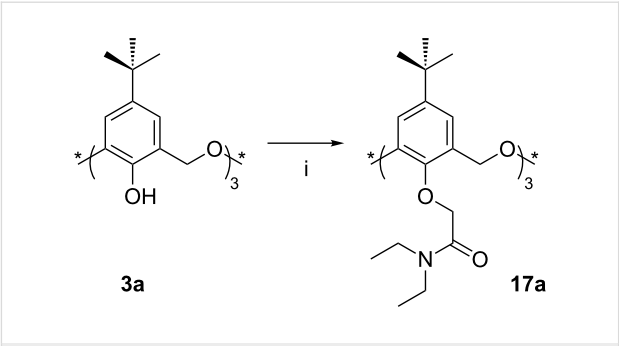

Scheme 10: Lower rim *N*,*N*-diethylamide **17a**: (i) *N*,*N*-Diethylchloroacetamide, NaH, *t*-BuOK or alkali metal carbonate, THF or DMF or acetone [25,26,33].

One consequence of this work is that the preferred route to C_3 symmetric *cone* derivatives is through tris(amide) derivative **17a**, which can readily be cleaved by hydrolysis employing sodium hydroxide in 1,4-dioxane/water to give *cone*-**14a**. In 2001 Yamato used *cone*-**14a** to form a C_3 symmetric hydrophobic receptor **18** in 13% yield through reaction with 1,3,5-tris(bromomethyl)benzene in the presence of Na_2CO_3 (Scheme 11) [33]. As the reaction failed to work when K_2CO_3 was used, the authors suggested that Na^+ may play a templating role in addition to that of a deprotonating agent.

The X-ray crystal structure of the product (Figure 9) shows that the carbonyl oxygen atoms point away from the cavity to create a large hydrophobic cavity. Extraction studies indicated a slight, and statistically insignificant, preference for K^+ over Cs^+ and Ag^+, with a much lower affinity for Na^+. The highest affinity was reserved for *n*-$BuNH_3^+$.

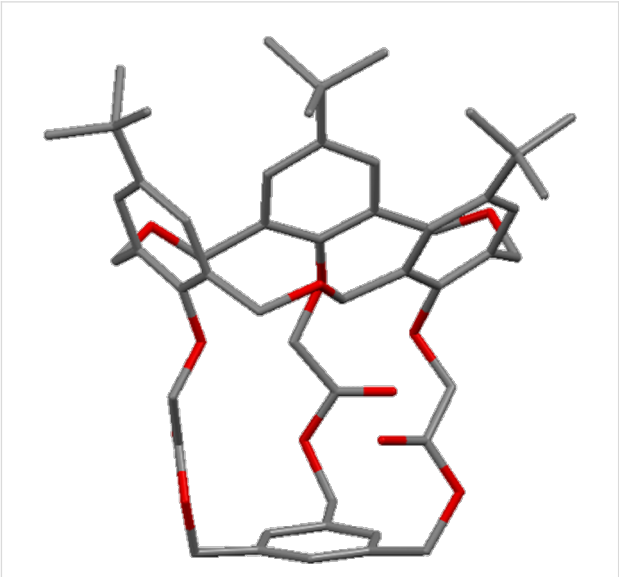

Figure 9: X-ray crystal structure of **18** (CCDC ID 142599) [33].

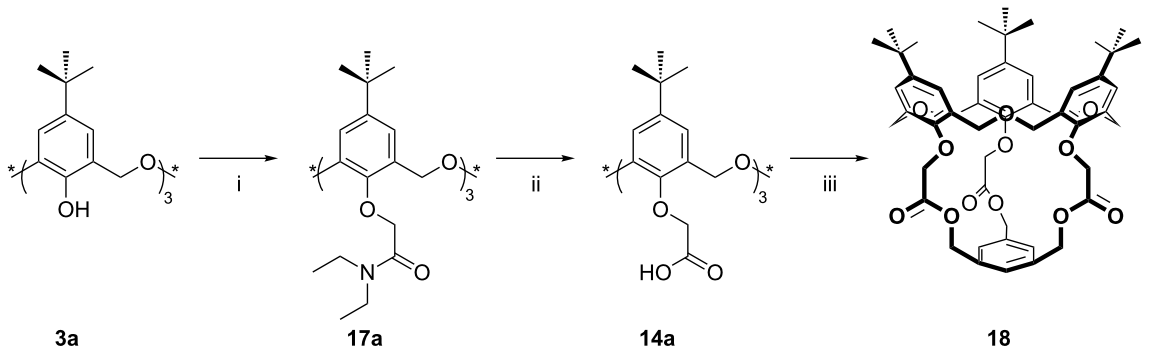

Scheme 11: Capping the lower rim: (i) *N*,*N*-Diethylchloroacetamide, NaH, THF; (ii) NaOH, H_2O/1,4-dioxane; (iii) 1,3,5-tris(bromomethyl)benzene, Na_2CO_3, DMF [33].

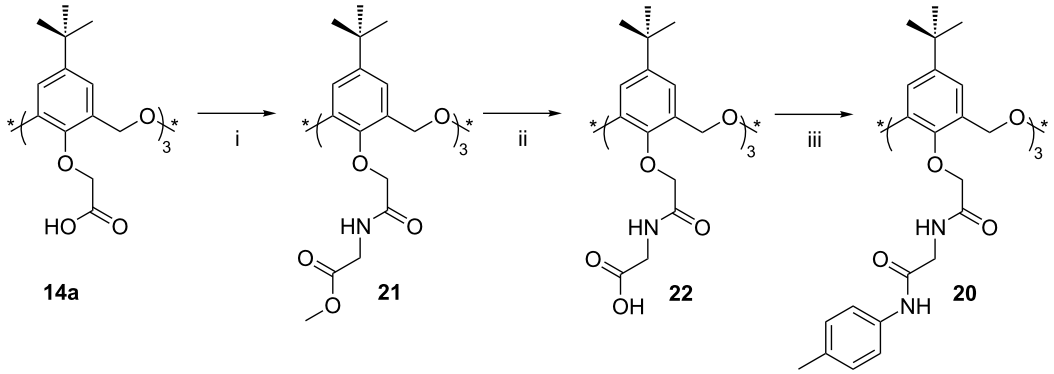

Scheme 12: Extending the lower rim: (i) Glycine methyl ester, HOBt, dicyclohexycarbodiimide (DCC), CH_2Cl_2; (ii) NaOH, H_2O/1,4-dioxane; (iii) *p*-toluidine, HOBt, DCC, CH_2Cl_2 [37].

An analogue of **18**, which showed little affinity for metal cations, was prepared with three 4-methylbenzyl substituents on the lower rim (**19**).

In 2001, Yamato reported an oxacalix[3]arene with pendant pyridines linked by amide bonds [34]. The intramolecular hydrogen bonds between neighbouring amide groups enforced a *flattened-cone* conformer for the macrocycle, which prevented binding to both metal cations and, to a large extent, alkyl ammonium cations. Extending the link between the macrocycle and aromatic termini did not disrupt the strong amide interactions, although binding was detected for Ag^+, as the triflate, and for *n*-$BuNH_3^+$, as the chloride salt [35]. Further work on this class of derivatives showed some anion selectivity in the presence of *n*-$BuNH_3^+$ through intermolecular hydrogen bonding with amide hydrogens [36].

In 2006, the same group used a similar route in order to synthesize the extended, uncapped derivative **20** incorporating three (phenylcarbamoyl)methylcarbamate substituents (Scheme 12), to mimic the binding sites in a protein, complete with hydrophobic region [37]. These amides were designed to act as heteroditopic receptors, capable of binding anions and cations separately and simultaneously in a cooperative way, and were shown to bind *n*-$BuNH_3^+$ halide salts in this manner.

N-Hydroxypyrazinones are known to function as bidentate ligands for metals such as iron or gallium that require an octahedral geometry. Katoh coupled *N*-hydroxypyrazinone substituents to *cone*-**14a** in order to prepare **23** (Scheme 13). Binding Ga^{3+} with remote lower-rim groups induced the cooperative binding of alkyl ammonium cations by the macrocycle [38].

Recently, Marcos reported the synthesis of an oxacalix[3]arene ketone derivative (Scheme 14) [39]. Treatment of **3a** with 1-adamantyl bromomethyl ketone and NaH in THF under reflux afforded adamantyl ketone **24** in the *cone* conformation only.

3.1.3 Phosphorus derivatives: Complete phosphorylation of **3a** was reported by Matt in 1999 and was achieved through reaction with NaH and $Ph_2P(O)CH_2OTs$ in toluene at 90 °C for three days (Scheme 15) [40]. The reaction resulted in the forma-

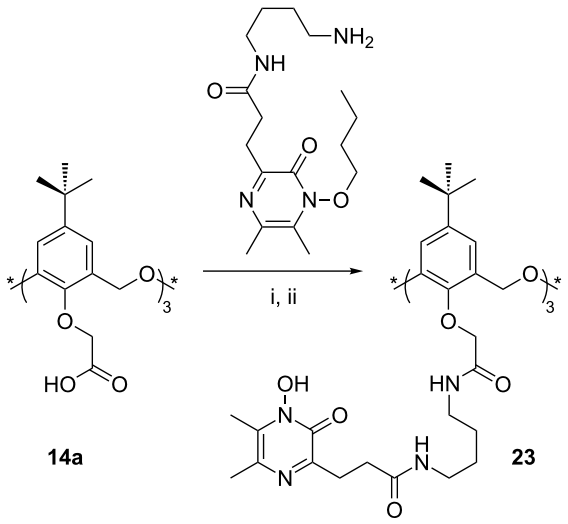

Scheme 13: Synthesis of *N*-hydroxypyrazinone derivative **23**: (i) 1-[3-(Dimethylamino)propyl]-3-ethylcarbodiimide hydrochloride, HOBt, Et_3N; (ii) H_2, 10% Pd-C, MeOH [38].

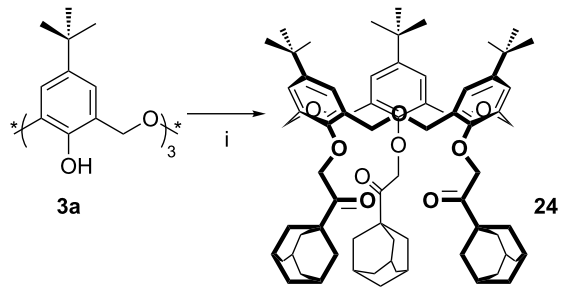

Scheme 14: Synthesis of **24**: (i) 1-Adamantyl bromomethyl ketone, NaH, THF [39].

tion of a 4:1 mixture of the *cone* and *partial-cone* diphenylphosphine oxide derivatives **25**: The preference for the *cone* formation is highly atypical but may be due to the templating effect of Na^+. Separation by column chromatography afforded the *cone* conformer in 72% yield although the *partial-cone* was never obtained in a pure form. Reduction by phenylsilane ($PhSiH_3$) gave the corresponding *cone* and *partial-cone* phosphines **26** quantitatively.

3.1.4 Silyl derivatives: In 1996, Hampton investigated the selectivity of silylation on oxacalix[3]arenes to determine the influence of the group in the *para*-position, the nature of the silylating agent and the reaction conditions [41]. Unsurprisingly, the formation of the *partial-cone* was favoured for all oxacalix[3]arenes, with small upper-rim substituents having the highest *partial-cone*:*cone* ratio (e.g., 100:1 for the Cl derivative) when bis(trimethylsilyl)trifluoroacetamide was used as the silylating reagent. When 1-(trimethylsilyl)imidazole was used, the ratios were 30 to 45:1 and were independent of the group in the *para*-position. A silylated *p*-*tert*-butyloxacalix[3]arene **27** was characterized by X-ray crystallography to confirm that it was in the *partial-cone* conformation as shown in Figure 10. These derivatives could serve as reaction intermediates, due to the ease with which the silicon–oxygen bond can be cleaved in the presence of fluoride, although this chemistry has yet to be explored.

3.1.5 Intramolecularly bridged derivatives: Linking two or more phenolic calixarene oxygen atoms together is a common method to improve selectivity and complex stability, and derivatives such as calixcrowns have been known for a considerable time [42]. Amido-di-*O*-bridged oxacalix[3]arenes were reported by Chen in 2005 through reaction of **3a** with *N*,*N'*-bis(chloroacetyl)-α,ω-alkylenediamines in refluxing acetone with K_2CO_3 as the base (Scheme 16) [43,44]. Those compounds linked by two (**28**) or three (**29**) methylene groups had a binding affinity for linear primary alkyl ammonium ions from *n*-$BuNH_3^+$ to *n*-$HexNH_3^+$.

3.2 Upper-rim derivatives

Although the lower rim has many advantages as a binding site for guests, not least in the relative ease with which substituents

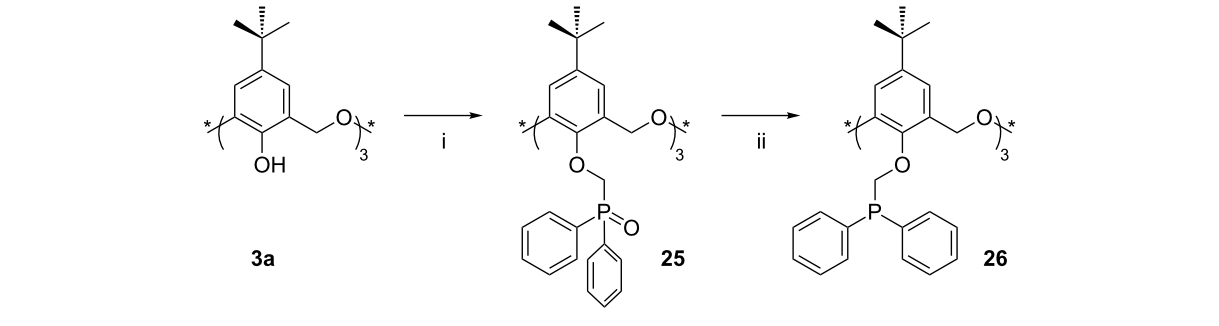

Scheme 15: Synthesis of **25** and **26**: (i) (Diphenylphosphino)methyl tosylate, NaH, toluene; (ii) phenylsilane, toluene [40].

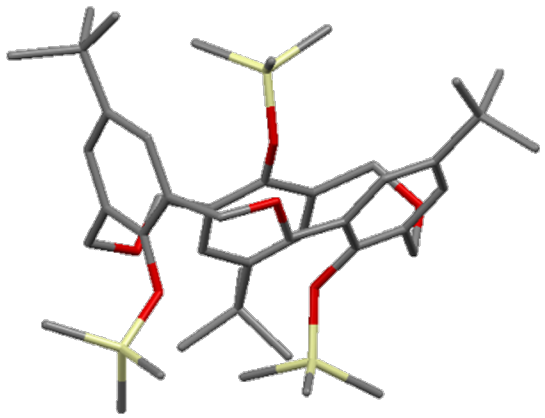

Figure 10: X-ray crystal structure of **27** in the *partial-cone* conformer (CCDC ID SUP 90399) [41].

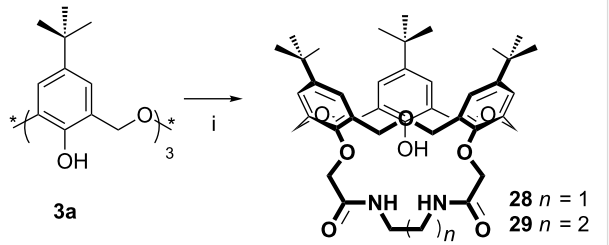

Scheme 16: Synthesis of strapped oxacalix[3]arene derivatives **28** and **29**: (i) *N*,*N*′-Bis(chloroacetyl)-1,2-ethylenediamine or *N*,*N*′-bis(chloroacetyl)-1,3-propylenediamine, K_2CO_3, acetone [43].

can be attached, the upper rim can also function as a molecular recognition centre. The cavity created by the lipophilic phenolic units, particularly when held in place through allosteric effects of lower-rim substituents bound to metals, can accommodate a number of quaternary ammonium ions or buckminsterfullerene, C_{60}. Consequently, the ability to vary the upper rim functional groups after cyclization is of some interest.

3.2.1 Asymmetric oxacalix[3]arenes: Using the synthetic routes described by Gutsche or Hampton it is possible to create oxacalixarenes with a range of upper-rim groups [14,15]; however, these methods can only yield threefold symmetric oxacalix[3]arenes. In order to introduce other groups and create asymmetric derivatives it is necessary to go through a stepwise synthetic route. Fortunately the strategy described by Fuji in 1998 [19] can be used to prepare linear trimers in which two or three different substituents are present. Using this method it was possible to prepare chiral oxacalix[3]arenes incorporating *t*-Bu, iPr, Et or H in the *para*-position of the phenolic moieties, as seen in example **30** in Figure 11 [45].

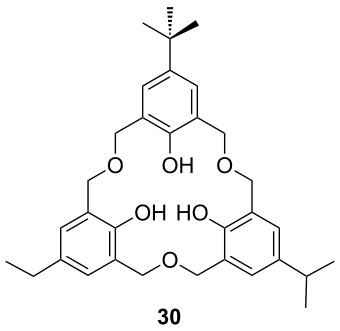

Figure 11: A chiral oxacalix[3]arene [45].

The enantiomers can be separated by a chiral HPLC column and give opposite circular dichroic spectra, and can be crystallized out for structural characterization. X-ray crystallography was again able to determine the structure of compound **30** (Figure 12).

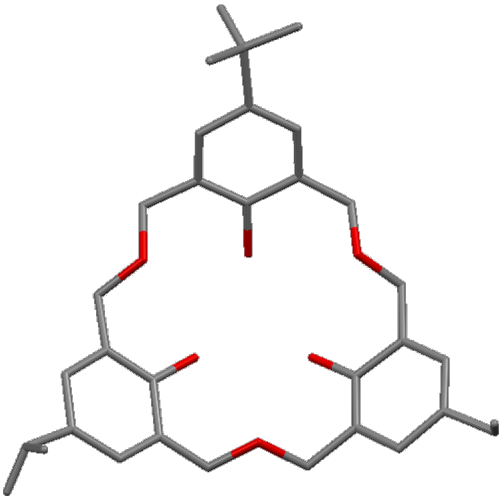

Figure 12: X-ray crystal structure of asymmetric oxacalix[3]arene **30** incorporating *t*-Bu, iPr and Et groups (CCDC ID 108839) [19].

The work was extended in 2001 [21], and expanded in 2002 [46] to include a single Br substituent (**31**), which led to an important advance in oxacalix[3]arene chemistry as debromination of **31** allowed the introduction of new groups in the vacant *para*-position via the mono-unsubstituted derivative **32** as shown in Scheme 17. The route introduced nitro (**33**), azide (**34**), imidazole (**35**), phthalimide (**36**), cyano (**37**) and methoxyether (**38**) groups, linked to one of the oxacalix[3]arene rings by a methylene spacer.

As noted earlier, in Scheme 3, Komatsu's diformylphenol approach also generates symmetric and asymmetric oxacalix[n]arenes, where n = 3 or 4 [22].

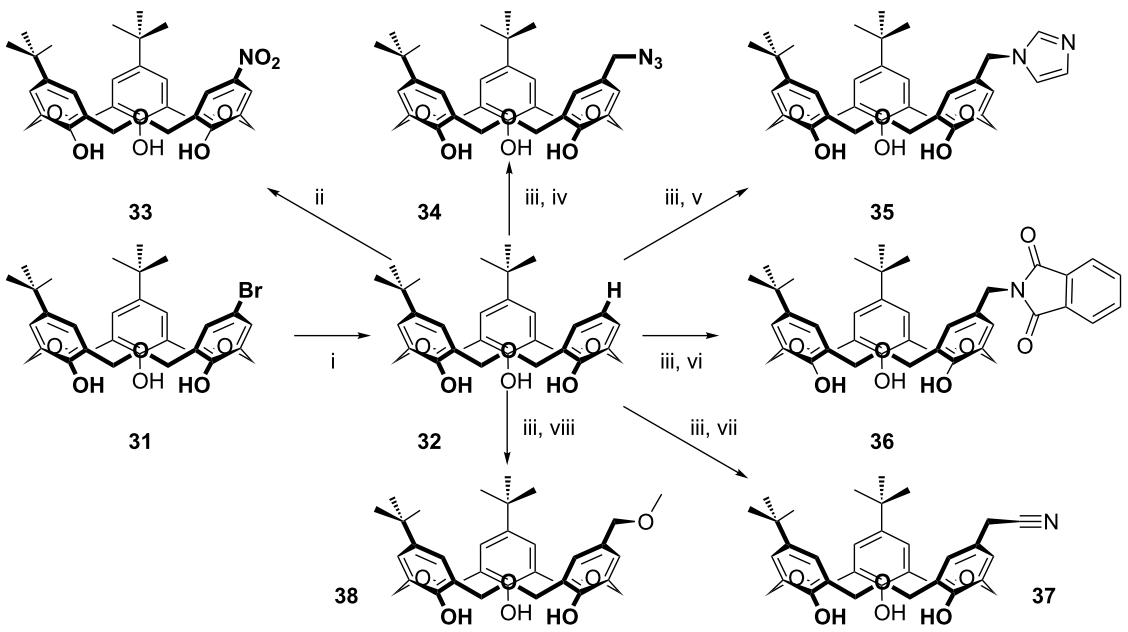

Scheme 17: Reactions of an oxacalix[3]arene incorporating an upper-rim Br atom with (i) $Pd(OAc)_2$, PPh_3, HCO_2H, Et_3N; (ii) NH_4NO_3, acetic anhydride; (iii) Et_2NH, H_2CO (aq), AcOH, MeI; (iv) NaN_3; (v) imidazole; (vi) potassium phthalimide; (vii) NaCN; (viii) NaOMe [46].

3.2.2 Upper-rim esters and their reactions: Formation of the oxacalix[3]arene **3k** with an upper-rim ester [47-49] makes further derivatives accessible by cleavage of the ester to leave the carboxylic acid **39** as shown in Scheme 18.

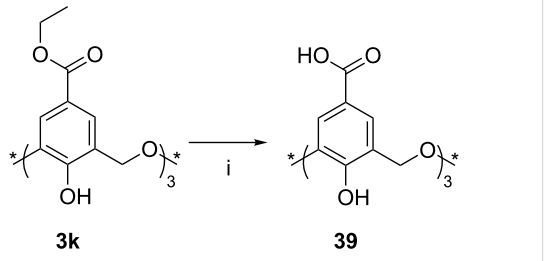

Scheme 18: Synthesis of acid **39**: (i) NaOH, EtOH/H_2O, HCl (aq) [47].

Shinkai used this methodology to prepare dimeric oxacalix[3]arene capsules linked by 1,4-xylylenediamine spacers. Derivatives of **39**, protected at the lower rim by methyl or *N*,*N*-diethylamide groups, were coupled to mono-*t*-Boc-protected 1,4-xylylenediamine. Subsequent deprotection and reaction with a second equivalent of the oxacalixarene acid gave the dimeric compound (capsule-**40**) shown in Figure 13. A nonencapsulating analogue was prepared through reaction of the acid derivative with benzylamine. The overall yield from the oxacalix[3]arene is less than 5%, but, given that the dimerization proceeds in only 14%, this is nevertheless quite impressive. However, in addition to the formation of the molecular capsule, a self-threaded dimer (rotaxane-**40**) was also isolated, which had resulted from an upper-rim substituent threading through the central cavity during dimerization. The existence of the rotaxane structure was deduced from the complexity of the patterns observed in the ^1H NMR spectrum compared to that of the capsule. A similar strategy was adopted to incorporate porphyrin linkers between two oxacalix[3]arenes, but, due to the size of the porphyrins and their rigidity, only the capsular form was found [50]. Treatment with zinc(II) acetate introduced three equivalents of the metal, one for each porphyrin unit.

3.2.3 Capping the upper rim: Capping the upper rim is also possible, as shown by Araki in 2000, through a complex synthetic pathway starting from bromooxacalix[3]arene [51]. As shown in Scheme 19, oxacalix[3]arene **3f** was treated with methyl iodide in the presence of NaH in THF at reflux to afford its methyl ether **41** in 41% yield. With the lower rim protected, the upper rim was converted to the aldehyde **42** and then reduced to the methylol **43**. Reaction with 1,3,5-tris(bromomethyl)benzene in a boiling suspension of NaH in THF/DMF afforded the upper-rim capped compound **44** in 26% yield. The sulfur-bridged analogue **45** was prepared in 36% yield by bromination of the methylol-terminated oxacalix[3]arene, employing PBr_3, and coupling with 1,3,5-tris(methanethiol)-benzene in the presence of Cs_2CO_3 in THF.

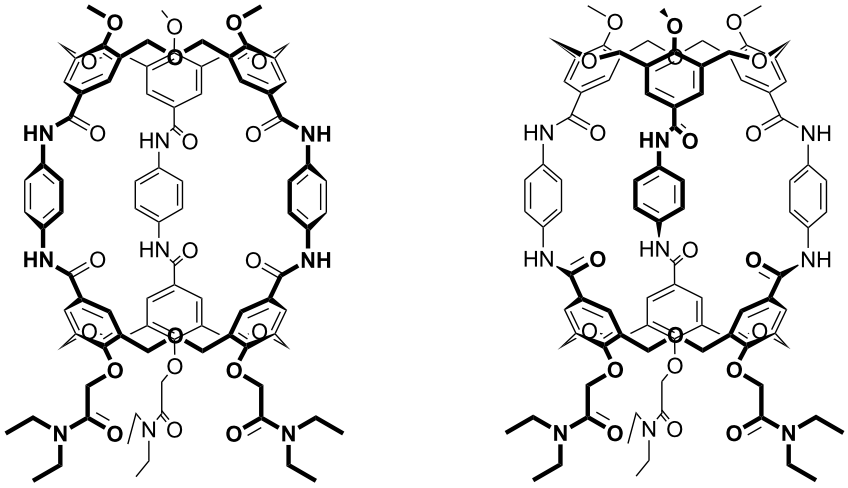

Figure 13: Two forms of dimeric oxacalix[3]arene **40** [47].

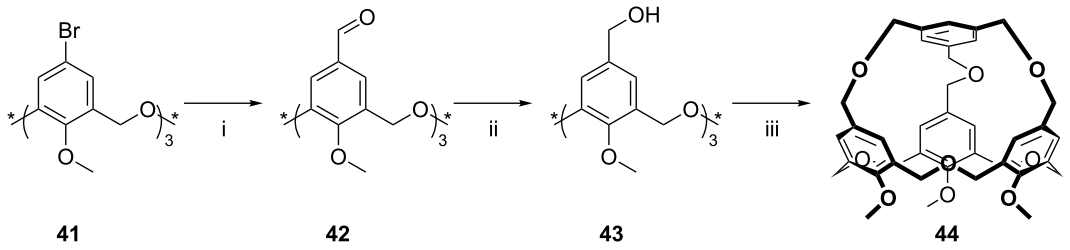

Scheme 19: Capping the upper rim: (i) *t*-BuLi, THF, −78 °C; (ii) $NaBH_4$, THF/EtOH; (iii) 1,3,5-tris(bromomethyl)benzene, Na_2CO_3, DMF [51].

3.2.4 Upper-rim coordination chemistry: The functionalization of the upper rims of oxacalix[3]arenes has also been achieved through classical inorganic coordination chemistry. Shinkai reported that the reactions of 4- and 3-pyridyloxacalix[3]arenes, protected on the lower rims by esters or methyl ethers, with [1,3-(diphenylphosphine)propane]palladium(II) salts gave dimeric capsules linked by three Pd(II) ions at the 4-pyridyl groups (**46**, Figure 14) or 3-pyridyl groups (**47**) [52,53]. The twist inherent in pyridylphenols, and by extension oxacalix[3]arenes incorporating these motifs, was expected to result in two chiral (*M* and *P*) forms of the capsules. The addition of Na^+ appeared to enhance the twisting of capsule **46**, presumably through an allosteric effect that occurred when the cations bound to the lower-rim esters, as indicated by increasingly complex ^{1}H NMR patterns. When **46** bound to *S*-2-methylbutylammonium triflate, the presence of a chiral complex was confirmed by circular dichroism [53].

4 Oxacalix[3]arene complexes

4.1 Complexation by parent oxacalix[3]arenes

4.1.1 Receptors for ammonium cations: The symmetric cavity of the oxacalix[3]arenes, with three CH_2OCH_2 bridges and electron-rich aromatic groups, makes them attractive macrocycles to bind ammonium cations. The affinity of **3a** for acetylcholine and several other quaternary ammonium ions was investigated by Masci in 1995 [54] who found that K_{assoc} values in $CDCl_3$ were modest, ranging from 38 M^{-1} for *N*,*N*,*N*-trimethylanilinium to 90 M^{-1} for *N*,*N*-dimethylpyrrolidinium, but significantly greater than those of the dihomocalix[4]arene and tetrahomooxacalix[4]arene analogues.

4.1.2 Alkali-metal complexes: The parent oxacalix[3]arenes (calixarenes with free OH groups) show little ability to bind alkali metals, and extraction studies from water to CH_2Cl_2 showed that this ability was enhanced only in the presence of strong bases [15]. Hampton's purification of **3a** involved the

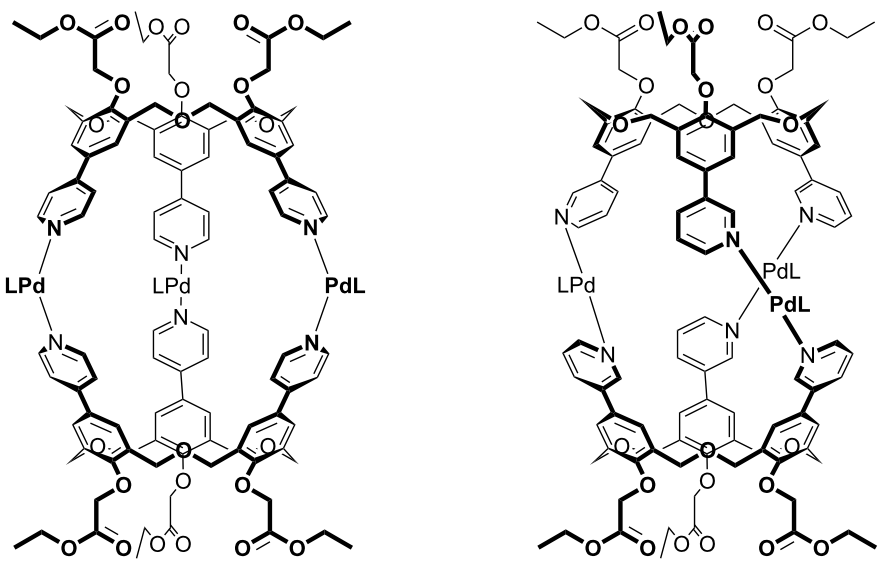

Figure 14: Oxacalix[3]arene capsules **46** and **47** formed through coordination chemistry [52,53].

formation and precipitation of the Na^+ salt, which would seem to indicate a significant affinity for metal cations. Surprisingly, only *para*-chlorooxacalix[3]arene, **3e**, was found to bind alkali metals and then only when triethylamine was used to promote salt formation. The binding constants were determined by ^{1}H NMR as 0.39 M^{-1} for Na^+, 0.32 M^{-1} for K^+ and 0.11 M^{-1} for Li^+ in the presence of 10 equiv of the triflate salts. However, those oxacalixarenes form stronger complexes with transition, lanthanide and uranyl cations.

Cragg employed the quartz-crystal-microbalance technique to investigate binding by Na^+, K^+ and Ca^{2+} to **3a** and **3k** [48]. Again, Na^+ was bound preferentially, with computer models suggesting that this was due to the depth to which the cation was drawn into the macrocyclic cavity when in the *cone* conformer.

4.1.3 Transition-metal complexes: The first example of transition-metal binding to an oxacalix[3]arene was Hampton's variable temperature ^{1}H NMR investigation of the interactions between titanium(IV) species and **3a** [55]. In the absence of crystallographic evidence the NMR splitting patterns were compared to simulated spectra. At ambient temperature the NMR-derived symmetry was C_{3v}, matching that of the macrocycle, but upon cooling an asymmetric C_s symmetry emerged. It was proposed that rapid interconversion between isomers occurred by a "turnstile" or Berry-pseudorotation mechanism. A subsequent paper from the group reported the crystal structure of the titanium(IV) isopropoxide ($Ti(iPrO)_4$) complex [56]. The structure was dimeric; each macrocycle was present as the trianion bound to the titanium by all three oxygens and pulled slightly into the cavity by $iPrO^-$. The paper also reported the result of a reaction between the lithium salt of **3b** and vanadyl chloride ($VOCl_3$). Based on powder diffraction and ^{51}V NMR data it was proposed that the VO group bound within the macrocyclic cavity, by analogy to the Ti(IV) complex, and that these units formed linear aggregates held together by V=O···V=O interactions. Ten years later, Redshaw was able to prove Hampton's assertion regarding the structure by X-ray analysis of the VO complex shown in Figure 15 [57].

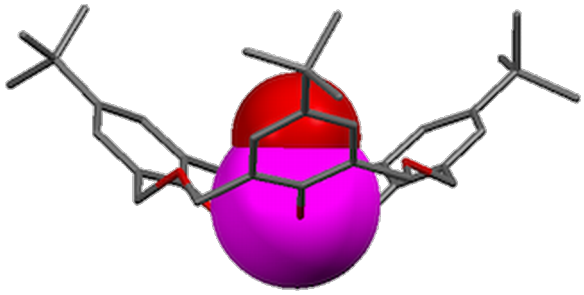

Figure 15: X-ray crystal structure of the **3b**-vanadyl complex (CCDC ID 240185) [57].

Katz used calixarenes to disperse reactive titanium on silica in order to prepare a catalytically active surface [58]. While *p-tert*-butylcalix[4]arene appeared to work successfully, oxacalix[3]arene **3a** first bound titanium and was then cleaved to give an acyclic surface-bound product with free methyl and aldehyde termini (Scheme 20).

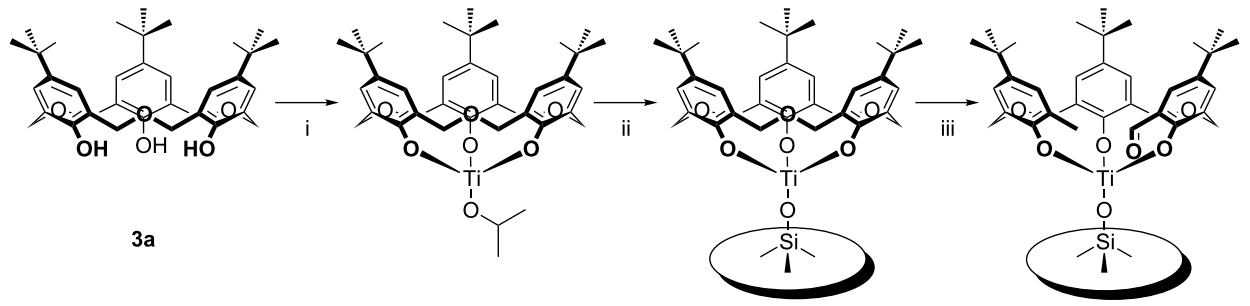

Scheme 20: Effect of Ti(IV)/SiO_2 on **3a**: (i) $Ti(OiPr)_4$, toluene; (ii) triphenylsilanol, toluene; (iii) partially dehydroxylated silica gel, toluene [58].

Klufers prepared complexes of **3b**, **3d** and **3k** through reaction of the macrocycles with $(Et_3N)_2[Re(CO)_3Br_3]$ in acetonitrile [49]. The X-ray crystal structures of the complexes with **3b** and **3d** showed binding by $Re(CO)_3$ to two deprotonated phenolic oxygen atoms as shown in Figure 16. Reaction with ester derivative **3k** at 85 °C resulted in decomposition of the macrocycle.

4.1.4 Lanthanide complexation: The first study of the binding affinities of lanthanides for oxacalix[3]arenes was in 1995 when Hampton reported the crystal structure and dynamic behaviour of a scandium(III) complex of **3a** [59]. Later, the X-ray structures of lanthanum, lutetium and yttrium complexes with the same macrocycle showed 2:2 complexes between the cations and macrocycles [60]. In these structures the lanthanides are either six-coordinate, with distorted octahedral metal centres, or eight-coordinate, as in the structure illustrated in Figure 17.

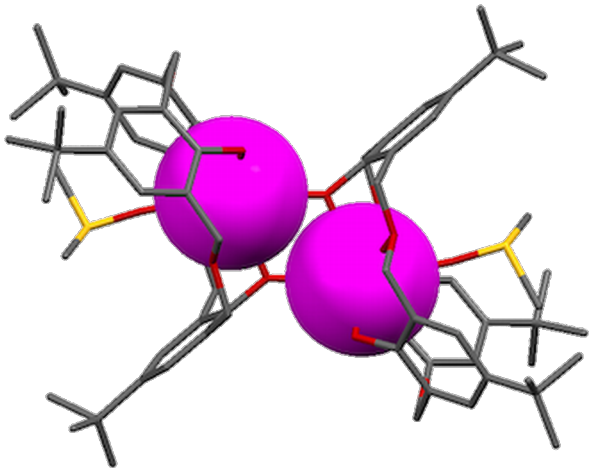

Figure 17: X-ray crystal structure of the La_2·**3a**$_2$ complex (CSD ID TIXXUT) [60].

The same group calculated the apparent binding constants of metal triflates with **3a** and **3e** [61]. Results showed that the binding constants for **3e** were slightly higher than **3a** and that the strength of binding increased in the sequence Ca^{2+}, Na^+, $Li^+ < Mg^{2+} < La^{3+} << Y^{3+} < Lu^{3+} << Sc^{3+}$. To reinforce this, the transporting ability of the oxacalixarenes was investigated.

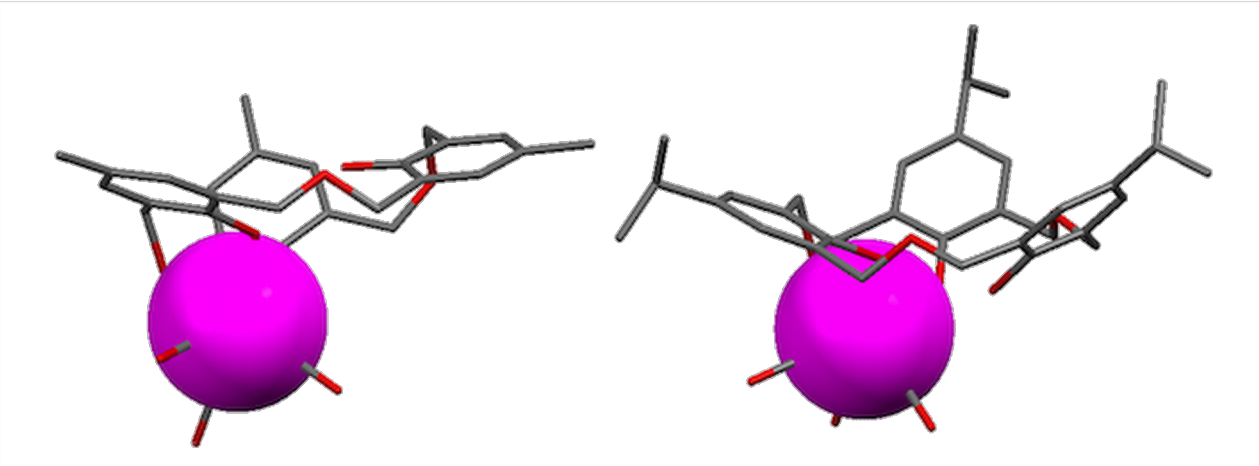

Figure 16: X-ray crystal structures of oxacalix[3]arene complexes with rhenium: **3b**·$Re(CO)_3$ (CCDC ID 620981, left) and **3d**·$Re(CO)_3$ (CCDC ID 620982, right) [49].

Aqueous/organic/aqueous liquid-membrane transport experiments were undertaken with both oxacalix[3]arenes in order to determine their cation selectivities. No transport of Li^+ or Mg^{2+} was observed, but **3e** transported 44% of the Sc^{3+} over 24 h when a mixture of three cations (Sc^{3+}, Mg^{2+} and Li^+) was used as the source phase.

4.1.5 Chelating behaviour with uranium: Complexation of the uranyl cation by oxacalix[3]arenes has been ongoing since 1999 when Thuéry reported a complex of uranyl (UO_2^{2+}) and **3a** [62]. The X-ray crystal structure showed that the cation was threaded through a single macrocycle in what was, at the time, an unprecedented pseudotrigonal geometry, which included a weak interaction between the nitrogen of Et_3N and a uranyl oxygen (Figure 18). Masci and Thuéry later reported more tetrahedrally and pentagonally distorted structures with **3a** and **3b** [63]. The nature of the alkylammonium counterion appeared to be influential in determining the final geometry around the uranium centre, yet in some cases it did not interact with the uranyl moiety (Figure 18).

Replacing the alkylammonium cations with protonated [2.2.2]cryptand resulted in 1:1 and 2:1 complexes in which the uranyl–oxacalix[3]arene moiety acts as a recognition site for the [2.2.2]cryptand [64]. Figure 19 shows the crystal structure of the 2:1 complex.

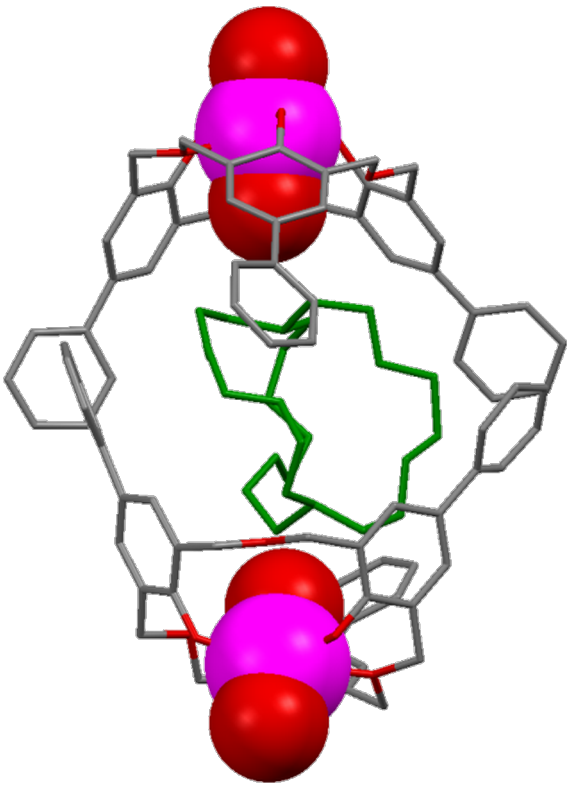

Figure 19: X-ray crystal structure of a supramolecule comprising two [**3g**·UO_2]$^-$ complexes that encapsulate a diprotonated cryptand (CCDC ID 181044) [64].

4.2 Binding properties of oxacalix[3]arene derivatives

One of the most important features of calixarenes in general and oxacalix[3]arenes in particular is their vast ability to selectively bind and carry ions and neutral species. This is achieved mainly with lower-rim derivatives in solution.

4.2.1 Receptors for ammonium cations: Although the simple parent oxacalix[3]arene **3a** is able to bind quaternary ammonium ions (as described above), several derivatives have also been studied with respect to these and other ammonium ions. Extrac-

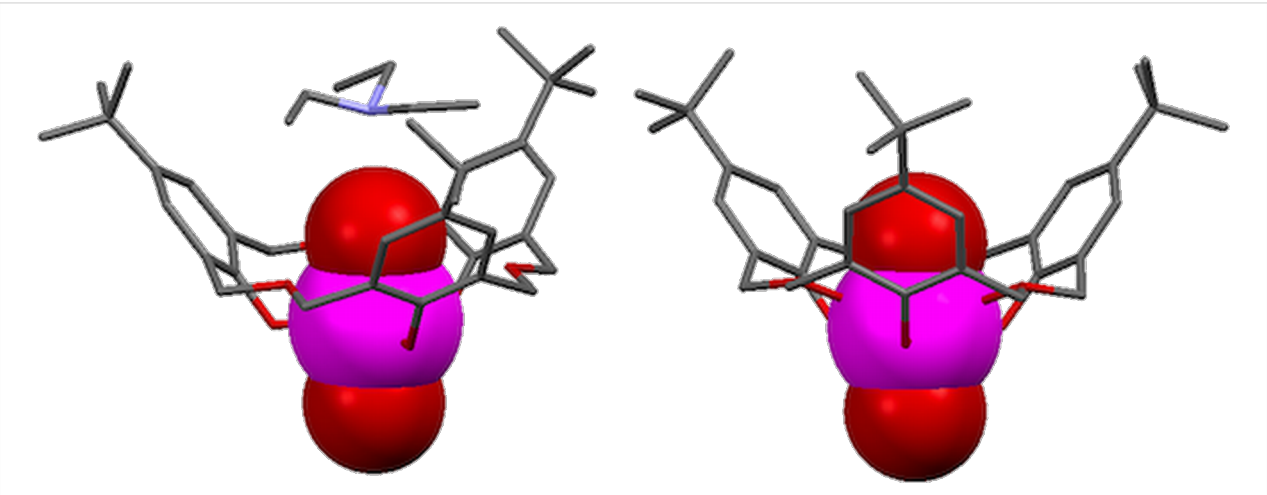

Figure 18: X-ray crystal structures of [**3a**·UO_2]$^-$ with a cavity-bound cation (CCDC ID 135575, left) and without a coordinated cation (CCDC ID 181042, right) [62,63].

tion studies from alkaline aqueous picrate solutions into CH_2Cl_2 indicated that the *n*-butyl ether derivative **10** showed a high affinity for *n*-$BuNH_3^+$ (82% *E*) as postulated by the authors, because both host and guest possess the same C_3-symmetry [24]. Ethyl ester **12a** was more efficient at extracting *n*-$BuNH_3^+$ picrate from water into CH_2Cl_2 than its calix[4]arene analogue was, in both the *cone* (77% vs 24% *E*) and *partial-cone* (42% vs 6% *E*) conformers [29]. In a wider study, Yamato determined extraction data for **17a** with *n*-$BuNH_3^+$ picrate (98% *E cone* vs 93% *E partial-cone*), i$BuNH_3^+$ picrate (48% *E cone* vs 37% *E partial-cone*) and *t*-$BuNH_3^+$ picrate (35% *E cone* vs 14% *E partial-cone*) [34]. The hexaamide derivative **20** bound *n*-$BuNH_3^+$ well, and an anion dependence was determined; K_{assoc} values in $CDCl_3$ were 536 ± 32 M^{-1} for Cl^- and 230 ± 17 M^{-1} for Br^- [37].

Studies of the C_3 symmetrically capped triamide **13** reported that this derivative acts as a well-preorganized host for binding primary ammonium ions, such as phenylalanine methyl ester [31]. Chiral recognition of optically active primary alkyl ammonium ions was also obtained with an ether derivative of oxacalix[3]arene **3a** with one methyl and two *n*-butyl lower-rim substituents **49**, as shown in Figure 20 [65]. The compound was shown to exist in (+) and (−) enantiomers, and in a *partial-cone* conformation, proof of which came from X-ray crystallography. The compound bound to α-amino acid ethyl esters and 1-arylethylamines with the methoxy and one *n*-butoxy oxygen. The (−)-4-*tert*-butyloxacalix[3]arene derivative bound L-alanine ethyl ester and L-phenylalanine ethyl ester better than their enantiomers, with association constants of 4500 M^{-1} and 2000 M^{-1}, respectively. (*R*)-1-Phenylethylamine and (*R*)-1-naphthylethylamine cations were bound more strongly by the (+)-enantiomer.

Allosteric effects can also be employed to affect the binding of ammonium cations. Katoh's *N*-hydroxypyrazinone-containing oxacalix[3]arene **23** extracted *n*-$BuNH_3^+$ picrate and *t*-$BuNH_3^+$ picrate better in the presence of Ga^{3+}, indicating cooperation between the two binding sites [38]. The association constant for *n*-$HexNH_3^+$ picrate was found to be 4375 M^{-1}, but when Ga^{3+} was present this dropped to 2833 M^{-1}, suggesting that the macrocyclic cavity, while preorganized for the smaller cations, was too rigid for the extended ammonium cation.

One of the more unusual derivatives to have been prepared, **50**, incorporates an *N*-pyridinium dye on one of the upper-rim positions, which, in combination with the phenolic unit of the macrocycle, forms a proton-ionizable Reichardt dye, illustrated in Figure 21 [66]. The other *p*-*tert*-butyl substituted phenols are blocked from ionization, as are the methyl ethers. The native oxacalix[3]arene dye is pale green and gives no response to benzylamine ($BzNH_2$) or triethylamine (Et_3N), but cyclohexylamine (*c*-$HexNH_2$) and *n*-butylamine (*n*-$BuNH_2$) bind with a concomitant colour change to blue.

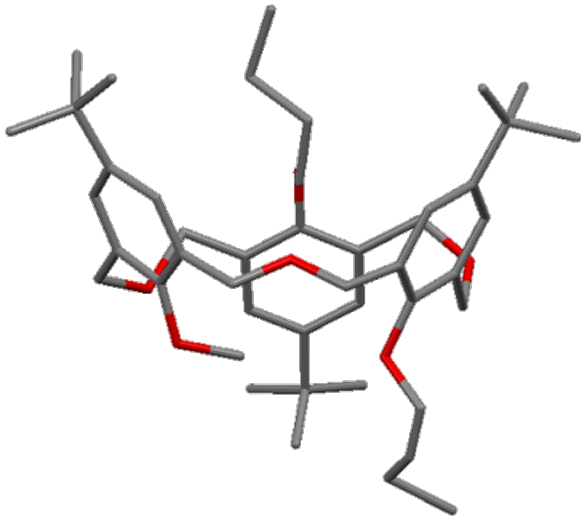

Figure 20: X-ray crystal structure of oxacalix[3]arene **49** capable of chiral selectivity (CSD ID HIGMUF) [65].

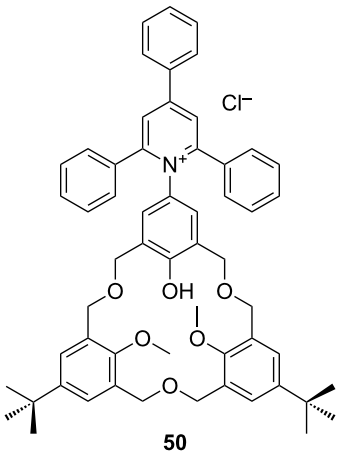

50

Figure 21: The structure of derivative **50** incorporating a Reichardt dye [66].

4.2.2 Alkali metals: The ionophoric properties of the conformationally mobile ethyl ether of **3a** (**8**) and both *cone* and *partial-cone* *n*-butyl ether **10** derivatives toward alkali-metal cations were estimated by extraction experiments from alkaline aqueous picrate solutions to CH_2Cl_2 [24], with the latter showing some preference for K^+ (59% *E*) over Na^+ (6%) and Cs^+ (35%).

Replacement of the alkyl groups by residues with additional binding sites, such as the carbonyl group, strongly affects the binding ability of calixarene derivatives. Thus, the binding properties of derivatives containing esters, amides and ketones, have been assessed. Extraction studies performed under the same conditions as described above reported that *cone* ester **12a** shows high selectivity for Na^+ whereas the *partial-cone* conformer shows K^+ selectivity (Table 1) [29]. Similar extraction experiments performed with amide **17a** [34] reported that this derivative is a better phase-transfer agent than **12a**, but shows the same trend as **12a**: *cone*-**17a** exhibits the highest preference for Na^+, while *partial-cone*-**17a** prefers K^+ (Table 1).

Table 1: Percentage extraction of alkali-metal picrates into CH_2Cl_2.[a,b]

	Li^+	Na^+	K^+	Cs^+
cone-**12a**	7	79	64	49
paco-**12a**[b]	0	26	88	82
cone-**17a**	–	93	72	–
paco-**17a**	–	28	73	–

[a]Data adapted from references [29] and [34]. [b]*partial-cone* denoted as *paco*.

The association constants, K_{assoc}, for both derivatives (**12a** and **17a**) were determined in THF/$CHCl_3$ (1:1) at 25 °C by UV absorption spectrophotometry (Table 2) [25].

Table 2: Association constants (log K_{assoc}) of alkali- and alkaline-earth-metal complexes.[a,b].

	Na^+	K^+	Rb^+	Cs^+	Mg^{2+}	Ca^{2+}	Ba^{2+}
cone-**12a**	4	4.7	4.2	3.9	<2	<2	<2
cone-**17a**	>7	5.9	5.5	5.2	4.9	>7	>7
paco-**17a**[b]	5.1	6.2	6.0	5.5	–	–	–

[a]Data adapted from reference [25]. [b]*partial-cone* denoted as *paco*.

Marcos [39,67] reported binding data for alkali- and alkaline-earth-metal cations with **17a** and **24** (Table 3). Extraction studies performed under different conditions than the previous ones (neutral aqueous picrate solutions to CH_2Cl_2), indicated that both derivatives show similar extraction profiles, although **17a** is a much stronger binder than **24**. Both exhibit highest selectivity for Na^+ (50 and 20% *E* for **17a** and **24**, respectively) and **17a** is also a good extractant for Ba^{2+} (55% *E*).

Derivatives with heteroatoms on the lower rim have also been tested as cation chelators. The binding properties of 2-pyridylmethyloxy derivative **11a** in both conformations, have been established [27,68]. Extraction studies from neutral aqueous picrate solutions to CH_2Cl_2 showed that, among all the cations studied, the *partial-cone* conformer is a better extractant than the *cone*.

As well as simple oxacalix[3]arenes and their derivatives, capped compounds have also been investigated. Association constants for several metal cations were determined for Yamato's lower-rim-capped derivative **18** [33]. Values were found for Na^+ (log K_{assoc} 5.3), K^+ (log K_{assoc} 6.7) and Cs^+ (log K_{assoc} 5.8). This contrasts with log K_{assoc} of 7.6 for *n*-$BuNH_3^+$ picrate. The extractability of metals from aqueous solution into CH_2Cl_2 by Araki's upper-rim-capped derivatives was also determined [51]. The complementary cavity size and the rigid structure of the cage molecule **44** probably led to the high Cs^+ selectivity (≈45% *E*) compared to negligible amounts of Na^+, K^+ or Rb^+ (<5% *E*); however, the sulfur-linked compound **45** failed to extract any cations.

4.2.3 Transition metals: The tris(diphenylphosphine) derivative **26** prepared by Matt [40] was reacted with [Mo(CO)$_3$(cycloheptatriene)] to give a complex that was determined to be the symmetrically bound Mo(CO)$_3$ complex involving all three of the phosphorus donors. The oxacalix[3]arene also formed a complex with rhodium. Elemental analysis supported a composition incorporating the H–Rh–C=O fragment. ^{1}H NMR indicated that this was threaded through the macrocyclic annulus, based on the presence of a peak at −9.70 ppm, and infrared analysis showed a carbonyl absorption band at 1977 cm^{-1}. This suggested an orientation in which the hydrogen was *endo*, and the carbonyl *exo*, to the macrocyclic cavity. Gold(I) and silver(I) complexes also form with the cations most likely adopting a trigonal planar C_{3v}

Table 3: Percentage extraction of alkali and alkaline earth metal picrates into CH_2Cl_2.

	Li^+	Na^+	K^+	Rb^+	Cs^+	Mg^{2+}	Ca^{2+}	Sr^{2+}	Ba^{2+}
cone-**17a**[a]	25	50	32	27	20	17	34	41	55
cone-**24**[b]	4	20	5	6	6	2	4	4	4

[a]Data adapted from references [67]. [b]Data adapted from reference [39].

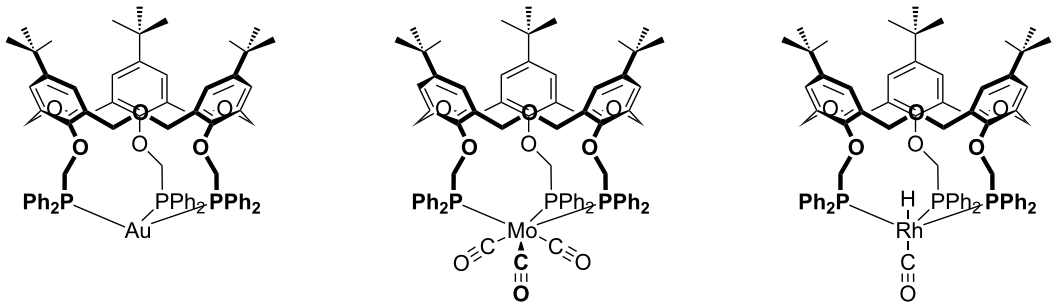

Figure 22: Phosphorylated oxacalix[3]arene complexes with transition metals: (Left to right) **26**·Au, **26**·$Mo(CO)_3$ and **26**·RhH(CO) [40].

geometry, as shown in Figure 22, based on the symmetric ^{31}P NMR pattern at ambient temperature. At lower temperatures, however, the A_3X pattern seen for the silver(I) complex changes to an A_2BX pattern, indicating that the apparent symmetry is a time-averaged effect.

Cragg reported the reaction of **17a** with mercury(II) chloride and the X-ray crystal structure of the product (Figure 23) [69]. The structure revealed that a $[HgCl_2]_2$ fragment bridged between two macrocycles through coordination to one amide group of each. The cations were thus *exo* to the macrocyclic cavity and represented the first example in which a cation was not bound within the annulus.

Marcos reported on the binding properties and theoretical studies of **17a** [67] and **24** [39] with transition and heavy metals. Extraction studies from neutral aqueous picrate solutions to CH_2Cl_2 indicated that amide **17a** is a good extractant for Ni^{2+}, Co^{2+}, and Ag^+, and mainly for Pb^{2+} with 80% *E*. The data in Table 4 also shows that ketone **24** is a weak extracting agent, with a slight preference for Ag^+. This is in agreement with the higher basicity of the carbonyl oxygen in the amide group compared with the ketone group.

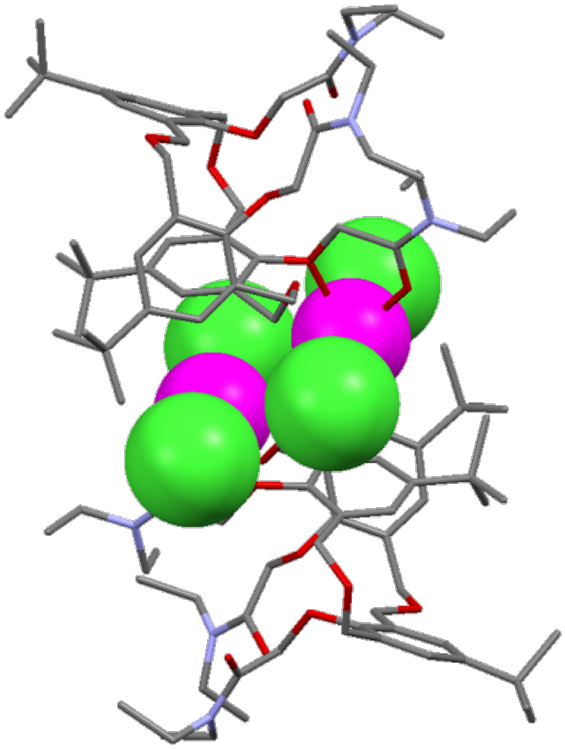

Figure 23: X-ray crystal structure of [**17a**·$HgCl_2]_2$ (CCDC ID 168653) [69].

4.2.4 Lanthanides: Marcos investigated the lanthanide extraction by both **17a** [70] and **24** [39] using the same conditions as described above (Table 5). Ketone **24** is a poor phase-transfer agent (% *E* ranges from 5 to 7), while amide **17a** clearly discriminates between the light and heavy lanthanides. The lower-weight cations, such as Ce^{3+}, Pr^{3+} and Nd^{3+} (34% *E*) are preferred over the heavier, such as Er^{3+} and Yb^{3+} (13% *E*). The stability constants for the 1:1 complexes with **17a** were also

Table 4: Percentage extraction of transition- and heavy-metal picrates into CH_2Cl_2.

	Mn^{2+}	Fe^{2+}	Co^{2+}	Ni^{2+}	Cu^{2+}	Zn^{2+}	Ag^+	Cd^{2+}	Pb^{2+}
17a[a]	19	19	39	45	24	15	40	37	80
24[b]	2	5	2	4	4	3	13	3	5

[a]Data adapted from reference [67]. [b]Data adapted from reference [39].

Table 5: Percentage extraction of lanthanide-metal picrates into CH_2Cl_2.

	La^{3+}	Ce^{3+}	Pr^{3+}	Nd^{3+}	Sm^{3+}	Eu^{3+}	Gd^{3+}	Dy^{3+}	Er^{3+}	Yb^{3+}
17a[a]	28	34	34	34	31	30	17	18	13	13
24[b]	6	5	5	6	6	6	6	5	6	7

[a]Data adapted from reference [70]. [b]Data adapted from reference [39].

determined by UV absorption spectrophotometry in methanol at 25 °C, by using chloride salts. The same positive discrimination for the light lanthanides was observed (log β = 5.5 and 3.4 for La^{3+} and Yb^{3+}, respectively).

The complexing ability of the ionizable tricarboxylic acid **14a** towards lanthanides Pr^{3+}, Eu^{3+} and Yb^{3+} and actinide Th^{4+} was established in methanol, by potentiometry measurements [71]. Results showed that the complex formed with Th^{4+} was more stable than the complexes of lanthanides (log β values are 20.5, 19.6, 21.3 and 23.1, respectively).

5 Other applications

5.1 Hosts for fullerenes

One of the remarkable characteristics of calixarenes is the bowl shape of the molecule. In the case of oxacalix[3]arenes, the bowl is quite shallow, which indicates that they may be good hosts for spherical guests and immediately suggests binding to fullerenes. Furthermore, the macrocyclic bowl is the perfect size for C_{60} and has a complementary threefold-symmetry element.

Based on the knowledge that *p-tert*-butylcalix[8]arene was able to complex C_{60} [72,73] Shinkai investigated the interaction of C_{60} with **3a** in 1997 by UV–vis spectroscopy [74]. In a later full paper, UV–vis absorption spectra of C_{60} were recorded with calix[*n*]arenes and oxacalix[3]arenes. The interaction of fullerenes with calixarenes affected the spectra between 420 and 450 nm [75]. By using the Benesi–Hildebrand method, **3a** was shown to bind to C_{60} with a K_{assoc} of 35.5 M^{-1} in toluene at 25 °C; however, when methylated on the lower rim, no binding was observed. Molecular modelling was employed to illustrate how the shallow cavity of **3a** allowed for optimum interactions between the oxacalix[3]arene aromatic rings and C_{60}.

While subtle spectroscopic features and computer models appeared to indicate fullerene binding, structural evidence was to be more compelling. In 1998, Fuji reported the solid-state structure of **3f** with C_{60} as proof of 1:1 binding [76]. Alignment of the oxacalix[3]arene C_3 axis with the same symmetry axis of the fullerenes is observed. This arrangement maximizes the number of points of contact within the supramolecular complex, thereby enhancing the van der Waals interactions. In the same paper, the association constants of several oxacalix[3]arenes were calculated by the Rose–Drago method based on absorption features at 425 or 430 nm in toluene. The strongest binding was observed for **3a** (35.6 M^{-1}) and the weakest for **3h** (9.1 M^{-1}).

Although spectroscopic methods are widely used to determine host–guest association constants, Georghiou has argued persuasively that spectral changes in solution may be due to a combination of several factors, of which host–C_{60} complex formation is only one [77]. Consequently, reported K_{assoc} values determined by this method should be treated with some caution.

Fullerene derivatives that lack some of the symmetry of the parent compound have been shown to bind to oxacalix[3]arenes, as in Fuji's X-ray structure of 1,4-bis(9-fluorenyl)-1,4-dihydro[60]fullerene with **3f** shown in Figure 24, in which the oxacalix[3]arene binds to the C_{60} derivative with the fluorenyl substituents oriented away from the macrocycle [78].

Raston reported that *p*-benzyloxacalix[3]arene (**3i**) formed a 2:1 complex with C_{60} in toluene [79]. The X-ray crystal structure showed how the two oxacalix[3]arenes bound on opposite sides of the fullerene, with their benzyl arms interdigitated. When the complex was isolated and added to CH_2Cl_2 then the fullerene was released. The method could be used to separate C_{60} from fullerite (a mixture of fullerenes of different sizes) in greater than 99.5% purity. A similar experiment was undertaken by Georghiou with **6a** leading to much higher association constants of 296 M^{-1} (toluene) and 441 M^{-1} (benzene) [23]. Crystallography revealed a similar interdigitated 2:1 complex to that observed by Raston for **3i** (Figure 25).

One area of interest has been the selective separation of C_{70} from a mixture of fullerenes. Komatsu proposed a method for the preferential precipitation of C_{70} over C_{60} with *p*-halooxacalix[3]arenes [80]. *p*-Iodooxacalix[3]arene (**3j**) was able to achieve 90% extraction with a selectivity approaching 90%.

An unexpected effect of fullerene complexation was that a water-soluble capsule formed from two *p-tert*-butyloxacalix[3]arenes with trimethylammonium groups on the lower

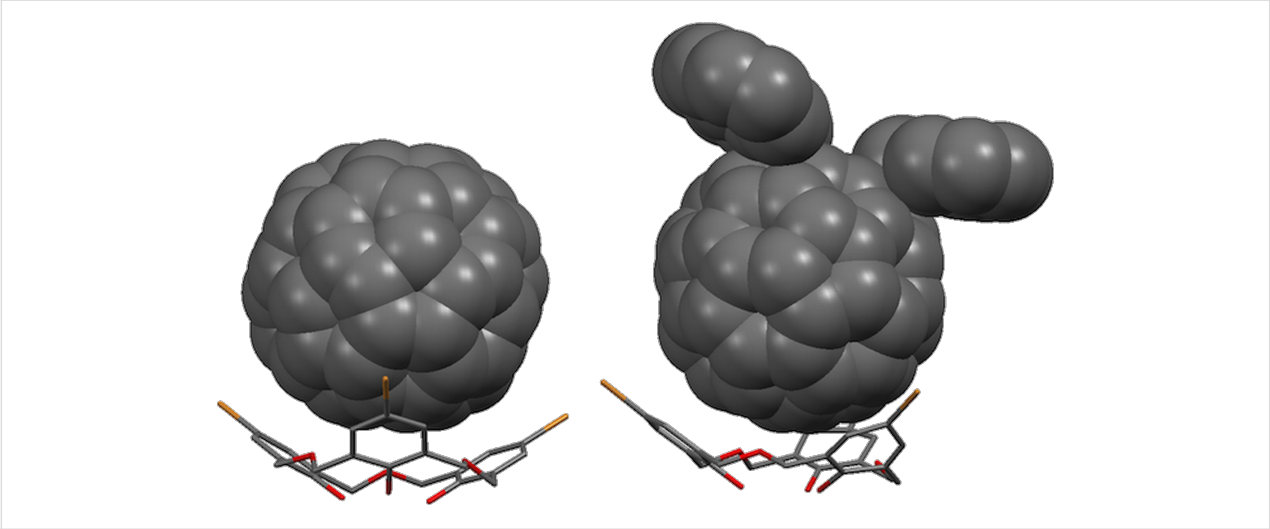

Figure 24: X-ray crystal structures of **3f** with C_{60} (CCDC ID 182801, left) [76] and a 1,4-bis(9-fluorenyl) C_{60} derivative (CCDC ID 139793, right) [78].

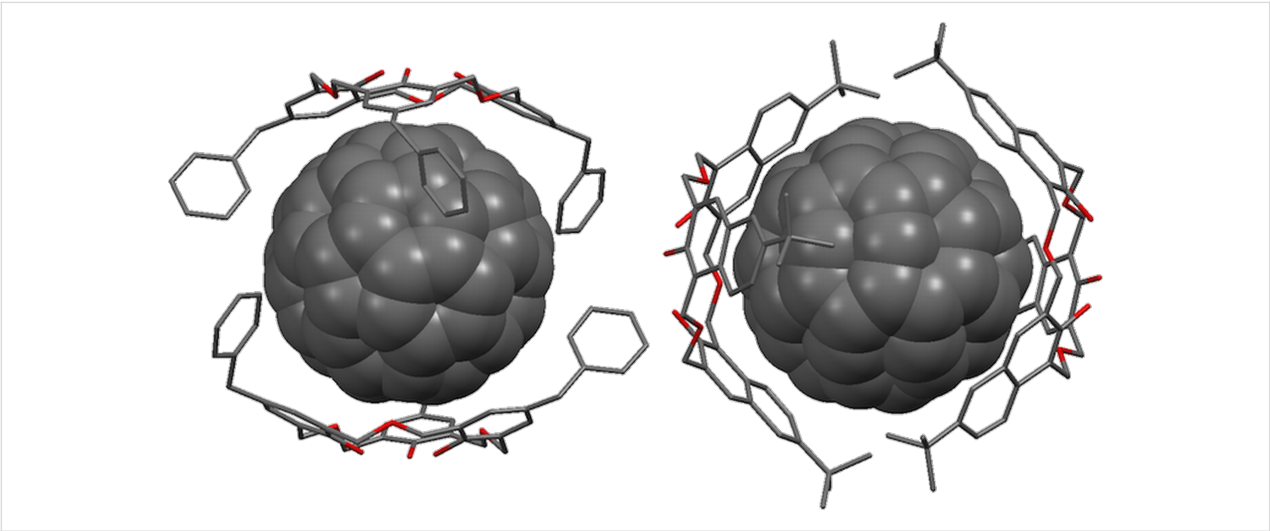

Figure 25: X-Ray crystal structure of **3i** and **6a** encapsulating C_{60} (CCDC ID 102473 and 166077) [23,79].

rims, **51**, which bound C_{60}, was able to cleave DNA (Figure 26) [81]. The capsule was solubilized as the MsO^- salt and applied to a supercoiled form of DNA. In the absence of light, no change was seen, but in the presence of visible light the DNA became "nicked", that is, a phosphodiester bond in one strand was broken. The authors speculated that the cationic complex was able to bind to the anionic DNA whereupon $^1O_2$ generated by photoinduced electron transfer from guanine and C_{60}, or alternatively photochemically by C_{60} alone, cleaves the DNA strand. Ikeda later advanced this line of research to carbohydrate-containing oxacalix[3]arenes that functioned in water [82].

The same cationic complex was deposited as a monolayer onto an alkylsulfonate coated gold surface and elicited both a redox response, as determined by cyclic voltammetry, and a photochemical response to visible light [83,84]. The optical response was studied further [85], and a transient band was observed at 545 nm, which was not present in the spectrum of C_{60} alone. The origin of the band was ascribed to C_{60}-capsule triplet–triplet absorption.

As discussed above, oxacalix[3]arenes with pyridine in the *para*-position and ethyl esters on the lower rim are able to form capsules through coordination to palladium [53]. Capsule **46** was shown to bind to C_{60} by the presence of two peaks in the ^{13}C NMR spectrum, which did not coalesce even at 90 °C. ^1H NMR was used to determine an association constant of 54 M^{-1} in $Cl_2CDCDCl_2$ at 60 °C. An asymmetric capsule incorporating an oxacalix[3]arene and three Zn(II)porphyrin

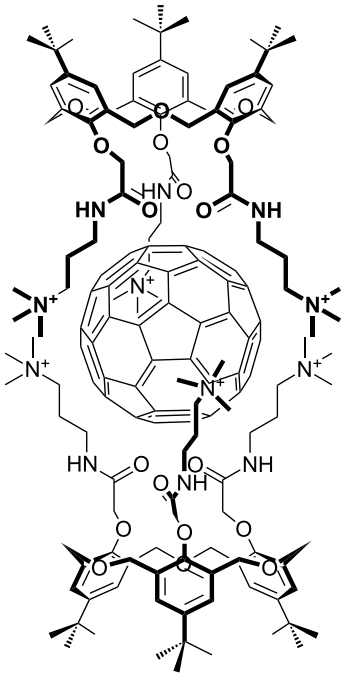

51

Figure 26: A C_{60} complexing cationic oxacalix[3]arene **51** [81].

moieties, **52**, was also able to bind C_{60} in a similar fashion with an association constant of 60 M^{-1} in toluene-d_8 at −30 °C [86].

Another strategy to promote fullerene inclusion in an oxacalix[3]arene was to link the two by a triethylene glycol tether to form a molecular cup-and-ball **53** [87]. In addition to self-inclusion, the authors also proposed the formation of higher order oligomers arising from C_{60} inclusion in a neighbouring oxacalixarene through the change in conformation illustrated in Figure 27.

5.2 Fluorescent chemosensors

In order to determine the equilibrium constants with quaternary ammonium ions, Shinkai [88] prepared an oxacalixarene with pendent pyrene groups, **54**, which fluoresced at 480 nm. Oxacalix[3]arene fluorescence was significantly quenched in the presence of *n*-hexyl ammonium cations (*n*-$HexNH_3^+$), but only in the *partial-cone* conformation, as the ammonium cation forced the lower-rim pyrene groups apart. The same cation had a much higher affinity for *cone*-**54** through its complementary binding sites, but approached these from the upper rim, leaving the excimer fluorescence unaffected. Yamato also pursued this path, preparing a tris(pyrenyl) derivative **55** in the *cone* conformer by employing "click" chemistry (Scheme 21) [89]. One interesting aspect of the synthesis was that the tris(propargyl) click precursor crystallized as a mixture of *cone* and *partial-cone* conformers, yet addition of *n*-$BuNH_3^+ClO_4^-$ to the conformers in solution pushed the equilibrium towards the *cone*. *Cone*-**55** gave a response to Pb^{2+} through the enhancement of minor fluorescence peaks between 370 and 400 nm, which were unaffected by other metal guests. The group also reported that the fluorescence intensity at 396 nm increased linearly when Zn^{2+} was added and that the 1:1 complex of this macrocycle gave an increasing linear response at 485 nm to $H_2PO_4^-$ [90].

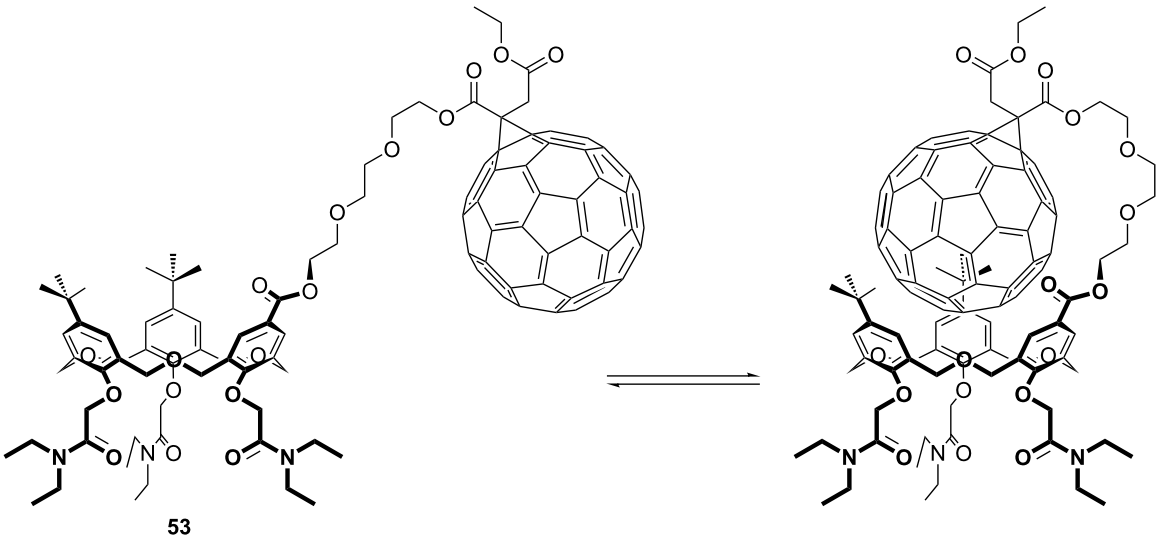

53

Figure 27: An oxacalix[3]arene-C_{60} self-associating system **53** [87].

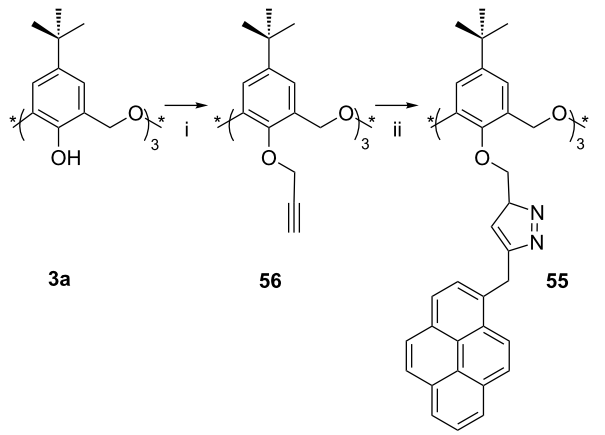

Scheme 21: Synthesis of fluorescent pyrene derivative **55**: (i) Propargyl bromide, acetone; (ii) CuI, 1-azidomethylpyrene, THF/H_2O [89].

Rhodamine substituents can be introduced to the lower rim of the *cone*-**14a** through the ethylamine derivative of the dye (Scheme 22) [91]. Fluorescence enhancement was observed between 500 nm and 600 nm upon addition of Fe^{3+}, Ni^{2+} and Sb^{3+} to **57**, turning the colourless solution fluorescent orange–yellow, together with a colourless-to-magenta colourimetric response.

Kang found that the reaction of **3a** with 1-bromo-4-nitrobenzyl acetate gave the trisubstituted nitrobenzene derivative **58** in 40% yield (Scheme 23) as the *partial-cone* conformer [92]. When a range of fluorescent ammonium cations incorporating pyrene, anthracene or naphthalene groups was tested, quenching was observed. Association constants were determined to be in the range of 1850 M^{-1} to 78000 M^{-1}. The uncharged

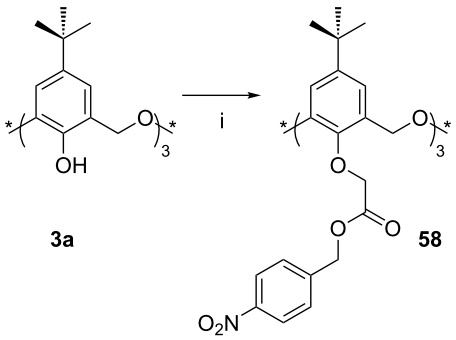

Scheme 23: Synthesis of nitrobenzyl derivative **58**: (i) 1-Bromo-4-nitrobenzyl acetate, K_2CO_3, refluxing acetone, 3 h [92].

pyrenemethylamine was not bound at all, and a trimethylpyrenium cation was weakly bound (K_{assoc} = 300 M^{-1}).

5.3 Ion-selective electrodes

Given the apparent oxacalix[3]arene selectivity for Na^+ and certain protonated amines it is likely that they can act as ion-selective agents in electrodes. This aspect of oxacalix[3]arene research demonstrates that they are not limited to fluorescent sensor applications but can also function in the electrochemical sphere.

5.3.1 Dopamine recognition: The first example of oxacalixarenes being used as electrode modifiers was in 1999 when Odashima incorporated *cone p-tert*-butyloxacalix[3]arene tri(*n*-butyl ether) (**10**) in a PVC matrix liquid membrane [93]. The electrode displayed excellent selectivity for dopamine over biologically important alkali-metal cations K^+, by a factor of 150, and Na^+, by a factor of 1600. Selectivity for dopamine against other catecholamine neurotransmitters, such as adrenaline and

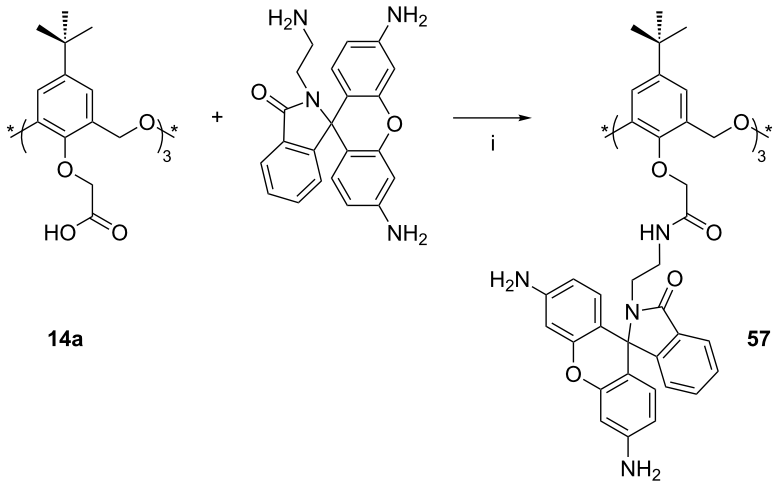

Scheme 22: Synthesis of responsive rhodamine derivative **57**: (i) DCC, CH_2Cl_2 [91].

noradrenaline, was also greater by a factor of at least 100. This selectivity obtained with **10** is a very promising result with the potential to be developed into a dopamine sensor for use under physiological conditions. The dopamine selectivity of the trimethyl ether analogue **7** was investigated by Arrigan at the interface between water and 1,2-dichloroethane using cyclic voltammetry [94]. The log K_{assoc} value obtained was 8.3, which was significantly higher than those for Na^+ and K^+. The log K_{assoc} comparative data for dibenzo-18-crown-6 were 7.6 for the dopamine complex and 10.1 for the K^+ complex, indicating that not only was **7** a better host for dopamine but also that K^+ would not be bound preferentially as is the case for the crown ether.

5.3.2 Sensing Pb^{2+}: In 2007, Yaftian incorporated Matt's phosphorylated derivative **26** in a membrane solution, prepared by dissolving PVC, $NaBF_4$, a plasticizer and the oxacalixarene in THF, which was then used to coat a graphite electrode [95]. This electrode gave a good Nernstian response of 29.7 mV/decade, over a concentration range of 1×10^{-8} M to 1×10^{-4} M of Pb^{2+} ions, with a detection limit of 0.4×10^{-8} M. When tested in mixtures of several competing cations (such as alkali, alkaline earth, transition, heavy metal, lanthanide and Th^{4+} ions) the electrode was able to determine the concentration of Pb^{2+} correctly within 5%, even when other ions were present in tenfold excess.

Diethylacetamide **17a** was also used as an active material in ion-selective electrodes to check the detection of different types of cations [96]. Optimization of the PVC membrane composition was achieved by using different plasticizers (DEHA, *o*-NPOE and BBPA). The performance of the ISE incorporating **17a** indicated a high affinity for Pb^{2+} and the use of DEHA as the best plasticizer.

5.4 Biological models

The crystal structure of the complex of **17a** with $NaPF_6$ (Figure 28) shows how the lower-rim binding site, composed of phenolic oxygen and amide nitrogen atoms, is predisposed to bind Na^+ in its ideal octahedral environment [97]. The compound has been proposed to be an artificial analogue for the filter region in cation channels formed by naturally occurring transmembrane proteins and has been shown to have some activity on transmembrane ion transport in cells.

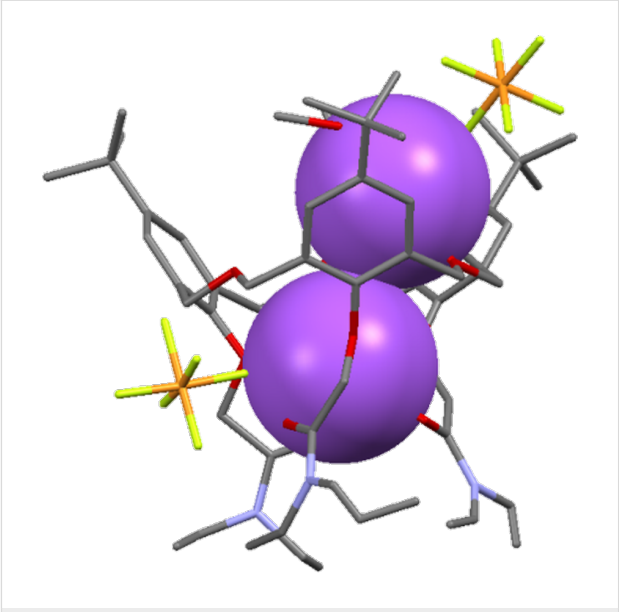

Figure 28: X-ray crystal structure of $[Na_2 \cdot \mathbf{17a}](PF_6)_2$ (CCDC ID 116656) [97].

Conclusion

Since their origins in the phenol-formaldehyde chemistry of the 1960s, oxacalix[3]arenes and their analogues have shown themselves to be interesting and useful additions to the large array of artificial macrocycles that has been developed by supramolecular chemists. The C_3 symmetry of oxacalix[3]arenes, commonly encountered in nature but relatively rare in synthetic host molecules, has made them valuable members of the calixarene family, with an affinity for guests with complementary binding requirements. While the parent compounds do not form particularly strong complexes with metal ions, their *O*-alkylated derivatives are easy to prepare and can show very efficient and selective cation binding, extending to alkyl ammonium salts. Advances in upper-rim functionalization allow for the formation of molecular capsules and chiral recognition sites, and applications have been found in fluorescence sensors, ion-selective electrodes and the extraction of pure C_{60} and C_{70} from crude fullerite. Fifty years on from their discovery by Hultzsch, oxacalix[3]arenes and their derivatives are still able to amaze chemists with their elegant symmetry and fascinating complexes.

Acknowledgements

The use of the EPSRC's Chemical Database Service at Daresbury is gratefully acknowledged. KC thanks the Rhône-Alpes Regional Council for an Explo'ra Sup scholarship.

References

1. Gutsche, C. D. *Calixarenes: An Introduction; Monographs in Supramolecular Chemistry,* 2nd ed.; Royal Society of Chemistry: Cambridge, U.K., 2008.
2. Sliwa, W.; Kozlowski, C. *Calixarenes and Resorcinarenes: Synthesis, Properties and Applications;* Wiley VCH: Weinheim, Germany, 2009.
3. Böhmer, V. *Angew. Chem., Int. Ed. Engl.* **1995,** *34,* 713–745. doi:10.1002/anie.199507131
4. Brodesser, G.; Vögtle, F. *J. Incl. Phenom. Mol. Recognit. Chem.* **1994,** *19,* 111–135. doi:10.1007/BF00708978

5. Gutsche, C. D.; Bauer, L. J. *J. Am. Chem. Soc.* **1985,** *107,* 6052–6059. doi:10.1021/ja00307a038
6. Cragg, P. J. Homocalixarenes. In *Encyclopedia of Supramolecular Chemistry;* Atwood, J. L.; Steel, J. W., Eds.; Marcel Dekker: New York, 2004; pp 649–657.
7. Späth, A.; König, B. *Beilstein J. Org. Chem.* **2010,** *6,* No. 32. doi:10.3762/bjoc.6.32
8. Yamato, D. J. *J. Inclusion Phenom. Mol. Recognit. Chem.* **1998,** *32,* 195–207. doi:10.1023/A:1008011410507
9. Shokova, E. A.; Kovalev, V. V. *Russ. J. Org. Chem.* **2004,** *40,* 607–643. doi:10.1023/B:RUJO.0000043707.97314.52
10. Shokova, E. A.; Kovalev, V. V. *Russ. J. Org. Chem.* **2004,** *40,* 1547–1578. doi:10.1007/s11178-005-0062-9
11. Hultzsch, K. *Kunststoffe* **1962,** *52,* 19–24.
12. Masci, B.; Finelli, M.; Varrone, M. *Chem.–Eur. J.* **1998,** *4,* 2018–2030. doi:10.1002/(SICI)1521-3765(19981002)4:10<2018::AID-CHEM2018>3.0.CO;2-I
13. Mukoyama, Y.; Tanno, T. *Org. Coat. Plast. Chem.* **1979,** *40,* 894–897.
14. Dhawan, D.; Gutsche, C. D. *J. Org. Chem.* **1983,** *48,* 1536–1539. doi:10.1021/jo00157a033
15. Hampton, P. D.; Bencze, Z.; Tong, W.; Daitch, C. E. *J. Org. Chem.* **1994,** *59,* 4838–4843. doi:10.1021/jo00096a026
16. Zerr, P.; Mussrabi, M.; Vicens, J. *Tetrahedron Lett.* **1991,** *32,* 1879–1880. doi:10.1016/S0040-4039(00)85986-9
17. Suzuki, K.; Minami, H.; Yamagata, Y.; Fuji, S.; Tomita, K.-I.; Asfari, Z.; Vicens, J. *Acta Crystallogr., Sect. C: Cryst. Struct. Commun.* **1992,** *48,* 350–352. doi:10.1107/S0108270191010399
18. Miah, M.; Romanov, N. N.; Cragg, P. J. *J. Org. Chem.* **2002,** *67,* 3124–3126. doi:10.1021/jo025597a
19. Tsubaki, K.; Otsubo, T.; Tanaka, K.; Fuji, K.; Kinoshita, T. *J. Org. Chem.* **1998,** *63,* 3260–3265. doi:10.1021/jo971945a
20. Ashram, M.; Mizyed, S.; Georghiou, P. E. *J. Org. Chem.* **2001,** *66,* 1473–1479. doi:10.1021/jo001518o
21. Tsubaki, K.; Morimoto, T.; Otsubo, T.; Kinoshita, T.; Fuji, K. *J. Org. Chem.* **2001,** *66,* 4083–4086. doi:10.1021/jo0100502
22. Komatsu, N. *Tetrahedron Lett.* **2001,** *42,* 1733–1736. doi:10.1016/S0040-4039(00)02336-4
23. Mizyed, S.; Ashram, M.; Miller, D. O.; Georghiou, P. E. *J. Chem. Soc., Perkin Trans. 2* **2001,** 1916–1919. doi:10.1039/B105019M
24. Araki, K.; Inada, K.; Otsuka, H.; Shinkai, S. *Tetrahedron* **1993,** *49,* 9465–9478. doi:10.1016/S0040-4020(01)80216-7
25. Matsumoto, H.; Nishio, S.; Takeshita, M.; Shinkai, S. *Tetrahedron* **1995,** *51,* 4647–4654. doi:10.1016/0040-4020(95)00165-5
26. Cragg, P. J.; Drew, M. G. B.; Steed, J. W. *Supramol. Chem.* **1999,** *11,* 5–15. doi:10.1080/10610279908048711
27. Yamato, T.; Haraguchi, H.; Nishikawa, J.-I.; Ide, S.; Tsuzuki, H. *Can. J. Chem.* **1998,** *76,* 989–996. doi:10.1139/v98-102
28. Yamato, T.; Zhang, F.; Sato, T.; Ide, S. *J. Chem. Res., Synop.* **2000,** 10–12. doi:10.3184/030823400103165707
29. Araki, K.; Hashimoto, N.; Otsuka, H.; Shinkai, S. *J. Org. Chem.* **1993,** *58,* 5958–5963. doi:10.1021/jo00074a021
30. Ashram, M.; Mizyed, S.; Georghiou, P. E. *Org. Biomol. Chem.* **2003,** *1,* 599–603. doi:10.1039/b209046p
31. Takeshita, M.; Inokuchi, F.; Shinkai, S. *Tetrahedron Lett.* **1995,** *36,* 3341–3344. doi:10.1016/0040-4039(95)00536-L
32. Khrifi, S.; Guelzim, A.; Baert, F.; Mussrabi, M.; Asfari, Z.; Vicens, J. *Acta Crystallogr., Sect. C: Cryst. Struct. Commun.* **1995,** *51,* 153–157. doi:10.1107/S0108270194008036
33. Yamato, T.; Zhang, F.; Tsuzuki, H.; Miura, Y. *Eur. J. Org. Chem.* **2001,** 1069–1075. doi:10.1002/1099-0690(200103)2001:6<1069::AID-EJOC1069>3.0.CO;2-R
34. Yamato, T.; Zhang, F. L. *J. Inclusion Phenom. Macrocyclic Chem.* **2001,** *39,* 55–64. doi:10.1023/A:1008196612553
35. Takimoto, M.; Ni, X.-L.; Rahman, S.; Xi, Z.; Yamato, T. *J. Inclusion Phenom. Macrocyclic Chem.* **2011,** *70,* 69–80. doi:10.1007/s10847-010-9863-8
36. Ni, X.-L.; Rahman, S.; Zeng, X.; Hughes, D. L.; Redshaw, C.; Yamato, T. *Org. Biomol. Chem.* **2011,** *9,* 6535–6541. doi:10.1039/c1ob05564j
37. Yamato, T.; Rahman, S.; Zeng, X.; Kitajima, F.; Gil, J. T. *Can. J. Chem.* **2006,** *84,* 58–64. doi:10.1139/v05-260
38. Ohkanda, J.; Shibui, H. *Chem. Commun.* **1998,** 375–376. doi:10.1039/a706869g
39. Marcos, P. M.; Ascenso, J. R.; Segurado, M. A. P.; Bernardino, R. J.; Cragg, P. J. *Tetrahedron* **2009,** *65,* 496–503. doi:10.1016/j.tet.2008.11.005
40. Dieleman, C. B.; Matt, D.; Neda, I.; Schmutzler, R.; Harriman, A.; Yaftian, R. *Chem. Commun.* **1999,** 1911–1912. doi:10.1039/a905677g
41. Hampton, P. D.; Daitch, C. E.; Duesler, E. N. *New J. Chem.* **1996,** *20,* 427–432.
42. Casnati, A.; Pochini, A.; Ungaro, R.; Ugozzoli, F.; Arnaud, F.; Fanni, S.; Schwing, M.-J.; Egberink, R. J. M.; de Jong, F.; Reinhoudt, D. N. *J. Am. Chem. Soc.* **1995,** *117,* 2767–2777. doi:10.1021/ja00115a012
43. Liu, S.-L.; Gong, S.-L.; Chen, Y.-Y. *Chin. J. Chem.* **2005,** *23,* 1651–1654. doi:10.1002/cjoc.200591651
44. Liu, S.-L.; Gong, S.-L.; Zheng, Q.; Chen, Y.-Y.; Wu, X.-J. *J. Chem. Res., Synop.* **2005,** 126–129. doi:10.3184/0308234054497218
45. Tsubaki, K.; Otsubo, T.; Kinoshita, T.; Kawada, M.; Fuji, K. *Chem. Pharm. Bull.* **2001,** *49,* 507–509. doi:10.1248/cpb.49.507
46. Tsubaki, K.; Otsubo, T.; Morimoto, T.; Maruoka, H.; Furukawa, M.; Momose, Y.; Shang, M.; Fuji, K. *J. Org. Chem.* **2002,** *67,* 8151–8156. doi:10.1021/jo026152p
47. Zhong, Z.; Ikeda, A.; Shinkai, S. *J. Am. Chem. Soc.* **1999,** *121,* 11906–11907. doi:10.1021/ja9925002
48. Miah, M.; Pavey, K. D.; Gun'ko, V. M.; Sheehan, R.; Cragg, P. J. *Supramol. Chem.* **2004,** *16,* 185–192. doi:10.1080/10610270310001644473
49. Hinrichs, M.; Hofbauer, F. R.; Klüfers, P.; Suhanji, M. *Inorg. Chem.* **2006,** *45,* 6688–6693. doi:10.1021/ic0603048
50. Kawaguchi, M.; Ikeda, A.; Shinkai, S. *Tetrahedron Lett.* **2001,** *42,* 3725–3728. doi:10.1016/S0040-4039(01)00463-4
51. Araki, K.; Hayashida, H. *Tetrahedron Lett.* **2000,** *41,* 1807–1810. doi:10.1016/S0040-4039(00)00034-4
52. Ikeda, A.; Yoshimura, M.; Tani, F.; Naruta, Y.; Shinkai, S. *Chem. Lett.* **1998,** *27,* 587–588. doi:10.1246/cl.1998.587
53. Ikeda, A.; Udzu, H.; Zhong, Z.; Shinkai, S.; Sakamoto, S.; Yamaguchi, K. *J. Am. Chem. Soc.* **2001,** *123,* 3872–3877. doi:10.1021/ja003269r
54. Masci, B. *Tetrahedron* **1995,** *51,* 5459–5464. doi:10.1016/0040-4020(95)00207-O
55. Hampton, P. D.; Daitch, C. E.; Alam, T. M.; Bencze, Z.; Rosay, M. *Inorg. Chem.* **1994,** *33,* 4750–4758. doi:10.1021/ic00099a028
56. Hampton, P. D.; Daitch, C. E.; Alam, T. M.; Pruss, E. A. *Inorg. Chem.* **1997,** *36,* 2879–2883. doi:10.1021/ic9611195

57. Redshaw, C.; Rowan, M. A.; Warford, L.; Homden, D. M.; Arbaoui, A.; Elsegood, M. R. J.; Dale, S. D.; Yamato, T.; Peréz Casas, C.; Matsui, S.; Matsuura, S. *Chem.–Eur. J.* **2007,** *13,* 1090–1107. doi:10.1002/chem.200600679
58. Notestein, J. M.; Andrini, L. R.; Kalchenko, V. I.; Requejo, F. G.; Katz, A.; Iglesia, E. *J. Am. Chem. Soc.* **2007,** *129,* 1122–1131. doi:10.1021/ja065830c
59. Hampton, P. D.; Daitch, C. E.; Duesler, E. N. *Inorg. Chem.* **1995,** *34,* 5641–5645. doi:10.1021/ic00126a038
60. Daitch, C. E.; Hampton, P. D.; Duesler, E. N.; Alam, T. M. *J. Am. Chem. Soc.* **1996,** *118,* 7769–7773. doi:10.1021/ja9605984
61. Hampton, P. D.; Daitch, C. E.; Shachter, A. M. *Inorg. Chem.* **1997,** *36,* 2956–2959. doi:10.1021/ic961445k
62. Thuéry, P.; Nierlich, M.; Masci, B.; Asfari, Z.; Vicens, J. *J. Chem. Soc., Dalton Trans.* **1999,** 3151–3152.
63. Masci, B.; Nierlich, M.; Thuéry, P. *New J. Chem.* **2002,** *26,* 120–128. doi:10.1039/b108947c
64. Masci, B.; Nierlich, M.; Thuéry, P. *New J. Chem.* **2002,** *26,* 766–774. doi:10.1039/b200734g
65. Araki, K.; Inada, K.; Shinkai, S. *Angew. Chem., Int. Ed. Engl.* **1996,** *35,* 72–74. doi:10.1002/anie.199600721
66. Tsubaki, K.; Morimoto, T.; Otsubo, T.; Fuji, K. *Org. Lett.* **2002,** *4,* 2301–2304. doi:10.1021/ol026019j
67. Marcos, P. M.; Ascenso, J. R.; Cragg, P. J. *Supramol. Chem.* **2007,** *19,* 199–206. doi:10.1080/10610270601026594
68. Marcos, P. M. et al., manuscript in preparation.
69. Cragg, P. J.; Miah, M.; Steed, J. W. *Supramol. Chem.* **2002,** *14,* 75–78. doi:10.1080/10610270290006592
70. Marcos, P. M.; Ascenso, J. R.; Segurado, M. A. P.; Cragg, P. J.; Michel, S.; Hubscher-Bruder, V.; Arnaud-Neu, F. *Supramol. Chem.* **2011,** *23,* 93–101. doi:10.1080/10610278.2010.510562
71. Arnaud-Neu, F.; Cremin, S.; Harris, S.; McKervey, M. A.; Schwing-Weill, M.-J.; Schwinté, P.; Walker, A. *J. Chem. Soc., Dalton Trans.* **1997,** 329–334. doi:10.1039/A602631A
72. Atwood, J. L.; Koutsantonis, G. A.; Raston, C. L. *Nature* **1994,** *368,* 229–231. doi:10.1038/368229a0
73. Suzuki, T.; Nakashima, K.; Shinkai, S. *Chem. Lett.* **1994,** *23,* 699–702. doi:10.1246/cl.1994.699
74. Ikeda, A.; Yoshimura, M.; Shinkai, S. *Tetrahedron Lett.* **1997,** *38,* 2107–2110. doi:10.1016/S0040-4039(97)00318-3
75. Ikeda, A.; Suzuki, Y.; Yoshimura, M.; Shinkai, S. *Tetrahedron* **1998,** *54,* 2497–2508. doi:10.1016/S0040-4020(98)00012-X
76. Tsubaki, K.; Tanaka, K.; Kinoshita, T.; Fuji, K. *Chem. Commun.* **1998,** 895–896. doi:10.1039/a800078f
77. Georghiou, P. E.; Tran, A. H.; Stroud, S. S.; Thompson, D. W. *Tetrahedron* **2006,** *62,* 2036–2044. doi:10.1016/j.tet.2005.09.151
78. Tsubaki, K.; Murata, Y.; Komatsu, K.; Kinoshita, T.; Fuji, K. *Heterocycles* **1999,** *51,* 2553–2556. doi:10.3987/COM-99-8650
79. Atwood, J. L.; Barbour, L. J.; Nichols, P. J.; Raston, C. L.; Sandoval, C. A. *Chem.–Eur. J.* **1999,** *5,* 990–996. doi:10.1002/(SICI)1521-3765(19990301)5:3<990::AID-CHEM990>3.0.CO;2-4
80. Komatsu, N. *Org. Biomol. Chem.* **2003,** *1,* 204–209. doi:10.1039/b208107e
81. Ikeda, A.; Hanato, T.; Kawaguchi, M.; Suenaga, H.; Shinkai, S. *Chem. Commun.* **1999,** 1403–1404. doi:10.1039/a903872h
82. Ikeda, A.; Ejima, A.; Nishiguchi, K.; Kikuchi, J.-i.; Matsumoto, T.; Hatano, T.; Shinkai, S.; Goto, M. *Chem. Lett.* **2005,** *34,* 308–309. doi:10.1246/cl.2005.308
83. Hatano, T.; Ikeda, A.; Akiyama, T.; Yamada, S.; Sano, M.; Kanekiyo, Y.; Shinkai, S. *J. Chem. Soc., Perkin Trans. 2* **2000,** 909–912. doi:10.1039/b000022l
84. Ikeda, A.; Hanato, T.; Shinkai, S.; Akiyama, T.; Yamada, S. *J. Am. Chem. Soc.* **2001,** *123,* 4855–4856. doi:10.1021/ja015596k
85. Islam, S. D.-M.; Fujitsuka, M.; Ito, O.; Ikeda, A.; Hanato, T.; Shinkai, S. *Chem. Lett.* **2000,** *29,* 78–79. doi:10.1246/cl.2000.78
86. Ikeda, A.; Sonoda, K.; Shinkai, S. *Chem. Lett.* **2000,** *29,* 1220–1221. doi:10.1246/cl.2000.1220
87. Ikeda, A.; Nobukuni, S.; Udzu, H.; Zhong, Z.; Shinkai, S. *Eur. J. Org. Chem.* **2000,** 3287–3293. doi:10.1002/1099-0690(200010)2000:19<3287::AID-EJOC3287>3.0.CO;2-R
88. Takeshita, M.; Shinkai, S. *Chem. Lett.* **1994,** *23,* 125–128. doi:10.1246/cl.1994.125
89. Ni, X.-L.; Wang, S.; Zeng, X.; Tao, Z.; Yamato, T. *Org. Lett.* **2011,** *13,* 552–555. doi:10.1021/ol102914t
90. Ni, X.-L.; Zeng, X.; Redshaw, C.; Yamato, T. *J. Org. Chem.* **2011,** *76,* 5696–5702. doi:10.1021/jo2007303
91. Wu, C.; Zhang, W.-J.; Zeng, X.; Mu, L.; Xue, S.-F.; Tao, Z.; Yamato, T. *J. Inclusion Phenom. Macrocyclic Chem.* **2010,** *66,* 125–131. doi:10.1007/s10847-009-9665-z
92. Kang, J.-M.; Cheong, N.-Y. *Bull. Korean Chem. Soc.* **2002,** *23,* 995–997. doi:10.5012/bkcs.2002.23.7.995
93. Odashima, K.; Yagi, K.; Tohda, K.; Umezawa, Y. *Bioorg. Med. Chem. Lett.* **1999,** *9,* 2375–2378. doi:10.1016/S0960-894X(99)00395-9
94. Herzog, G.; McMahon, B.; Lefoix, M.; Mullins, N. D.; Collins, C. J.; Moynihan, H. A.; Arrigan, D. W. M. *J. Electroanal. Chem.* **2008,** *622,* 109–114. doi:10.1016/j.jelechem.2008.05.006
95. Yaftian, M. R.; Parinejad, M.; Matt, D. *J. Chin. Chem. Soc.* **2007,** *54,* 1535–1542.
96. Bocheńska, M.; Cragg, P. J.; Guziński, M.; Jasiński, A.; Kulesza, J.; Marcos, P. M.; Pomećko, R. *Supramol. Chem.* **2009,** *21,* 732–737. doi:10.1080/10610270902853043
97. Cragg, P. J.; Allen, M. C.; Steed, J. W. *Chem. Commun.* **1999,** 553–554. doi:10.1039/a808492k

License and Terms

Beilstein Journal of Organic Chemistry

Synthesis of multivalent host and guest molecules for the construction of multithreaded diamide pseudorotaxanes

Nora L. Löw[‡1], Egor V. Dzyuba[‡1], Boris Brusilowskij[‡1], Lena Kaufmann[1], Elisa Franzmann[2], Wolfgang Maison[2], Emily Brandt[3,4], Daniel Aicher[3,5], Arno Wiehe[1,3] and Christoph A. Schalley[*1]

Full Research Paper

Open Access

Address:
[1]Institut für Chemie und Biochemie der Freien Universität Berlin, Takustr. 3, 14195 Berlin, Germany, [2]Pharmazeutische und Medizinische Chemie, Universität Hamburg, Bundesstr. 45, 20146 Hamburg, Germany, [3]Biolitec research GmbH, Otto-Schott-Str. 15, 07745 Jena, Germany, [4]Charité – Universitätsmedizin, International Graduate Program Medical Neurosciences, Charitéplatz 1, 10117 Berlin, Germany and [5]WITEGA Laboratorien Berlin-Adlershof GmbH, Magnusstr. 11, 12489 Berlin, Germany

Email:
Christoph A. Schalley[*] - christoph@schalley-lab.de

* Corresponding author ‡ Equal contributors

Keywords:
multivalency; pseudorotaxanes; Sonogashira coupling; supramolecular chemistry; tetralactam macrocycles

Beilstein J. Org. Chem. **2012,** *8,* 234–245.
doi:10.3762/bjoc.8.24

Received: 21 November 2011
Accepted: 23 January 2012
Published: 09 February 2012

This article is part of the Thematic Series "Supramolecular chemistry II".

Associate Editor: N. Sewald

Abstract

A series of di-, tri- and tetravalent axles and wheels for the synthesis of pseudorotaxanes bearing the tetralactam macrocycle/diamide axle binding motif was prepared. Starting from iodinated monovalent precursors, Sonogashira cross-coupling reactions were utilized to couple the binding sites to appropriate spacer groups. Through this “Lego” or “toolbox” approach, the convergent synthesis of host and guests with a well-defined number of the binding sites is possible. In addition, the spatial arrangement of the binding sites can be controlled through the quite rigid connections between linker and binding sites. Although a quantitative assessment of binding strengths was not possible by NMR titration experiments, typical and significant shifts of the signals of the diamide moiety indicate qualitatively the formation of pseudorotaxanes from the axle and wheel precursors.

Introduction

Synthetic supramolecular complexes have the great potential to put those concepts to the test that govern much of the noncovalent chemistry in nature. Among these concepts are not only molecular recognition and the noncovalent bonds themselves, but also self-assembly, self-sorting, templation and multivalent binding [1-8]. Consequently, the reductionist investigation of synthetic supramolecules can help us to understand biological systems better. Such a synthetic approach can also help in the

investigation of multivalent binding [9-12], because the number of binding sites can be altered at will, and studies can be done with a suitable series of host and guest molecules in which the nature and number of binding sites is systematically varied.

Interlocked molecules [13-28] are interesting not only because of their particular topology or the mechanical bond, but also as they have been intensely investigated with respect to the construction of molecular machines [29-32]. The mechanical bond appears particularly suited for this goal, because it connects the axle and wheel strongly, but leaves freedom for the relative movement of the two components. Pseudorotaxanes are the precursors for both rotaxane syntheses by stoppering reactions or catenanes by macrocyclization. The use of weak interactions, e.g., metal complexation [33-47], charge-transfer interactions [48-63], or hydrogen bonding [64-79], between the single building blocks is necessary for efficient templating effects, which aim at assembling higher-order molecular architectures. The synthesis of a multiply threaded architecture [80,81] thus requires multivalent wheel and axle components as precursors, which are also interesting with respect to their binding properties. Among the examples of such multivalent pseudorotaxanes [80-82], the “molecular elevators” reported by Stoddart et al. [83,84] are particularly fascinating, because they combine multivalency with the ability of a molecular device to respond to external stimuli, in this case to acids and bases, which induce motion of the wheel and axle components relative to each other.

Tetralactam macrocycles (TLMs) [65,66] have widely been used in the synthesis of amide catenanes and rotaxanes [85-92] and represent excellent hosts for dicarbonyl compounds [93-101]. They bear four converging amide groups, which in each case can form hydrogen bonds to suitable axle molecules in aprotic and not too strongly competitive solvents such as CH_2Cl_2 or $CHCl_3$. In this contribution, we report the synthesis and binding behaviour of di-, tri- and tetravalent diamide-axle–TLM complexes. The design is based on the two building blocks **1** and **2** (Figure 1). Compound **1** is the wheel component, and **2** is the axle, which comprises a diamide moiety that binds to the wheel as indicated in the center of Figure 1 through the formation of four (wheel)N–H···O=C(axle) hydrogen bonds.

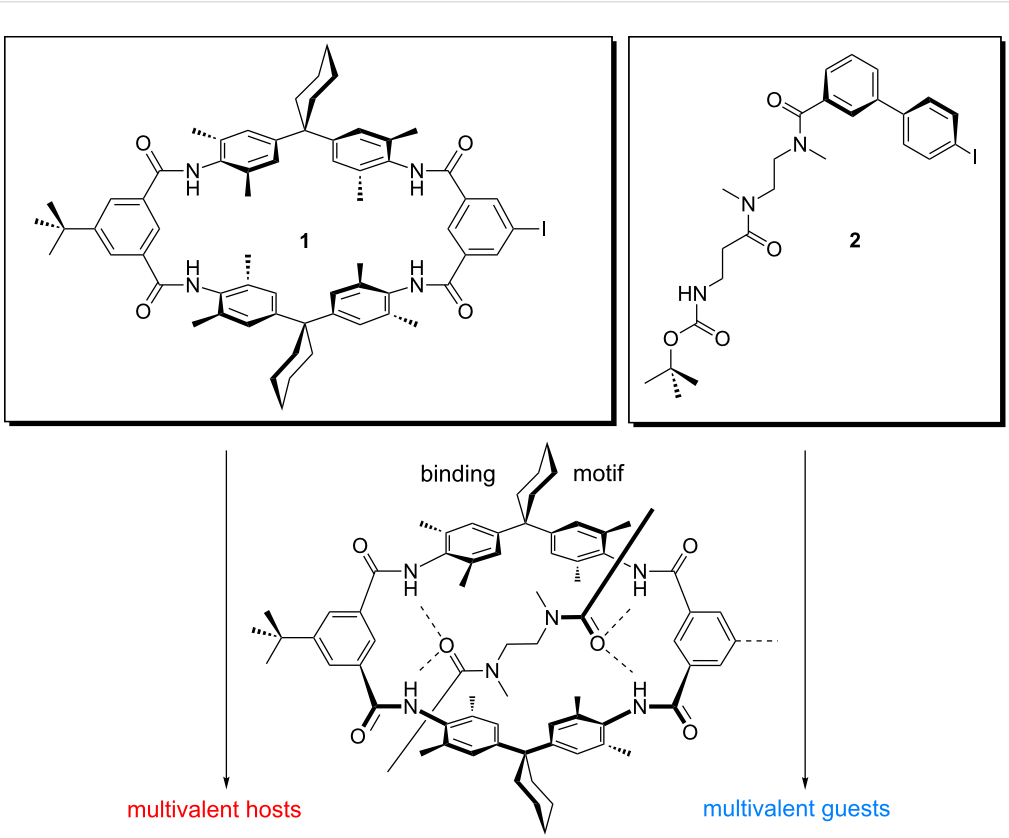

Figure 1: Hunter/Vögtle-type tetralactam macrocycle **1** bearing an iodo substituent at one of the isophthaloyl groups, and the diamide axle piece **2**. The iodoaryl groups in both building blocks are suitable for Sonogashira cross-coupling reactions. Therefore, these monovalent precursors can be connected to different suitable spacers so that a "toolbox" of multivalent hosts and guests can be synthesized convergently. The center shows the binding motif, which connects the axle and wheel by four N–H···O hydrogen bonds.

Through the iodine substituents, both building blocks can be connected to appropriate spacers in Sonogashira cross-coupling reactions [102].

This coupling strategy creates rather rigid connections to the spacers and helps in reducing the entropic penalties that arise from conformational fixing of the spacers upon multivalent binding. The building blocks were chosen based on simple force-field calculations of the resulting pseudorotaxanes and permit us to synthesize a series of different hosts and guests in a convergent way. Thus, a "toolbox" [103,104] of multivalent host and guest molecules becomes available with this synthetic strategy. In the future, the pseudorotaxanes designed here should be easily converted into rotaxanes after cleavage of the Boc protective group at the axle ends and attachment of stopper groups to the terminal amines.

Results and Discussion

Synthesis of monovalent precursors

Although aryl bromides, triflates and sometimes even chlorides react efficiently in Sonogashira cross-coupling reactions, our previous studies [103,104] showed that only the iodinated TLM, and in some rare cases the corresponding triflate-substituted wheel, is reactive enough to provide sufficiently high yields. This is particularly important when the same precursor is to be multiply connected to the same spacer. Low-yielding reaction steps would result in mixtures of the desired compounds with incompletely substituted side products. Therefore, iodo-substituted TLM **1** was prepared according to well-documented literature procedures [64-103] and used for the cross-coupling reactions in this study.

The synthesis of the iodo-substituted monovalent diamide axle centerpiece **2** was realized by the four-step synthesis shown in Scheme 1. The free amino group in mono-Cbz-protected *N*,*N*'-dimethylethylene diamine **3** [105] was elongated with the commercially available *N*-Boc-protected β-alanine **4** in the presence of EDC and HOBt as activating coupling reagents. This step provides the basis for future stopper attachment to the axle termini, as mentioned above. Product **5** was formed with a yield of 92% without the need for time-consuming purification steps. This molecule now contains two orthogonal protecting groups, and hydrogenation of **5** deprotects the amino group at the *N*,*N*'-dimethylethylene diamine site to yield **6** in 98% yield. The iodo-substituted acid **8** can easily be prepared under mild conditions from the iodine-free precursor **7** [106] by using I_2 and phenyliodine diacetate (PIDA) and is then available for amide coupling with **6** yielding binding site **2** in 73% yield. Since an excess of **7** was used and the 2'/6'-positions are sterically hindered, only monoiodination in the 4'-position was observed. This synthetic pathway thus gives reasonable overall yields.

It should be mentioned that the diamide moiety bears two tertiary amides. All attempts to prepare a similar axle with secondary amide groups failed because of the low solubility of the

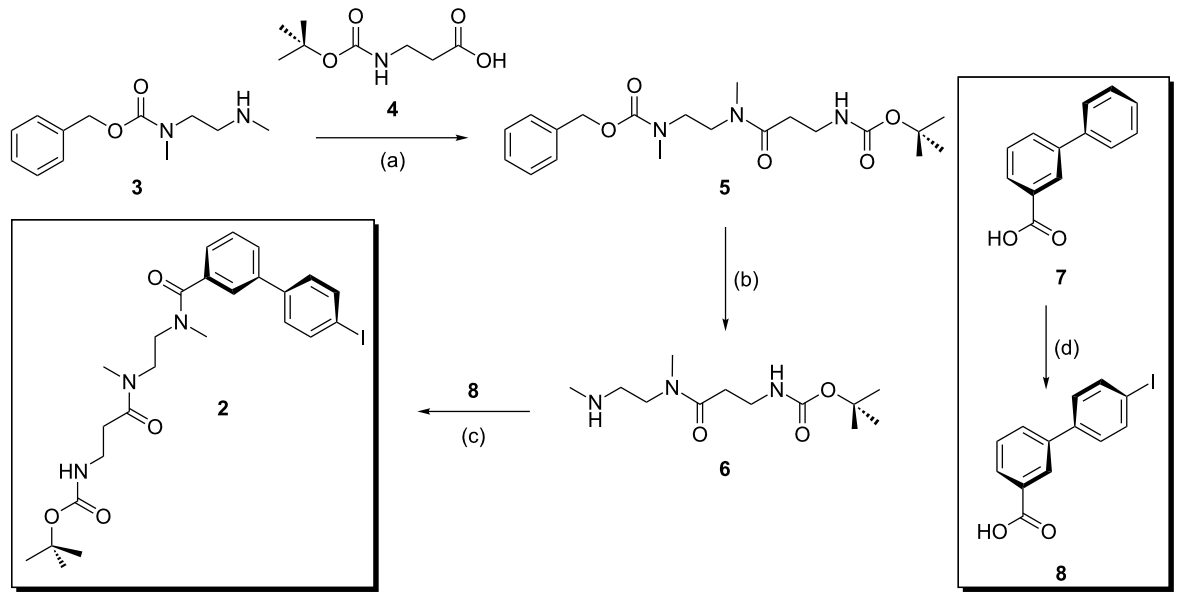

Scheme 1: Synthesis of the monovalent diamide axle **2**, which was used for Sonogashira coupling to the appropriate spacers: (a) EDC, HOBt, DMF, 22 h, 92%; (b) H_2, Pd/C, EtOH, 3 d, 98%; (c) EDC·HCl, HOBt, DMF, 24 h, 73%; (d) I_2, PIDA, AcOH/Ac_2O, 1 h, 67%; (EDC = 1-ethyl-3-(3-dimethylaminopropyl)carbodiimide, HOBt = 1-hydroxybenzotriazole, DMF = *N*,*N*'-dimethylformamide, PIDA = phenyliodine diacetate).

products. This is an important aspect, because the threading of the station into the TLMs requires noncompetitive solvents such as CH_2Cl_2 or $CHCl_3$. Consequently, any polar aprotic solvent, such as acetone, acetonitrile, DMF or DMSO, which would solubilize the axles sufficiently well, would interfere strongly with pseudorotaxane formation. The tertiary amides are much more soluble and, therefore, appear to be the more appropriate binding site. However, the better solubility comes at a price. While secondary amides prefer the *trans*-conformation, in which the carbonyl oxygen and the NH proton diverge, the tertiary amides do not exhibit a similarly strong preference for one of the conformations. The axle binding sites thus exist in equilibrium between (*trans*,*trans*)-, (*trans*,*cis*)- and (*cis*,*cis*)-isomers in solution, which complicates the analysis of the binding properties.

Synthesis of multivalent wheels

Monovalent axle **2** and TLM **1** are designed to give a good complementary fit, when both are connected to the same flat spacer molecules through Sonogashira cross-coupling reactions. Therefore, ethynyl-substituted benzene spacers **9**, **11** and **13** were used to synthesize a bent divalent (**10**), a linear divalent (**12**), and a trivalent wheel (**14**) [103] (Scheme 2 and Scheme 3). From the enormously broad choice of different

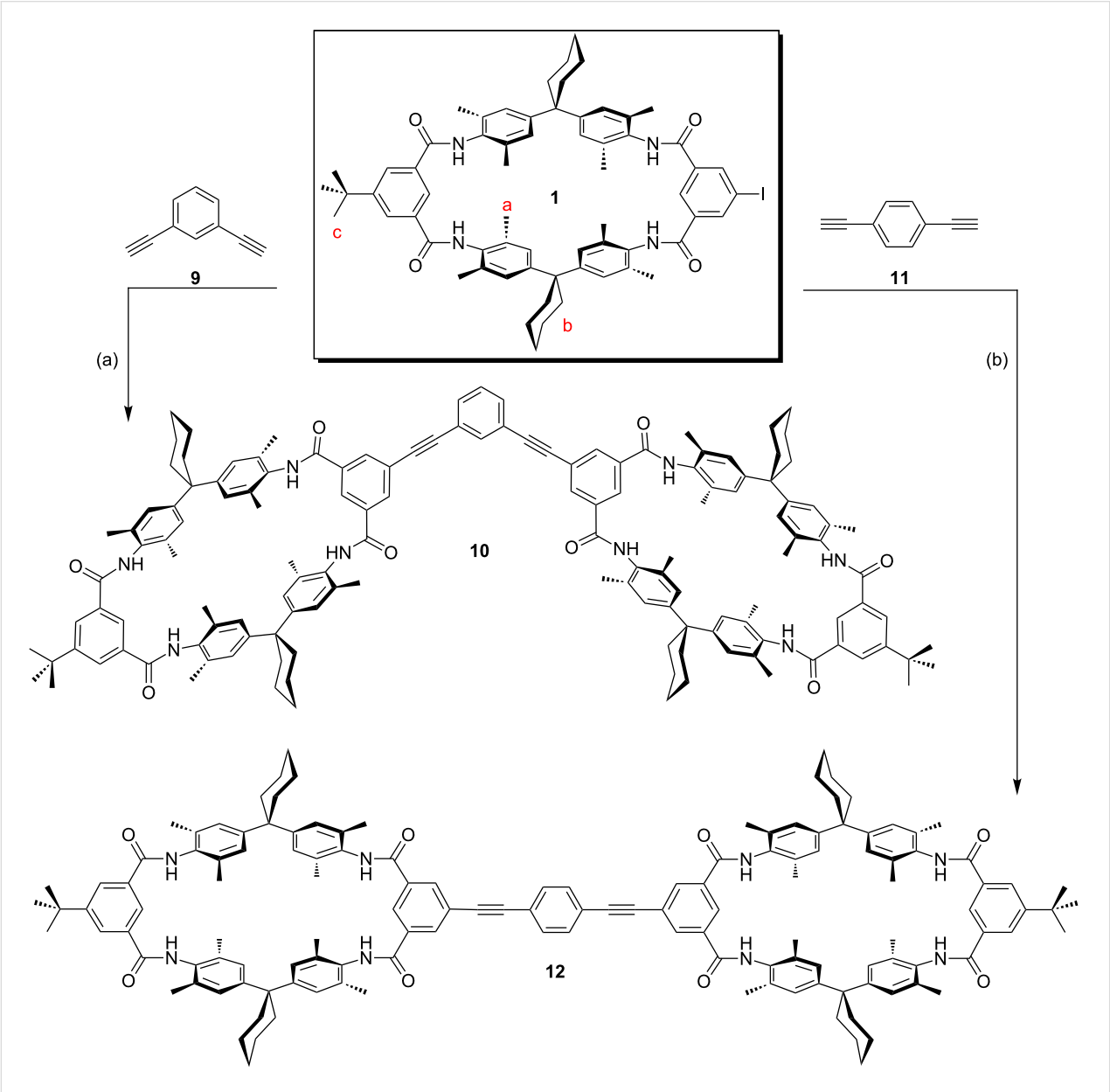

Scheme 2: Synthesis of divalent wheels from TLM **1**: (a), (b) $(Ph_3P)_2PdCl_2$, CuI, PPh_3, NEt_3, DMF, 25 °C, 24 h, 90% (**10**), 78% (**12**).

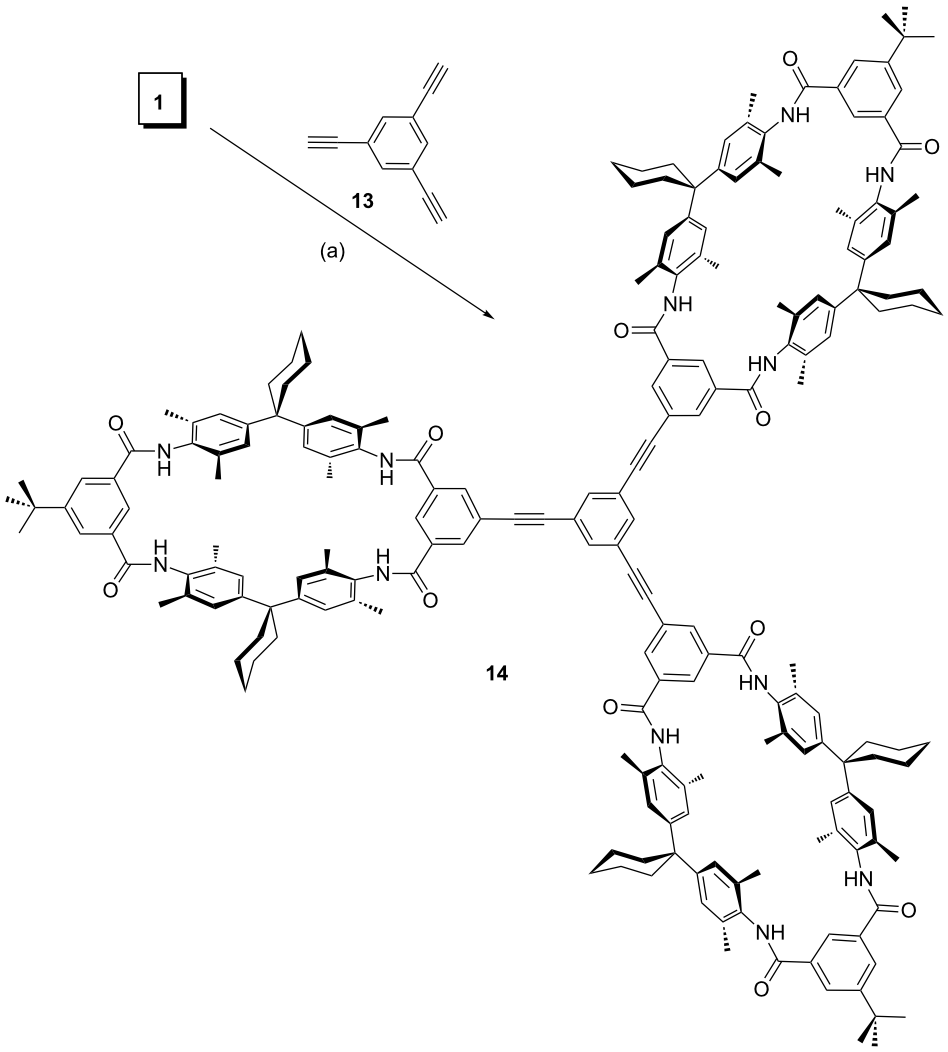

Scheme 3: Synthesis of trivalent wheel **14** from TLM **1**: (a) $(Ph_3P)_2PdCl_2$, CuI, PPh_3, NEt_3, DMF, 25 °C, 24 h, 40% (**14**). Compound **14** was described previously [103] and is included to complete the series.

Pd-catalysts and reaction conditions, we used $(Ph_3P)_2PdCl_2$ and CuI in the presence of PPh_3 as the coligand, NEt_3 as the base, and DMF as the solvent. This protocol was successfully applied previously for the synthesis of **14** [103]. The yields of 90% and 78% obtained for the divalent hosts **10** and **12**, respectively, were even higher than that for **14** (40%).

All attempts to use the same conditions for the fourfold coupling of **1** to **15** to synthesize tetravalent wheel **16** were unsuccessful, and we finally used another procedure for the cross-coupling reaction [107]. Because the Cu(I) catalyst may interfere with the Zn core of porphyrin **15** or lead to Glaser coupled side-reaction products, a copper-free Sonogashira procedure [107,108] employing $Pd_2(dba)_3$ as the catalyst and $AsPh_3$ as the coligand in NEt_3/DMF was applied (Scheme 4). This reaction unfortunately provided only 7% of the desired tetravalent wheel **16**; however, this amount sufficed for characterization by ^1H NMR and ESI mass spectrometry. There may be several reasons for this observation. One reason for the low yield may be solubility, which in our experience is always low for tetralactam wheels connected through nicely stacking spacers.

Synthesis of multivalent axles

In order to prepare the multivalent axles that fit to the wheels described above, the same spacers **9**, **11** and **13** were also used

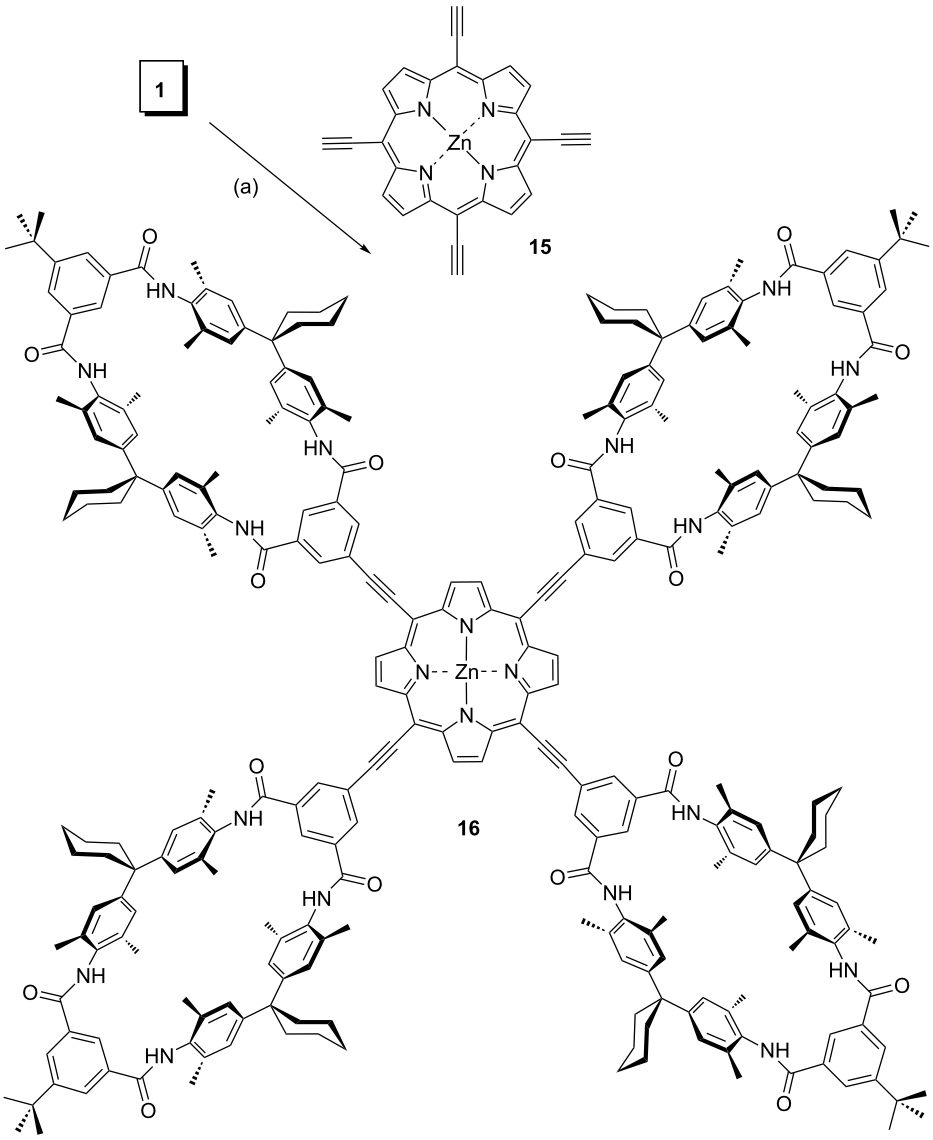

Scheme 4: (a) $Pd_2(dba)_3$, $AsPh_3$, NEt_3, DMF, 120 °C, 12 h, 7% (**16**).

for the synthesis of multivalent guests **17**–**19**, respectively (Scheme 5). In addition, a triethynyl-adamantane derivative **20** [109,110] was employed in order to prepare an axle component with a slightly different, nonflat spacer geometry.

For the axle preparation, neither the use of $(Ph_3P)_2PdCl_2$/CuI/PPh_3 nor that of $Pd_2(dba)_3$/$AsPh_3$ provided the desired products, and therefore the conditions of the Sonogashira cross-coupling reactions had to be optimized again. Finally, the mixture of $Pd_2(dba)_3$/CuI/PPh_3 gave the di- and tritopic axles **17**–**19** and **21** in DMF/NEt_3 with decent yields when the temperature was raised to 70 °C. The copper-free Sonogashira procedure was again applied for the synthesis of tetravalent guest **23** (Scheme 6) and yielded 17% of the product. Interestingly, a homocoupling of axle **2** gave rise to divalent axle **22**, which was isolated as a side product in 37% yield. This molecule may be useful for other divalent hosts, such as two macrocycles connected through a butadiyne spacer or a thiophene unit. Such hosts have been reported previously [103] and are not included here.

Formation of pseudorotaxanes

In order to determine the binding strengths quantitatively, NMR titrations, dilution experiments, and ITC experiments were attempted. The NMR titrations suffer from the fact that different conformations of the tertiary amide groups hamper an in-depth

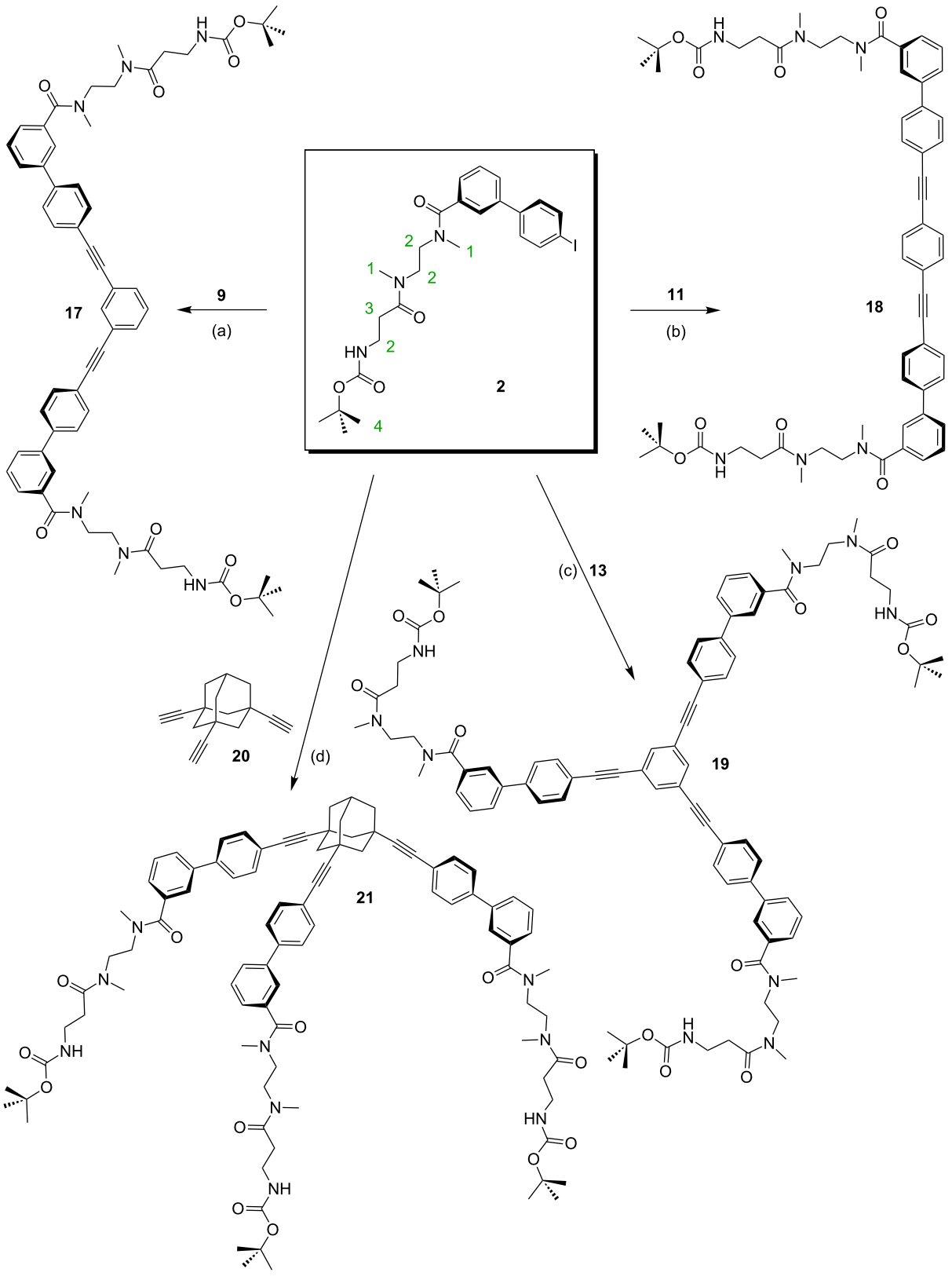

Scheme 5: Synthesis of a series of multivalent guests starting from the axle **2**. (a), (b), (c), (d): $Pd_2(dba)_3$, CuI, PPh_3, NEt_3, DMF, 70 °C, 3 d; 32% (**17**), 37% (**18**), 24% (**19**), 64% (**21**), respectively.

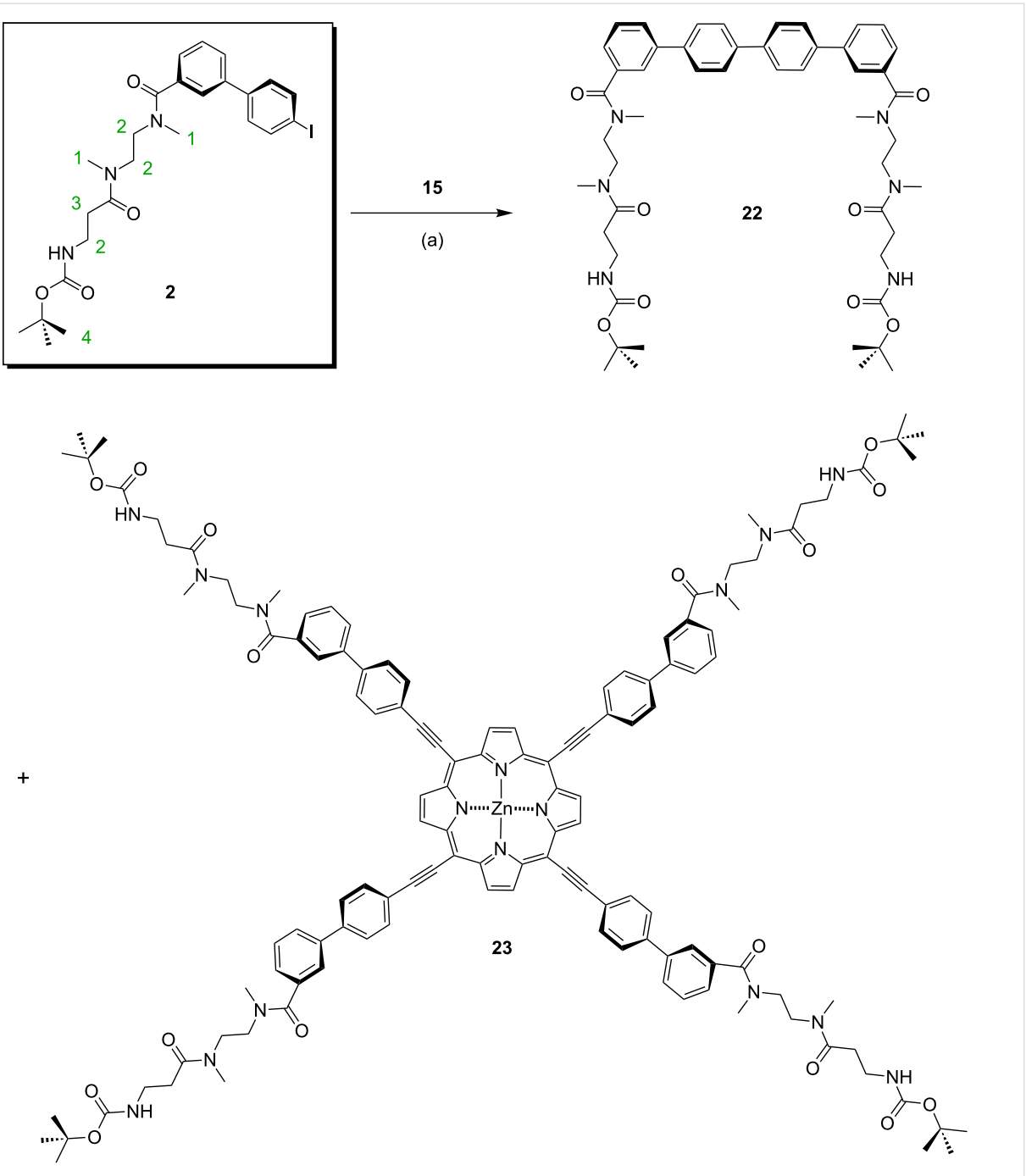

Scheme 6: Synthesis of the tetravalent axle **23** and its divalent side product: (a) $Pd_2(dba)_3$, $AsPh_3$, NEt_3, DMF, 80 °C, 2 d, 37% (**22**), 17% (**23**).

evaluation of the titration data. The diamide *N*-CH_3 and *N*-CH_2 protons appear with four sets of signals, one for the (*trans*,*trans*)-, two for the asymmetric (*trans*,*cis*)- and one for the (*cis*,*cis*)-isomer. This, and significant signal overlaps, make it impossible to quantify the NMR titration data. For ITC measurements, the concentration range in which one can expect reasonable heats to evolve upon binding could not be reached, due to the low solubility of the wheel components. Furthermore, mass spectrometry was attempted in order to show the formation of 1:1 complexes qualitatively, but this was without success. This does not come as a surprise in view of previous theoretical calculations on amide/tetralactam macrocycle complexes [111], which show that simple amide axles dethread in the gas phase because of a favourable entropy term arising from the increase in particle number upon complex dissociation. This entropic contribution overcompensates for the enthalpic

contribution to the binding. As the calculations were done for monovalent complexes and monoamide, we nevertheless attempted to ionize complexes of our di- and trivalent systems, but unfortunately without success.

However, when ^{1}H NMR spectra of the free axles are compared with the ^{1}H NMR spectra of 1:1 mixtures of axles and wheels, structure-indicative signal shifts are observed that demonstrate the axles to be threaded through the wheels (Figure 2). Consequently, the binding event cannot easily be quantified, but there is qualitative evidence for pseudorotaxane formation. With ^{1}H/^{1}H-COSY NMR experiments, an assignment of, for example, the *N*-CH_3 groups to two singlets at ca. 3.1 ppm is possible (protons labelled "1" in the spectra of **17**, **18** and **19** in Figure 2). These signals shift to higher field by ca. 0.9 ppm when 1 equiv of the wheel component is added. These complexation-induced signal shifts are even stronger than similar shifts observed for other rotaxanes with a diamide moiety [101]. The fact that proton "3" also shifts significantly indicates that binding may also involve the carbonyl group of the Boc protective group. A reversible shuttling between both the diamide station and the outer carbonyl group of that moiety and the Boc group would rationalize this shift easily. Consequently, this preliminary NMR evidence qualitatively provides evidence for binding, while a quantification is not easily possible.

Conclusion

In conclusion, the synthesis of a "toolbox" of multivalent host and guest molecules has been described, which can be obtained from the two easy-to-prepare building blocks **1** and **2** by Sonogashira coupling reactions to ethynyl-substituted spacers. This synthetic approach is convergent, and thus the sometimes limited yields do not detract from this approach. With our toolbox, the number and position of binding sites can be varied systematically; hence, the toolbox provides a means to examine multivalency. However, despite the fact that there is qualitative evidence for pseudorotaxane formation, the binding motif is not yet optimal for a quantitative study. Two problems need to be solved: On one hand, the solubility of the hosts needs to be increased such that a concentration range can be reached that enables us to obtain thermochemical data from ITC experiments. On the other hand, a more suitable binding moiety would be advantageous for use in the axles. The tertiary amides obscure a precise analysis of NMR titrations because of the interconverting *trans* and *cis* amide conformations. Secondary amides again cause solubility problems. However, as described in a recent article [112], diketopiperazines are quite tightly bound to the TLMs. Equipping our wheels with better solubilizing groups and using diketopiperazine axles should therefore help us to go beyond the limitations encountered in the present study.

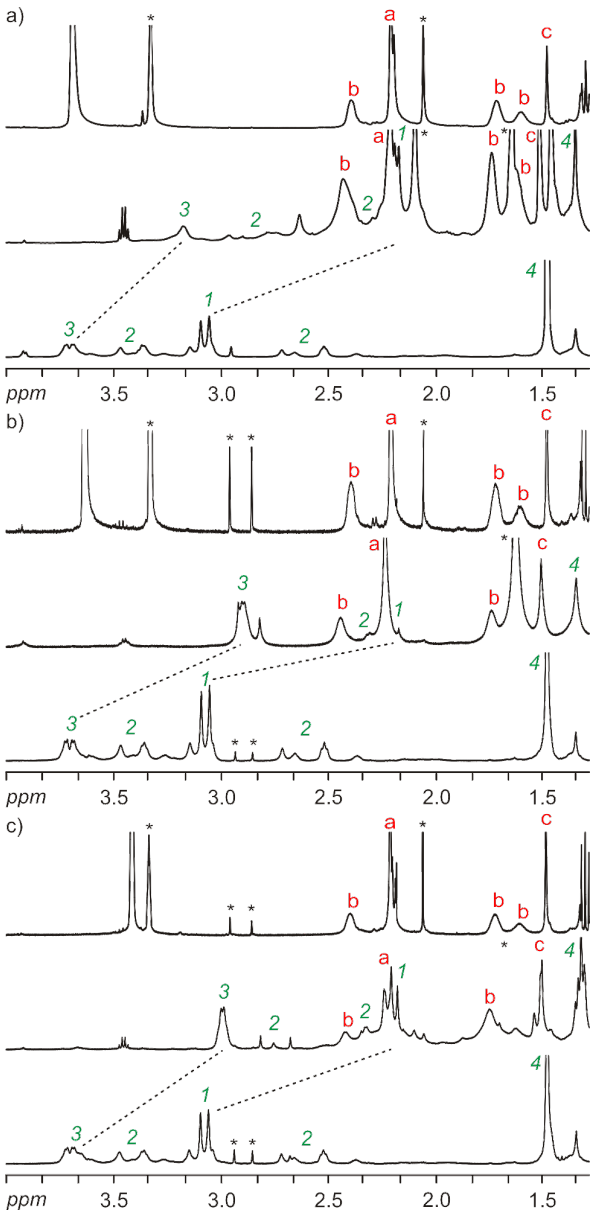

Figure 2: Aliphatic regions of the ^{1}H NMR spectra (CD_2Cl_2, 500 MHz, 298 K, 2.3 mM) of (a) **10** (top), **17@10** (center) and **17** (bottom), (b) **12** (top), **18@12** (center) and **18** (bottom), and (c) **14** (top), **19@14** (center) and **19** (bottom). Because of the low solubility of the wheel components **10**, **12** and **14**, the samples were dissolved in CD_2Cl_2/CD_3OD (10:1). Red letters assign signals of the wheels as shown in Scheme 2, green numbers those of the axles as shown in Scheme 5.

Supporting Information

Supporting Information File 1

Experimental details and characterization data.
[http://www.beilstein-journals.org/bjoc/content/supplementary/1860-5397-8-24-S1.pdf]

Acknowledgements

This research was funded by the Deutsche Forschungsgemeinschaft (SFB 765 "multivalency") and the Fonds der Chemischen Industrie (FCI). E.V.D. and L. K. thank the Studienstiftung des deutschen Volkes for a PhD scholarship. We thank Gülsah Ayvalik, B.Sc. for her help with the synthesis of starting materials and Dr. Andreas Schäfer for helpful comments on the interpretation of the NMR experiments.

References

1. Lehn, J.-M. *Supramolecular Chemistry - Concepts and Perspectives;* Wiley-VCH: Weinheim, Germany, 1995.
2. Sauvage, J.-P.; Dietrich-Buchecker, C. O., Eds. *Molecular Catenanes, Rotaxanes, and Knots;* Wiley-VCH: Weinheim, Germany, 1999.
3. Gerbeleu, N. V.; Arion, V. B.; Burgess, J. *Template Synthesis of Macrocyclic Compounds;* Wiley-VCH: Weinheim, Germany, 1999.
4. Diederich, F.; Stang, P. J., Eds. *Templated Organic Synthesis;* Wiley-VCH: Weinheim, Germany, 2000.
5. Steed, J. W.; Turner, D. R.; Wallace, K. *Core Concepts in Supramolecular Chemistry and Nanochemistry;* Wiley-VCH: Weinheim, Germany, 2007.
6. Diederich, F.; Stang, P. J.; Tykwinski, R. R., Eds. *Modern Supramolecular Chemistry: Strategies for Macrocycle Synthesis;* Wiley-VCH: Weinheim, Germany, 2008.
7. Atwood, J. L.; Steed, J. W. *Supramolecular Chemistry,* 2nd ed.; Wiley: Chichester, U.K., 2009.
8. Ariga, K.; Nalwa, H. S., Eds. *Bottom-up Nanofabrication: Supramolecules, Self-Assemblies, and Organized Films;* American Scientific Publishers: Valencia, USA, 2009.
9. Mammen, M.; Choi, S.-K.; Whitesides, G. M. *Angew. Chem.* **1998,** *110,* 2908–2953. doi:10.1002/(SICI)1521-3757(19981016)110:20<2908::AID-ANGE2908>3.0.CO;2-2
   Angew. Chem., Int. Ed. **1998,** *37,* 2754–2794. doi:10.1002/(SICI)1521-3773(19981102)37:20<2754::AID-ANIE2754>3.0.CO;2-3
10. Mulder, A.; Huskens, J.; Reinhoudt, D. N. *Org. Biomol. Chem.* **2004,** *2,* 3409–3424. doi:10.1039/b413971b
11. Kiessling, L. L.; Gestwicki, J. E.; Strong, L. E. *Angew. Chem.* **2006,** *118,* 2408–2429. doi:10.1002/ange.200502794
    Angew. Chem., Int. Ed. **2006,** *45,* 2348–2368. doi:10.1002/anie.200502794
12. Reczek, J. J.; Kennedy, A. A.; Halbert, B. T.; Urbach, A. R. *J. Am. Chem. Soc.* **2009,** *131,* 2408–2415. doi:10.1021/ja808936y
13. Sauvage, J.-P. *Acc. Chem. Res.* **1998,** *31,* 611–619. doi:10.1021/ar960263r
14. Blanco, M.-J.; Jiménez, M. C.; Chambron, J.-C.; Heitz, V.; Linke, M.; Sauvage, J.-P. *Chem. Soc. Rev.* **1999,** *28,* 293–305. doi:10.1039/a901205b
15. Balzani, V.; Credi, A.; Raymo, F. M.; Stoddart, J. F. *Angew. Chem.* **2000,** *112,* 3484–3530. doi:10.1002/1521-3757(20001002)112:19<3484::AID-ANGE3484>3.0.CO;2-O
    Angew. Chem., Int. Ed. **2000,** *39,* 3348–3391. doi:10.1002/1521-3773(20001002)39:19<3348::AID-ANIE3348>3.0.CO;2-X
16. Schalley, C. A.; Beizai, K.; Vögtle, F. *Acc. Chem. Res.* **2001,** *34,* 465–476. doi:10.1021/ar000179i
17. Ballardini, R.; Balzani, V.; Credi, A.; Gandolfi, M. T.; Venturi, M. *Acc. Chem. Res.* **2001,** *34,* 445–455. doi:10.1021/ar000170g
18. Harada, A. *Acc. Chem. Res.* **2001,** *34,* 456–464. doi:10.1021/ar000174l
19. Collin, J.-P.; Dietrich-Buchecker, C.; Gaviña, P.; Jiménez-Molero, M. C.; Sauvage, J.-P. *Acc. Chem. Res.* **2001,** *34,* 477–487. doi:10.1021/ar0001766
20. Clemente-León, M.; Credi, A.; Martínez-Díaz, M.-V.; Mingotaud, C.; Stoddart, J. F. *Adv. Mater.* **2006,** *18,* 1291–1296. doi:10.1002/adma.200502265
21. Balzani, V.; Credi, A.; Silvi, S.; Venturi, M. *Chem. Soc. Rev.* **2006,** *35,* 1135–1149. doi:10.1039/b517102b
22. Credi, A. *Angew. Chem.* **2007,** *119,* 5568–5572. doi:10.1002/ange.200700879
    Angew. Chem., Int. Ed. **2007,** *46,* 5472–5475. doi:10.1002/anie.200700879
23. Kay, E. R.; Leigh, D. A.; Zerbetto, F. *Angew. Chem.* **2006,** *119,* 72–196. doi:10.1002/ange.200504313
    Angew. Chem., Int. Ed. **2007,** *46,* 72–191. doi:10.1002/anie.200504313
24. Mateo-Alonso, A.; Guldi, D. M.; Paolucci, F.; Prato, M. *Angew. Chem.* **2007,** *119,* 8266–8272. doi:10.1002/ange.200702725
    Angew. Chem., Int. Ed. **2007,** *46,* 8120–8126. doi:10.1002/anie.200702725
25. Champin, B.; Mobian, P.; Sauvage, J.-P. *Chem. Soc. Rev.* **2007,** *36,* 358–366. doi:10.1039/b604484k
26. Silvi, S.; Venturi, M.; Credi, A. *J. Mater. Chem.* **2009,** *19,* 2279–2294. doi:10.1039/b818609j
27. Bodis, P.; Panman, M. R.; Bakker, B. H.; Mateo-Alonso, A.; Prato, M.; Buma, W. J.; Brouwer, A. M.; Kay, E. R.; Leigh, D. A.; Woutersen, S. *Acc. Chem. Res.* **2009,** *42,* 1462–1469. doi:10.1021/ar9000845
28. Durot, S.; Reviriego, F.; Sauvage, J.-P. *Dalton Trans.* **2010,** *39,* 10557–10570. doi:10.1039/c0dt00457j
29. Schliwa, M., Ed. *Molecular Motors;* Wiley-VCH: Weinheim, Germany, 2003.
30. Balzani, V.; Venturi, M.; Credi, A. *Molecular Devices and Machines. A Journey into the Nano World;* Wiley-VCH: Weinheim, Germany, 2003. doi:10.1002/3527601600
31. Balzani, V.; Credi, A.; Venturi, M. *Molecular Devices and Machines: Concepts and Perspectives for the Nanoworld,* 2nd ed.; Wiley-VCH: Weinheim, Germany, 2008. doi:10.1002/9783527621682
32. Sauvage, J.-P.; Gaspard, P., Eds. *From Non-Covalent Assemblies to Molecular Machines;* Wiley-VCH: Weinheim, Germany, 2010. doi:10.1002/9783527632817
33. Dietrich-Buchecker, C. O.; Sauvage, J.-P. *Chem. Rev.* **1987,** *87,* 795–810. doi:10.1021/cr00080a007
34. Anderson, S.; Anderson, H. L.; Sanders, J. K. M. *Acc. Chem. Res.* **1993,** *26,* 469–475. doi:10.1021/ar00033a003
35. Chambron, J.-C.; Collin, J.-P.; Heitz, V.; Jouvenot, D.; Kern, J.-M.; Mobian, P.; Pomeranc, D.; Sauvage, J.-P. *Eur. J. Org. Chem.* **2004,** 1627–1638. doi:10.1002/ejoc.200300341
36. Amman, M.; Rang, A.; Schalley, C. A.; Bäuerle, P. *Eur. J. Org. Chem.* **2006,** 1940–1948. doi:10.1002/ejoc.200500938
37. Hutin, M.; Schalley, C. A.; Bernardinelli, G.; Nitschke, J. R. *Chem.–Eur. J.* **2006,** *12,* 4069–4076. doi:10.1002/chem.200501591
38. Bäuerle, P.; Ammann, M.; Wilde, M.; Götz, G.; Mena-Osteritz, E.; Rang, A.; Schalley, C. A. *Angew. Chem.* **2007,** *119,* 367–372. doi:10.1002/ange.200602652
    Angew. Chem., Int. Ed. **2007,** *46,* 363–368. doi:10.1002/anie.200602652

39. Yamashita, K.-i.; Kawano, M.; Fujita, M. *J. Am. Chem. Soc.* **2007,** *129,* 1850–1851. doi:10.1021/ja067132y
40. Meyer, C. D.; Joiner, C. S.; Stoddart, J. F. *Chem. Soc. Rev.* **2007,** *36,* 1705–1723. doi:10.1039/b513441m
41. Bonnet, S.; Collin, J.-P. *Chem. Soc. Rev.* **2008,** *37,* 1207–1217. doi:10.1039/b713678c
42. Crowley, J. D.; Goldup, S. M.; Lee, A.-L.; Leigh, D. A.; McBurney, R. T. *Chem. Soc. Rev.* **2009,** *38,* 1530–1541. doi:10.1039/b804243h
43. Faiz, J. A.; Heitz, V.; Sauvage, J.-P. *Chem. Soc. Rev.* **2009,** *38,* 422–442. doi:10.1039/b710908n
44. Collin, J.-P.; Durola, F.; Heitz, V.; Reviriego, F.; Sauvage, J.-P.; Trolez, Y. *Angew. Chem.* **2010,** *122,* 10370–10373. doi:10.1002/ange.201004008
45. Clever, G. H.; Shionoya, M. *Chem.–Eur. J.* **2010,** *16,* 11792–11796. doi:10.1002/chem.201002013
46. Megiatto, J. D., Jr.; Schuster, D. I.; Abwandner, S.; de Miguel, G.; Guldi, D. M. *J. Am. Chem. Soc.* **2010,** *132,* 3847–3861. doi:10.1021/ja910149f
47. Hänni, K. D.; Leigh, D. A. *Chem. Soc. Rev.* **2010,** *39,* 1240–1251. doi:10.1039/b901974j
48. Amabilino, D. B.; Stoddart, J. F.; Williams, D. J. *Chem. Mater.* **1994,** *6,* 1159–1167. doi:10.1021/cm00044a014
49. Amabilino, D. B.; Stoddart, J. F. *Chem. Rev.* **1995,** *95,* 2725–2828. doi:10.1021/cr00040a005
50. Glink, P. T.; Stoddart, J. F. *Pure Appl. Chem.* **1998,** *70,* 419–424. doi:10.1351/pac199870020419
51. Nepogodiev, S. A.; Stoddart, J. F. *Chem. Rev.* **1998,** *98,* 1959–1976. doi:10.1021/cr970049w
52. Lee, J. W.; Samal, S.; Selvapalam, N.; Kim, H.-J.; Kim, K. *Acc. Chem. Res.* **2003,** *36,* 621–630. doi:10.1021/ar020254k
53. Kim, K.; Selvapalam, N.; Ko, Y. H.; Park, K. M.; Kim, D.; Kim, J. *Chem. Soc. Rev.* **2007,** *36,* 267–279. doi:10.1039/b603088m
54. Dichtel, W. R.; Miljanić, O. Š.; Zhang, W.; Spruell, J. M.; Patel, K.; Aprahamian, I.; Heath, J. R.; Stoddart, J. F. *Acc. Chem. Res.* **2008,** *41,* 1750–1761. doi:10.1021/ar800067h
55. Griffiths, K. E.; Stoddart, J. F. *Pure Appl. Chem.* **2008,** *80,* 485–506. doi:10.1351/pac200880030485
56. Isaacs, L. *Chem. Commun.* **2009,** 619–629. doi:10.1039/b814897j
57. Appel, E. A.; Biedermann, F.; Rauwald, U.; Jones, S. T.; Zayed, J. M.; Scherman, O. A. *J. Am. Chem. Soc.* **2010,** *132,* 14251–14260. doi:10.1021/ja106362w
58. Zhang, M.; Zhu, K.; Huang, F. *Chem. Commun.* **2010,** *46,* 8131–8141. doi:10.1039/c0cc02717k
59. Au-Yeung, H. Y.; Pantoş, G. D.; Sanders, J. K. M. *Angew. Chem.* **2010,** *122,* 5459–5462. doi:10.1002/ange.201000807 *Angew. Chem., Int. Ed.* **2010,** *49,* 5331–5334. doi:10.1002/anie.201000807
60. Cougnon, F. B. L.; Au-Yeung, H. Y.; Pantoş, G. D.; Sanders, J. K. M. *J. Am. Chem. Soc.* **2011,** *133,* 3198–3207. doi:10.1021/ja111407m
61. Fang, L.; Basu, S.; Sue, C.-H.; Fahrenbach, A. C.; Stoddart, J. F. *J. Am. Chem. Soc.* **2011,** *133,* 396–399. doi:10.1021/ja1087562
62. Biedermann, F.; Rauwald, U.; Zayed, J. M.; Scherman, O. A. *Chem. Sci.* **2011,** *2,* 279–286. doi:10.1039/c0sc00435a
63. Niu, Z.; Huang, F.; Gibson, H. W. *J. Am. Chem. Soc.* **2011,** *133,* 2836–2839. doi:10.1021/ja110384v
64. Hunter, C. A. *J. Chem. Soc., Chem. Commun.* **1991,** 749–751. doi:10.1039/C39910000749
65. Hunter, C. A. *J. Am. Chem. Soc.* **1992,** *114,* 5305–5311. doi:10.1021/ja00039a047
66. Vögtle, F.; Meier, S.; Hoss, R. *Angew. Chem.* **1992,** *104,* 1628–1631. doi:10.1002/ange.19921041212 *Angew. Chem., Int. Ed.* **1992,** *31,* 1619–1622. doi:10.1002/anie.199216191
67. Ottens-Hildebrandt, S.; Meier, S.; Schmidt, W.; Vögtle, F. *Angew. Chem.* **1994,** *106,* 1818–1821. doi:10.1002/ange.19941061712 *Angew. Chem., Int. Ed.* **1994,** *33,* 1767–1770. doi:10.1002/anie.199417671
68. Vögtle, F.; Dünnwald, T.; Schmidt, T. *Acc. Chem. Res.* **1996,** *29,* 451–460. doi:10.1021/ar950200t
69. Kim, K. *Chem. Soc. Rev.* **2002,** *31,* 96–107. doi:10.1039/a900939f
70. Schalley, C. A.; Weilandt, T.; Brüggemann, J.; Vögtle, F. *Top. Curr. Chem.* **2004,** *248,* 141–200.
71. Kay, E. R.; Leigh, D. A. *Top. Curr. Chem.* **2005,** *262,* 133–177. doi:10.1007/128_011
72. Jiang, W.; Winkler, H. D. F.; Schalley, C. A. *J. Am. Chem. Soc.* **2008,** *130,* 13852–13853. doi:10.1021/ja806009d
73. Jiang, W.; Schalley, C. A. *Proc. Natl. Acad. Sci. U. S. A.* **2009,** *106,* 10425–10429. doi:10.1073/pnas.0809512106
74. Stoddart, J. F. *Chem. Soc. Rev.* **2009,** *38,* 1802–1820. doi:10.1039/b819333a
75. Lee, C.-F.; Leigh, D. A.; Pritchard, R. G.; Schultz, D.; Teat, S. J.; Timco, G. A.; Winpenny, R. E. P. *Nature* **2009,** *458,* 314–318. doi:10.1038/nature07847
76. Jiang, W.; Mohr, P. C.; Schäfer, A.; Schalley, C. A. *J. Am. Chem. Soc.* **2010,** *132,* 2309–2320. doi:10.1021/ja9101369
77. Jiang, W.; Schalley, C. A. *Beilstein J. Org. Chem.* **2010,** *6,* No. 14. doi:10.3762/bjoc.6.14
78. Fang, L.; Olson, M. A.; Benítez, D.; Tkatchouk, E.; Goddard, W. A., III; Stoddart, J. F. *Chem. Soc. Rev.* **2010,** *39,* 17–29. doi:10.1039/b917901a
79. Ma, X.; Tian, H. *Chem. Soc. Rev.* **2010,** *39,* 70–80. doi:10.1039/b901710k
80. Jiang, W.; Han, M.; Zhang, H.-Y.; Zhang, Z.-J.; Liu, Y. *Chem.–Eur. J.* **2009,** *15,* 9938–9945. doi:10.1002/chem.200901206
81. Chen, C.-F. *Chem. Commun.* **2011,** *47,* 1674–1688. doi:10.1039/c0cc04852f
82. Badjić, J. D.; Nelson, A.; Cantrill, S. J.; Turnbull, W. B.; Stoddart, J. F. *Acc. Chem. Res.* **2005,** *38,* 723–732. doi:10.1021/ar040223k
83. Badjić, J. D.; Balzani, V.; Credi, A.; Silvi, S.; Stoddart, J. F. *Science* **2004,** *303,* 1845–1849. doi:10.1126/science.1094791
84. Badjić, J. D.; Ronconi, C. M.; Stoddart, J. F.; Balzani, V.; Silvi, S.; Credi, A. *J. Am. Chem. Soc.* **2006,** *128,* 1489–1499. doi:10.1021/ja0543954
85. Reuter, C.; Vögtle, F. *Org. Lett.* **2000,** *2,* 593–595. doi:10.1021/ol990350u
86. Affeld, A.; Hübner, G. M.; Seel, C.; Schalley, C. A. *Eur. J. Org. Chem.* **2001,** 2877–2890. doi:10.1002/1099-0690(200108)2001:15<2877::AID-EJOC2877>3.0.CO;2-R
87. Schalley, C. A.; Silva, G.; Nising, C.-F.; Linnartz, P. *Helv. Chim. Acta* **2002,** *85,* 1578–1596. doi:10.1002/1522-2675(200206)85:6<1578::AID-HLCA1578>3.0.CO;2-L
88. Li, X.-y.; Illigen, J.; Nieger, M.; Michel, S.; Schalley, C. A. *Chem.–Eur. J.* **2003,** *9,* 1332–1347. doi:10.1002/chem.200390153
89. Linnartz, P.; Bitter, S.; Schalley, C. A. *Eur. J. Org. Chem.* **2003,** 4819–4829. doi:10.1002/ejoc.200300466

90. Felder, T.; Schalley, C. A. *Angew. Chem.* **2003,** *115,* 2360–2363. doi:10.1002/ange.200350903
Angew. Chem., Int. Ed. **2003,** *42,* 2258–2260. doi:10.1002/anie.200350903
91. Linnartz, P.; Schalley, C. A. *Supramol. Chem.* **2004,** *16,* 263–267. doi:10.1080/1061027042000204010
92. Ghosh, P.; Federwisch, G.; Kogej, M.; Schalley, C. A.; Haase, D.; Saak, W.; Lützen, A.; Gschwind, R. M. *Org. Biomol. Chem.* **2005,** *3,* 2691–2700. doi:10.1039/b506756a
93. Seel, C.; Parham, A. H.; Safarowsky, O.; Hübner, G. M.; Vögtle, F. *J. Org. Chem.* **1999,** *64,* 7236–7242. doi:10.1021/jo990042+
94. Chang, S.-Y.; Kim, H. S.; Chang, K.-J.; Jeong, K.-S. *Org. Lett.* **2004,** *6,* 181–184. doi:10.1021/ol035954j
95. Herrmann, U.; Jonischkeit, T.; Bargon, J.; Hahn, U.; Li, Q.-Y.; Schalley, C. A.; Vogel, E.; Vögtle, F. *Anal. Bioanal. Chem.* **2002,** *372,* 611–614. doi:10.1007/s00216-001-1230-6
96. Bargon, J.; Braschoß, S.; Flörke, J.; Herrmann, U.; Klein, L.; Lörgen, J. W.; Lopez, M.; Maric, S.; Parham, A. H.; Piacenza, P.; Schäfgen, H.; Schalley, C. A.; Silva, G.; Schlupp, M.; Schwierz, H.; Vögtle, F.; Windscheif, G. *Sens. Act. B* **2003,** *95,* 6–19. doi:10.1016/S0925-4005(03)00395-2
97. Kleefisch, G.; Kreutz, C.; Bargon, J.; Silva, G.; Schalley, C. A. *Sensors* **2004,** *4,* 136–146. doi:10.3390/s40900136
98. Kossev, I.; Reckien, W.; Felder, T.; Kishan, M. R.; Schalley, C. A.; Sokolowski, M. *J. Phys. Chem. C* **2009,** *113,* 12870–12877. doi:10.1021/jp903668x
99. Kossev, I.; Reckien, W.; Kirchner, B.; Felder, T.; Nieger, M.; Schalley, C. A.; Vögtle, F.; Sokolowski, M. *Adv. Funct. Mater.* **2007,** *17,* 513–519. doi:10.1002/adfm.200600540
100. Kossev, I.; Felder, T.; Schalley, C. A.; Vögtle, F.; Sokolowski, M. *Springer Proc. Phys.* **2009,** *127,* 235–245. doi:10.1007/978-3-540-88201-5_27
101. Hunter, C. A.; Packer, M. J. *Chem.–Eur. J.* **1999,** *5,* 1891–1897. doi:10.1002/(SICI)1521-3765(19990604)5:6<1891::AID-CHEM1891>3.0.CO;2-G
102. Chinchilla, R.; Nájera, C. *Chem. Rev.* **2007,** *107,* 874–922. doi:10.1021/cr050992x
103. Baytekin, B.; Zhu, S. S.; Brusilowskij, B.; Illigen, J.; Ranta, J.; Huuskonen, J.; Russo, L.; Rissanen, K.; Kaufmann, L.; Schalley, C. A. *Chem.–Eur. J.* **2008,** *14,* 10012–10028. doi:10.1002/chem.200801289
104. Dzyuba, E. V.; Baytekin, B.; Sattler, D.; Schalley, C. A. *Eur. J. Org. Chem.*, in press.
105. Liu, H.-X.; Shao, F.; Li, G.-Q.; Xun, G.-L.; Yao, Z.-J. *Chem.–Eur. J.* **2008,** *14,* 8632–8639. doi:10.1002/chem.200801298
106. Kabalka, G. W.; Wang, L. *Tetrahedron Lett.* **2002,** *43,* 3067–3068. doi:10.1016/S0040-4039(02)00437-9
107. Kuo, M.-C.; Li, L.-A.; Yen, W.-N.; Lo, S.-S.; Lee, C.-W.; Yeh, C.-Y. *Dalton Trans.* **2007,** 1433–1439. doi:10.1039/b617170b
108. Ljungdahl, T.; Bennur, T.; Dallas, A.; Emtenäs, H.; Mårtensson, J. *Organometallics* **2008,** *27,* 2490–2498. doi:10.1021/om800251s
109. Maison, W.; Frangioni, J. V.; Pannier, N. *Org. Lett.* **2004,** *6,* 4567–4569. doi:10.1021/ol048055j
110. Pannier, N.; Maison, W. *Eur. J. Org. Chem.* **2008,** 1278–1284. doi:10.1002/ejoc.200701003
111. Spickermann, C.; Felder, T.; Schalley, C. A.; Kirchner, B. *Chem.–Eur. J.* **2008,** *14,* 1216–1227. doi:10.1002/chem.200700479
112. Dzyuba, E. V.; Kaufmann, L.; Löw, N. L.; Meyer, A. K.; Winkler, H. D. F.; Rissanen, K.; Schalley, C. A. *Org. Lett.* **2011,** *13,* 4838–4841. doi:10.1021/ol201915j

License and Terms

Beilstein Journal of Organic Chemistry

A ferrocene redox-active triazolium macrocycle that binds and senses chloride

Nicholas G. White and Paul D. Beer*

Full Research Paper

Open Access

Address:
Chemistry Research Laboratory, Mansfield Road, Oxford, OX1 3TA, United Kingdom

Email:
Paul D. Beer* - paul.beer@chem.ox.ac.uk

* Corresponding author

Keywords:
anion binding; C–H···anion interactions; electrochemistry; ferrocene; triazolium

Beilstein J. Org. Chem. **2012,** *8,* 246–252.
doi:10.3762/bjoc.8.25

Received: 21 December 2011
Accepted: 30 January 2012
Published: 13 February 2012

This article is part of the Thematic Series "Supramolecular chemistry II".

Guest Editor: C. A. Schalley

Abstract

A ferrocene bis(triazole) macrocycle was synthesised in good yield by the Eglinton coupling of an acyclic bis(alkyne) precursor and characterised in the solid state by X-ray crystallography. Alkylation gives the corresponding triazolium macrocycle, which binds chloride and benzoate strongly in CD_3CN solution through favourable charge-assisted C–H···anion interactions, as evidenced by ^1H NMR titration experiments. Preliminary electrochemical studies reveal that the redox-active macrocycle is capable of sensing chloride in CH_3CN solution.

Introduction

The copper(I)-catalysed cycloaddition of alkynes and azides (CuAAC) [1,2] to give the 1,2,3-triazole group is increasingly being exploited in the synthesis of a vast array of materials since its discovery [3]. Several seminal studies have demonstrated the ability of acyclic and macrocyclic bis- and poly(triazole) containing systems to bind anions in organic solvents through triazole C–H···anion interactions [4-7]. More recently, we [8], and others [9,10], have shown that alkylating the triazole group to give the triazolium group increases the strength of anion binding significantly by further polarising the C–H bond of the heterocycle.

With one notable recent exception of an acyclic ferrocene-appended aryl triazole receptor, which selectively senses phosphate species electrochemically in dichloromethane [11], to the best of our knowledge, redox-active triazole and triazolium receptors are unprecedented. Herein we describe the synthesis of a novel ferrocene bis-triazolium macrocyclic receptor and investigate its anion binding and electrochemical-sensing properties.

Results and Discussion

Synthesis

The CuAAC reaction of ferrocene bis(azide) **1** [12], with a large excess of 1,6-heptadiyne afforded **2** in 50% yield. An intramolecular Eglinton cyclisation reaction was used to prepare the ferrocene bis(triazole) macrocycle **3**, in surprisingly good yield (54%) after purification by column chromatography, as

well as a small amount (12%) of the corresponding larger tetra(triazole) macrocycle, **4** (Scheme 1).

The reaction of macrocycle **3**, with an excess of trimethyloxonium tetrafluoroborate gave a crude product, which was difficult to purify. Chromatographic purification was required, but this was complicated by the doubly positively charged macrocycle. Nevertheless, preparative thin-layer chromatography in 17:2:1 acetonitrile:water:saturated $KNO_{3(aq)}$ solution, followed by removal of the organic solvents under reduced pressure and precipitation of the product as its bis(hexafluorophosphate) salt from the remaining aqueous solution (using NH_4PF_6), gave the desired bis(triazolium) macrocycle **5**, in moderate yield (Scheme 2). Alternatively, **2** could be readily alkylated to give

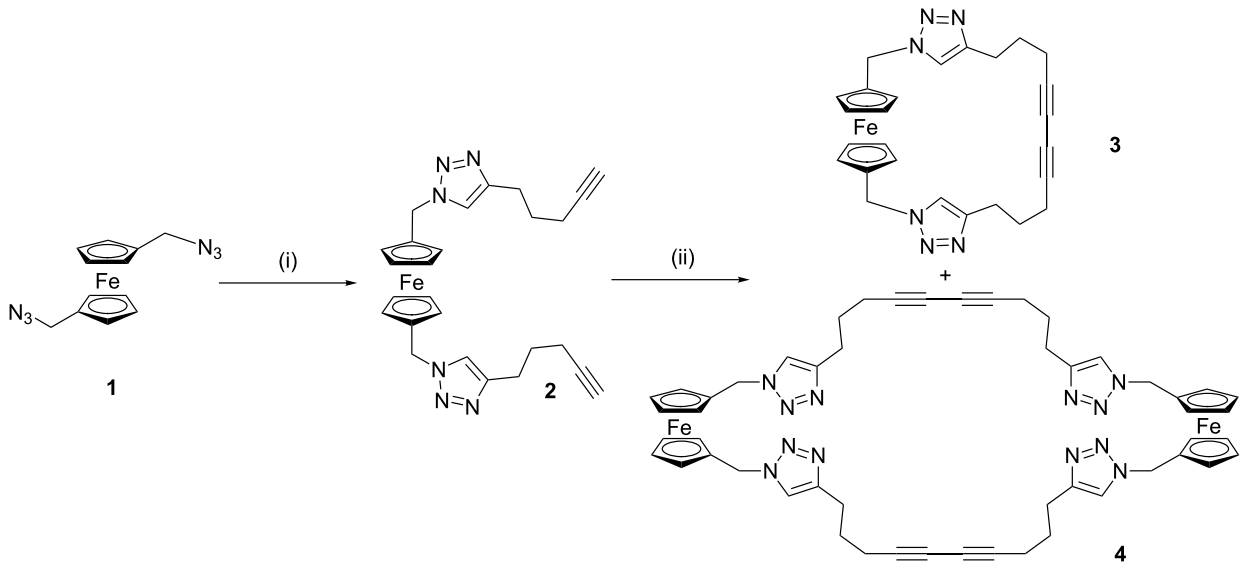

Scheme 1: Synthesis of bis(triazole) macrocycle **3** and tetra(triazole) macrocycle **4**. Conditions and reagents: (i) 1,6-Heptadiyne, $[Cu^{I}(CH_3CN)_4](PF_6)$, tris[(benzyltriazol-4-yl)methyl]amine (TBTA), diisopropylamine (DIPEA), CH_2Cl_2, 50%; (ii) $Cu^{II}(OAc)_2{\cdot}H_2O$, CH_3CN, reflux, 54% of **3**, 12% of **4**.

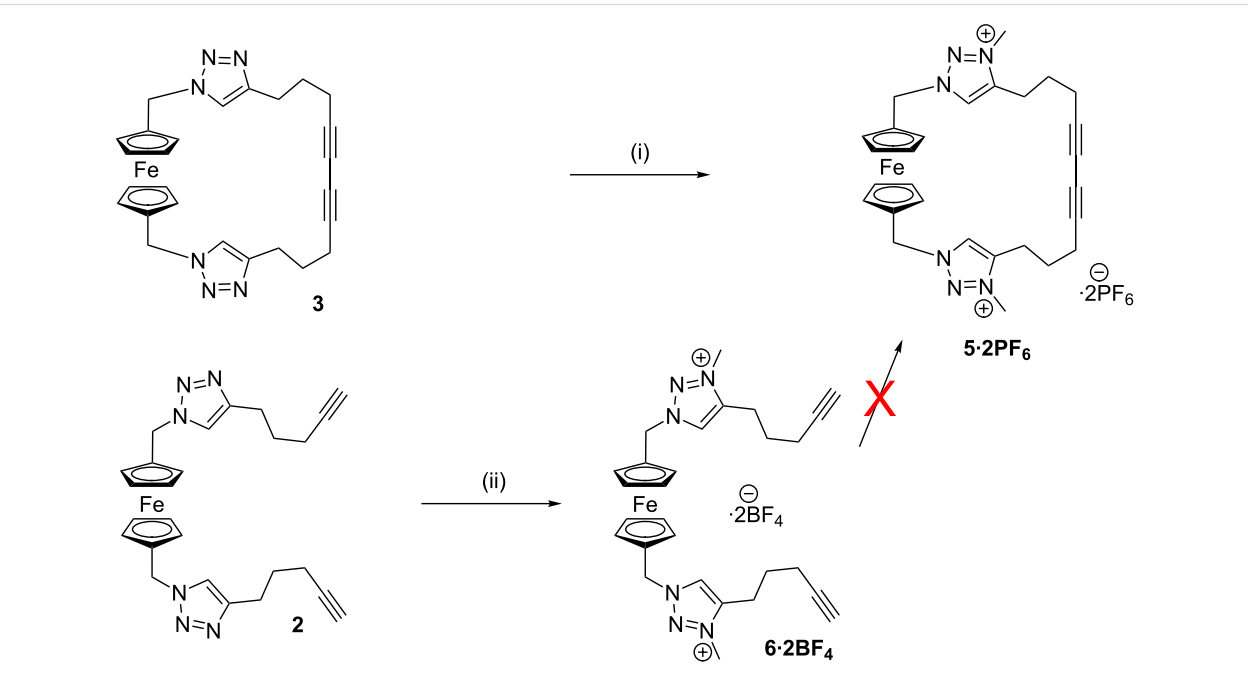

Scheme 2: Synthesis of bis(triazolium) macrocycle, **5**. Conditions and reagents: (i) (a) $(Me_3O)(BF_4)$, CH_2Cl_2, (b) chromatography with 17:2:1 CH_3CN:H_2O: sat. $KNO_{3(aq)}$, then $NH_4PF_{6(aq)}$, 12%; (ii) $(Me_3O)(BF_4)$, CH_2Cl_2, 77%.

bis(triazolium)-bis(alkyne), **6**, in good yield; however, attempts to cyclise under analogous conditions to those used to produce **3** were unsuccessful, resulting in decomposition of the ferrocene motif.

All new compounds were characterised by ^{1}H and ^{13}C NMR spectroscopy and high-resolution ESI mass spectrometry, as well as by ^{19}F and ^{31}P NMR spectroscopy where appropriate. Single crystals of **3** were grown by the vapour diffusion of diethyl ether into an acetone solution of the macrocycle, and of macrocycle **4** by vapour diffusion of pentane into a chloroform/methanol solution. The solid-state structures were determined by synchrotron X-ray crystallography (Figure 1). The structure of **3** shows that the diyne unit appears to enforce a reasonably rigid geometry on the rest of the macrocycle, due to its sterically demanding nature, which may help to constrain the anion binding cleft and lead to selective anion binding. In contrast, the larger size of **4** gives a much more open structure, with a diameter of approximately 17 Å (Figure 1). Despite this open structure, no solvent cocrystallises with the macrocycle, with the structure being tightly packed due to a series of intermolecular hydrogen bonds between triazole C–H donors and triazole N-acceptors on adjacent molecules.

Anion-binding investigations

The anion-binding properties of **5**·**2PF$_6$** were investigated in CD_3CN solution by ^{1}H NMR titration experiments. Aliquots of anions as their *N*-tetrabutylammonium (TBA) salts were added to **5**·**2PF$_6$** and the chemical shift of the (chemically equivalent) triazolium protons was monitored. As shown in Figure 2, the addition of chloride to the macrocyclic receptor resulted in large downfield shifts of the triazolium signal, d, concomitant with relatively smaller perturbations of proton c, which suggests that halide binding occurs in proximity to the ferrocene group.

WINEQNMR2 [13] analysis of the titration data (Figure 3) shows that the cyclic receptor, **5**·**2PF$_6$**, binds both chloride and benzoate strongly with 1:1 stoichiometries in CD_3CN (association constants are shown in Table 1), with the more basic carboxylate anion forming the strongest complex. The larger halide, iodide, is only weakly bound. The addition of small amounts (<1 equiv) of dihydrogen phosphate caused precipitation and, hence, no association constant could be calculated.

Table 1: Anion association constants for **5**·**2PF$_6$** calculated by using WINEQNMR2 [13] based on ^{1}H NMR titration data (500 MHz, 293 K, CD_3CN).

Anion[a]	K_a (M^{-1})[b]
Benzoate	$4.6(2) \times 10^3$
Chloride	$2.5(2) \times 10^3$
Iodide	$2.0(2) \times 10^2$
Dihydrogen phosphate	Precipitation

[a]All anions added as TBA salts. [b]Estimated standard errors given in parentheses.

Electrochemical Investigations

The ability of **5**·**2PF$_6$** to sense anions electrochemically was investigated by cyclic voltammetry in 0.1 M TBA·PF_6 in CH_3CN. The macrocycle displays a quasi-reversible oxidation of the ferrocene/ferrocenium couple, which is shifted to a more positive potential by 0.38 V relative to ferrocene by virtue of

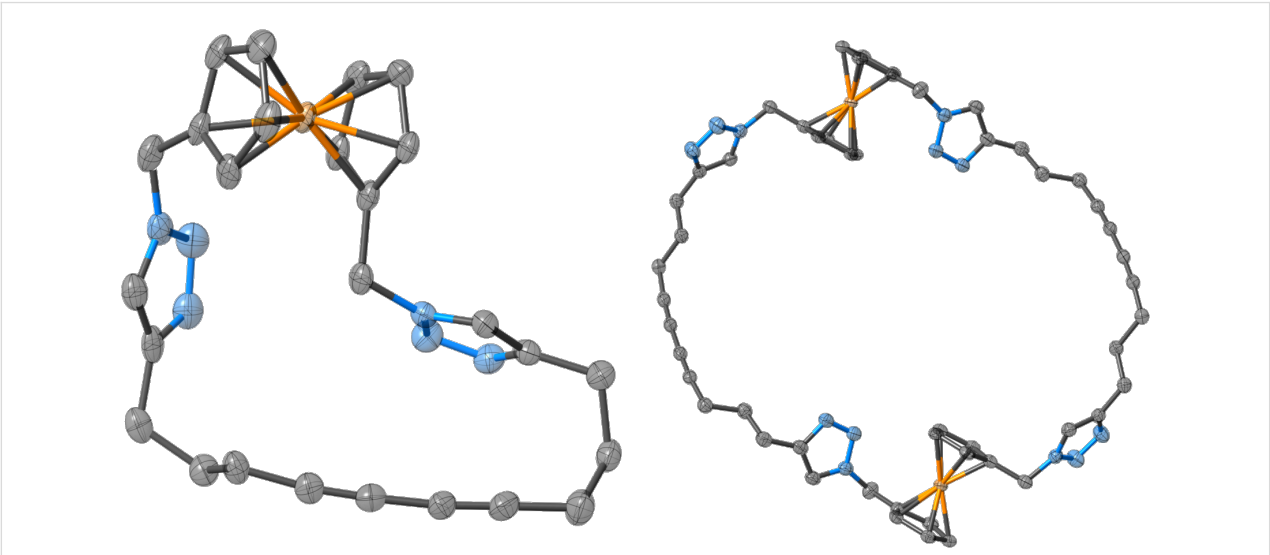

Figure 1: Solid-state structure of **3** (left) and **4** (right). Hydrogen atoms omitted for clarity, ellipsoids are shown at 50% probability; only one of the two independent molecules in the asymmetric unit of **3** is shown. Colour scheme: grey = carbon, blue = nitrogen, orange = iron.

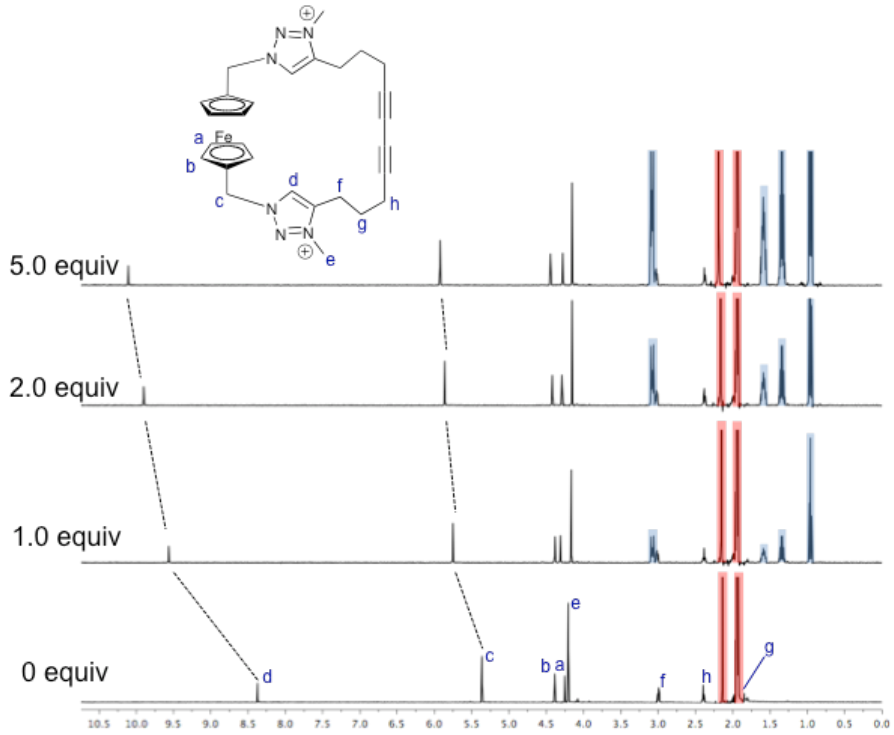

Figure 2: ^{1}H NMR spectra of **5**·**2PF$_6$** after the addition of 0, 1.0, 2.0 and 5.0 equiv of TBA·Cl (500 MHz, 293 K, CD_3CN). Red-shaded peaks correspond to solvent signals (H_2O and CH_3CN); blue-shaded peaks correspond to signals from TBA cations.

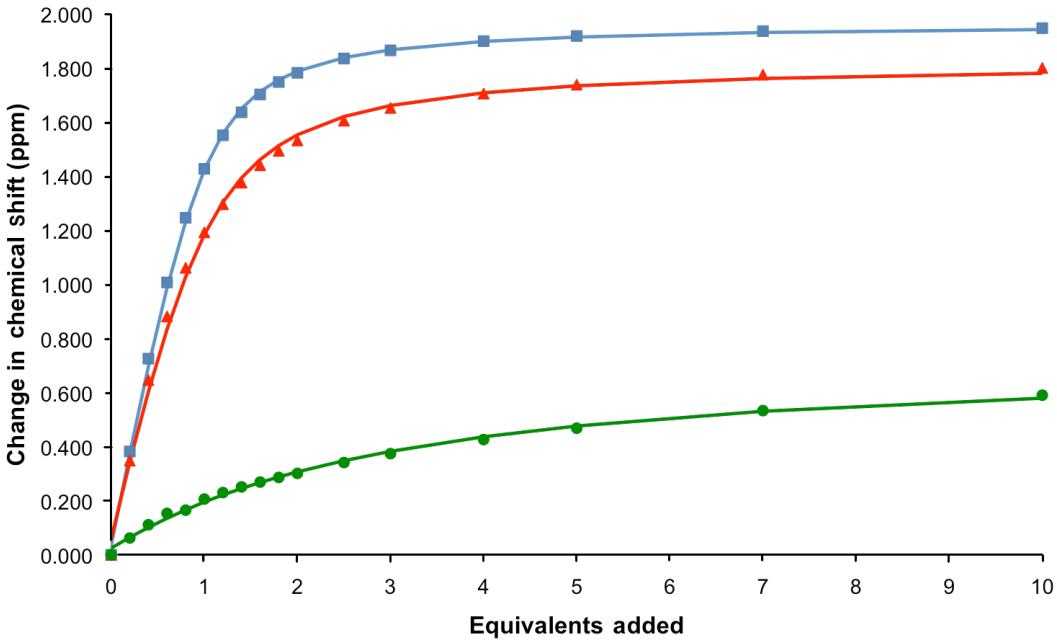

Figure 3: Titration data (solid points) and fitted binding isotherms (curves) monitoring the triazolium proton, d, for titration of benzoate, chloride and iodide into a solution of **5**·**2PF$_6$** (500 MHz, 293 K, CD_3CN).

the positively charged triazolium groups of the receptor. Addition of one equiv of TBA·Cl caused a cathodic shift of the oxidation potential of 25 mV and a loss of reversibility, which may be indicative of an EC mechanism [14] (Figure 4). Further addition of TBA·Cl led to increasing cathodic perturbations of the E_{pa} oxidation wave of up to 40 mV after five equiv. As noted with other ferrocene based anion receptors [15-17], chloride-anion binding stabilises the ferrocenium oxidation state, which results in the cathodic perturbation observed. Analogous electrochemical experiments with benzoate caused an immediate disappearance of the redox signal, which indicates precipitation of an insoluble ferrocenium complex upon oxidation.

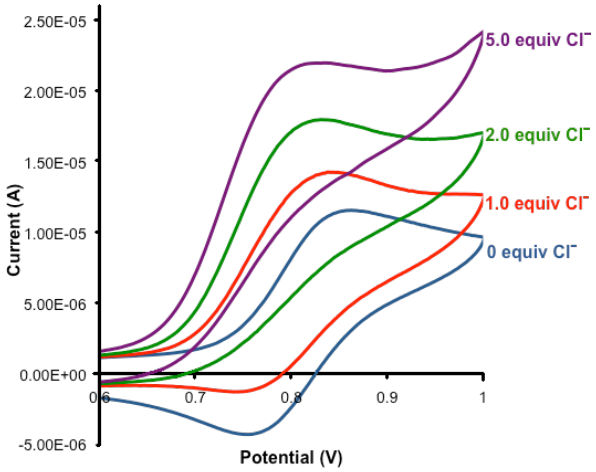

Figure 4: CV of **5·2PF$_6$** upon the addition of TBA·Cl (electrolyte: 0.1 M TBA·PF$_6$/CH$_3$CN, [**5·2PF$_6$**] = 0.50 mM, 293 K. Potential vs. Ag/AgCl reference).

Conclusion

A new ferrocene bis(triazole) macrocycle was readily synthesised by intramolecular Eglinton coupling of an acyclic 1,1'-bis(triazolylalkyne) ferrocene precursor. Alkylation of this macrocycle gave the dicationic bis(triazolium) macrocycle, which was demonstrated by ^{1}H NMR titration experiments to bind chloride and benzoate in CD$_3$CN, solely through charge-assisted C–H···anion hydrogen-bonding interactions. The redox-active macrocycle was also shown to sense chloride electrochemically via a cathodic shift of the E_{pa} wave of the ferrocene/ferrocenium redox couple.

Experimental

General Remarks

Bis(azide) **1** [12], and TBTA [18] were prepared as described in the literature. Dry dichloromethane and acetonitrile were purged with nitrogen and passed through a MBraun MSP-800 column. Water was deionised and microfiltered in a Milli-Q® Millipore machine. Tetrabutylammonium salts were stored in a vacuum desiccator under reduced pressure. All other compounds were bought commercially and used as received. Routine NMR spectra were recorded on a Varian Mercury 300 spectrometer with ^{1}H NMR operating at 300 MHz, ^{13}C at 75.5 MHz. Spectra for anion-binding titrations were recorded on a Varian Unity Plus 500 spectrometer with ^{1}H operating at 500 MHz. Mass spectra were recorded on a Bruker microTOF spectrometer.

Bis(alkyne) 2

Bis(azide) **1** (0.148 g, 0.500 mmol) and 1,6-heptadiyne (0.69 mL, 0.55 g, 6.0 mmol) were dissolved in dichloromethane (50 mL). DIPEA (0.17 mL, 0.13 g, 1.0 mmol), TBTA (0.053 g, 0.10 mmol) and [Cu^I(CH$_3$CN)$_4$](PF$_6$) (0.037 g, 0.10 mmol) were added, and the yellow solution was stirred at room temperature under a nitrogen atmosphere for three days. It was then taken to dryness under reduced pressure and purified by column chromatography (silica, 2% methanol in dichloromethane) to give **2** as a yellow solid. Yield: 0.120 g (50%). ^{1}H NMR (CDCl$_3$) δ 7.24 (s, 2H, trz-*H*), 5.19 (s, 4H, Fc-C*H*$_2$-trz), 4.23 (t, ^3J = 1.6 Hz, 4H, Fc-*H*), 4.19 (t, ^3J = 1.6 Hz, 4H, Fc-*H*), 2.80 (t, ^3J = 7.6 Hz, 4H, trz-C*H*$_2$-CH$_2$), 2.22 (dt, ^3J = 7.0 Hz, ^4J = 2.6 Hz, 4H, C*H*$_2$-C≡CH), 1.95 (t, ^4J = 2.6 Hz, 2H, C≡C*H*), 1.87 (m, 4H, trz-CH$_2$-C*H*$_2$); ^{13}C NMR (CDCl$_3$) δ 147.3, 120.6, 83.9, 82.7, 69.9, 69.6, 69.0, 49.5, 28.1, 24.6, 18.0; HRMS–ESI (*m*/*z*): [M + Na]$^+$ calcd for C$_{26}$H$_{28}$N$_6$Fe·Na, 503.1617; found, 503.1614.

Bis(triazole) macrocycle 3

The bis(alkyne) **2** (0.120 g, 0.250 mmol) and copper(II) acetate monohydrate (0.125 g, 0.625 mmol) were heated under reflux in acetonitrile (150 mL) under a nitrogen atmosphere overnight. The green solution was cooled to room temperature and then taken to dryness under reduced pressure. It was taken up in water (20 mL) and extracted with dichloromethane (4 × 20 mL). The combined organic fractions were dried (magnesium sulfate), taken to dryness under reduced pressure and then purified by column chromatography (silica, gradient: 3% methanol in dichloromethane) to give **3** as an orange powder. Yield: 0.065 g (54%). ^{1}H NMR (CDCl$_3$) δ 7.44 (s, 2H, trz-*H*), 5.06 (s, 4H, Fc-C*H*$_2$-trz), 4.15 (t, ^3J = 1.9 Hz, 4H, Fc-*H*), 4.10 (t, ^3J = 1.9 Hz, 4H, Fc-*H*), 2.91 (t, ^3J = 6.6 Hz, 4H, trz-C*H*$_2$-CH$_2$), 2.31 (t, ^3J = 6.6 Hz, 4H, C*H*$_2$-C≡C), 1.92–2.01 (m, 4H, trz-CH$_2$-C*H*$_2$); ^{13}C NMR (CDCl$_3$) δ 146.9, 121.9, 110.9, 84.0, 69.3, 69.1, 66.6, 49.1, 26.6, 24.2, 18.4; HRMS–ESI (*m*/*z*): [M + Na]$^+$ calcd for C$_{26}$H$_{26}$N$_6$Fe·Na, 501.1461; found, 501.1467.

Tetra(triazole) macrocycle 4

The same procedure as for the synthesis of **3** but switching to 7% methanol in dichloromethane as eluent gave **4** as an orange powder. Yield: 0.014 g (12%). ^{1}H NMR (CDCl$_3$) δ 7.33 (s, 4H, trz-*H*), 5.11 (s, 8H, Fc-C*H*$_2$-trz), 4.14 (t, ^3J = 1.7 Hz, 8H, Fc-*H*),

4.11 (t, ^3J = 1.7 Hz, 8H, Fc-*H*), 2.74 (t, ^3J = 6.6 Hz, 4H, trz-C*H*$_2$-CH$_2$), 2.23 (t, ^3J = 6.6 Hz, 4H, C*H*$_2$-C≡C), 1.76–1.86 (m, 8H, trz-CH$_2$-C*H*$_2$); ^{13}C NMR (DMSO-d_6) δ 145.8, 121.9, 83.6, 77.6, 69.3, 69.0, 65.7, 48.3, 27.7, 24.0, 17.9; HRMS–ESI (*m*/*z*): [M + Na]$^+$ calcd for $C_{52}H_{52}N_{12}Fe_2$·Na, 979.3029; found, 979.3038.

Bis(triazolium) macrocycle **5·2PF$_6$**

The neutral macrocycle **3** (0.048 g, 0.10 mmol) was dissolved in dry dichloromethane (10 mL). Trimethyloxonium tetrafluoroborate (0.032 g, 0.22 mmol) was added and the orange solution stirred at room temperature under a nitrogen atmosphere overnight, during which time it took on a brown tinge. Methanol (1 mL) was added to quench the alkylating agent, and the mixture was evaporated to dryness under reduced pressure. The crude mixture was purified by preparative thin layer chromatography (silica, eluent: 17:2:1 CH_3CN/H_2O/sat. $KNO_{3(aq)}$). The band containing the product was scraped from the plate and washed off the silica with the same solvent mixture, and the acetonitrile was removed under reduced pressure to give an orange aqueous solution. Addition of NH_4PF_6 (0.15 g in 0.5 mL H_2O) caused the precipitation of a yellow solid. This was extracted into dichloromethane (2 × 15 mL), washed with water (2 × 15 mL) and thoroughly dried in vacuo to give **5** as a glassy orange solid. Yield: 0.0098 g (12%). ^{1}H NMR (CD_3CN) δ 8.32 (s, 2H, H_d), 5.34 (s, 6H, H_c), 4.37 (t, $^3J_{a,b}$ = 1.9 Hz, 4H, H_b), 4.24 (t, $^3J_{a,b}$ = 1.9 Hz, 4H, H_a), 4.19 (s, 6H, H_e), 2.99 (t, $^3J_{f,g}$ = 6.6 Hz, 4H, H_f), 2.40 (t, $^3J_{g,h}$ = 6.5 Hz, 4H, H_h), 1.95–2.03 (m, partially obscured by residual acetonitrile solvent peak, 4H, H_g). Compound lettering shown in Figure 2. ^{13}C NMR (CD_3CN) δ 145.1, 129.1, 81.6, 77.6, 71.2, 70.3, 66.6, 53.6, 38.7, 25.6, 22.7, 18.4; ^{19}F NMR (CD_3CN) δ −144.6 (heptet, $J_{P,F}$ = 707 Hz); ^{31}P NMR (CD_3CN) δ −73.4 (d, $J_{P,F}$ = 707 Hz); HRMS–ESI (*m*/*z*): [M + PF_6]$^+$ calcd for $C_{28}H_{32}N_6Fe$·PF_6, 653.1674; found, 653.1693

Bis(triazolium)-bis(alkyne) **6·2BF$_4$**

The neutral bis(alkyne) **2** (0.096 g, 0.20 mmol) was dissolved in dichloromethane (15 mL). Trimethyloxonium tetrafluoroborate (0.065 g, 0.44 mmol) was added and the orange solution stirred at room temperature under a nitrogen atmosphere overnight. Methanol (1 mL) was added to quench the alkylating agent, and the mixture was evaporated to dryness under reduced pressure. Purification by preparative thin-layer chromatography (silica, eluent: 10% methanol in dichloromethane) gave **6·2BF$_4$** as an orange powder. Yield: 0.106 g (77%). ^{1}H NMR (acetone-d_6) δ 8.60 (s, 2H, trz$^+$-*H*), 5.75 (s, 4H, Fc-C*H*$_2$-trz$^+$), 4.64 (t, ^3J = 1.9 Hz, 4H, Fc-*H*), 4.42 (t, ^3J = 1.9 Hz, 4H, Fc-*H*), 4.34 (s, 6H, trz$^+$-C*H*$_3$), 3.08 (t, ^3J = 7.7 Hz, 4H, trz$^+$-C*H*$_2$-CH$_2$), 2.41 (t, ^4J = 2.6 Hz, 2H, C≡C*H*), 2.35 (dt, ^3J = 6.8 Hz, ^4J = 2.6 Hz, 4H, C*H*$_2$-C≡CH), 1.93–2.02 (m, 4H, CH$_2$-C*H*$_2$-CH$_2$-C≡CH); ^{13}C NMR (acetone-d_6) δ 145.0, 128.6, 83.5, 80.9, 71.6, 71.5, 71.2, 53.7, 38.1, 26.5, 22.8, 18.0; ^{19}F NMR (acetone-d_6) δ −150.9 (m); HRMS–ESI (*m*/*z*): [M + BF_4]$^+$ calcd for $C_{28}H_{34}N_6Fe$·BF_4, 597.2218; found, 597.2239.

X-ray crystallography

Single crystal X-ray diffraction data for **3** were collected by using synchrotron radiation (λ = 0.6889 Å) at the Diamond Light Source, Beam I19. The diffractometer was equipped with a Cryostream N_2 open-flow cooling device [19] and the data were collected at 100(2) K. A series of ω-scans was performed in such a way as to collect a half-sphere of data to a maximum resolution of 0.77 Å. Cell parameters and intensity data (including interframe scaling) were processed with CrysAlis Pro [20].

The structures were solved by charge-flipping methods with SUPERFLIP [21] and refined using full-matrix least-squares on F^2 within the CRYSTALS suite [22]. All nonhydrogen atoms were refined with anisotropic displacement parameters. Hydrogen atoms were generally visible in the difference map, and their positions and displacement parameters were refined by using restraints prior to inclusion into the model employing riding constraints [23].

Crystallographic data for the structures have been deposited with the Cambridge Crystallographic Data Centre, CCDC: 859564 and 859565. Copies of these data can be obtained free of charge from The Cambridge Crystallographic Data Centre at http://www.ccdc.cam.ac.uk/data_request/cif.

NMR titration protocols

Initial sample volumes were 0.50 mL and concentrations were 2.0 mmol L^{-1} of host. Solutions (100 mmol L^{-1}) of anions as their tetrabutylammonium salts were added in aliquots, the samples thoroughly shaken and spectra recorded. Spectra were recorded at 0, 0.2, 0.4, 0.6, 0.8, 1.0, 1.2, 1.4, 1.6, 1.8, 2.0, 2.5, 3.0, 4.0, 5.0, 7.0 and 10 equivalents. Stability constants were obtained by analysis of the resulting data with the WinEQNMR2 [13] computer program, following the triazolium C–H protons in all cases.

Electrochemistry protocols

Cyclic voltammetry was performed on an Autolab Potentiostat/Galvanostat model PG-STAT 12, controlled by General Purpose Electrochemical System Software v. 4.9 (Eco Chemie). A standard one-compartment three-electrode electrochemical cell, located inside a Faraday cage, was used with a glassy carbon solid-disc working electrode, a platinum-wire auxiliary electrode and an Innovative Instruments, Inc. LF-2 leak-free silver/silver chloride reference electrode. A 0.50 mM ferrocene

sample was used in order to check the reference electrode and internal resistance of the equipment. The electrolyte solution used in all experiments was 0.10 M TBA·PF_6 in CH_3CN. CVs were recorded with a 1 s equilibration time and a step potential of 1 mV.

The receptor **3** was dissolved in 3.0 mL of the electrolyte solution, such that the receptor concentration was 0.50 mM, and cyclic voltammograms were recorded. Scan rates of 25, 50, 100, 200, 300, 400 and 500 mV s^{-1} were used in order to test for reversibility. Aliquots of TBA·Cl or TBA·BzO (as a 0.50 M solution of electrolyte solution) were added to the receptor solution, stirred and the cyclic voltammograms recorded at a scan rate of 100 mV s^{-1}.

Supporting Information

Supporting Information File 1

NMR-spectra of new compounds.
[http://www.beilstein-journals.org/bjoc/content/supplementary/1860-5397-8-25-S1.pdf]

Supporting Information File 2

X-ray data of macrocycles **3** and **4**.
[http://www.beilstein-journals.org/bjoc/content/supplementary/1860-5397-8-25-S2.cif]

Acknowledgements

We thank the Clarendon Fund and Trinity College, Oxford for funding and Diamond Light Source for the award of beam time on Beamline I19. Ben Mullaney is thanked for assistance with electrochemistry experiments.

References

1. Rostovtsev, V. V.; Green, L. G.; Fokin, V. V.; Sharpless, K. B. *Angew. Chem., Int. Ed.* **2002,** *41,* 2596–2599. doi:10.1002/1521-3773(20020715)41:14<2596::AID-ANIE2596>3.0.CO;2-4
2. Tornøe, C. W.; Christensen, C.; Meldal, M. *J. Org. Chem.* **2002,** *67,* 3057–3064. doi:10.1021/jo011148j
3. Juríček, M.; Kouwer, P. H. J.; Rowan, A. E. *Chem. Commun.* **2011,** *47,* 8740–8749. doi:10.1039/c1cc10685f
4. Li, Y.; Flood, A. H. *J. Am. Chem. Soc.* **2008,** *130,* 12111–12122. doi:10.1021/ja803341y
5. Li, Y.; Flood, A. H. *Angew. Chem., Int. Ed.* **2008,** *47,* 2649–2652. doi:10.1002/anie.200704717
6. Meudtner, R. M.; Hecht, S. *Angew. Chem., Int. Ed.* **2008,** *47,* 4926–4930. doi:10.1002/anie.200800796
7. Juwarker, H.; Lenhardt, J. M.; Castillo, J. C.; Zhao, E.; Krishnamurthy, S.; Jamiolkowski, R. M.; Kim, K.-H.; Craig, S. L. *J. Org. Chem.* **2009,** *74,* 8924–8934. doi:10.1021/jo901966f
8. Mullen, K. M.; Mercurio, J.; Serpell, C. J.; Beer, P. D. *Angew. Chem.* **2009,** *48,* 4781–4784. doi:10.1002/anie.200901313
9. Kumar, A.; Pandey, P. S. *Org. Lett.* **2008,** *10,* 165–168. doi:10.1021/ol702457w
10. Schulze, B.; Friebe, C.; Hager, M. D.; Günther, W.; Kohn, U.; Jahn, B. O.; Görls, H.; Schubert, U. S. *Org. Lett.* **2010,** *12,* 2710–2713. doi:10.1021/ol100776x
11. Cao, Q.-Y.; Pradhan, T.; Kim, S.; Kim, J. S. *Org. Lett.* **2011,** *13,* 4386–4389. doi:10.1021/ol201722d
12. Casas-Solvas, J. M.; Ortiz-Salmerón, E.; Giménez-Martínez, J. J.; García-Fuentes, L.; Capitán-Vallvey, L. F.; Santoyo-González, F.; Vargas-Berenguel, A. *Chem.–Eur. J.* **2009,** *15,* 710–725. doi:10.1002/chem.200800927
13. Hynes, M. J. *J. Chem. Soc., Dalton Trans.* **1993,** 311–318.
14. Bard, A. J.; Faulkner, L. R. *Electrochemical methods: fundamentals and applications;* John Wiley & Sons, 1980.
15. Evans, N. H.; Serpell, C. J.; Beer, P. D. *Chem. Commun.* **2011,** *47,* 8775–8777. doi:10.1039/c1cc13247d
16. Wong, W. W. H.; Curiel, D.; Lai, S.-W.; Drew, M. G. B.; Beer, P. D. *Dalton Trans.* **2005,** 774–781. doi:10.1039/b416851h
17. Beer, P. D.; Hayes, E. J. *Coord. Chem. Rev.* **2003,** *240,* 167–189. doi:10.1016/S0010-8545(02)00303-X
18. Lee, B.-Y.; Park, S. R.; Jeon, H. B.; Kim, K. S. *Tetrahedron Lett.* **2006,** *47,* 5105–5109. doi:10.1016/j.tetlet.2006.05.079
19. Cosier, J.; Glazer, A. M. *J. Appl. Crystallogr.* **1986,** *19,* 105–107. doi:10.1107/S0021889886089835
20. *CrysAlis Pro;* Oxford Diffraction: Yarnton, U.K., 2010.
21. Palatinus, L.; Chapuis, G. *J. Appl. Crystallogr.* **2007,** *40,* 786–790. doi:10.1107/S0021889807029238
22. Betteridge, P. W.; Carruthers, J. R.; Cooper, R. I.; Prout, K.; Watkin, D. J. *J. Appl. Crystallogr.* **2003,** *36,* 1487. doi:10.1107/S0021889803021800
23. Cooper, R. I.; Thompson, A. L.; Watkin, D. J. *J. Appl. Crystallogr.* **2010,** *43,* 1100–1107. doi:10.1107/S0021889810025598

License and Terms

Beilstein Journal of Organic Chemistry

Self-assembly of Ru_4 and Ru_8 assemblies by coordination using organometallic $Ru(II)_2$ precursors: Synthesis, characterization and properties

Sankarasekaran Shanmugaraju, Dipak Samanta and Partha Sarathi Mukherjee*

Full Research Paper

Open Access

Address:
Department of Inorganic and Physical Chemistry, Indian Institute of Science, Bangalore-560 012, India. Fax: 91-80-2360-1552; Tel: 91-80-2293-3352

Email:
Partha Sarathi Mukherjee* - psm@ipc.iisc.ernet.in

* Corresponding author

Keywords:
cages; macrocycles; ruthenium(II); self-assembly; self-sorting

Beilstein J. Org. Chem. **2012,** *8,* 313–322.
doi:10.3762/bjoc.8.34

Received: 20 December 2011
Accepted: 08 February 2012
Published: 28 February 2012

This article is part of the Thematic Series "Supramolecular chemistry II".

Guest Editor: C. A. Schalley

Abstract

Coordination-driven self-assembly of binuclear half-sandwich *p*-cymene ruthenium(II) complexes $[Ru_2(\mu\text{-}\eta^4\text{-}C_2O_4)(MeOH)_2(\eta^6\text{-}p\text{-cymene})_2](O_3SCF_3)_2$ (**1a**) or [Ru$_2$(μ-η^4-*N*,*N*′-diphenyloxamidato)(MeOH)$_2$(η^6-*p*-cymene)$_2$](O$_3$SCF$_3$)$_2$ (**1b**) separately with an imidazole-based tetratopic donor **L** in methanol affords two tetranuclear metallamacrocycles **2a** and **2b**, respectively. Conversely, the similar combination of **L** with 2,5-dihydroxy-1,4-benzoquinonato (dhbq) bridged binuclear complex $[Ru_2(\mu\text{-}\eta^4\text{-}C_6H_2O_4)(MeOH)_2(\eta^6\text{-}p\text{-cymene})_2](O_3SCF_3)_2$ (**1c**) in 1:2 molar ratio resulted in an octanuclear macrocyclic cage **2c**. All the self-assembled macrocycles **2a**–**2c** were isolated as their triflate salts in high yields and were characterized fully by multinuclear (^{1}H, ^{13}C and ^{19}F) NMR, infrared (IR) and electrospray ionization mass spectrometry (ESIMS). In addition, the molecular structure of macrocycle **2a** was established unequivocally by single-crystal X-ray diffraction analysis and adopts a tetranuclear rectangular geometry with the dimensions of 5.53 Å × 12.39 Å. Furthermore, the photo- and electrochemical properties of these newly synthesized assemblies have been studied by using UV–vis absorption and cyclic voltammetry analysis.

Introduction

Self-assembly of metal-based molecular architectures through coordination has emerged as an active field of research as large numbers of intricate structural motifs can easily be derived in a single step from predesigned molecular building units. In the last two decades several interesting molecular architectures of defined shapes, sizes and functionality have been discovered with the aid of this powerful protocol [1,2]. The basic requirement for successful metal–ligand-directed self-assembly resides

in the judicious designing of information-encoding molecular building blocks having complementary binding sites. Large numbers of molecular polygons and polyhedra have been synthesized mostly from *cis*-blocked Pd(II)- and Pt(II)-based building units due to their rigid square-planar coordination geometry as well as to their interesting photophysical properties [3-5]. However, we and others have recently reported several shape-persistent discrete macrocycles/cages using half-sandwich octanuclear Ru(II) piano-stool complexes in combination with polypyridyl or polycarboxylate donors [6-10]. Ligands with an imidazole functionality are of considerable interest due to the presence of imidazole in many biological systems, and also the better donor character of imidazole compared to widely used pyridyl donors. Owing to these properties, we were interested in incorporating an imidazole functionality into discrete molecules of defined shapes, and also to investigate their influence in terms of directionality in controlling the geometry of the resulting molecular architectures. Herein, we report the self-assembly reactions of $[Ru_2(\mu\text{-}\eta^4\text{-}C_2O_4)(MeOH)_2(\eta^6\text{-}p\text{-cymene})_2](O_3SCF_3)_2$ (**1a**) or $[Ru_2(\mu\text{-}\eta^4\text{-}N,N'\text{-diphenyloxamidato})(MeOH)_2(\eta^6\text{-}p\text{-cymene})_2]$ $(O_3SCF_3)_2$ (**1b**) and $[Ru_2(\mu\text{-}\eta^4\text{-}C_6H_2O_4)(MeOH)_2(\eta^6\text{-}p\text{-cymene})_2](O_3SCF_3)_2$ (**1c**) with a tetratopic imidazole-based donor **L** in methanol at room temperature to generate two tetranuclear macrocycles of general formula $[Ru_4(\mu\text{-}\eta^4\text{-}C_2O_4$ or *N,N'*-diphenyloxamidato$)_2$(**L**)$(\eta^6\text{-}p\text{-cymene})_4](O_3SCF_3)_4$ (**2a**, **2b**) and an octanuclear macrocyclic cage $[Ru_8(\mu\text{-}\eta^4\text{-}C_6H_2O_4)_4$(**L**$)_2(\eta^6\text{-}p\text{-cymene})_8](O_3SCF_3)_8$ (**2c**), respectively in quantitative yields [**L** = 1,2,4,5-*tetrakis*(imidazol-1-yl)benzene]. The final assemblies were characterized by multinuclear (^{1}H, ^{13}C and ^{19}F) NMR, IR and ESIMS analyses. The molecular structure of tetranuclear macrocycle **2a** was determined by single-crystal X-ray diffraction analysis, which reveals a tetranuclear geometry with the dimensions of 5.53 Å × 12.39 Å. In addition to their synthesis and characterization, the UV–vis absorption and cyclic voltammetry studies are reported.

Results and Discussion

Synthesis and characterization of the tetranuclear complexes

According to the "directional-bonding approach" and "symmetry-interaction model", one can expect the formation of either a [4 + 2] assembled octanuclear tetragonal prism or a [2 + 1] assembled tetranuclear 2D structure upon reaction of a binuclear "clip"-type acceptor and a tetratopic donor (Scheme 1) [11].

Instead, the exclusive formation of two tetranuclear assemblies (**2a**, **2b**) upon mixing of binuclear $Ru(II)_2$ acceptors **1a** or **1b** with an imidazole-based tetratopic donor **L** is interesting. The exclusive self-sorting of tetranuclear macrocycles (**2a** and **2b**) rather than the expected octanuclear molecular cage is, presumably, due to the perfect matching of the distance between two Ru(II) metal centers with the distance between the adjacent imidazole donor sites in **L**. Moreover, from an entropic point of view such [2 + 1] self-assembly is expected to be preferred over [4 + 2] assembly as the loss of entropy in the latter case is more. As shown in Scheme 2, the binuclear acceptor **1a** or **1b** was treated separately with an imidazole-based tetratopic donor **L** in a 2:1 molar ratio in methanol at room temperature to obtain [2 + 1] self-assembled macrocycles **2a** and **2b**, respectively, in high yields. The addition of solid **L** into a methanolic solution of the acceptor (**1a** or **1b**) lead to the immediate consumption of the solid and showed a sharp visible color change from light yellow to intense yellow. Both **2a** and **2b** are isolated as their triflate salts and are highly soluble in common organic solvents such as $(CH_3)_2CO$, CH_3CN, CH_3OH and CH_2Cl_2. The formation of the complexes (**2a** and **2b**) was initially characterized by IR, multinuclear (^{1}H, ^{13}C and ^{19}F) NMR and ESIMS spectrometric analyses.

The IR spectra (Figure S1, Supporting Information File 1) of the macrocycles showed strong bands at 1624.6 cm^{-1} (**2a**) and

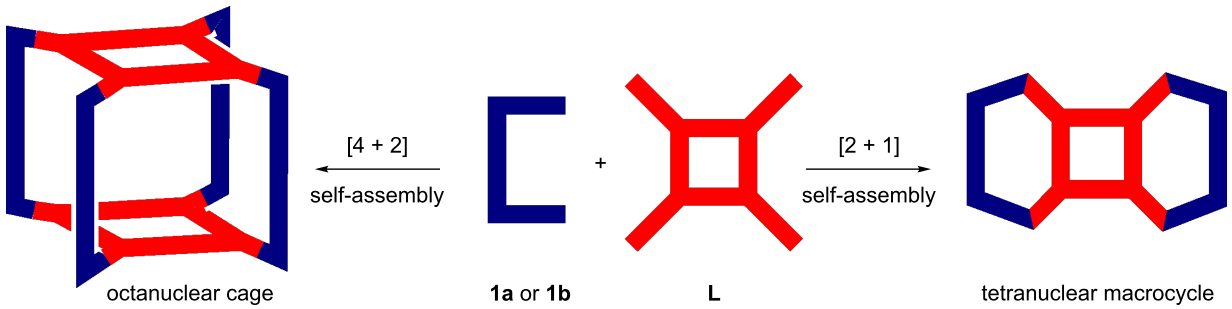

Scheme 1: Possible octanuclear prism and tetranuclear macrocycle resulting from the combination of a tetradendate donor with a clip-type acceptor unit.

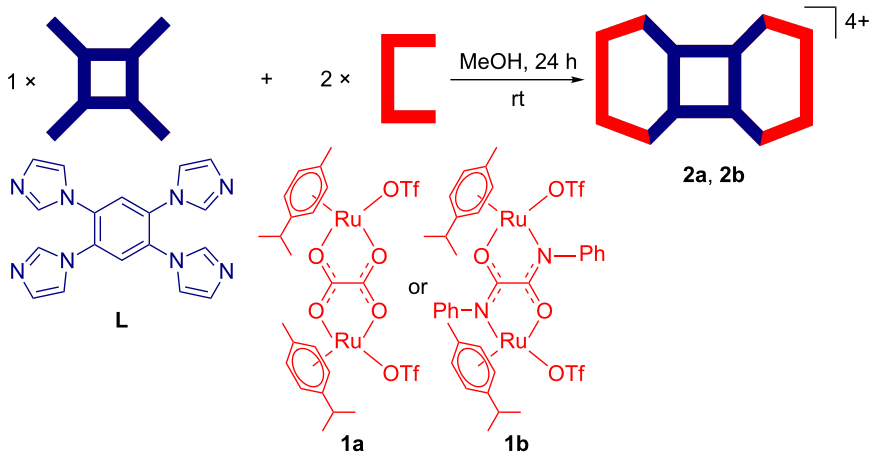

Scheme 2: Formation of the tetranuclear complexes (**2a** and **2b**) upon the reaction of Ru(II)$_2$ based acceptors **1a** or **1b** and tetraimidazole ligand **L** in methanol at room temperature.

1602 cm^{-1} (**2b**) corresponding to the symmetrical stretching frequencies (ν_{CO}) of the carbonyl groups of the coordinated bis-bidentate oxalato (**2a**) or *N*,*N*′-diphenyloxamidato (**2b**) ligands. These bands, due to symmetrical stretching (ν_{CO}) in the complexes, are slightly shifted to a higher energy region compared to those of the starting acceptors (**1a**, ν_{CO} = 1623.7 cm^{-1}; **1b**, ν_{CO} = 1605.0 cm^{-1}) due to the ligand-to-metal coordination. The appearance of a single peak in the ^{19}F NMR spectrum at −81.03 ppm (**2a**) or −79.8 ppm (**2b**) indicated the presence of triflate counter anions in the same chemical environment in the resultant complexes (Figure 1 and Figure S3, Supporting Information File 1).

Four peaks correspond to the donor **L** in the aromatic region (δ 6.95–8.10 ppm) were found in the ^{1}H NMR spectra of **2a** and **2b**. Protons corresponding to the capped *p*-cymene moiety appeared in the range of δ 5.14–5.81 ppm. Notably, the ^{1}H signals of the protons of **L** exhibited a significant downfield shift compared to the unbound linker due to the loss of electron density upon ligand-to-metal coordination (Figure 1 and Figure S2, Supporting Information File 1). The high solubility of the assemblies in common organic solvents and the symmetric nature of ^{1}H NMR spectra primarily ruled out the formation of a polymer with extended coordination. Although the initial characterization of the self-assembled species by NMR spec-

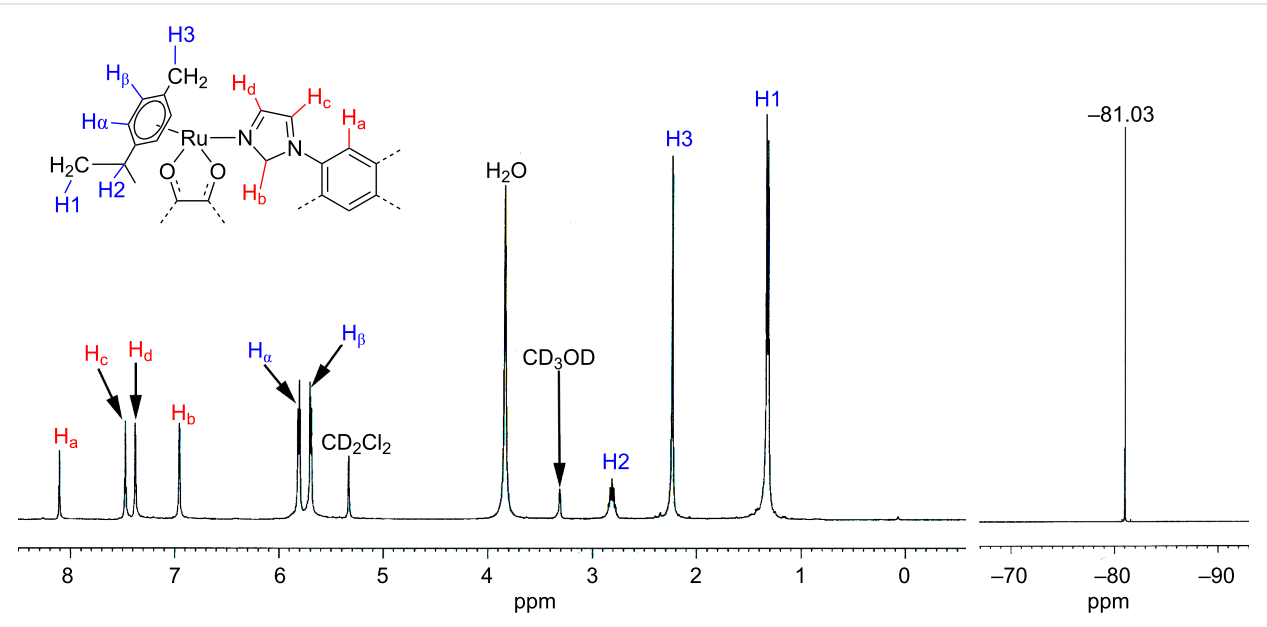

Figure 1: ^{1}H (left) and ^{19}F (right) NMR spectra of tetranuclear macrocycle **2a** recorded in CD_2Cl_2–CD_3OD with peak assignments.

troscopy intimated the ligand-to-metal coordination, it does not provide any information about the exact composition and nuclearity of the final products.

Electrospray ionization mass spectrometry (ESIMS) can be used as a soft-ionization method to elucidate the exact composition of the product [12]. The ESIMS analysis confirmed the formation of the rather unexpected [2 + 1] self-assembled tetranuclear macrocycles **2a** and **2b** by the appearance of multiply charged fragmented ions (Figure 2 and Figure S4, Supporting Information File 1). The multiply charged ions for **2a** at m/z = 1906.9 [**2a** − $O_3SCF_3^-$]$^+$, 879.0 [**2a** − $2O_3SCF_3^-$]$^{2+}$; for **2b** at m/z = 1029.53 [**2b** − $2O_3SCF_3^-$]$^{2+}$, 637.27 [**2b** − $3O_3SCF_3^-$]$^{3+}$ were observed and these peaks were well resolved isotopically (Figure 2 and Figure S4, Supporting Information File 1). The appearance of the expected peaks along with the isotopic patterns was in strong support of the formation of [2 + 1] self-assembled products in both cases.

Finally, the molecular structure of the tetranuclear metallamacrocycle [(*p*-cymene)$_4$Ru$_4$(μ-η^4-oxalato)$_2$(**L**)]$^{4+}$($O_3SCF_3^-$)$_4$ (**2a**) was unambiguously determined by single-crystal X-ray diffraction analysis. Single crystals of **2a** of high enough quality for X-ray diffraction were grown by slow vapor diffusion of diethyl ether into a methanolic solution of **2a** at room temperature. Macrocycle **2a** was crystallized in a tetragonal crystal system with *I*41/*a* space group having sixteen formula units per unit cell. A perspective view of the macrocycle **2a** is depicted in Figure 3 with atom numbering, and its selected bond parameters are summarized in Table S1, Supporting Information File 1.

The crystal-structure analysis of **2a** shows a tetranuclear geometry with dimensions of 5.53 Å × 12.39 Å, and the coordination geometry around each Ru(II) is octahedral. Capped *p*-cymene occupies three coordinating sites of each Ru(II). The bridging dianionic oxalato ($C_2O_4^{2-}$) ligand binds through its two oxygen atoms. The imidazole nitrogen of the donor **L** occupies the sixth

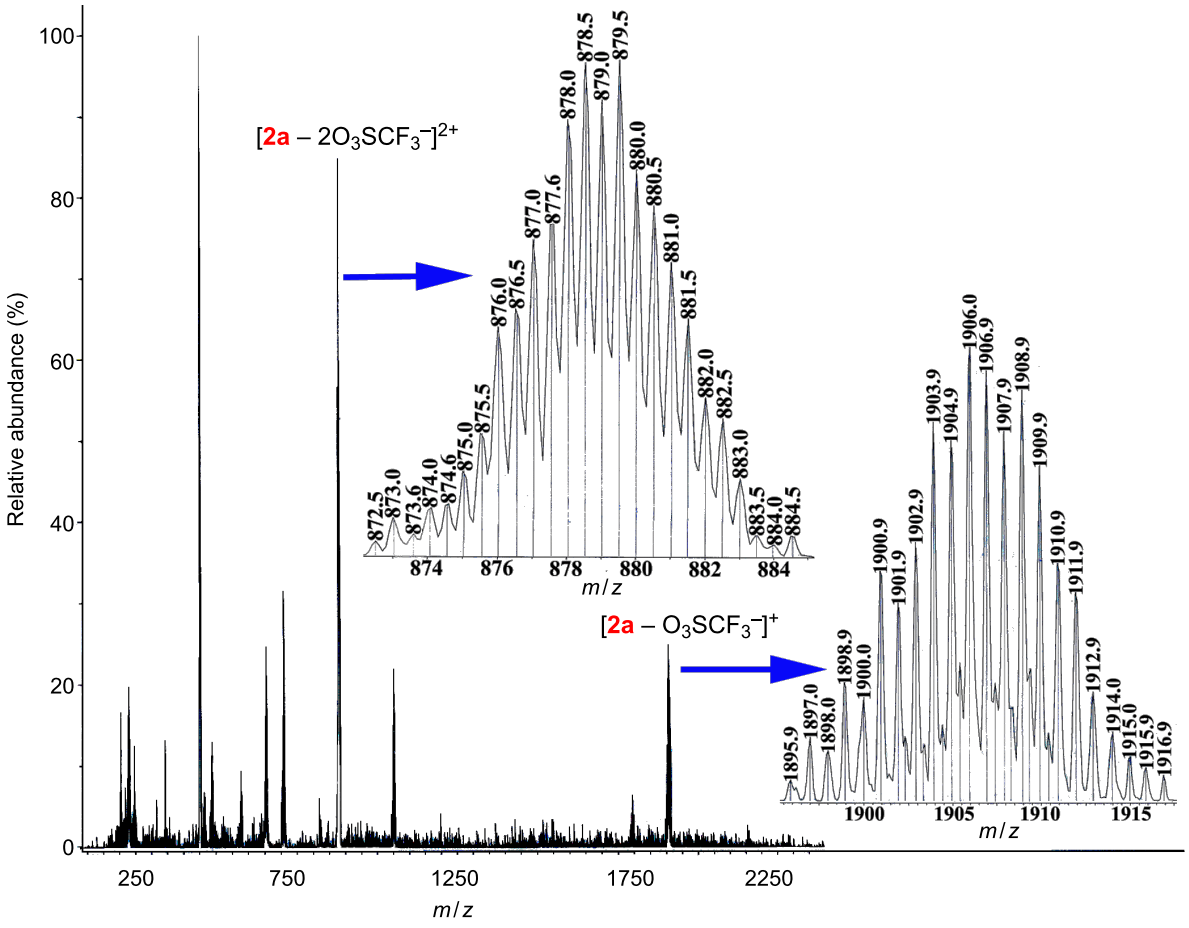

Figure 2: ESIMS spectrum of the macrocycle **2a** recorded in acetonitrile. Inset: Experimentally observed isotopic distribution for [**2a** − $O_3SCF_3^-$]$^+$ and [**2a** − $2O_3SCF_3^-$]$^{2+}$ fragments.

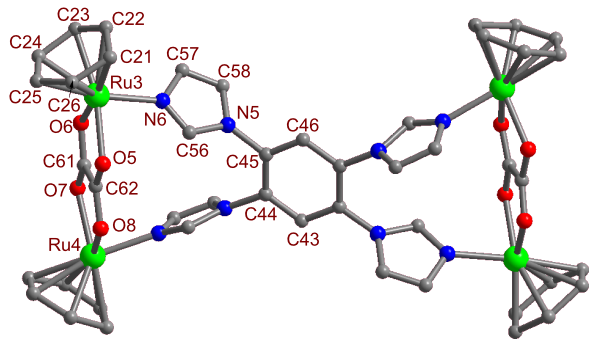

Figure 3: A ball and stick representation of **2a** with atom numbering. Color code: Ru = green; O = red; N = blue; C = dark gray. All hydrogen atoms, triflate counter anions, isopropyl and methyl groups of the *p*-cymene moiety are omitted for the sake of clarity.

coordination site. The oxalato ligand connects to two ruthenium metal centers through four oxygen atoms. The average Ru–N and Ru–O bond distances are 2.140 Å and 2.141 Å, respectively. The four donor sites of **L** are coordinated to four different Ru(II) metal centers and thereby it adopts a tetranuclear rectangular geometry. The solid-state packing of macrocycle **2a** along the crystallographic *c*-axis results in a highly porous structure with square-type channels due to the π–π interactions between the adjacent macrocycles (Figure S8, Supporting Information File 1). Triflate ($O_3SCF_3^-$) counter anions are located outside of the porous channel (Figure S8, Supporting Information File 1).

Synthesis and characterization of the octanuclear cage

The construction of an octanuclear macrocyclic cage **2c** was accomplished following a similar procedure as adopted for the synthesis of tetranuclear rectangular complexes **2a** and **2b**. Drop-wise mixing of a methanolic solution of binuclear acceptor **1c** into a suspension of tetradendate linker **L** in methanol in 2:1 molar ratio afforded the exclusive formation of the [4 + 2] self-assembled macrocyclic cage **2c** in good yield after 24 h of stirring at room temperature (Scheme 3). The obvious reason for the formation of an octanuclear macrocyclic cage **2c** in contrast to the tetranuclear rectangles **2a** and **2b** is attributed to the increased length of the acceptor unit **1c** compared to **1a** or **1b**. The immediate consumption of the suspended donor **L** in the clear solution and the observable color change from purple to deep red indicated the progress of the self-assembly reaction. The initial characterization of the isolated macrocycle by multinuclear (^{1}H, ^{13}C and ^{19}F) NMR suggested the formation of a single and symmetric macrocyclic complex.

The infrared spectra (Figure S1, Supporting Information File 1) of the macrocycle (**2c**) showed a strong band at 1521.2 cm^{-1} corresponding to the symmetric stretching frequency (ν_{CO}) of the carbonyl groups of the coordinated bis-bidentate quinonato ligand, and this symmetric stretching frequency (ν_{CO}) in the isolated macrocycle is slightly shifted to the higher energy region compared to that of the starting acceptor (**1c**, ν_{CO} =

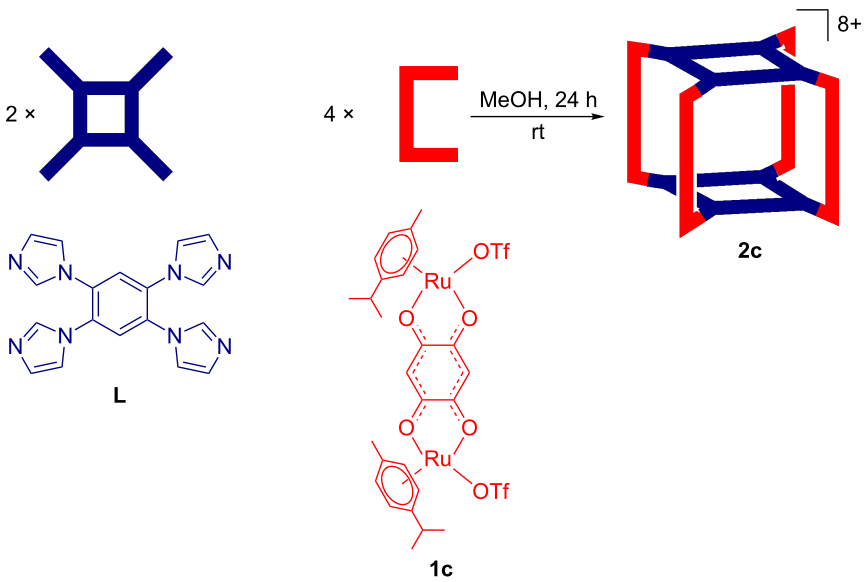

Scheme 3: Formation of an octanuclear macrocycle **2c** upon reaction of $Ru(II)_2$-based acceptors **1c** with imidazole-based tetratopic donor **L** in methanol at room temperature.

1515.8 cm^{-1}) due to the ligand-to-metal coordination. The ^1H NMR spectra of the macrocycle **2c** established the expected peaks in the aromatic region corresponding to the tetratopic donor **L** and the proton resonance of capped *p*-cymene ligand. Moreover, the peak of **L** in the macrocyclic complex exhibits a significant downfield shift due to the ligand–metal coordination (Figure 4). The assignment of the proton signals in the ^1H NMR spectra was confirmed by the ^1H–^1H COSY NMR (Figure S5, Supporting Information) spectral analysis. Furthermore, the appearance of prominent peaks in the ESIMS spectra of the multiply charged ions for **2c** at m/z = 2008.0 [**2c** − $2O_3SCF_3^-]^{2+}$, 1288.0 [**2c** − $3O_3SCF_3^-]^{3+}$, 928.9 [**2c** − $4O_3SCF_3^-]^{4+}$ indicated the formation of a [4 + 2] self-assembled octanuclear macrocyclic cage. The peaks corresponding to the [**2c** − $2O_3SCF_3^-]^{2+}$ and [**2c** − $3O_3SCF_3^-]^{3+}$ fragments are well resolved isotopically (Figure S6, Supporting Information File 1).

Unfortunately, all efforts to obtain diffraction-quality single crystals of the macrocycle **2c** have so far been unsuccessful. However, the analysis of multinuclear NMR (^1H, ^{13}C and ^{19}F) in concurrence with the ESIMS study is fully consistent with the formation of a [4 + 2] self-assembled octanuclear metallacage. In view toward gaining further insight into the structural characteristics of the newly designed macrocycle, the energy-minimized structure of the macrocycle **2c** was obtained by means of molecular mechanics universal-force-field simulation (MMUFF) [13]. A perspective view of the energy-minimized structure of the macrocycle **2c** is depicted in Figure 5. The optimized structures of the macrocycle **2c** suggested the formation

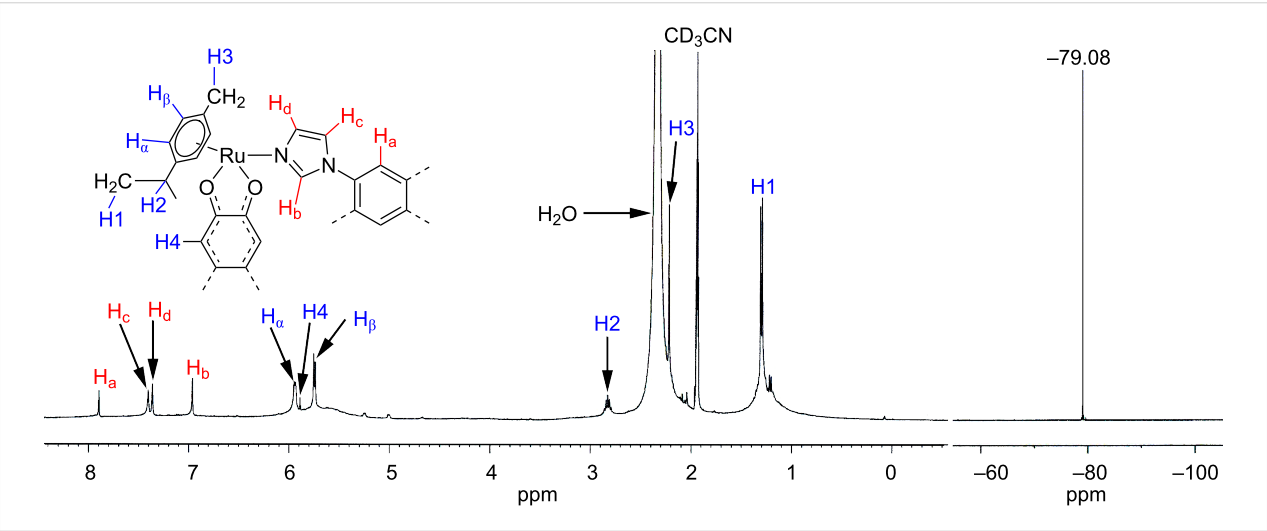

Figure 4: ^1H (left) and ^{19}F (right) NMR spectrum of the macrocycle **2c** recorded in CD_3CN with the peak assignments.

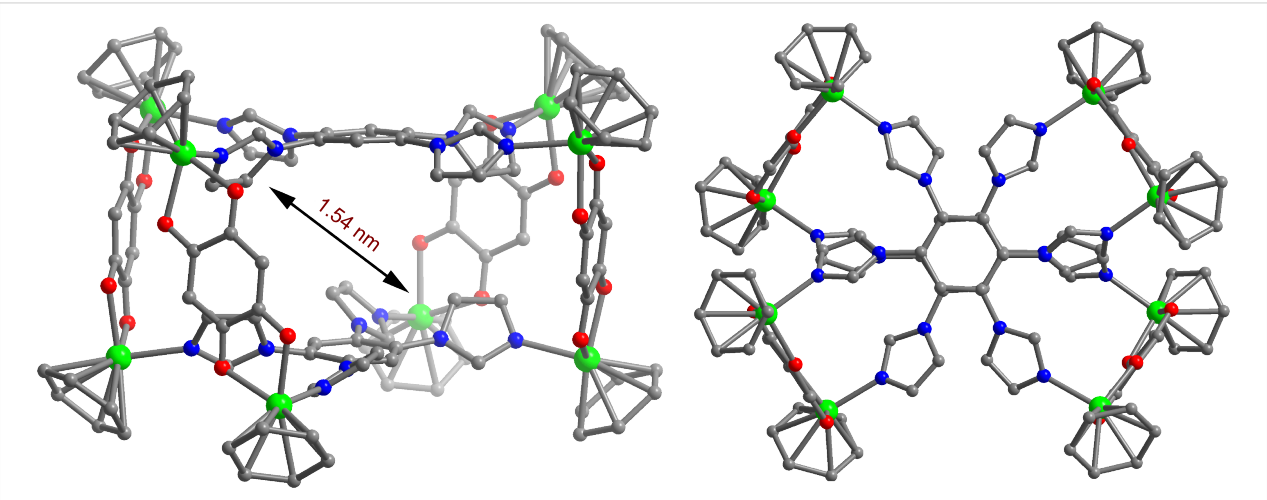

Figure 5: Side (left) and top (right) view of the energy-minimized structures of the octanuclear macrocycle **2c**. Color code: green = Ru, blue = N, red = O, gray = C. The hydrogen atoms, methyl and isopropyl group of the cymene moiety have been removed for the sake of clarity.

of an octanuclear macrocycle having an internal diameter of 1.54 nm. Notably, the quinonato-bridged ruthenium clips are tilted out of the plane of the imidazole donor in **2c** in order to minimize the steric influence between the acceptor clips. Therefore, macrocycle **2c** adopts a staggered conformation as was observed in similar types of 3D cages [14].

UV–vis absorption and electrochemical studies

One of the strongest driving factors to design multifarious functional supramolecular complexes is attributed to their interesting functional properties. In general, the utilization of functional properties would be realized more from macrocycles containing transition metals, due to their high sensitivity towards various external stimuli, compared to purely organic macrocycles. In this regard, substantial efforts have been devoted to the design of novel, nanoscopic and functional metallamacrocycles and also to the study of their functional properties [15]. The photo- and electrochemical properties of our newly synthesized macrocycles (**2a** and **2b**) are studied by UV–vis absorption and cyclic voltammetry investigations and the obtained results are summarized in Table 1.

The UV–vis absorption spectra were recorded from a CH_3CN solution (1.0×10^{-5} M) of the macrocycles at room temperature. The electronic absorption spectra (Figure 6) of the macrocycles **2a**–**2c** exhibit intense bands at λ_{max} (ε) 309 nm (2.3×10^4 M^{-1} cm^{-1}), 383 nm (6.8×10^3 M^{-1} cm^{-1}) for **2a**; λ_{max} (ε) = 328 nm (5.8×10^4 M^{-1} cm^{-1}) for **2b** and λ_{max} (ε) = 293 nm (6.3×10^4 M^{-1} cm^{-1}), 499 nm (3.2×10^4 M^{-1} cm^{-1}) for **2c**. The peaks in the ranges of 293–309 nm and 328–499 nm can be ascribed to both intra- and intermolecular π–π* and metal-to-ligand charge-transfer transitions associated with the capped *p*-cymene–ruthenium moiety, respectively. The electrochemical behavior of the macrocycles (**2a**–**2c**) was examined by using a Pt-disk electrode in dichloromethane with 0.1 M *n*-Bu_4NPF_6 as the supporting electrolyte and at 100 mV s^{-1} scan rate. The obtained redox responses of the macrocycles were found to be entirely different. Macrocycle **2c** shows three well-anchored quasi-reversible reductions at −0.39, −1.09 and −1.54 V and their corresponding anodic peak current at −0.16, −0.81 and −1.38 V (Figure 6). On the other hand, complex **2b** showed a single quasi-reversible redox response of the cathodic peak current at −1.53 V and the anodic peak counterpart potential approximately at −1.24 V (Figure S7, Supporting Information

Table 1: Results of UV–vis absorption (in CH_3CN, 1.0×10^{-5} M) and electrochemical (in CH_2Cl_2, 0.1 M *n*-Bu_4NPF_6) studies of macrocycles **2a**–**2c** at 298 K.

Macrocycle	Absorption maxima[a] λ_{max} (nm)	Molar extinction coefficient ε × 10^3 $M^{-1}cm^{-1}$ λ_{max} (nm)	$E_{1/2}$ (*V* vs SCE)
2a	**309**, 383	23 (309)	–
2b	**328**	58 (328)	−0.15
2c	**293**, 499	63 (293)	−0.08, −0.14, −0.12

[a]Values in bold represent the highest absorption (λ_{max}) maxima.

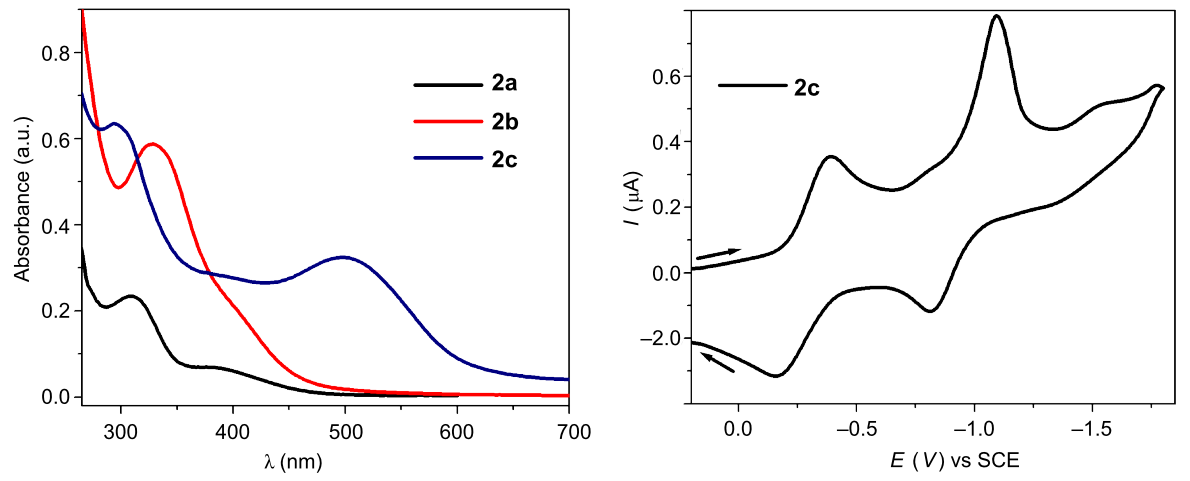

Figure 6: UV–vis absorption spectrum (left) of macrocycles (**2a**–**2c**) recorded in CH_3CN at 298 K, and cyclic voltammogram of **2c** (right) performed in CH_2Cl_2/0.1 M $(n\text{-Bu})_4NPF_6$ with a scan rate of 100 mV s^{-1} versus SCE at 298 K.

File 1). Surprisingly, macrocycle **2a** showed no anodic or cathodic peak current intensity within the range of +0.2 to −0.2 V, which implies the electrochemical inertness of **2a** (Figure S7, Supporting Information File 1). The observed anodic and cathodic peak currents of **2c** are almost equal, indicating the high chemical stability on the time scale of the voltammetry experiments. Notably, the cathodic peak current intensity of **2b** is much higher than its anodic peak current, and this can be attributed to the deposition of macrocycles on the electrode surface. Based on the electrochemical activity of other reported ruthenium complexes, the observed cathodic peaks are roughly assigned to one-electron reductions of the bridged quinonato or diphenyloxamidato ligands, and the oxidation is attributed to the Ru(II)/Ru(III) redox couples [16,17].

Conclusion

In conclusion, we synthesized two new tetranuclear macrocycles **2a**, **2b** and an octanuclear molecular prism **2c**, by coordination-driven self-assembly of an imidazole-based tetratopic donor linker **L** in combination with Ru(II)-based binuclear "clip" acceptors. All three of the self-assembled macrocycles were fully characterized by multinuclear (^{1}H, ^{13}C and ^{19}F) NMR, IR and ESIMS spectroscopic studies. In addition, the formation of a tetranuclear structure of **2a** was unambiguously established by analysis of single-crystal X-ray diffraction data. Though the formation of discrete structures from pyridyl donors has been well established, the quantitative formation of **2a**, **2b** and **2c** from an imidazole-type donor is new and suggests the feasibility of using imidazole derivatives as potential building units. The lengths of **1a** and **1b** fit well with the distance between two imidazole units in **L** to form the entropically favored [2 + 1] self-assembled structures **2a** and **2b**, respectively. As the distance between the two Ru(II) in **1c** is greater compared to the distance between the neighboring imidazole units in **L**, a similar reaction with **1c** allowed the formation of the 3D cage **2c**. The use of imidazole-based donor linkers in combination with organometallic half-sandwich ruthenium(II) precursors may generate a wide variety of complex molecular architectures with interesting functional properties.

Experimental

Materials and methods

The acceptor clips $[Ru_2(\mu\text{-}\eta^4\text{-}C_2O_4)(MeOH)_2(\eta^6\text{-}p\text{-cymene})_2](O_3SCF_3)_2$ (**1a**), $[Ru_2(\mu\text{-}\eta^4\text{-}N,N'\text{-diphenyloxamidato})(MeOH)_2(\eta^6\text{-}p\text{-cymene})_2](O_3SCF_3)_2$ (**1b**) and $[Ru_2(\mu\text{-}\eta^4\text{-}C_6H_2O_4)(MeOH)_2(\eta^6\text{-}p\text{-cymene})_2](O_3SCF_3)_2$ (**1c**) were synthesized under a dry nitrogen atmosphere by means of a standard Schlenk technique following the reported procedures [18-20]. The solvents were dried and distilled according to the standard literature procedures. 1,2,4,5-tetrabromobenzene and α-phellandrene were purchased from commercial sources and used without further purification. 1,2,4,5-Tetrakis(imidazol-1-yl)benzene (**L**) was synthesized by following the reported procedure [21]. NMR spectra were recorded on a Bruker 400 MHz spectrometer. The chemical shifts (δ) in the ^{1}H NMR spectra are reported in ppm relative to tetramethylsilane (Me_4Si) as the internal standard (0.0 ppm) or the proton resonance resulting from incomplete deuteration of the NMR solvents: CD_3CN (1.94), CD_3OD (3.33) and CD_2Cl_2 (5.33). ^{19}F NMR were recorded at 376.5 MHz and the chemical shifts (δ) are reported in ppm relative to the external standard Cl_3CF (0.00). ESIMS experiments were performed on a Bruker Daltonics (Esquire 300 Plus ESI model) with standard spectroscopic grade solvents CH_3CN or CH_3OH. IR spectra were recorded on a Bruker ALPHA FT-IR spectrometer. Electronic absorption studies were carried out on a Perkin Elmer LAMBDA 750 UV–vis spectrophotometer. The electrochemical measurements were performed in a three-electrode system consisting of a platinum electrode, a glassy-carbon counter electrode and a standard calomel reference electrode. All the potentials of the macrocycles (1.0×10^{-3} M in DCM) were measured with 0.1 M n-Bu_4NPF_6 as the supporting electrolyte at room temperature with a scan rate of 100 mV s^{-1}.

General procedure for the synthesis of 2a–2c: To a solid form of the tetratopic donor **L** was added separately a clear solution of the binuclear acceptor clip (**1a**–**1c**) in methanol (4 mL) in 1:2 molar ratio, and the mixture was stirred at room temperature for 24 h in a closed 4 mL glass vial. Immediate consumption of the suspended tetratopic donor (**L**) and significant visual color changes from light yellow to intense yellow for **2a** and **2b** or purple to deep red for **2c** evidenced the progress of the reactions. The solvent was removed under vacuum and the residue was dissolved in the minimum amount of dichloromethane (DCM) (~2 mL). Diethyl ether was mixed with concentrated clear solutions to precipitate out the expected macrocycles in pure form.

2a: Acceptor clip **1a** (29.5 mg, 0.032 mmol) and tetratopic donor **L** (5.5 mg, 0.016 mmol) were stirred in methanol (4 mL) to obtain **2a**. Isolated yield: 85%. ^{1}H NMR (400 MHz, CD_2Cl_2/CD_3OD) δ 8.10 (s, 2H, H_a-phenyl), 7.47 (s, 4H, H_c-imidazole), 7.37 (s, 4H, H_d-imidazole), 6.95 (s, 2H, H_b-imidazole), 5.81 (d, J = 6.0 Hz, 8H, H_α-cymene), 5.70 (d, J = 6.0 Hz, 8H, H_β-cymene), 2.84–2.77 (septet, 4H, H2-cymene), 2.23 (s, 12H, H3-cymene), 1.33 (d, 24H, H1-cymene); ^{19}F NMR (376.5 MHz, CD_2Cl_2/CD_3OD) δ −81.03 ppm; ^{13}C NMR (100 MHz, CD_3COCD_3) δ 171.65, 140.12, 136.08, 131.62, 129.14, 126.36, 124.65, 101.55, 98.10, 82.85, 81.12, 54.51, 31.56, 22.03, 17.79; IR (neat) ν (cm^{-1}): 3128.8 (w, C=C of aromatic), 1624.6 (s, CO-oxalate), 1254.9 (s, C–F of CF_3); ESIMS (m/z): 1907.16

[**2a** − $O_3SCF_3^-$]$^+$, 879.0 [**2a** − $2O_3SCF_3^-$]$^{2+}$; UV–vis (1.0×10^{-5} M, CH_3CN) λ_{max} nm (ε): 309 (2.3×10^4 M^{-1} cm^{-1}), 383 (6.8×10^3 M^{-1} cm^{-1}); Anal. calcd for $C_{66}H_{70}F_{12}N_8O_{20}Ru_4S_4$: C, 38.56; H, 3.43; N, 5.45; found: C, 38.84; H, 3.68; N, 5.71.

2b: Acceptor clip **1b** (34.3 mg, 0.032 mmol) and tetratopic donor **L** (5.5 mg, 0.016 mmol) were stirred in methanol (4 mL) to obtain **2b**. Isolated yield: 88%. ^{1}H NMR (400 MHz, CD_3OD) δ 8.19 (s, 4H, H_c-imidazole), 8.17 (s, 4H, H_d-imidazole), 7.82 (s, 4H, H_b-imidazole), 7.46–7.21 (m, 20H, *N*-phenyl), 7.17 (s, 2H, H_a-imidazole), 5.63–5.14 (m, 16H, $H_{\alpha,\beta}$-cymene), 2.50–2.48 (septet, 4H, H2-cymene), 1.71 (s, 12H, H3-cymene), 1.12 (d, 24H, H1-cymene); ^{19}F NMR (376.5 MHz, CD_3OD) δ −79.84; ^{13}C NMR (100 MHz, CD_3NO_2) δ 170.89, 147.02, 139.76, 135.54, 132.74, 129.87, 128.63, 127.03, 125.45, 123.82, 123.00, 119.81, 104.32, 99.43, 85.27, 83.99, 82.23, 81.35, 65.70, 31.47, 22.30, 20.99, 17.16, 14.70; IR (neat) ν (cm^{-1}): 3136 (w, C=C of aromatic), 1602 (s, CO-oxamide), 1262 (s, C–F of CF_3); ESIMS (*m*/*z*): 1029.53 [**2b** − $2O_3SCF_3^-$]$^{2+}$, 637.27 [**2b** − $3O_3SCF_3^-$]$^{3+}$; UV–vis (1.0×10^{-5} M, CH_3CN) λ_{max} nm (ε): 328 (5.8×10^4 M^{-1} cm^{-1}); Anal. calcd for $C_{90}H_{90}F_{12}N_{12}O_{16}Ru_4S_4$: C, 45.88; H, 3.85; N, 7.13; found: C, 46.59; H, 4.17; N, 7.43;

2c: Acceptor clip **1c** (31.1 mg, 0.032 mmol) and tetratopic donor **L** (5.5 mg, 0.016 mmol) were stirred in methanol (4 mL) to obtain **2c**. Isolated yield: 80%.^{1}H NMR (400 MHz, CD_3CN) δ 7.89 (s, 4H, H_a-phenyl), 7.40 (s, 8H, H_c-imidazole), 7.36 (s, 8H, H_d-imidazole), 6.96 (s, 8H, H_b-imidazole), 5.94 (d, *J* = 5.6 Hz, 16H, H_α-cymene), 5.88 (s, 4H, H4-quinone), 5.75 (d, *J* = 6.0 Hz, 16H, H_β-cymene), 2.86–2.79 (septet, 8H, H2-cymene), 2.22 (s, 24H, H3-cymene), 1.31 (d, 48H, H^1-cymene); ^{19}F NMR (376.5 MHz, CD_3CN) δ −79.08; ^{13}C NMR (100 MHz, CD_3NO_2) δ 183.92, 140.62, 134.75, 131.45, 124.09, 122.92, 119.74, 103.76, 99.10, 84.88, 83.65, 79.47, 78.00, 31.78, 22.27, 17.70; IR (neat) ν (cm^{-1}): 3128.8 (w, C=C of aromatic), 1521.2 (s, CO-oxalate), 1252.1 (s, C–F of CF_3); ESIMS (*m*/*z*): 2008.0 [**2c** − $2O_3SCF_3^-$]$^{2+}$, 1288.0 [**2c** − $3O_3SCF_3^-$]$^{3+}$, 928.9 [**2c** − $4O_3SCF_3^-$]$^{4+}$; UV–vis (1.0×10^{-5} M, CH_3CN) λ_{max} nm (ε): 293 (6.3×10^4 M^{-1} cm^{-1}), 499 (3.2×10^4 M^{-1} cm^{-1}); Anal. calcd for $C_{148}H_{148}F_{24}N_{16}O_{40}Ru_8S_8$: C, 41.23; H, 3.46; N, 5.20; found: C, 41.83; H, 4.16; N, 5.60.

X-ray data collection and structure refinements: Crystallographic data for **2a** were collected on a Bruker SMART APEX CCD diffractometer with the SMART/SAINT software [22]. X-ray-quality crystals were mounted on a glass fiber with traces of viscous oil. Intensity data were collected by using graphite-monochromatized Mo Kα radiation (0.7107 Å) at 150 K. The structures were solved by direct methods using SHELX-97 incorporated in WinGX [23-27]. Empirical absorption corrections were applied with SADABS [25]. All nonhydrogen atoms were refined with anisotropic displacement coefficients. Hydrogen atoms were assigned isotropic displacement coefficients, U(H) = 1.2U(C) or 1.5U (C-methyl), and their coordinates were allowed to ride on their respective carbons.

CCDC-845980 (for complex **2a**) contains the supplementary crystallographic data reported in this paper. The data can be obtained free of charge from the Cambridge Crystallographic Data Center via http://www.ccdc.cam.ac.uk/data_request/cif.

Crystallographic data: $C_{66}H_{70}F_{12}N_8O_{20}Ru_4S_4$, M_r = 2055.86, tetragonal, space group *I*41/*a*, *a* = 27.975(5) Å, *b* = 27.975(5) Å, *c* = 48.786(17) Å, α = 90°, β = 90°, γ = 90°, *V* = 38179(16) Å^3, *Z* = 16, $\rho_{calcd.}$ = 1.431 g cm^{-1}, Mo Kα radiation (graphite monochromatic, λ = 0.71073 Å), *T* = 150 K, final R indices [I > 2σ(I)]: R_1 = 0.1152 (5366), wR_2 = 0.4337 (18769).

Supporting Information

Supporting Information File 1

Infrared and NMR spectra of the macrocycles **2a**, **2b** and **2c** and solid-state packing diagram of macrocycle **2a**.
[http://www.beilstein-journals.org/bjoc/content/supplementary/1860-5397-8-34-S1.pdf]

Supporting Information File 2

Crystallographic details of **2a**.
[http://www.beilstein-journals.org/bjoc/content/supplementary/1860-5397-8-34-S2.cif]

Acknowledgements

S.S. and D.S. gratefully acknowledge the Council of Scientific and Industrial Research, New Delhi, India for the award of a research fellowship. P.S.M. thanks the Department of Science and Technology (DST), India, for financial support. S.S. sincerely thanks Mr. R. Sathish Kumar (SSCU, IISc) and Mr. Yogesh P. Patil (IPC, IISc) for their kind help in the X-ray data collection and structure solving. S.S. thanks Mr. Tridip (IPC, IISc) for his assistance in the cyclic voltammetry study. The authors are grateful to Johnson Matthey Pvt. Ltd. U.K. for their generous donation of $RuCl_3$.

References

1. Northrop, B. H.; Yang, H.-B.; Stang, P. J. *Chem. Commun.* **2008,** 5896–5908. doi:10.1039/b811712h
2. Yoshizawa, M.; Klosterman, J. K.; Fujita, M. *Angew. Chem., Int. Ed.* **2009,** *48,* 3418–3438. doi:10.1002/anie.200805340
3. Chakrabarty, R.; Mukherjee, P. S.; Stang, P. J. *Chem. Rev.* **2011,** *111,* 6810–6918. doi:10.1021/cr200077m

4. Shanmugaraju, S.; Bar, A. K.; Chi, K.-W.; Mukherjee, P. S. *Organometallics* **2010,** *29,* 2971–2980. doi:10.1021/om100202c
5. Shanmugaraju, S.; Joshi, S. A.; Mukherjee, P. S. *Inorg. Chem.* **2011,** *50,* 11736–11745. doi:10.1021/ic201745y
6. Therrien, B. *Eur. J. Inorg. Chem.* **2009,** 2445–2453. doi:10.1002/ejic.200900180
7. Han, Y.-F.; Jia, W.-G.; Yu, W.-B.; Jin, G.-X. *Chem. Soc. Rev.* **2009,** *38,* 3419–3434. doi:10.1039/b901649j
8. Wang, M.; Vajpayee, V.; Shanmugaraju, S.; Zheng, Y.-R.; Zhao, Z.; Kim, H.; Mukherjee, P. S.; Chi, K.-W.; Stang, P. J. *Inorg. Chem.* **2011,** *50,* 1506–1512. doi:10.1021/ic1020719
9. Shanmugaraju, S.; Bar, A. K.; Mukherjee, P. S. *Inorg. Chem.* **2010,** *49,* 10235–10237. doi:10.1021/ic101823s
10. Shanmugaraju, S.; Bar, A. K.; Joshi, S. A.; Patil, Y. P.; Mukherjee, P. S. *Organometallics* **2011,** *30,* 1951–1960. doi:10.1021/om2000019
11. Northrop, B. H.; Chercka, D.; Stang, P. J. *Tetrahedron* **2008,** *64,* 11495–11503. doi:10.1016/j.tet.2008.08.062
12. Fujita, M.; Yu, S.-Y.; Kusukawa, T.; Funaki, H.; Ogura, K.; Yamaguchi, K. *Angew. Chem., Int. Ed.* **1998,** *37,* 2082–2085. doi:10.1002/(SICI)1521-3773(19980817)37:15<2082::AID-ANIE2082>3.0.CO;2-0
13. *ArgusLab 4.0;* Planaria Software LLC: Seattle, WA, http://www.arguslab.com.
14. Govindaswamy, P.; Linder, D.; Lacour, J.; Süss-Fink, G.; Therrien, B. *Chem. Commun.* **2006,** 4691–4693. doi:10.1039/b610155k
15. Amijs, C. H. M.; van Klink, G. P. M.; van Koten, G. *Dalton Trans.* **2006,** 308–327. doi:10.1039/b505354d
16. Mattsson, J.; Govindaswamy, P.; Renfrew, A. K.; Dyson, P. J.; Stěpnička, P.; Süss-Fink, G.; Therrien, B. *Organometallics* **2009,** *28,* 4350–4357. doi:10.1021/om900359j
17. Kitagawa, S.; Kawata, S. *Coord. Chem. Rev.* **2002,** *224,* 11–34. doi:10.1016/S0010-8545(01)00369-1
18. Barry, N. P. E.; Govindaswamy, P.; Furrer, J.; Süss-Fink, G.; Therrien, B. *Inorg. Chem. Commun.* **2008,** *11,* 1300–1303. doi:10.1016/j.inoche.2008.08.007
19. Zhang, W.-Z.; Han, Y.-F.; Lin, Y.-J.; Jin, G.-X. *Dalton Trans.* **2009,** 8426–8431. doi:10.1039/b909357e
20. Yan, H.; Süss-Fink, G.; Neels, A.; Stoeckli-Evans, H. *J. Chem. Soc., Dalton Trans.* **1997,** 4345–4350. doi:10.1039/A704658H
21. Rit, A.; Pape, T.; Hepp, A.; Hahn, F. E. *Organometallics* **2011,** *30,* 334–347. doi:10.1021/om101102j
22. *SMART/SAINT;* Bruker AXS, Inc.: Madison, WI, 2004.
23. Sheldrick, G. M. *SHELX-97,* Program for the Solution and Refinement of Crystal Structures; University of Göttingen: Göttingen, Germany, 1998.
24. *WinGX: An Integrated System of Windows Programs for the Solution, Refinement; Analysis for Single Crystal X-ray Diffraction Data,* Version 1.65.04; Department of Chemistry: University of Glasgow: Glasgow, UK, 2003.
Farrugia, L. J. *J. Appl. Crystallogr.* **1999,** *32,* 837–838. doi:10.1107/S0021889899006020
25. Sheldrick, G. M. *SADABS,* Bruker Nonius Area Detector Scaling and Absorption Correction; Version 2.05; University of Göttingen: Göttingen, Germany, 1999.
26. *ORTEP-3 for Windows, Version, 1.08.*
Farrugia, L. J. *J. Appl. Crystallogr.* **1997,** *30,* 565. doi:10.1107/S0021889897003117
27. Spek, A. L. *Acta Crystallogr.* **1990,** *A46,* C34.

License and Terms

Beilstein Journal of Organic Chemistry

Azobenzene dye-coupled quadruply hydrogen-bonding modules as colorimetric indicators for supramolecular interactions

Yagang Zhang and Steven C. Zimmerman*

Full Research Paper

Open Access

Address:
Department of Chemistry, 600 South Mathews Avenue, University of Illinois, Urbana, IL 61801, USA

Email:
Steven C. Zimmerman* - sczimmer@illinois.edu

* Corresponding author

Keywords:
azobenzene dye; colorimetric indicators; 7-deazaguanine urea (DeUG); 2,7-diamido-1,8-naphthyridine (DAN); polymer; quadruply hydrogen bonding; supramolecular

Beilstein J. Org. Chem. **2012,** *8,* 486–495.
doi:10.3762/bjoc.8.55

Received: 04 January 2012
Accepted: 08 March 2012
Published: 02 April 2012

This article is part of the Thematic Series "Supramolecular chemistry II".

Guest Editor: C. A. Schalley

Abstract

The facile coupling of azobenzene dyes to the quadruply hydrogen-bonding modules 2,7-diamido-1,8-naphthyridine (DAN) and 7-deazaguanine urea (DeUG) is described. The coupling of azobenzene dye **2** to mono-amido DAN units **4**, **7**, and **9** was effected by classic 4-(dimethylamino)pyridine (DMAP)-catalyzed peptide synthesis with *N*-(3-dimethylaminopropyl)-*N*'-ethyl carbodiimide hydrochloride (EDC) as activating agent, affording the respective amide products **5**, **8**, and **10** in 60–71% yield. The amide linkage was formed through either the aliphatic or aromatic ester group of **2**, allowing both the flexibility and absorption maximum to be tuned. Azobenzene dye **1** was coupled to the DeUG unit **11** by Steglich esterification to afford the product amide **12** in 35% yield. Alternatively, azobenzene dye **16** underwent a room-temperature copper-catalyzed azide–alkyne Huisgen cycloaddition with DeUG alkyne **17** to give triazole **18** in 71% yield. Azobenzene coupled DAN modules **5**, **8**, and **10** are bright orange–red in color, and azobenzene coupled DeUG modules **12** and **18** are orange–yellow in color. Azobenzene coupled DAN and DeUG modules were successfully used as colorimetric indicators for specific DAN–DeUG and DAN–UPy (2-ureido-4(1*H*)-pyrimidone) quadruply hydrogen-bonding interactions.

Introduction

Lehn's pioneering studies [1] have advanced supramolecular chemistry to the point where complex hierarchical self-assembled [2] and even dynamically assembled structures are routinely described [3]. Noncovalent hydrogen bonding, electrostatic interactions, π–π stacking and metal coordination have been used alone and in concert to assemble a broad range of building blocks, from small molecules [4-7] to polymers [8,9] including dendrimers [10,11]. Among these noncovalent inter-

actions, hydrogen bonding is especially useful, not only because of its predictability both in terms of strength and geometry, but also because of its intrinsically dynamic and reversible nature. Of the hydrogen-bonding units developed for assembly, those that feature multiple hydrogen bonding sites are particularly desirable because they usually pair with high affinity and high fidelity [12]. High-affinity hydrogen-bonding units have found particular applications in supramolecular polymers [13,14], in which the presence of fewer hydrogen bonds means that the desired assemblies are not achieved, or results in polymers of lower molecular weight. The utility of these units is further demonstrated in the broad range of supramolecular architectures that have emerged and the materials to which these units have been attached, including dendrimers [15-17], polymer chain-ends [18-20] and polymer side-chains [21,22], modified polymeric materials, functionalized nano-structures [23] and surfaces [24].

Of the numerous supramolecular coupling agents developed those that pair using quadruply hydrogen bonding have arguably received the most attention in the context of supramolecular polymer chemistry. In particular, the highly stable UPy dimers developed by Meijer and Sijbesma [9,14,25] and the high-stability and high-fidelity DAN·UG heterodimers developed in our laboratory [26,27] are appealing because beyond the stable complexes that they form, they are synthetically quite accessible (Figure 1) [28]. Indeed, several syntheses of the DAN unit are now available [29-34]. The original UG unit contains a labile nucleoside unit, but a DeUG unit [35] and more recently a DeUG module bearing a range of synthetic handles for further elaboration [36] were both reported with more scalable syntheses. With regard to applications, the DAN·UG (DeUG) heterodimer has been used to drive the formation of: (1) polymer blends [37], (2) a supramolecular multi-

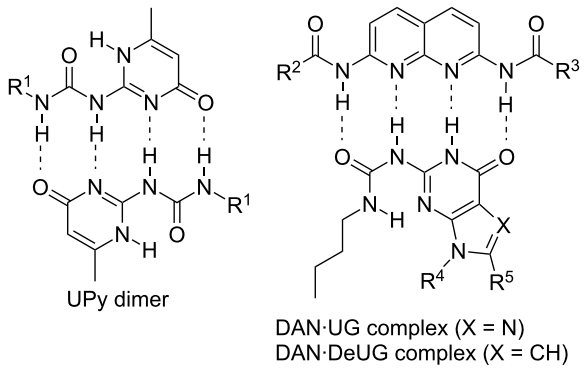

Figure 1: Chemical structures of UPy dimer and DAN complexes with UG and DeUG.

block copolymer with a high propensity for alteration [38], and (3) a supramolecular ABC triblock polymer [39]. Further, a structure–property relationship has been developed for DAN·UG-based supramolecular-network polymer blends [40], and a redox-active eDAN unit was described wherein a $>10^4$-fold drop in binding affinity occurred upon reversible oxidation [41].

Herein, we extend the chemistry of the heterocyclic hydrogen bonding units (DAN and DeUG) by their coupling to azobenzene dyes allowing them to serve as colorimetric indicators for supramolecular interactions. Beyond reporting the straightforward coupling of DAN and DeUG to azobenzene dyes, we show that the dye-recognition-unit conjugates act as selective polymer colorants (Figure 2). The development of a recognition unit opens the possibility of their use as a colorimetric handle for monitoring and investigating quadruply hydrogen-bonding interactions at molecular levels and in materials applications.

Results and Discussion

The azobenzene units were chosen because they are widely used as dyes and exhibit a range of vivid colors. Furthermore, the application of azobenzenes in chemistry is quite broad and includes their use as switches [42], in nonlinear optics [43], sensing devices [44], and in nanostructured films for optical storage [45]. Although this work does not focus on switching, the ability to synthesize these recognition units containing azobenzene units opens up the possibility to turn hydrogen bonding on and off. With regard to synthesis, aromatic azo compounds are commonly prepared by an electrophilic substitution reaction, the best partners being an electron-rich aromatic ring and an aryl diazonium cation.

The synthesis of azobenzene-dye-coupled DAN **5** began with 4-aminobenzoic acid *tert*-butyl ester (Scheme 1). Diazotization and coupling with phenol afforded **1** in 60% yield, which was comparable to the reported synthesis [46]. Compound **1** was alkylated with ethyl 4-bromobutyrate to give **2** in 72% yield [47]. Acid-catalyzed deprotection of **2** afforded carboxylic acid **3** in 85% yield [48]. The coupling of **3** with the mono-heptanamide of 2,7-diamino-1,8-naphthyridine (DAN **4**) was effected by using a standard peptide-coupling method. Thus, 1-(3-dimethylaminopropyl)-3-ethylcarbodiimide hydrochloride (EDC) was used as an activating agent and 4-(dimethylamino)pyridine (DMAP) was used as a catalyst [49]. Azobenzene–DAN conjugate **5** was obtained in 71% yield as an orange–red solid following chromatography.

Deprotection of azobenzene **2** under mildly basic conditions was also investigated, which afforded compound **6** in 88% yield

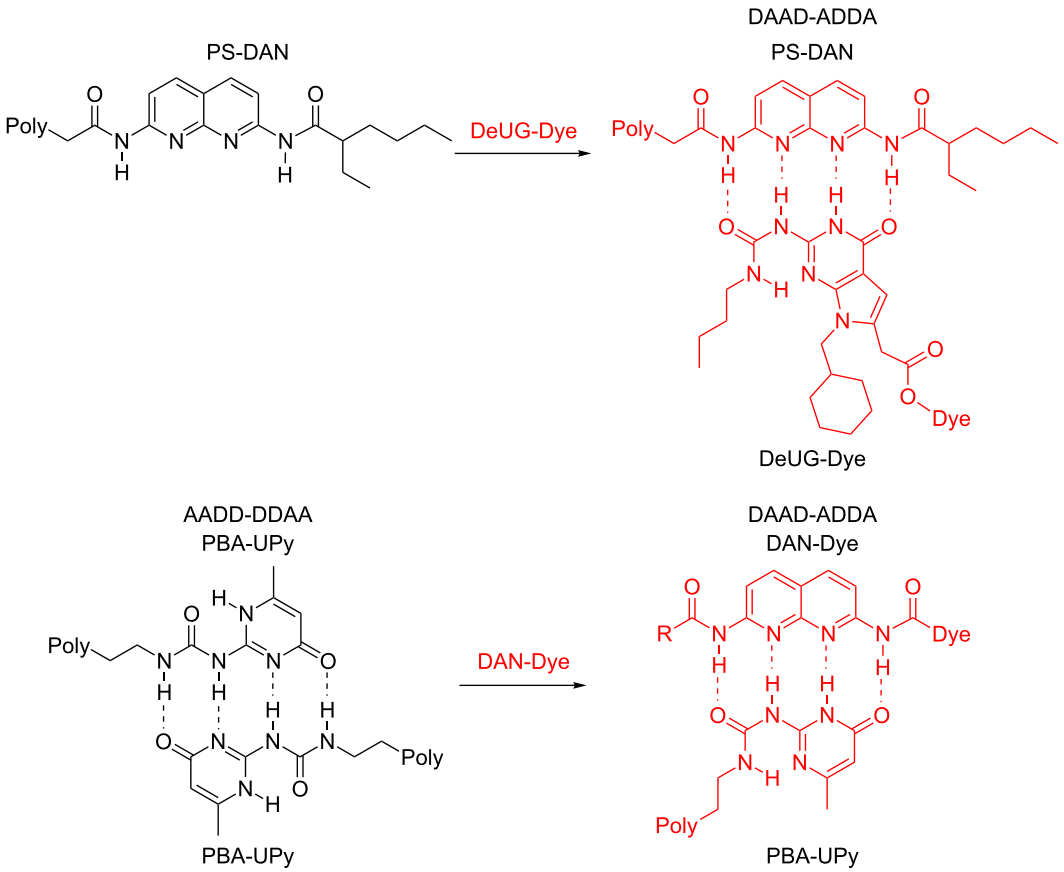

Figure 2: Illustration of the use of DeUG-Dye and DAN-Dye as colorimetric indicators for supramolecular interactions through specific quadruply hydrogen-bonding interactions. Top: DeUG-Dye interacts with DAN modified polystyrene (PS). Bottom: DAN-Dye interacts with UPy modified poly-butyl acrylate (PBA).

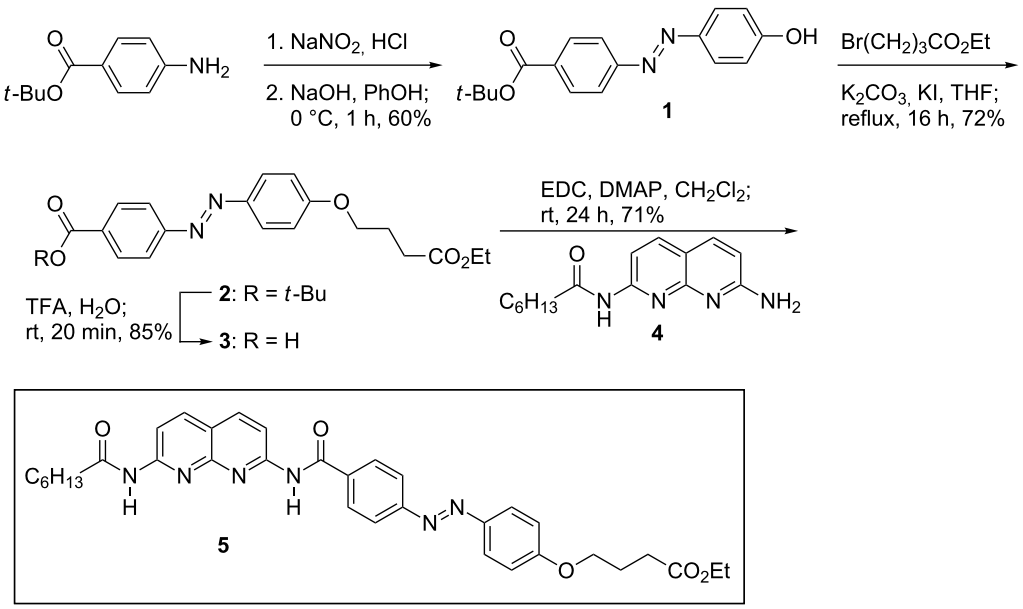

Scheme 1: Synthesis of azobenzene-dye-coupled DAN **5**.

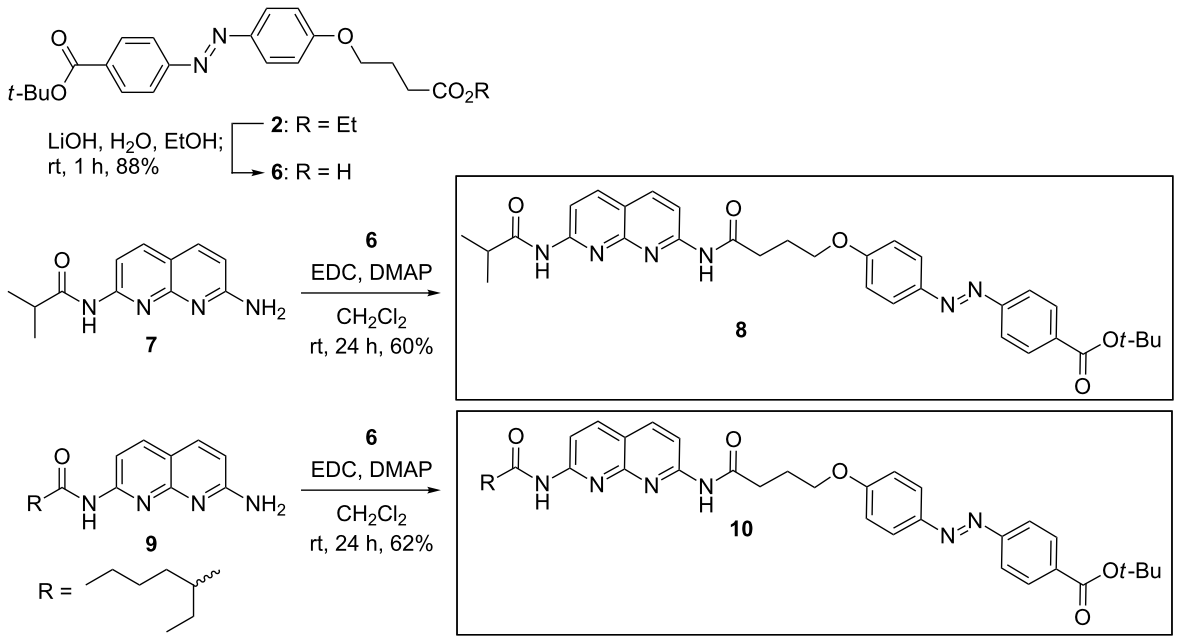

Scheme 2: Synthesis of azobenzene-dye-coupled DAN **8** and **10**.

(Scheme 2). The coupling of monoamide derivatives of 2,7-diamido-1,8-naphthyridine (DAN), i.e., **7** and **9** with **6** under similar coupling conditions, yielded **8** and **10** in 60% and 62% yield, respectively. All three azobenzene-coupled DAN modules were vivid orange–red in color and had excellent solubility in a range of nonpolar organic solvents.

The initial attempt to couple DeUG unit **11** to azobenzene dye **1** utilized the established Steglich esterification procedure [50] with DMAP as the catalyst [51]. Thus, DeUG carboxylic acid **11** was coupled with **1** by using EDC and DMAP in methylene chloride, and the orange–yellow product **12** was isolated in a relatively low 35% yield (Scheme 3). No attempt was made to optimize the coupling conditions; instead, attention was turned to the possibility of coupling the partners by using the copper-catalyzed azide–alkyne Huisgen cycloaddition (click reaction).

The click approach began with the readily available and inexpensive starting material, 4-aminobenzoic acid (Scheme 4), which was diazotized and treated with phenol to afford **13** in 65% yield, comparable to published procedures [52-54]. To install the azide functionality, **13** was treated with 1,5-dibromopentane and potassium carbonate to afford bromide **14** in 62% yield. Because of its poor solubility, **14** was esterified to afford ethyl ester **15** in 76% yield. Treatment of **15** with sodium azide in the presence of tetrabutyl ammonium bromide as a

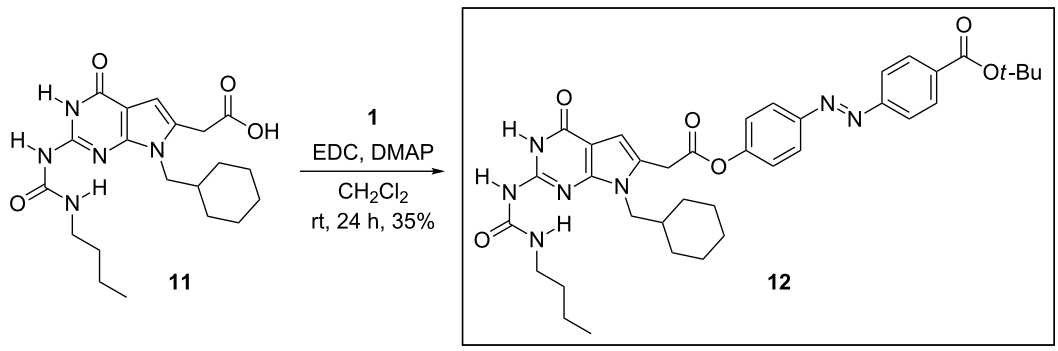

Scheme 3: Synthesis of azobenzene dye-coupled DeUG **12**.

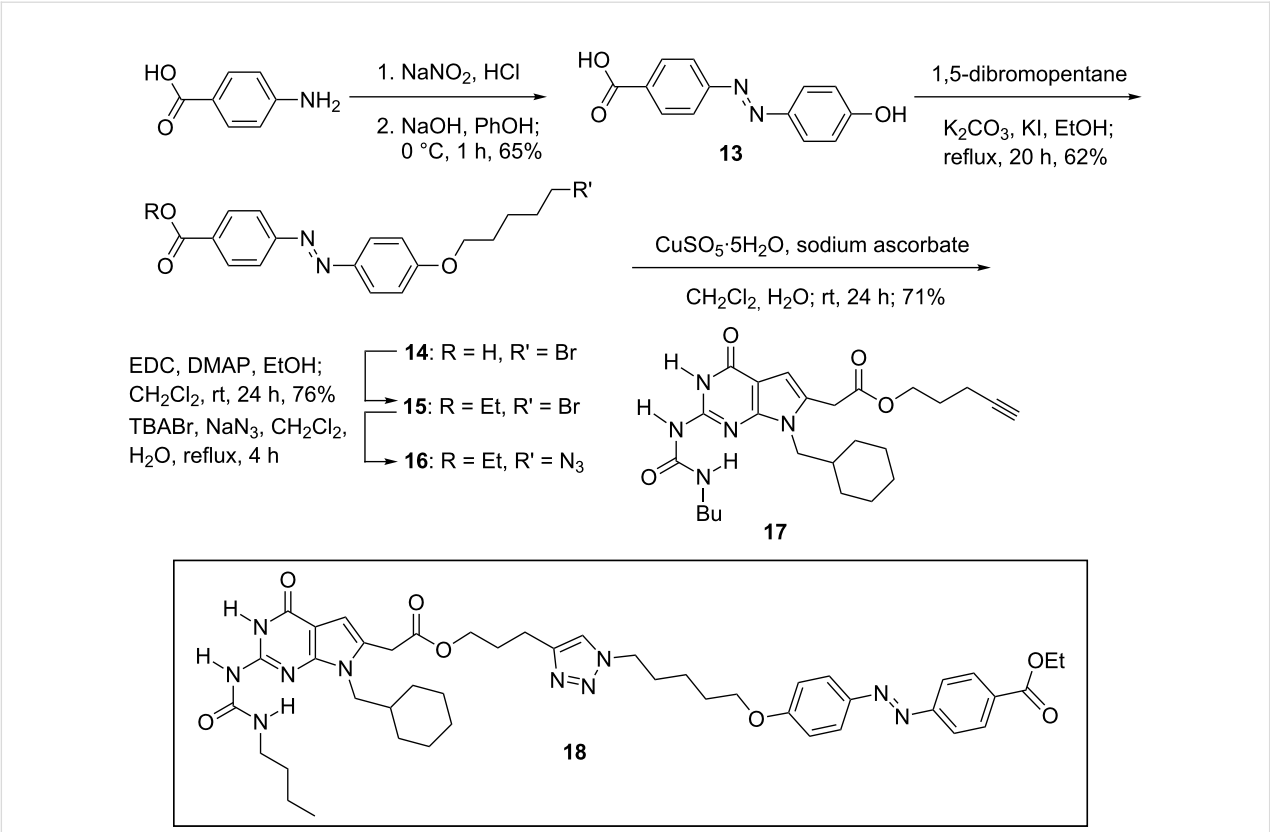

Scheme 4: Synthesis of azobenzene dye-coupled DeUG **18**.

phase-transfer reagent produced crude **16**, which was used directly in the next step without purification. Coupling of azide **16** with the known **17** [34] was successfully effected under standard conditions for the copper-catalyzed azide–alkyne cycloaddition [55]. Azobenzene dye-coupled DeUG module **18** was obtained as an orange–yellow solid in 71% yield. The product was assigned as the 1,4-substituted triazole by analogy to that seen in other such cycloaddition reactions [56].

Azobenzene-coupled DAN modules **5**, **8**, and **10** are bright orange–red in color and azobenzene-coupled DeUG modules **12** and **18** are orange–yellow in color (Figure 3). All of the azobenzene coupled DAN and DeUG modules have excellent solubility in nonpolar organic solvents, wherein their supramolecular recognition is most effective.

Figure 3: Solution (20 mmol) of azobenzene-dye-coupled DAN and DeUG in CH_2Cl_2; a = compound **5**, b = compound **8**, c = compound **10**, d = compound **12**, e = compound **18**.

To study the ability of the DAN and DeUG-coupled azobenzene dyes to engage in quadruply hydrogen-bonding interactions and demonstrate the possibility of using these compounds as colorimetric indicators, two types of polymers bearing DAN and UPy were used (Figure 4). The DAN modified polystyrene (PS-DAN) was a gift from Dr. Cyrus Anderson and its synthesis will be published elsewhere. Commercially available polystyrene (PS) was used as a control polymer and purified by dissolving in CH_2Cl_2 and precipitating out with MeOH.

PS and PS-DAN were characterized by SEC with THF as eluent, with PS molecular weight standards. The loading of the DAN unit was determined by ^{1}H NMR (Table 1). Poly(butyl

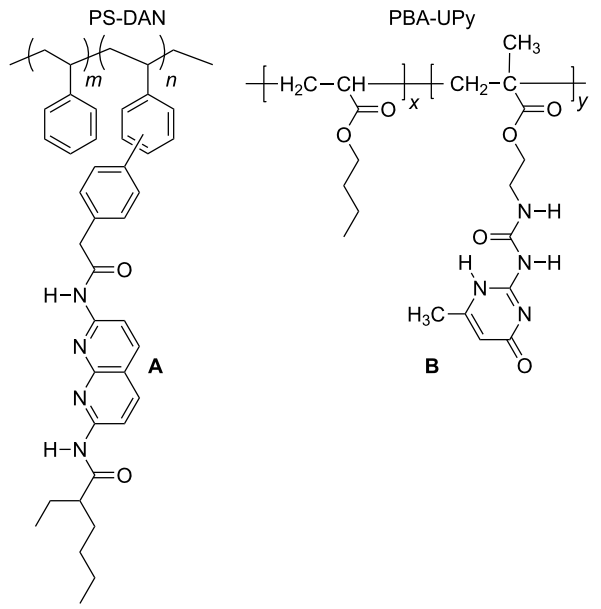

Figure 4: Structure of DAN-modified PS and Upy-modified PBA.

acrylate) (PBA) and 2-ureido-4(1*H*)-pyrimidone (UPy) modified poly(butyl acrylate) (PBA-UPy) were prepared and characterized by THF SEC against PS standards according to a known procedure [57]. The loading of the UPy units, determined by ^{1}H NMR, is listed in Table 1.

PS and DAN-modified PS were obtained as white powders whereas PBA and UPy-modified PBA ranged from viscous liquids to gels depending on the loading of UPy groups on the polymer backbone (Figure 5). The supramolecular coupling of DAN and DeUG units and DAN and UPy units has been well studied. Thus, the association constant (K_{assoc}) for the DAN–DeUG heterocomplex was measured as $K_{assoc} \approx 10^8$ M^{-1} [36], whereas for the DAN–UPy heterocomplex K_{assoc} = 10^6 M^{-1} [58-60].

Table 1: Molecular weight, molecular weight distribution and mol % loading of DAN modified PS and UPy modified PBA.

entry	polymer	M_w (kDa)	M_n (kDa)	PDI
A0	PS	138	69	2.0
A1	PS-DAN (2.0 mol %)	148	114	1.3
A2	PS-DAN (5.0 mol %)	131	73	1.8
B0	PBA	84	38	2.2
B1	PBA-UPy (2.6 mol %)	84	38	2.2
B2	PBA-UPy (4.1 mol %)	80	38	2.1
B3	PBA-UPy (7.1 mol %)	110	55	2.0

Whether these complex stabilities allow for the selective coloration of the functional polymers was examined by mixing CH_2Cl_2 solutions of polymer and dye-coupled recognition units, evaporation of the solvent, and repeated washing of the residue with CH_2Cl_2–hexanes in an attempt to remove the color. These conditions were selected because they were effective at removing dye from the unfunctionalized polymer. Thus, as seen in Figure 6 (left panel, vial A), PS did not retain DeUG-Dye compound **12** after washing. However, PS-DAN (2 mol %) retained both compound **12** and **18** (vial B and C, respectively), showing intense coloration. The designed supramolecular recognition (DAN–DeUG heterocomplex) was shown to be the key factor by a control experiment featuring PS-DAN and azobenzene dyes **2** and **15**, both of which lack the DeUG unit. As seen in Figure 6 (left panel, vial D and E), the dye was washed away from the polymer. Not surprisingly the 5 mol %

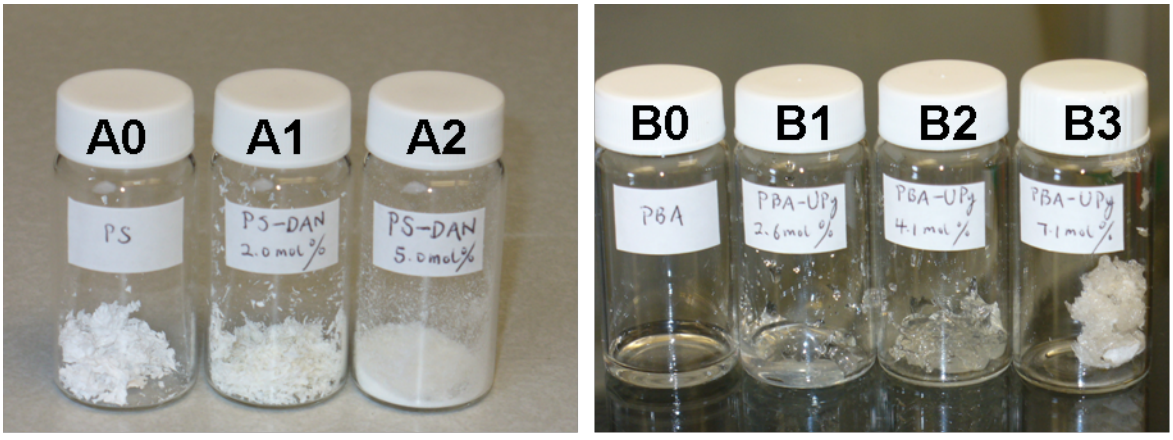

Figure 5: Physical appearance of DAN-modified PS and UPy-modified PBA. Left: A0 = PS, A1 = PS-DAN 2.0 mol %, A2 = PS-DAN 5.0 mol %. Right: B0 = PBA, B1 = PBA-UPy 2.6 mol %, B2 = PBA-UPy 4.1 mol %, B3 = PBA-UPy 7.1 mol %.

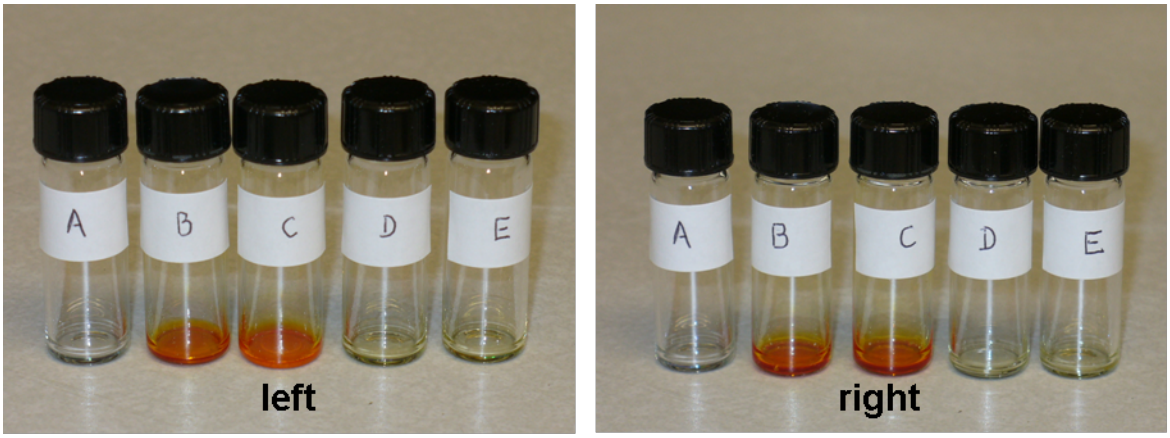

Figure 6: Color change after the interaction of azo-benzene dye-coupled DeUG modules with different DAN modified PS, followed by washing. Left: (A) PS with compound **12**, (B) PS-DAN (2.0 mol %) with compound **12**, (C) PS-DAN (2.0 mol %) with compound **18**, (D) PS-DAN (2.0 mol %) with compound **2**, (E) PS-DAN (2.0 mol %) with compound **15**. Right: (A) PS with compound **18**, (B) PS-DAN (5.0 mol %) with compound **12**, (C) PS-DAN (5.0 mol %) with compound **18**, (D) PS-DAN (5.0 mol %) with compound **2**, (E) PS-DAN (5.0 mol %) with compound **15**.

PS-DAN performed at least as well in the same series of experiments (Figure 6, right panel). The overall approach is meant to illustrate the strength and specificity of the recognition process, not to provide a quantitative method. Thus, although the washing procedure with a mixed nonpolar solvent (CH_2Cl_2–hexanes) proved to be effective in removing non-specifically associated compounds, over 50% of the polymer was also lost during the multiple washings.

The generality of this recognition process was demonstrated by observing the same trend with DAN-Dyes **5**, **8** and **10** and UPy-modified PBA (Figure 7). Thus, after mixing of DAN-Dyes **5**, **8** and **10** with UPy modified PBA (both 4.1 mol % and 7.1 mol %) the polymers became highly colored. However, after being washed repeatedly with CH_2Cl_2–hexanes, unfunctionalized PBA lost its color (Figure 7, left and right panels, vial A) whereas PBA-UPy retained an intense orange color (Figure 7 left and right panels, vials B and C). Control studies with PBA-UPy (both 4.1 mol % and 7.1 mol %) mixed with azobenzene dye **2** and **15** lacking a DAN-recognition unit, showed a complete loss of color following extensive washing (Figure 7 left and right panels, vials D and E).

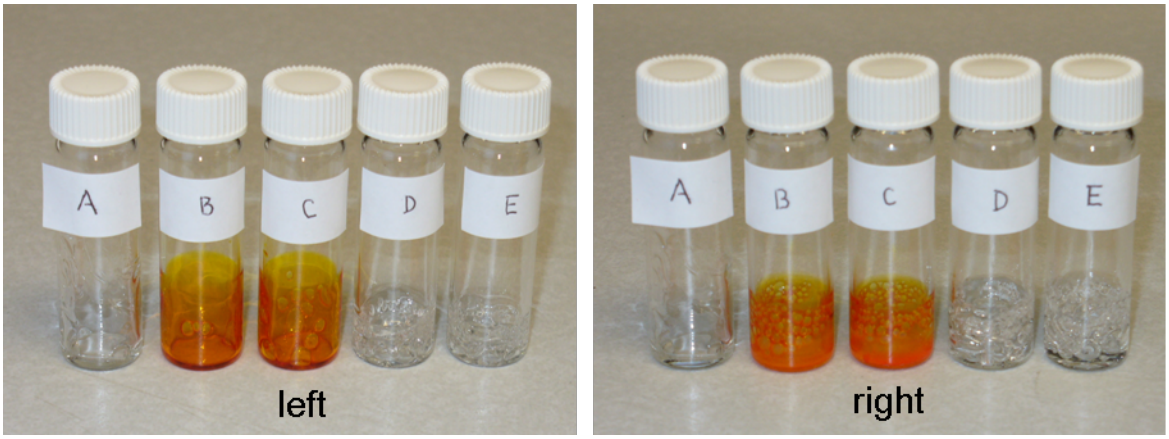

Figure 7: Color change after the interaction of azobenzene dye-coupled DAN modules with different UPy-modified PBA, followed by washing. Left: (A) PBA with compound **5**, (B) PBA-UPy (4.1 mol %) with compound **5**, (C) PBA-UPy (4.1 mol %) with compound **8**, (D) PBA-UPy (4.1 mol %) with compound **2** (E) PBA-UPy (4.1 mol %) with compound **15**. Right: (A) PBA with compound **5**, (B) PBA-UPy (7.1 mol %) with compound **8**, (C) PBA-UPy (7.1 mol %) with compound **10**, (D) PBA-UPy (7.1 mol %) with compound **2**, (E) PBA-UPy (7.1 mol %) with compound **15**.

Conclusion

In conclusion, we have demonstrated straightforward and scalable syntheses of azobenzene dye-coupled quadruply hydrogen-bonding recognition modules. Specifically, the 2,7-diamido-1,8-naphthyridine (DAN) unit was linked to azobenzene dyes through one of its amide groups, giving compounds **5**, **8**, and **10**, and the 7-deazaguanine urea (DeUG) unit was linked to an azobenzene dye by a Steglich esterification, giving **12**, or by the copper-catalyzed azide–alkyne cycloaddition (click reaction) to give **18**. The synthesis provides access to highly colored recognition units that may serve as useful probes of recognition events. In this work we have successfully demonstrated that these units colored two polymers, PBA and PS, but only when they contain the complementary recognition units along their backbone.

Experimental

General

With the exception of 1-(3-dimethylaminopropyl)-3-ethylcarbodiimide hydrochloride (EDC), which was purchased from Advanced ChemTech and used as received, all other chemicals were purchased from Sigma-Aldrich and used without further purification. Compounds **4**, **7**, and **9** were synthesized according to the published procedures [34], as were compounds **11** and **17** [36]. Solvents were reagent grade and used without further purification except as follows: Tetrahydrofuran (THF) was distilled from sodium benzophenone ketyl immediately prior to use. Methylene chloride (CH_2Cl_2) was obtained from an MB-SPS Solvent Purification System and stored over 4 Å molecular sieves. All reactions were carried out under a dry nitrogen atmosphere, except for the preparation of compounds **1** and **13**. Ambient or room temperature refers to 25 ± 3 °C.

Representative procedure for testing polymer coloration

One representative example each of coloration experiments with (a) DeUG-Dye **18** with PS-DAN and (b) DAN-Dye **5** with PBA-UPy: (a) 0.30 g PS-DAN (5.0 mol %) was dissolved in 25 mL of CH_2Cl_2, then 5.0 mL of a solution of DeUG-Dye **18** in CH_2Cl_2 (20 mM) was added and the mixture was stirred for 3 h. The solvent was removed in vacuo. The resulting solid was washed with 0.2% CH_2Cl_2–hexanes (v/v) (10 × 12 mL). Each washing was carried out in a 20 mL scintillation vial under stirring for 40 min. After settling of the polymer, the washing solvent was decanted and removed with a pipette. The final polymer was transferred into a small vial and dried at room temperature. (b) To a solution of 0.30 g PBA-UPy (4.1 mol %) in 25 mL CH_2Cl_2 was added 5.0 mL of a solution of DAN-Dye **5** in CH_2Cl_2 (20 mM) and the mixture was stirred for 3 h. The solvent was removed in vacuo. The resulting solid was washed with 1% CH_2Cl_2–hexanes (v/v) (10 × 12 mL). Each washing was carried out in a 20 mL scintillation vial under stirring for 40 min. After settling of the polymer, the washing solvent was decanted and removed with a pipette. The final polymer was transferred into a small vial and dried at room temperature.

Supporting Information

Supporting Information File 1

General experimental procedures, detailed synthetic procedures and characterization data.
[http://www.beilstein-journals.org/bjoc/content/supplementary/1860-5397-8-55-S1.pdf]

Acknowledgements

The authors gratefully acknowledge support of this work by the NSF (CHE-1012212) and compounds that were provided by Dr. Cyrus A. Anderson and Dr. Darrell W. Kuykendall.

References

1. Lehn, J.-M. *Angew. Chem., Int. Ed. Engl.* **1988,** *27,* 89–112. doi:10.1002/anie.198800891
2. Lawrence, D. S.; Jiang, T.; Levett, M. *Chem. Rev.* **1995,** *95,* 2229–2260. doi:10.1021/cr00038a018
3. Lehn, J.-M. *Chem. Soc. Rev.* **2007,** *36,* 151–160. doi:10.1039/b616752g
4. Whitesides, G. M.; Simanek, E. E.; Mathias, J. P.; Seto, C. T.; Chin, D.; Mammen, M.; Gordon, D. M. *Acc. Chem. Res.* **1995,** *28,* 37–44. doi:10.1021/ar00049a006
5. Fang, L.; Olson, M. A.; Benítez, D.; Tkatchouk, E.; Goddard, W. A., III; Stoddart, J. F. *Chem. Soc. Rev.* **2010,** *39,* 17–29. doi:10.1039/b917901a
6. Hof, F.; Craig, S. L.; Nuckolls, C.; Rebek, J., Jr. *Angew. Chem., Int. Ed.* **2002,** *41,* 1488–1508. doi:10.1002/1521-3773(20020503)41:9<1488::AID-ANIE1488>3.0.CO;2-G
7. Jung, J. H.; Park, M.; Shinkai, S. *Chem. Soc. Rev.* **2010,** *39,* 4286–4302. doi:10.1039/c002959a
8. Zimmerman, N.; Moore, J. S.; Zimmerman, S. C. *Chem. Ind.* **1998,** 604–610.
9. Brunsveld, L.; Folmer, B. J. B.; Meijer, E. W.; Sijbesma, R. P. *Chem. Rev.* **2001,** *101,* 4071–4097. doi:10.1021/cr990125q
10. Zeng, F.; Zimmerman, S. C.; Kolotuchin, S. V.; Reichert, D. E. C.; Ma, Y. *Tetrahedron* **2002,** *58,* 825–843. doi:10.1016/S0040-4020(01)01113-9
11. Zimmerman, S. C. *Curr. Opin. Colloid Interface Sci.* **1997,** *2,* 89–99. doi:10.1016/S1359-0294(97)80013-1
12. Todd, E. M.; Quinn, J. R.; Park, T.; Zimmerman, S. C. *Isr. J. Chem.* **2005,** *45,* 381–389. doi:10.1560/DQCJ-1K9J-1TBT-DK5M
13. Zimmerman, S. C.; Zeng, F.; Reichert, D. E. C.; Kolotuchin, S. V. *Science* **1996,** *271,* 1095–1098. doi:10.1126/science.271.5252.1095
14. Sijbesma, R. P.; Beijer, F. H.; Brunsveld, L.; Folmer, B. J. B.; Hirschberg, J. H. K. K.; Lange, R. F. M.; Lowe, J. K. L.; Meijer, E. W. *Science* **1997,** *278,* 1601–1604. doi:10.1126/science.278.5343.1601
15. Wong, C.-H.; Chow, H.-F.; Hui, S.-K.; Sze, K.-H. *Org. Lett.* **2006,** *8,* 1811–1814. doi:10.1021/ol0603716

16. Corbin, P. S.; Lawless, L. J.; Li, Z.; Ma, Y.; Witmer, M. J.; Zimmerman, S. C. *Proc. Natl. Acad. Sci. U. S. A.* **2002,** *99,* 5099–5104. doi:10.1073/pnas.062641199
17. Wang, Y.; Zeng, F.; Zimmerman, S. C. *Tetrahedron Lett.* **1997,** *38,* 5459–5462. doi:10.1016/S0040-4039(97)01222-7
18. Yamauchi, K.; Kanomata, A.; Inoue, T.; Long, T. E. *Macromolecules* **2004,** *37,* 3519–3522. doi:10.1021/ma049913u
19. Yang, X.; Hua, F.; Yamato, K.; Ruckenstein, E.; Gong, B.; Kim, W.; Ryu, C. Y. *Angew. Chem., Int. Ed.* **2004,** *43,* 6471–6474. doi:10.1002/anie.200460472
20. Yang, S. K.; Ambade, A. V.; Weck, M. *Chem. Soc. Rev.* **2011,** *40,* 129–137. doi:10.1039/c0cs00073f
21. Feldman, K. E.; Kade, M. J.; de Greef, T. F. A.; Meijer, E. W.; Kramer, E. J.; Hawker, C. J. *Macromolecules* **2008,** *41,* 4694–4700. doi:10.1021/ma800375r
22. Pollino, J. M.; Weck, M. *Chem. Soc. Rev.* **2005,** *34,* 193–207. doi:10.1039/b311285n
23. Subramani, C.; Dickert, S.; Yeh, Y.-C.; Tuominen, M. T.; Rotello, V. M. *Langmuir* **2011,** *27,* 1543–1545. doi:10.1021/la1039514
24. Viswanathan, K.; Ozhalici, H.; Elkins, C. L.; Heisey, C.; Ward, T. C.; Long, T. E. *Langmuir* **2006,** *22,* 1099–1105. doi:10.1021/la052253h
25. Sijbesma, R. P.; Meijer, E. W. *Chem. Commun.* **2003,** 5–16. doi:10.1039/b205873c
26. Park, T.; Todd, E. M.; Nakashima, S.; Zimmerman, S. C. *J. Am. Chem. Soc.* **2005,** *127,* 18133–18142. doi:10.1021/ja0545517
27. Park, T.; Zimmerman, S. C.; Nakashima, S. *J. Am. Chem. Soc.* **2005,** *127,* 6520–6521. doi:10.1021/ja050996j
28. Wilson, A. J. *Soft Matter* **2007,** *3,* 409–425. doi:10.1039/b612566b
29. Corbin, P. S.; Zimmerman, S. C. *J. Am. Chem. Soc.* **1998,** *120,* 9710–9711. doi:10.1021/ja981884d
30. Lüning, U.; Kühl, C.; Uphoff, A. *Eur. J. Org. Chem.* **2002,** 4063–4070. doi:10.1002/1099-0690(200212)2002:23<4063::AID-EJOC4063>3.0.CO;2-L
31. Li, X.-Q.; Feng, D.-J.; Jiang, X.-K.; Li, Z.-T. *Tetrahedron* **2004,** *60,* 8275–8284. doi:10.1016/j.tet.2004.06.104
32. Park, T.; Mayer, M. F.; Nakashima, S.; Zimmerman, S. C. *Synlett* **2005,** 1435–1436. doi:10.1055/s-2005-868507
33. Ligthart, G. B. W. L.; Ohkawa, H.; Sijbesma, R. P.; Meijer, E. W. *J. Org. Chem.* **2006,** *71,* 375–378. doi:10.1021/jo051864b
34. Anderson, C. A.; Taylor, P. G.; Zeller, M. A.; Zimmerman, S. C. *J. Org. Chem.* **2010,** *75,* 4848–4851. doi:10.1021/jo100476x
35. Ong, H. C.; Zimmerman, S. C. *Org. Lett.* **2006,** *8,* 1589–1592. doi:10.1021/ol0601803
36. Kuykendall, D. W.; Anderson, C. A.; Zimmerman, S. C. *Org. Lett.* **2009,** *11,* 61–64. doi:10.1021/ol802344w
37. Park, T.; Zimmerman, S. C. *J. Am. Chem. Soc.* **2006,** *128,* 11582–11590. doi:10.1021/ja0631854
38. Park, T.; Zimmerman, S. C. *J. Am. Chem. Soc.* **2006,** *128,* 13986–13987. doi:10.1021/ja064116s
39. Todd, E. M.; Zimmerman, S. C. *J. Am. Chem. Soc.* **2007,** *129,* 14534–14535. doi:10.1021/ja075453j
40. Park, T.; Zimmerman, S. C. *J. Am. Chem. Soc.* **2006,** *128,* 14236–14237. doi:10.1021/ja065469u
41. Li, Y.; Park, T.; Quansah, J. K.; Zimmerman, S. C. *J. Am. Chem. Soc.* **2011,** *133,* 17118–17121. doi:10.1021/ja2069278
42. Beharry, A. A.; Woolley, G. A. *Chem. Soc. Rev.* **2011,** *40,* 4422–4437. doi:10.1039/c1cs15023e
43. Yesodha, S. K.; Pillai, C. K. S.; Tsutsumi, N. *Prog. Polym. Sci.* **2004,** *29,* 45–74. doi:10.1016/j.progpolymsci.2003.07.002
44. Ishi-i, T.; Shinkai, S. *Top. Curr. Chem.* **2005,** *258,* 119–160. doi:10.1007/b135554
45. Oliveira, O. N., Jr.; dos Santos, D. S., Jr.; Balogh, D. T.; Zucolotto, V.; Mendonça, C. R. *Adv. Colloid Interface Sci.* **2005,** *116,* 179–192. doi:10.1016/j.cis.2005.05.008
46. Yildiz, I.; Ray, S.; Benelli, T.; Raymo, F. M. *J. Mater. Chem.* **2008,** *18,* 3940–3947. doi:10.1039/b806247a
47. Kreger, K.; Wolfer, P.; Audorff, H.; Kador, L.; Stingelin-Stutzmann, N.; Smith, P.; Schmidt, H.-W. *J. Am. Chem. Soc.* **2010,** *132,* 509–516. doi:10.1021/ja9091038
48. Lee, K.; Pan, F.; Carroll, G. T.; Turro, N. J.; Koberstein, J. T. *Langmuir* **2004,** *20,* 1812–1818. doi:10.1021/la0358163
49. Nakajima, N.; Ikada, Y. *Bioconjugate Chem.* **1995,** *6,* 123–130. doi:10.1021/bc00031a015
50. Neises, B.; Steglich, W. *Angew. Chem., Int. Ed. Engl.* **1978,** *17,* 522–524. doi:10.1002/anie.197805221
51. Höfle, G.; Steglich, W.; Vorbrüggen, H. *Angew. Chem., Int. Ed. Engl.* **1978,** *17,* 569–583. doi:10.1002/anie.197805691
52. Landi, F.; Johansson, C. M.; Campopiano, D. J.; Hulme, A. N. *Org. Biomol. Chem.* **2010,** *8,* 56–59. doi:10.1039/b916693a
53. Leriche, G.; Budin, G.; Brino, L.; Wagner, A. *Eur. J. Org. Chem.* **2010,** 4360–4364. doi:10.1002/ejoc.201000546
54. Shimpuku, C.; Ozawa, R.; Sasaki, A.; Sato, F.; Hashimoto, T.; Yamauchi, A.; Suzuki, I.; Hayashita, T. *Chem. Commun.* **2009,** 1709–1711. doi:10.1039/b819938h
55. Rostovtsev, V. V.; Green, L. G.; Fokin, V. V.; Sharpless, K. B. *Angew. Chem., Int. Ed.* **2002,** *41,* 2596–2599. doi:10.1002/1521-3773(20020715)41:14<2596::AID-ANIE2596>3.0.CO;2-4
56. Himo, F.; Lovell, T.; Hilgraf, R.; Rostovtsev, V. V.; Noodleman, L.; Sharpless, K. B.; Fokin, V. V. *J. Am. Chem. Soc.* **2005,** *127,* 210–216. doi:10.1021/ja0471525
57. Yamauchi, K.; Lizotte, J. R.; Long, T. E. *Macromolecules* **2003,** *36,* 1083–1088. doi:10.1021/ma0212801
58. Ligthart, G. B. W. L.; Ohkawa, H.; Sijbesma, R. P.; Meijer, E. W. *J. Am. Chem. Soc.* **2005,** *127,* 810–811. doi:10.1021/ja043555t
59. Zhao, X.; Wang, X.-Z.; Jiang, X.-K.; Chen, Y.-Q.; Li, Z.-T.; Chen, G.-J. *J. Am. Chem. Soc.* **2003,** *125,* 15128–15139. doi:10.1021/ja037312x
60. Wang, X.-Z.; Li, X.-Q.; Shao, X.-B.; Zhao, X.; Deng, P.; Jiang, X.-K.; Li, Z.-T.; Chen, Y.-Q. *Chem.–Eur. J.* **2003,** *9,* 2904–2913. doi:10.1002/chem.200204513

Beilstein Journal of Organic Chemistry

Enantioselective supramolecular devices in the gas phase. Resorcin[4]arene as a model system

Caterina Fraschetti*[1,§], Matthias C. Letzel[2], Antonello Filippi[1], Maurizio Speranza[1] and Jochen Mattay[2,¶]

Review

Open Access

Address:
[1]Sapienza University of Rome, Department of Chemistry and Technologies of Drug, Piazzale Aldo Moro, 5, 00185, Rome, Italy and [2]Bielefeld University, Department of Chemistry, Organic Chemistry I, P.O. Box 100131, 35501 Bielefeld, Germany

Email:
Caterina Fraschetti* - caterina.fraschetti@uniroma1.it;
Jochen Mattay - mattay@uni-bielefeld.de

* Corresponding author
§ Fax: +39-06 4991 3602, Phone: +39-06 4991 3634
¶ Fax: +49-521-106-6146, Phone: +49-521-106-2072

Keywords:
diastereomeric complexes; gas phase enantioselectivity; kinetics; mass spectrometry; resorcin[4]arene receptor

Beilstein J. Org. Chem. **2012,** *8,* 539–550.
doi:10.3762/bjoc.8.62

Received: 02 December 2011
Accepted: 15 March 2012
Published: 12 April 2012

This article is part of the Thematic Series "Supramolecular chemistry II".

Guest Editor: C. A. Schalley

Abstract

This review describes the state-of-art in the field of the gas-phase reactivity of diastereomeric complexes formed between a chiral artificial receptor and a biologically active molecule. The presented experimental approach is a ligand-displacement reaction carried out in a nano ESI-FT-ICR instrument, supported by a thermodynamic MS-study and molecular-mechanics and molecular-dynamics (MM/MD) computational techniques. The noncovalent ion–molecule complexes are ideal for the study of chiral recognition in the absence of complicating solvent and counterion effects.

Review

Enzymes are macromolecular assemblies that make up the machinery whose structures and dynamics enable and support life functions. They are invariably characterized by more-or-less flexible structures with asymmetric cavities of appropriate shape and size possessing suitable functionalities in specific positions. The large number of existing enzymes characterized by a specific function has provided chemists with both the stimulus and inspiration to design "synthetic enzymes" in order to provide exemplars suitable for improving the understanding of the amazing properties of natural biomolecules and for attempts to reproduce them for practical applications. Thus, noncovalent complexes between chiral receptors and biomolecules represent an important class of life's supramolecular systems in which the guest molecule (e.g., amino acids, neurotransmitters, drugs) is selectively captured into the host macromolecular structure (molecular recognition) and transformed catalytically at a specific "active site" (enzyme catalysis) [1-3]. Furthermore, the biorecognition may require the partial or complete desolvation of the guest molecule and of the polar groups of the active site by greatly enhancing its reactivity [4].

An important step towards the elucidation of enzyme mechanisms requires a comprehensive study of the structure, dynamics, and reactivity of simplified models under conditions, such as the gas phase, in which the noncovalent interactions in the guest–host complex are not perturbed by effects owing to the medium. As biological function and morphology are strongly correlated, knowledge of the supramolecular host–guest structures is expected to shed light on their biological functions. From the beginning of evolutionary processes right up to the present biodiversity, life relies on biological specificity, which arises from the fact that individual biomolecules "communicate" through noncovalent interactions. Resorcin[4]arenes are an important class of tunable macrocycles largely studied in the context of host–guest chemistry, as cavitands [5] and capsules [6]. The great ability of resorcin[4]arenes to trap several classes of compounds makes them very suitable for the subtle study of the chemicophysical properties of their host–guest systems, even in the gas phase. The most recent advances in this field include several gas-phase investigations: (i) The size and structure selectivity of tetraethyl and tetraphenyl resorcin[4]arenes in the recognition of mono, di-, and oligosaccharides by electrospray coupled with Fourier transform ion cyclotron resonance mass spectrometry (FT-ICR) [7]; (ii) the gaseous (and solution) selectivity towards several organic and inorganic anions [8], and tetramethylphosphonium cation [9]; and (iii) the complexation of saturated, nonsaturated, and aromatic dicarboxilic acids by a tetraammonium C1-resorcinarene, strongly dependent on the isomeric structure of the used guest [10].

Resorcin[4]arene molecules are characterized by three main contact regions [11]: (1) The *down*-region is the cavity of the receptor, which can be hydrophilic or lipophilic depending on the nature of the lateral chains; (2) The *external*-region is located in the proximity of lateral chains; and (3) The *up*-region is defined by the upper rim of the receptor crown. Furthermore, the nature of the pendants allows for subtle tuning of the polarity of both the *down*- and the *external*-regions, and the size of the *up*-region. The capability to discriminate biomolecules such as the zwitterionic forms of aromatic amino acids [12], basic amino acids [13-15], aliphatic and aromatic native amino acids [16-18], and amines and peptides [19], by acting as an artificial receptor [20-30], is thanks to this structural versatility.

The kinetic measurement of ligand-displacement reactions [31-37] is one of the different mass-spectrometric approaches used to promote an efficient chiral recognition [38], as already mentioned in the last review published in this field [31]. In the present review the attention will be focussed on the most recent results obtained by our group with this particular kinetic method.

Methodology

The proton-bound $[\boldsymbol{M}\cdot\mathrm{H}\cdot\mathrm{G}]^+$ aggregates ($\boldsymbol{M}$: chiral hosting resorcin[4]arene; G: guest biomolecule) were generated by electrospray ionization (ESI) of $\boldsymbol{M}$/G methanolic mixtures (where the $\boldsymbol{M}$ to G ratio lies in the range of 0.1–1), and then transferred into the resonance cell of a FT-ICR mass spectrometer by using an accumulation hexapole and two gradients: (1) The electrostatic gradient was kept by a system of potentials and lenses, and (2) the pressure gradient was maintained by a differential pumping system along the ion trajectory. The proton-bound $[\boldsymbol{M}\cdot\mathrm{H}\cdot\mathrm{G}]^+$ complex of interest was isolated by broad-band ejection of the other ions and then quenched by collisions with an inert gas (e.g., methane, argon), which pulsed into the cell through a magnetic valve. After the thermalization, the complex was allowed to stay in the cell for a variable reaction delay and then made to collide with a chiral or achiral reagent B introduced into the cell at a fixed pressure (10^{-10} to 10^{-8} mbar, Equation 1).

$$[\boldsymbol{M}\cdot\mathrm{H}\cdot\mathrm{G}]^+ + \mathrm{B} \rightarrow [\boldsymbol{M}\cdot\mathrm{H}\cdot\mathrm{B}]^+ + \mathrm{G} \qquad (1)$$

The extraction of the ligand-exchange rate constant is based on the decay of the isolated precursor ion $[\boldsymbol{M}\cdot\mathrm{H}\cdot\mathrm{G}]^+$ as a function of time t. If I is the intensity of the precursor $[\boldsymbol{M}\cdot\mathrm{H}\cdot\mathrm{G}]^+$ at the delay time t and I^0 is the sum of the signals of $[\boldsymbol{M}\cdot\mathrm{H}\cdot\mathrm{G}]^+$ and $[\boldsymbol{M}\cdot\mathrm{H}\cdot\mathrm{B}]^+$, a monoexponential $\ln(I/I^0)$ versus t plot is often obtained, whose slope provides the pseudo-first-order rate constant k_{exp} for the reaction in Equation 1. The monoexponential decay of an isolated system indicates that either just one reacting species exists or that more than one structure exists but that they react with similar rate constants (different species with a rate-constant ratio of less than 10 are kinetically indistinguishable, Figure 1).

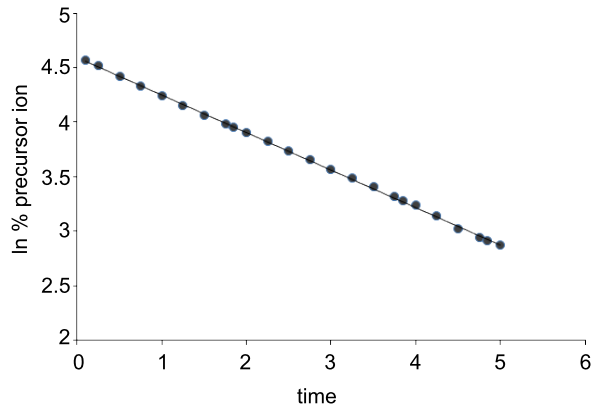

Figure 1: Examples of monoexponential decay: The slope of the line directly provides the reaction pseudo-first-order rate constant.

The bimolecular rate constant (k_{bi}) in monoexponential kinetics was calculated by solving Equation 3:

$$k_{exp} = k_{bi}[X] = k_{bi}\frac{P_{obs}}{S_{N_2}\cdot R_X\cdot k_B\cdot T} \quad (2)$$

$$k_{bi} = \frac{\left(k_{exp} \pm \delta k_{exp}\right)\cdot\left(S_{N_2} \pm \delta S_{N_2}\right)\cdot R_X\cdot k_B\cdot T}{\left(P_{obs} \pm \delta P_{obs}\right)} \quad (3)$$

P_{obs}: Observed pressure corrected for the background pressure.

$S_{N_2}\left(P_{obs}/P_{true}\right)_{N_2}$: Chemical sensitivity of vacuum gauge for N_2.

R_X (S_X / S_{N_2}; reacting gas dependent): Calibration factor of the vacuum gauge.

k_B = Boltzmann constant

Less frequently a biexponential decay was observed. This kinetic behavior indicates the presence of at least two different reacting structures: One of them decays faster (k_{fast}) than the other (k_{slow}: Figure 2).

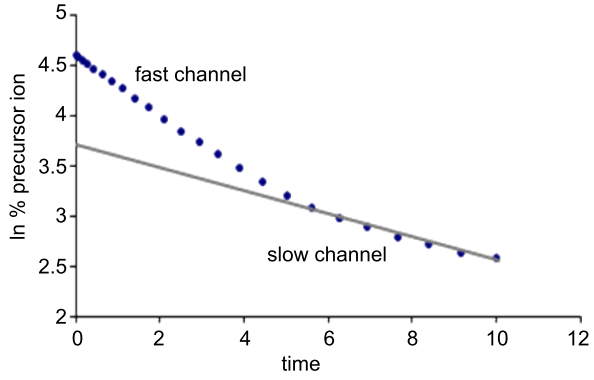

Figure 2: Example of biexponential decay.

In the latter case the following expression was used:

$$I = I^0_{fast}e^{-k_{slow}t} + I^0_{slow}e^{-k_{slow}t} \quad (4)$$

I^0_{fast} = intensity of the fast reacting structure at $t = 0$

I^0_{slow} = intensity of the slow reacting structure at $t = 0$

I^0_{slow} is extractable from the intercept of the slow component with the y-axis, with its slope giving k_{slow}. At this point Equation 4 also provides k_{fast}, considering that $I^0_{fast} + I^0_{slow} = 100$. The bimolecular $k_{(bi)fast}$ and $k_{(bi)slow}$ are obtained from k_{fast} and k_{slow} by using Equation 3. Finally, the calculated k_{bi} were compared with the thermal capture rate with the neutral bath (k_{cap}) in order to obtain the efficiency of the reaction as $k_{bi}/k_{cap} \times 100$. For this purpose the ion was treated as a point charge and the polar molecule as a two-dimensional rigid rotor by using the classical trajectory model (CT) of Su and Chesnavich [39,40].

When the host and the guest in the complex have the same absolute configuration, the rate constant of reaction described by Equation 1 is denoted as k_{homo}; when instead they have opposite configuration, the rate constant is denoted as k_{hetero}. The kinetic enantioselectivity of Equation 1 is obtained by comparing the second-order rate constants k for the same reaction involving the diastereomeric $[\boldsymbol{M}\cdot H\cdot G]^+_{homo}$ and $[\boldsymbol{M}\cdot H\cdot G]^+_{hetero}$ complexes, by means of the ρ factor (= k_{homo}/k_{hetero}). Furthermore, when the guest exchange of Equation 1 involves a chiral reactant B (either B_S or B_R), another enantioselectivity factor ξ can be extracted from the kinetic results, based on the ratio of the rate constants of the same reaction involving B_R (k_R) and B_S (k_S), namely $\xi = k_R/k_S$. Obviously a $\rho > 1$ value indicates that the reactant B displaces the guest from the homochiral complex faster than from the heterochiral one. The opposite is true when $\rho < 1$, whereas a $\rho = 1$ indicates a lack of enantioselectivity. Analogously, a $\xi > 1$ value indicates that the displacement of the guest from a given complex is faster with B_R than with B_S. Again, the opposite is true when $\xi < 1$. A $\xi = 1$ value corresponds to equal displacement rates irrespective of the configuration of B.

Chiral calixarenes, and their resorcinarene relatives, can be characterized by a variable conformational flexibility. They may exist in a highly symmetric bowl-shaped conformation, a so-called cone conformation, or in several other asymmetric conformations. In general, the chirality of resorcin[4]arenes can be due to (1) the presence of stereogenic centers in their side chains, or (2) the hindered spatial arrangement of achiral subunits forming a chiral macrocyclic scaffold.

Chiral centers in the side chains

Flexible peptidoresorcin[4]arenes as chiral selectors of dipeptides. In 2002, the first investigations of chiral recognition by calixarenes in the gas phase were carried out in Rome by the group of Prof. Speranza by using ESI-FT-ICR-MS. They published several other studies [11,41,42] on the displacement of selected amino acids (G) from a type-1 chiral amidoresorcin[4]arene $\mathbf{Y_S}$ (Figure 3) whose molecular asym-

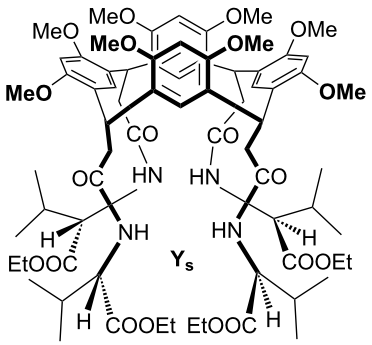

Figure 3: Amidoresorcin[4]arene $\mathbf{Y_S}$.

metry is due to the four axial pendants containing the chiral L-valine group. Two chiral effects were experimentally considered: The configuration of the amine B and that of the guest G. According to theoretical calculations, the chiral effects are insignificant if the guest molecule in the $[\mathbf{Y_S}{\cdot}H{\cdot}G]^+$ complex is located outside the cavity of the host, while a bimodal kinetic is mirrored by the coexistence of a different guest position depending on the G configuration.

In 2009, the lengths and the complexity of the lateral chains were modified in order to investigate the effect of the nature, and the sequence of the *N*-linked amino acid residues in the *down*-region of the host. The resorcin[4]arene octamethyl ethers were functionalized with leucyl-valine and valyl-leucine (**I** and **III**; Scheme 1a) methyl esters, and the enantioselectivity toward the same dipeptide esters used in their synthesis, namely, leucyl-valine-OMe and valyl-leucine-OMe (**1** and **3**; Scheme 1b) was investigated [43].

A configurational preference was pointed out from previous NMR experiments [44]: In $CDCl_3$ solution the neutral homochiral aggregate is significantly more stable than the heterochiral one, while NMR 1D ROESY results indicated that the dipeptidic guest is not located in the cavity of the host, but that the interaction that is mainly involved is hydrogen bonding occurring on the external surface of the resorcin[4]arene. These preliminary results motivated the gas-phase enantioselectivity study reported in [43], in which the guest displacement between proton-bound diastereomeric $[\boldsymbol{M}{\cdot}H{\cdot}G]^+$ ($\boldsymbol{M}$: **I**–**IV**; G = **1**–**3**) complexes and (*R*)-(−)-2-butylamine (B) (Equation 5 and Equation 6) was monitored. In addition to the displacement

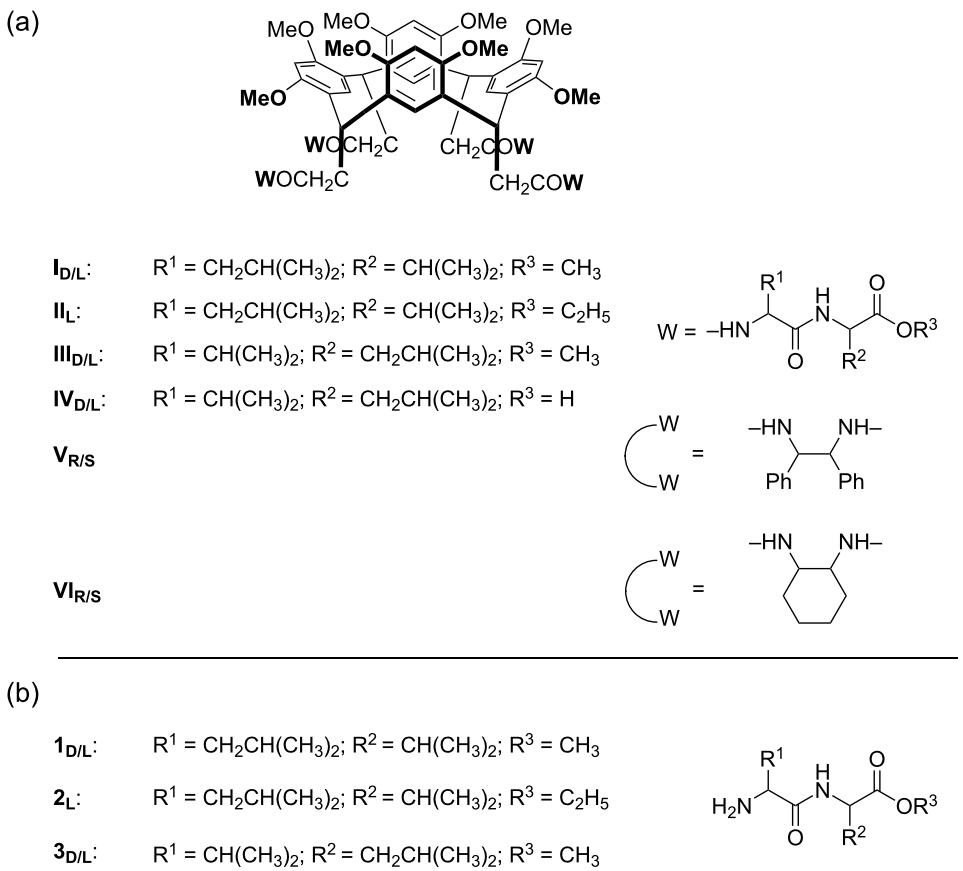

Scheme 1: Studied (a) peptidoresorcin[4]arenes and (b) dipeptidic guests.

enantioselectivity, the structural analogies between the resorcinarene and the dipeptides made other evaluations possible as, for instance, the effect of the –R in the CO_2R groups of the host and the guest (–CH_3 versus –C_2H_5), and the aminoacidic-sequence effect of the host pendants and the guest.

$$[\boldsymbol{M}_{\mathrm{L}}\cdot\mathrm{H}\cdot\mathrm{B}]^+ \xrightarrow[+\mathrm{B}-\mathrm{G}_{\mathrm{L}}]{k^{\mathrm{LL}}} [\boldsymbol{M}_{\mathrm{L}}\cdot\mathrm{H}\cdot\mathrm{G}]^+ \xleftarrow[+\mathrm{B}-\mathrm{G}_{\mathrm{D}}]{k^{\mathrm{LD}}} [\boldsymbol{M}_{\mathrm{L}}\cdot\mathrm{H}\cdot\mathrm{B}]^+ \quad (5)$$

$$[\boldsymbol{M}_{\mathrm{D}}\cdot\mathrm{H}\cdot\mathrm{B}]^+ \xrightarrow[+\mathrm{B}-\mathrm{G}_{\mathrm{L}}]{k^{\mathrm{DL}}} [\boldsymbol{M}_{\mathrm{D}}\cdot\mathrm{H}\cdot\mathrm{G}]^+ \xleftarrow[+\mathrm{B}-\mathrm{G}_{\mathrm{D}}]{k^{\mathrm{DD}}} [\boldsymbol{M}_{\mathrm{D}}\cdot\mathrm{H}\cdot\mathrm{B}]^+ \quad (6)$$

The $[\boldsymbol{M}\cdot\mathrm{H}\cdot\mathrm{G}]^+$ (***M***: **I**–**III**) complexes invariably reveal linear $\ln(I/I^0)$ versus *t*. In contrast, biexponential kinetics are observed with $[\mathbf{IV}\cdot\mathrm{H}\cdot\mathrm{G}]^+$. As pointed out in the methodology paragraph, the latter kinetic behavior is ascribed to the occurrence of at least two stable isomeric $[\boldsymbol{M}\cdot\mathrm{H}\cdot\mathrm{G}]^+$ structures, one less reactive ($[\mathbf{IV}\cdot\mathrm{H}\cdot\mathrm{G}]^+_{\mathrm{slow}}$) and the other more reactive ($[\mathbf{IV}\cdot\mathrm{H}\cdot\mathrm{G}]^+_{\mathrm{fast}}$). The configuration of B does not appreciably influence the reactions kinetics of Equation 5 and Equation 6 [43], thus suggesting that the amine does not need to enter the cavity to interact with the chiral lower portion of the host before displacing the dipeptide G from the complex. This hypothesis agrees well with the external location of G in the $[\boldsymbol{M}\cdot\mathrm{H}\cdot\mathrm{G}]^+$ complex that was observed in independent solution experiments [44].

The heterochiral $[\boldsymbol{M}\cdot\mathrm{H}\cdot\mathrm{G}]^+$ (***M***: **I**–**III**) complexes react more efficiently than their homochiral analogues, with the exception of the "slow" population of the heterochiral $[\mathbf{IV}\cdot\mathrm{H}\cdot\mathbf{3}]^+$. Both the populations of the diastereomeric $[\mathbf{IV}\cdot\mathrm{H}\cdot\mathbf{1}]^+$ react with scarce or absent enantioselectivity.

Concerning the structural effect of the ester tail, the kinetics of the reactions in Equation 5 and Equation 6 are appreciably affected by the nature of the –CO_2R function of the dipeptidic guest, while they are not subject to the influence of the specific ester functions of the host pendants [43], thus, providing further evidence that the guest is placed outside the host cavity in $[\boldsymbol{M}\cdot\mathrm{H}\cdot\mathrm{G}]^+$ (***M*** = **I**–**III**). The negligible effect observed between $[\mathbf{IV}\cdot\mathrm{H}\cdot\mathrm{G}]^+_{\mathrm{fast}}$ and their $[\mathbf{III}\cdot\mathrm{H}\cdot\mathrm{G}]^+$ analogues (G = **1**, **3**) was correlated to a similar spatial arrangement of the guests with respect to their receptors, while the relatively slow population of $[\mathbf{IV}\cdot\mathrm{H}\cdot\mathrm{G}]^+$ (G = **1**, **3**) reacts with an efficiency that is definitely lower than $[\mathbf{III}\cdot\mathrm{H}\cdot\mathrm{G}]^+$. This diverging behavior suggests that the guest in $[\mathbf{IV}\cdot\mathrm{H}\cdot\mathrm{G}]^+_{\mathrm{slow}}$ is arranged in a completely different orientation, and this particular feature is due to the presence of the COOH tail in **IV** pendants, which acts as a protonated "hook" for dipeptides [43]. Indeed, the reaction enantioselectivity factors reflect these differences ($[\boldsymbol{M}\cdot\mathrm{H}\cdot\mathrm{G}]^+$ (***M*** = **I**–**III**): $\rho < 1$; $[\mathbf{IV}\cdot\mathrm{H}\cdot\mathrm{G}]^+_{\mathrm{slow}}$: $\rho \geq 1$). Based on the NMR measurements [44], in which the homochiral $[\boldsymbol{M}\cdot\mathrm{H}\cdot\mathrm{G}]^+$ complexes appear to be more stable than the heterochiral ones, a $\rho < 1$ factor measured with $[\boldsymbol{M}\cdot\mathrm{H}\cdot\mathrm{G}]^+$ (***M*** = **I**–**III**) was rationalized from a thermodynamic point of view. The most enantioselective receptor towards guests **1** and **3** was **III**, while the lowest selectivity was observed with their $[\mathbf{I}\cdot\mathrm{H}\cdot 3]^+$ analogues. Irrespective of the nature of the host pendants (**III** or **I**), the complex of the guest **3** is more reactive than those of **1**, with the only exception of the heterochiral $[\mathbf{I}\cdot\mathrm{H}\cdot\mathrm{G}]^+$ (G = **1**, **3**). This enantioselectivity trend was ascribed to structural and steric factors, given the similar basicity of **1**–**3** [45-47]. The access of the amine B to the supramolecular assembly may be influenced by both steric and orientation factors, which can split the thermodynamic stability of the complexes and/or determine the dynamics of the displacement. In summary, the kinetic results [43] indicate that a dipeptidic guest is located outside the cavity of an analogous resorcin[4]arene, with the NH_2 terminus coordinated by the amido group of a pendant and the estereal terminus H-bonded to the adjacent pendant. When the estereal tail is substituted by a –CO_2H group, the hydrogen-bonding network is deeply modified. This gas phase arrangement, reproducing quite well the previous NMR experiments, is strongly influenced by the configuration of the partners in the charged aggregate.

Flexible peptidoresorcin[4]arenes as chiral selectors of vinca alkaloids. The interactions of the vinca alkaloids with the same resorcin[4]arenes were investigated in order to shed some light on the origin of the anticancer activity, by focusing on the drug/receptor interaction. Vinblastine and vincristine are "dimeric" molecules, comprising two subunits, i.e., rearranged (+)-catharanthine (T) and (−)-vindoline (D) (Figure 4) [48]. The gas-phase ligand-displacement approach was employed to investigate the intrinsic properties of these monomers on a molecular level [49]. First of all **I**, **III**, and **IV** were employed as artificial receptors characterized by more flexible lateral chains. The effect of the skeleton rigidity was evaluated by further investigation of the kinetic behavior of the rigid **V** and **VI** resorcin[4]arenes as chiral receptors.

The reaction with (*R*)-(−)-2-butylamine as the neutral gas B exhibited a significant enantioselectivity (Table 1).

In all cases the displacement reaction of $[\boldsymbol{M}\cdot\mathrm{H}\cdot\mathrm{T}]^+$ and $[\boldsymbol{M}\cdot\mathrm{H}\cdot\mathrm{D}]^+$ (***M*** = **I**–**III**) exhibited a monoexponential decay, while $[\mathbf{V_{R/S}}\cdot\mathrm{H}\cdot\mathrm{D}]^+$ diastereoisomers react by following a bimodal kinetic. When the COOMe terminus was replaced by the COOH group ($[\mathbf{IIIV_{D/L}}\cdot\mathrm{H}\cdot\mathrm{T}]^+ \rightarrow [\mathbf{VI_{D/L}}\cdot\mathrm{H}\cdot\mathrm{T}]^+$) an appreciable increase of enantioselectivity in the B-to-T displacement process was observed, while the inversion of the pendant sequence ($[\mathbf{I_{D/L}}\cdot\mathrm{H}\cdot\mathrm{T}]^+ \rightarrow [\mathbf{III_{D/L}}\cdot\mathrm{H}\cdot\mathrm{T}]^+$) induced a significant

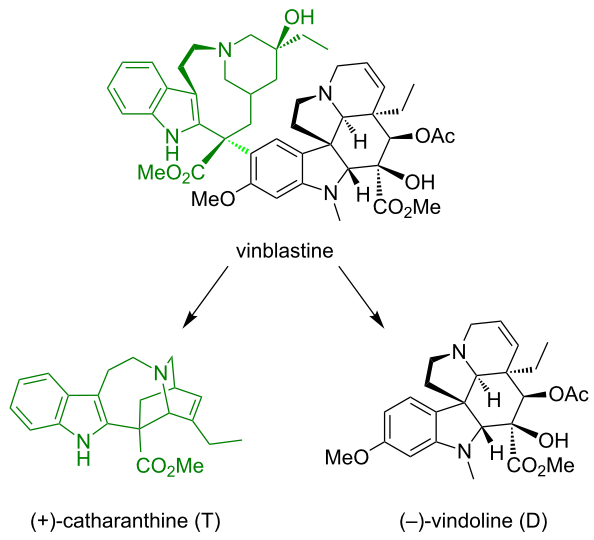

Figure 4: Catharanthine and vindoline, monomers constituting the anticancer vinblastine and the analogous vincristine.

Table 1: Exchange rate constants ($k \times 10^{-11}$ cm^3 molecule^{-1} s^{-1}).

Complex	ρ
$[\mathbf{I_D}\cdot H\cdot T]^+_{homo}$ $[\mathbf{I_L}\cdot H\cdot T]^+_{hetero}$	1.70 ± 0.22
$[\mathbf{III_D}\cdot H\cdot T]^+_{homo}$ $[\mathbf{III_L}\cdot H\cdot T]^+_{hetero}$	1.02 ± 0.14
$[\mathbf{IV_D}\cdot H\cdot T]^+_{homo}$ $[\mathbf{IV_L}\cdot H\cdot T]^+_{hetero}$	0.70 ± 0.14
$[\mathbf{V_R}\cdot H\cdot T]^+_{homo}$ $[\mathbf{V_S}\cdot H\cdot T]^+_{hetero}$	16.9 ± 2.8
$[\mathbf{VI_R}\cdot H\cdot T]^+_{homo}$ $[\mathbf{VI_R}\cdot H\cdot T]^+_{homo}$	0.56 ± 0.07

reduction of the reaction enantioselectivity. The investigated $[\boldsymbol{M}\cdot H\cdot D]^+$ complexes basically showed enantioselective parallels to that of the corresponding $[\boldsymbol{M}\cdot H\cdot T]^+$ adduct.

Rigid resorcin[4]arenes as chiral selectors of vinca alkaloids. Further attention was focused on the diastereomeric $[\mathbf{V_{R/S}}\cdot H\cdot T]^+$ complexes whose large enantioselectivity (ρ = 16.9 ± 2.8) must be essentially promoted by substantial differences in the relevant reaction pathway [49]. Indeed, from the computational analysis performed on catharanthine (T), two families of conformers resulted as stable from the study performed in vacuum as well as in water: The skew-boat conformation of catharanthine is about 1 kcal mol^{-1} more stable than the chair conformation (Figure 5).

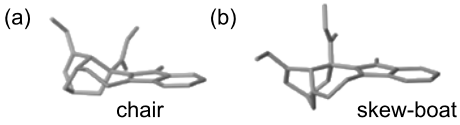

Figure 5: Stable conformers of catharanthine.

The skew-boat structure of both T and TH^+ is persistent during all the MD simulations, while the chair→skew-boat interconversion very easily occurs in aqueous TH^+. Furthermore, in all simulations the position of the CO_2Me function oscillates between two orientations differing by 180°, except for TH^+ in vacuum, while the ethyl group is invariably free to rotate in the three-dimensional space [49].

The computational results indicated that the chair conformation is better stabilized by the solvation and torsional energy terms than the skew-boat one is. In contrast, the electrostatic factor may induce a stronger stabilization of the skew-boat minimum, surpassing all the other effects. It can be concluded that in vacuum, electrostatic interactions prevail against the other energy terms, such that the T molecule, and the TH^+ ion even more, are locked in the skew-boat. When the dielectric constant becomes high (water), torsional and solvation factors may become comparable to intramolecular electrostatic factors, with the consequence that conformational flexibility of the structure may increase.

According to the MM and MD calculations, both the $[\mathbf{V_{S/R}}\cdot H\cdot T]^+$ enantiomers of the host tend to orientate two adjacent carbonyl oxygen atoms to the basic site of the guest. This arrangement requires that the structure of the host is strongly distorted from the uncomplexed form, by formation of a modified intramolecular hydrogen-bonding network at the lower rim [49]. The hosting regions of resorcin[4]arenes appear to be one the mirror image of the other, as does the hydrogen-bonding network involved in the interaction. Nevertheless, the marked differences, which finally justify the exceptional enantioselectivity measured, concern the orientation of the catharanthine in the lower rim of the cavity (Figure 6).

An aspect deserving more attention is the relative energies of the diastereomeric minima, which are very similar to each other, and thus this excludes an important contribution of thermodynamic control in the FT-ICR-MS experiments. The large enantioselectivity could be explained on the grounds of the pre-exponential term of Arrhenius, because depending on the orientation of catharanthine in the cavity there is more or less space for the approaching amine, which thus strongly influences the effective probability that the necessary proton transfer from T to B occurs.

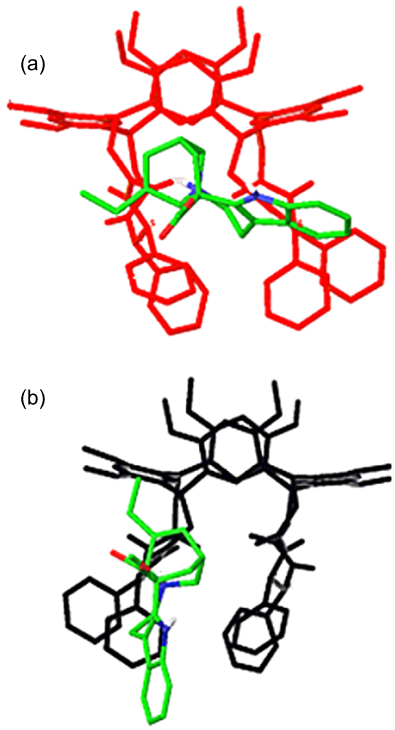

Figure 6: Global minima of (a) $[\mathbf{V_S}\cdot H\cdot T]^+$ and (b) $[\mathbf{V_R}\cdot H\cdot T]^+$ complexes.

Rigid resorcin[4]arenes as chiral selectors of amino acids and neurotransmitters. Further insights into the molecular recognition of basket resorcin[4]arene **V** towards representative chiral molecules were gathered. For this purpose, the proton-bonded diastereomeric $[\mathbf{V}\cdot H\cdot G]^+$ complexes [G = tyrosine methyl ester (tyr^{OMe}), and amphetamine (amph); Figure 7] were generated in the ESI source of an FT-ICR-MS to measure the kinetics of their ligand displacement towards the enantiomers of the neutral 2-aminobutane (B) (Table 2) [50].

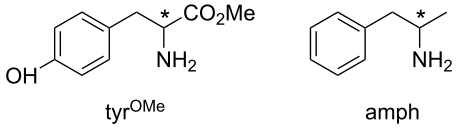

Figure 7: Guests studied in [47].

Irrespective of the configuration of B the $[\mathbf{V}\cdot H\cdot tyr^{OMe}]^+_{hetero}$ complex reacts faster than its homochiral counterpart. In contrast, the selectivity of the amphetamine aggregate strictly depends on the configuration of the approaching amine, as it shows $\rho > 1$ factors in the reaction with B_R and $\rho < 1$ factors in that with B_S.

To verify whether the measured enantioselectivity is determined by the relative stability of the starting diastereomeric complexes or by the transition states involved in the reaction path, the collision-induced dissociation spectra of the $[\mathbf{V}\cdot H\cdot tyr^{OMe}]^+$ and $[\mathbf{V}\cdot H\cdot amph]^+$ complexes were recorded ($[\mathbf{V}\cdot H]^+$ is the unique CID fragment, arising from the loss of the guest molecule) [50]. The *R* [51] values obtained in the CID of the $[\mathbf{V}\cdot H\cdot tyr^{OMe}]^+$ and $[\mathbf{V}\cdot H\cdot amph]^+$ complexes are definitely far from unity (0.32 and 0.48, respectively). These results indicate that both the homochiral $[\mathbf{V}\cdot H\cdot tyr^{OMe}]^+$ and $[\mathbf{V}\cdot H\cdot amph]^+$ complexes are significantly more stable than their heterochiral analogues. Based on the CID results, it can be concluded that the displacement reaction of the $[\mathbf{V}\cdot H\cdot tyr^{OMe}]^+$ complexes is mainly controlled by the relative stability of the starting diastereoisomers, while the ligand-exchange enantioselectivity of $[\mathbf{V}\cdot H\cdot amph]^+$ is determined by the effects of the chiral resorcin[4]arene scaffold upon the transition-state structures involved in the reaction, similarly to the complex of **V** with catharanthine.

Rigid resorcin[4]arenes as chiral selectors of nucleosides. Nucleosides are the elementary units of the RNA and DNA biomacromolecules, and their physiological importance at many different levels [52-54] makes them potential candidates as anticancer drugs. The gas-phase study of the intimate interactions between the resorcin[4]arene **V** and several pyrimidine nucleosides can be an inspiration for both the design of new drug carriers, characterized by high solubility and selectivity, and a better understanding of the selective uptake of nucleosides by their respective membrane receptors [55]. The selected pyrimidine nucleosides are reported in Figure 8, i.e., 2'-deoxycytidine dC, cytidine, Cy, cytarabine CT, an epimer of cytidine, and gemcitabine GC, which is the *gem*-difluoro derivative of 2'-deoxycytidine (Figure 8).

Table 2: Exchange rate constants ($k \times 10^{-10}$ cm^3 $molecule^{-1}$ s^{-1}).

$[M\cdot H\cdot G]^+$	B = (*R*)-(–)-$C_4H_9NH_2$ $\rho = k_{homo}/k_{hetero}$	B = (*S*)-(+)-$C_4H_9NH_2$ $\rho = k_{homo}/k_{hetero}$
$[\mathbf{V}\cdot H\cdot tyr^{OMe}]^+$	0.93 ± 0.03	0.78 ± 0.04
$[\mathbf{V}\cdot H\cdot amph]^+$	1.26 ± 0.09	0.91 ± 0.06

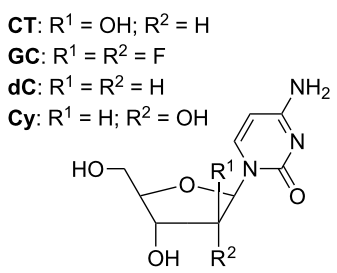

Figure 8: Selected nucleosides.

Two reaction products were observed in the reaction with the enantiomers (2)-aminobutane: the addition $[\boldsymbol{M}\cdot H\cdot G\cdot B]^+$ and the ligand-exchange $[\boldsymbol{M}\cdot H\cdot B]^+$ derivative. The experimental data was successfully fitted by using the integrated equation describing the kinetic Equation 7 [55].

$$[\boldsymbol{M}\cdot H\cdot G]^+ + B \underset{k_{-1}}{\overset{k_1}{\rightleftharpoons}} [\boldsymbol{M}\cdot H\cdot G\cdot B]^+ \xrightarrow{k_2} [\boldsymbol{M}\cdot H\cdot B]^+ + G \quad (7)$$

This profile indicates that, once formed, the $[\boldsymbol{M}\cdot H\cdot G\cdot B]^+$ three-body complex can either back dissociate to $[\boldsymbol{M}\cdot H\cdot G]^+$ and B (k_{-1}), or "kick out" G in order to leave the protonated resorcin[4]arene coordinating to B (k_2). The $10^{11}k_1/k_{-1}$ and k_{-1}/k_2 ratios are reported in Table 3.

The basicity of the nucleosides decreases in the order: dC < CT = Cy < GC, and in the same order the $10^{11}k_1/k_{-1}$ ratio tends to increase, most probably because the partial positive charge on the host pendants becomes larger, thus making the uptake of the third body B more efficient. The k_{-1}/k_2 ratio is invariably above unity, thus indicating that the release of B in general prevails on its uptake. Nevertheless, this ratio strongly depends on the electron demand of the 2'-substituent and on its orientation (Cy versus CT).

The more relevant result was observed for the complexes with G = dC as guest [55]. Indeed, when the host was in the *R*-configuration no reaction products were detected even after 300 s reaction time ([B] = 7.4×10^9 molecule cm^{-3}), whereas, under the same experimental conditions, the reaction carried out on the $[\mathbf{V_S}\cdot H\cdot dC]^+$ complex occurred and proceeded to over 20%. These findings indicate that the pre-equilibrium step involving $[\mathbf{V_R}\cdot H\cdot dC]^+$ (Equation 6) is ca. 200 times more shifted towards the reactants than that involving $[\mathbf{V_S}\cdot H\cdot dC]^+$ (dynamic range of the FT-ICR: ca. 10^3:1). In other words the $[\mathbf{V_R}\cdot H\cdot dC]^+$ complex does not uptake B, whereas its diastereoisomers are able to efficiently capture B and to proceed to the nucleoside displacement.

This very sensitive system strongly resembles the electronic concept of a logic gate. Indeed, depending on the relative configuration of the supramolecular device and of the neutral gas B, the transported nucleoside can or cannot be released. This effect is outstanding for the $[\mathbf{V_{R/S}}\cdot H\cdot dC]^+$ aggregates, which, if "stimulated" by a reactant characterized by the correct configuration, can selectively release one enantiomer of a chiral guest and keep the other enantiomer bound (Figure 9).

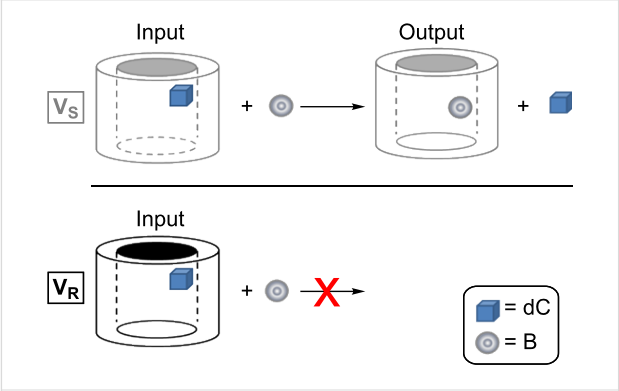

Figure 9: Example of molecular logic gate.

Table 3: Rate constant ratios (Equation 6).

Complexes	$10^{11}k_1/k_{-1}$ (cm^3 molecule^{-1})		k_{-1}/k_2	
	B = $\mathbf{B^R}$	B = $\mathbf{B^S}$	B = $\mathbf{B^R}$	B = $\mathbf{B^S}$
$[\mathbf{V_R}\cdot H\cdot CT]^+$	2.4	0.5	4.6	21.5
$[\mathbf{V_S}\cdot H\cdot CT]^+$	1.1	0.9	7.6	12.7
$[\mathbf{V_R}\cdot H\cdot GC]^+$	18.4	23.4	6.2	5.3
$[\mathbf{V_S}\cdot H\cdot GC]^+$	4.3	7.6	22.2	4.1
$[\mathbf{V_R}\cdot H\cdot dC]^+$	$<2 \times 10^{-3}$	$<2 \times 10^{-3}$	$>5 \times 10^3$	$>5 \times 10^3$
$[\mathbf{V_S}\cdot H\cdot dC]^+$	0.5	0.5	25.1	24.4
$[\mathbf{V_R}\cdot H\cdot Cy]^+$	1.8	2.4	43.1	70.1
$[\mathbf{V_S}\cdot H\cdot Cy]^+$	6.4	9.8	1.3	2.1

Cyclochiral resorcin[4]arenes as chiral selectors

A cyclochiral resorcin[4]arene is characterized by four identical subunits noncovalently coordinated by hydrogen bonds [56], three-dimensionally arranged either clockwise or counterclockwise. The authors investigated the effect of the mentioned source of asymmetry by generating, in a nanoESI-FT-ICR mass spectrometer, proton-bound complexes between resorcinarenes **C** (Figure 10) [57] and several polyfunctionalized biomolecules (G, Table 4), and then by measuring their gas-phase reactivity towards some primary amines (B: $CH_3CH\Omega NH_2$ with Ω = H, CH_3, C_2H_5) [58].

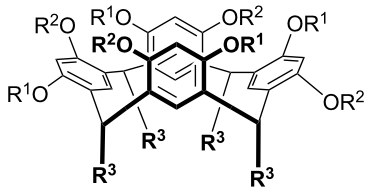

R^1 = H; R^2 = CH_3; R^3 = $(CH_3)_9CH_3$: $\mathbf{C}_{M,R}^{H}$
R^1 = H; R^2 = CH_3; R^3 = $(CH_3)_9CD_3$: $\mathbf{C}_{M,R}^{D}$
R^1 = H; R^2 = CH_3; R^3 = $(CH_3)_9CH_3$: $\mathbf{C}_{P,S}^{H}$
R^1 = H; R^2 = CH_3; R^3 = $(CH_3)_9CD_3$: $\mathbf{C}_{P,S}^{D}$

Figure 10: Cyclochiral resorcin[4]arenes.

The presence of four decamethylene lateral chains in the structure of **C** favored the arrangement of guests on the upper aromatic cavity of **C**, and the remote position of labeled or unlabeled methyl groups enables the kinetic measurements of the corresponding quasi-diastereomeric complexes under the same experimental conditions (Equation 8 and Equation 9; B: $CH_3CH\Omega NH_2$ with Ω = H, CH_3, C_2H_5) [59,60].

$$[\mathbf{C}_{P,S}^{\mathbf{H}} \cdot \mathrm{H} \cdot \mathrm{G}]^+ + \mathrm{B} \longrightarrow [\mathbf{C}_{P,S}^{\mathbf{H}} \cdot \mathrm{H} \cdot \mathrm{B}]^+ + \mathrm{G} \quad (8)$$

$$[\mathbf{C}_{M,R}^{\mathbf{D}} \cdot \mathrm{H} \cdot \mathrm{G}]^+ + \mathrm{B} \longrightarrow [\mathbf{C}_{M,R}^{\mathbf{D}} \cdot \mathrm{H} \cdot \mathrm{B}]^+ + \mathrm{G} \quad (9)$$

The selected $[\mathbf{C}\cdot H\cdot G]^+$ complexes exist as single kinetically distinguishable structures. The heterochiral complexes mostly react faster than their homochiral homologues, with the exception of the $[\mathbf{C}\cdot H\cdot G]^+$ complexes with G = A_4, N_2, N_4 (Table 5) [58].

As previously mentioned, the origin of the enantioselectivities showed in Table 5 can be due to a thermodynamic and/or kinetic control of the reaction coordinates. It has been found that when the proton affinity of the neutral amine increases, and the reaction becomes enthalpically favored, the measured enantioselectivity tends to decrease. This finding indicates that the main reaction control factor is the kinetic one, because the system is less enantioselective if the involved transition structures become more similar to the starting diastereomeric reactant complexes, by following the proton affinity order of B. This interpretation was supported by independent MS tandem measurements carried out on the $[\mathbf{C}_{M,R}^{\mathbf{a}}\cdot\mathbf{C}_{P,S}^{\mathbf{b}}\cdot H\cdot G]^+$ (G = N_1; N_2; a,b = H,D or D,H) ternary adducts yielding $[\mathbf{C}_{M,R}^{\mathbf{a}}\cdot H\cdot G]^+$ and $[\mathbf{C}_{P,S}^{\mathbf{b}}\cdot H\cdot G]^+$ as the fragmentation products. The distribution of the quasi-enantiomer fragments points to the same relative stability for the starting diastereomeric $[\mathbf{C}\cdot H\cdot N_1]^+$ complexes and an appreciable energy difference between the diastereoisomers of $[\mathbf{C}\cdot H\cdot N_2]^+$ ($[\mathbf{C}\cdot H\cdot N_2]^+_{hetero}$ > $[\mathbf{C}\cdot H\cdot N_2]^+_{homo}$). The combination of the dependence of ρ on the proton affinity of the amine and the independent CID data clearly indicates that the kinetics of the $[\mathbf{C}\cdot H\cdot N_1]^+$ adducts is mostly controlled by the cyclochirality determining the differential energies of the involved transition structures. In contrast,

Table 4: Overview of investigated amino acids, amino alcohols and amino acid esters.

Free AA[a]		Amino alcohols	
L-Phenylalanine	A_1	L-Tyrosinol	N_1
3,4-Dihydroxy-L-phenylalanine	A_2	(1*R*,2*R*)-2-Amino-1-phenyl-1,3-propandiol	N_2
L-Tryptophan	A_3	L-Epinephrine	N_3
5-Hydroxy-L-tryptophan	A_4	L-Norepinephrine	N_4
L-Tyrosine	A_5		
AA ester			
L-Phenylalanine ethyl ester	E_1		
L-Tyrosine methyl ester	E_2		

[a]amino acid.

Table 5: k_{homo}/k_{hetero} measured for reactions of $[\mathbf{C}^{H}\cdot H\cdot G]^+/[\mathbf{C}^{D}\cdot H\cdot G]^+$ complexes with **B**.

	Ω = H	Ω = CH_3	Ω = C_2H_5	Ω = C_2H_5 (*S*)-
P.A.	210	212.5	214.1	214.1
G		k_{homo}/k_{hetero} (ρ)		
A_1	0.99 ± 0.07	—	1.10 ± 0.04	1.10 ± 0.08
A_2	0.39 ± 0.01	0.70 ± 0.05	0.93 ± 0.06	0.94 ± 0.04
A_3	0.56 ± 0.02	—	0.95 ± 0.06	1.08 ± 0.07
A_4	—	2.03 ± 0.11	1.31 ± 0.08	1.44 ± 0.09
A_5	—	—	0.95 ± 0.05	0.99 ± 0.06
E_1	0.53 ± 0.03	0.74 ± 0.03	0.77 ± 0.03	0.82 ± 0.08
E_2	—	0.80 ± 0.04	0.82 ± 0.04	0.84 ± 0.05
N_1	0.59 ± 0.03	0.47 ± 0.02	0.54 ± 0.03	0.76 ± 0.03
N_2	—	3.89 ± 0.29	3.94 ± 0.23	2.65 ± 0.38
N_3	—	0.89 ± 0.04	1.02 ± 0.04	0.78 ± 0.03
N_4	—	1.51 ± 0.09	1.57 ± 0.09	1.32 ± 0.08

the significant enantioselectivity exhibited by the diastereomeric $[\mathbf{C}\cdot H\cdot N_2]^+$ complexes is due to the synergy between their different stabilities and the effect of the asymmetric architecture of the cyclochiral resorcin[4]arene.

The presented evidence represents the first example of a kinetic enantiorecognition mainly due to an exclusive structural factor: the cyclochirality of the receptor's cavity.

Conclusion

The high enantioselectivity found in biochemical systems is essentially due to several intimate noncovalent interactions. In living systems a covalent bond between a neurotransmitter and its macromolecular target cannot be imagined, because it would produce an irreversible inactivation of the receptor primary functions, which is incompatible with the existence of living matter itself. In fact, the pharmacological mechanism, so called suicide, of many drugs (e.g., anticancer molecules) consists in the formation of a covalent, and thus irreversible, bond with their target. The main advantage of a gaseous environment is the exclusion of any counterion and/or solvent effect, while at the same time the chemicophysical properties of the isolated system can be subtly studied.

Finally, the application of the displacement-reaction methodology provides a variety of information on the dynamic behavior of a supramolecular device: (1) The decay curve of a selected precursor indicates whether one or several kinetically distinguishable structures exist; (2) The effect of the neutral configuration suggests the actual location of the substituted guest (external or internal); (3) the effect of the neutral proton affinity on the measured enantioselectivity indicates the prevalence of kinetic or thermodynamic reaction control. Further energetic details can be gained by an independent mass-spectrometric approach (Cook's method on a three-body complex), and by several computational supports (molecular dynamics and ab initio optimization). The dynamic point of view is fundamental for supramolecular ionic aggregates, because the synergy of several noncovalent interactions confers a pronounced stability even to very flexible aggregates, and the lifetime of the same interactions determines the reaction pathway.

The reviewed papers point to the crucial role of the nature and sequence of the resorcin[4]arene pendants, even in the case of gas-phase biorecognition, analogous to the enzymatic behavior. Furthermore, the high selectivity in the reaction of $[\boldsymbol{M}\cdot H\cdot \text{drug}]^+$ towards an organic base could efficiently reproduce the driving forces for the intimate contact between the same drug and its biotarget.

Acknowledgements

The authors from Bielefeld University gratefully acknowledge the support from the Deutsche Forschungsgemeinschaft (SFB 613). The authors from Rome gratefully acknowledge the support of the Ministero dell'Istruzione dell'Università e della Ricerca (MIUR-PRIN-2007H9S8SW) and the Consiglio Nazionale delle Ricerche (CNR).

References

1. Kauzmann, W. *Rev. Mod. Phys.* **1959,** *31,* 549–556. doi:10.1103/RevModPhys.31.549

2. Schnier, P. D.; Klassen, J. S.; Strittmatter, E. F.; Williams, E. R. *J. Am. Chem. Soc.* **1998,** *120,* 9605–9613. doi:10.1021/ja973534h
3. Pichierri, F.; Aida, M.; Gromiha, M. M.; Sarai, A. *J. Am. Chem. Soc.* **1999,** *121,* 6152–6157. doi:10.1021/ja984124b
4. Hollfelder, F.; Kirby, A. J.; Tawfik, D. S. *Nature* **1996,** *383,* 60–63. doi:10.1038/383060a0
5. Jain, V. K.; Kanaiya, P. H. *Russ. Chem. Rev.* **2011,** *80,* 75–102. doi:10.1070/RC2011v080n01ABEH004127 And references therein.
6. Winkler, H. D. F.; Dzyuba, E. V.; Sklorz, J. A. W.; Beyeh, N. K.; Rissanen, K.; Schalley, C. A. *Chem. Sci.* **2011,** *2,* 615–624. doi:10.1039/c0sc00539h
7. Kalenius, E.; Kekäläinen, T.; Neitola, R.; Beyeh, K.; Rissanen, K.; Vainiotalo, P. *Chem.–Eur. J.* **2008,** *7,* 5220–5228. doi:10.1002/chem.200800075
8. Salorinne, K.; Weimann, D. P.; Schalley, C. A.; Nissinen, M. *Eur. J. Org. Chem.* **2009,** 6151–6159. doi:10.1002/ejoc.200900814
9. Beyeh, N. K.; Valkonen, A.; Rissanen, K. *Supramol. Chem.* **2009,** *21,* 142–148. doi:10.1080/10610270802308411
10. Mäkinen, M.; Kalenius, E.; Neitola, R.; Rissanen, K.; Vainiotalo, P. *Rapid Commun. Mass Spectrom.* **2008,** *22,* 1377–1383. doi:10.1002/rcm.3522
11. Tafi, A.; Botta, B.; Botta, M.; Delle Monache, G.; Filippi, A.; Speranza, M. *Chem.–Eur. J.* **2004,** *10,* 4126–4135. doi:10.1002/chem.200305772
12. Antipin, I. S.; Stoikov, I. I.; Pinkhassik, E. M.; Fitseva, N. A.; Stibor, I.; Konovalov, A. I. *Tetrahedron Lett.* **1997,** *38,* 5865–5868. doi:10.1016/S0040-4039(97)01305-1
13. Douteau-Guével, N.; Coleman, A. W.; Morel, J.-P.; Morel-Desrosiers, N. *J. Phys. Org. Chem.* **1998,** *11,* 693–696. doi:10.1002/(SICI)1099-1395(1998100)11:10<693::AID-POC18>3.0.CO;2-8
14. Douteau-Guével, N.; Coleman, A. W.; Morel, J.-P.; Morel-Desrosiers, N. *J. Chem. Soc., Perkin Trans. 2* **1999,** *3,* 629–634. doi:10.1039/A806855K
15. Selkti, M.; Tomas, A. W.; Coleman, A. W.; Nicolis, I.; Douteau-Guével, N.; Villain, F.; Tomas, A.; de Rango, C. *Chem. Commun.* **2000,** *2,* 161–162. doi:10.1039/a906546f
16. Arena, G.; Contino, A.; Gulino, F. G.; Magri, A.; Sansone, F.; Sciotto, D.; Ungaro, R. *Tetrahedron Lett.* **1999,** *40,* 1597–1600. doi:10.1016/S0040-4039(98)02654-9
17. Araki, K.; Inada, K.; Shinkai, S. *Angew. Chem., Int. Ed. Engl.* **1996,** *108,* 92–94. doi:10.1002/anie.199600721
18. Ito, K.; Kida, A.; Ohba, Y.; Sone, T. *Chem. Lett.* **1998,** *27,* 1221–1222. doi:10.1246/cl.1998.1221
19. Buschmann, H.-J.; Mutihac, L.; Jansen, K. *J. Inclusion Phenom. Macrocyclic Chem.* **2001,** *39,* 1–11. doi:10.1023/A:1008155823862
20. Gutsche, C. D. In *Calixarenes in Monographs in Supramolecular Chemistry;* Stoddart, J. F., Ed.; Royal Society of Chemistry: Cambridge, 1989.
21. Gutsche, C. D. In *Calixarenes Revisited in Monographs in Supramolecular Chemistry;* Stoddart, J. F., Ed.; Royal Society of Chemistry: Cambridge, 1998.
22. Vicens, J.; Böhmer, V., Eds. *Calixarenes: A Versatile Class of Macrocyclic Compounds;* Topics in Inclusion Science, Vol. III; Kluwer Academic Publishers: Dordrecht, 1991.
23. Böhmer, V. *Angew. Chem., Int. Ed. Engl.* **1995,** *34,* 713–745. doi:10.1002/anie.199507131
24. van Wageningen, A. M. A.; Verboom, W.; Reinhoudt, D. N. *Pure Appl. Chem.* **1996,** *68,* 1273–1277. doi:10.1351/pac199668061273
25. Ikeda, A.; Shinkai, S. *Chem. Rev.* **1997,** *97,* 1713–1734. doi:10.1021/cr960385x
26. Mandolini, L.; Ungaro, R., Eds. *Calixarenes in Action;* Imperial College Press: London, 2000.
27. Asfari, M.-Z.; Böhmer, V.; Harrowfield, J.; Vicens, J., Eds. *Calixarenes;* Kluwer Academic Publishers: Dordrecht, 2001.
28. Harrowfield, J. M.; Richmond, W. R.; Sobolev, A. N.; White, A. H. *J. Chem. Soc., Perkin Trans. 2* **1994,** *1,* 5–9. doi:10.1039/p29940000005
29. Ludwig, R.; Fresenius, J. *Anal. Chem.* **2000,** *367,* 103–128. doi:10.1007/s002160051611
30. Arena, G.; Contino, A.; Magri, A.; Sciotto, D.; Spoto, G.; Torrisi, A. *Ind. Eng. Chem. Res.* **2000,** *39,* 3605–3610. doi:10.1021/ie000220l
31. Speranza, M.; Gasparrini, F.; Botta, B.; Villani, C.; Subissati, D.; Fraschetti, C.; Subrizi, F. *Chirality* **2009,** *21,* 69–86. doi:10.1002/chir.20606
32. Lebrilla, C. B. *Acc. Chem. Res.* **2001,** *34,* 653–661. doi:10.1021/ar980125x
33. Ramirez, J.; He, F.; Lebrilla, C. B. *J. Am. Chem. Soc.* **1998,** *120,* 7387–7388. doi:10.1021/ja9812251
34. Ramirez, J.; Ahn, S.; Grigorean, G.; Lebrilla, C. B. *J. Am. Chem. Soc.* **2000,** *122,* 6884–6890. doi:10.1021/ja000717m
35. Gal, J. F.; Stone, M.; Lebrilla, C. B. *Int. J. Mass Spectrom.* **2003,** *222,* 259–267. doi:10.1016/S1387-3806(02)00992-2
36. Ahn, S.; Ramirez, J.; Grigorean, G.; Lebrilla, C. B. *J. Am. Soc. Mass Spectrom.* **2001,** *12,* 278–287. doi:10.1016/S1044-0305(00)00220-8
37. Grigorean, G.; Lebrilla, C. B. *Anal. Chem.* **2001,** *73,* 1684–1691. doi:10.1021/ac001135q
38. Splitter, J. S.; Turecek, F. *Applications of Mass Spectrometry to Organic Stereochemistry;* John Wiley & Sons, 1993.
39. Su, T.; Chesnavich, W. J. *J. Chem. Phys.* **1982,** *76,* 5183–5185. doi:10.1063/1.442828
40. Su, T. *J. Chem. Phys.* **1988,** *89,* 5355. doi:10.1063/1.455750
41. Botta, B.; Botta, M.; Filippi, A.; Tafi, A.; Delle Monache, G.; Speranza, M. *J. Am. Chem. Soc.* **2002,** *124,* 7658–7659. doi:10.1021/ja020232t
42. Botta, B.; Caporuscio, F.; D'Acquarica, I.; Delle Monache, G.; Subissati, D.; Tafi, A.; Botta, M.; Filippi, A.; Speranza, M. *Chem.–Eur. J.* **2006,** *12,* 8096–8105. doi:10.1002/chem.200600102
43. Botta, B.; Fraschetti, C.; D'Acquarica, I.; Speranza, M.; Novara, F. R.; Mattay, J.; Letzel, M. C. *J. Phys. Chem. A* **2009,** *113,* 14625–14629. doi:10.1021/jp904374h
44. Botta, B.; D'Acquarica, I.; Delle Monache, G.; Subissati, D.; Uccello-Barretta, G.; Mastrini, M.; Nazzi, S.; Speranza, M. *J. Org. Chem.* **2007,** *72,* 9283–9290. doi:10.1021/jo7016636
45. Nold, M. J.; Cerda, B. A.; Wesdemiotis, C. *J. Am. Soc. Mass Spectrom.* **1999,** *10,* 1–8. doi:10.1016/S1044-0305(98)00120-2
46. Pingitore, F.; Polce, M. J.; Wang, P.; Wesdemiotis, C.; Paizs, B. *J. Am. Soc. Mass Spectrom.* **2004,** *15,* 1025–1038. doi:10.1016/j.jasms.2004.03.014
47. Val-Leu and Leu-Val dipeptides exhibit the same gas phase basicity (GB = 211.2 kcal mol^{-1}; http://webbook.nist.gov). It is plausible that their relative esters display the same BG as well.
48. Wilson, L.; Bamburg, J. R.; Mizel, S. B.; Grisham, L. M.; Creswell, K. M. *Fed. Proc.* **1974,** *33,* 158–166.

49. Botta, B.; Fraschetti, C.; Novara, F. R.; Tafi, A.; Sacco, F.; Mannina, L.; Sobolev, A. P.; Mattay, J.; Letzel, M. C.; Speranza, M. *Org. Biomol. Chem.* **2009,** *7,* 1798–1806. doi:10.1039/b900735k
50. Botta, B.; D'Acquarica, I.; Nevola, L.; Sacco, F.; Valbuena Lopez, Z.; Zappia, G.; Fraschetti, C.; Speranza, M.; Tafi, A.; Caporuscio, F.; Letzel, M. C.; Mattay, J. *Eur. J. Org. Chem.* **2007,** 5995–6002. doi:10.1002/ejoc.200700829
51. $$R = \frac{\left(\frac{[\mathrm{V}\cdot\mathrm{H}]^+}{[\mathrm{V}\cdot\mathrm{H}\cdot\mathrm{G}]^+}\right)_{\mathrm{homo}}}{\left(\frac{[\mathrm{V}\cdot\mathrm{H}]^+}{[\mathrm{V}\cdot\mathrm{H}\cdot\mathrm{G}]^+}\right)_{\mathrm{hetero}}}$$
52. Van Belle, H. *Cardiovasc. Res.* **1993,** *27,* 68–76. doi:10.1093/cvr/27.1.68
53. Baldwin, S. A.; Mackey, J. R.; Cass, C. E.; Young, D. J. *Mol. Med. Today* **1999,** *5,* 216–224. doi:10.1016/S1357-4310(99)01459-8
54. da Rocha, A. B.; Lopes, R. M.; Schwartsmann, G. *Curr. Opin. Pharmacol.* **2001,** *1,* 364–369. doi:10.1016/S1471-4892(01)00063-7
55. Botta, B.; Fraschetti, C.; D'Acquarica, I.; Sacco, F.; Mattay, J.; Letzel, M. C.; Speranza, M. *Org. Biomol. Chem.* **2011,** *9,* 1717–1719. doi:10.1039/c0ob00664e
56. Szumna, A. *Org. Biomol. Chem.* **2007,** *5,* 1358–1368. doi:10.1039/b701451a
57. Buckley, B. R.; Boxhall, J. Y.; Bulman Page, P. C.; Chan, Y.; Elsegood, M. R. J.; Heaney, H.; Holmes, K. E.; McIldowie, M. J.; McKee, V.; McGrath, M. J.; Mocerino, M.; Poulton, A. M.; Sampler, E. P.; Skelton, B. W.; White, A. H. *Eur. J. Org. Chem.* **2006,** 5117–5134. doi:10.1002/ejoc.200600590
58. Fraschetti, C.; Letzel, M. C.; Paletta, M.; Mattay, J.; Speranza, M.; Filippi, A.; Aschi, M.; Rozhenko, A. B. *J. Mass Spectrom.* **2012,** *47,* 72–78. doi:10.1002/jms.2028
59. Sawada, M. *Mass Spectrom Rev* **1997,** *16,* 73–90. doi:10.1002/(SICI)1098-2787(1997)16:2<73::AID-MAS2>3.0.CO;2-6
60. Nikolaev, E. N.; Denisov, E. V.; Rakov, V. S.; Futrell, J. H. *Int. J. Mass Spectrom.* **1999,** *182–183,* 357–368. doi:10.1016/S1387-3806(98)14275-6

License and Terms

Beilstein Journal of Organic Chemistry

Investigation of the network of preferred interactions in an artificial coiled-coil association using the peptide array technique

Raheleh Rezaei Araghi[1,§], Carsten C. Mahrenholz[2,§], Rudolf Volkmer[2] and Beate Koksch[*1]

Full Research Paper

Open Access

Address:
[1]Institute of Chemistry and Biochemistry, Freie Universität Berlin, Takustrasse 3, 14195 Berlin, Germany and [2]Institute of Medical Immunology, Charité-Universitätsmedizin Berlin, Augustenburger Platz 1, 13353, Berlin, Germany

Email:
Beate Koksch[*] - koksch@chemie.fu-berlin.de

* Corresponding author
§ These authors contributed equally to this work.

Keywords:
β- and γ-amino acids; coiled coil; foldamer; screening libraries; SPOT technique

Beilstein J. Org. Chem. **2012,** *8,* 640–649.
doi:10.3762/bjoc.8.71

Received: 29 January 2012
Accepted: 03 April 2012
Published: 25 April 2012

This article is part of the Thematic Series "Supramolecular chemistry II".

Guest Editor: C. A. Schalley

Abstract

We screened a randomized library and identified natural peptides that bound selectively to a chimeric peptide containing α-, β- and γ-amino acids. The SPOT arrays provide a means for the systematic study of the possible interaction space accessible to the αβγ-chimera. The mutational analysis reveals the dependence of the binding affinities of α-peptides to the αβγ-chimera, on the hydrophobicity and bulkiness of the side chains at the corresponding hydrophobic interface. The stability of the resulting heteroassemblies was further confirmed in solution by CD and thermal denaturation.

Introduction

Coiled-coil domains, which consist of two or more α-helices, are the most common representatives of α-helix-mediated protein–protein interactions, which regulate many important biological pathways [1]. Coiled coils have several advantageous features that, on the one hand, allow them to fulfill a wide range of important cellular functions [2] and, on the other hand, make them ideal building blocks in protein design: They are ubiquitous proteins that have the ability to oligomerize with high selectivity, forming stable multimers with strong interhelical interactions. Recently, their potential as drug targets has become the focus of medical research [3]. Their effectiveness in the successful inhibition of membrane fusion proteins of viruses, such as HIV [4] and avian influenza [5], also supports the concept of rational drug design based on coiled-coil

proteins [6]. In this context, the use of unnatural amino acids in peptidomimetics is advisable, to enhance enzymatic stability, limit conformational flexibility, and improve pharmacodynamics and bioavailability [7]. In order to manipulate helix-mediated interactions to achieve high specificity levels, a pioneering approach is to design helical foldameric sequences containing β- and γ-amino acids. Foldamers are shown to form, successfully, a variety of conformations at secondary, tertiary, and quaternary structure levels [8-10]. In spite of the increasing number of helical assemblies made of peptidic foldamers, the combination of artificial oligomers with natural peptides remains a challenge. The main difficulties arise in the prediction of a suitable side-chain composition and the geometry of the foldameric binding groove that interacts with α-peptides [11]. Therefore, elucidating the side-chain compositions responsible for selective intermolecular interactions in an otherwise natural coiled-coil assembly should facilitate the design of helix–helix interaction motifs. We broadly surveyed interaction properties in order to improve the association between artificial and natural patterns by means of SPOT technology, which is a simple high-throughput method shown to be useful for the characterization of intermolecular domains in general and coiled coils in particular at the amino-acid level [12-15]. This method assisted in the mapping of α-residues of a natural peptide strand that interact with key β- and γ-amino acids of a chimeric peptide. A wide range of analogues of wild-type α-partners were synthesized and analyzed in order to evaluate affinity, selectivity, and the binding determinants of the αβγ-chimeric backbone. Further, the stability and the stoichiometry of selected sequences were examined by CD and SEC in solution.

Results and Discussion

Screening system: Coiled coils are a highly populated class of protein-folding motifs that exhibit a distinctive heptad repeat sequence, conventionally labeled with the letters *a*–*g* [16,17]. The set of hydrophobic residues at the first (i.e., *a*) and fourth (i.e., *d*) positions pack into the coiled-coil interfaces and play the main role in helical association, while the *e* and *g* positions frequently consist of polar or charged residues forming the electrostatic interface. A preliminary structural investigation revealed that one such characteristic heptad can be substituted by a pentad repeat sequence of alternating β- and γ-amino acids, while retaining folding stability [18,19]. The backbone-engineered coiled-coil system comprises two peptides: A glutamic acid-rich α-poly peptide (Acid-pp) and a lysine-rich chimeric B3β2γ sequence. These systems have a high propensity for heterooligomerization (Figure 1). In B3β2γ, the two central turns of the α-helix are substituted by a pentad of alternating β- and γ-amino acids. Our previous study revealed the heteromeric assembly of natural and chimeric sequences with 1:1 stoichiometry [18]. The heterooligomerization is driven by the burial of the hydrophobic surface area and is directed by electrostatic interactions between charged residues that flank the hydrophobic core. However, substituting an α-heptad with a pentad of β- and γ-amino acids has structural consequences, such as disruption of the local packing, or conformational chaos due to the loss of one peptide bond and therewith one H-bond donor and one H-bond acceptor. More recently, it has been shown that a careful choice of side chains can provide key residue contacts and a sufficient number of van der Waals interactions to enable the chimeric sequence to form helical interfaces interacting with a native peptidic partner [20]. These

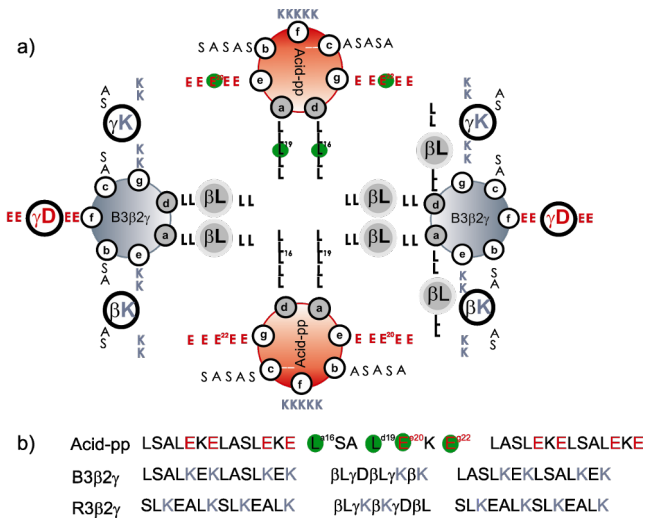

Figure 1: (a) Helical wheel representation of the tetrameric Acid-pp/B3β2γ helix bundle, (b) sequences of Acid-pp, B3β2γ, R3β2γ. Red and blue letters indicate the acidic residues in Acid-pp and the basic residues in B3β2γ and R3β2γ, respectively. The randomized positions are designated by green circles.

instructive investigations have revealed that side-chain and backbone characteristics are tuneable elements for control of the interaction between αβγ-chimera and their native partners. To extend these studies, in the current report, we screen the "interaction space" of chimeric coiled coils using a large library of native peptides in order to search for more efficient interacting partners.

Library design and synthesis: To investigate the Acid-pp–chimera interaction, a peptide array (1764 spots), featuring multiple substitutions at positions *a*/*d*/*e*/*g* of the central heptad of the *wt* Acid-pp sequence (Figure 2a), was created on cellulose membrane and probed for binding to the αβγ-chimera. The chimeric sequence B3β2γ, containing three β- and two γ-amino acids, was synthesized by standard solid-phase peptide synthesis and labeled at the N-terminus with the fluorophore 5(6)-tetramethylrhodamine (TAMRA). As described above, the chimera has a modified pentad (β- and γ-amino acids) at the center of its 31-residue sequence (positions 15–19). Thus, the positions in the complementary heptad of Acid-pp (positions 15–21) were mutated, as shown in Figure 1a and Figure 1b. In order to investigate the contact elements on the

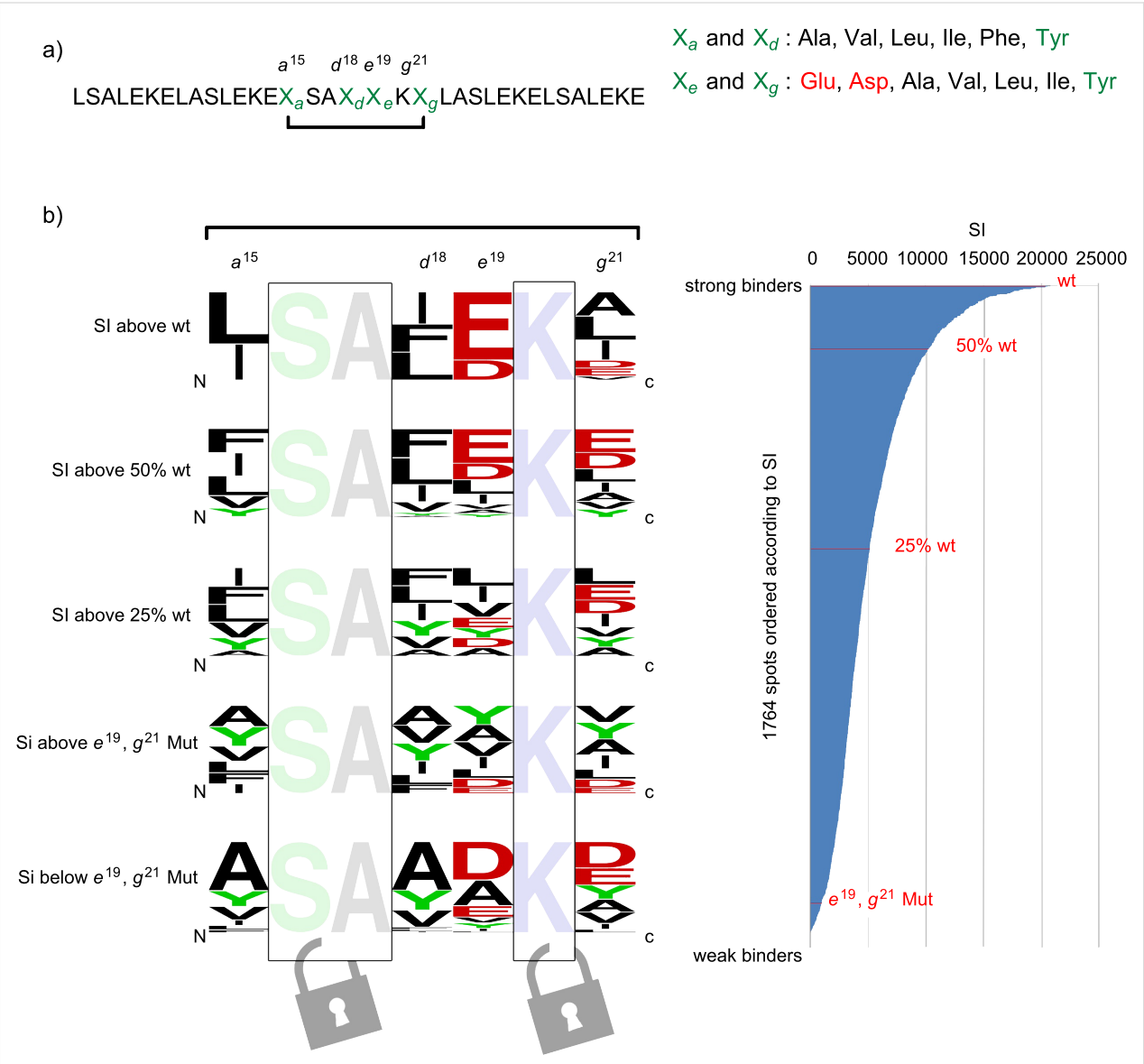

Figure 2: (a) Sequence for random mutation resulting in 1764 spots. The randomized positions are denoted by X_a, X_d, X_e, and X_g, and the amino acids selected for randomization are listed on the right. (b) The sequence logos (left) indicate the frequencies of specific *a*/*d*/*e*/*g* substitutions within a class (the larger the letter, the higher the frequency). The mutated positions *a*, *d*, *e*, and *g* are denoted by 15, 18, 19, and 21, respectively. The graph (right) displays the signal intensity (SI) of the 1764 spots and is ordered from strong to weak binders. Indicated are the four interaction classes grouped according to SIs relative to the Acid-pp wt SI and the e^{19},g^{21} mutant.

natural peptide that are crucial for the coiled-coil interaction with the chimeric sequence, the residues located close to and within the interhelical core (*a*,*d*,*e*,*g*), which are most important for molecular recognition, were mutated. More specifically, hydrophobic (a^{15},d^{18}) and electrostatic (e^{19},g^{21}) positions were mutated simultaneously (Figure 2). The 35mer mutants on the membrane only differ in the positions that interact with side chains of the β- and γ-residues.

Mutational analysis of the selected positions (a^{15},d^{18},e^{19} and g^{21}) was carried out with a chosen set of amino acids (Figure 2a, right) to characterize the suitable side-chain composition for optimal interaction with the βγ-foldameric pattern on the chimeric αβγ-sequence.

Thereby, the most favorable amino acid side chains at each key position were identified. Since the *a* and *d* positions are typically occupied by hydrophobic residues in most of the naturally occurring coiled-coil sequences, the mutations at a^{15} and d^{18} positions incorporated only hydrophobic amino acids, including the sterically bulky ones. To support heteroassembly between the αβγ-chimeric sequences and their natural counterparts, the complementary negative side chains of Glu and Asp residues as well as a series of hydrophobic side chains were considered at the e^{19} and g^{21} positions. Interactions between the chimera and immobilized α-mutants were measured by using a peptide array assay.

Additionally, to ensure that the chimera interacts with the surface-bound peptides at the aforementioned hydrophobic (*a* and *d*) and electrostatic (*e* and *g*) positions, several positions relevant to coiled-coil binding were replaced with glycine. As depicted in Figure 3, both/either (i) hydrophobic (a^{15},d^{18}) and/or electrostatic (e^{19},g^{21}) positions of the central heptad or (ii) essential hydrophobic positions in the flanking heptads were substituted with glycine. This set of sequences was used to evaluate the quality of interaction between the side chains of immobilized α-mutants and the complementary αβγ-chimeric sequence.

Spot analysis: A peptide array containing the multiple substitutions was incubated with the chimera, and spot signal intensities of the resulting heteromeric associations were measured and evaluated. The measured signal intensities (SI) obtained from the TAMRA-labeled modified sequence interacting selectively with immobilized α-peptides, were classified as described above. Remarkably, despite their limited sequence variability, the α-mutants exhibited various degrees of binding affinity to the chimera. Based on the SI values, the α-mutants were classified into five interaction groups. As depicted in Figure 2 on the right-hand side, sequences with equal or slightly higher SI values compared to Acid-pp were classified as strong binders (only 22 representatives). The second and third classes contain the mutants with SI values lower than those of the strong binders but still above 50% and 25% of that of Acid-pp, respectively. The poor binders have SI values below 25% of that of Acid-pp. This group also contains the aforementioned glycine-mutants. For each class we computed the residue frequencies at the mutated positions *a*, *d*, *e*, and *g* of the central heptad and summarized the results as sequence logos (Figure 2, left). At

Figure 3: Glycine scanning of Acid-pp sequences. The substituted glycines are highlighted in red. Each sequence is followed by its corresponding spot (three replicas each). White spots indicate interactions between cellulose membrane-bound variants of Acid-pp and the TAMRA-labeled chimera.

each position, the residues are arranged in order of predominance from top to bottom, and the mutants we selected are named after the respective combinations of four mutated residues. The frequencies of specific side chains in the recognition domain indicate the preferred interactions between the β- and γ-amino acids and the complementary side chains of the natural α-partners. These results suggest that only a few mutants are able to interact efficiently with B3β2γ.

The glycine-scan (Figure 3) reveals the nature of the chimeric coiled-coil interaction. Only the acid-pp *wt* shows strong binding to B3β2γ. If the hydrophobic or electrostatic regions essential for coiled-coil binding are blocked by glycine, the signal breaks down. As expected, the glycine scanning of the hydrophobic residues at *a* and *d* positions of the flanking heptads (a,d^{flank}Mut) results in a diminishing of interactions between chimera and the natural partner peptide. Remarkably, the replacement of only two hydrophobic side chains located at the central heptad is equally destabilizing for the entire assembly, indicating the key role of the interhelical interactions between the third heptad of the native sequences and foldameric section of the chimera. Manipulation of the interacting native amino acids on the third heptad (a^{15},d^{18}Mut), (e^{19},g^{21}Mut), (a^{15},d^{18},e^{19},g^{21}Mut) resulted in a loss of binding, which strongly suggests that the quaternary structure does not only tolerate but is in fact dependent on the interaction of the central heptad of natural peptides with side chains of the unnatural amino acids on the chimera.

As a negative control, the binding affinity of the modified sequences was tested against a randomly designed αβγ-chimeric sequence, R3β2γ (Figure 1b). In the R3β2γ sequence, all of the amino acids including β- and γ-residues are randomly distributed. The screening of the peptide library against this chimeric peptide results in a poor binding profile. Interestingly, and in contrast to the randomly designed R3β2γ, the sequences on the membrane show remarkable selectivity in the binding to B3β2γ.

In general, a direct relation exists between the observed light intensity and the heteroassociation between chimera and mutants on the membrane. More importantly, the implicit binding affinities are highly consistent with previously published data [18]. In our previous study we reported a gradual destabilization of the chimeric coiled-coil assembly with gradual truncation of the β- and γ-side chains at the hydrophobic core due to a loss of hydrophobic interactions between the αβγ-peptide and its natural α-partner. Similarly, the interactions between the peptides on the array and the chimera decrease drastically in sequences presenting the shorter side chains of Val and Ala at *a* and *d* positions, compared to mutants with the longer and more bulky side chains of Leu, Ile, and Phe (Figure 4, right). Furthermore, the negligible binding affinities between the chimera and the control sequences, in which the hydrophobic and electrostatic residues were replaced with glycine residues, indicate that B3β2γ prefers mutants that provide sufficient side-chain–side-chain contact.

The peptide array detected many new side-chain combinations, the investigation of which provides useful insights into the complex contact networks of an αβγ-chimeric folding motif. Enlarging the interior cavity of coiled coils by positioning the backbone extended β- and γ-amino acids in the hydrophobic

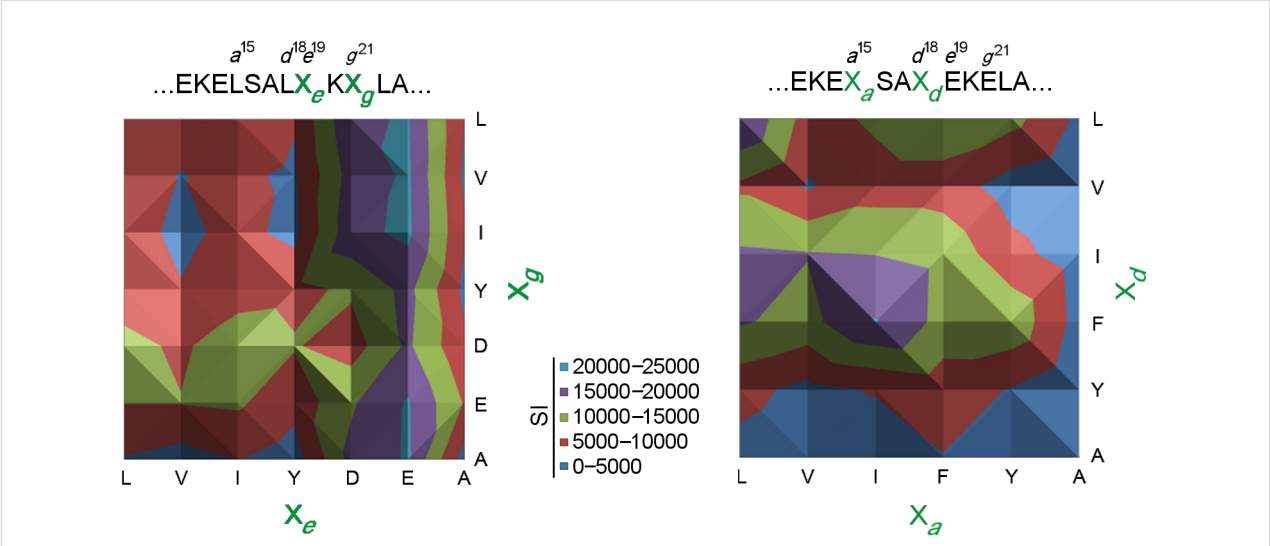

Figure 4: Heat-map diagrams depicting the quantitatively measured SIs for Acid-pp sequences containing mutations at positions e^{19} and g^{21} (left) and at positions a^{15} and d^{18} (right) in heptad III. The SIs corresponding to each color are displayed between the heat maps.

core necessitates compatible coverage. This requirement is confirmed by the sequence logo for strong binders (Figure 2b, first on top): A stronger peptide–peptide interaction was observed between the chimeric pattern of B3β2γ and the α-mutants with large and bulky hydrophobic residues, for instance the aromatic Phe, the long and bulky Leu, and the β-branched Ile.

Remarkably, the preference for hydrophobic residues is highly position-dependent (Figure 3b and Figure 4); Phe is favored at the *d* position, while Leu is more prevalent in the *a* position. Moreover, substitution of a single hydrophobic position with tyrosine ($L^{15}Y$) in the $Y^aL^dE^eE^g$ mutant results in a significant reduction in the spot intensity compared to that of *wt* Acid-pp. As already discussed, despite the similarity in size between Phe and Tyr residues, they exhibit prominent differences in the coiled-coil formation that are probably due to the destabilizing orientation of the polar hydroxyl group towards the hydrophobic core [21]. The clear decrease in binding affinity between chimera and Tyr-comprising mutants shows that the side chains at the artificial interface of the helix bundle experience an environment similar to that of natural coiled coils.

Another important observation is that, although they provide sufficient hydrophobicity at the interhelical domain, the mutants with two Phe residues are among the weaker binders (Figure 4, right). This is also true for the β-branched Ile; substitution with two Ile residues results in a medium binding affinity (Figure 4). This can be explained by the fact that, similarly to that of native coiled coils, the chimeric hydrophobic core is disrupted by excessively bulky side chains [22]. However, the preference for specific hydrophobic side chains in *a* and *d* positions and of unique combinations thereof indicates that the selection of residues in the hydrophobic core is determined not only by side-chain hydrophobicity but also by side-chain packing. The packing geometry is thus an important aspect influencing the stability of artificial coiled coils. These results additionally confirm the impact of electrostatic interactions at the *e* and *g* positions. The SI values of sequences mutated in these positions show that shortening of the negatively charged side chain in the case of the $Glu^{e19}Asp$ exchange, results in a general decline in binding affinity for almost all mutants presented on the membrane (Figure 2, left and Figure 4, left). However, there is a discrepancy between the two core-flanking positions; the *e* position was found to be significantly more sensitive to replacement than the supposedly similar *g* position. This fact has also been observed and reported for natural coiled coils [23]. The different interaction profiles of the side chains at *e* and *g* positions (Figure 4, left) can be caused by the asymmetrical geometry of complementary Lys side chains on the βγ-foldameric interaction partner. A further interesting observation is that hydrophobic residues populate the core-flanking positions, which suggests that the side chains at these positions lead to an extension of the hydrophobic core.

Solution study: To gain more insight into the relationship between hetero-selective binding and structural stability, several mutants from different classes were studied further in solution (Figure 5a). These sequences were synthesized on resin, purified, and finally investigated by CD and size-exclusion chromatography. We chose $I^aF^dE^eE^g$ as a representative of the strong binders to be tested in solution because of the frequently repeated positioning of Phe in the hydrophobic core, that is, more specifically at the *d* positions. Moreover, the behavior of $V^aV^dE^eE^g$ and $G^aG^dE^eE^g$, belonging to the medium and poor binder classes, respectively, was tested in solution (Figure 4). Another mutant we selected is $L^aL^dD^eD^g$, in which both e^{19} and g^{21} positions are occupied by Asp, which, according to the observed SIs, leads to weaker binding affinity to the chimera compared to Acid-pp.

An extremely weak interaction between B3β2γ and $G^aG^dE^eE^g$, indicated by a low spot signal intensity, was further confirmed in solution by a drastic decrease in helical content and structural stability (Figure 5b). This result identifies the side chains at a^{16} and d^{19} positions and their complementary β^3Leu side chains on the chimera as hot spots in the chimeric recognition motif; interaction with these residues could lead to an increase in binding selectivity and stability.

An equimolar solution of B3β2γ/$L^aL^dD^eD^g$ and B3β2γ/$V^aV^dE^eE^g$ showed medium spot intensities (SIs of 7568 and 4487, respectively) with minima at 222 nm and 208 nm, which are less intense when compared with B3β2γ/Acid-pp (Figure 5a). Furthermore, the thermal melt T_m values of B3β2γ/$L^aL^dD^eD^g$ (T_m = 64 °C) and B3β2γ/$V^aV^dE^eE^g$ (T_m = 52 °C) also dropped in comparison to the parental system (Figure 5c). As expected, shortening of the side chains in the hydrophobic core, by replacing Leu side chains with Val in $V^aV^dE^eE^g$, had a more pronounced destabilizing effect on selectivity and stability of the resulting quaternary structure than did substitution of Glu side chains with Asp in core-flanking positions in the $L^aL^dD^eD^g$ mutant. This fact is also reflected in their different spot intensities; the signal intensity of the $L^aL^dD^eD^g$ mutant is almost half of that observed for $V^aV^dE^eE^g$.

In an analogous manner, the highly intense spot provided by interaction of the $I^aF^dE^eE^g$ mutant with B3β2γ was confirmed further in solution by the intensive canonical minima of the α-helical coiled-coil structure at 222 and 208 nm and the relatively high thermal stability (Figure 5b, Figure 5c). The combi-

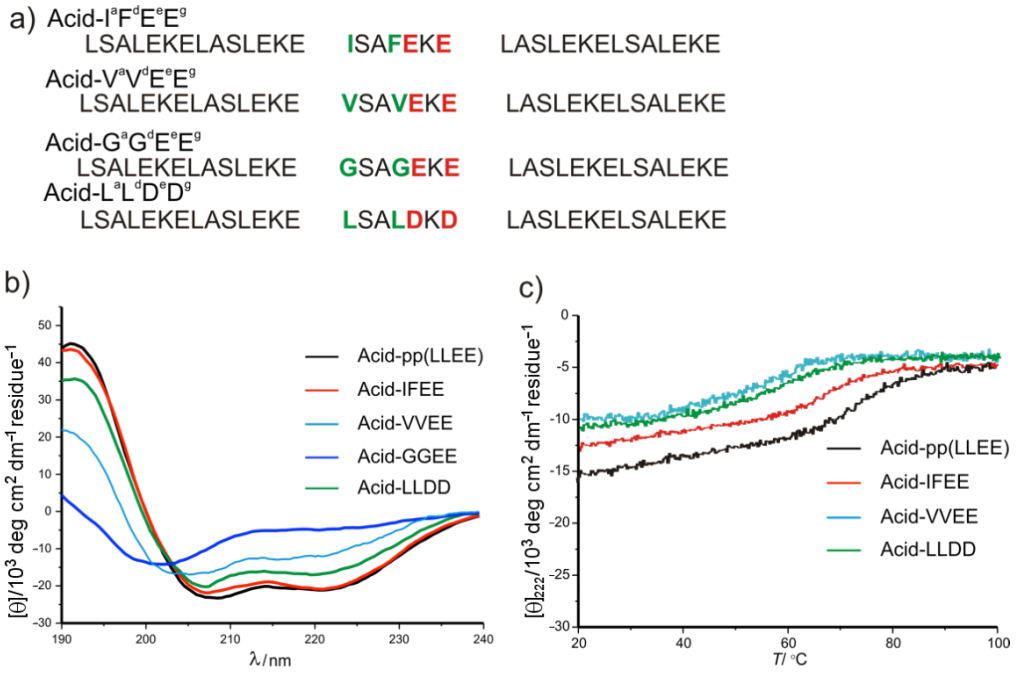

Figure 5: (a) The complete sequences of the selected α-mutants. (b) CD and (c) thermal denaturation spectra of an equimolar mixture of B3β2γ and the α-mutants (25 μM of peptide concentration in phosphate buffer 50mM in presence of 250 mM GndHCl).

nation of Phe at *d* and Ile at *a* positions resulted in a significantly high binding affinity between I^{a}F^{d}E^{e}E^{g} and the chimera. Thermal denaturation of an equimolar mixture of B3β2γ and I^{a}F^{d}E^{e}E^{g} resulted in relatively high T_m values of 70 °C, which are close to those of an equimolar mixture of B3β2γ and Acid-pp (T_m values of 74 °C).

In order to compare both the packing effects and the burial of the hydrophobic surface of various side-chain compositions, the oligomerization states of the corresponding helix bundles of B3β2γ with native mutants were further studied by size-exclusion chromatography (SEC).

The retention-time (T_R) value of each mixed system was compared with an equimolar solution of B3β2γ/Acid-pp as a tetrameric reference structure (Figure 6) [18]. The SEC results show that, in analogy to B3β2γ/Acid-pp, tetramers are the predominant oligomerization state in all probed equimolar mixtures of B3β2γ/L^{a}L^{d}D^{e}D^{g}, B3β2γ/V^{a}V^{d}E^{e}E^{g}, and B3β2γ/I^{a}F^{d}E^{e}E^{g} in aqueous solution (59 min). In the case of B3β2γ/I^{a}F^{d}E^{e}E^{g}, despite the presence of tetrameric helix bundles, other species consistent with a higher order of oligomers can be observed; this has also been indicated by SEC at about 45 min. Whereas the stoichiometry of the interaction on the membrane is considered to be 1:1, the geometry of Phe residues at the

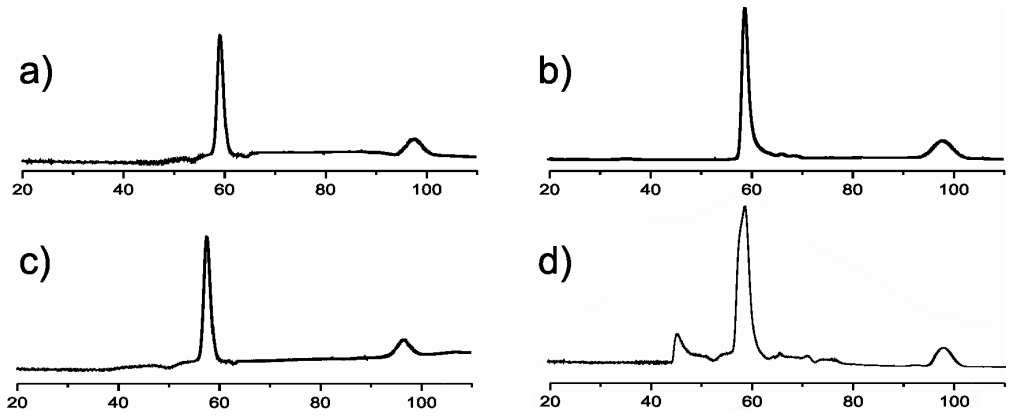

Figure 6: Size-exclusion chromatograms of equimolar mixtures of B3β2γ with (a) Acid-pp, (b) V^{a}V^{d}E^{e}E^{g}, (c) L^{a}L^{d}D^{e}D^{g}, and (d) I^{a}F^{d}E^{e}E^{g} (50 μM of peptide concentration in phosphate buffer 100 mM). The chromatogram of the tetrameric B3β2γ/Acid-pp helix bundle serves as the reference.

hydrophobic core suggests the possibility of aromatic ring stacking in solution. This type of side chain has the distinct feature of being largely indiscriminate in defining a specific oligomerization state; however, it is tolerant of large assemblies [24,25].

Overall, the binding affinities between native mutants and B3β2γ in solution follow the same trends found for the spot intensities on the membrane. The great sequence similarity between synthesized mutants and *wt* sequence allows the study of the impact of new side-chain compositions at *a* and *d* positions.

Conclusion

A challenge associated with the design of artificial quaternary structures formed by foldameric sequences is to find a suitable α-partner that selectively binds with high affinity. The fact that amino acid side chains exhibit different characteristics depending on the sequence (i.e., structural) context, further complicates the recognition of well-suited side-chain compositions required for a specific interaction between bioactive foldamers and natural targets. This report has presented the application of a simple and sensitive peptide array technique to selectively form stable α-helical coiled-coil structures with an αβγ-chimera. The overall analysis of the interaction between α-partners and αβγ-chimera provides valuable information about the interaction environment accessible to the chimeric motif. Interestingly, small changes (even single mutations) in the sequence of the immobilized α-mutants result in drastic changes in the interaction profile of the αβγ-chimera. Furthermore, this study has identified the residues crucial for forming the recognition epitope of the foldameric βγ-pattern in dependence of the interaction affinities resulting from side-chain mutations in *a* and *d* positions, as well as *e* position of the interacting α-partners. It is also important to note that the coiled-coil pairing selectivity is profoundly increased by bulky hydrophobic side chains at core and core-flanking positions. In terms of binding affinities, the intolerance of these positions to substitution with small or polar amino acids is evidence for the existence of an enlarged interior cavity formed by extended-backbone amino acids, which requires more-space-filling side chains to exclude the surrounding aqueous solution. Finally, these observations suggest that spot technology is an excellent and reliable technique for generating natural sequences that suitably interact with unknown patterns forming artificial coiled-coils.

Experimental

SPOT-synthesis (analogous to a procedure from [26])**:** Cellulose-bound peptide arrays were prepared according to standard SPOT synthesis protocols by using a SPOT synthesizer (Intavis, Köln, Germany) as described in detail in [15]. The peptides were synthesized on amino-functionalized cellulose membranes (Whatman, Maidstone, Great Britain) of the ester type prepared by modifying cellulose paper with Fmoc-β-alanine as the first spacer residue. In the second coupling step, the anchor position Fmoc-β-alanine-OPfp in dimethylsulfoxide (DMSO) was used. Residual amino functions between the spots were capped by acetylation. The Fmoc group was cleaved by using 20% piperidine in dimethylformamide (DMF). The cellulose-bound peptide arrays were assembled on these membranes by using 0.3 M solutions of Fmoc-amino acid-OPfp in 1-methyl-2-pyrrolidone (NMP). The side-chain protection of the Fmoc-amino acids used was as follows: Glu, Asp (O*t*-Bu); Ser, Thr, Tyr (*t*-Bu); His, Lys, Trp (Boc); Asn, Gln, Cys (Trt); Arg (Pbf). After the last coupling step, the acid-labile protection groups of the amino acid side chains were cleaved by using 90% trifluoroacetic acid (TFA) for 30 min and 60% TFA for 3 h. To ensure adequate quality, the peptides to be analyzed were cleaved from the membrane by using the standard protocol as described by Wenschuh et al. [15] and dissolved in water (using 10% acetonitrile to increase solubility, if necessary). HPLC analysis (Waters, Milford, USA) was conducted by using a linear solvent gradient (A: 0.05% TFA in water; B: 0.05% TFA in acetonitrile; gradient: 5–60% B over 30 min; UV detector at 214 nm; RP-18 column). α-cyanocinnamic acid was used as a matrix for MALDI–TOF (Applied Biosystems, Forster City, USA) MS analysis.

Binding studies on cellulose membranes [26]**:** All incubation and washing steps were carried out under gentle shaking and at room temperature. After washing of the membrane with ethanol once for 10 min and three times for 10 min with tris-buffered saline (TBS: 50 mM tris(hydroxymethyl)aminomethane, 137 mM NaCl, 2.7 mM KCl, adjusted to pH 8 with HCl/0.05%), the membrane-bound peptide arrays were blocked (3 h) with blocking buffer (casein-based blocking buffer concentrate (Sigma-Genosys, Cambridge, UK), 1:10 in TBS containing 5% (w/v) sucrose), and then washed with TBS (1 × 10 min). Subsequently, the peptide arrays were incubated with the labeled analytes (c = 10 μM) for 10 min in TBS blocking buffer. After washing for 120 min with TBS, analysis and quantification of peptide-bound TAMRA was carried out by using a Lumi-Imager.

Measurement of spot signal intensities [26]**:** Binding events (TAMRA-fluorescence) were recorded on a cooled CCD-camera by using a Lumi-Imager (Roche, Indianapolis, USA). The signal intensity (SI) of each spot was calculated by defining a spot radius that can be optimally applied to all spots in the image and taking the median value of the pixel intensity. The

background signal was determined with a safety margin to the circular region of each spot, and then the global background mean was subtracted from each individual spot signal. This parameter is referred to as SI. Grid layer and SI were calculated by using dedicated image analysis software: GeneSpotter has a fully automatic grid-finding routine resulting in reproducible signal intensities. The median value of the intraspot distribution was sufficient to avoid saturation. Results are shown as the interspot global background-corrected mean value over three replica spots for each sequence. TAMRA was measured at 645 nm. The aforementioned wavelength was chosen to detect TAMRA at lower background noise.

Peptide synthesis and characterization (analogous to [18])**:** Peptides were synthesized by using standard, automated Fmoc solid-phase synthesis (0.05 mM scale) using a SyroXP-I peptide synthesizer (MultiSyn Tech GmbH, Witten, Germany) and HOBT/TBTU activation. Manual coupling of β- and γ-amino acids was carried out by HOAT/DIC activation. The molar excess of amino acid and coupling reagents was reduced for β- and γ-residues to twofold for the first and onefold for the second coupling. The completion of these couplings was indicated by a negative Kaiser test. Prior to each deprotection step, capping of the possibly nonacylated N-termini was carried out by treatment with 10% acetic anhydride and 10% DIEA in DMF (3 × 10 min). Peptide cleavage from resin was performed by using 95% trifluoroacetic acid, 2.5% triisopropylsilane, and 2.5% water. Peptides were purified by HPLC on a C-18 preparative column using gradients between 0.1% TFA in water and 0.1% TFA in acetonitrile. All peptides were >95% pure by analytical HPLC on a C-8 column (Phenomenex® Luna C8, 10 μM, 250 mm × 21.2 mm). The identities of peptides were confirmed using an ESI–TOF instrument.

Circular-dichroism (CD) spectroscopy [18]**:** Peptide samples were analyzed in 10 mM phosphate buffer (pH 7.4). Far-ultraviolet circular-dichroism spectra and GndHCl unfolding profiles were recorded on a J-810 spectropolarimeter (Jasco GmbH, Gross-Umstadt, Germany) equipped with a temperature controlled quartz cell of 0.1 cm path length. The recorded spectra were evaluated with the Jasco software package. The spectra were the average of three scans obtained by collecting data from 190–240 nm at 0.2 nm intervals, 2 nm bandwidth, and 1 s response time. Ellipticity data in mdeg were converted to conformation parameters by the following equation: $[\theta] = [\theta]_b \times mrw/10 \times l \times c$, where $[\theta]_b$ is the ellipticity measured in degrees, mrw is the mean residue molecular weight (molecular weight of the peptide divided by the number of amino acid residues), c is the peptide concentration in g/mL, and l is the optical path length of the cell in cm. Denaturation was carried out in 0.5 °C intervals with a heating rate of 3 °C min^{-1}. The midpoints of the thermal melts, T_ms, were taken as the maximum of the derivative d(Fraction unfolded)/dT.

Size-exclusion chromatography (SEC) [18]**:** The measurements were performed on a VWR-Hitachi Elite LaChrome system (Pump L-2130, UV Detector L-2400, VWR, Germany) equipped with a Superdex 75 PC 3.2/30 column from Amersham Biosciences. The peptides were analyzed in 100 mM sodium phosphate pH 7.4 with a flow rate of 0.025 mL/min. Peptide absorbance was registered at 220 nm. The retention times were corrected with internal and external references. Glyanthranilic acid was used as an internal reference. GCN4-pLI was employed as a reference for tetrameric coiled coils [27], because its monomer size is comparable to that of the model system used in this study.

Supporting Information

Supporting Information File 1

Complete set of SPOT intensities.
[http://www.beilstein-journals.org/bjoc/content/supplementary/1860-5397-8-71-S1.pdf]

References

1. Lupas, A. *Trends Biochem. Sci.* **1996,** *21,* 375. doi:10.1016/S0968-0004(96)10052-9
2. Burkhard, P.; Stetefeld, J.; Strelkov, S. V. *Trends Cell Biol.* **2001,** *11,* 82. doi:10.1016/S0962-8924(00)01898-5
3. Strauss, H. M.; Keller, S. –Pharmacological Interference with Protein–Protein Interactions Mediated by Coiled-Coil Motifs. In *Protein–Protein Interactions as New Drug Targets;* Klussmann, E.; Scott, J., Eds.; Handbook of Experimental Pharmacology, Vol. 186; Springer: Berlin, Heidelberg, 2008; pp 461 ff. doi:10.1007/978-3-540-72843-6_19
4. Bianchi, E.; Finotto, M.; Ingallinella, P.; Hrin, R.; Carella, A. V.; Hou, X. S.; Schleif, W. A.; Miller, M. D.; Geleziunas, R.; Pessi, A. *Proc. Natl. Acad. Sci. U. S. A.* **2005,** *102,* 12903. doi:10.1073/pnas.0502449102
5. Russell, R. J.; Kerry, P. S.; Stevens, D. J.; Steinhauer, D. A.; Martin, S. R.; Gamblin, S. J.; Skehel, J. J. *Proc. Natl. Acad. Sci. U. S. A.* **2008,** *105,* 17736. doi:10.1073/pnas.0807142105
6. McFarlane, A. A.; Orriss, G. L.; Stetefeld, J. *Eur. J. Pharmacol.* **2009,** *625,* 101. doi:10.1016/j.ejphar.2009.05.034
7. Gentilucci, L.; De Marco, R.; Cerisoli, L. *Curr. Pharm. Des.* **2010,** *16,* 3185. doi:10.2174/138161210793292555
8. Gellman, S. H. *Acc. Chem. Res.* **1998,** *31,* 173. doi:10.1021/ar960298r
9. Cheng, R. P.; DeGrado, W. F. *J. Am. Chem. Soc.* **2001,** *123,* 5162. doi:10.1021/ja010438e
10. Seebach, D.; Beck, A. K.; Bierbaum, D. J. *Chem. Biodiversity* **2004,** *1,* 1111. doi:10.1002/cbdv.200490087
11. Farmer, P. S.; Ariëns, E. J. *Trends Pharmacol. Sci.* **1982,** *3,* 362. doi:10.1016/0165-6147(82)91184-1

12. Volkmer, R. *ChemBioChem* **2009,** *10,* 1431. doi:10.1002/cbic.200900078
13. Przezdziak, J.; Tremmel, S.; Kretzschmar, I.; Beyermann, M.; Bienert, M.; Volkmer-Engert, R. *ChemBioChem* **2006,** *7,* 780. doi:10.1002/cbic.200500408
14. Portwich, M.; Keller, S.; Strauss, H. M.; Mahrenholz, C. C.; Kretzschmar, I.; Kramer, A.; Volkmer, R. *Angew. Chem.* **2007,** *119,* 1682. doi:10.1002/ange.200603246
15. Wenschuh, H.; Volkmer-Engert, R.; Schmidt, M.; Schulz, M.; Schneider-Mergener, J.; Reineke, U. *Biopolymers* **2000,** *55,* 188. doi:10.1002/1097-0282(2000)55:3<188::AID-BIP20>3.0.CO;2-T
16. Lupas, A. N.; Gruber, M. *Adv. Protein Chem.* **2005,** *70,* 37. doi:10.1016/S0065-3233(05)70003-6
17. Moutevelis, E.; Woolfson, D. N. *J. Mol. Biol.* **2009,** *385,* 726. doi:10.1016/j.jmb.2008.11.028
18. Rezaei Araghi, R.; Jäckel, C.; Cölfen, H.; Salwiczek, M.; Völkel, A.; Wagner, S. C.; Wieczorek, S.; Baldauf, C.; Koksch, B. *ChemBioChem* **2010,** *11,* 335. doi:10.1002/cbic.200900700
19. Rezaei Araghi, R.; Baldauf, C.; Gerling, U. I. M.; Cadicamo, C. D.; Koksch, B. *Amino Acids* **2011,** *41,* 733. doi:10.1007/s00726-011-0941-z
20. Rezaei Araghi, R.; Koksch, B. *Chem. Commun.* **2011,** *47,* 3544. doi:10.1039/c0cc03760e
21. Sakurai, Y.; Mizuno, T.; Hiroaki, H.; Oku, J.-I.; Tanaka, T. *J. Pept. Res.* **2005,** *66,* 387. doi:10.1111/j.1399-3011.2005.00304.x
22. Betz, S. F.; Bryson, J. W.; DeGrado, W. F. *Curr. Opin. Struct. Biol.* **1995,** *5,* 457. doi:10.1016/0959-440X(95)80029-8
23. Mahrenholz, C. C.; Abfalter, I. G.; Bodenhofer, U.; Volkmer, R.; Hochreiter, S. *Mol. Cell. Proteomics* **2011,** *10,* M110. doi:10.1074/mcp.M110.004994
24. Tripet, B.; Wagschal, K.; Lavigne, P.; Mant, C. T.; Hodges, R. S. *J. Mol. Biol.* **2000,** *300,* 377. doi:10.1006/jmbi.2000.3866
25. Yoder, N. C.; Kumar, K. *J. Am. Chem. Soc.* **2006,** *128,* 188. doi:10.1021/ja055494k
26. Mahrenholz, C. C.; Tapia, V.; Stigler, R. D.; Volkmer, R. *J. Pept. Sci.* **2010,** *16,* 297. doi:10.1002/psc.1237
27. Harbury, P. B.; Zhang, T.; Kim, P. S.; Alber, T. *Science* **1993,** *262,* 1401. doi:10.1126/science.8248779

License and Terms